Hydraulics of Spillways and Energy Dissipators

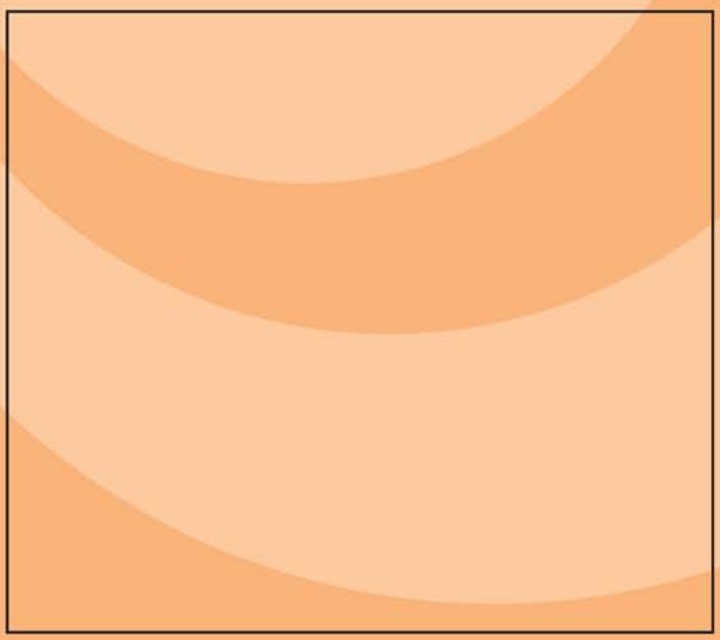

R. M. Khatsuria

Hydraulics of Spillways and Energy Dissipators

Civil and Environmental Engineering

A Series of Reference Books and Textbooks

Editor

Michael D. Meyer

Department of Civil and Environmental Engineering
Georgia Institute of Technology
Atlanta, Georgia

1. Preliminary Design of Bridges for Architects and Engineers
   Michele Melaragno
2. Concrete Formwork Systems
   Awad S. Hanna
3. Multilayered Aquifer Systems: Fundamentals and Applications
   Alexander H.-D. Cheng
4. Matrix Analysis of Structural Dynamics: Applications and Earthquake Engineering
   Franklin Y. Cheng
5. Hazardous Gases Underground: Applications to Tunnel Engineering
   Barry R. Doyle
6. Cold-Formed Steel Structures to the AISI Specification
   Gregory J. Hancock, Thomas M. Murray, Duane S. Ellifritt
7. Fundamentals of Infrastructure Engineering: Civil Engineering Systems: Second Edition, Revised and Expanded
   Patrick H. McDonald
8. Handbook of Pollution Control and Waste Minimization
   Abbas Ghassemi
9. Introduction to Approximate Solution Techniques, Numerical Modeling, and Finite Element Methods
   Victor N. Kaliakin
10. Geotechnical Engineering: Principles and Practices of Soil Mechanics and Foundation Engineering
    V. N. S. Murthy

Additional Volumes in Production

Chemical Grouting and Soil Stabilization: Third Edition, Revised and Expanded
Reuben H. Karol

Estimating Building Costs
Calin M. Popescu, Kan Phaobunjong, Nuntapong Ovararin

Hydraulics of Spillways and Energy Dissipators

R. M. Khatsuria

Marcel Dekker New York

Library of Congress Cataloging-in-Publication Data
A catalog record for this book is available from the Library of Congress.

ISBN: 0-8247-5789-0

This book is printed on acid-free paper.

Headquarters
Marcel Dekker, 270 Madison Avenue, New York, NY 10016, U.S.A.
tel: 212-696-9000; fax: 212-685-4540

Distribution and Customer Service
Marcel Dekker, Cimarron Road, Monticello, New York 12701, U.S.A.
tel: 800-228-1160; fax: 845-796-1772

World Wide Web
http://www.dekker.com

Current printing (last digit):

10 9 8 7 6 5 4 3 2 1

PRINTED IN THE UNITED STATES OF AMERICA

To My Parents

Preface

The need for a comprehensive book dealing in hydraulics of spillways and energy dissipators has been realized since long. Various topics pertaining to the spillways and energy dissipators are available in the sources devoted mainly to the design of dams, text books on hydraulics and open channel flow and handbooks of hydraulics. However, advances in research and design, generally published through papers presented at the specialty conferences and journals, are seldom disseminated wide enough for application on a general scale. Consequently, the rift between the advancements in knowledge and its formal documentation in the books and treatise grows wider. Of the many examples illustrating this lag, a typical one is the aerator on spillways to mitigate cavitation damage. Although, the beneficial effects of aeration were known in the early fifties, considerable research had been pursued, to understand hydraulics of the phenomenon, from the sixties and aeration devices were installed on the existing structures in the late seventies, it was not until the eighties that aeration devices became an integral part of spillway design. It is noteworthy that no book on spillways published until the late eighties included the topic of aeration, and reference sources remained scattered in journals and proceedings.

This practice of lag continues, as several topics of vital significance have not been embodied comprehensively and coherently into any of the book literature. A few to mention include: spillway construction stages, spillways serving dual purpose of flood as well as sediment disposal, overtopping protection of earth dams used as spillways, prediction of and protection against detrimental forces such as uplift, cavitation, scour etc. It is obvious that such a book would be the easiest way for a reader to access the information on the latest developments in the field. The present book is the outcome of such an attempt.

The book has been organized into four sections dealing with spillways, energy dissipators, cavitation and air entrainment, and hydraulic modeling. Emphasis has been on discussing first the hydraulics of different types of spillways and energy dissipators and to illustrate its application to practical design problems. To this end, illustrative examples have been included at appropriate places.

The first two chapters in section I introduce the topic and broad design philosophy. The chapter on spillway design flood defines two distinct aspects: the estimation, which is hydrologist's regime and the selection, which is the responsibility of the designer. Subsequent chapters have been devoted to discussion on hydraulics and general design features of different types of spillways such as ogee, chute and side channel, stepped, siphon, shaft, tunnel, labyrinth and duck bill, free jet and fuse plug etc. Special features such as spillways for flood and sediment disposal, inflatable rubber weirs and overtopping protection of dams used as spillways have also been included. Separate chapters on spillway crest gates and spillway construction stages have been written.

Discussions on the three most common types of energy dissipators for spillways, viz. hydraulic jump stilling basins, trajectory buckets and submerged roller buckets in section II, have been quite elaborate, obviously in view of the large amount of information published during recent years. Energy dissipators for shaft and tunnel spillways warrant a special chapter in view of peculiar hydraulic conditions at the outfalls. Separate chapters have been devoted to the discussion of impact type energy dissipators and some unconventional or special designs of energy dissipators.

Section III includes chapters on the topics of cavitation and air entrainment and aerators concerning the design of spillways and energy dissipators.

Hydraulic modeling of spillways and energy dissipators has been covered in section IV. No attempt has been made to discuss the theory of similitude and hydraulic models, found in many books. On the other hand, emphasis has been placed on topics of scale effect; dynamic flow measurement and aspects of analysis and interpretation of model results. It is hoped that this will be useful, to not only research engineers, but also to the designers and practicing engineers directing the model studies.

In the field of technology, a continuous stream of development and improvement adds to the knowledge. Therefore, nothing can be claimed as exhaustive or final. Similarly, it is equally difficult to decide what is old or obsolete. The difficult task was therefore to evaluate every piece of information from the standpoint of practical utility, be it for the researcher, designer, practicing engineer or student. While this book is not intended to be a textbook to cater to any specific curriculum, nor a handbook, it is expected to serve as a comprehensive reference source for all concerned. It is hoped that the reader will be able to obtain an extensive exposure of the topic, beyond which the references listed at the end of the chapters will be useful for locating additional details.

Experience gained during my association, of nearly four decades, with the Central Water and Power Research Station, Pune—an institution of international reputation and discussions with several experts in the field of their own specialist knowledge, have greatly contributed to writing of the book. Thanks are also due to friends and colleagues for their help and encouragement which lent a strong

impetus toward the completion of this book. My wife Kala, daughters Pallavi, Reshma, and son-in-law Praveen extended support throughout the writing of the book.

I have pleasure in placing on record, my appreciation for the excellent coordination by Mr. B.J. Clark, Executive Acquisitions Editor, Mr. E.F. Stannard, Senior Production Editor and Ms. Kerry Doyle, Director, Book Editorial, Marcel Dekker, Inc. at various stages of publication of the book.

Feedback from the readers in respect of any omission or error as also their comments and suggestions to improve upon the contents of the book, shall be gratefully appreciated.

R. M. Khatsuria
5/4, Krutarth Society
Behind Sharda Bank
Off: Satara Road,
PUNE - 411 037, INDIA
Email - rmkhatsuria@rediffmail.com

Acknowledgments

The author acknowledges with thanks, the following institutions, organizations and individuals who permitted to refer/reproduce their publications in this book. The details of the materials have been listed in the appropriate reference sections within the chapters.

- American Society of Civil Engineers, New York, USA
- Aqua-Media International Ltd, UK (Jnl of Hydropower and Dams)
- Bacchiega, J.D, Fattor, C.A and Barrionuevo, H.C (INA, Argentina)
- Back, Paul, Berks, UK
- BHR Group Limited, Cranfield, UK
- Canadian Society of Civil Engineers, Canada
- Central Board of Irrigation and Power (CBIP), New Delhi, India
- Chanson, H (The University of Queensland, Australia)
- Damulevicius, V and Ruplys, B (LZUU, Lithuania)
- Ervine, D.A. (The University of Glasgow, UK)
- Gao, JiZhang, IWHR, Beijing, China
- Hager, W.H., ETH, Switzerland
- Iguacel, C.M, CEDEX, Spain
- Indian Institute of Science, Bangalore, India
- Indian Society for Hydraulics, Pune, India
- Institution of Civil Engineers, London, UK
- Institution of Engineers Australia, Melbourne, (XXI IAHR 1985)
- Institution of Engineers (India), Kolkata, India
- International Association for Hydraulic Research, (IAHR), Madrid, Spain (Jnl of Hyd Res, VI–VII IAHR, 1955, 1957)
- International Congress on Large dams (ICOLD), Paris, France (ICOLD Publications)
- Japan Society of Civil Engineers, Tokyo, Japan
- Jongeling, T (Delft Hydraulics), The Netherlands
- National Hydroelectric Power Corporation Ltd, New Delhi, India

– National University of Singapore (IX APD-IAHR, 1994)
– Rathgeb, A (Wasser-und Schiffahrtsamt, Stuttgart), Germany
– SAF Laboratory, University of Minnesota, USA
– Sardar Sarovar Narmada Nigam Ltd (SSNNL), Gandhinagar, India
– Schleiss, A, EPFL, Switzerland (XXII IAHR 1987)
– Swets and Zeitlinger Publishers, (Balkema Publishers), The Netherlands
– Technische Akademie Esslingen (TAE), Germany (IAHR Symp 1984)
– Thomas Telford Publishing, London, UK (XXVI IAHR 1995)
– Plate, E, University of Karlsruhe, Germany (XVII IAHR 1977)
– United States Army Corps of Engineers (USACE), USA
– UNESCO Publishing, Paris, France
– United States Bureau of Reclamation (USBR), USA
– United States Society on Dams (USCOLD), USA
– Virginia Polytechnic Institute, USA
– Wang, Lianxiang IWHR, China (XXIX IAHR 2001)
– Wilmington Publishing, Kent, UK (Jnl of Water Power and Dam Construction)
– Wilmington Publishing, Kent, UK (Dam Engineering)
– Yugoslav Association for Hydraulic Research (YAHR), Belgrade, Serbia
– Yasuda, Y (Nihon University), Japan

Contents

Section II: Energy Dissipators

1
Spillways: Functions and Classification

1.1 INTRODUCTION

> ''He who creates a potential danger is responsible for doing everything within human power to control it.''

The function of a spillway can be best illustrated as emanating from the above well-known legal argument. Impounding large quantity of water behind a dam creates the danger of a dam-break flood wave, which could have catastrophic consequences. The safe design of a dam to avoid such a danger includes a spillway, aptly described as the safety valve of the dam-reservoir system.

1.2 NECESSITY OF A SPILLWAY

A spillway is designed to prevent overtopping of a dam at a place that is not designed for overtopping. Vischer et al. (1988) discuss the necessity of a spillway with reference to the following questions:

> Is overflowing of the reservoir possible?
> Could overtopping cause a dam failure?
> Could overtopping cause any other damage?

A reservoir will overflow if its capacity is less than the difference between the volumes of inflow and outflow. If a dam can, economically, be made high enough to provide a retention space above Full Supply Level (FSL) to absorb the entire volume of inflow design flood, no spillway would be required and an outlet such as a turbine or sluice would only be needed for regulating/utilizing storage. There are indeed a few dams where spillways were dispensable or a nominal spillway facility was all that was needed; Moric (1997) has reported two such cases. However, in a majority of cases, it is impractical to provide retention capacity

above FSL large enough to absorb the inflow design flood and, hence, a special device to surplus the extra quantity of water is required, namely a spillway.

Whether a dam would fail due to overtopping depends largely on the type of the dam in question. The most sensitive structures are earth-fill dams, which—if not specially protected—are destroyed by even a small overtopping. Masonry and concrete dams, as well as gravity and arch dams can withstand overtopping up to certain extent before they fail due to excessive stresses. However, the indirect threat to their stability due to erosion from an immediate downstream, mainly by overflowing impinging jet, would be of more concern. Overtopping of a dam may also cause other damages to the nearby structures that are not designed for such overtopping.

Considering the above, one can conclude that all dams should be constructed with a safety device, in the form of a spillway, against overtopping. The question then arises as to what portion of the total cost of the dam a spillway constitutes. The available information indicates a large variation, ranging from 4% (unlined rock spillways) to 22% (spillways for earth and rock-fill dams). Generally, spillways account for a small portion of the cost in concrete and arch dams as compared to those with earth or rock-fill dams. However, it seems more appropriate to consider the cost of a spillway in terms of each cumec released rather than the cost of the complete spillway structure in relation to the total cost of the dam. A pertinent observation in this regard is provided by Mriouah (1988), of the spillway of Oued el Makhazine dam (Morocco), where increasing the design flood 2.5 times from 3500 to 8600 cumec (dam height increased by 0.5 m) raised the overall cost of the structure by only 3%. This issue can also be considered in terms of dam safety. A United States Bureau of Reclamation (USBR) report (1983) states that spillway inadequacy represents about 40% of the dam failure hazards. Compared with this figure, the percentage cost of the spillway, especially from the standpoint of marginal cost, is usually much lower.

1.3 FUNCTIONS OF A SPILLWAY

While the principal function of a spillway is to pass down the surplus water from the reservoir into the downstream river, there are precisely seven functions that can be assigned to spillway as discussed by Takasu et al. (1988).

1. Maintaining normal river water functions (compensation water supply)
2. Discharging water for utilization
3. Maintaining initial water level in the flood-control operation
4. Controlling floods
5. Controlling additional floods

6. Releasing surplus water (securing dam and reservoir safety)
7. Lowering water levels (depleting water levels in an emergency)

It may be mentioned that the above functions have been defined for spillways and regulating outlets as per the Cabinet Orders Concerning Structural Criteria for River Administration Facilities and have been applied to all dams constructed in Japan. Part of the function under (1), (2), and (3) are combined with outlets for low water. Facilities providing function (5) are added to (4) or (6) and are collectively called outlets for high water. Function (7) is essentially for reservoir depletion, which is generally accomplished by low-level outlets. Figure 1 shows graphically the above functions in water level–discharge domain.

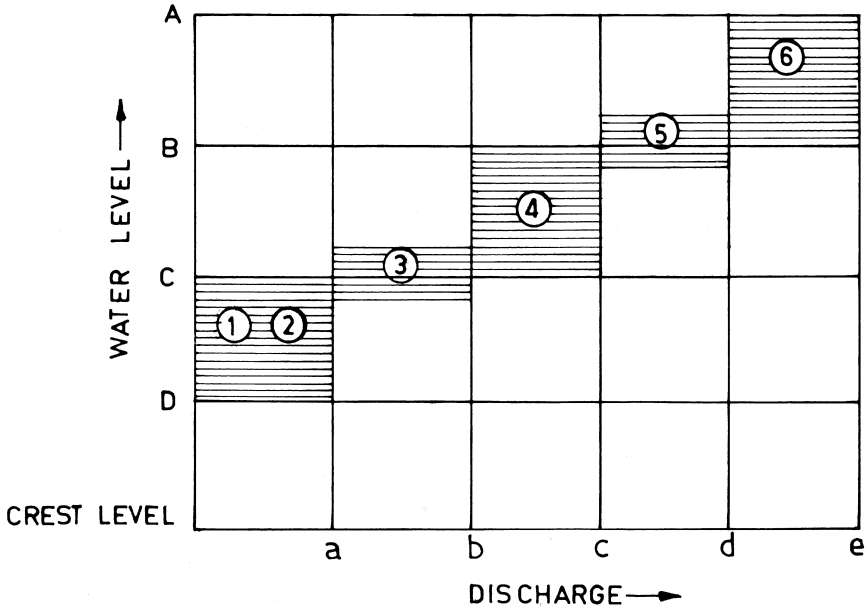

Figure 1 Functions of Spillways and Regulating Outlets. (Takasu et al.-1988) A: Design flood level, B: Surcharge level, C: Initial water level in flood-control operation, D: Minimum operating level, a: Maximum outflow for water supply, b: Initial inflow discharge in the flood-control operation, c: Maximum outflow discharge in the flood-control operation, d: Standard project flood discharge, e: Spillway design flood discharge, 1: Maintenance of normal river water functions (compensation water), 2: Discharge for water utilization, 3: Maintaining initial water level in flood-control operation, 4: Flood control, 5: Additional flood control, 6: Release of surplus water.

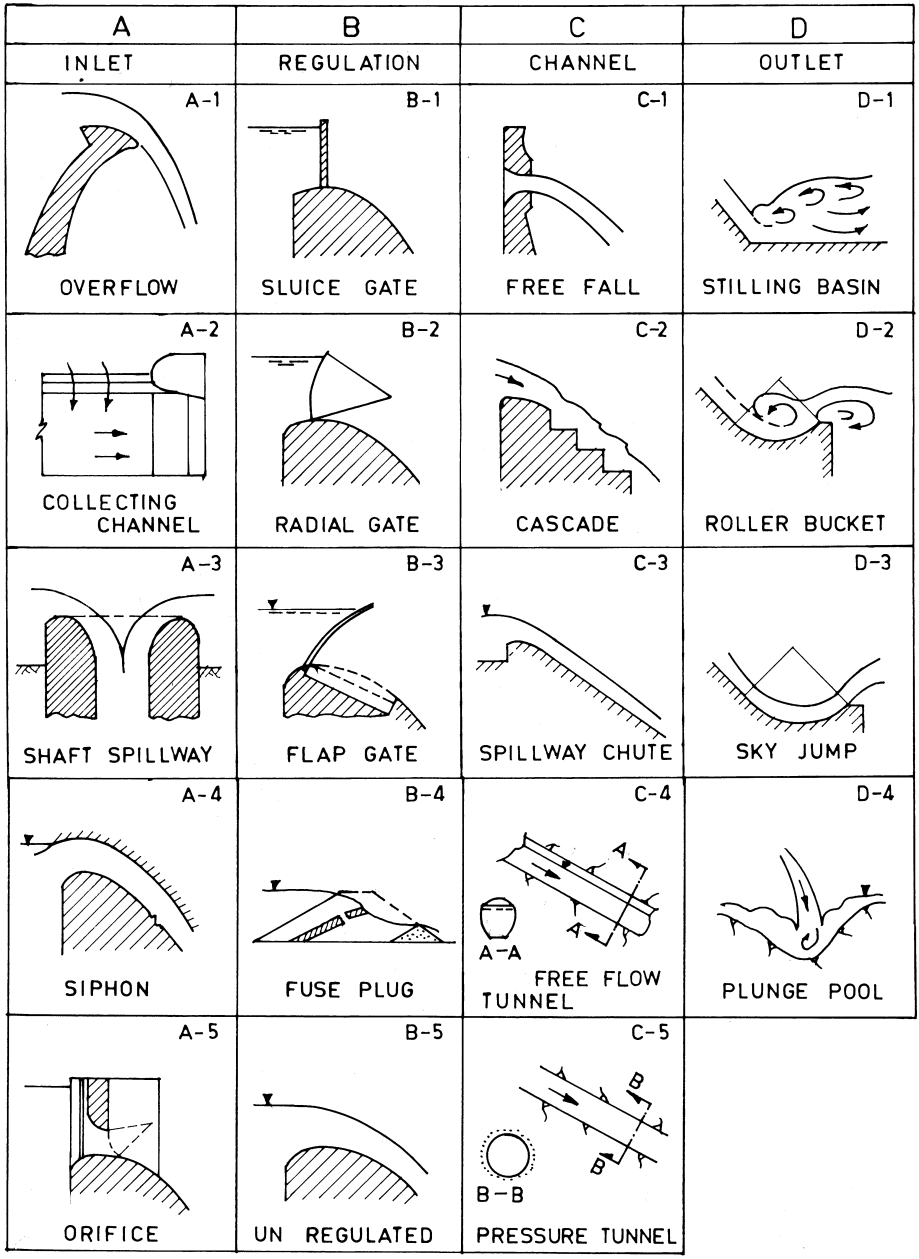

Figure 2 Classification of Spillway (shown in Vischer et al, San Francisco,1988).

1.4 CLASSIFICATION OF SPILLWAYS

Spillways have been classified according to various criteria

I. According to the most prominent feature
   A. Ogee spillway
   B. Chute spillway
   C. Side channel spillway
   D. Shaft spillway
   E. Siphon spillway
   F. Straight drop or overfall spillway
   G. Tunnel spillway/Culvert spillway
   H. Labyrinth spillway
   I. Stepped spillway
II. According to Function
   A. Service spillway
   B. Auxiliary spillway
   C. Fuse plug or emergency spillway
III. According to Control Structure
   A. Gated spillway
   B. Ungated spillway
   C. Orifice of sluice spillway

Vischer et al. (1988) have proposed a more comprehensive classification that seeks to include essentially all components of the spillway: inlet, regulation or control, discharge carrier, and outlet (including energy dissapators). Their classification—with minor modifications—lists the following alternatives in each component and is shown schematically in Figure 2.

It would seem that if every element could be combined with all the others, (i.e., $5 \times 5 \times 5 \times 3$), 375 combinations would be possible, or 375 different types of spillways. However, several combinations are not meaningful, such as radial gate, siphon; free fall, ski jump; etc. Only about 65 combinations seem meaningful, and very few are of practical interest.

REFERENCES

1. Moric, P. ''Questioning the need for spillways'', International Water Power & Dam Construction, January, 1997.
2. Mriouah, D. ''Crues Importantes imprevues: cas du barrage de Oued el Makhazine all Maroc'', Q-63, R-82 Proc. 16th ICOLD. San Francisco, June 1988.

3. Takasu, S.; Yamaguchi, J. ‘‘Principle for selecting type of spillway for flood control dams in Japan’’, Q-63, R-19, ibid, 1988.
4. ‘‘Seminar on Safety Evaluation of Existing Dam for Foreign Engineers – History of Dam Safety Development in the U.S.’’ USBR, 1983.
5. Vischer, D.; Rutschmann, P. ‘‘Spillway facilities – Typology and General Safety Questions’’, Q-63, R-23, Proc. 16th ICOLD:. San Francisco, June, 1988.

2
Spillway Design: An Overview

2.1 INTRODUCTION

The object of spillway design, which involves two steps, is to provide a safe and adequate spillway structure for the lowest combined cost of the spillway and the dam. The first step in the design involves determining the type and overall size of the spillway structure to suit the anticipated requirements and conditions of the site. A detailed hydraulic and structural design of the spillway structure is the next step. This chapter is concerned with the general procedure of an overall design. An evaluation of the basic data should be the first step in the preparation of the design. This includes the topography and geology as well as flood hydrography, storage, and release requirements. The type, size, and elevation of the crest and whether it will be controlled can also be tentatively decided. Several alternative arrangements might be possible and a final layout could be created on the basis of economic analysis. However, considering analyses of existing spillways could be useful in understanding trends towards the types of spillways for a given set of conditions.

2.2 ANALYSIS OF EXISTING STRUCTURES

It would be of interest to analyze existing structures to see if there was a trend for adopting a particular type of spillway in a given set of condition. Semenkov (1979) analyzed more than 400 projects in terms of parameters L/H and N for the three main types of spillways: gravity spillways, chute spillways, and tunnel spillways for concrete and earth-fill dams. Here, L and H are the length and height of the dam crest respectively, and N is the power of the flow from the

spillway given by 0.0098 × Q × H_b, MW, where Q (cumec) is the discharge and H_b (m)—the difference between the upstream water level and natural river bed. The results are shown in Figure 1.

In the projects with concrete dams, the spillways were mainly located within the channel portion of the river valley with any combinations of L/H and N. About 35% of spillways of concrete dams are used in combination with sluices and bottom outlets and the use of chute spillways and tunnel spillways makes up about 10% and 5% respectively.

In the projects with earth-fill dams, gravity spillways were used with L/H from 8 to 1700. In the narrow valleys, gravity spillways were used when the power of the flow discharged was small. In the case of great flows, chute spillways were preferred. On wide valleys, spillway tunnels gave way to chute spillways,

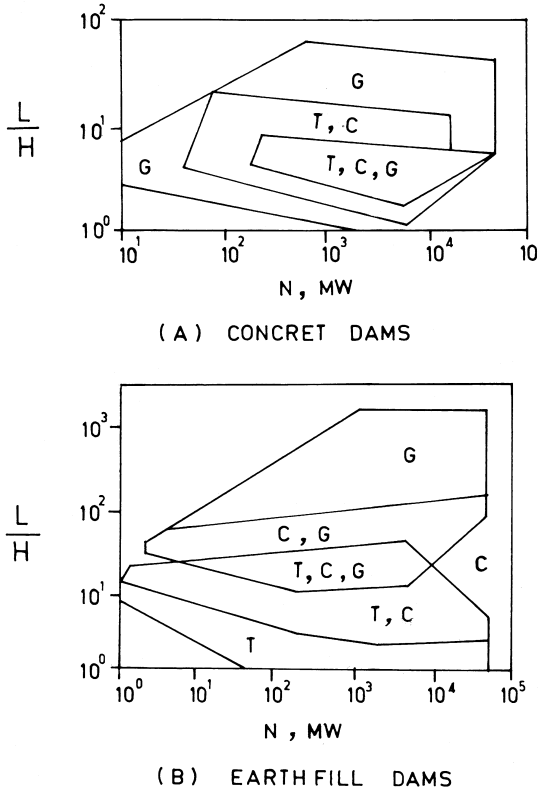

Figure 1 Types of spillways for concrete and earth-fill dams. T: Tunnel spillways, C: Chute spillways, G: Gravity spillways (shown in Semenkov, New Delhi, 1979).

as the power of the flow discharged was more than 5000 MW. Tunnel spillways make up about a quarter of all flow-release structures of earth-fill dams.

2.3 VARIOUS ASPECTS INVOLVED IN A SPILLWAY DESIGN

The following aspects are involved in the design of spillways:

Hydrology
Topography and geology
Utility and operational aspects
Constructional and structural aspects

2.3.1 Hydrology

The hydrological aspects relevant to the spillway design are:

Estimation of inflow design flood (IDF)
Selection of spillway design flood
Determination of spillway outflow discharge
Determination of frequency of spillway use

Estimation of inflow design flood for a given dam site is an exercise in hydrology, therefore, procedures are fairly standardized. The earlier approaches of regional flood formulae (such as Inglis, Dickens, etc.) and envelope curves have now been replaced with refined methods involving statistical analyses (flood frequency series) and numerical modeling of rainfall–runoff relationships. On the other hand, selection of the spillway design flood is a function of social, moral, and economic, as well as technological considerations. While the previous design flood–selection criteria considered factors such as dam height, storage volume, and downstream development, current practice is to select a design inflow flood on the basis of the consequences of dam failure. This is one of the most debated issues of spillway design and different countries have their own standards or procedures for selecting spillway design flood. A detailed discussion on this topic is included in the chapter, ''Spillway Design Flood: Estimation and Selection''.

The spillway outflow discharge corresponding to an inflow flood is determined from the flood-routing analysis. At least a tentative design of the spillway—Full Reservoir Level (FRL), crest level, number of spans, and an approximate discharge rating curve for the spillway—is necessary for a flood-routing analysis. The design of various elements of the spillway such as crest profile, sidewalls, energy dissapator and downstream protection are all based on spillway outflow discharge.

The frequency of spillway usage is determined by the run-off characteristics of the drainage area and the flood storage capacity available in the reservoir. Ordinary river flows are usually stored in a reservoir, diverted through head works, or released through outlets; therefore, the spillway may not be required to function. At diversion dams, where storage space is limited and diversion flows are relatively small compared to flood flows, a spillway is used more frequently. When the flood flows are generally restricted to a small duration and are flashy in nature, the spillways are expected to operate more frequently. The design philosophy for such spillways favors a more elaborate and fail-safe design.

2.3.2 Topography and Geology

Topography and geology, with selected subsurface explorations, have greater influence on the location and type of spillway than any other factors. The class and amount of excavation, possibility of seepage and piping, value of excavated material for other purposes, possibility of scour and subsequent need for lining, location of faults, type of foundation, and bearing pressures allowed are some of the items considered.

These considerations thus determine the type and location of a spillway as follows:

1. Ogee spillway: Most commonly used as the integral overflow section of a concrete or a masonry dam.
2. Chute spillway: Adopted in a site where a suitable foundation with moderate depth of excavation is available, where topography of the site permits the use of a relatively short channel, or where spillway excavation can be used economically in the dam.
3. Side channel spillway: Suitable for earth or rock-fill dams in narrow canyons and for other situations where direct overflow is not permissible.
4. Shaft spillway/Tunnel spillway: Used advantageously at dam sites in narrow canyons where abutments rise steeply or where a diversion tunnel or conduit is available for use as the downstream leg.
5. Siphon spillway: Used when there is a desire for an automatic operation without mechanical parts and the discharge to be passed is small.
6. Free over-fall spillway: Suitable for arch dams
7. Duck bill spillway: Used when the waterway and foundation for the spillway are limited and a curved crest-projection into the reservoir is possible.

2.3.3 Utility and Operational Aspects

From the standpoint of serviceability, spillways may be defined in three broad classes as follows.

Service Spillways

Include any spillway that may be utilized without significant damage to the structure or downstream channel. As a general rule, service spillways have paved channels and suitable energy dissipators.

Limited Service and Additional Spillways

Include any spillway that may be utilized infrequently for operation of the reservoir without incurring excessive damage. Some extraordinary maintenance at infrequent intervals would be acceptable in order to reduce initial construction costs, but not to the extent of imposing significant limitations on the optimum utilization of the reservoir's controlled storage capacity under normal operating conditions.

Emergency Spillways

Include any spillway, the use of which to be avoided as long as possible, used to prevent major damage to the spillway structure or to downstream areas. Emergency spillways may involve partial control by so-called ''Fuse Plugs'' or ''Flash Boards.''

The overall advantages and disadvantages of service, additional, and emergency spillways should be considered in the planning and design of a reservoir project. Besides the aforementioned, the spillways can be classified according to the control structure, namely controlled or gated crest and uncontrolled or ungated crest.

Uncontrolled Crest

Uncontrolled crests permit water to discharge whenever the reservoir surface is higher than the crest. The height of the dam is determined from the maximum flood required to be discharged and the necessary free board. Since the longest crest requires the least head, an economic balance may be found between length and height of spillway if the topography does not limit the length of the crest.

Controlled Crest

Gates may be used to control the reservoir water surface. The top of the gates is usually at the normal water-surface elevation of the reservoir; to keep the maximum elevation constant, the gates are opened sufficiently to pass the floods.

While an uncontrolled crest requires a dam higher than a controlled crest, an uncontrolled crest offers the following advantages: flood storage is always available, the necessity of gates and their maintenance is eliminated, and the crest has a greater ability to pass the logs and other debris without interference. An

uncontrolled crest requires less discharge capacity than a controlled crest for a given flood, since part of the flood is stored in order to acquire a head necessary to pass the discharge. An uncontrolled crest also becomes necessary for some dams located in distant valleys or where, for some reason, spillways are not accessible during floods. A completely controlled crest immediately passes all incoming floodwater if the flood starts when the reservoir is at maximum stage, but it also offers a means of draining the water level in anticipation of floods or allowing induced surcharge at the time of floods. A choice between a controlled and an uncontrolled spillway would require consideration of the above aspects.

Spillways for Flood and Sediment Disposal

While the prime objective of a spillway is disposal of floods, if designed specifically, it may also serve for the disposal of sediment deposited in the reservoir. Mountainous streams with dependable flows and considerable heads favor selection of run-off river plants. However, such streams carry large amount of sediment that could ultimately settle in the reservoir and reduce its capacity. In such projects, spillways can be designed to serve the dual purpose of flood disposal and sediment disposal to flush material deposited in the reservoir downstream, but these requirements are often conflicting. While flood disposal warrants a larger spillway capacity with a wider waterway, sediment disposal requires low-level spillways or bottom outlets of large capacity placed deep below the water surface. A detailed discussion on this topic is included in the chapter ''Spillways for Flood and Sediment Disposal.''

2.3.4 Constructional and Structural Aspects

River valley projects with multiple purposes are usually phased over long periods of time to suit the requirements of irrigation and power, financial allocations, and progress of rehabilitation of the project-affected population. The construction of major dams and spillways involves large quantities of excavation, earthwork, and concreting, and may be required to be constructed in stages. The flood flows in the intervening periods, diverted over partly constructed spillways, may set up undesirable flow conditions, thus resulting in damage to the adjacent structures already constructed by then. It would therefore be necessary to plan the construction schedule, as well as spillway features, in such a way that the temporary passages of flow do not cause undesirable flow conditions. Hydraulic model study is the best means to visualize these effects and to evolve suitable designs.

The choice of earth- and rock-fill dams is often based on the availability of material from the excavation for the spillways. In such situations, unlined rock spillways and unlined cascade spillways may be preferred over chute and side channel spillways. A detailed discussion on this is presented in the chapter ''Unlined Rock Spillways.''

Many future dams are likely to adopt the technology of roller-compacted concrete. This method of construction is cost-effective, typically faster, and causes minimum project disruption. This technique also facilitates the provision of stepped spillways since the rolling in lifts of 30 to 60 cm favors the construction of a stepped surface as the height increases. The stepped spillways ensure energy dissipation on the flow surface itself at almost double that of an unstepped, smooth spillway. The theory and case studies on stepped spillways are discussed in the chapter, ''Stepped Spillways.''

2.4 ECONOMIC ANALYSIS

The procedure for economic analysis has been illustrated by the USBR (1960). The analysis seeks to identify an optimum combined cost of the dam-spillway combination. In determining the best combination of storage and spillway capacity to accommodate the selected design flood, all pertinent factors of hydrology, hydraulics, design cost, and probable damage should be considered. Such factors may be: (1) the characteristics of the flood hydrograph; (2) the damages that would result if a flood occurred without the dam; (3) the damages that would result if such a flood occurred with the dam in place; (4) the damages that would occur if the dam or spillway were breached; (5) the effects of various dam-spillway combinations on the probable increase or decrease of damages above or below the dam; (6) the relative cost of increasing the spillway capacity; and (7) the use of outlet facilities to serve more than one function, such as control of releases and control or passage of floods.

The costs of dams are worked out as functions of maximum reservoir level. For a given inflow flood, an increase in the maximum reservoir level increases the height and hence, the cost of the dam. However, the flood absorption capacity of the reservoir also increases, which results in a smaller outflow discharge for the spillway—whether gated or ungated—resulting in a smaller size of the spillway and hence, a reduction in the cost. The results are plotted as shown in Figure 2. The curves representing the combined costs of dam-spillway combinations indicate the optimum height of the dam that gives the minimum cost.

However, the costs considered in the economic analysis described before only include the first cost. The analysis ought to include the probable cost of repair and maintenance of the spillway structure. Regan (1979) commented on this procedure citing examples of the spillways of Libby and Dworshak dams, United States. The initial costs of both of these structures decreased with the reduction in number of spillway spans and sluices. However, the increase in the unit discharge that contributed to an enormous damage, and necessitated huge expenditure in repairs, was not reflected in the cost of the spillway at the time of planning. The repair cost in each case was about five million dollars. Perhaps,

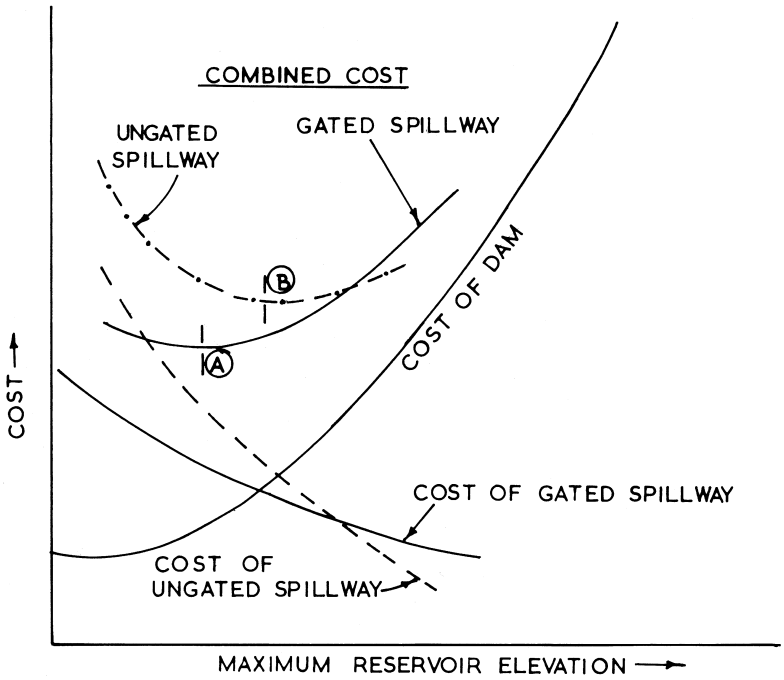

Figure 2 Comparative costs: spillway-dam combinations. A:Minimum cost: gated spillway, B: Minimum cost: ungated spillway (shown in USBR, United States,1960).

a wider spillway with undersluices, though resulting in an increased intial cost, would have avoided high-energy concentration in the discharge channel and would have substantially minimized the damage and subsequent efforts for repairs, if not eliminated them altogether. Admittedly, such visualization in advance requires experience and foresight on the part of the designer, and there lies the complexity of the hydraulics of high velocity flows.

REFERENCES

1. Regan, R. P. Comments on the paper- Cavitation and erosion damage of sluices and stilling basins at two high-head dams- 13th ICOLD, New Delhi, 1979; Vol. V, 580.
2. Semenkov, V. M. General Report on Q 50- Large capacity outlets and spillways, 13th ICOLD, New Delhi, 1979; Vol. V, 94.
3. Design of Small Dams, United States Bureau of Reclamation. USBR, USA, 1960.

3
Spillway Design Flood: Estimation and Selection

3.1 INTRODUCTION

The overtopping of dams causes more than a third of all dam failures. Equipment malfunctions or operational errors are sometimes to blame, but the principal cause is inadequate spillway capacity. Thus, the importance of spillway design flood cannot be over emphasized. In many cases, because the consequences of dam failure would be so severe, no significant level of failure can be tolerated, and protection should be provided up to the maximum flood levels. However, where the consequences would be less serious, the probability of slight failure would be acceptable, and the expenditure for protecting the dam can be reduced. Besides, the distinction can also be made between dam safety and works discharge capacity. This approach, in practical terms, leads to two design floods and their spillway discharge capacity.

The Safety Check Flood

This flood is often made equal to the Probable Maximum Flood (PMF). It is considered acceptable practice for the crest structure, waterway, and energy dissapator to be on the verge of failure, but to exhibit marginally safe performance and an accepted risk of damage without total failure.

The Design Flood

This flood strictly represents the inflow, which must be discharged under normal conditions with a safety margin provided by the free board. The design flood is usually taken as a percentage of PMF or is a flood with a given probability of exceeding its capacity, such as 1:100, 1:1000, etc.

Two aspects concerning the spillway design flood, estimation and selection, have been discussed here. The first falls within the responsibilities of a hydrologist, the latter within those of a dam designer.

3.2 ESTIMATION OF SPILLWAY DESIGN FLOOD

The estimation of spillway design flood or the inflow design flood is an exercise involving diverse disciplines of hydrology, meteorology, statistics and probability. There is a great variety of methods used around the world to determine exceptional floods and their characteristics. ICOLD (1992) groups all these methods under the two main categories:

Methods based mainly on flow data.
Methods based mainly on rainfall data.

Historical methods, empirical and regional formulas, envelope curves, and flood frequency analysis are included in the first catergory whereas rainfall-runoff analysis, based on unit hydrograph and hydrologic modeling, is included in the second category.

It is beyond the scope of this book to present each method thoroughly and their peculiarities, which depend on location, climate and usage, as well as the size and importance of the structure. Only an overview of the methods has been presented; refer to the bibliography for further reading on these methods.

3.3 METHODS BASED MAINLY ON FLOW DATA

In ancient times, the most commonly used site–specific measurement was marking the water level, still preserved in several places, from which a rough estimate of the corresponding discharge could be made along with suitable assumptions of waterway, slope, and friction. Next, the direct measurement of discharge along with water levels was taken followed by series of measurements for several more years. The following methods are based on the analysis of flow data.

3.3.1 Historical Method

This method is based on the assessment of flood discharge over periods of history and determined from the water levels/marks available at sections of rivers, bridges, or buildings. Their only value is in supplementing existing hydrologic data and in comparing results obtained by other methods.

3.3.2 Empirical and Regional Formulas

During the early stages of the development of hydrology, flood estimation was primarily carried out by using empirical relationships between the observed flood peaks and easily measured variables such as the catchment area, rainfall intensity, etc. Empirical formulas may be classified into the following three groups:

1. Formulas in which the discharge holds a simple relation with the catchment area:

$$Q = f(A) \tag{1}$$

2. Formulas in which the discharge is a function of the catchment area and other topographical and meteorological characteristics:

$$Q = f(A,P) \text{ where P is the precipitation} \tag{2}$$

3. Formulas in which other parameters such as intensity of rainfall (I), time of concentration (t_c), and return period (T) are involved:

$$Q = f(A, I, t_c, T) \tag{3}$$

Though simple to use, these formulas are derived from small catchments and are characterized by local and regional conditions; therefore, their use is limited. Chow (1988), Raudkivi (1979), and Garde (1998) list several such formulas.

3.3.3 Envelope Curves

Based on the data of observed flood peaks in rivers located in the same region, for a number of rivers with different catchment areas, the flood peak discharges and respective catchment areas are plotted on a log-log graph and are enveloped by a smooth curve; curves given by Creager, Justin, and Hinds (1944) are examples.

Francou and Rodier (1967) applied this method at a world-wide scale and proposed the formula

$$Q/Q_o = (A/A_o)^{1-K/10} \tag{4}$$

where

Q = maximum flood peak (cumec)
A = catchment area (sq.km)
$Q_o = 10^6$ (cumec)
$A_o = 10^8$ (sq.km)
K = regional coefficient which varies generally between 0 and 6.

A graph representing this formula is given in Figure 1. It can be seen that, in the graph log Q against log A, the K equals constant lines that are envelopes of maximum observed flood peaks in hydrologically homogenous regions. These lines converge to a single point F, whose coordinates ($A_o = 10^8$ sq.km and

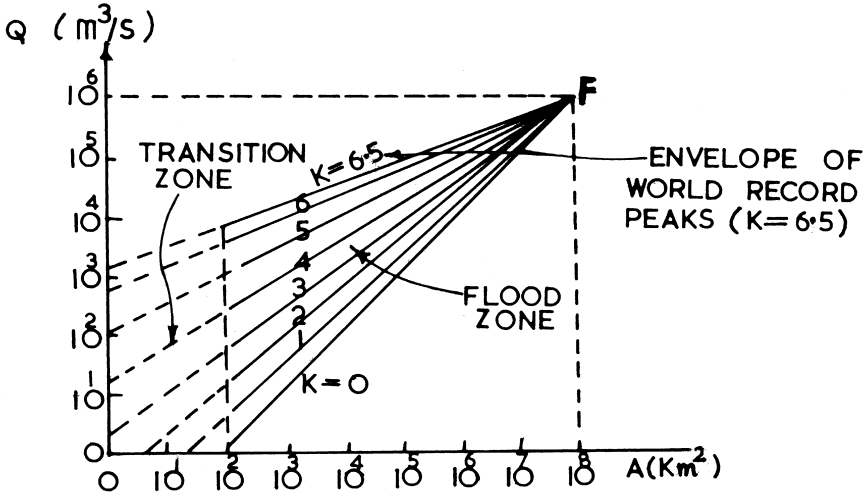

Figure 1 Francou-Rodier Envelope Curves.

$Q_o = 10^6$ cumec) represent the approximate total catchment surface of the earth experiencing precipitation (including lakes but excluding deserts and ice-caps) and the mean annual discharge of all rivers draining these surfaces. The equation is valid only in a flood zone whose lower limit is about 100 sq.km. Below this limit, the maximum flow peak tends to depend only on the maximum rainfall intensity alone.

3.3.4 Flood Frequency Analysis

The occurrence of annual floods at a given site cannot be predicted with certainty because the magnitude of flood discharge is a random variable. Hence, statistical methods are used to predict the design flood for large structures like spillways, bridges, etc. The prediction of the design flood is made by analyzing the data of the past floods for 20 to 60 years. The data is a sample from the population, which consists of annual floods that have occurred at the site, provided that the population considered complies with the following two conditions:

The population is homogeneous; for example, the flood records are not affected by dams, diversions, urbanization, etc.

The characteristics of the population are stationery, that is, independent of time.

Two types of flood series are used by hydrologists for such predictions. The first one is the Annual Flood Series (AFS) in which the highest peak occurring every year is selected. The second series is formed by taking peaks above a certain threshold and is called Partial Duration Series (PDS). AFS is more relevant when it is required to determine risk according to the time of the year while PDS is used for estimation of flows of a low return period. Generally, the two analyses give almost the same results beyond return periods of 10 years.

In the frequency analysis, a probability of occurrence has to be assigned to each flood magnitude. Assigning such a probability is known as determination of the plotting position. For this, the sample data are arranged in descending order of magnitude and rank is given to each value as 1, 2, 3, etc. If two or more observations have the same value, each one is assigned a unique rank assuming them to be different. If m is the rank and there are N observations in the series, the plotting position $m/(N+1)$ is more often used by hydrologists. Once the plotting position is assigned to each flood magnitude in the sample, the probability distribution law that the data follows is determined. The probability of exceedance, $p\ (X>x)$, is related to the return period as

$$T = 1/p\ (X>x) \tag{5}$$

The most commonly used probability distribution or laws used in hydrology are: Gassian or normal, log-normal, log-Pearson type III, and Extreme value-I, or Gumbel distribution. There is, however, no satisfactory logical basis for preferring one distribution to the other and usually the one that best fits the data of that region is recommended for use.

In developing countries, where long-term AFS are not available, the method of regional flood frequency analysis is useful. At present, the most used method for regional analysis is the index flood method, due to a US Geological Survey (1960). Garde (1998) gives a brief account of regional flood frequency studies carried out in India.

3.4 METHODS BASED MAINLY ON RAINFALL DATA

These methods are based on the rational analysis of rainfall and run-off data and are considered more reliable for estimating floods. These methods not only give the peak discharge, but also provide the complete flood hydrograph and thereby give flood volume and a decided advantage in the design of storage reservoirs. Continuous discharge data for at least 4 to 5 rainy seasons with adequate concurrent rainfall data are essential. In addition, rainfall data for as many rain gauge stations in and around the catchment area, including hourly rainfall data, would

be very valuable for assessing areal and time distribution of rainfall. For very large basins, the methods can be applied to their sub-basins with hydrologic or hydraulic routing of the resultant flows.

In this connection, the definitions of the maximum flood are quite relevant and are listed next.

Probable Maximum Flood (PMF)

This is the flood that may be expected from the most severe combination of critical meteorological and hydrological conditions that are reasonably possible in the region. This is computed by using the Probable Maximum Storm, which is an estimate of the physical upper limit to maximum precipitation in the basin. This is obtained from transposition studies of the storms that have occurred over the region and maximizing them for the most critical atmospheric conditions.

The storms are maximized to ascertain how rainfall of a particular storm could have been increased by an increase in the meteorological factors producing the storm. These are the mechanical efficiency of the storm and the moisture content of rain producing air mass involved in the storm.

Standard Project Flood (SPF)

This is the flood that may be expected from the most severe combination of hydrological and meteorological factors that are considered reasonably characteristic of the region and is computed by using the Standard Project Storm (SPS). While transposition of storms from outside the basin is permissible, very rare storms that are not characteristics of the region concerned are excluded from the SPS. Also, the process does not involve maximization of the factors, as done for the PMS.

There are basically two methods of rainfall-runoff analysis used to derive flood hydrographs of the desired characteristics:

Unit hydrograph method
Hydrologic modeling; also known as Conceptual Rainfall-Runoff (CRR) model

However, the first step in the analysis is the determination of PMS or SPS.

3.4.1 Development of the PMS and PMP

The Probable Maximum Participation (PMP) is defined as the theoretically greatest depth of precipitation for a given duration that is physically possible over

a given size storm area at a particular geographic location at a certain time of a year. For each drainage basin there is a PMP, which produces a critical flood at the dam site. To select this PMP, run-off hydrographs produced by large, historic storms are examined. These storms usually constitute the greatest rainfall depths on record for the particular location or surrounding region. Such storms are frequently associated with significant flooding and damage. Having obtained a suitable severe storm database, areal-durational rainfall depths from these storms are adjusted in developing estimates of PMP.

There are three basic adjustments made to the observed rainfall data:

Moisture maximization
Transposition
Envelopment

Moisture maximization is a process whereby observed precipitation is increased to a value consistent with the maximum moisture in the atmosphere for the storm location. The basic storm moisture maximization is expressed as:

$$P_a = P_o \frac{W_{p(\max)}}{W_{p(storm)}}$$

where

P_a = adjusted moisture maximized precipitation
P_o = observed precipitation,
$W_p\,(_{storm})$ = observed precipitable water
$W_p\,(_{max})$ = maximum precipitable water

Application of this adjustment results in storm rainfall depths that are considered to have reached conditions represented by the physical maximum of moisture available in the air above a basin and the rate at which wind may carry the humid air into the basin.

Storm transposition involves relocating individual storm precipitation within a region considered homogeneous relative to topographic and meteorologic characteristics deemed significant to that storm. Since each location of interest has not likely experienced the number of severe storms necessary for PMP development, storm transposition becomes an important tool for providing additional data at a particular site.

Storm envelopment involves the selection of the greatest likely value from a set of data. This step becomes a requirement due to the lack of a uniform storm database for every duration, area, location, and season of interest.

For more details, refer to the excellent treatment of the subject by the World Meterologic Organisation (1986), Cudworth (1989), and Myers (1967).

Once the PMP depth has been calculated, it must be distributed chronologically into a logical storm sequence. Studies of rainfall occurrences have shown

that the variation of rainfall depths in a storm is random. However, conservative considerations have been developed for time wise distribution of rainfall depths, which must vary from zero, at the beginning and end of the storm, to a maximum at some intermediate time increment, generally near the mid-point of the storm. Data available from national weather services or meteorological departments in respect to time distribution of rainfall data, as well as guide lines offered by USBR (1987), may prove to be helpful for further reading.

3.4.2 Unit Hydrograph Method

Unit hydrograph is defined as the hydrograph of direct run-off (excluding ground water) from a given basin resulting from 1 inch of excess rainfall, generated uniformly over the basin area at a uniform rate during a specified time period (duration) such as 1 hour, 2 hour, etc. Thus, a 6 hour unit hydrograph is the rainfall excess generated at 1/6 inch per hour. A unit hydrograph thus represents the integrated effects of all the basin characteristics such as drainage area, shape, stream channel pattern, channel capacities, land slope. and other physical factors. The theory of unit hydrograph assumes that excess rainfall is distributed uniformly over time and over the basin.

A direct run-off hydrograph resulting from an isolated, intense, short duration storm, of nearly uniform distribution in space and time, is the most desirable to satisfy the above assumptions in the theory. If stream flow records are not available, synthetic unit hydrograph can be obtained from known physical characteristics of the basin. Snyder (1938) has developed relationships for synthetic unit hydrographs.

Compiling a design hydrograph from a unit hydrograph of a specified duration involves, superimposing on the unit hydrograph ordinates, the effect of rainfall excess of the design storm. Various segments of the storm are superimposed and added to obtain the design flood hydrograph.

For large catchments, unit hydrographs are worked out for several sub-areas, rainfall excess is applied to the unit hydrographs of each area and flooding from each sub-area is routed to the outlet point of the whole catchment.

Several program packages are available for the combined calculations of rainfall excess, unit hydrograph transfer and river routing, which facilitate computations involved in the process. The most preferred is the HEC-1 flood hydrograph package, developed by the US Army Corps of Engineers (1990).

3.4.3 Hydrologic Modelling

Generalized approaches to model water resources systems also exist. These models are classified into two categories: deterministic and stochastic. Deterministic models are those whose operational characteristics are in terms of known

physical laws or empirical relationships, while stochastic models are expressed by probability functions. Both of these model types play important roles in hydrologic simulation and analysis. However, a deterministic model is more readily adaptable to the examination of land use changes and provides more insight into the physical processes of the hydrologic cycle.

Deterministic models are further classified as empirical models, conceptual models, and physical distribution models.

Relationships developed for physical processes without significant importance to constituents are known as empirical relationships. Models based on such relationships are called empirical models. Such models usually depend on establishing a relationship between input and output, directly or indirectly, using a few parameters; as for example, the rainfall-runoff function. Within the range of calibration data, such models may be successful owing to an implied mathematical structure inherent in the analysis. However, in extrapolating beyond the range of calibration, the physical link is weakened and the prediction then relies on mathematical technique alone. Since no physical process is simulated, such models cannot be used to predict the effect of a future changes in land use patterns.

Conceptual models are based on some consideration of the physical processes in the catchment, as for example, an elaborate Conceptual Rainfall-Runoff (CRR) model. CRR models comprise a series of functions that mimic the water movement within a basin such as: infiltration, overland flow, sub-surface flow, and evapotranspiration. Important features of CRR models include keeping track of the present state of moisture conditions of the watershed and modeling some of the dominant non-linearity of the system such as those associated with saturation of soil mass. The major data required for CRR models include: stream flow data (such as hourly gauge-discharge data), channel configurations, rating curves, particulars of flow diversion, hourly and daily data of precipitation, evaporation, evapotranspiration, and basin characteristics such as area, travel-time in reaches, soil types, etc.

Models based on mathematical relationships using the basic equations governing the system are called physically based models. Such models simulate the complete regime and provide multiple outputs. These models are spatially distributed as the equations formed involve one or more space coordinates. Such models require large data and computation time.

Stochastic models are based on the premise that all hydrological processes are more or less stochastic in nature. If the available record (i.e., a time series) is of sufficient length to be considered as a representative sample, the statistical parameters derived from it will enable formulation of a reliable stochastic model. The data generated by this model will not be qualitatively better than the historical observed data. The major advantage is that many combinations of patterns of data sequences can be synthetically generated for a length longer than the observed data.

Once a hydrological model is selected, it needs to be calibrated and calibration is invariably data demanding. The models use mathematical equations containing parameters representing different phases of the hydrological cycle. A general rule in the case of CRR models is that for calibration, about 5 years of continuously recorded hydrometeorological data should be used. Once the model is satisfactorily calibrated it needs to be further tested for its accuracy. This time, a new set of data is required called validation data, obviously for a different time period than used for calibration.

CRR models can be broadly divided into explicit soil moisture accounting (ESMA) and implicit soil moisture accounting (ISMA). Some of the well-known CRR models under ESMA are Stanford Watershed Model (SWM), Kentucky Water Shed Model (KWM), and Streamflow Synthesis and Reservoir Regulation (SSARR); whereas the Tank model falls under ISMA. The self-calibrating version of KWM is the OPSET (for evaluation of Optimum SET of parameters) model written in Fortran. For detailed information on various models, refer to Singh (1982) and (1989).

3.4.4 Gradex Method

The most recently developed method in France is the method of Gradient of Extreme values or Gradex method. It involves a major simplification of the rainfall-runoff process and identifying the most pertinent characteristics dealt with in a statistical model. One of the basic assumptions of the Gradex method is that the cumulative distribution functions of the areal rainfall in the catchment hold within a very large range of probabilities. The Gradex method may be used for the basins whose base time or time of concentration is smaller than about three days. The method requires the availability of flood records for10 years to derive the quantities relative to return periods of 20 to 50 years. This method cannot be used in areas where storm events may be of cyclonic type which are not amenable to a single cumulative distribution function. For a detailed discussion on this method, see Duband et al. (1988).

3.5 FLOOD ESTIMATION METHODS: CRITICAL ANALYSIS

Basic flood estimation methods with comments on application were covered earlier. While there is a need for consistent standards, there is no single method or methods to embrace all factors, particularly where data are scarce, where flows are highly variable, and where rare meteorological conditions can produce exceptional storms. For large dams with major consequences of failure, the design flood annual exceedance probability is generally in the range of 1:1000 to 1:100000. Such probabilities are well outside the range of the limited data bank

available to develop and calibrate any flood estimation method. It would be practicable to use a combination of frequency analysis and hydrological modeling to obtain a wide range of flows expected and to determine the most suitable value considering relevant factors that characterize the basin as a whole.

The discussion on flood estimation is concluded with the case study of the Sardar Sarovar dam where various approaches were used for the estimation of PMF.

3.5.1 Estimation of Design Flood for the Sardar Sarovar Dam on River Narmada, India

River Narmada in Central India flows almost West-Southwest over 1300 km to join the Arabian Sea and is the largest west flowing river in India. The river's basin has an elongated shape with a maximum length of 953 km (East to West), a maximum width of 234 km (North to South), and is oriented almost parallel to the storm tracks originating from the Bay of Bengal. The storm and river flows have, at times, synchronized to cause record floods with disproportionately large peak discharges. The Sardar Sarovar dam forms a terminal reservoir at 1153 km from the source and intercepts an area of about 88000 sq.km. The climate of the basin is humid and tropical. The normal annual rainfall for the basin is 1178 mm, nearly 90% of that occurring from June to October. The river has 41 tributaries, of which 22 are on the left bank and 19 are on the right bank. Approximately, 75% of the basin area is covered by either the black soils or medium black soils whose infiltration rates are quite low.

The estimation of PMF is based on the following approaches:

I. Flood frequency analysis
II. Hydrological modelling using
    A. SSARR
    B. OPSET coupled with Muskingum Kinematic routings
    C. HEC-1 model based on Clark's instantaneous unit hydrograph

Flood Frequency Analysis

The observed stream flow data at the Garudeswar gauge site, 11.3 km downstream of Sardar Sarovar dam, for the period 1948 to 1980 were subjected to statistical analysis for the purpose of developing distributional models. The flood discharges in the series varied from 10,364 cumec to 69,405 cumec. Figure 2 shows the relationship between the discharge (Q) and the return period (T) using LP-III and Gumbel distribution under AFS as well as the relationship obtained with PDS approach.

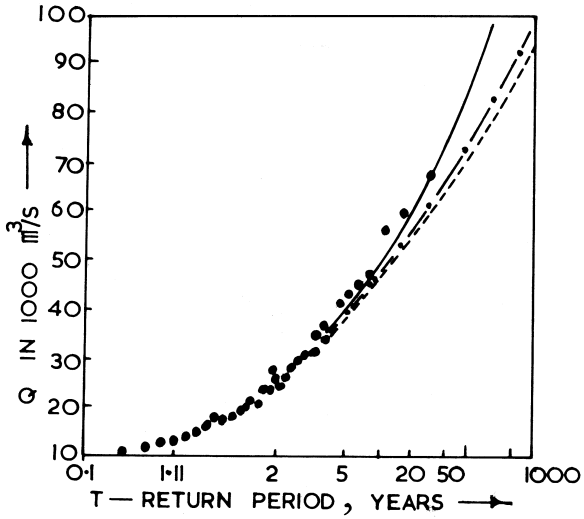

Figure 2 Flood frequency analysis of flood data for Narmada at Garudeswar.
● Observed
——— LP III
—·— P.D.S
– – – – Gumbel

In this particular case, LP-III distribution proved to be a better fit than Gumbel distribution. Comparison between flood discharges estimated for different return periods are shown below.

Return Period, Years	Estimated flood, cumec		
	AFS		PDS
	Gumbel	LP-III	
100	73,260	84,020	71,380
500	90,710	112,430	92,850
1000	98,210	124,510	101,660
10000	123,130	154,030	130,880

Hydrological modeling

The entire basin was divided into 20 sub-basins and the PMP adopted for the initial studies was based on an August 1973 storm using a maximization factor of 1.35. The SSARR model gave a peak flood of about 102,874 cumec whereas OPSET model gave a peak flood of about 112,000 cumec. In the subsequent studies, in addition to the insitu storm over the basin, storms over the

adjacent basins were also considered and transposed. A July 1927 storm with a maximization factor of 1.13 (Storm A) and the August (1973) storm with maximization factor of 1.59 (Storm B) were adopted with OPSET model and Muskingum and Kinematic routing procedures.

The summary of results is given below:

Storm A		Storm B	
Muskingum	Kinematic	Muskingum	Kinematic
165,650	170,990	144,420	146,940

The unit hydrographs for 28 sub-basins were derived and routed by Muskingum method. For this, the 1973 flood with a maximization factor of 1.35 and the 1927 flood from the adjacent basin, which was transposed, with a maximization factor of 1.13 were used. The PMF derived from the above analysis was assumed to be preceded by a flood of a 25-year return period–a 1968 flood observed with a peak of about 58000 cumec. The peak values obtained were 133,480 cumec and 174,290 cumec, respectively. For further details, see Desai et al. (1984).

It would be interesting to compare the above values with those obtained by application of various envelope curves for flood estimation. Some of the results are given below:

Envelope curve	Maximum flood (cumec)
Creager, Justin and Hinds	58,000
Kanvar Sen and Karpov (for Northern and Central Indian rivers)	41,060
Francou and Rodier (with highest value of 6 for the regional coefficient K)	59,950

3.6 SELECTION OF SPILLWAY DESIGN FLOOD

While the estimation of spillway design flood is an exercise in hydrology and related disciplines, selection of Spillway Design Flood (SDF) involves social, moral, economical, as well as technological judgment. In the cases, where clearly defined criteria or methodologies do not exist, selection of the SDF may prove to be difficult and controversial.

While too small a spillway capacity involves a high risk of total failure of the dam by overtopping, an excessively large capacity will involve higher cost and in addition, endanger the lives and properties of downstream inhabitants due

to erroneous reservoir operation (the so-called man-made flood) or due to the malfunction of spillway gates, allowing discharges in excess of the carrying capacity of the downstream valley. Graham (2000) mentions that while modifications to existing dams can reduce economic losses from dam failure, they can also lead to economic losses due to large spillway flows in non-failure events. Thus, selection of the design flood is governed not only by the degree of risk judged acceptable in the event of it being exceeded but also during normal periods.

3.6.1 Economic Risk Analysis (ERA)

The earlier approaches to determining the design flood relied heavily on the economic approach, balancing the cost of providing protection against losses that would occur when protection is insufficient. Smith (1993) has illustrated an example of selection of the design flood frequency by incorporating in the analysis the parameters of annual cost, annual damage, and the B/C (benefit to cost) ratio. Annual cost is worked out considering the expected life of the project and also includes interest, amortization, operation, maintenance, etc. Average annual damage (natural) represents the cost of replacing lost goods and restoring services, government expenses for flood fighting, evacuation, etc., had the dam not been built. Conceptually, the average annual damage may be thought of as the damage in 100 years divided by 100. With the construction of a dam, the extent and frequency of damage will be reduced. The damage that still occurs is referred to as the residual damage. The benefit derived from the dam is equal to the value of the damage prevented or the original damage minus the residual damage. The benefits and costs corresponding to various frequencies of floods are calculated and the B/C ratios are marked against those frequencies as shown in Figure 3. The analysis thus helps in selecting the most economic proposal.

The methods proposed by Fahlbusch (1979), Von Thun (1985), and Afshar and Marino (1990) are based on Economic Risk Analysis (ERA). The basic idea

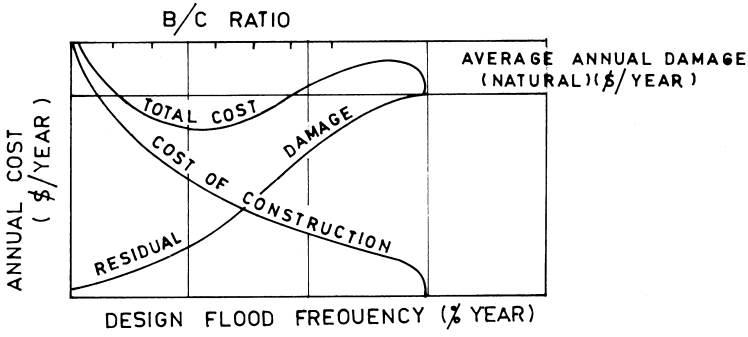

Figure 3 Optimum Design Flood Frequency by Economic Analysis (after Smith 1993).

of economic risk analysis as reported by Bouvard (1988) is in optimizing the maximum flow Q_o that has to be transferred downstream without endangering the dam. A flow Q higher than Q_o will lead to overtopping, the probability of the occurring in any year being

$$\int_{Qo}^{\infty} \rho(q)dq \tag{6}$$

In which p(q) is the probability density of the flow-function considered. The expected cost of overtopping over a long period is given by

$$\frac{A}{a}\int_{Qo}^{\infty} p(q)dq \tag{7}$$

where

a = Discount rate

A = Direct and indirect cost of overtopping to be evaluated in each case

Floods above Q_o would overtop and destroy an earth dam, empty the reservoir, and release downstream a devastating flood of a size determined by the reservoir capacity. Parameter A may be considered independent of the flood discharge because the downstream surge wave from a large reservoir will be produced essentially by the release of the stored water. This considerably simplifies the equation and enables the expected value of C, the cost of the damage to be written as

$$C = \frac{A}{a}F(Q_0) \tag{8}$$

Where $F(Q_o)$ is the total probability of occurrence of a flow greater than Q_o — in a sense the reciprocal of the return period—the function decreases as Q_o increases. Adding the cost of the spillway to the expected value of the damage caused by dam failure yields a plot of the total cost. This passes through a minimum, which in theory corresponds to the optimum cost of the spillway and the magnitude of Q.

3.6.2 Comments on ERA

A comprehensive ERA investigation was conducted for the French earth dam at Serre-Poncon. The analysis revealed some practical difficulties in choosing a range of values of A due to the fact that the resulting optimum was extremely flat. The total cost defined above rose only by 7% when Q_o increased by 40% from 2900 to 4000 cumec; while at the same time, increase in the flow considerably altered the safety situation. It was considered that the expression for A ought to have reflected an extremely important consideration: the equivalent in financial terms of the loss of life resulting from dam failure and an agreed monetary value for each life lost. There is, however, general reluctance among practicing

engineers in assigning monetary values to human lives and objective difficulty of detailing data of this kind. As Lafitte (1989) opines, one could attempt to carry out ERA but the matter is, broadly speaking, a political one. This includes arbitrary components with respect to another crucial question: at what cost does society rate the protection of human life? There cannot be a universal answer because it depends on the competence of each country or region to determine its own safety criteria. Several countries have adopted a judicious approach method; they classify dams in different categories of potential hazard and specify for each one of them the design flood. This approach brings out a new trend; if loss of human life is expected because of community or other significant developments downstream, the dam classified in the ''high hazard'' category has to be designed for the PMF (as in USA, UK, India, and many other countries). However, for the same hazard conditions, some would recommend a flood with frequency of more than 1/10000 (as in Australia).

3.6.3 Design Flood Standards and Regulations

Several countries have formed their own guidelines or regulations for determination of spillway design flood.

Countries like Poland (Balcerski et al. 1967), Czechoslovakia (Broza 1988), Japan (Takasu et. al. 1988), and Norway (Saelthun 1988) have stipulated laws and regulations for setting the design flood.

Some countries like France (CIGB-1973) have no formal rules, but use accepted practice, which is modified to suit specific conditions. Others like United States (Wang 1988), Great Britain (Kennard et al 1988), Canada (NRCC 1990), Australia (Cantwell et al. 1988), Switzerland (Biedermann et al. 1988), India, and South Africa (SANCOLD 1991) issue guidelines from Scientific Committees or regulatory authorities. Countries like China (Pan et al 1988), Finland (Reither 1988), Spain (Delgrado 1988), Sweden (Bergstorm 1988), Zimbabwe, and the former USSR have some standard practices for selection of design flood.

Some typical guidelines are described in the following paragraphs

United States

Wang (1988) has discussed main provisions relating to the updated approach on selection of safety standards. Accordingly, dams are classified into three categories based on the height (small, intermediate, and large), storage capacity, and the hazard potential of the extent and nature of damage due to dam failure (low, significant, and high).

Generally, large dams are designed for PMF, intermediate for SPF/PMF, and small dams for floods of return period of 100 years to SPF.

For concrete dams, zero minimum free board is accepted for the top of the dam in most cases, when a standard 1 m high parapet wall is constructed.

For embankment dams, the minimum free board should not be less than about 1 m. The use of a parapet wall to provide free board allowance may be considered on a case-by-case basis. However, the following safe guards must be met.

The maximum water surface resulting from routing of inflow design flood should not exceed the top of the impervious zone.
The parapet wall should only replace the portion of the free board needed to prevent overtopping from wave run-up.
The top of the parapet wall should be determined after considering future foundation and embankment settlement.

Russia (former USSR)

The design flood discharge and volume of annual run-off which effect the safety and economy of dams are specified by government-approved codes. According to these codes, probability of maximum flood discharge is specified in relation to the class of dam, which is governed by the type and height of a dam, foundation condition, and consequences of malfunction.

The main design case discharge (varying from 0.1 to 5% probability) should pass through the spillway at normal reservoir level. An excess of normal reservoir level would be justified for the verifying design case (probability varying from 0.01 to 1.0%) by techno-economic comparisons of alternative versions.

Switzerland

Biedermann (1988) has discussed the general procedure for the selection of design flood. Two different design criteria are used:

1. Probable maximum flood (PMF) assumed at 150% of the 1000 year flood discharge.
2. A flood with a given return period (i.e., 1000 years) taking into account an appropriate reserve against higher floods or unforeseen events.

Preference is generally given to case (1) because it is believed to ensure absolute safety. In actual practice, however, since the estimation of PMF is highly problematic, procedure (2) is preferred whenever sufficient representative precipitation and discharge measurements are available.

The safety of the dam against floods is based on a 1000-year flood assuming that the flood will impinge on the normal full reservoir level. All discharge facilities besides the spillway including river outlets, and even the headrace tunnels feeding the turbines, are assumed to be functioning. In this case, a discharging capacity corresponding to (n-1) turbines or pumps is assumed. Out of all the

outlet works with mechanical controls, such as gears and valves, the one with the highest discharging capacity is assumed to be blocked and non-operative.

Another important criterion followed is to ensure that the resulting reservoir level with flood routing (when the reservoir is at normal operating level) should remain at least 0.5 m to 1.0 m below the top of the concrete dam and 1.5 m to 3.0 m below the top of the embankment dam. The determination of the maximum free board is based, however, on the estimated PMF discharge.

Norway

Saelthun (1988) has briefly described comprehensive regulations for dam designs that have been enforced since 1981. These regulations comprise hydrological investigations aimed at bringing the procedures of flood estimation in line with internationally accepted procedures. These regulations apply to all the dams with heights more than 4 m or gross storage capacity of more than 0.5 million cubic meters. They apply equally to increased gradation of existing dams.

Regulations define two standard floods, namely, PMF and Design Inflow Flood. The design inflow flood is defined as the inflow with a return period of 1000 years, whereas the PMF is calculated from PMP. The design flood is to be applied to the calculations of water level and discharges that form the basis for the design of spillway and outlet works, whereas the PMF forms the basis for calculations to check the safety of the dam against failure. Since the concrete dams are supposed to withstanding overtopping for a short period, but earth/rock-fill dams cannot be allowed to be overtopped, PMF becomes, in practice, the design standard for spillways of earth/rock-fill dams.

For the dams in cascades, the flood calculations should take into account the advantageous effect of the time difference between the outflow flood from the upstream reservoir and the local inflow flood due to the areal distribution of rainfall. The rules specify not to start the flood calculations with the flood of the upstream reservoir, but to estimate the inflow flood for the total catchment area and then route the flood through the reservoirs and the river course.

India

Various design organizations, at the center and state level, follow procedures more or less similar to the US practice. A detailed review of evaluation and criteria for spillway design flood has been reported by Gole et al. (1979). Dams are classified according to hydraulic head (MWL minus the normal annual average flood level in the downstream) and gross storage capacity. All major reservoirs with storage capacity more than 51.7 million cubic meters are required to be designed for PMF, while barrages and dams with less than 51.7 million cubic meters are required to be designed for SPF or the 100 year flood, whichever is

higher. For weirs, aqueducts, etc., floods having a return period of 50–100 years have been recommended. It requires assuming that the flood impinges at full reservoir level. It also specifies that the spillway design flood can be assumed to be preceded or succeeded by a 25-year frequency flood within an interval of 3 to 5 days. In addition, the performance should be acceptable for at least 10% of the gates with a minimum of one gate inoperative. For important projects, dam break analysis is also carried out when deciding whether PMF needs to be adopted.

China

Pan et al. (1988) have discussed in detail the procedure adopted in China for determining the spillway design flood. To achieve reasonable balance between economy and risk, dams are classified into five categories (A, B, C, D, and E) according to their magnitude and importance. The classification considers reservoir capacity, power installation, irrigated area, and type of development to be protected from floods. Hydraulic structures are classified (Class 1, 2, 3, 4, and 5) depending on whether it is a permanent, auxiliary, or temporary structure.

All hydraulic structures are usually designed to fulfill two different flood-handling requirements

Normal operating condition (Design condition)
Extra ordinary condition (Check condition)

For structures where failure would cause heavy loss of life and property, PMF should be considered as the extra ordinary condition (Check condition). For less important structures, the extra ordinary operating conditions specified depend on whether the dam is an embankment dam or concrete dam. Embankment dams can be designed for floods of return period varying from 300 to 10,000 years whereas concrete dams can be designed for 200 to 5000 year floods, based on the class of the structure. For the above conditions, the safety factor of the dam or the free board can also be reduced.

Australia

Cantwell et al. (1988) discuss the procedure followed in Australia with reference to the guidelines published by the Australian National Committee on Large Dams (ANCOLD) in 1986. Accordingly, dams are classified into three categories:

1. Large dams: 15 m or more in height and storage at least 1 million cubic meters
2. Referable dams: 10 m or more in height and storage at least 20,000 cubic meters or 5 m or more in height and storage at least 50,000 cubic meters
3. Small dams: Smaller than referable dams and of low height

The design flood recommended is related to Incremental Flood Hazard Category (IFHC):

If loss of identifiable life would occur, Annual Exceedance Probability (AEP) should be between PMF and a flood corresponding to a return period 1 in 10,000.

If loss of life is not expected but is possible, AEP should be between 1 in 10000 and 1 in 1000.

Referable dams generally should have a design flood with AEP not exceeding 1 in 100, except possibly for small remote storages.

3.6.4 Comments on Design Standards

It would be seen that the design standards being used broadly reflect social, political, economical, and technological judgement in the respective countries. They also reflect the degree of control that is exercised by the governments of those countries.

In almost all cases, PMF is recommended as the design flood if the failure of a dam during flood entails loss of human life. In some cases, PMF is recommended on the basis of height of the dam or storage capacity even without reference to human life. This is based on the assumption that the probability of exceedance of either the PMP or the PMF is zero. They are hypothesized as the most severe conditions that can physically be expected to occur and hence PMF design ensures absolute safety. Graham (2000), however, raises a question: does increase in spillway size always accompany increased safety? Large spillways can actually make downstream flooding worse. He suggests that a new strategy that considers both positive and negative aspects of dam safety standards should be evolved.

When failure of a dam during a flood would not entail the loss of human life, but may put only some part of the population at risk, a flood smaller than PMF could be adopted as design flood. This smaller design flood is usually specified to be SPF or some percentage of PMF. Although the guidelines specify such a provision, more refined analyses based on risk analysis have been developed. Two such approaches used in the United States, namely Quantitative Risk Assessment and Incremental Hazard Evaluation, have been briefly discussed.

3.6.5 Quantitative Risk Assessment

Quantitative risk assessment is the appropriate methodology to support selection of dam safety design floods according to the American Society of Civil Engineers (ASCE) Task Committee on Spillway Design Flood Selection (1988).

Dams are assigned to one of three categories, depending on the extent and nature of the adverse consequences of failure.

1. Category 1 contains dams whose failures, based on reconnaissance-level assessments, would cause a loss of life or other social or economic losses which unarguably warrant the use of PMF as the safety design flood.
2. Category 2 contains dams where a reconnaissance-level assessment of failure consequences is not adequate to select a safety design flood. Unless a rigorous analysis shows that it is possible to conclude that a lesser flood is appropriate, PMF should be adopted as the safety design flood.
3. Category 3 contains dams which are usually small with low cost and where failures, based on reconnaissance-level assessments, will produce damage confined to the owner. Default safety design floods are suggested for this category.

   The procedure is summarized in the flow chart.

3.6.6 Incremental Hazard Evaluation

Incremental hazard evaluation is more sophisticated than ERA in that it attempts to consider only the additional damage caused by the additional discharge due to dam failure. For some dams, the consequences of failure are clearly unacceptable under any flow conditions. At the other extreme would be a low dam in an isolated area, where a failure would have no significant impact other than economic loss to the owner. The spillway design flood determination for these dams is not a complex process. The design flood in the first case is the PMF; for the other flood, flood frequency and risk-based analyses may be used, with the minimum standard being the 100-year event.

Many dams fall somewhere in the middle. A typical example would be a dam for which a reconnaissance-level examination or a limited-breach analysis demonstrates that failure under either normal operating conditions or during a PMF would not result in increased hazard, but for which the nature and location of downstream development indicate that failure under intermediate flow conditions may have a significant effect. Sometimes, the damage caused by the PMF alone—in the absence of a dam—may be considerable, whereas by contrast, release of stored water from a small reservoir following a failure would cause only a small amount of extra damage. For such dams, it is necessary to determine the flood level beyond which dam failure would not significantly increase the threat to downstream life and property. This flood event is the spillway design flood.

The Federal Energy Regulatory Commission (FERC), US, has developed a flow chart for such an analysis. Hawk (1992) has described this procedure in detail, as shown in the flow chart (page 37).

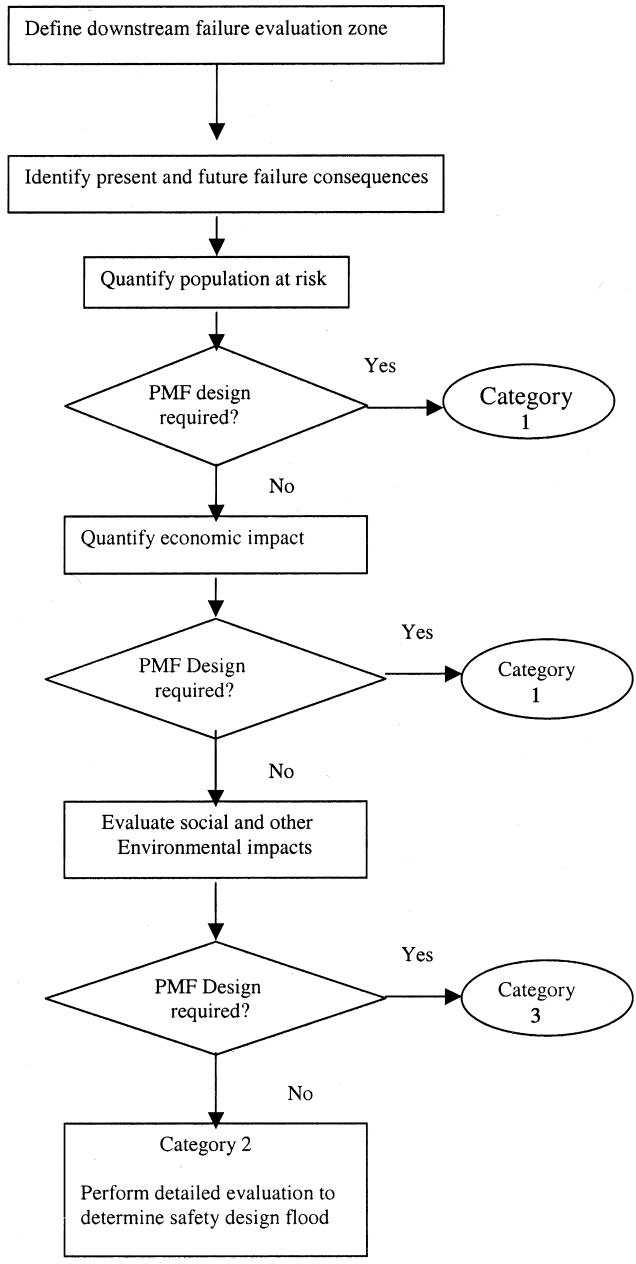

Quantitative Risk Assessment (ASCE, 1988)

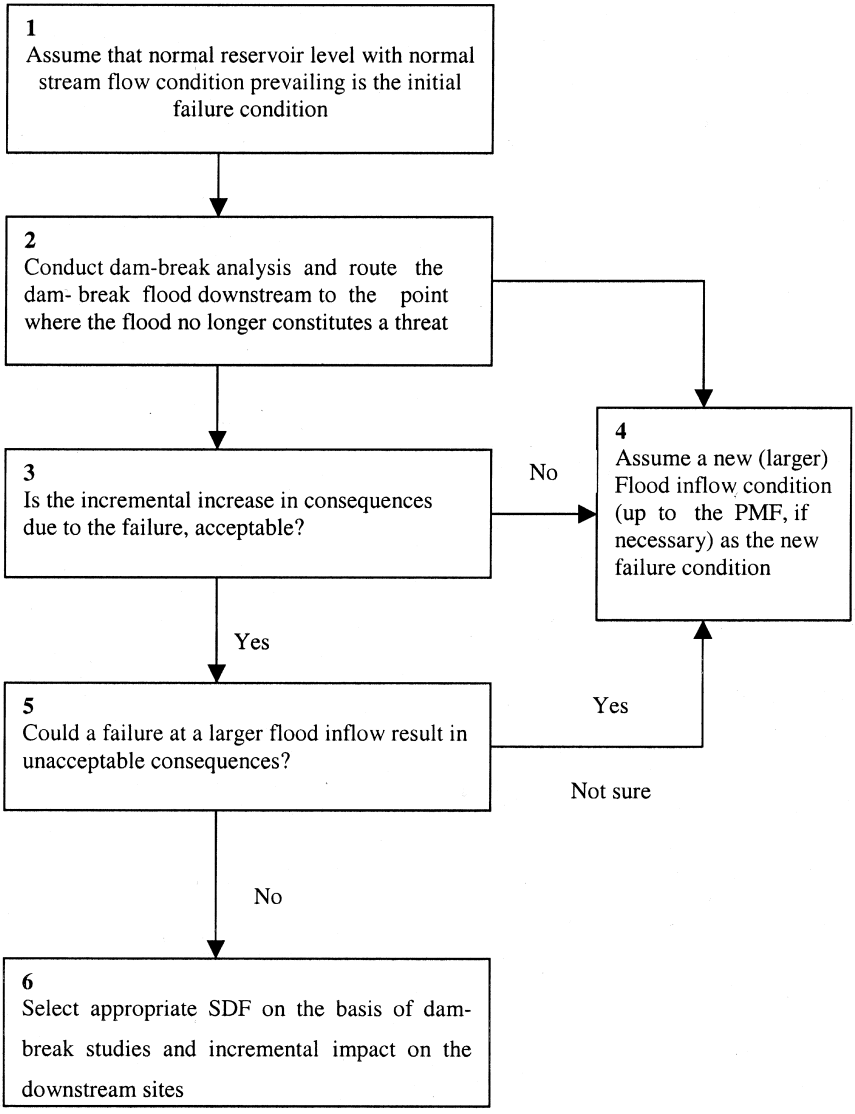

Incremental Hazard Evaluation (Hawk, 1992)

The discussion of selection of a spillway design flood is concluded with the following remarks by the ICOLD (1982):

Project engineers and hydrologists must never forget the following when dealing with design floods, size and type of spillways, and rules for reservoir operation:

1. The exceptional floods actually experienced in Nature and that are likely to occur in the future far exceed those which we have on record.
2. The combination of rare events with a very low probability of occurrence is a real possibility.
3. And that, in the final analysis, human life is of great value and our most important asset.

Notations

A = Catchment area
= Direct and indirect cost of overtopping of a dam.
A_o = Total catchment surface of earth, 10^8 sq.km.
a = Discount rate
c = Cost of damage
I = Intensity of rainfall (mm/hr etc)
K = Regional co-efficient in Francou – Rodier envelope equation
m = rank
N = Number of observations.
P = Precipitation
P_o = Observed precipitation
P_a = Adjusted moisture maximized precipitation
Q = Discharge
Q_o = Mean annual discharge of all rivers on the earth = 10^6 cumec
T = Return period, years
t_c = time of concentration, hours
V = Volume of water under unit hydrograph
$W_{p\,(max)}$ = Observed precipitable water
$W_{p\,(storm)}$ = Maximum precipitable water

REFERENCES

Estimation of Design Flood

1. Chow, V. T.; Maidment, D. R.; Mays, L. W. Applied Hydrology; McGraw-Hill, New York, 1988.

2. Creager, W. P.; Justin, J. D.; Hinds, J. Engineering for Dams; John Wiley & Sons, New York, 1944; Vol. 1.
3. Cudworth, A. G. Flood Hydrology Manual – A Water Resources Technical Publication, USBR; Denver, USA, 1989.
4. Desai, N. B.; Rao, S. G. V.; Mathew, N. T. Estimation of probable maximum flood in the Narmada at Sardar Sarovar, 41st Annual Research and Development Session, CBI&P, Vol. II-Hydraulics, Vadodara, India, 1984.
5. Duband, D.; Michel, C.; Garros, H.; Astier, J. Estimating exteme value floods and the design flood by the Gradex method – ICOLD, 16th Congress; San Francisco, USA, 1988; Vol. IV, Q 63, R 60.
6. Francou, J.; Rodier, J. A. Tentative classification of maximum observed floods, Proc. Leningred Symposium on floods and their computation, UNESCO, 1967.
7. Garde, R. J. Floods and Flood Control : Engineering Approach, Memoir Geological Society of India, No.41, 1998, 173–193.
8. ICOLD. Selection of Design Flood – Current Methods Bulletin 82, 1992.
9. Myers, V. A. Meteorological estimation of extreme precipitation for spillway design floods. Weather Bureau Technical Memorandum WBTM Hydro-5, 1967.
10. Raudkivi, A. Hydrology; Pergamon Press, Oxford, 1979.
11. Singh, V. P. Rainfall – Runoff relationships, Water Resources Publication, 1982.
12. Singh, V. P. Hydrologic Systems – Watershed Modelling; Prentice Hall, New Jersey, 1989; Vol. II, 237–254.
13. Snyder, F. F. Synthetic unit Graphs _ Trans. American Geophysics Union, Part I, 1938.
14. United States Bureau of Reclamation Design of Small Dams, Revised Edition, 1987.
15. USGS Flood frequency analysis – Manual of Hydrology, Part 3, Flood flow techniques, USGS Water supply paper 1543, 1960, 11–25.
16. US Army Corps of Engineers HEC-1 – Flood Hydrograph Package 723-X6-L-2010, 1990.
17. World Meterological Organisation Manual for estimation of probable maximum precipitation, Operation Hydrology Report No.1, WMO – 332, 1986.

Selection of Design Flood

1. Afshar, A.; Marino, M. A. Determining optimum spillway capacity based on estimated flood distribution – International Water Power and Dam Construction, January 1990.
2. ASCE Evaluation procedures for hydrologic safety of dams – A report of Task Committee on spillway design flood selection, 1988.
3. Balcerski, W.; Bolesta, S. Evaluation de debits maxima pour le dimensionnement d'ouvrages des crues dans les barrages, CIGB, 9th Congress. Istanbul, 1967.
4. Bergstrom, S.; Ohlsson, P. E. Towards new guidelines on spillway design in Sweden – ICOLD 16th Congress, Q 63, RG7; San Francisco, USA, 1988.
5. Biedermann, R. Safety of Swiss dams against floods – design criteria and design flood – Q 63, R 22; San Francisco, USA,, 1988.

6. Bouvard, M. C. Design flood and operational flood control – General Report, ibid, 1988.
7. Broza, V. Q 63, R 42; San Francisco, USA, 1988.
8. Cantwell, B. L.; Murley, K. A. Design flood guidelines, Australia – Q 63, R 15; San Francisco, USA, 1988.
9. CIGB 11th Congress; Madrid, Spain, 1973; Vol. II, Q 41, R8.
10. Delgrado, G. J. Basic criteria for sizing large dam spillways – ICOLD 16th Congress, Q.63, R 65; San Francisco, USA, 1988.
11. Fahlbusch, F. E. Optimum design flood for spillways – International Water Power and Dam Construction, 1979, 79–84.
12. Gole, C. V.; Krishnamurthy, K. Evaluation and criteria for spillway design flood and adequacy in relation to safety of dams, ICOLD, 13th Congress, Q 50, R 50, 1979.
13. Graham, W. J. Placing risks in perspective, International Water Power and Dam Construction, December, 2000.
14. Hawk, J. K. Evaluating Spillway Adequacy, Civil Engineering, May 1992, 74–76.
15. ICOLD Selection of design flood – Current Methods, Bulletin 82, 1992.
16. Kennard, M. F.; Bass, K. T. Determination of design flood and its application to existing dams, ICOLD, 16th Congress, Q 63, R 53; San Francisco, USA, 1988.
17. Lafitte, R. Dam safety in relation to floods – International Water Power & Dam Construction, April 1989.
18. NRCC Hydrology of floods in Canada – A guide to planning and design NR 16–15/ 1988 – National Research Council of Canada, 1990.
19. Pan, J.; Terg, W. Determination of design flood in China – 16th ICOLD, Q 63, R 88; San Francisco, USA, 1988.
20. Reither, P. H. Experience in design flood analysis of dams in Finland, Q63, R 57; San Francisco, USA, 1988.
21. Saelthun, N. R. Norwegian procedures for flood estimation, Q 63, R 28; San Francisco, USA, 1988.
22. SANCOLD South African National Committee on Large Dams, SANCOLD guidelines on safety in relation to floods, Report No.4, 1991.
23. Smith, C. D. Selection of design flood frequencies for hydraulic structures, Canadian Journal of Civil engineering, August 1993.
24. Takasu, S.; Yamaguchi, J. Principle for selecting type of spillway for flood control dams in Japan, 16th ICOLD, Q 63, R 19; San Francisco, USA, 1988.
25. Von Thun, J. L. Use of risk based analysis in making decision on dam safety; NATO Advanced Study Institute on Engineering Reliability and Risk, Tuscon, USA, 1985.
26. Wang, B. H. Determination of design flood for spillways, ICOLD, 16th Congress, Q 63, R 39; San Francisco, USA, 1988.

4
Ogee or Overflow Spillways

4.1 INTRODUCTION

The ogee or overflow spillway is the most common type of spillway. It has a control weir that is ogee or S-shaped. It is a gravity structure requiring sound foundation and is preferably located in the main river channel, although there are many spillways located on the flanks in excavated channels due to foundation problems. The structure divides naturally into three zones: the crest, the rear slope, and the toe. An ogee crest and apron may comprise an entire spillway, such as the overflow portion of a concrete gravity dam, or the ogee crest may only be the central structure for some other type of spillway. Because of its high discharge efficiency, the nappe-shaped profile is used for most spillway control crests.

4.2 THE SPILLWAY CREST PROFILE

Normally the crest is shaped to conform to the lower surface of the nappe from a fully aerated sharp-crested weir as shown in Figure 1. The pressures on the crest will then be atmospheric. The shape of such a profile depends upon the head, the inclination of the upstream face of the overflow section, and the height of that section above the floor of the entrance channel. Bazin (1886 to 1888) made the first comprehensive laboratory investigation of nappe shapes. Early crest shapes were usually based on a simple parabola designed to the fit the trajectory of the falling nappe in the general form

$$y/H = A\,(x/H)^2 + B\,(x/H) + C + D \qquad (1)$$

wherein the values of various constants have been evaluated by Creager, Justin and Hinds, Ippen and Blaisdell. Grzywienski (1951) has discussed at length the development of various profiles.

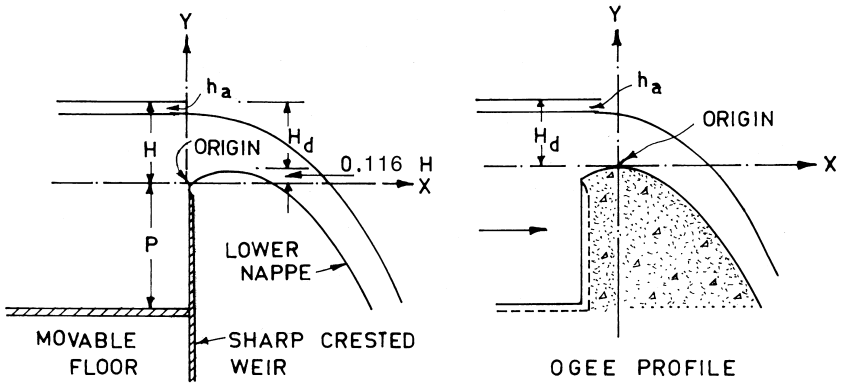

Figure 1 Principle of derivation of crest profile

Crest shapes have been studied extensively in the USBR hydraulic laboratories with various approach depths. The upper and lower nappe surfaces were carefully measured for various discharges and velocities of approach. On the basis of experimental data including Bazin's, the Bureau has developed coordinates of nappe surfaces for vertical and upstream sloped weirs. The results are well documented in the USBR publication 'Design of Small Dams' (1960). The profiles are defined as they relate to the coordinate axes at the apex of the crest. The portion upstream of the origin is defined as a compound circular arc. The portion downstream is defined by the equation

$$(y/H_d) = -K\,(x/H_d)^n \qquad (2)$$

where

H_d = Design head

K & n are constants whose values depend on the upstream inclination and velocity of approach.

Typical profiles are shown in Figure 2.

On the basis of the USBR data, the US Army Corps of Engineers, WES (1952) has developed several standard shapes, designated as WES standard spillway shapes, represented on the downstream of the crest axis by the equation:

$$X^n = K\,H_d^{n-1}\,Y \qquad (3)$$

where

X and Y are coordinates of crest profile with origin at the highest point of the crest.

H_d = design head including velocity head of the approach flow.

K and n are parameters depending on the slope of the upstream face.

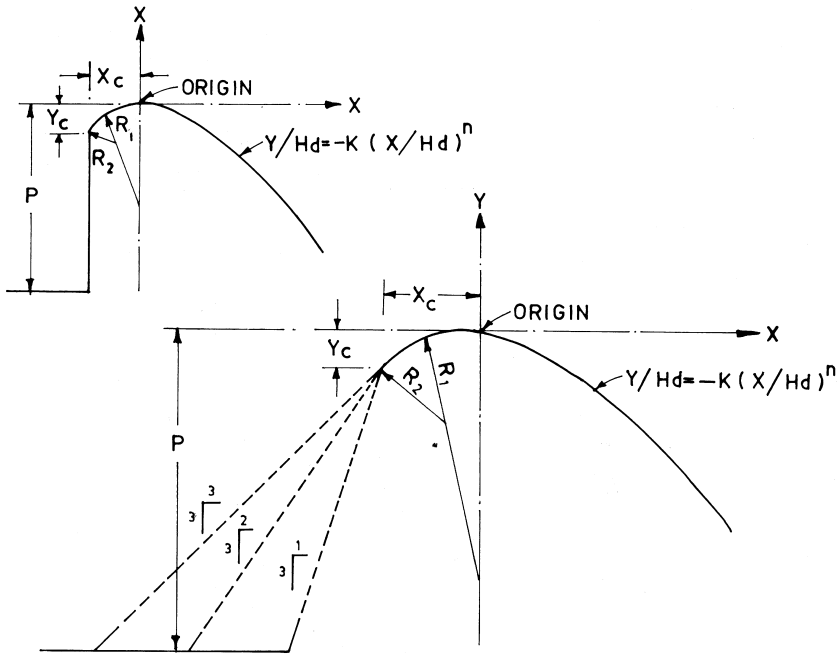

Figure 2 Typical USBR crest profiles.

Typical WES standard shapes are shown in Figure 3.

Murphy (1973), of WES, observed that there was no simple universal procedure for design of overflow spillway crests and that the designers followed one set of rules if the approach depth was deep and another if the approach depth was shallow. Also, there were different sets of rules depending on the inclination of the upstream face of the spillway. Murphy felt the need of eliminating the discontinuity at the intersection of the spillway crest and the upstream face of the dam. In the revised procedure developed by Murphy, using the same basic data of USBR, the upstream quadrant was shaped as an ellipse with the equation

$$X^2/A^2 + Y^2/B^2 = 1 \quad (4)$$

where

A = Semi-major axis (functions of the ratio of approach depth to design head)

B = Semi-minor axis (-do-)

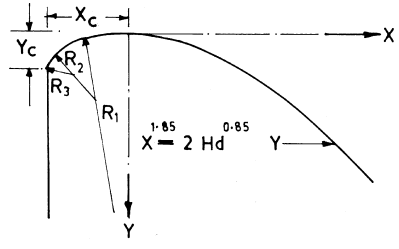

Xc = 0·2818 Hd ; Yc = 0·136 Hd .
R_1 = 0·5 Hd ; R_2 = 0·2 Hd ; R_3 = 0·04 Hd .

A– VERTICAL UPSTREAM FACE.

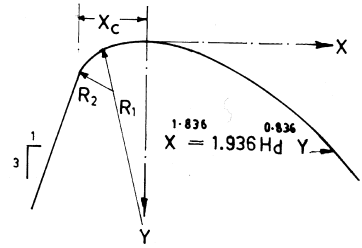

Xc = 0·257 Hd .
R_1 = 0·68 Hd ; R_2 = 0·21 Hd .

B – 3-ON-1 UPSTREAM FACE.

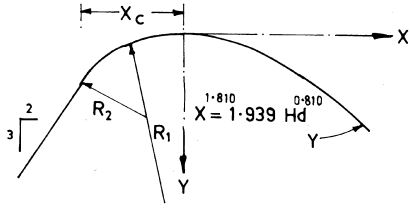

Xc = 0·214 Hd
R_1 = 0·48 Hd ; R_2 = 0·22 Hd

C– 3-ON-2 UPSTREAM FACE.

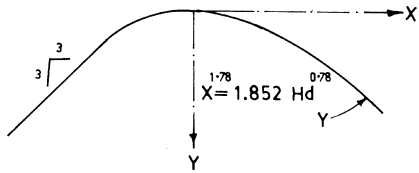

UPSTREAM QUADRANT DETAILS
AS PER H D C 111-7 TO 111-10

D– 3-ON-3 UPSTREAM FACE

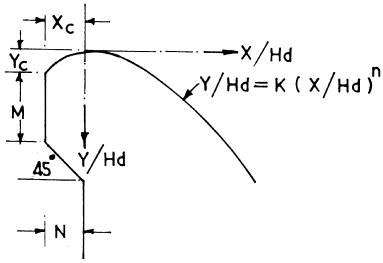

DETAILS AS PER H D C
111-19 AND 111-19/1

E– CREST WITH OFFSET AND RISER.

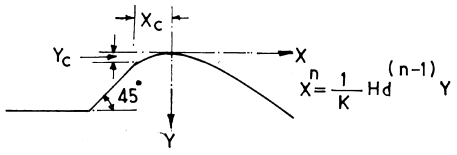

DETAILS AS PER H D C 122-3/1 TO 122-3/5

F – LOW OGEE CREST

Figure 3 Typical WES crest profiles.

and the downstream profile conformed to the equation

$$X^{1.85} = K H_d^{0.85} Y \quad (5)$$

where K is a parameter depending on the ratio approach depth and design head.

The design curves suggested by Murphy are reproduced in Figure 4.

It would be seen that these curves cover both the governing parameters namely design head and approach velocity head while also facilitating any desired upstream face slope (including vertical) without introducing discontinuity at the intersection of the crest with upstream slope.

For $P/Hd \geq 2$, A and B become constant with values of 0.28 Hd and 0.164 Hd respectively.

It would be interesting to see how the three profiles compare. Table 1 shows the comparison of the profiles of two typical cases: a low ogee spillway ($P/H_d = 0.5$) and a high overflow spillway ($P/H_d = 4$) for the same depth of overflow of 10 m and with appropriate heads due to the velocity of approach.

Although all three procedures for defining crest shapes described earlier are based on the same set of data (viz. USBR), there is some dissimilarity. While the profiles as per the USBR and WES (original) procedures show insignificant differences, the WES (Murphy) profile appears to exhibit a somewhat larger upstream quadrant than that given by the other two profiles, especially for sloping upstream faces. This is mainly because of the elaborate transition from an elliptical profile to a sloping upstream face.

Sometimes spillway crests are provided with offsets and risers to effect appreciable economy in the construction of concrete gravity or arch dam spillways, provided the concrete mass eliminated from the standard crest shape is not required for structural stability. WES (1952) has developed design charts based on the basic data from the USBR study of overhanging crests produced by an offset in a sharp crested weir. The design charts are given in HDC 111–19 to 111–19/2. Generally, the vertical depth of projection M should be equal to 0.5 H_d and the ratio of riser (M) to offset (N) should not be less than 0.5, unless this value is zero, in which case it results in a 45° backward sloping weir. Some of the spillways provided with riser and offset are: Monteynard (France), San Esteban (Spain), San Jacinto (Bolivia) for arch dams, Al Massira (Morocco) for buttress dams, and Ukai, Jawaharsagar (India) for gravity dams. Spillways with backward sloping faces have been provided on the arch dams of P.K.le. Roux dam (South Africa) and Victoria dam (Sri Lanka).

All the crest profiles described above still have two sets of equations, i.e., one for the upstream quadrant and another for the downstream. Hager (1987) has developed an equation, which is applicable to both of the quadrants as given by WES, i.e., compound circular arcs of three radii on the upstream and the standard equation for the downstream.

Hager's equation is

$$Z^* = -X^*. \ln X^* \ (X^* > -0.2818) \quad (6)$$

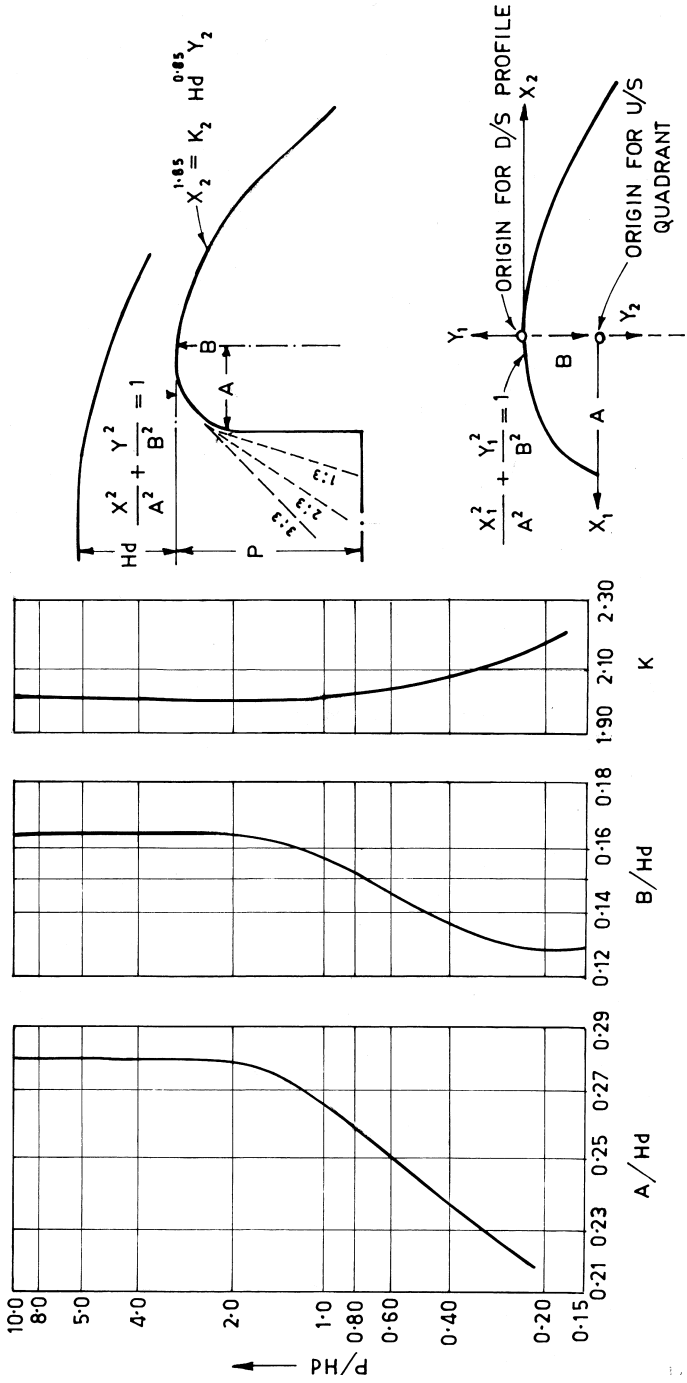

Figure 4 Design curves suggested by Murphy. (Ref-7)

Table 1 Comparison of Spillway Crest Profiles

Case I	Low Ogee Crests: P=5m, H_d=10m, P/H_d =0.5											
U/S Face	USBR				WES (Original)				WES (Elliptical)			
	X_c	Y_c	K	n	X_c	Y_c	K	n	X_c	Y_c	K	n
Vertical	2.595	0.968	0.511	1.835	not defined				2.683	1.572	0.488	1.85
1 : 3	2.465	0.836	0.511	1.815	not defined				2.633	1.271	0.488	1.85
2 : 3	2.282	0.628	0.51	1.764	not defined				2.498	1.0	0.488	1.85
3 : 3	2.139	0.463	0.51	1.748	2.135	0.445	0.524	1.748	2.314	0.777	0.488	1.85
Case II	High Overflow Spillways: P=40m,Hd=10m, P/Hd = 4											
Vertical	2.817	1.242	0.5	1.868	2.818	1.36	0.5	1.85	2.800	1.64	0.5	1.85
1 : 3	2.474	0.91	0.5	1.848	2.57	0.875	0.516	1.836	2.748	1.326	0.5	1.85
2 : 3	2.161	0.667	0.53	1.795	2.14	0.75	0.516	1.810	2.608	1.043	0.5	1.85
3 : 3	2.019	0.454	0.54	1.776	2.0	0.454	0.54	1.776	2.416	0.811	0.5	1.85

where

$X^* = 1.3055\ (X + 0.2818)$

$Z^* = 2.7050\ (Z + 0.136)$

$X = x/H_d;\ Z = z/H_d$

x and *z* are coordinates of the profile on horizontal and vertical axis respectively and the origin is at the crest. The coordinates at the beginning of the upstream vertical face are $(-0.2818,\ -0.136)$, i.e., the same coordinates for standard WES crest shape. This equation has the advantage of being smooth and having a gradually varied curvature. The difference between the original WES profile and this profile is only about 1% of the design head. It is, however, unclear whether the same can be applied to any inclination of the upstream slope other than vertical or with riser and offset, etc.

4.3 DISCHARGE CHARACTERISTICS

Similar to the crest profile, the discharge characteristics of the standard spillway can also be derived from the characteristics of the sharp crested weir. The weir equation in the form

$$Q = C_d \cdot \frac{2}{3} . b . \sqrt{\left(2gH^3\right)} \tag{7}$$

contains the coefficient of discharge C_d which is the product of coefficient of contraction C_c and coefficient of velocity C_v.

$$C_d = C_c \times C_v \tag{8}$$

For an infinitely high weir, the velocity of approach is negligible, the value of C_v is unity and C_d takes on the value $[\pi/(\pi + 1)] \approx 0.611$, as derived from potential flow theory. The more general expression for C_d derived by Rehbock relates the effect of velocity of approach in terms of height of the weir, thus

$$C_d = 0.611 + 0.08\ H/P \tag{9}$$

For the case of very high weir, H/P approaches zero and substitution of Equation 9 into Equation 7 gives

$$Q = 1.804\ b.\ H^{3/2} \tag{10}$$

H in Equation 10 refers to the crest of the sharp crested weir. If one considers the crest of the spillway, the head H_d on the spillway crest is found experimentally to be about 0.884 times the head on the sharp crest (see Fig. 1). The spillway discharge coefficient would then be equal to 2.17. The depth of overflow H_d for this condition is referred to as the design head for which the pressures over the

crest profile are expected to be atmospheric. However, the spillway will also have to operate at lower or higher heads. The former will result in higher than atmospheric pressures and a lower discharge coefficient; in the latter, the reverse of that will happen.

The coefficient of discharge C_d is not a dimensionless quantity. Its standard value for the design head, in British units is 3.98, which is equivalent to metric units, of 2.198. It is, however, convenient to use the non-dimensional coefficient C from the expression

$$Q = \frac{2}{3}.C.L.\sqrt{\left(2gH_o^3\right)} \tag{11}$$

The range of variation of C is then from 0.578, corresponding to the broad crested weir, to 0.75 or so, corresponding to the highest attainable value without exceeding permissible sub-atmospheric pressures on the crest.

Figure 5 shows the variation of coefficient of discharge with respect to head for high overflow spillway with vertical upstream face and negligible velocity of approach for the crest profiles conforming to USBR, WES (Original), and WES (Elliptical). It would be seen that the variation between the values corresponding to the three profiles is insignificant.

Factors Affecting Coefficient of Discharge

The values of the coefficient of discharge mentioned before are for the ideally shaped profile that operates uncontrolled and under a negligible velocity of approach; i.e., very high value of the ratio P/H_d. The coefficient is influenced by a number of factors such as (1) the relation of the actual crest shape to the ideal nappe shape, (2) the depth of approach, (3) the inclination of the upstream face, (4) the contraction caused by the crest piers and abutment, (5) the interference due to downstream apron, and (6) the submergence of the crest due to downstream water level.

The effects of heads other than design head, depth of approach, inclination of upstream face, interference due to downstream apron, and submergence by downstream water level have been studied and well documented by USBR (1960). Figure 6 shows the variation of C for an uncontrolled spillway with upstream vertical face, with respect to depth of approach, in the case of USBR and WES (Elliptical) profiles for $H_e/H_d = 1.0$. Figure 7 shows similar comparison in respect of inclination of the upstream face. Magalhaes (1979), commenting on the study reported by Lemos (1979), has stated that the crest with best hydraulic performance was one with vertical upstream face, followed by the crest with 3:3 slope upstream face; whereas the crest with a 2:3 upstream face poses some problems of cavitation and flow separation, which become worse in the case with a 1:3 slope upstream face. However, the observations were concerning a WES

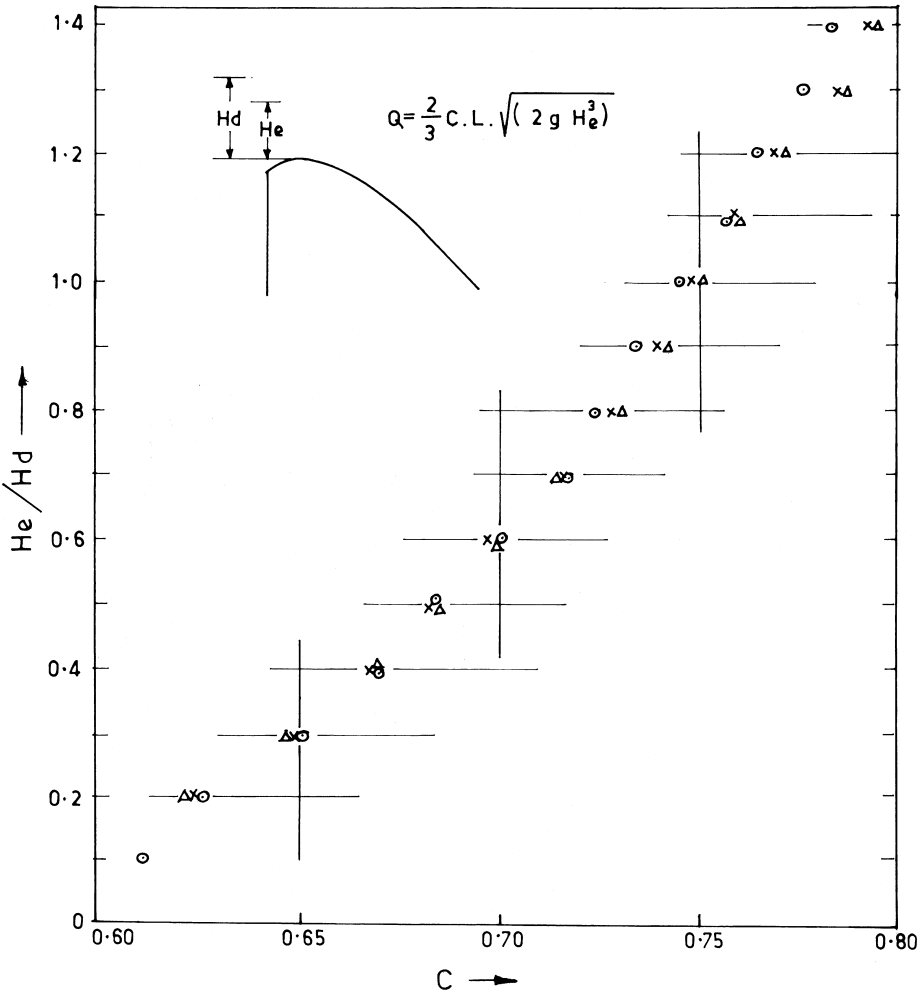

Figure 5 Discharge coefficient for design head for vertical upstream face: ⊙USBR, × WES(Original), △ WES(Elliptical).

crest profile of an earlier design that had an upstream quadrant made of two radii. It may be mentioned that no data is available in respect of WES elliptical profile for inclination of upstream face.

The effect of heads other than the design head have been studied by WES (HDC-111-3/3) utilizing the model data for ten widely varying spillway designs to generalize the relationship

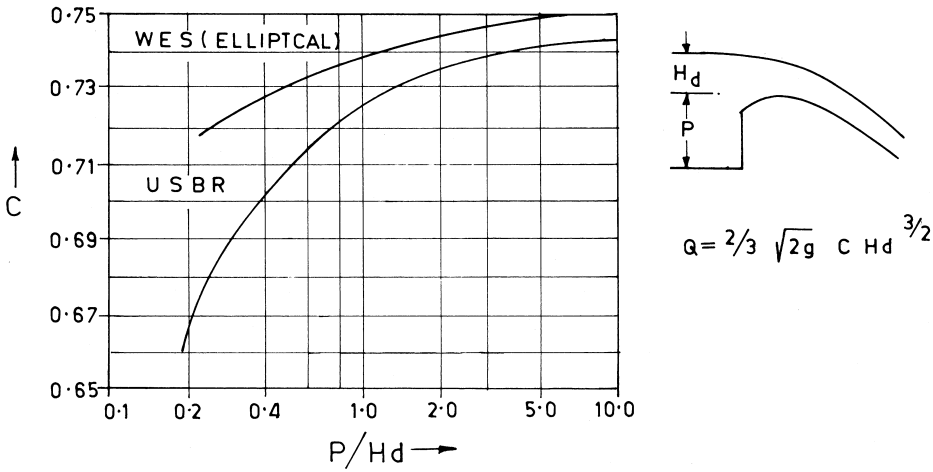

Figure 6 Effect of approach depth on coefficient of discharge.

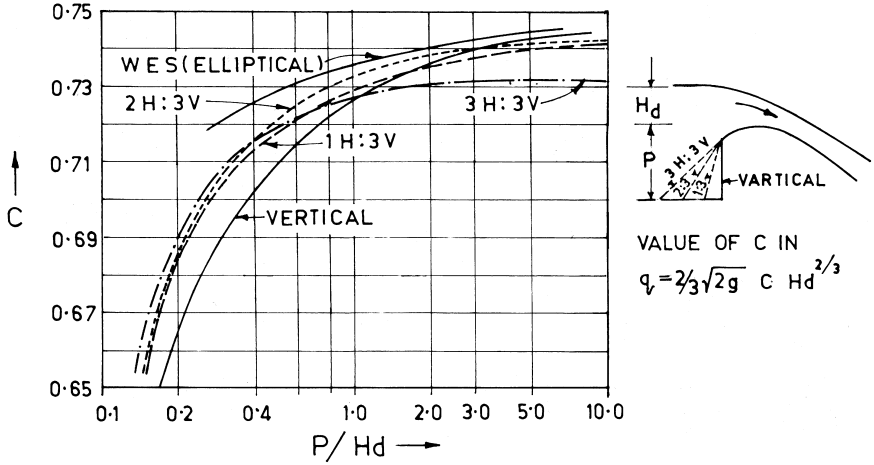

Figure 7 Effect of inclination of upstream face on coefficient of discharge.

$$Q = Q_d (H_e/H_d)^{1.6} \quad (12)$$

where

H_d = Design head
Q_d = Discharge corresponding to the design head
H_e = Head other than design head, including head due to velocity of approach
Q = Discharge corresponding to H_e

Crest piers and abutments cause contraction of the flow, reduction in the effective length of the crest, and cause reduction in the discharge as compared to that of an otherwise uncontrolled crest. The following relationship applies:

$$L' = L - 2 (NK_p + K_a) H_e \quad (13)$$

where

L = Effective length of crest for calculating discharge
L' = Net length of crest
N = Number of piers
K_p = Pier contraction coefficient
K_a = Abutment contraction coefficient
H_e = Total head on crest

As a result of extensive studies based on hydraulic model investigations of a number of spillways, WES has developed design charts for different configurations of piers and abutments. Generally, the pier contraction coefficient is affected by the shape and location of the pier nose, thickness of the pier, the head in relation to the design head, and the approach velocity. For condition of design head H_d, average pier contraction coefficients can be taken as follows:

For square-nosed piers with rounded corners 0.02
For round-nosed piers 0.02
For pointed-nose piers 0

The abutment contraction coefficient is affected by the shape of the abutment, the angle between the upstream approach wall and the axis of flow, the head in relation to the design head H_d, and the approach velocity. For condition of design head H_d, average coefficients can be taken as follows:

For square abutments with head wall at 90° to direction of flow. . .0.20
For round abutment with head wall at 90° to direction of flow and the radius of rounding the abutment corner between 0.15 H_o and 0.5 H_o. . .0.10
For rounded abutments with radius larger than 0.5 H_o and head wall is placed not more than 45° to direction of flow. . .0

For more details, reference may be made to WES-HDC 111-3/1, 111-3/2, 111-5, and 111-6. Refer to 122-2 for WES original profile and chart WES-HDC 11-22 for the elliptical crest spillway.

The effect due to interference caused by the downstream apron, in terms of variation of (C_a/C), the ratio of modified coefficient to free discharge coefficient, with respect to apron effect, has been studied in terms of variation of the parameter (h_d + d)/H_e as shown in Figure 8a. It can be seen that when this parameter exceeds about 1.7, the downstream floor has practically no effect on the discharge coefficient. The effect of submergence of crest by tail water on discharge coefficient is studied in terms of parameter (h_d/H_e), also called degree of submergence. Figure 8b also shows the variation of the factor (Cs/C), the ratio of modified coefficient to free discharge coefficient with respect to degree of submergence. It can be seen that the coefficient of discharge begins to be influenced by the submergence when the degree of submergence (expressed as the depth of TW above the crest/head on crest) exceeds about 40%.

A similar study by the WES (HDC-4/1), shown in Figure 9, indicates that for the spillway operating at the design head, the transition from the free uncontrolled flow to the submerged uncontrolled flow takes place at approximately 40% submergence of the crest.

The coefficient of discharge, among other parameters, is also influenced by the depth of approach on the upstream. Reference to Figures 6 and 7 indicates that the coefficient of discharge would decrease as the depth of approach decreases. However, there is no indication as to the expected value for a depth of

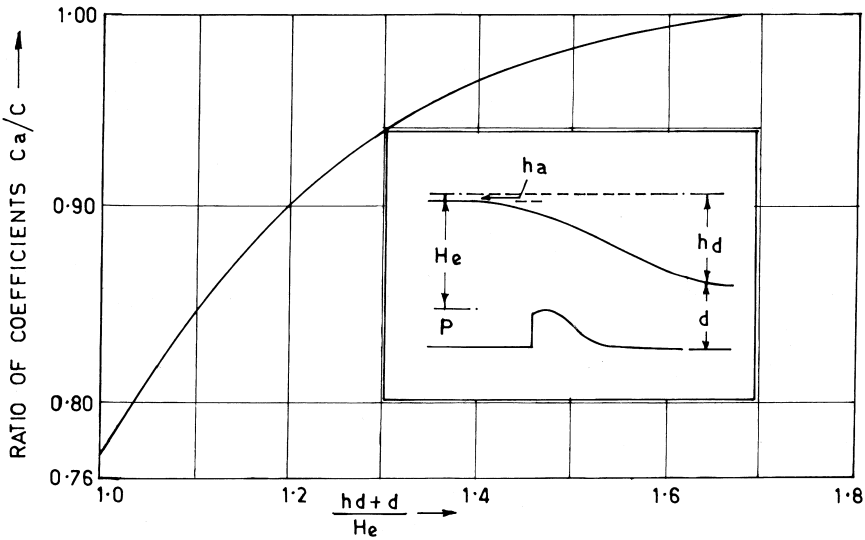

Figure 8a Effect of downstream apron. (USBR, Ref-11)

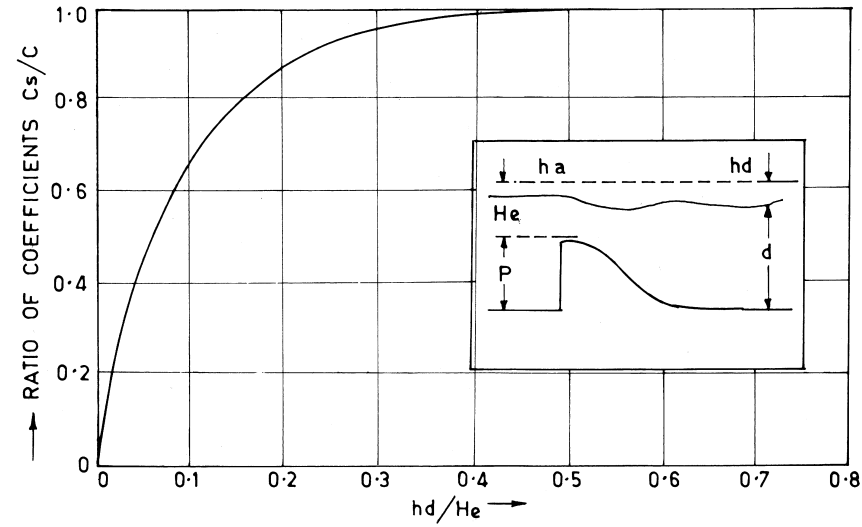

Figure 8b Effect of submergence by tail water. (USBR, Ref-11)

approach equal to zero, i.e., for the condition when the level of deposition has reached the crest level of the spillway. The question is particularly relevant to the low height spillways where the reservoir could be silted up to near about crest level. In this connection, Suryavanshi (1972) conducted model experiments for a 8 m high ungated weir, reproducing upstream bed profile as it originally existed at the time of construction, as per the deposition that took place after

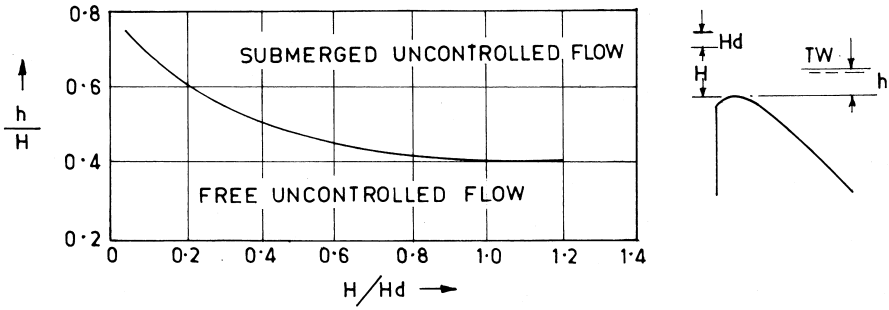

Figure 9 Transition from free to submerged flow. (WES, Ref-10)

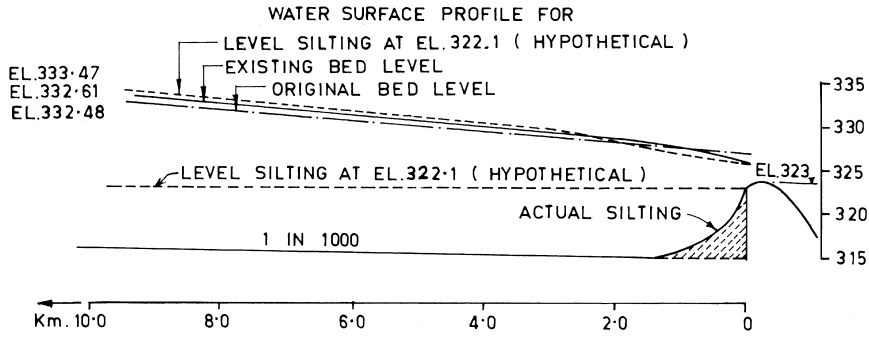

Figure 10 Effect of silting upstream of the spillway. (Suryavanshi, Ref-9)

45 years, and corresponding to a hypothetical case of the deposition occurring horizontally up to the crest level of the spillway. It was found that the coefficient of discharge of 2.143, corresponding to the original bed level, decreased to a value of 1.96 corresponding to the bed filled up to the crest level, i.e., a reduction of about 9.5%. The coefficient of discharge in both the cases was computed while taking into account the velocity of approach. However, the water level immediately upstream of the weir dropped from 5.27 m to 4.52 m corresponding to the design discharge intensity of 28.1 cumec/m, i.e., a reduction of about 14%. It was also found that although the water levels immediately upstream of the weir were lower, the afflux on the upper reach increased as the bed levels increased. Figure 10 shows the pertinent results of the studies by Suryavanshi.

Application of the design charts and values mentioned above would provide fairly accurate values for the purpose of preliminary designs. Hydraulic model investigations for a number of spillways have indicated close conformity between the calculated and observed values within $+/-$ 5%.

4.4 DISCHARGE COEFFICIENT VERSUS CREST PRESSURES

Figure 11 shows pressure distribution for various heads for the profiles with upstream vertical face. It is seen that the head on the crest influences the pressure distribution predominantly more than other factors such as P/H_d or slope of the upstream face. All other conditions remaining the same, pressures along the side of the crest piers are always lower than those along the center line of the span.

When a spillway operates with heads larger than the design head, the discharge coefficient increases while the pressures on the crest decrease. This can

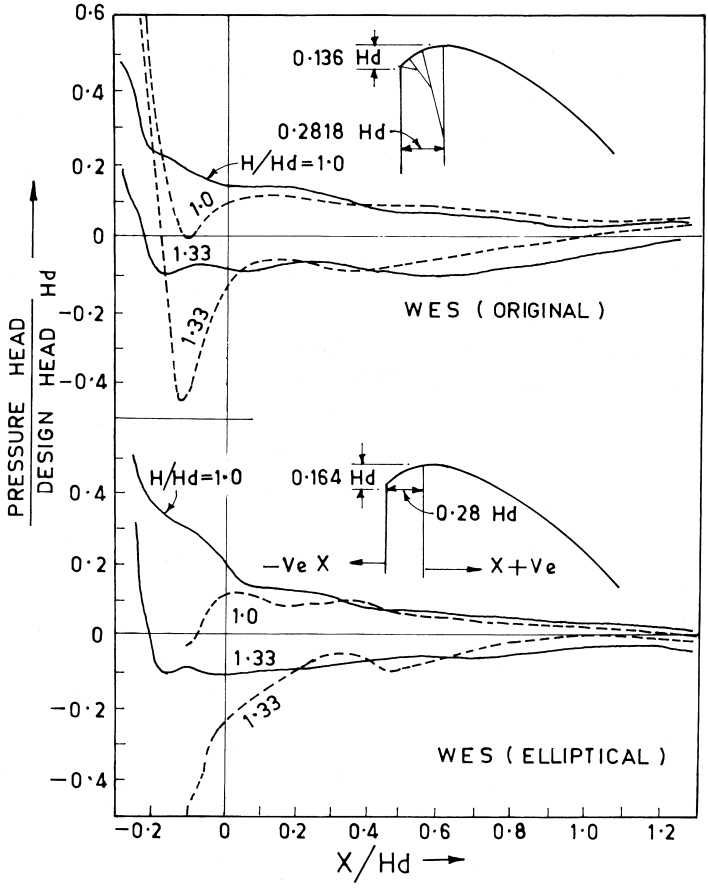

Figure 11 Pressure distribution on crest profiles: —— Pressure along CL of span and – – – Pressure along side of piers. (WES, Ref-10)

be explained with reference to Bernoulli equation where a reduction in pressure accompanies an increase in the flow velocity over the crest. Increasing the coefficient of discharge by operating the spillway with heads larger than the design heads, or designing the crest profile for a head smaller than a normal operating head, can help reduce the size of the structure. During the 1930s and 1940s, researchers had concentrated on this aspect of spillway design. The results of experiments conducted by Rouse and Reid (1935) plotted in Figure 12 show the increase in the coefficient of discharge with increase in the head, which also

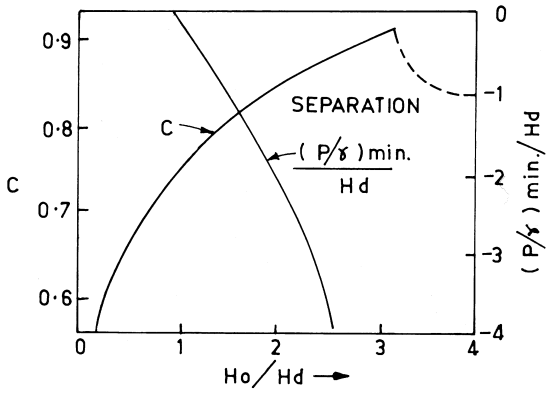

Figure 12 Discharge coefficient versus crest pressures. (Rouse et al.-Ref 8)

reduces the crest pressures. It would be seen that for heads higher than three times the design head, the coefficient of discharge drops sharply because of separation of the flow from weir surface.

4.5 DETERMINATION OF DESIGN HEAD

The increase in discharge capacity of a given crest shape as a result of an increase in the operating head, and consequently a reduction in crest pressure, would be restricted by the possibility of cavitation. In this regard, the minimum crest pressure and its location in relation to the operating head are relevant. WES suggest that the maximum negative pressure on the crest should be restricted to -20 ft (-6m) of water and that the crest profile be designed for a head $H_d = 0.309\ (He)^{1.2186}$ (in ft units), where He is the maximum operating head. Hager (1991) has generalized the results of studies of various research workers as follows:

The absolute minimum of crest pressure P_{min}

$$(P_{min}/H_o) = \gamma(1 - \chi) \tag{14}$$

where

$\chi = H_o/H_d$

H_o = Operating head

H_d = Design head, and

γ = Coefficient of proportionality

= 1 for WES profile with 45° downstream slope

= 0.9 for WES profile with 30° downstream slope

The location of zero bottom pressure, X_o from crest axis

$$X_o / H_d = 0.9 \tan \alpha \, (H_o/H_d - 1)^{0.43} \quad (15)$$

where

α = Angle of downstream slope

The coefficient of discharge

$$C_d = \frac{2}{3\sqrt{3}}\left[1 + \frac{4\chi}{9+5\chi}\right] \quad (16)$$

in the equation $Q = Cd.\, b.\sqrt{(2gH^3)}$

or

$$C = \frac{1}{\sqrt{3}}\left[1 + \frac{4\chi}{9+5\chi}\right] \quad (16a)$$

in the equation $Q = 2/3.C.b.\sqrt{(2gH^3)}$

The limiting operating head H_L for a given crest profile is governed by the magnitude of the minimum pressure on the crest which could induce cavitation. Theoretically, this pressure is the vapour pressure P_v. Inserting P_v in place of P_{min} in Equation 14 yields

$$H_L = [\gamma(1 - \chi)]^{-1} P_v \quad (17)$$

where

H_L = Limiting operating head in meters

P_v = Vapor pressure of water in meter of water

Cavitation is also dependent on the air content and particularly on the local turbulence level and smoothness of the flow surfaces. Considering the uncertainties of these factors, Abecasis (1970) assumed a minimum pressure of -7.6 m (25 ft) for incipient cavitation. Experimental results of Abacasis in a test facility creating an incipient cavitation condition are shown in Figure 13, which define

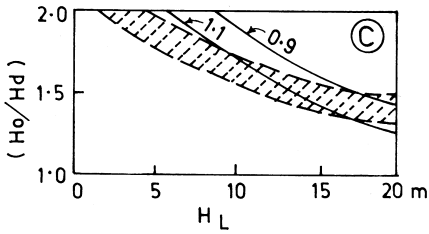

Figure 13 Experimental results of Abacasis 1970:—— Equation 4.17 with $\gamma = 1.1$ and 0.9— — Limit head Vs Relative head © Domain of definite cavitation.

H_L in terms of susceptibility to cavitation. However, a reliable indicator of cavitation is the cavitation index discussed in the chapter ''Cavitation in Spillways and Energy Dissipators.''

4.6 CREST PIERS

Crest piers are required when gates are to be installed to control the flow passing down the spillway. Piers may still be required for an ungated spillway for a road bridge. The most common shape of the pier includes a semi-circular upstream end kept flush with the upstream face of crest. Piers projecting upstream of the spillway face may be required from structural considerations and have smaller contraction coefficients. Generally, the crest piers have a consistent thickness but those that taper in the flow direction are preferred, if permissible by structural considerations. On the other hand, piers with gradually flared ends—more common in China—are adopted to expand the flow coming out of the gates in order to aerate it as much as possible and to prevent cavitation damage on the downstream face. This is discussed in detail in the chapter ''Air Entrainment and Forced Aeration''.

4.7 DOWNSTREAM SLOPE OR REAR SLOPE

The downstream slope is made tangential to the crest profile with the angle of the slope generally determined by requirement of structural stability. Slopes are usually in the range of 0.6:1 to 1.1:1. The rear slope together with sidewalls constitutes the discharge channel leading the flow from the crest to the energy dissipator. Because of the acceleration of the flow and the gradual increase in the velocity, extreme care is required to ensure that the profile of the discharge channel, both in elevation and plan, strictly conforms to the design profile. Deviations in these have resulted in severe damage in some projects. Also, the specified tolerances of surface finish is to be adhered to, as otherwise cavitation damage can be inflicted if flow velocity exceeds 25 m/s. Discussion on this aspect is, however, deferred until the chapter ''Cavitation in Spillways and Energy Dissipators''.

4.8 WATER SURFACE PROFILE

Water surface profiles in the crest region of standard spillway profiles, including the effects of piers and abutments, have been given in WES, HDC No. 111–11

to 111–14/1. Hager's (1991) generalized relationship for a freely overflowing spillway without piers, etc. is

$$S = 0.75\ [\chi^{1.1} - (1/6)X] \tag{18}$$

where

$S = s/H_d$
s = Vertically measured flow depth
$X = x/H_d$
x = Longitudinal coordinate
and $-2 < X < +2$

4.9 SPILLWAY TOE

The spillway toe is the junction between the discharge channel and the energy dissipator. Its function is to guide the flow passing down the spillway and smoothly in the energy dissipator—particularly hydraulic jump stilling basin apron—without unacceptable flow conditions. A toe curve is made up of a circular arc, tangential to both the rear slope and the apron as shown in Figure 14. The radius of such a curve should be such that the high velocity flow can change its direction smoothly, without hurdling. A minimum radius of 3 times the depth of flow entering the toe is recommended.

The pressures on the floor and sidewalls in the region of the curvature increase due to centrifugal action. The resulting pressure is the summation of the hydrostatic pressure and the centrifugal pressure, given by

$$P_b = y_1 + \frac{y_1 V_1^2}{gR} \tag{19}$$

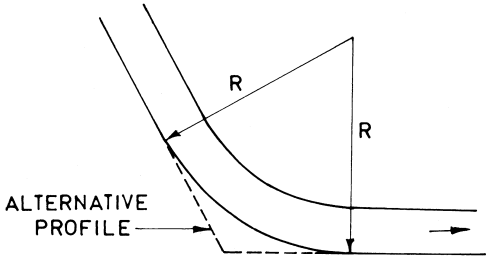

Figure 14 Toe curve at the base of spillway.

where

y_1 = Depth of flow at the toe
V_1 = Velocity of the flow at the toe
R = Radius of the toe curve

A spillway toe may also be without any curvature, as in the form of an intersection of the rear slope and the apron, as shown in Figure 14. This is, however, restricted to small and medium height spillways, as otherwise, the flow from the spillway would impinge on the apron and exert fluctuating pressures of high amplitude, leading to damage.

Notations

A = Constant
= Semi-major axis
B = Constant
= Semi-minor axis
b = Width of spillway
C = Coefficient of discharge
(Dimensionless)
C_c = Coefficient of contraction
C_d = Coefficient of discharge
C_v = Coefficient of velocity
C_s = Coefficient of discharge of submerged crest
d = Depth of water over apron
H = Depth of overflow
H_d = Design head for crest profile
H_e = Depth of overflow inclusive of head due to velocity of approach
H_o = Head on crest other than design head (operating head)
hd = Head drop between upstream water level and downstream water level
K = Constant
K_a = Abutment contraction coefficient
K_p = Pier contraction coefficient
L = Effective length of crest
L′ = Net length of crest
N = Number of piers
n = Constant
P = Height of crest from upstream bed
P_b = Total pressure at the toe of the spillway
P_{min} = Minimum pressure on crest profile
P_v = Vapor pressure of water
Q = Discharge

R = Radius of the toe curve
s = Vertically measured flow depth
S = s/H_d
V = Velocity of flow
V_1 = Velocity of flow entering the toe of the spillway
X = x − co-ordinate
= Normalized x − coordinate (χ/Hd)
X* = 1.3055 (X + 0.2818)
x = x − co-ordinate
Y = y − co-ordinate
y = y − co-ordinate
y_1 = Depth of flow at the toe
Z = Normalized Z − co-ordinate (Z/Hd)
Z* = 2.7050 (Z + 0.136)
α = Angle of downstream slope
γ = Coefficient of proportionality
χ = (H_o/H_d)

REFERENCES

1. Abecasis, F. M. Discussion on – Designing spillway crest for high-head operation. Jnl. ASCE, Hyd. Engg, 1970, 96(No.12).
2. Grzywienski, A. Anti-vacuum profiles for spillways of large dams; Trans. 4th ICOLD, New Delhi: India, 1951; Vol. 2.
3. Hager, W. H. Continuous crest profiles for standard spillway. Jnl. ASCE, Hyd. Engg, 1987, 113(No.11).
4. Hager, W. H. Experiments on standard spillway flow. Proc. Instn. Civil Engrs, Part 2, Sept. 1991.
5. Lemos, F. O. Criteria for the hydraulic design of overflow dams with 2:3 upstream face slope-13th ICOLD, Q 50, R 1 New Delhi, 1979.
6. Magalhaes, A. Comments on the paper- Criteria for the hydraulic design of overflow dams with 2:3 upstream face slope, by Lemos, Q 50, R1, in Vol 5, page 517, 13th ICOLD, New Delhi, 1979.
7. Murphy, T. E. Spillway crest design - Misc Paper No. H-73–5, U.S. Army Engineer Waterways Experiment Station, 1973.
8. Rouse, H.; Reid, L. Model research on spillway crests – Civil Engineering, January 1935.
9. Suryavanshi, R. D. The effect of silting on flow profile upstream of weirs- A case study- Irrigation and Power (CBIP), October, 1972.
10. US Army Engineer – Waterways Experiment Station – Hydraulic Design Criteria – 1952 and subsequent editions.
11. United States Bureau of Reclamation (USBR) – Design of small dams – 1960 and subsequent editions.

5
Chute and Side Channel Spillways

5.1 INTRODUCTION

Whenever possible, spillways are located in the main gorge of a river as this has an inherent advantage of confining flood flows within the banks of a river. Except for the creation of a reservoir upstream of the dam, the main direction of the flow in the downstream is maintained unchanged, as far as possible, by a proper alignment and location of a spillway in the main gorge. Although hydraulically more suitable, it would not be always possible to design heavy structures such as spillways, if a suitable foundation is not available in the main gorge. Then, a choice has to be made to locate the spillway structure on the flank.

Constructing a spillway at any place other than the main gorge involves considering the topography and geology of the site. Topography may favor a spillway located in a saddle away from the main dam with the flow from the spillway led to the main river in the downstream. However, it may also be advantageous to locate the spillway on one of the flanks connecting the crest structure by an artificially created approach channel on the upstream and chute on the downstream. This arrangement results in a chute or a side channel spillway, depending on the type of the control structure, which is governed by the local topography. In a chute spillway, the discharge passing down the crest is conveyed to the river downstream, with the flow taking place in a direction almost normal to the width of the spillway. In a side channel spillway, the crest structure is placed along the side of, and approximately parallel to, the upper portion of the spillway discharge channel. Flow over the crest falls into a narrow trough opposite the crest, turns approximately at a right angle, and then continues into the main discharge channel. Except for the control structure and the portion immediately downstream, the design of other elements such as approach channel, chute, energy dissipater, etc. is identical in both the cases.

5.2 PRINCIPAL ELEMENTS

A chute or side channel spillway generally consists of an approach channel, a flow control structure, a discharge channel or chute, energy dissipater, and a tail channel. Since the spillway is located on the flanks, which are at higher levels than the gorge, it becomes necessary to lead the water from the reservoir by means of an open channel called an approach channel. Because of the higher ground levels, the spillway structure is usually short and it may be gated or ungated. The discharge then passes down the carrier channel or chute which leads the flow to the energy dissipator. The energy dissipators are usually designed as a stilling basin, flip bucket or roller bucket, etc. The flow from the energy dissipator is led to the main river through a tail channel which may be a natural or artificial waterway.

Figure 1 and Figure 2 respectively show typical layouts and details of chute spillway and side channel spillway.

5.3 APPROACH CHANNEL

The approach channel is an artificial channel leading the flow from the reservoir to the spillway. Since chute spillways are located in the flanks it becomes necessary to create a flow passage from the reservoir to the spillway structure. There are two main hydraulic considerations in the design of approach channel. First, the length and layout of the channel should be such as to result in minimum loss of head. Secondly, the flow approaching the spillway should be distributed as uniformly as possible. This is important since uneven flow over the spillway would create unsatisfactory flow conditions on the chute and in the energy dissipator.

Several layouts are possible depending upon the topography and other site conditions. However, hydraulic model study is generally conducted to evolve a satisfactory layout accomplishing the objectives stated above. Based on the results of a number of model studies, some guidelines are available for preparing a preliminary layout.

The bed of the approach channel below spillway crest may be at least 1/5th the design head on the spillway and the approach velocity for the design discharge may be generally not more than 3 m/s. In some cases, a velocity up to 6 m/s has been allowed (Beas dam, India).

A straight alignment of the approach channel would result in nearly uniform distribution of discharge over the spillway. However, in a majority of designs, the straight length immediately upstream of the spillway has to be restricted to a minimum owing to huge hill excavations and, therefore, a curved layout becomes inevitable. A minimum straight length of the order of 1 to 1.5 times the width

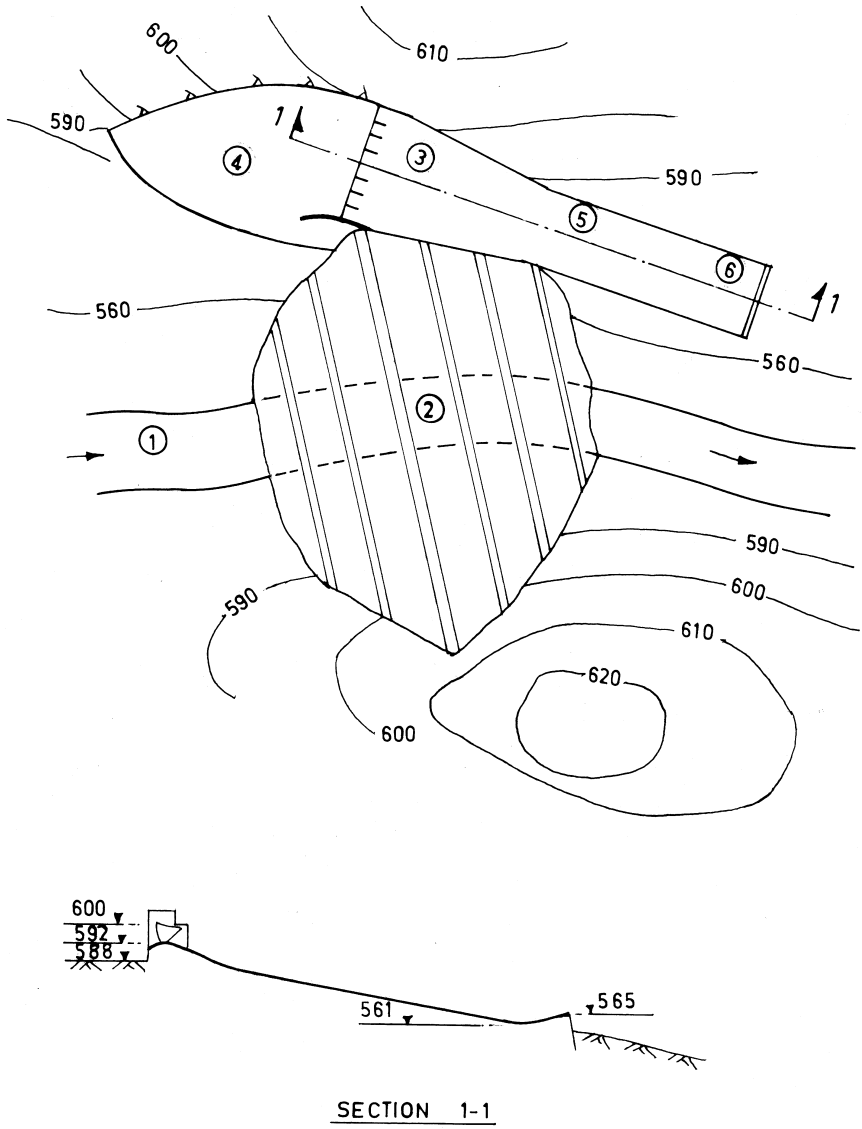

Figure 1 **Typical layout of a chute spillway**: (1) River, (2) Earth dam, (3) Spillway, (4) Approach channel, (5) Chute, (6) Flip bucket.

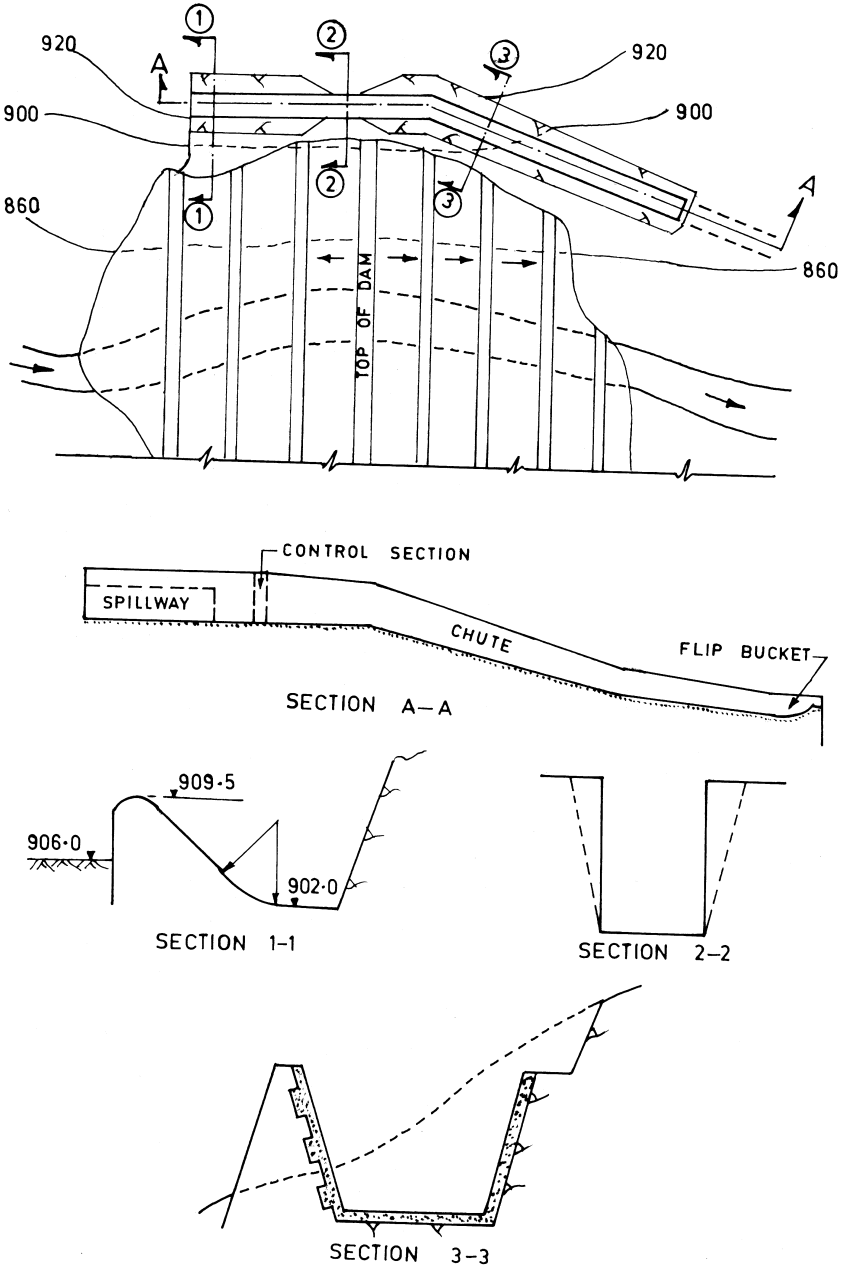

Figure 2 Typical layout of a side channel spillway.

of the spillway is recommended. The ratio (R/y) radius of curvature to the depth of flow at the crest should be as large as possible, but no smaller than about 3.

In some cases, a converging alignment towards the crest, from a wider channel to a channel width equal to the spillway width at crest, is also found to be effective in equalizing the flow distribution.

Because of obliquity, flow parallel to an earth dam may be induced, causing disruption of the stone pitching on the upstream face. Incorporating a training wall on the flank of the spillway (between the spillway and the earth dam) and extending the same on the upstream helps create a stagnant zone upstream of the earth dam and also improves approach conditions near the spillway. This effect can be studied on a hydraulic model.

5.4 SPILLWAY STRUCTURE

In both the types of spillways, the structures consist of a standard ogee shaped crest, although unconventional shapes of crest have been used in special conditions, as for example, an existing earth dam was concrete lined to act as a spillway at Bearspaw project, Canada. The crest structure in chute spillways is generally low in height to take advantage of the higher ground levels on the flank. In design, the majority of chute spillway structures have a straight alignment, with a few on a circular arc to facilitate converging chutes.

Side channel spillways may have straight, L-shaped, or U-shaped layouts in plan. Hajdin (1979) has described a special form of a Y-shaped side channel spillway. Balbacher et al. (1979) have described a U-shaped layout of a side channel spillway for Al Ibtissam dam (Algeria) where part of the spillway crest is gated, with an ungated portion at a higher crest elevation

Figure 3 shows various plan forms of chute and side channel spillways.

In a chute spillway, the crest structure is joined to the discharge channel (chute) through a toe curve. However, in many cases, the rear slope of the spillway continues as the chute. Supercritical flow expands after flowing past the downstream end of a spillway pier. The expanding flow from each side of a pier will intersect and form a disturbance, which is termed a pier end wave. These waves travel laterally as they move downstream. Multiple piers will cause a formation in a diamond pattern of waves within the chute. The impact at the intersection of the flow can be so severe that a rooster tail-like plume of water will form. The US Army Corps of Engineers (1990) suggests the following equation for the location on the sidewall where the wave from the first pier intersects the wall:

$$z = \frac{x}{Tan\left\{Sin^{-1}\dfrac{\sqrt{gy}}{V_s}\right\}} \ldots. \tag{1}$$

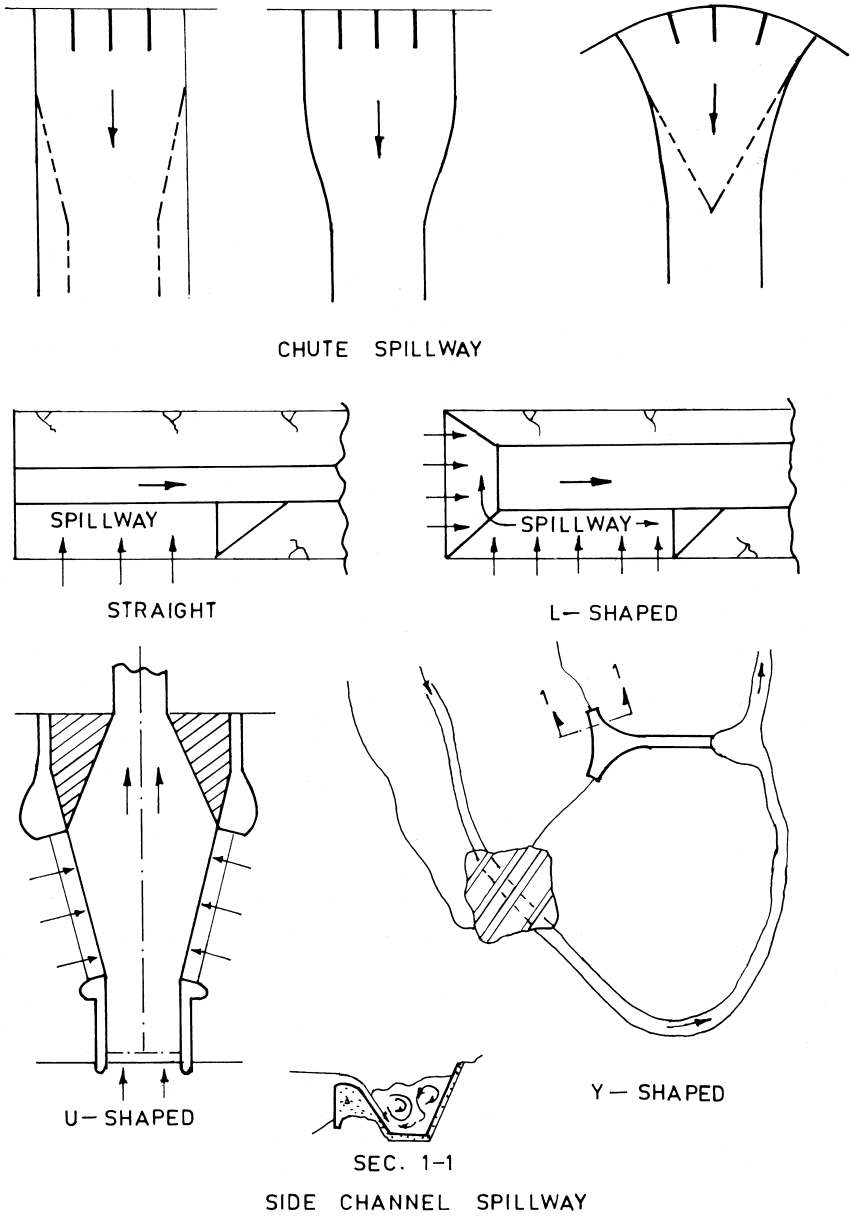

Figure 3 Plan forms of chute and side channel spillways.

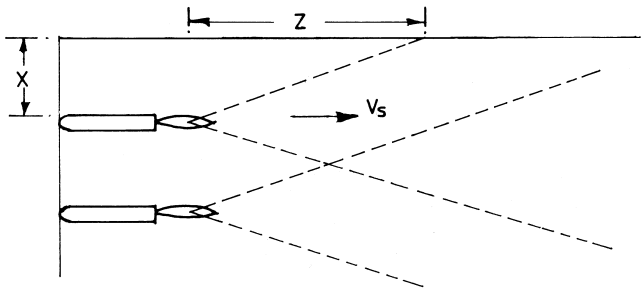

Figure 4 **Pier end waves downstream of spillway piers** (courtesy of WES 1990)

Referring to Figure 4, where

z = Distance from downstream end of pier to wave and wall intersection
x = Distance from first pier to the wall
y = Depth of flow
V_s = Surface velocity

It is suggested that wave height should be relatively small compared to the depth of the flow, and the velocity should be taken as the surface velocity, which can be approximated as twice the average velocity. The magnitude of pier end wave is difficult to determine without a model study. For a design without the benefit of the model study, it is suggested that an additional 25% of the depth of flow should be included in the sidewall height to account for the pier end waves.

5.5 SIDE CHANNEL SPILLWAY-TROUGH AND CONTROL SECTION

As shown in Figure 2, a side channel spillway combines an overfall section with a channel parallel to it, which carries the spillway discharge away to a chute or a tunnel. The analysis of flow in a side channel spillway has undergone gradual refinement over the years. The simplest form of analysis is based on the law of conservation of linear momentum, assuming that the only force producing motion in the channel results from the fall of water surface in the direction of spillway axis. The energy of the flow falling down the crest is assumed to be dissipated through its intermingling with the channel flow and offers no assistance in moving the water. Basic criteria for the design of side channel spillways have been proposed by Hinds (1926) and Favere (1933). Farney et al. (1962) pointed out the importance of the momentum correction coefficient.

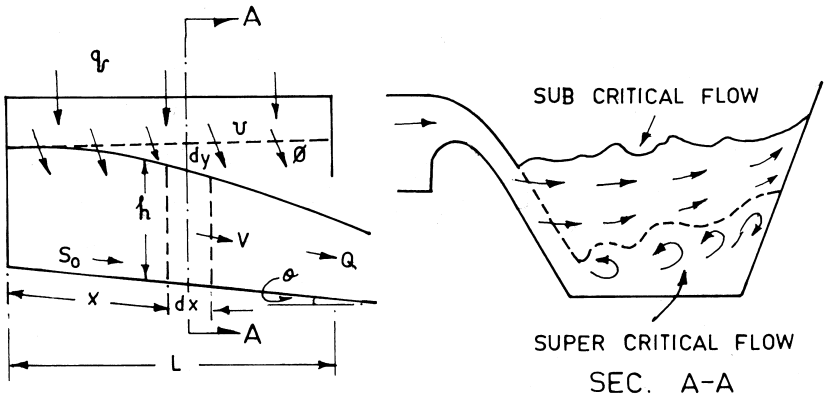

Figure 5 **Analysis of flow in a trough.**

Referring to Figure 5, the differential equation of the flow profile ignoring channel friction is given by

$$\frac{dy}{dx} = \frac{1}{g}\left(V\frac{dV}{dx} + \frac{V^2}{x} \right).. \tag{2}$$

where

dy = Fall in the water surface along the channel length dx
V = Average velocity at the cross-section under consideration
x = Distance measured along the channel from upstream end

Since the discharge increases linearly with the distance, the velocity can also be assumed to vary with x in some arbitrary manner, provided that the channel is designed to produce such a relation. An exponential type of relationship can be assumed as

$$V = a\,x^n \tag{3}$$

from which

$$\frac{dV}{dx} = nax^{n-1} = \frac{nV}{x} \tag{4}$$

With this, equation (2) would be

$$y = \frac{a^2(n+1)}{g(2n)}x^{2n}. \tag{5}$$

Or

$$y = \left(\frac{n+1}{n}\right)\left(\frac{V^2}{2g}\right)... \tag{5a}$$

To satisfy this, the channel cross-section and bottom profile must be designed in such a way as to make the water surface drop proportionately to its velocity head.

The constants a and n are arbitrary and may be selected in such a way as to produce a profile that will most economically conform to the site conditions. From Equation 5, it can be seen that when n = 1/2, the profile will be linear, concave downward for n >1/2 and concave upward for n <1/2. The flow profile can be computed from the velocity and cross-sectional area. The equation of the channel bottom can be determined by accounting for the depth of flow with reference to the flow profile. Usually, the water level at the outlet end would be fixed by the control section leading to the discharge channel. This will automatically fix the constant a if the exponent n is assumed.

Illustrative Examples

A 50 m long side channel spillway will have a maximum discharge of 200 cumec with a depth of overflow of 1.5 m. The channel cross-section is trapezoidal with a bed width of 12 m and side slopes of 2V:1H. The depth of flow at the end of the spillway will be 5 m (with a suitable control in the downstream). The velocity of flow is to vary linearly as the distance from the beginning of the spillway. Determine the equation of the flow profile and channel bottom, neglecting the effects due to uneven distribution of velocity and channel friction.

Referring to Figure 6, the cross-sectional area of the flow is 72.5 sq.m and hence the velocity will be 200/72.5 = 2.76 m/s.

Also, V = a $x^{1/2}$ from which, a = $2.76/50^{1/2}$ = 0.39 and the equation of the flow profile will be

$$y = \frac{a^2(n+1)}{2ng}x^{2n} = \frac{(0.152)(1.5)}{2(0.5)(9.81)}x = 0.0233x \quad \text{or} \quad y = 0.0233x \tag{5b}$$

Thus, the water surface will be (0.0233 × 50 =) 1.16 m below the spillway crest at the end of the spillway and at the level of the crest at the beginning of the spillway. The channel bottom, similarly, is 5 m below the respective water level, i.e., on a slope of 1V: 43.1H, as shown in Figure 6.

A procedure without imposing any relationship between the average velocity V and distance x has been suggested by USBR (1977), as

$$\Delta y = \frac{Q_1}{g}\frac{(v_1+v_2)}{(Q_1+Q_2)}\left[(v_2-v_1)+\frac{v_2(Q_2-Q_1)}{Q_1}\right] \tag{6}$$

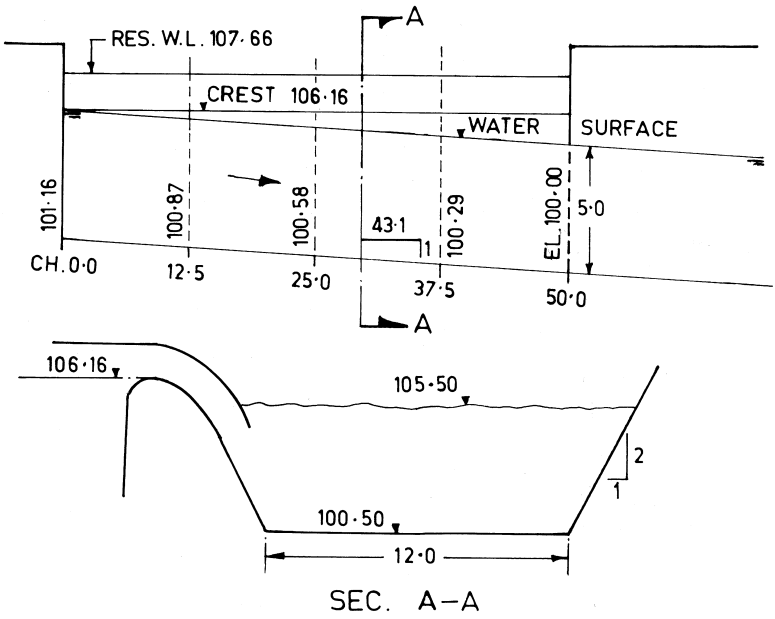

Figure 6 **Side channel spillway: illustrative example.**

which can be applied to calculate the water surface profile in a step-by-step manner. Here Q_1 and v_1 and Q_2 and v_2 are the discharge and velocity at the beginning and end of a small distance $\triangle$x.This procedure has been illustrated by a few steps, for the above example, with the channel bottom slope of 1V: 43.1H and depth of flow of 5 m, as shown in Table 1.

The effect of channel friction and uneven velocity distribution can be introduced considering that A = Q/V (at respective locations), $h_f = S_f$ .dx, and x = S_0.dx etc.

$$\frac{dy}{dx} = \frac{S_0 - S_f - 2\alpha Qq / gA^2}{1 - \alpha Q^2 / gA^2 D}. \tag{7}$$

where

S_0 = Bed slope
S_f = Friction slope
α = Energy correction coefficient
A = Cross-sectional area
D = Hydraulic depth A/B, where B = water surface width

Table 1 Solution of Equation 6 in a Stepwise Manner

St	Δx	Bed El	Trial Δy	W.S El	h	A	Q	v	Q_1+Q_2	$Q_1/[g(Q_1+Q_2)]$	(v_1+v_2)	(v_2-v_1)	(Q_2-Q_1)	$(Q_2-Q_1)/Q_1$	$v_2(Q_2-Q_1)/Q_1$	(13)+(16)	Δy=(11)×(12)×(17)	Remarks
(1)	(2)	(3)	(4)	(5)	(6)	(7)	(8)	(9)	(10)	(11)	(12)	(13)	(14)	(15)	(16)	(17)	(18)	(19)
50	–	100	–	105	5	72.5	200	2.76	–	–	–	–	–	–	–	–	–	–
37.5	12.5	100.29	0.5	105.5	5.21	76.1	150	1.97	350	0.0437	4.73	0.79	50	0.333	0.92	1.71	0.353	too large
			0.3	105.3	5.01	72.67	150	2.06	350	0.0437	4.82	0.70	50	0.333	0.92	1.62	0.340	OK
25	12.5	100.58	0.24	105.59	5.01	72.67	100	1.38	250	0.041	3.42	0.66	50	0.50	1.02	1.68	0.236	OK

The procedure of calculation has been illustrated by a few steps in the case of the same example with energy correction coefficient $\alpha = 1.1$ and Manning's $n = 0.015$, (Table 2).

An alternative form of Equation 7 is

$$\frac{dy}{dx} = \frac{S_0 - S_f - 2Qq / gA^2}{1 - F^2} \ldots \tag{8}$$

$$F^2 = Q^2B/gA^2$$

Location of critical flow section X_c in an uncontrolled channel is given by

$$X_c = \frac{8q^2}{g\,B^2\left(S_0 - \dfrac{gP}{C^2B}\right)} \tag{9}$$

where

P = Wetted perimeter
C = Chezy coefficient

This can be solved by a trial method, in conjunction with the relationship for the critical depth, for a given channel section, assuming the total discharge Q at a trial distance x. With the critical depth so obtained, values of B, P, and C can be worked out to get Xc from Equation 9. If this is not the same as the assumed distance X, calculations should be repeated with other value of X till the desired agreement is obtained.

If $X_c < L$, the total length of the channel, it would mean that the flow upstream of the critical flow section would be sub-critical and downstream of it will be supercritical. In such a case, it would be desirable to provide a control section in the downstream to ensure sub-critical flow in the entire length of the trough. In fact, a water surface in the trough that is as high as possible would be desirable to generate maximum intermingling of the flow and adequate dissipation of energy and hence smoother water surface in the trough (Fig. 5). The practical upper limit of water surface is the level that causes no more than 50–60% submergence of the spillway crest.

Other parameters in the analysis include the stream wise velocity component of the lateral inflow and the momentum correction coefficient β which replaces the energy correction coefficient α. Although, in the preliminary analysis, it is assumed that the lateral inflow has no component in the channel direction, experiments have indicated that such a component exists, especially if the channel bed has a slope in the direction of flow.

Yen and Wenzel (1970) have presented a generalized equation for the free surface flow in a trough as

Table 2 Solution of Equation 7

St (1)	Δx (2)	Bed El (3)	Trial Δy (4)	WS El (5)	h (6)	A (7)	Q (8)	v (9)	P (10)	Δy (11)	αΔy (12)	R=A/P (13)	$h_t=\Delta x\,[n^2 v^2/R^{4/3}]$ (14)	Δy=(12)+(14) (15)	Remarks (16)
50		100		105.0	5.0	72.5	200	2.76	–	–	–	–	–	–	–
37.5	12.5	100.29	0.5	105.5	5.21	76.1	150	1.97	23.65	0.353	0.388	3.218	0.0023	0.39	too low
			0.4	105.4	5.11	74.37	150	2.01	23.42	0.348	0.382	3.174	0.0024	0.385	low
			0.37	105.37	5.08	73.86	150	2.03	23.36	0.345	0.379	3.16	0.0025	0.38	OK

$$\frac{dh}{dx} = \frac{S_0 - S_f + \frac{\beta V^2}{gA}\frac{\partial A}{\partial x} - \frac{V^2}{g}\frac{d\beta}{dx} + \frac{q}{gA}(UCos\phi - 2\beta V)}{Cos\theta - \frac{\beta V^2}{g\bar{h}}} \tag{10}$$

where

β = Momentum correction coefficient
θ = Bottom slope angle
A = Cross sectional area
ϕ = Angle formed by U with the channel axis
U = Velocity vector of the spilling flow

$$\bar{h} = \frac{A}{\partial A / \partial h}$$

= Hydraulic depth

The above relationship is quite complex and cannot be solved unless adequate information regarding the momentum correction coefficient β, its variation with respect to channel length, and the stream wise component of the lateral inflow are available.

Guercio and Magini (1998) have presented comparisons between experimental and computed water surface profiles. Experiments were conducted with a 1 m long side channel spillway placed parallel to a 0.2 m wide horizontal rectangular channel. The flow over the weir was assumed to be in a direction normal to the channel axis. The momentum correction coefficient β was evaluated from measurements of U and V. The equation was solved on a one-dimensional numerical model with $\theta = 0°$, $\Phi = 90°$ and S_f evaluated using Manning's formula.

The results of both the models agreed well. It was also seen that the difference between the computed and observed water levels, at the beginning of the channel, considering the value of β as unity and β as a function $\beta = \beta$ (U), was 15–20% of the depth of flow h and that at the end of the spillway there was practically no difference. Figure 7 shows typical variations of β as functions of distance x and mean velocity V, as obtained from experiments. It would be seen that solution of Equation 10 would require more precise information about the variation of β with reference to other parameters.

Bremen and Hager (1989) have presented comparisons between experimental and computed surface profiles based on Equation 10, for the case of a rectangular channel with linear width variation $B = b + \theta_x$ and constant bottom slope. It is stated that the lateral inflow velocity U depends on the difference of elevations between the head H on the spillway and the free surface profile h (x) and the lateral inflow angle Φ is equal to the bottom slope S_0. Thus, the stream wise momentum contribution per unit weight of fluid is (U Cosθ/V).

As can be seen, this relationship does not account for the momentum correction coefficient β. It was found that the experimental observations agreed fairly

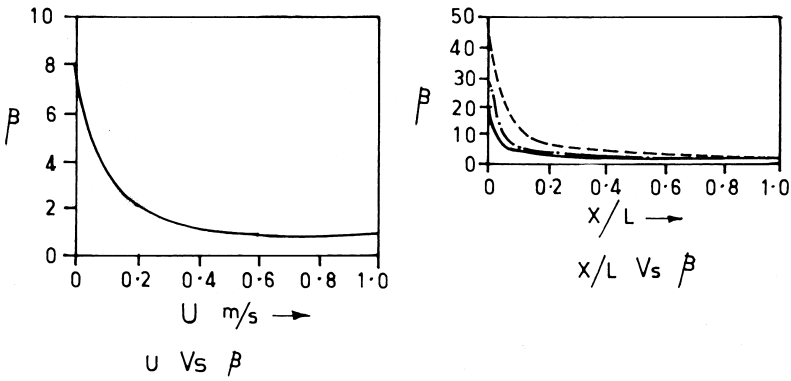

Figure 7 **Typical variations of momentum correction coefficient β:** —— Unsubmerged crest — · — · — -do- with storage in the trough –––– Submerged crest (courtesy of Guercio et al. 1998)

well with the predicted levels; however, notable deviations appeared between the water surface profiles along the channel axis and channel sidewalls. It was indicated that for agreement, effects of non-hydrostatic pressure and uneven velocity distribution, along with better simulation of the lateral inflow characteristics must be incorporated.

Knight (1989) states that using a weir that is L-shaped in a plan can reduce the amount of excavation and concrete required for a side channel spillway. The floor of the collecting trough rises to nearly the level of the end weir crest so that the downstream batter is almost continuous with the invert. The invert profile is curved or consists of a series of chords as shown in Figure 8. Knight has presented a modified momentum equation to include the downstream component of velocity of approach of lateral flow. For practical purposes, his analysis assumes momentum correction coefficient and cos θ equal to unity while neglecting channel friction. Knight's method can be used to design a side channel spillway that is U-shaped. An algorithm for the solution of momentum equation is also suggested.

A control section of the trough downstream is required to ensure sub-critical flow conditions in the trough but, more importantly, adequate volume of water in the trough to affect proper energy dissipation and smoother water surface. The most common form of control section is a contraction in the plan. Any change in the direction of the flow, contraction or expansion, could be accomplished easily if the flow in the concerned reach is sub-critical. Khatsuria et al. (1988) have described model studies incorporating chute sill to improve conditions in the trough as well as downstream chute, followed by a curvature in plan.

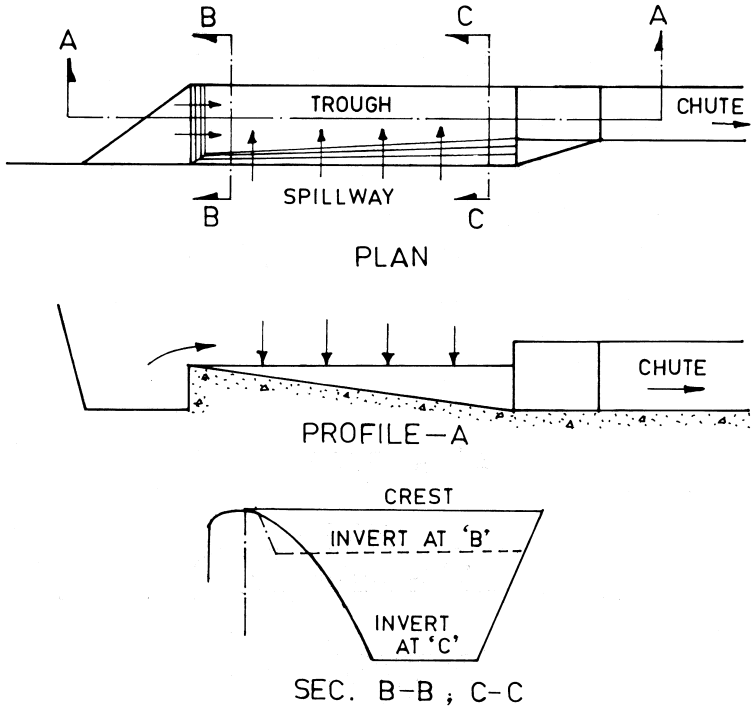

Figure 8 **L-shaped side channel spillway** (shown in Knight 1989).

5.6 CHUTE

A discharge channel downstream of the control structure, known as a chute, may be straight or curved with sides parallel, converging, or diverging. It may be either rectangular or trapezoidal in cross-section and may have either a constant or a variable bottom width.

Discharge channel dimensions are governed primarily by hydraulic requirements but the selection of profile, cross-sectional shapes, widths, and lengths is influenced by geological and topographical features at the site. Open channels excavated in the abutment usually follow the ground surface profile.

Since the flow in the chute is always supercritical, it is advisable to have a straight alignment without transitions such as constriction, expansion, or curvature. It is well known that such features induce shock waves that materially effect the flow profile and the entire characteristics of the flow. However, in many cases, deviation from a straight alignment or inclusion of transitions becomes necessary. When a chute spillway is located on a flank adjacent to the dam

abutment, curvature in the chute alignment often proves to be expedient in leading the flow from the spillway to the river downstream of the dam. Similarly, contraction or expansions may be necessary not only from topographical, geological, or economical considerations, but may also be dictated by hydraulic considerations, for example, to obtain the required intensity of discharge for the energy dissipator.

5.6.1 Contraction and Expansion

Contracting the width of a chute immediately downstream of the chute spillway is not recommended since the flow from the end spans will be obstructed by the converging walls and will create unacceptable flow conditions. A straight length of the chute, of at least one spillway width, is provided before introducing convergence of the chute.

Spillway chutes may have to be contracted or expanded in width, usually to obtain discharge intensity suitable for an energy dissipator that may have to be provided according to the site or hydraulic conditions. Basically, three types of contractions are used: funnel, fan, and nozzle, as shown in Figure 9. Usually, the first two types of contractions are common and have been investigated in detail. An excellent review including general design principles has been discussed in Bulletin No. 81 of ICOLD (1992).

Any attempt to deflect the supercritical flow, either into or away from the main flow, by a sidewall or other means, generates a standing wave-like feature also called a cross-wave. A positive cross-wave is generated at the point where the deflection is into the flow and results in an increased depth of flow downstream of the cross-wave. On the other hand, a negative cross-wave is generated at a point where the deflection is away from the flow. In this case, depth of flow downstream of the wave decreases. Both, the positive and negative waves have

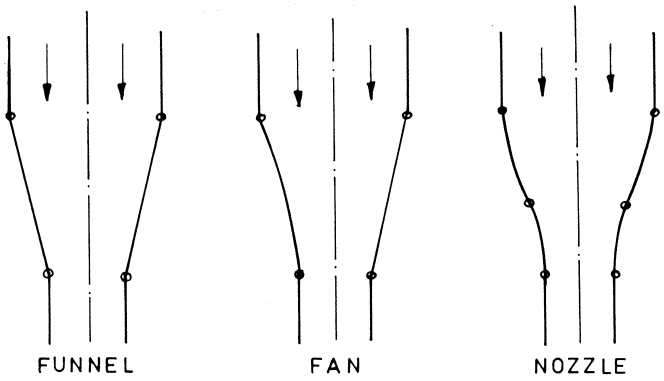

Figure 9 Types of contraction.

a tendency to reflect at the opposite wall and change the flow regime. The resulting flow conditions in the downstream are characterized by uneven water surface, unequal distribution of discharge across the width, and excessive air entrainment necessitating higher sidewalls. The main consideration in the design of channel contraction or expansion is to ensure uniform, parallel flow in the transition reach and further downstream as far as possible. For achieving this, the waves of opposite characteristics must be made to interfere with each other to compensate for the increase or decrease in the flow depth.

Funnel Type Contraction

The simplest, most effective, widely used contraction is the funnel type, consisting of straight-lined contracting walls, as shown in Figure 10. The general flow pattern resulting from such a contraction has been described by ICOLD (1992) with reference to the studies by Ippen and Dawson (1951) and has been shown in Figure 10a.

Here, θ is the angle of contraction and β_1 is the angle of cross-wave. As can be seen, the series of reflection of positive and negative waves creates disturbance in the flow downstream of the contraction. This can be eliminated if positive cross-waves generated at points A and B are directed to points C and D, where

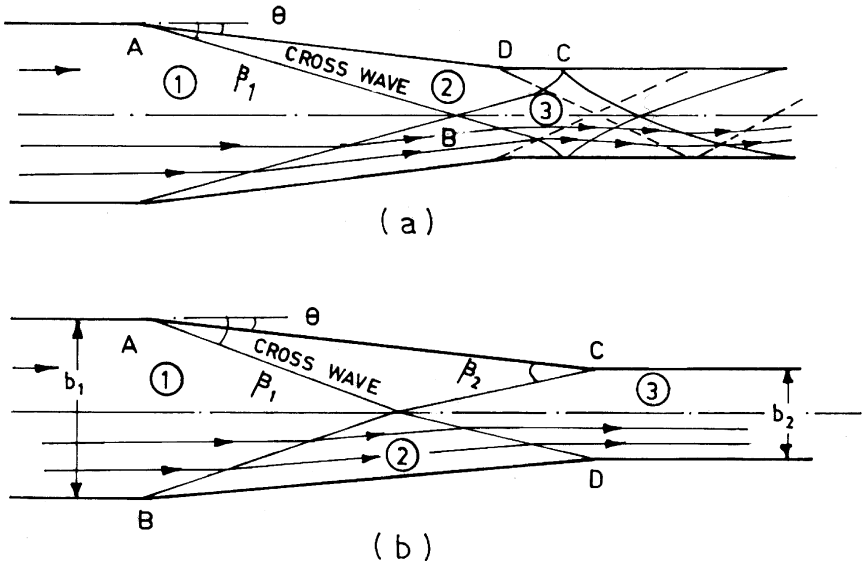

Figure 10 Flow in funnel type contraction (shown in Ippen et al. 1951).

negative cross-waves are generated, as shown in Figure 10b. The flow in domain (2) then will only be non-axial and will tend to be axial and parallel to sidewalls further downstream. For a given contraction ratio b_1/b_2 and the entrance Froude number F_1, there is a unique contraction angle θ for achieving the above condition. A set of equations relating θ, β_1, β_2, F_1, and F_2 exists that have to be solved either by trial method or graphically following the four-quadrant diagram proposed by Ippen (1951). ICOLD (1992) suggests an approximate expression, with reference to Hager and Bretz (1987), for contraction angles $< 10°$ which is

$$\theta = Tan^{-1}\frac{1}{2F_1}\left(\frac{b_1}{b_2}-1\right) \tag{11}$$

The ratio of Froude numbers is

$$\frac{F_2}{F_1}=\frac{1}{2}\left(1+\frac{b_2}{b_1}\right) \tag{12}$$

It is also suggested that for larger θ, the result should be checked against the possibility of the choking of the flow, if F_2 is close to unity. In such a case, hydraulic jump may take place in the contraction. The design should therefore, be based on $F_2 > 2$.

On the basis of experimental results, USBR (1977) have suggested an angle corresponding to

$$Tan\,\theta = \frac{1}{3F_a} \tag{13}$$

Where F_a equals the Froude number of the flow, based on average values of velocities and depths of flow, at the beginning and end of contraction.

It is stated that Equation 13 gives slightly conservative values and has also been recommended for expansion.

USACE (1990) suggest that the ratio $\Delta L/\Delta W \geq 5$, where ΔL is the change in centerline length and ΔW is the corresponding change in width. The contraction should not exceed beyond the section where $F > 1.5$.

Although simple and effective, the above design has a limitation in that the desired interference of waves exist only at one value of F_1; for other values of F_1, the reflected waves do not strike at C, D, etc. However, it may still give good results at the downstream end of chutes, which are long enough for the flow to become uniform.

Fan-shaped Contraction

For the spillway crests aligned on circular arcs, a fan-shaped contraction becomes necessary in order to guide the flow smoothly from the end spans. Typical details of a fan-shaped contraction are shown in Figure 11. The channel bed downstream

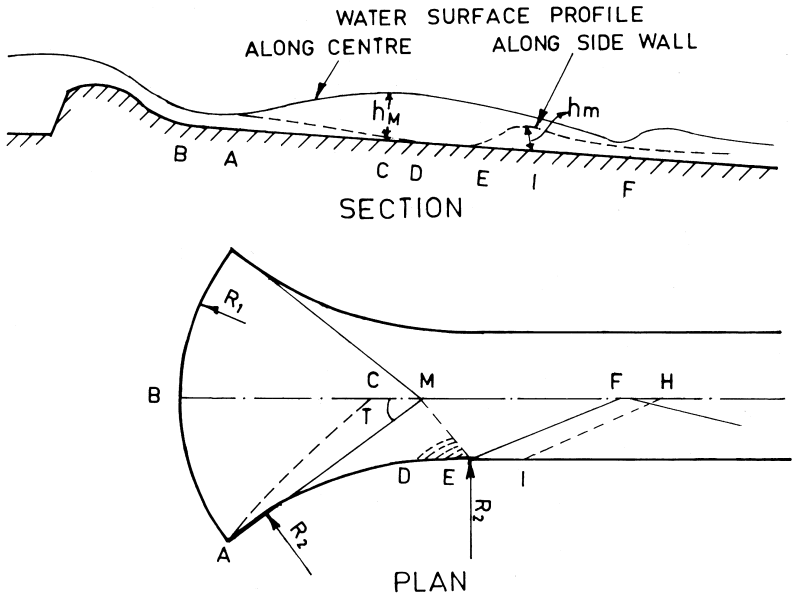

Figure 11 **Fan-shaped contraction.**

of the spillway, including the contraction, is planar and normally of constant longitudinal slope. The flow tends to concentrate to the center of curvature M, associated with a domain of almost zero flow along the sidewall DE. The maximum flow depth h_M occurs at point C. Further downstream the axial surface profile decreases to a minimum at point F and reaches a second maximum at H. The cross-wave from point M intersects the wall at point E and its maximum h_m is slightly downstream at I. Hartung and Knauss (1967) have analyzed this design for a bottom slope of 10% and subtended angle of 40°. In general, this design is not efficient in terms of equal distribution of flow. WES (1952) developed a design to obtain an even distribution of flow by incorporating triangular sill at the chute entrance and by realigned sidewalls.

Anastasi et al. (1979) evolved a modified design in which cross-waves were largely suppressed by a transversally curved bottom geometry, as shown in Figure 12. The wall curvature along the contracting sidewalls varies according to a clothoid, i.e., R_u is finite and $R_d \rightarrow \infty$. A design procedure has also been given. It is shown (ICOLD-1992) that the design has been satisfactory in ensuring even distribution of flow.

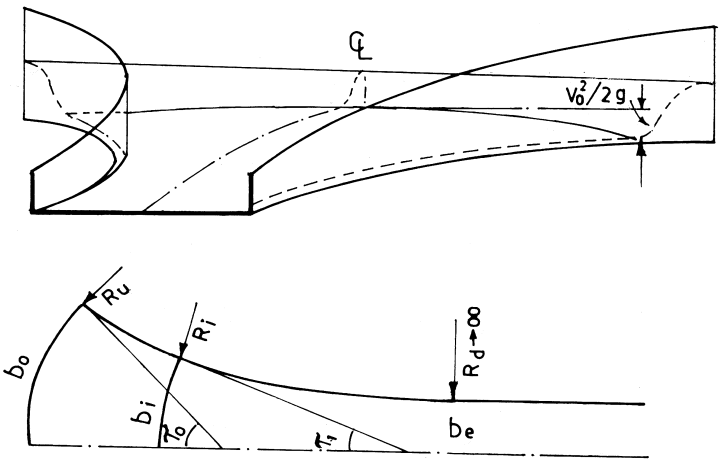

Figure 12 **Modified design of fan-shaped contraction** (shown in Anastasi et al. 1979).

USACE (1990) suggests that chute walls curved horizontally with long radii should be used when F exceeds 1.5. The curved walls should be designed such that

$$\frac{\Sigma\Delta L}{\Sigma\Delta W} \geq \frac{1}{0.382 - 0.116F} (\text{ft units}) \tag{14}$$

where

$\Sigma\Delta L$ = Center line distance from the intersection of crest axis with sidewall
$\Sigma\Delta W$ = Accumulated sidewall conversion beginning at the intersection of the sidewall with spillway crest
F = Local Froude number at the section $\Sigma\Delta L$ for design discharge

Experience shows that straight-lined contracting sidewalls that run for some length downstream from the spillway crest, followed by curved transitions that lead to the desired channel width, as shown in Figure 13, give better flow conditions than the curved sidewalls immediately at the spillway crest (Fig. 11). However, generalized procedure for such a design has not been established as of yet.

Expansion

For flows emerging from a closed conduit, spillway or steep chute, a downstream channel with a larger width may often be desired. If the transition from the narrow channel to the wide channel is abrupt, large cross-waves may occur. If on the

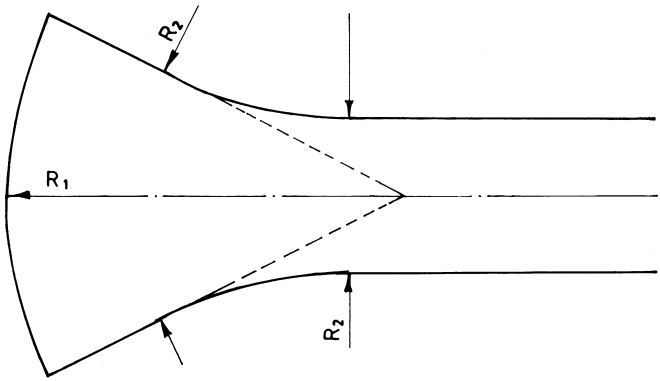

Figure 13 **Alternative layout of fan-shaped contraction.**

other hand, the transition is too gradual, a longer and, consequently uneconomic design results.

Both, the experimental and numerical approaches have been applied to design expansions. ICOLD (1992) have summarized the experimental results of Rouse et al. (1951). A typical curve consists of an expanding portion, a point of inflection, and a reversed curve joining the expanded portion of the channel, as shown in Figure 14. The length L_p of the initial portion is given by

$$\frac{L_p}{b_1 F_1} = 0.7 \left(\frac{b_2}{b_1}\right)\ldots. \tag{15}$$

and that of the total length L_t is

$$\frac{L_t}{b_1 F_1} = 1 + 3.25 \left(\frac{b_2}{b_1} - 1\right) \tag{16}$$

Mazumder and Hager (1993) have reported that the transition length, as per the original Rouse curves, was too long for practical purposes and recommended that the design Froude number F_D be made equal to

$$F_D = F_1 \,/\, 2.5 \tag{17}$$

without any significant loss of efficiency and at the same time affecting a reduction in the length to about 40%.

It must be noted, however, that this expansion will perform satisfactory for mild bottom slopes and that the flow will concentrate along the center for steep slopes. Equation 13 is applicable for expansion also.

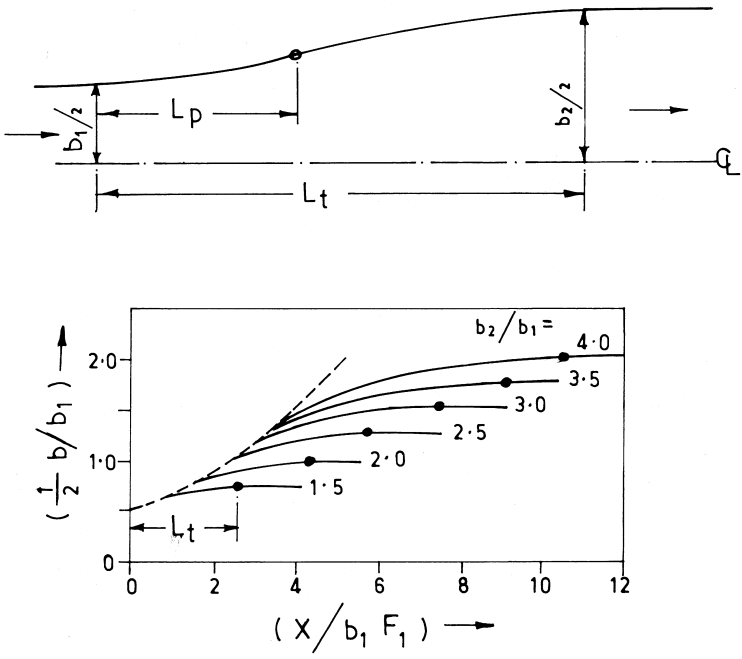

Figure 14 **Generalize boundary curves for supercritical expansion** (shown in Rouse et al. 1951).

Illustrative Examples

1. The discharge channel of a rectangular cross-section downstream of a spillway, passing a unit discharge of 800 cumec, has a width of 30 m, slope of 5%, and flow depth of 1.42 m. If a funnel-shaped contraction is to be provided with a contracted width of 16 m, what should be the optimum angle of contraction? What will be the depth of flow downstream of the contraction?

$$\text{With } F_1 = 5.03, \text{ Equation 11 gives } \theta = Tan^{-1}\frac{1}{2F_1}\left[\frac{b_1}{b_2} - 1\right] = 0.087 \rightarrow \tag{17a}$$

$$\theta = 4.97^{\circ}$$

From Equation 12

$$\frac{F_2}{F_1} = \frac{1}{2}\left[1 + \frac{b_2}{b_1}\right] \rightarrow F_2 = 5.03\left[\frac{1}{2}\left(1 + \frac{16}{30}\right)\right] = 3.86, \text{ which} \tag{17b}$$

which gives $h_2 = 2.57$m.

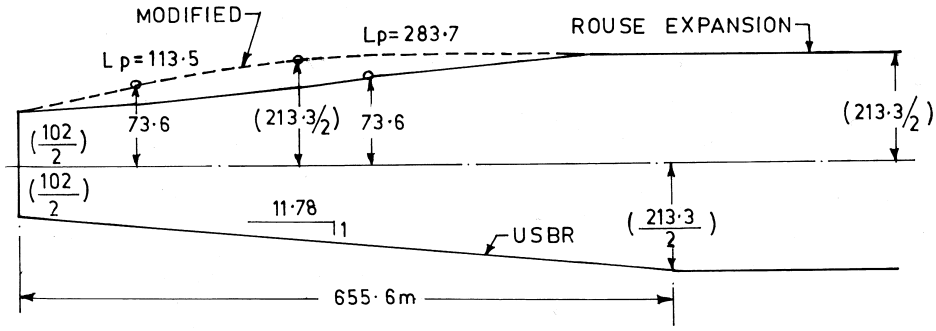

Figure 15 Comparison of Expansions (Example 2).

2. Design an expansion from a 102 m wide discharge channel of rectangular cross-section, to 213.3 m width, with initial flow depth 7.45 m, initial velocity 16.25 m/s, i.e,. a Froude number of 1.9.

Rouse expansion: Equation 15

$$L_t = b_1 F_1 \left[1 + 3.25 \left(\frac{b_2}{b_1} - 1 \right) \right] = 881\text{m}. \tag{17c}$$

Hager et al. Modified Equation 17; $F_D = F_1/2.5 = 0.76$ gives Lt = 352.4 m.

The application of USBR Equation 13 requires a Froude number based on the average values of depths and velocities at the beginning and end of expansion. The values obtained from model experiments at the end of expansion were 1.32 m and 44 m/s respectively, giving $F_a = 4.59$. Thus, flaring would be $1/3F_a = 1:13.77$

The actual flaring adopted was 1:11.78 giving a length of transition Lt = 655.6 m. It was observed from model studies that this expansion performed satisfactory, even with the combination of bottom slopes of 9.55:1, 20:1 and a plunge slope of 2:1 just upstream of the entrance to the stilling basin. Figure 15 shows comparison of all the three expansions.

5.6.2 Curvature in Plan

In a channel of curved alignment, the super elevation due to centrifugal force gives rise to an uneven distribution of flow in addition to the disturbance pattern of cross-waves.

The transverse rise in the water surface in a channel bend as shown in Figure 16 can be estimated from

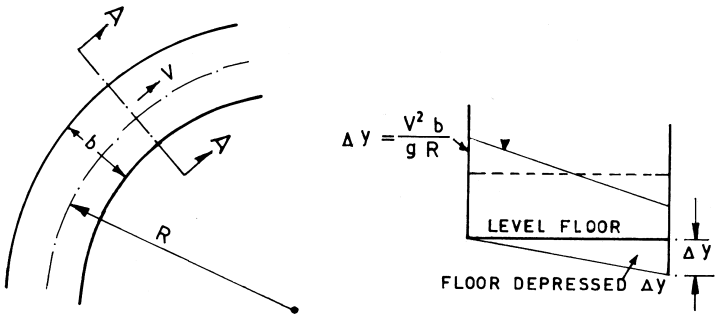

Figure 16 **Super elevation and banking.**

$$\Delta y = \frac{V^2 b}{gR} \tag{18}$$

where

V = Average channel velocity
b = Width of the channel
R = Radius of curvature at center line

WES (1970 a) recommends a minimum radius of a simple curve as

$$R_{\min} = \frac{4V^2 b}{gy} \tag{19}$$

and maximum allowable super elevation for acceptable flow condition in rectangular channel as

$$\Delta y_{\max} = 0.09b \tag{20}$$

where y is the flow depth for the minimum expected friction factor.

Three different methods are being used to produce improved flow conditions in curved chutes.

The most effective method seems to be the banking of the channel bottom as shown in Figure 16. The effect of this is to impart centripetal forces to the fluid elements opposing the centrifugal forces. Banking involves use of a bottom cross-slope, by dropping the inside bottom elevation by an amount

$$S_t = \frac{V^2 b}{gR} \tag{21}$$

and leaving the outside at the same elevation. A spiral transition (WES-1970 b) should be used before and after the main curve to accomplish the desired banking. The recommended length of transition on each side is given by

$$L_t = 30\Delta y \tag{22}$$

Another method is to use a compound curve for the bend as shown in Figure 17. If the total direction change is θ, then

$$\theta = 2\theta_t + \theta_c \tag{23}$$

where θ_t is the angle subtending each transition curve and θ_c is the central angle for the main curve and

$$\theta_t = \tan^{-1}\left[\frac{b/\tan\beta_1}{R_t + b/2}\right]. \tag{24}$$

$\beta_1 = \text{Sin}^{-1}(1/F_1)$
$R_t = 2\,R_c$
R_c = radius of central curve
F_1 = Froude number of the flow at the beginning of the transition

Alternatively, placing of diagonal sills and curved vanes to mitigate the wave disturbance pattern, thereby equalizing the discharge distribution across the section, could also be tried. This method is seldom adopted because of the high

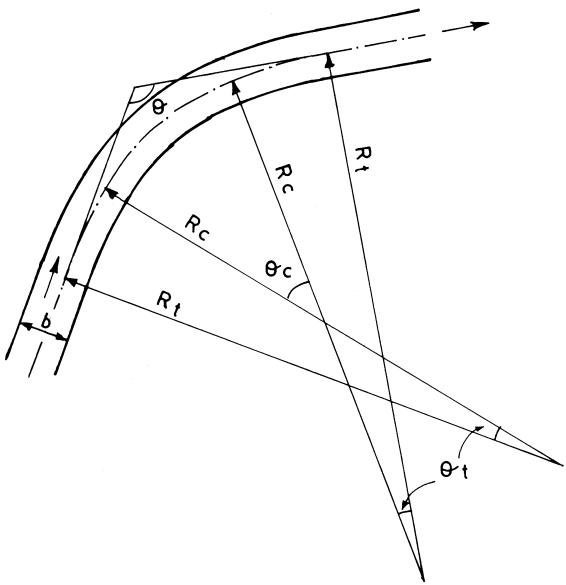

Figure 17 Compound curve at a bend.

maintenance cost, pronounced disturbance at low flows, possible cavitation at high velocity, and problems of silting, abrasion, etc.

5.6.3 Special Layouts

Some special forms of contractions and expansions have also evolved that keep in view specific requirement of the projects. A plan form for the chute spillway of M'Jara project.(Morocco), combining the contraction, expansion, and curvature to deflect the flow leaving the spillway into a plunge pool has been reported by Quintela (1979), as also shown in Figure 18. Such layouts necessarily require studies on hydraulic models.

5.6.4 Longitudinal Profiles

The topographical and geological features of the site govern longitudinal profile of the chute. The main concern is the curvature introduced at the change of grade.

Concave curvature, generally accompanied by circular arcs tangential to the upstream and downstream portions, as shown in Figure 19, present no difficulty, provided the radius of the curvature is not smaller than 10 y_1, where y_1 is the depth of flow at the beginning of curvature. But a larger radius would still be better.

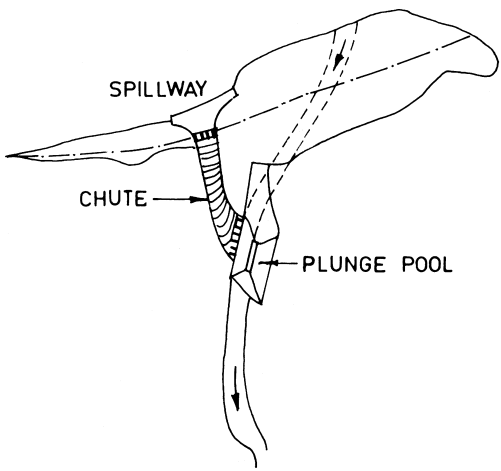

Figure 18 Chute spillway of M'jara Project, Morroco (shown in Ouintela 1979).

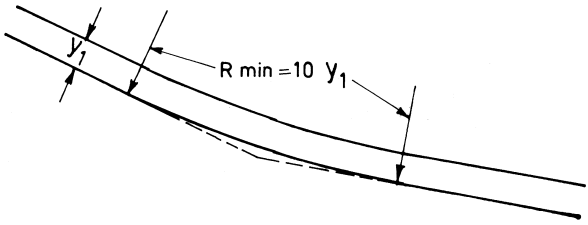

Figure 19 **Vertical curvature (concave) in a chute.**

Convex curves should be flat enough to maintain positive pressures and avoid the tendency for separation of flow from the floor. The curvature should approximate the shape conforming to

$$y = x\tan\theta + \frac{x^2}{K\left[4(y_1 + h_v)\cos^2\theta\right]} \tag{25}$$

where

$\theta =$ Slope angle of the floor upstream of the curve
$h_v =$ Velocity head at the beginning of the curvature
$K =$ A coefficient equal to or greater than 1.5

Figure 20 shows pertinent details of a convex curvature.

When long and flat chutes precede a stilling basin the slope of the chute immediately upstream from the stilling basin should be steep (2:1 or so). In long and flat chutes, frictional resistance on the sidewalls reduces the velocities there rather than at the center. This uneven distribution reflects on the performance of the stilling basin. The steep entrance slope helps making velocity distribution reasonably uniform.

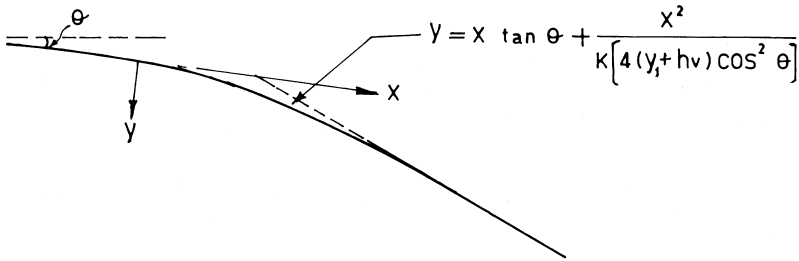

Figure 20 **Vertical curvature (convex) in a chute.**

5.6.5 Tail Channel

The flow leaving the energy dissipator is led to the river downstream of the main dam, either through a natural stream or an artificial channel. It is customary to provide a partial section, namely a pilot cut in the beginning, and allow it to attain its stable configuration in due course of time, provided erosion in the vicinity is not a problem.

5.7 NUMERICAL AND PHYSICAL MODELING

In the last few years, numerical modeling of supercritical flow in channels with curved alignments and steep bottom slopes has rapidly evolved. This would greatly facilitate in refining preliminary designs derived from the simple relationships given above. Yet, there is still a necessity for a physical model study to optimize the design, identifying there from the localized flow conditions, which are often crucial in deciding the efficiency of the design. Model study will be an indispensable tool, particularly for finalizing the approach channel configurations and dealing with supercritical flows and transitions involving such flows. The modeling of long and flat chutes terminating into hydraulic jump stilling basins creates problems of proper simulation of frictional losses; as often, the energy of flow entering the stilling basin is disproportionately smaller in the model as compared to the prototype. In such cases, special techniques of simulation are required.

Notations

A = Cross sectional area of trough
a = constant in relation $V = a\, x^n$
B = Water surface width
b = Width of channel
b_1 = Width of channel before transition
b_2 = Width of channel after transition
C = Chezy coefficient
D = Hydraulic depth = A/B
F = Froude number of flow
F_1 = Froude number of flow before transition
F_a = Average value of Froude number
F_D = Design Froude number for channel expansion
h = Depth of flow
h_M = Depth of flow in the center of contraction
h_m = Depth of flow along the side of contraction
$\overline{h}$ = Hydraulic depth (Eq. 10)
h_v = Velocity head
K = A constant in equation of convex curve

L = Total length of channel
L_p = Length of expanding segment of transition (Rouse)
L_t = Total length of transition (Rouse)
n = A constant in $V = a\ x^n$
= Mannings roughness
P = Wetted perimeter
Q = Total discharge
Q = Discharge per unit width, discharge intensity
R = Hydraulic radius
R_c = Radius at the center of curve
R_{min} = Minimum radius of channel transition
S_0 = Bed slope of trough
S_f = Friction slope of flow in trough
S_t = Amount of banking in channel curvature
U = Velocity vector of the spillway flow
V = Average local velocity of flow in trough
V_s = Surface velocity of the flow downstream of the piers
v = Velocity of flow
X_c = Location of critical flow section
x = Distance measured along trough from upstream end
= Distance from first pier to the sidewall (Fig 4)
y = Fall in water surface in trough
= Depth of flow downstream of the pier
y_c = Critical depth
z = Distance from downstream end of pier to wave and wall intersection Fig (4)
α = Energy coefficient
α = Momentum correction coefficient
β_1 = Wave angle in supercritical flow
Δ_y = Transverse rise of water surface in channel bend
Δ_{ymax} = Maximum allowable value of Δ_y
ϕ = Angle formed by U with the channel axis
θ = Bottom slope angle
θ = Angle of contraction
θ_c = Angle subtending main curve
θ_t = Angle subtending transition curve

REFERENCES

1. Anastasi, G.; Bisaz, E.; Gerodetti, M.; Schaad, F.; Soudrier, F. Essiis sur modele hydraulique et etudes d'evacuateurs par rapport aux conditions de restitution-13th ICOLD, Q 50, R 32, 1979.

2. Balbacher, K.; Lafitte, R. Evacuateur de crue du barrage al Ibtissam (Algerie)- 13th ICOLD, Q 50, R 54, New Delhi, 1979.
3. Bremen, R.; Hager, W. H. Experiments in side channel spillways. ASCE of Jnl of Hyd Engg, May 1989; Vol. 115, No 5.
4. Farney, H. S.; Markus, A. Side channel spillway design. ASCE Jnl of Hyd Div, 1962; Vol. 88, 3.
5. Favere, H. Contribution a l'etude des courants liquides-; Rascher & Cie, Zurich: Switzerland, 1933.
6. Guercio, R.; Magini, R. Modelling Side Channel Spillways- Hydropower and Dams, 1998, Issue 4.
7. Hager, W. H; Bretz, N. V. Discussion to ''Simplified design of contractions in supercritical flow''. ASCE Jnl of Hyd Engg, 1987; Vol. 113, 3.
8. Hajdin, G. Two contributions to spillway designing based on experimental studies- 13th ICOLD, Q50, R 45, 1979.
9. Hartung, F.; Knauss, J. Developments to improve economy, capacity and efficiency of structures controlling the passage of flood water through reservoirs-9th ICOLD, Istanbul, Q 33, R 14, 1967.
10. Hinds, J. Side Channel Spillways- Hydraulic theory, economic factors and experimental determination of losses. Trans ASCE, 1926; Vol. 89.
11. ICOLD (International Congress On Large Dams) Spillways, Shockwaves and Air entrainment, Bulletin No 81, 1992.
12. Ippen, A. T. Mechanics of supercritical flow, 1st paper of High velocity flow in open channels: A symposium. Trans, ASCE, 1951; Vol. 116.
13. Ippen, A. T.; Dawson, J. H. Design of channel contractions- High velocity flow in open channels, A symposium. Trans, ASCE, 1951; Vol. 116.
14. Khatsuria, R. M.; Deolalikar, P. B. Problems encountered in the hydraulic design of a side channel spillway- 6th Congress, APD- IAHR, Kyoto, Japan, 1988.
15. Knight, A. C. E. Design of efficient side channel spillway. ASCE Jnl of Hyd. Div, Sept, 1989; Vol. 115, 9.
16. Mazumder, S. K.; Hager, W. H Supercritical Expansion flow in Rouse modified and reversed transitions. ASCE Jnl of Hyd. Eng., Feb. 1993; Vol. 119, 2.
17. Quintela, A. C.; Mohemed, J.; Magalhaes, A. P.; Almeida, A. B.; Costa, J. V. L'evacuateur de crue et les vidanges de fond du barrage de M'Jara- 13th ICOLD, Q 50, R 40, 1979.
18. Rouse, H.; Bhoota, B. V.; Hsu, E. Y. Design of channel expansion. Trans ASCE, 1951; Vol. 116.
19. USBR Design of Small Dams, 1977.
20. WES Spillway for Genegantslet dam,. New York, Tech Memo 2–351, 1952.
21. WES Hydraulic Design Criteria, Chart 660–1, 1970a.
22. WES Hydraulic Design Criteria, Chart 660–2, 1970b.
23. USACE Engineering and Design; Hydraulic design of Spillway, Engineer Manual EM 1110–2–1603, January 1990.
24. Yen, B. C.; Wenzel, H. G. Dynamic equations for steady spatially varied flow. ASCE Jnl of Hyd Div, March, 1970; Vol. 96, 3.

6
Stepped Spillways

6.1 INTRODUCTION

In the last two decades, there has been an increasing interest in the stepped spillways in various laboratories around the world. This is partly because of technical advances in the construction of Roller Compacted Concrete (RCC) dams and considerable amount of energy dissipation along the chute leading to reduction in the size of the stilling basin. As a part of rehabilitation program of some earth dams, steps have been added to dam embankments, utilizing RCC technique, to allow safe passage of overtopping flows. While hydraulic characteristics have been extensively studied on scale models and design procedures finalized, limited amount of prototype verification has been found to be encouraging. At present, use of stepped spillways is limited to unit discharge up to 30 cumec/m, because of apprehension of cavitation damage for higher discharges.

6.2 HISTORICAL BACKGROUND

Contrary to the belief that the use of stepped channels for energy dissipation purposes is a new concept (developed along with the introduction of new construction techniques, e.g., roller compacted concrete, gabions), stepped chutes have been used since antiquity. Stepped channels were designed to contribute to the stability of structures (e.g. overflow weir) and to dissipate flow energy. In fact, the technique of stepped channels was developed independently by several ancient civilizations. Some 16 dams with stepped spillways were built during ancient times, ranging in height from 1.4 m to 50 m, width from 3.7 m to 150 m, maximum discharge up to about 9000 cumec, and with step height varying from 0.6 m to 5 m while the number of steps varied from 2 to 14.

6.3 FLOW REGIMES ON A STEPPED CHUTE

The flow over a stepped chute can be classified into three types: nappe flow, transition flow, and skimming flow.

Nappe Flow

Nappe flow is characterised by a succession of free falling jets impinging on the steps and followed by a fully or partially developed hydraulic jump. This situation may apply to small discharges or relatively flat spillways. In the case of large discharges, the jump may not occur but the nappe hits the step directly and falls on to the next. Hydraulic jump may also be formed, aided by the provision of weirs at the end of the steps. Energy dissipation in nappe flow occurs by jet break up in air and jet mixing on the step with or without formation of a hydraulic jump on the step.

Transition Flow

With the increase in the discharge, the cavity beneath the falling nappe starts disappearing with the jet still striking near the edge of the step, causing a condition similar to stagnation. This regime is characterized by significant aeration, splashing, and chaotic appearance. It is also observed that flow properties vary from step to step. Further increase in the discharge results in skimming flow.

Skimming Flow

Skimming flow occurs when, with the increase in the discharge, the cavity beneath the falling nappe completely disappears; that is, when the water pool on the step fills the entire step height Water flows as a coherent stream skimming over the steps. Stable recirculating vortices develop between the steps filling the zone between the main flow and the step edges. Most of the energy is dissipated to maintain stable horizontal vortices beneath the pseudo-bottom formed by the external edges of the steps. The vortices are maintained by turbulent stress between the skimming stream and the recirculating fluid underneath.

Figure 1 shows different flow regimes on stepped spillway.

6.4 CHARACTERISTICS OF THE NAPPE FLOW

The following characteristics of the nappe flow are relevant to the design of stepped spillways:

Upper limit for the occurrence of isolated nappe flow with or without a hydraulic jump.
Energy dissipation and residual head.

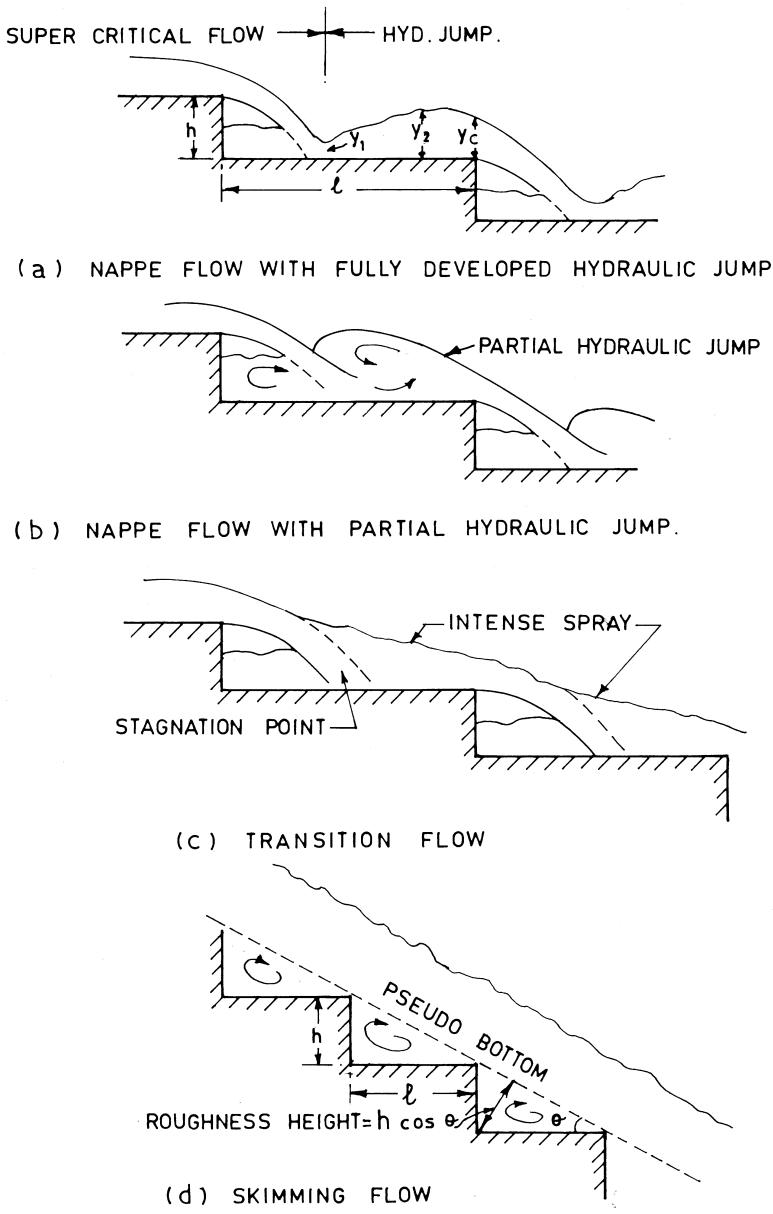

Figure 1 Flow regimes on stepped spillways.

6.4.1 Nappe Flow Occurrence

The flow conditions on a stepped chute are governed by the step height, step length, inclination of the chute with horizontal, and the unit discharge. Most investigators have developed empirical relationships with parameters (y_c/h) and (h/l), where y_c is critical depth, h is step height, and l the step length. The parameter (h/l) represents the chute slope.

Based on the results presented by Rand (1955) concerning flow geometry at straight drop spillways, Chanson (1994-a) proposed the following condition for the occurrence of isolated nappe flow with a fully developed hydraulic jump, deduced for the interval $0.2 \leq h / l \leq 0.6$.

$$\frac{y_c}{h} \leq 0.0916\,(h/l)^{-1.276} \tag{1}$$

Hydraulic jump would not form with increase in discharge or chute slope.

Yasuda et al. (2001) developed the following relationship for the lower limit of the step height for the formation of nappe flow

$$\left(\frac{h}{y_c}\right) = 0.57\left(\frac{h}{l}\right)^3 + 1.3 \tag{2}$$

for $0.1 \leq (h/l) \leq 1.43$ and $0 < (h/y_c) \leq 1.37$.

Chanson (2001-a) defined upper limit of nappe flow regime as

$$\left(\frac{y_c}{h}\right) = 0.89 - 0.4\left(\frac{h}{l}\right) \tag{3}$$

The above relationship is valid for uniform or quasi-uniform flow (not rapidly varied flow) and within the range $0.05 \leq (h/l) \leq 1.7$.

Chinnarasri (2002) states upper limit of nappe flow as

$$\left(\frac{y_c}{h}\right) = 0.98(0.55)^{h/l} \tag{4}$$

It would be seen that an increase in discharge would require flattening of the chute slope for the flow to be maintained as nappe flow, with a given step height. In addition, reducing the step height (without changing the chute slope) would require decrease in discharge.

The above relationships plotted superimposed in Figure 2 show a fair degree of consistency in the results obtained by different investigators.

6.4.2 Energy Dissipation and Residual Head for Nappe Flow

For a stepped channel with nappe flow, having enough steps so that uniform flow can be reached in the last step, the residual head H_r, immediately downstream of the channel can be expressed as

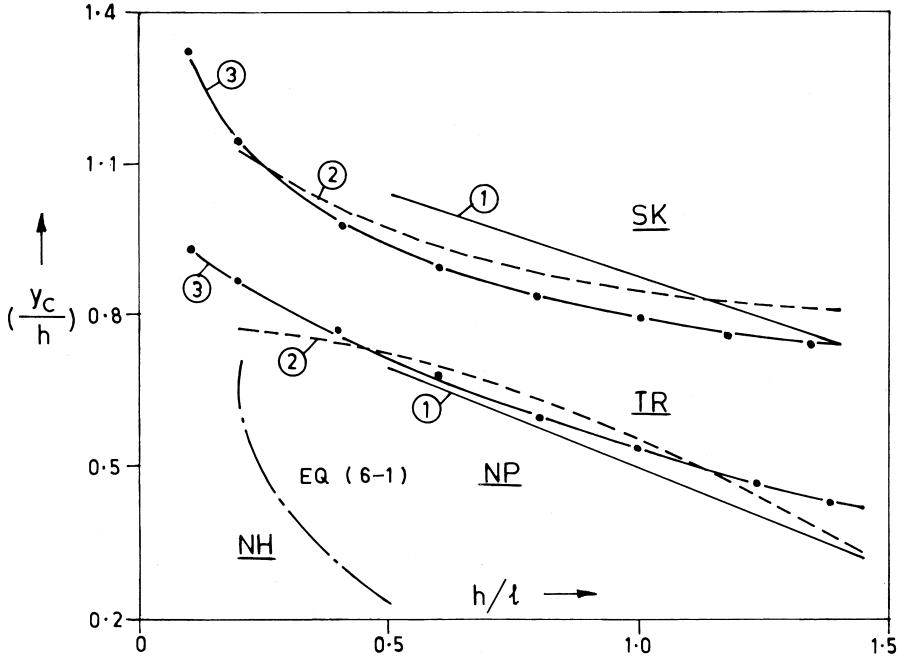

Figure 2 **Flow regimes on stepped spillways**: ① Chanson (2001), ② Yasuda et al. (2001), ③ Chinnarasi (2002), NH is nappe flow with hydraulic jump, NP is nappe flow, TR is transition flow, and SK is skimming flow.

$$H_r = y_1 + (q_2/2g\ y_1^2) \tag{5}$$

Where y_1 is the flow depth and q is the discharge per unit width.

The energy dissipation ΔH is expressed as

$$\Delta H = H_{max} - H_r \tag{6}$$

Where H_{max} is the maximum head.

Chanson (1994-b) developed the following expression valid for free flow spillways and nappe flow with fully developed hydraulic jump

$$\frac{Hr}{H_{max}} = \frac{0.54(y_c/h)^{0.275} + 1.715(y_c/h)^{-0.55}}{1.5 + (H_d/y_c)} \tag{7}$$

Where H_d is the dam height from the toe up to the spillway crest.

Fratino et al (2000) analyzed energy dissipation at the base of a stepped spillway under nappe flow as follows:

$$\frac{\Delta H}{H_{\max}} = 1 - \frac{H_r}{H_{\max}} = 1 - \frac{y_1 + \frac{1}{2}\frac{y_c^3}{y_1^2}}{H_d + \frac{3}{2}y_c} = 1 - \frac{\lambda + \frac{1}{2}\lambda^{-2}}{\frac{H_d}{y_c} + \frac{3}{2}} \tag{8}$$

λ is a dimensionless parameter expressing the relationship between y_1 and y_c and is given by

$$\lambda = \frac{\sqrt{2}}{\frac{3}{2\sqrt{2}} + \sqrt{\frac{h}{y_c} + \frac{3}{2}}} \tag{9}$$

Figure 3 shows the results of experiments on a model containing 14 steps of 24 mm height each with three slopes, i.e. (h/λ) ranging from 0.12 to 0.48 in comparison with Equation 8. The agreement between the theory and experiment is quite satisfactory.

Chamani and Rajaratnam (1994) investigated energy dissipation for nappe flow on inclined steps shown in Figure 4. They have pointed out that the provision of adverse slope helps to form at least a partial jump that makes additional contribution to energy dissipation. The increase in energy dissipation with step angle is due to the possibility of the formation of jump and increase in the depth of the recirculating water over the steps, which is due to increase in the vertical distance between the toe and heel of two consecutive steps.

The relative energy loss $\Delta E/E_o$, for nappe flow on horizontal stepped spillway is given by

$$\frac{\Delta E}{E_o} = 1 - \frac{\left[(1-\alpha)[1+1.5(y_c/h)] + \sum_{i=1}^{N-1}(1-\alpha)^i\right]}{N + 1.5(y_c/h)} \tag{10}$$

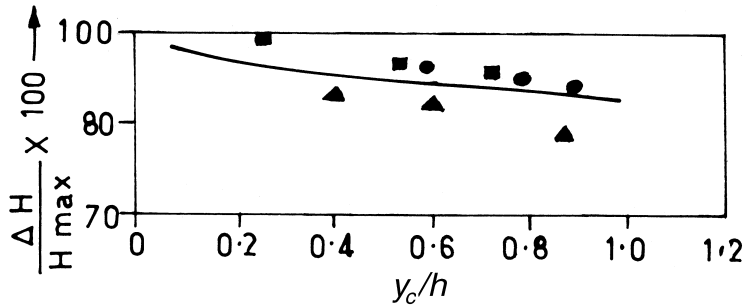

Figure 3 **Energy dissipation in nappe flow regime:** ● h/l = 0.12 ▲ h/l = 0.24 ■ h/l = 0.48 Eq. (7)

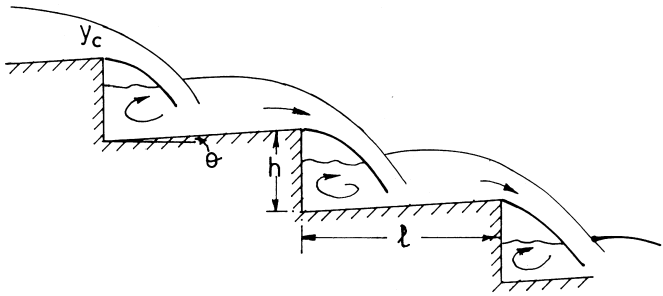

Figure 4 Nappe flow on inclined steps.

where

N = number of steps
H_0 = upstream head referred to step elevation
α = average energy loss per step

The proportion of energy loss per step α, is not a constant but varies with (h/λ) and (y_c/h) for a horizontal stepped spillway. In the case of spillway with steps inclined at an angle of ϕ, α varies also with ϕ. Tatewar and Ingle (1999) evolved a relationship for α by regression analysis, as

$$\alpha = -0.1169 - 0.822 \log(y_c/h) + 0.0675 \log\Phi - 0.5481 \log(h/l) \quad (11)$$

θ is expressed in degrees.

The coefficients in the expression for α in Equation 11 have been evaluated for the range of Φ from 5° to 20°, (h/λ) from 0.421 to 0.842, and (y_c/h) from 0.05 to 0.833.

For horizontal steps, further regression analysis using the same set of data gave the relationship

$$\alpha = -0.746 \log(y_c/h) - 0.5481 \log(h/\mathrm{l}) - 0.0455 \quad (12)$$

6.4.3 Pooled Step Cascades

A stepped spillway can be designed so that each step corresponds to an independent stilling basin with hydraulic jump, formed with the provision of an overflow weir at the end of each step, as shown in Figure 5. Aigner (2001) has suggested a procedure for the design of such a spillway. For a given unit discharge (and hence y_c) and step height h, the conjugate depth y_2 of hydraulic jump is calculated on the basis of the total energy entering the step:

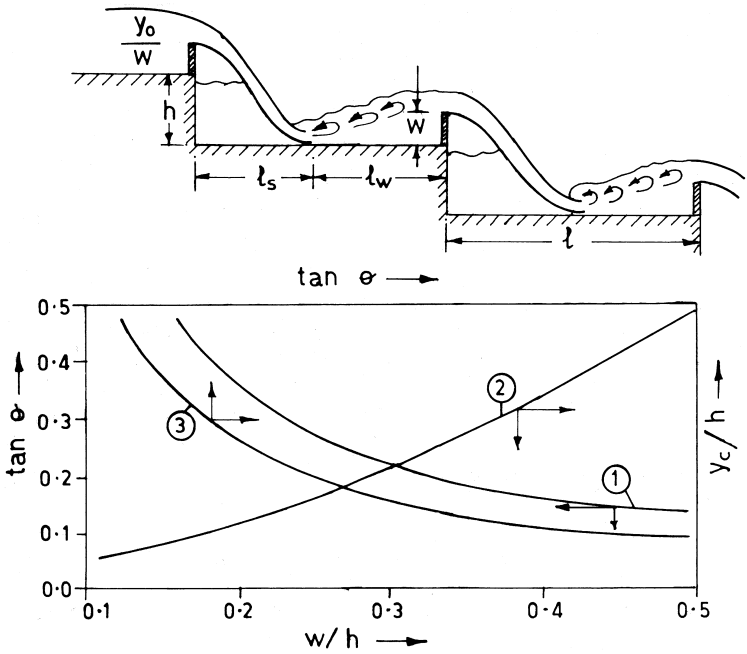

Figure 5 **Pooled step cascades–Design charts:** ① Tan θ Vs W/h, ② y_c/h Vs W/h, ③Tan θ Vs y_c/h (courtesy of Aigner 2001)

$$E_0 = h + w + y_0 + \frac{y_c^3}{2(w + y_0)^2} \tag{13}$$

where

y_0 = depth of flow over the weir

$\frac{y_c^3}{2(w + y_0)^2}$ = head due to velocity of approach

w = height of the weir

A safety margin of 5% has been suggested, so that

$$w = 1.05\ y_2 - h \tag{14}$$

The length l of the step is then

$$l = l_s + l_w \tag{15}$$

where l_s = throw length of the jet from the downstream
l_w = length of hydraulic jump, usually equal to 6 y_2

A design chart has also been presented (Fig. 5) for the range of parameters

tan θ 0.1 to 0.5
Y_c/h 0 to 0.5
w/h 0.1 to 0.5

The design charts enable the determination of stepped spillway configurations if discharge and chute slope are given or for given spillway configurations, the maximum discharge that can be passed, ensuring hydraulic jump at all steps.

Illustrative Examples

1. A stepped spillway consisting of 10 steps, 1 m high and 2 m long each, is to pass a unit discharge of 0.3 cumec/m. Assess the type of flow conditions on the chute and energy dissipation at the base of the spillway.

$y_c = 0.209$, $y_c/h = 0.209$, $h/l = 0.5$, $H_d = 10$ m, $H_{max} = H_d + 3/2\ y_c = 10.313$ m

Starting with Equation 1, $y_c/h = [0.0916\ (h/l)^{-1.276}] = 0.222$ which is larger than the existing value of 0.209. Therefore, a nappe flow with fully developed hydraulic jump on each step would occur. Residual head at the base of the spillway is

$$\frac{Hr}{H_{max}} = \frac{0.54(y_c/h)^{0.275} + 1.715(y_c/h)^{-0.55}}{1.5 + (H_d/y_c)} = 0.0893 \quad (15a)$$

and hence $$\frac{\Delta E}{H_{max}} = 1 - \frac{H_r}{H_{max}} = 0.91 \quad (15b)$$

Energy dissipation efficiency is 91%.

2. If the discharge is increased to 0.6 cumec/m, estimate the efficiency of energy dissipation.

$y_c = 0.332$, $y_c/h = 0.332$, $h/l = 0.5$

Equation 2 gives lower limit of step height $h = 0.332[0.57(0.5)^3 + 1.3] = 0.455$ m, against actual step height of 1 m.

Equation 3 gives upper limit of $y_c/h = 0.89 - 0.4(0.5) = 0.69$, against actual value of 0.332.

Equation 4 also gives $y_c/h = 0.98(0.55)^{0.5} = 0.726$.

Therefore, nappe flow would still prevail, but hydraulic jump would not form.

As per Equation 7 and 8,

$$\lambda = \frac{\sqrt{2}}{\frac{3}{2\sqrt{2}} + \sqrt{\frac{h}{y_c} + \frac{3}{2}}} = 0.444 \tag{15c}$$

$$\text{and } \frac{\Delta H}{H_{\max}} = 1 - \frac{H_r}{H_{\max}} = 1 - \frac{y_1 + \frac{1}{2}\frac{y_c^3}{y_1^2}}{H_d + \frac{3}{2}y_c} = 1 - \frac{\lambda + \frac{1}{2}\lambda^{-2}}{\frac{H_d}{y_c} + \frac{3}{2}} = 0.906 \tag{15d}$$

Efficiency of energy dissipation is 90.6%.

As per Equation 10 and 12, horizontal steps

$$\alpha = -0.746 \log(y_c/h) - 0.5481 \log(h/l) - 0.0455 = 0.476 \tag{15e}$$

and

$$\frac{\Delta E}{E_o} = 1 - \frac{\left[(1-\alpha)[1+1.5(y_c/h)] + \sum_{i=1}^{N-1}(1-\alpha)^i\right]}{N + 1.5(y_c/h)} \text{ work out to}$$

$$= 1 - [0.524\{1 + (1.5 \times 0.332)\} + (0.524 + 0.524^2 + \cdots\cdots + 0.524^9) / \{10 + 1.5(0.332)\}] = 0.84$$

Efficiency of energy dissipation is 84%.

3. If the steps are inclined at an angle of

a. 10°
b. 15°
c. 20°

with the horizontal, estimate the efficiency of energy dissipation.

As per Equation 10 and 11,

$$\alpha = -0.1169 - 0.822 \log(y_c/h) + 0.0675 \log \Phi - 0.5481 \log(h/l)$$

$\phi°$	α	H_r/H_{max}	Energy diss efficiency
10	0.508	0.147	85%
15	0.520	0.141	86%
20	0.450	0.138	86.2%

4. A stepped spillway with a step height of 1.2 m is to be laid on a slope of 15°. Design a pooled step cascade such that hydraulic jump forms on each step.

Step height and chute slope determine the step length l. There is, therefore, only one combination of unit discharge q and weir height w, which would result in a combination of throw length of the jet and length of hydraulic jump, equal to the step length l. Referring to the design chart (Fig. 5):

Curve 1 – $\tan 15^\circ = 0.268$ gives w/h = 0.26 or w = 0.312 m.
Curve 2 – w/h = 0.26 gives $y_c/h = 0.17$ or $y_c = 0.204$ m i.e. q = 0.29 cumec/m
Curve 3 – $\tan \theta = 0.268$ also gives $y_c/h = 0.17$

Therefore, unit discharge up to 0.29 cumec/m can be passed with weir height of 0.312 m.

If the slope of the chute is reduced to 10°, i.e. $\tan \Phi = 0.176$,

Curve 1 – $\tan\theta = 0.176$ gives w/h = 0.38 or w = 0.456 m.
Curve 2 – w/h = 0.38 gives $y_c/h = 0.3$, $y_c = 0.36$ i.e. q = 0.676 cumec/m
Curve 3 also gives $y_c/h = 0.3$

It would be seen that weir height also increases with the increase in the discharge.

6.4.4 Transition Flow Regime

Earlier investigators either had ignored the existence of a transition flow regime or did not precisely demarcate between the nappe and skimming flow regimes. Relationships developed for the onset of skimming flow include

$$\text{Rajaratnam (1990)} \left(\frac{y_c}{h}\right) > 0.8 \qquad 0.4 < (h/l) < 0.9 \tag{16}$$

$$\text{Chanson (1994 - a)} \left(\frac{y_c}{h}\right) = 1.057 - 0.465\left(\frac{h}{l}\right) \quad 0.2 \leqq (h/l) \leqq 1.25 \tag{17}$$

$$\text{Mondardo et al. (1995)} \left(\frac{y_c}{h}\right) > 1.1974 - 0.59501\left(\frac{h}{l}\right) \tag{18}$$

$$\text{Boes (2000)} \quad 0.91 - 0.14\left(\frac{h}{l}\right) \qquad 0.47 < \left(\frac{h}{l}\right) < 1.43 \tag{19}$$

However, the above relationships do not demarcate distinct boundaries between the flow regimes as shown by the relationships of Chanson (2001-a), Yasuda et al.(2001), and Chinnarsri (2002) in Figure 2

Chanson (2001-a) has studied characteristics of transition flow pattern and air entrainment. This regime is characterized by strong stagnation on the horizontal step faces associated with chaotic behavior and pressure fluctuations. In a further study, Chanson et al. (2001-b) observed very large aeration, in excess of

acknowledged limits observed in smooth chute flows, accompanied by irregular variations in depth and flow properties on each step. This would imply that chute sidewalls must be designed higher than in nappe flow or skimming flow for identical flow rates. Quoting some incidents of prototype failures experienced with transition flows, Chanson has also recommended avoiding the design of stepped spillways with transition flows regime, unless a rigorous hydraulic and structural modeling of the flow instabilities is conducted.

6.5 CHARACTERISTICS OF THE SKIMMING FLOW

In skimming flow, two different flow zones can be clearly distinguished (Fig. 6.1):

1. An upper region over the external edges of the steps, which form a pseudo bottom.
2. A lower area, beneath the pseudo-bottom, formed by almost triangular cell where the water remains caught, except water exchanged with the upper flow due to intense turbulence.

On stepped chutes with skimming flow regime, the flow is highly turbulent and the conditions for free surface aeration are satisfied. The boundary layer starts at the crest section and grows along the chute until its outer edge reaches the free surface. At this point, turbulence initiates natural free surface aeration. The location of the start of air entrainment is called the point of inception. Downstream of the inception point, a layer containing a mixture of both, air, and water extends gradually through the flow. Far downstream, the flow will become uniform and for a given discharge, the flow depth, air concentration, and velocity distribution will not vary along the chute. This region is defined as the uniform equilibrium flow region. These are shown in Figure 6.

Yasuda et al. (1999), have introduced the concept of quasi-uniform flow and equilibrium condition as applied to skimming flows. For a given chute slope, discharge, and step height, as the downstream distance along the chute becomes long, a quasi-uniform flow is reached at a certain section of the channel. With the quasi-uniform flow, the parameter (h_2/y_c), that is the ratio of the sub-critical depth of the hydraulic jump, formed at the toe, to the critical depth, is independent of the relative dam height (H_d/y_c) for a given chute slope θ and relative step height (h/y_c). This is also called equilibrium condition, where, the total head of the quasi-uniform flow in the stepped channel, given by $[u_0^2/(2g) + y_0 \cos\theta]$ coincides with that at the toe of the jump expressed as $[(u_1^2 / 2g) + \lambda h_1]$. Here u_0 and y_o and u_1 and y_1 are respectively the velocity and flow depth on the chute and at the toe, and λ is the pressure distribution coefficient at the toe. The flow depth y_1 has been determined indirectly by measuring y_2. It has been verified

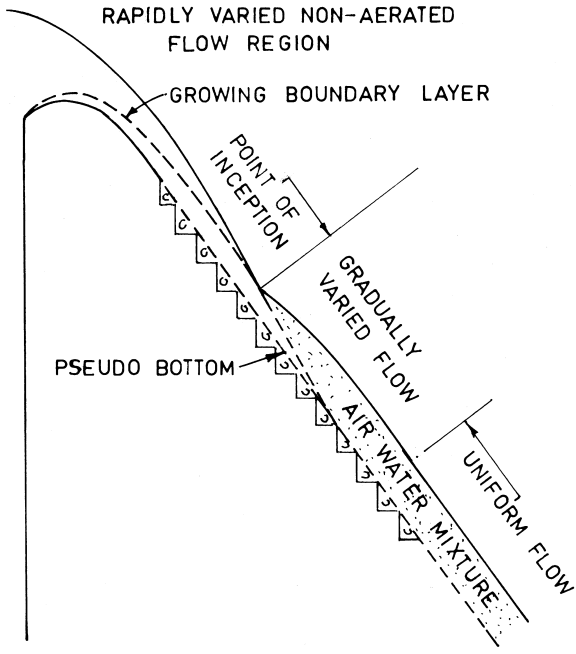

Figure 6 **Flow regions in skimming flow.**

experimentally that the supercritical depth, y_0 coincides with the clear water depth y_w, within $\pm$ 10% error.

Since skimming flow is the most dominant flow condition for the stepped spillway, it has been extensively studied by various research workers. The following characteristics are relevant to the design of stepped spillways:

Estimation of flow resistance to assess frictional energy loss.
Energy dissipation.
Air entrainment and aerated flow properties.
Pressure fluctuations and cavitation considerations.

6.5.1 Estimation of Flow Resistance

Estimation of flow resistance is necessary for assessing frictional energy loss. Flow resistance in skimming flows depends on a number of factors. Besides the flow depth and stepped chute geometry, such as chute slope, the factors include condition of flow (gradually varied, uniform etc), relative step height, intake

condition (whether gated or uncontrolled), and degree of air entrainment. Estimation of flow resistance is based on the measurement of flow depth and velocity. These measurements are often difficult and inconclusive, because of the turbulence and air entrainment and result in overestimation of energy dissipation.

When the flow over the spillway is fully developed and uniform, it is reasonable to use the Strickler formula to calculate friction losses along the chute. Nigus et al. (2000) analyzed the results of model studies of McClure dam of USBR conducted by Christodoulou (1993) and by Rice and Kadavy (1996). A large variation of the values obtained—from 15 $m^{1/3}/s$ to 55 $m^{1/3}/s$—however, made the results less reliable. Many investigators, therefore, preferred to analyze the resistance phenomenon in terms of either the coefficient of fluid friction C_f or Darcy-Weisbach friction factor f ($=4\ C_f$).

In the developed flow region, The Reynolds shear stress τ between the skimming flow and the recirculating flow on the steps can be expressed as

$$\tau = C_f \overline{\rho_m}\ u_m^2/2 \tag{20}$$

where u_m is the mean velocity and $\overline{\rho_m}$ is the mean density averaged over the flow depth $y_{0.9}$. It can be shown that

$$C_f = \frac{2gy_{0.9}\sin\theta}{u_m^2} \tag{21}$$

Rajaratnam (1990) analyzed results of Sorensen (1985) (on a 1:25 scale model of Monskville dam spillway) and Rajaratnam and Katopodis (1984) based on Equation 21. It was concluded that C_f varied in the range of 0.05 to 0.18 with Reynolds number in the range of $5000 - 10^6$. The average value of 0.18 can be compared with the smooth, unstepped spillway C_f of 0.0065, to obtain an indication of the energy dissipation potential of the stepped spillway.

Tozzi (1994) evaluated variations of the friction factor in a closed conduit model to avoid the problems associated with air entrainment. The Darcy friction factor f (which is equal to 4 C_f) was given by

$$\frac{1}{\sqrt{f}} = 2.16 + 1.24\log\frac{y}{k} \tag{22}$$

where

y = depth of flow

k = roughness produced by the step = $h\ \cos\theta = hl/\sqrt{h^2+l^2}$ (22a)

Chamani and Rajaratnam (1999) conducted studies on a 2.5 m high stepped spillway model with chute slopes of 0.6 and 0.8, and with y_c/h in the range of 0.7–4.4. They analyzed the data of Sorenson (1985), Christodoulou (1993), Sikora (1997), and their own investigations in the fully developed flow to relate C_f with the term ($y_{0.9}/k$). However, the plot of the results exhibited a large degree of

scatter. In the later analysis, C_f was averaged for every specific roughness height for a range of flow depths. It was then possible to draw a mean curve through most of the data, which gave the relationship

$$\frac{1}{\sqrt{C_f}} = 3.85\log\left(\frac{y}{k}\right) + 3.53 \tag{23}$$

Chanson et al. (2001-b) conducted studies on a steep flume ($\theta = 21.8°$, $h = 0.1$ m, $W = 1$ m), estimating the friction factor by using the equation $f = \frac{4\tau_0}{1/2\rho_w u_w^2}$. It was found that the friction factor data presented no obvious correlation with the relative step roughness, Reynolds, Froude, or Weber numbers. He concluded that form drag and shear instability developed at each step edge and could generate different cavity regimes, associated with different drag coefficients. In this study, three dominant values of f (0.105, 0.17, and 0.30) were obtained.

Yasuda et al. (2001) present the following relationship valid for the equilibrium condition

$$f = 4C_{fw} = \frac{4\tau_0}{1/2\rho_w u_w^2} = \frac{8gy_w \sin\theta}{u_w^2} = 8\left(\frac{y_w}{y_c}\right)^3 \sin\theta \tag{24}$$

where

ρ_w = mass density of water
C_{fw} = clear water skin friction coefficient
y_w and u_w are clear water depth and velocity

Chinnarasri (2002) suggests

$$\frac{1}{\sqrt{f}} = 2.0 + 1.19\log\frac{y_0}{k}. \tag{25}$$

for $0.1 \leq k/y_0 \leq 2.1$ and $\theta = 15°$ to $59°$.

Boes and Minor (2002) suggest the following relationship for the uniform flow:

$$\frac{1}{\sqrt{f}} = \frac{1}{\sqrt{0.5 - 0.42Sin(2\theta)}}\left[1.0 - 0.25\log\left(\frac{k}{D_{hwu}}\right)\right] \tag{26}$$

where $D_{hwu} = 4\,y_{wu}$, is the hydraulic diameter for the uniform clear water flow in wide rectangular channels, also given by

$$\frac{y_{wu}}{y_c} = 0.215(Sin\theta)^{-1/3} \tag{27}$$

Some of these relationships have been plotted in Figure 7. It would be seen that the relationships proposed by Tozzi (Eq. 22), Chamani and Rajaratnam

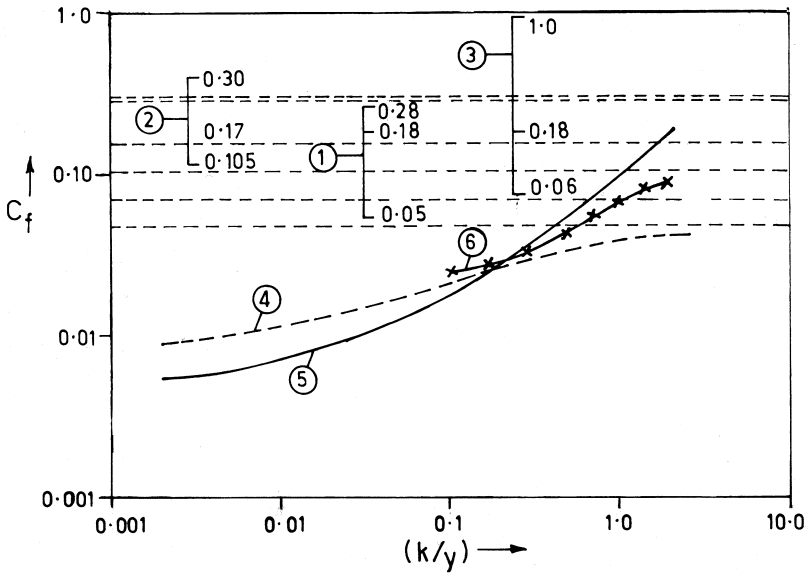

Figure 7 Variation of average skin friction coefficient:

① Rajaratnam (1990) C_f 0.05–0.28 Avg 0.18
② Chanson et al. (2001) C_f 0.105, 0.17, 0.30
③ Matos et al. (1995) C_f 0.06–1.0 Avg 0.18
④ Tozzi (1994)
⑤ Chamani & Rajaratnam (1999)
⑥ Chinnarasri (2002)

(Eq. 23), and Chinnarasri (Eq. 25) follow a similar trend, whereas the average values suggested by others appear to be on the higher side. While assessing frictional energy loss at the toe of a stepped spillway, for designing energy dissipator, it would be advisable to use conservative values of the friction factor.

Air entrainment influences the phenomenon of flow resistance by way of drag reduction. It is believed that drag reduction occurs from interaction between the entrained bubbles and a mixing layer in the flow caused by separation at the step edge.

6.5.2 Air Entrainment

Air entrainment occurs on stepped spillways, for both the nappe flow and skimming flow regimes. However, the mechanism of air entrainment is different on

both. On nappe flow, the entrainment is caused by the turbulence generated at the point of impingement of the nappe on step bottom, whereas in the skimming flow, aeration commences when the turbulent boundary layer emerges at the free surface. This process is similar to that on the smooth, unstepped spillway chutes, with flow regimes characterized by non-aerated, gradually varied, and uniform flows, as shown in Figure 1, Chapter 27. In calculations of air entrainment on stepped chutes, the pseudo-bottom formed by the external edges of steps is taken as the chute invert profile and the parameter (h cosα) is the surface roughness, instead of the usual sand grain roughness k_s as in the case of unstepped spillways.

Point of Inception

In the case of skimming flow on stepped spillways, the distance L_i, from the start of boundary layer to the inception point of air entrainment, is relatively shorter than with the smooth unstepped spillways, because of roughness of the surface and turbulence.

Chanson (1994-a) suggests

$$\frac{L_i}{k} = 9.719(\sin\alpha)^{0.796} F_h^{0.713} \tag{28}$$

$$\frac{y_i}{k} = \frac{0.4034}{(\sin\alpha)^{0.04}} F_h^{0.592} \tag{29}$$

where k = h cosα is the roughness height perpendicular to the pseudo-bottom. F_h is in terms of step height h instead of k_s, so that

$$F_h = q_w/\sqrt{g \cdot \sin\theta \cdot (h\cos\alpha)^3} \tag{29a}$$

Chamani (2000) found that his observations agreed well with those of Chanson's and modified Equation 28 as

$$\frac{L_i}{k} = 8.29 F_i^{0.85} \tag{30}$$

where $F_i = q_w/\sqrt{g \cdot (h/l) \cdot k}$

Matos et al. (2000) obtained

$$\frac{L_i}{k} = 6.289 F_s^{0.734} \tag{31}$$

$$\frac{y_i}{k_s} = 0.361 F_s^{0.606} \tag{32}$$

where $F_s = q_w/\sqrt{g.h^3}$

Boes and Minor (2000) give

$$\frac{L_i}{k} = 9.72 F_h^{0.86} \tag{33}$$

This has been modified by Boes and Minor (2002) as

$$L_i = \frac{5.90 y_c^{1.2}}{(Sin\theta)^{1.4} h^{0.2}} \tag{34}$$

$$y_i = \frac{0.4 y_c^{0.9} h^{0.1}}{(Sin\theta^{0.3})} \tag{35}$$

Depth averaged air concentration at L_i is

$$\overline{C}_i = 1.2x10^{-3} (240^\circ - \theta) \tag{36}$$

Aerated Flow Depth

Downstream of the point of inception, the flow passes through the gradually varied flow regime to uniform equilibrium flow. Hager and Boes (2000) have proposed the following relationship for the characteristic air-water mixture flow depth y_{90} in terms of uniform mixture flow depth $y_{90(u)}$

$$\frac{y_{90(x)}}{y_{90(u)}} = \text{Tanh}\left[1.1 \frac{y_{90(u)}^2 \sin\alpha}{y_c^3}(x - L_i)\right] \tag{37}$$

where $y_{90,u}$ is the uniform flow depth corresponding to 90% air concentration. Boes and Minor (2002) suggest

$$\frac{y_{90,u}}{h} = 0.50\left(F_h^*\right)^{0.1Tan\theta+0.5} \tag{38}$$

$$\text{where } F_h^* = \frac{q}{(g\, Sin\theta\, h^3)} \tag{38a}$$

The normalized vertical distance below crest, required for uniform flow to be attained is given by Boes and Minor (2002)

$$\frac{H_{d,u}}{y_c} = 24(Sin\theta)^{2/3} \tag{39}$$

Tatewar et al. (2000) also propose an empirical relationship derived from the results of Chamani and Rajaratnam (1999)

$$\log\left(\frac{y_{90(u)}}{h}\right) = 0.3011 \log\left(\frac{q^2}{gh^3}\right) + 0.01696 \log\left(\frac{h}{l}\right) - 0.2053 \tag{40}$$

It will be seen from Equation 40 that the flow reaches uniform regime asymptotically at the end of long channels of constant slope. It must, however, be noted that this equation has been derived from the results of experiments that covered the range $\alpha = 51^\circ - 59^\circ$ and $y_c/h = 0.8$ to 4.4 and that for some of the discharges, flow had not reached uniform regime.

Air Concentration

It is observed that air concentration distribution in skimming flow on stepped spillways is similar to that in self-aerated flow on smooth, unstepped spillways.

Matos et al. (2000) conducted experiments on stepped spillway models 2.9 m and 4.3 m high, with step heights of 8 cm and 10 cm, and with chute slopes of 53° and 51° respectively. They concluded that mean air concentration at the point of inception could be expressed as

$$C_{mean}(_i) = 0.163\ F_h^{0.154} \tag{41}$$

It was seen that its variation, with respect to F_h (between 3 and 7), was insignificant and was approximately constant at about 0.2. As for the air concentration, further downstream, Matos derived

$$C_{\text{mean}} = 0.210 + 0.297 \exp\left[-0.497(\ln s' - 2.972)^2\right] \tag{42}$$

for $0 < s' < 30$,

$$C_{mean} = \left[0.888 - \frac{1.065}{\sqrt{s'}}\right]^2 \quad for\ s' \geq 30 \tag{43}$$

where

$$s' = \frac{L \quad L_i}{y_i} \tag{43a}$$

The non-dimensional depth (y/y_i) is given by

$$\frac{y}{y_i} = \frac{1}{1 + \xi\sqrt{s'}} \tag{44}$$

where ξ is given by

$$\xi = \left[21.338 - \frac{13.815}{(y_c h)^2}\right]^{-1} \tag{45}$$

Frizell et al. (2000) conducted studies on a 15 m high flat chute ($\theta = 26.6°$) laid with concrete blocks 5 cm high. Their measurements gave a relationship for C_{mean}, downstream of the point of inception.

$$C_{\text{mean}} = 0.23 + 0.017\left(\frac{L - L_i}{y_i}\right)^{0.46} \tag{46}$$

where L is the distance measured along the chute.

Matos (2000) has shown that the mean air concentration also approaches asymptotically to that, corresponding to the uniform equilibrium concentration $\overline{C}_e$, given by Hager (1991) as $\overline{C}_e = 0.75 Sin\alpha^{0.75}$. A qualitative relationship suggested by Matos (2000) is

$$\overline{C} = 0.62 - 55.9\,(H_d/y_c)^2 \quad (47)$$

for $\alpha = 53°$ and $10 < (H_d/y_c) < 100$

Air concentration close to the pseudo-bottom is of relevance to safety precautions against cavitation. Matos (2000) reported that a conservative value of air concentration of 8% close to the boundary could be realized for $(L - L_i/y_i)$ greater than 6. Boes and Minor (2000) obtained

$$C_b = 0.068 - 6.21 \times 10^{-4} \times F_h \quad (\theta = 30°) \quad (48)$$

$$C_b = 0.268 - 6.69 \times 10^{-3} \times F_h \quad (\theta = 50°) \quad (49)$$

Chanson (2001-b) has shown that although the air concentration distribution in skimming flow followed a similar trend to that seen on the smooth, unstepped chutes, a comparison of his experimental results ($\alpha = 21.8°$) with analytical solution showed that skimming flows were more aerated in the upper layers and less aerated in the lower layers, than in the smooth chute flows.

Velocity Distribution

Velocity distribution in skimming flows follows typical power law, namely

$$\frac{u}{u_{90}} = \left(\frac{y}{y_{90}}\right)^{1/n} \quad (50)$$

Various investigators have obtained values of n in the range of 3.5 to 6. Experiments of Matos (2000) were performed in a longer chute, under uniform flow regime, where n was approximately 4. Chanson's (2001-b) studies were conducted in a relatively short flume, where uniform conditions were not achieved, and the values of n ranged from 5.1 to 6 for y_c/h varying from 1.5 to 1.1.

Friction Factor

As with the smooth, unstepped chutes, aeration tends to reduce shear stress at the boundary, as in the case of skimming flows on stepped spillways also. A correlation function proposed by Chanson (2001-b) is:

$$\frac{f_e}{f} = 0.5\left[1 + Tanh\left(0.68\frac{0.5 - C_{mean}}{C_{mean}(1 - C_{mean})}\right)\right] \quad (51)$$

This relationship has been compared with the corresponding functions for the smooth, unstepped spillways, in Figure 7 (Chapter 27).

6.5.3 Energy Dissipation

In the skimming flow, in addition to the recirculation between the main flow and the water trapped on the steps, large vortex elements are continuously produced

that break off and get carried into the skimming flow. These two features enhance the energy dissipation in the skimming flow.

Uniform Flow Condition

Yashuda et al. (2001) have derived a general expression for the energy loss at the base of a stepped spillway with skimming flow, regardless of whether the flow is uniform or not:

$$\frac{\Delta H}{H_{\max}} = \frac{H_{\max} - H_r}{H_{\max}} = 1 - \frac{\left(\frac{y_w}{y_c}\right)^{-2} + 2\left(\frac{y_w}{y_c}\right) Cos\theta}{3 + 2\left(\frac{H_d}{y_c}\right)} \tag{52}$$

Where y_w is the clear water depth of flow referred to the pseudo-bottom.

This has been expressed by Chanson (1994-b), in the case of uniform/quasi-uniform flow under an ungated flow condition, as

$$\frac{\Delta H}{H_{\max}} = 1 - \frac{\left(\frac{f_a}{8Sin\theta}\right)^{1/3} Cos\theta + \frac{1}{2}\left(\frac{f_a}{8Sin\theta}\right)^{-2/3}}{\frac{3}{2} + \frac{H_d}{y_c}} \tag{53}$$

For gated flow, the expression is

$$\frac{\Delta H}{Ho} = 1 - \frac{(f_a / 8\sin\theta)^{1/3} Cos\theta + \frac{1}{2}(f_a / \sin\theta)^{-2/3}}{\frac{H_d + H_p}{y_c}} \tag{54}$$

Where f_a is the friction factor for uniform aerated flow and H_p is the depth of overflow.

Chamani and Rajaratnam (1999) assessed the energy loss at the base of a 2.5 m high stepped spillway model, with the measurement of velocity and depths of fully developed flow, and concluded that the energy loss varied in the range of 48–63%. It was also implied from the analysis that the value of f_a varied from 0.16 to 0.28.

Figure 8 shows a plot of the Equation 53 with $f_a = 0.18$ and $\theta = 53°$ along with the results of the theoretical study by Stephenson (1991) for $\theta = 54.4°$ with step height $h = y_c/2$. It will be seen that both the results agree well, indicating that the average value of $f_a = 0.18$ is a reliable estimation of energy dissipation.

Non-uniform Flow Condition

When the flow had not reached uniform/quasi-uniform condition, energy dissipation was assessed by experimental means. This was usually done on hydraulic

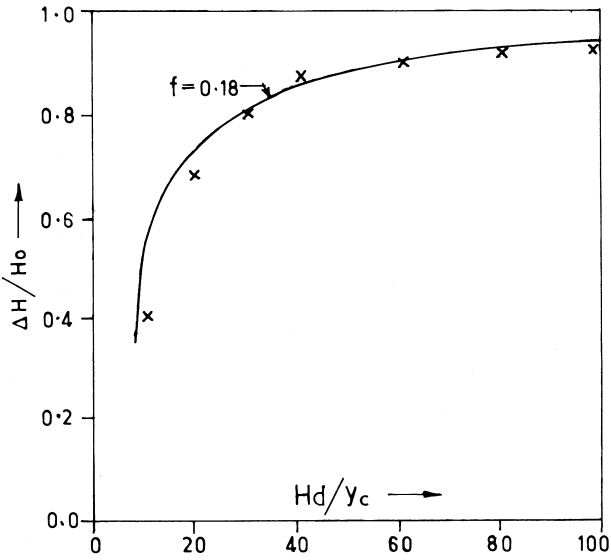

Figure 8 Energy dissipation on stepped spillways with uniform flow:
——— Equation 53: f = 0.18, $\theta = 53°$
× Stephenson: $h = y_c/2$, $\theta = 54.4°$

models, based on measurements on aerated flows, which often resulted in overestimation of energy loss. Some of the investigations are: Sorenson (1985) for the Monksville dam (energy dissipation 88–94%), Rice and Kadavy (1996) for the Salado dam (48–71%), and Yildiz (1998) on a 3.23 m high spillway model (80–95%).

Christodoulou (1993) conducted experiments on a moderately sized stepped spillway model. He presented a general diagram for the energy loss considering the number of steps, for $\theta \approx 35°$ and y_c/h in the range of 1–4. Shu-Xun et al. (1994) conducted experiments on a 1.6 m high stepped spillway model with $\theta = 53°$ and four alternative step heights and y_c in the range of 0.3–2.2. Although, their measurements were in aerated flow, the depths were corrected for the aerated upper region and volume of bubbles contained in the flow. Bindo et al. (1993) conducted studies on a 1.5 m high stepped spillway model of the M'Bali dam ($\theta = 51°$) and presented results in a generalized design chart. Ghare et al. (2002) conducted model studies, where different step heights were incorporated on a constant chute slope. They propose the following relationship:

$$\frac{\Delta H}{H_{\max}} = -0.0209 \ln \left[\frac{y_c}{h}\right] + 0.9055 \tag{55}$$

It would be seen that the above relationship does not include the parameter of chute slope (θ). This therefore results in the energy grade line of a constant slope, depending only on the step height and discharge, regardless of the flow regime—whether rapidly varying, gradually varying, or uniform. Theoretically, this is not possible.

Yashuda et al. (2001) have suggested functional relationship from dimensional consideration

$$\frac{\Delta H}{H_{\max}} = f\left[\frac{H_d}{y_c}, Tan\,\theta, \frac{h}{y_c}\right] \tag{56}$$

They conducted a series of experiments in which three different chute slopes were used with the other parameters as

θ°	H_d/y_c	h/y_c
5.73	8.09–38.5	0–0.688
19.0	6.18–83.8	0–0.913
55.0	6.48–84.0	0–1.37

The range of discharges covered non-uniform as well as quasi-uniform flow. Energy loss at the base of the spillway was calculated for the quasi-uniform flow, based on friction factor and energy loss equation (Eq. 53). For the non-uniform flow, the energy loss was determined experimentally, evaluating clear water depths of flow based on air concentration measurements. The results are shown in Figure 9.

Boes and Minor (2002) suggest Equation 53 for calculating energy dissipation, in the case of uniform flow, with friction factor f corresponding to clear water uniform flow given by Equation 26.

For the non-uniform flow, they propose

$$\frac{H_r}{H_{\max}} = \exp\left[\left(-0.045\left[\frac{k}{D_{h,w}}\right]^{0.1}(Sin\theta)^{-0.8}\right)\frac{H_d}{y_c}\right] \tag{57}$$

where $D_{h,w}$ is the clear water depth of flow at the location concerned. As a first approximation, it is also suggested that this depth can be linearly interpolated from the depth of flow at the point of inception and the uniform depth $y_{go,u}$, given by Equation 38, and occurring at a normalized vertical distance $H_{d,u}$, given by Equation 39.

Illustrative Example

A 90 m high stepped spillway has a slope of 0.7H: 1V, and has been designed for a maximum unit discharge of 23 cumec/m. The step height is 1.2 m.

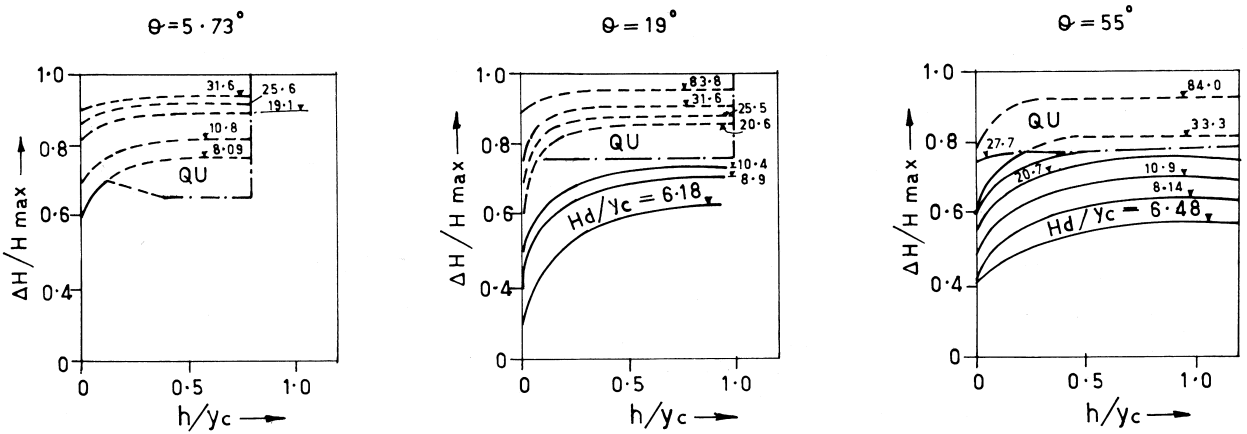

Figure 9 **Energy dissipation-Design charts** (courtesy of Yasuda et al. 2001): – – – – Calculated curve, —— Experimental curve, QU: Quasi-uniform flow region

1. Estimate the energy dissipation at:

   the point of inception
   a location 50 m below the crest
   the location where the flow becomes uniform
   the base of the spillway

2. Calculate the aerated flow depths at the above locations.

Energy dissipation.

$\theta = \text{Tan}^{-1}$ (1/0.7) = 55°; k = h Cosθ = 0.69; y_c = 3.78 m; H_d = 90 m; $H_{max} = 90 + 1.5y_c = 95.67$m

At the point of inception, Equation 34 $L_i = \dfrac{5.90y_c^{1.2}}{(Sin\theta)^{1.4}h^{0.2}}$ gives L_i = 37.1 m and Equation 35 $y_i = \dfrac{0.4y_c^{0.9}h^{0.1}}{(Sin\theta^{0.3})}$ gives y_i = 1.43 m. Also, Chanson's Equations 28 and 29 give respectively 37.87 m and 1.35 m.

Average velocity at the point of inception = 23/1.43 = 16.08 m/s.

Energy at the point of inception $= 1.43(Cos\theta) + \dfrac{16.08^2}{2g} = 14m$ (57a)

Energy level = [90 − (37.1 $Sin\theta$) + 14] = 73.16m with datum at the base of the spillway.

Alternatively, Equation 57 for non-uniform flow

$\dfrac{H_r}{H_{max}} = \exp\left[\left(-0.045\left[\dfrac{k}{D_{h,w}}\right]^{0.1}(Sin\theta)^{-0.8}\right)\dfrac{H_d}{y_c}\right]$ where $D_{h,\,w}$ may be taken as the depth of water. $H_d = (37.1\ Sin\theta) = 30.39$ m and $H_{max} = 30.39 + 1.5\ y_c = 36.06$ m.

$\dfrac{H_r}{36.06} = \exp\left[\left(-0.045\left(\dfrac{0.69}{1.43}\right)^{0.1}(0.819)^{-0.8}\right)\dfrac{30.39}{3.78}\right] \Rightarrow H_r = 36.06\exp(-0.3947) =$ $0.674 \Rightarrow H_r = 24.3m$. Energy level = (90 − 30.59) + 24.3 = 83.91 m. (57b)

At 50 m below crest.

Normalized vertical distance required for uniform flow to be attained is given by Equation 39: $\dfrac{H_{d,u}}{y_c} = 24(Sin\theta)^{2/3} \Rightarrow H_{d,\,u}$ = 79.42 m. Thus,uniform flow has not been reached at this elevation. The uniform clear water depth according to Equation 27, $\dfrac{y_{wu}}{y_c} = 0.215(Sin\theta)^{-1/3} \Rightarrow y_{w,\,u} = 0.868$ m.By interpolation, the clear water depth at 50 m below crest, i.e. at a distance of (50/ Sin θ) = 61 m, is 1.206 m. Then, from Equation 57 with $H_{max} = 50 + 1.5 \times 3.78 = 55.67$ m and H_d = 50 m, H_r = 28.76 m.

At the location of uniform flow.

Friction factor f is given by Equation 26

$\frac{1}{\sqrt{f}} = \frac{1}{\sqrt{0.5 - 0.42Sin(2\theta)}}\left[1.0 - 0.25\log\left(\frac{k}{D_{hwu}}\right)\right]$. With D_{hwu}=4x 0.868m, f= 0.076 and Equation 53, $\frac{\Delta H}{H_{\max}} = 1 - \frac{\left(\frac{f_a}{8Sin\theta}\right)^{1/3} Cos\theta + \frac{1}{2}\left(\frac{f_a}{8Sin\theta}\right)^{-2/3}}{\frac{3}{2} + \frac{H_d}{y_c}}$. With H_d= 79.42*m and* $H_{\max} = 79.42 + 1.5 \times 3.78 = 85.09m$, $H_r = 37.35$ m.

Friction factor f can also be calculated from Equation 6.24, which, in the present case works out to be 0.079.

At the base of the spillway.

The flow depth and friction factor remain the same. $H_d = 90$ m and $H_{max} = 95.67$ m give Hr = 37.36 m. It would thus be seen that the energy content in the uniform flow remains the same. Energy dissipation has been also assessed applying the results of Yasuda et al. (2001), Figure 9. The results of both the methods are shown in Figure 10. It will be seen that there is considerable difference in the

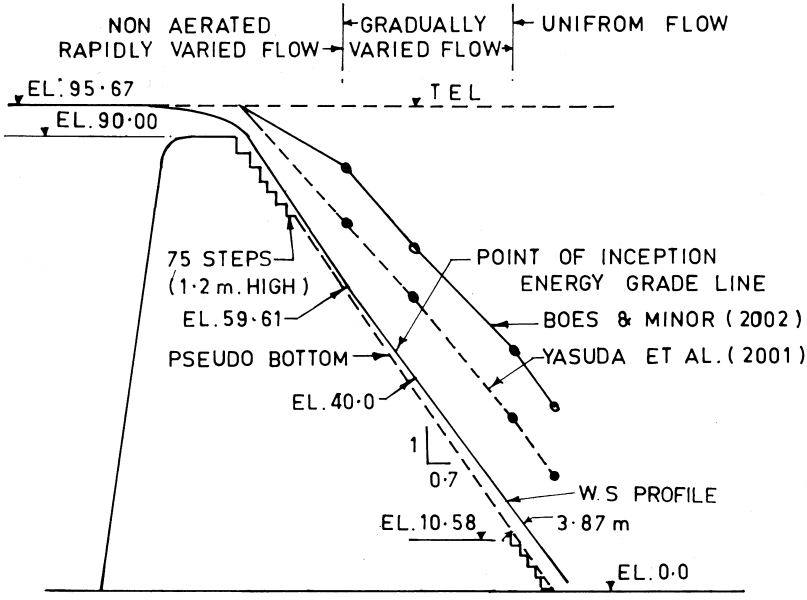

Figure 10 Illustrative example: Energy dissipation

results. For the present, it would be advisable to adopt conservative values for the design of stilling basin at the base of a spillway.

Aerated flow depths.

Up to the point of inception, the flow is non-aerated. The uniform mixture depth $y_{90,u}$ is given by Eq (38) $\frac{y_{90,u}}{h} = 0.50\left(F_h^*\right)^{0.1Tan\theta+0.5}$ where $F_h^* = \frac{q}{(g\ Sin\theta\ h^3)}$ = 6.173, $y_{90,u}$ =3.87m, at x=79.42m and furtherdown.

At location 50 m below crest, Equation 37

$\frac{y_{90(x)}}{y_{90(u)}} = \text{Tanh}\left[1.1\frac{y_{90(u)}^2 \sin\alpha}{y_c^3}(x - L_i)\right]$, with x = (50 / Sin θ=61m, $y_{90(61)}$ =3.83 m.

6.5.4 Pressure Fluctuations and Cavitation Susceptibility

In the skimming flow, the lower area beneath the pseudo-bottom, formed by almost triangular cells, contains maximum turbulence. The pressure field in these cells is expected to exhibit intense pressure fluctuations and therefore, it is important to know whether fluctuating pressure depressions can cause intermittent cavitation inception. This is particularly important in the region between the crest and the point of inception, because this region does not contain air to mitigate cavitation damage. It is believed that in this reach, a velocity of about 20 m/s can cause cavitation, which could be attained with a unit discharge of about 25 cumec/m. Far below, in the region of uniform flow, air has reached the bottom layer and hence, this reach is well protected against cavitation damage.

Sanchez et al. (2000) studied pressure distribution in the stepped region, with a piezo-resistive pressure transducer and flow visualizing technique. It was found that the upper half of the vertical face of the steps was subjected to negative pressures whereas horizontal faces of the steps were free of negative pressures, except a small part corresponding to the minimum fluctuating amplitude. The severity of pressure fluctuations was more on the upstream of the point of inception. Shu-Xun et al. (1994) have also reached the same conclusion. They also computed cavitation index σ based on minimum pressures, which ranged from 2.43 to 13.1 and concluded that these being substantially larger than the incipient cavitation index based on minimum pressures, σ_i = 1.1, cavitation would not occur. Chinnarasri (2002) has presented results of experiments in regard to the maximum time averaged pressure P_{max} on the horizontal face of the step, located at H_i below the crest level as

$$\frac{P_{\max}}{\gamma\ H_i} = 1.28\left(\frac{q^2}{gH_i^3}\right)^{0.31} \tag{58}$$

6.6 GUIDELINES FOR DESIGN OF STEPPED SPILLWAYS

Current interest in stepped spillways is in part due to the RCC (Roller Compacted Concrete) horizontal lift placement techniques, of which a stepped spillway is a natural outcome. Also of major importance is the fact that a significant proportion of energy can be dissipated over the stepped face of the dam, and thus economizing on the size of the stilling basin at the toe. General guidelines for the design of concrete stepped spillways and weirs have been discussed here. Design of earth dam spillway with pre-cast concrete blocks will be discussed in Chapter 16, ''Overtopping Protection of Dams Used as Spillways.''

A survey of existing structures indicates that concrete stepped spillways have been designed and constructed up to about 75 m in height and specific discharge of 30 cumec/m.

It is important to avoid transition flow regime as far as possible. Referring to Figure 2, this implies that flow conditions with (y_c/h) in the range of approximately 0.8 to 1.2 should be avoided. This, however, would be possible only for gated spillways. For ungated spillways, the nappe flow regime corresponding to low discharges would pass through transition regime with increasing discharges, to skimming flow regime. In such a case, necessary precautions should be taken as discussed in Paragraph 6.4.4.

Designing concrete stepped spillways involves following:

Transition from ogee crest to stepped profile.
Determination of the step geometry, particularly step height.
Identification of flow conditions: occurrence of nappe flow, transition from nappe flow to skimming flow, and assessment of residual energy at the toe.
Estimation of air entrainment and air concentration close to the pseudo-bottom of the chute.
Requirement of free board for the side walls.
Design of energy dissipator, i.e. stilling basin

6.6.1 Crest Profile and Transition

A typical stepped spillway can be divided into two zones: the conventional ogee crest profile and the stepped chute. The crest profile is dimensioned for a flow close to or at maximum head. For lower discharges, flow takes place like a jet on to the first step and is likely to spring clear of the step if proper transition is not provided. Generally, the ogee profile is continued up to the tangent point, from where the chute slope commences downward. However, with this, part of the energy dissipation potential is lost, especially for low spillways. The objective, therefore, would be to design a transition in such a way that the advantages of a standard ogee profile (such as WES or USBR) are retained and the stepped profile is introduced at as

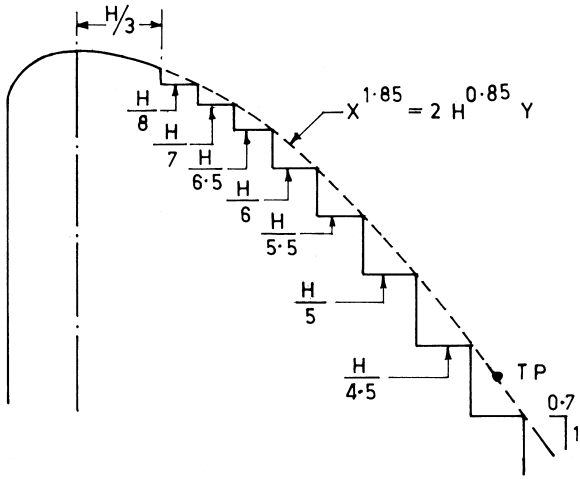

Figure 11 Crest profile and transition.

high of an elevation as possible. Iguacel et al. (1995) have evolved a profile, often designated as CEDEX* profile in which the first step starts at a horizontal distance of $H_d/3$ from the crest axis, its length being $H_d/8$. The step height is determined by the profile of the crest. Subsequent steps are at $H_d/7$, $H_d/6.5$, $H_d/6$, $H_d/5.5$, $H_d/5$, etc., until the rear slope is met, where steps of identical rise and tread are provided. The details are shown in Figure 11.

6.6.2 Step Height

For RCC stepped spillways, the step height is often governed by the dam construction procedure. For example, the step height is usually one to four times the thickness of a compacted lift of typically 0.3 m, i.e., between 0.3 m and 1.2 m. Hydraulic considerations are cavitation potential and energy dissipation. If $C_b = 0.05$ is considered a minimum value to avoid cavitation, the roughness Froude number F_h must not exceed 29 and 38.3 for $\theta = 30°$ and 50° respectively. Assuming that the maximum unit discharge does not exceed 30 m^2/s, the step height would then be about 0.6 m for $\theta = 30°$ and 0.5 m for $\theta = 50°$. Tatewar et al. (2000) suggest that optimum value of Froude number at the toe should be about 5.3 and deduce that step height would be 1.557 y_c for chute slope of 1:0.6, 2.622

* Centro de Estudios y Experimentación de Obras Públicas (CEDEX), Spain.

y_c for 1:0.7, and 4.01 y_c for 1:0.8. These of course give excessive values of step height. Matos (2000) recommend optimum step height as 0.3 dc.

6.6.3 Freeboard for Sidewalls

Considerable aeration on stepped chutes leads to bulking of the flow that has to be taken into account in the design of spillway training walls. The characteristic mixture flow depth y_{90} with a surface air concentration of 90%, given by Equation 37 and 38, serve as a guide for the design in the aerated or white water region. A factor of safety varying from 1.2 to 1.5 has also been suggested.

6.6.4 Design of Energy Dissipator

Hydraulic jump stilling basin is the obvious choice for an energy dissipator at the toe of a stepped spillway. There is significant energy dissipation with stepped spillways. Experimental results by several researchers indicate that the length of hydraulic jump can be reduced by 10 to 50% as compared to that resulting from a smooth, unstepped spillway. The equivalent clear water depth and corresponding velocity can be used to estimate the specific energy at the toe.

6.7 HYDRAULIC MODEL STUDIES

The hydraulics of stepped channels and chutes differs substantially from classical, smooth chute calculations. It is therefore advisable to have the preliminary design based on the above guidelines as studied on a hydraulic model. Unlike clear water, open channel flow, highly turbulent air-water flow cannot be modeled precisely without scale effect, using Froudian similarity, because of the effects of viscosity and surface tension. Boes (2000) has extensively studied the scale effects involved in such modelling on scales of 1:26.4, 1:13.2. and 1:6.6 with chute slopes of 30° and 50°. He concluded that the scale effects would be insignificant if model Reynolds number and Weber number are at least 10^5 and 10^2 respectively. For typical unit discharge of about 20 m^2/s and step height of 0.6 m, this implies a minimum scale of 1:10 to 1:15.

Notations

C_b = Air concentration close to bed.
C_{mean} = Mean air concentration
C_f = Coefficient of skin friction
$D_{h,w}$ = Clear water depth of flow
D_{hwu} = -do- for uniform flow condition
E_o = Total energy
F_h = Froude number based on step height
$F_h = q_w/g \cdot \sin\theta\,(h\cos\theta)^3$

Fr = Froude number defined in terms of roughness height
$Fr = q_w / \sqrt{g \cdot \sin\theta \cdot k_s^3}$
Fs = Froude number based on step height
$F_s = q_w / \sqrt{gh^3}$
f = Darcy – Weisbach friction factor.
H_o = Upstream head referred to step elevation
H_d = Dam height from toe
$H_{d,u}$ = Vertical distance below crest, required for uniform flow to be attained.
H_{max} = Maximum head
H_p = Depth of overflow
H_r = Residual energy head
h = Height of step
k = h cosθ
L = Distance from the crest measured along chute
k_s = Nikuradse equivalent sand roughness
L_i = Distance from the start of boundary layer
L_u = Distance from crest, along chute, at the point where flow becomes uniform
l = Length of step
l_s = Throw length of the jet
l_w = Length of hydraulic jump
N = Number of steps
q = Discharge per unit width
q_w = Water discharge per unit width
$s' = (L - L_i)/y_i$
U_w = clear water velocity
W = Height of the weir at the end of the step
x = Distance from the crest measured along chute
y = Depth of flow
y_{90} = Characteristic depth where the air concentration is 90%.
y_c = Crticial depth
y_i = Depth of flow at the point of inception
y_w = clear water depth
y_{wu} = Uniform flow clear water depth
α = Kinetic energy coefficient
Average energy loss per step
λ = Dimensionless parameter
τ_0 = Shear stress
θ = Angle of inclination of chute
θ_b = Initial angle of stream lines
ϕ = Angle of inclination of step

ξ = A parameter
ΔH = Loss of head

REFERENCES

1. Aigner, D. Hydraulic design of pooled step cascades-29th IAHR Congress, Beijing, China. 2001.
2. Boes, R. M. Scale effects in modelling two-phase stepped spillway flow – Hydraulics of stepped spillways; © Swets & Zeitlinger, Balkema. 2000, 53–60.
3. Boes, R. M.; Minor, H. E. Guidelines for the hydraulic design of stepped spillways – ibid –; © Swets & Zeitlinger. 2000, 163–170.
4. Boes, R. M.; Minor, H. E. Hydraulic design of stepped spillways for RCC dams-Intnl.Jnl of Hydropower and Dams. 2002, Issue 3.
5. Bindo, M.; Gautier, J.; Lacroix, F. The stepped spillway of M'Bali dam, International Water power and dam construction. January, 1993.
6. Chamani, M. R. Air inception in skimming flow regime over stepped spillways, Proc.Intl. Workshop on Hydr of stepped Spillways, Balkema, Rotterdam; © Swets & Zeitlinger. 2000.
7. Chamani, M. R.; Rajaratnam, N. Jet flow on stepped spillways. J. Hydr. Engg. 1994, 120(2), 254–259.
8. Chamani, M. R.; Rajaratnam, N. Characteristics of skimming flow over stepped spillways. J. Hydrulic Engineering. 1999, 125(4), 361–368.
9. Chanson, H. State of the art of the hydraulic design of stepped chute spillways. Hydropower and Dams Journal. 1994a, 33–42.
10. Chanson, H. Comparison of energy dissipation between nappe and skimming flow regimes on chutes. IAHR Jnl. of Hydraulic Research. 1994b, 32(2), 213–218.
11. Chanson, H. A Transition flow regime on stepped spillways. The facts; 29th IAHR Congress, Beijing, China. 2001a.
12. Chanson, H. Experimental investigations of air entrainment in transition and skimming flows down a stepped chute, Research report no CE 158; The University of Queensland, Australia. July, 2001b.
13. Christodoulou, G. C. Energy dissipation on stepped spillways. Journal of Hyd. Engg. 1993, 119(No.3), 644–650.
14. Chinnarasri, C. Assessing the flow resistance of skimming flow on the step faces of stepped spillways - Dam Engineering, 2002.
15. Fratino, U.; Piccinni, A. F.; de Marinis, G. Dissipation efficiency of stepped spillways, Hydraulics of stepped spillways; © Swets & Zeitlinger, Netherlands. 2000.
16. Frizell, K. H.; Matos, J.; Pinheiro, A. N. Design of concrete stepped overlay protection for embankment dams – ibid.; © Swets & Zeitlinger. 2000.
17. Ghare, A. D.; Porey, P. D.; Ingle, R. N. Experimental studies on energy dissipation over stepped spillways, Proc Hydro 2002; Indian Society for Hydraulics, Mumbai. Dec 2002.
18. Hager, W. H. Uniform aerated chute flow. ASCE Jnl of Hyd Engg. April, 1991.
19. Hager, W. H.; Boes, R. M. Backwater and drawdown curves in stepped spillway flows, Proc.Intl. Workshop on Hydr of stepped Spillways; © Swets & Zeitlinger, Balkema, Rotterdam. 2000.

20. Iguacel, C. M.; Garcia, V. E. Stepped spillways – Design for the transition between the spillway crest and steps. HYDRA 2000. 1995, I, 260–65, Thomas Telford, London.
21. Matos, J. Hydraulic design of stepped spillways over RCC dams, Hydraulics of stepped spillways; © Swets & Zeitlinger, Netherlands. 2000.
22. Matos, J.; Sanchez, M.; Quintela, A.; Dolz, J. Air entrainment and safety against cavitation damage in spillways over RCC dams – Hydraulics of stepped spillways – Balkema Publishers; © Swets & Zeitlinger, Netherlands. 2000.
23. Mondardo, J. M.; Fabiani, A. L. Comparison of energy dissipation between nappe and skimming flow regimes on stepped chutes. IAHR Journal of Hydraulic Research. 1995, 33(No.1), 119–122.
24. Nigus, L. A.; Steiger, K. M.; Marti, C. Ashton stepped spillway – Design and Construction, Hydraulics of Stepped Spillways, Balkema Publishers; © Swets & Zeitlinger, Netherlands. 2000.
25. Rajaratnam, N.; Katopodis, C. Hydraulics of Denil fishways. Proc ASCE J Hyd Engg. Sept 1984.
26. Rajaratnam, N. Skimming flow in stepped spillways. Journal of Hyd. Engg. 1990, 116(4), 587–91.
27. Rand, W. Flow geometry at straight drop spillways. Pros. ASCE, Hyd. Dn. 1955, 81(No.791, Sept.), 1–13.
28. Rice, G. E.; Kadavy, K. C. Model study of a roller compacted concrete stepped spillway. Journal of Hyd. Engg. 1996, 122(12), 292–7.
29. Sanchez, M.; Pomares, J.; Dolz, J. Pressure field in skimming flow over a stepped spillway, Hydraulics of stepped spillways, Balkema Publishers; © Swets & Zeitlinger, Netherlands. 2000.
30. Shu-Xun, R.; Chao-Yang, T.; Rui-Wan, P.; Xue-Min, H. Stepped dissipator on spillway face, Proc. 9th APD-IAHR, Singapore; 1994.
31. Sikora, G. J. An experimental study of the flow regimes in pool and weir fishways; M.Sc Thesis, University of Alberta, Canada. 1997.
32. Soreson, R. M. Stepped spillway, Hydraulic Model Investigation, Discussion. Journal of Hyd. Engg. 1985, III(No.12), 1095–97.
33. Stephenson, D. Energy dissipation down stepped spillways, Intnl Water Power and Dam Construction. Sept. 1991.
34. Tatewar, S. P.; Ingle, R. N. Nappe flow on inclined stepped spillways. Journal of Institution of Engineers (India), – CV. Feb. 1999, 79, 175–179.
35. Tatewar, S. P.; Ingle, R. N.; Porey, P. D. Discussion on paper Sr no 8 above. ASCE Jnl of Hyd Engg. 2000.
36. Tozzi, M. J. Residual energy in stepped spillways, Intl Water Power and Dam Construction, May 1994.
37. Yasuda, Y.; Otshu, I. Flow resistance in skimming flow in stepped channels, Proc. 28th IAHR Congress; Theme B, Austria. 1999.
38. Yasuda, Y.; Takahashi, M.; Ohtsu, I. Energy dissipation of skimming flows on stepped-channel chutes, 29th IAHR Congress, Beijing, China. 2001.
39. Yildiz, D.; Kas, I Hydraulic performance of stepped chute spillways. Intl Jnl of Hydropower and Dams. 1998(Issue 4).

7
Siphon Spillways

7.1 INTRODUCTION

The discharge over an overflow spillway is a function of the head measured over its crest. Enclosing the crest and making the resulting conduit flow full can substantially increase this effective head. The head on the spillway is then the difference in elevation between the reservoir surface and the spillway outlet. However, the flow near the crest of the spillway would then be under a negative pressure. In other words, the conduit becomes a siphon. All necessary precautions must be taken to ensure that the vacuum is maintained and that it does not become so excessive as to cause cavitation. The maximum negative pressure at the spillway crest is theoretically 10 m of water at sea level. Allowing for the vapor pressure of water, loss due to turbulence, etc., the maximum net effective head is rarely more than about 7.5 m. This corresponds to a velocity of $\sqrt{2 \times 9.81 \times 7.5} \approx 12 m/s$. Which means that the initial velocity in any siphon cannot exceed about 12 m/s at the inlet. The essence of the hydraulic design of siphon spillways, therefore, lies in ensuring maximum discharge capacity without harmful negative pressures.

7.2 TYPES OF SIPHON

Siphons can be classified in several ways (Govind Rao 1956).

I. According to the configuration
   A. Hood or Saddle siphon (as shown in Figure 1)
   B. Volute siphon (as shown in Figure 2)

II. According to the operating head
   A. Low head siphon, operating at net head (difference between the upstream and downstream water levels) less than atmospheric pressure, i.e., about 10 m.
   B. High head siphon exceeding the above value

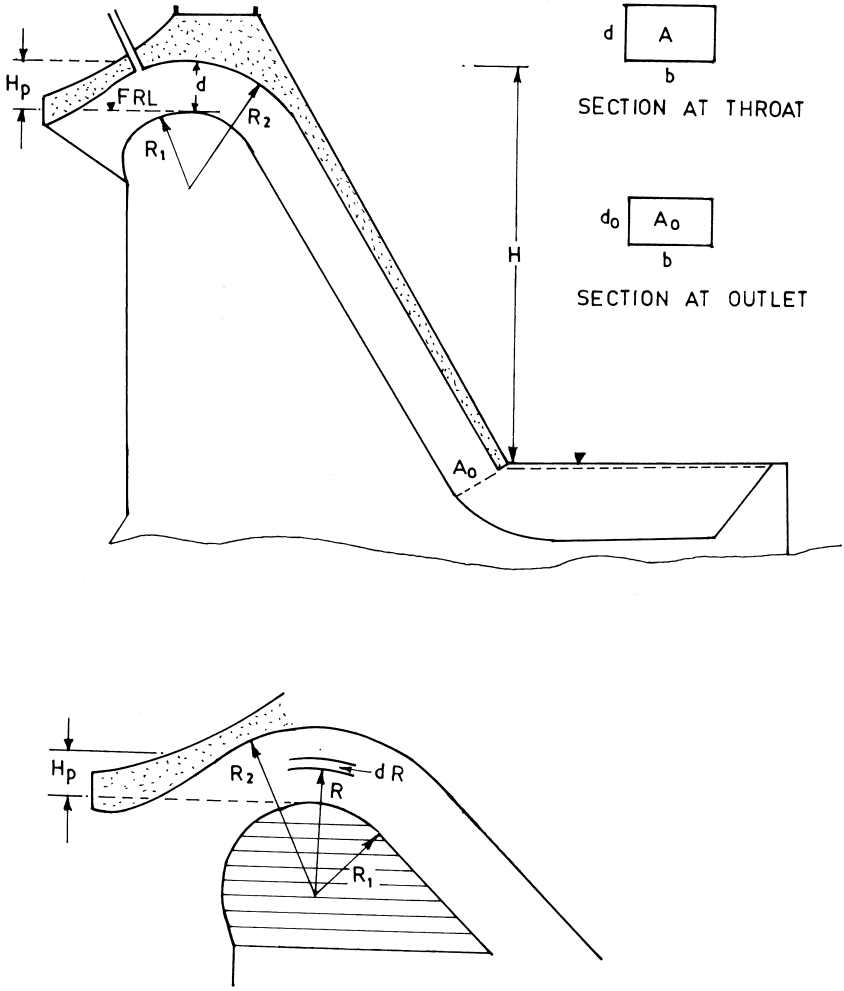

Figure 1 Typical saddle siphon.

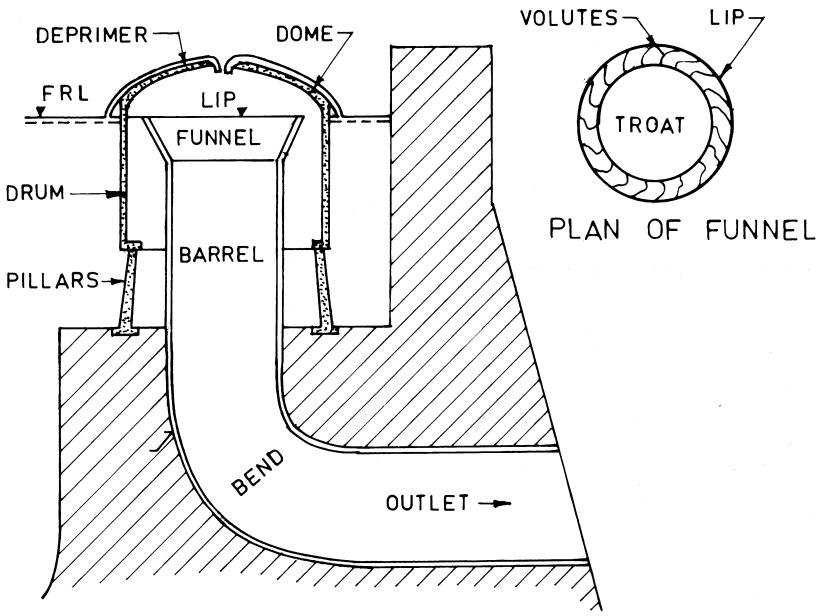

Figure 2 **Typical siphon volute.**

III. According to arrangement of priming
   A. Water seal type
   B. Tilted outlet
   C. Baby siphon
   D. Tudel or stepped type, etc.
IV. According to regulation
   A. Unregulated
   B. Air-regulated

7.3 HYDRAULIC ACTION

Siphons have been used as spillways for reservoirs and canals since the middle of 18th century. Their advantages over simple weirs, gated weirs and gated orifices are: automatic control of head water level within close limits, concentration of flow within restricted space, operation without mechanical parts, independence from outside power supply, and low maintenance costs.

Some disadvantages are: the discharge is inhibited or reduced if obstructed by debris or ice and the sudden increase of discharge on priming might cause fluctuations in head water level and flash floods downstream.

In a hood or saddle siphon (Fig. 1) the crest is set at the FRL (Full Reservoir Level). It has a bell-mouth entry and exit, and a water seal to prevent air from entering from the downstream. When the water rises above FRL, i.e., above the crest, the discharge passed down through the lower limb carries away air in the throat. This action is similar to the weir overflow. With increase in the head and discharge, more and more air is dragged out resulting in fall in pressure. The difference between the atmospheric pressure on the outside and reduced pressure in the siphon creates more flow and a higher pressure drop until the entire throat starts flowing full, when it is said to have primed. To stop the siphonic action, there is an air inlet pipe with its mouth at FRL or a higher elevation. As soon as the water in the reservoir goes below the desired elevation, air rushes through this pipe into the siphon and breaks the vacuum, stopping the flow. The air inlet pipe is called a deprimer.

Various devices are used to induce early priming of the siphon. The two most commonly used are the step or deflector (Fig. 3) and the baby siphon (Fig. 4).

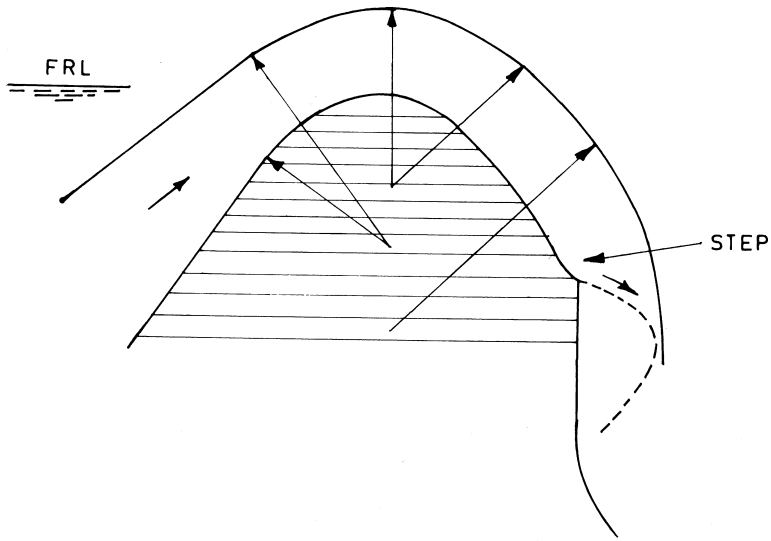

Figure 3 **Siphon with step.**

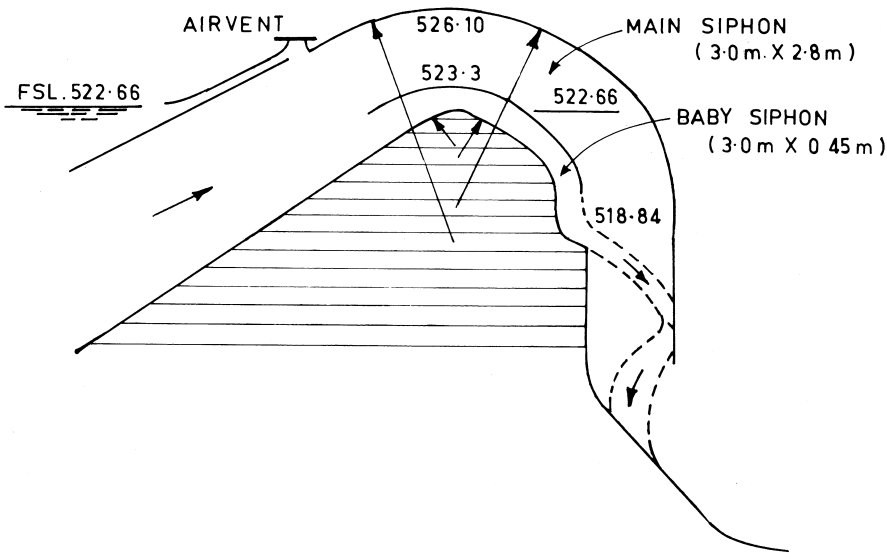

Figure 4 **Siphon with a baby siphon.**

In a volute siphon, (Ganesh Iyer 1950) shown in Figure 2, the lip of the funnel is kept at FRL and a number of volutes (like the blades of pumps or turbines) are placed on the funnel to induce a spiral motion of water passing along them. When the water rises above FRL, it spills, over the circumference of the lip of the funnel and flows along the volutes with a spiral motion, forming a vortex in the vertical pipe. This induces a strong suction pool creating a powerful vacuum, which sets the siphon in action. To stop the siphonic action, air is let in through small pipes taking off from the crown of the dome with their inlet opened at FRL.

7.4 HYDRAULIC DESIGN CONSIDERATIONS

The following characteristics are relevant in the hydraulic design of siphon spillways:

Discharging capacity
Priming depth
Regulating flow

Stabilizing function
Effect of waves in the reservoir
Cavitation
Vibration

7.5 DISCHARGING CAPACITY

The flow in the throat section of a saddle siphon can be idealised as a free vortex, so that

$$R = V_1 R_1 = V_2 R_2 = \text{constant} \quad (1)$$

where

V = Velocity of flow
R = Radius

Subscript 1 refers to quantities at the crest and subscript 2 refers to the crown of the siphon.

$$V = V_1 \frac{R_1}{R} \quad (2)$$

Referring to Figure 1, discharge through an elemental area dA formed by a strip dR and throat width b is

$$Q_A = V_1 \frac{R_1}{R} dA = V_1 \frac{R_1}{R} b\, dR \quad (2a)$$

and hence

$$Q = \int_{R_1}^{R_2} V_1 \frac{R_1}{R} b\, dR = V_1 R_1 b \int_{R_1}^{R_2} \frac{dR}{R} = V_1 R_1 b \left[1\text{n} \frac{R_2}{R_1} \right] \quad (3)$$

Since, the maximum value of V_1 is 12 m/s,

$$Q_{\max} = 12\, R_1\, b \left[1\text{n} \frac{R_2}{R_1} \right] \quad (4)$$

and the average velocity will be

$$V_a = \frac{Q}{A} = \frac{12 R_1 b}{(R_2 - R_1) b} \left[1\text{n} \frac{R_2}{R_1} \right] = \frac{12 R_1}{(R_2 - R_1)} \left[1\text{n} \frac{R_2}{R_1} \right] \quad (5)$$

This velocity should be the same at all sections along the siphon barrel unless there is expansion or contraction of the section. However, when the siphon is running full, the velocity is given by the total head H (from reservoir level up to the tail water level or crown of the outlet section, as the case may be),

$$V = \mu \sqrt{2g\, H} \quad (6)$$

μ = siphon-coefficient accounting for various losses such as inlet, friction, bend, etc.

If the siphon barrel is of constant cross section without constriction or expansion,

$$\mu = \frac{1}{\sqrt{k}} = \frac{1}{\sqrt{(1 + k_i + k_f + k_b + ...)}} \tag{7}$$

Where k_i etc. are loss coefficients for inlet, friction, bend and outlet.

It may be necessary to limit the head in some manner to prevent V from exceeding the value specified in Equation 5. This can be done either by increasing the outlet loss by constricting the outlet section or by decreasing the total head by raising the elevation of the outlet.

When the outlet section is constricted, the exit velocity V_0 is given by

$$H = \frac{V_0^2}{2g} + \frac{V_a^2}{2g}(k_i + k_f + k_b + ..) \tag{8}$$

Where V_a is obtained from Equation 5. The required outlet area A_o can then be calculated from V_0. The above procedure can also be represented by a single relationship

$$A_0 = \frac{Q}{V_0} = \frac{AV_a}{V_0} = \frac{A}{\sqrt{\frac{2gH}{V_a^2} - (k_i + k_f + k_b + ...)}} \tag{9}$$

The discharge in the volute siphon can also be calculated in the same way by assuming that the flow entering the funnel at the lip (Fig. 5) takes a circular path (Govind Rao 1956).

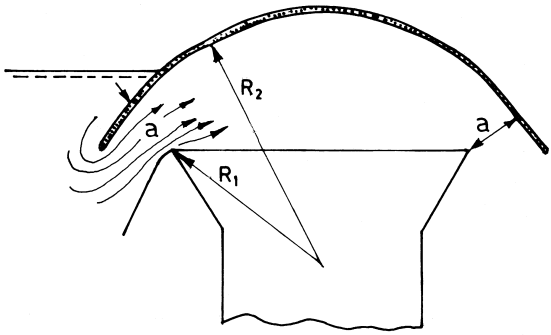

Figure 5 **Calculation of discharge in a volute siphon.**

$$Q = C_d.a.\frac{V_1 R_1 \log e \frac{R_2}{R_1}}{R_2 - R_1} \tag{10}$$

where

C_d = Coefficient of discharge ≈ 0.7

a = Area of the annular space

If the area at the outlet section is A_o and H is the operating head available,

$$Q = C_d.\, A_o \sqrt{2g\, H} \tag{11}$$

C_d may be assumed to be 0.70, however, model observations have shown this to be as high as 0.85.

Ackers et.al. (1975) have summarized the discharge characteristics in a non-dimensional form as shown in Figure 6, applicable for all air-regulated siphons. Initially, the discharge rises slowly as relative to upstream head. When priming occurs, the curve flattens, representing a wide range of discharge for a small difference in head.

This is the range within which the siphon will operate flowing full of air-water mixture, until the upstream level falls below the depriming head. To avoid hunting it is desirable for the curve in the operating range to gently rise with

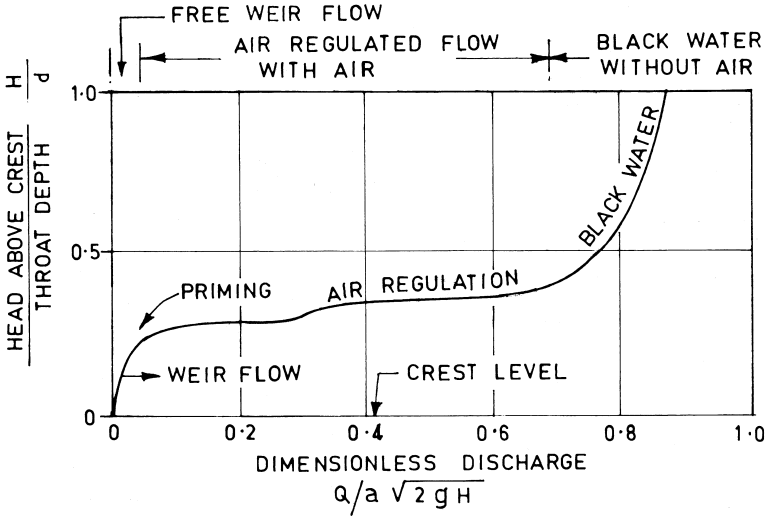

Figure 6 Discharge characteristics of an air regulated siphon. (Ackers et al. 1975)

increase in the discharge. If the upstream level rises beyond this operating range, the siphon will run to black water (a term used to define flow without air), when the discharge will increase in proportion to only $\sqrt{H}$. Generally, the siphon should be designed such that the black water condition is not reached.

Prettyjohns et al. (1989) have reported experiments with air regulation through two pipes, which dip into the surface of the headwater. One of these dip pipes admits air to the crown of the siphon passage and the other admits air at the crest. This form of air admission produces good dispersion of air into the flow. This results in a head-discharge characteristic that is considerably flat, showing large change in discharge for very little change in headwater level as shown in Figure 7.

Illustrative Examples

1. A reservoir requires a spillway to surplus a maximum discharge of 450 cumec with its FRL 20 m above the tail water elevation.

   a. If an overflow spillway with a WES crest profile is used with crest elevation 5 m below the FRL, what should be the length of such a spillway?
   b. If a siphon spillway is used, with a constant cross section 5 m in depth and formed by radii of 5 m and 10 m, what should be the width of such a siphon?
   c. If the total head loss through the siphon (excluding velocity head at outlet) is 10 m, how far above or below the tail water level should the siphon discharge in order to avoid cavitation?

a. For overflow spillway, the coefficient of discharge may be taken as 2.20.

$$L = \frac{Q}{C_d H^{3/2}} = \frac{450}{2.20\, x5^{3/2}} = 18.3\, m \tag{11a}$$

b. With $R_1 = 5$ m and $R_2 = 10$ m, average velocity allowed through the siphon is given by Equation 5,

$$V_a = \frac{Q}{A} = \frac{12 R_1 b}{(R_2 - R_1) b}\left[1\mathrm{n}\frac{R_2}{R_1}\right] = \frac{12 R_1}{(R_2 - R_1)}\left[1\mathrm{n}\frac{R_2}{R_1}\right] \tag{11b}$$

$$V_a = \frac{12x5}{5}\left[1\mathrm{n}\frac{10}{5}\right] = 8.32 m/s \tag{11c}$$

and hence the required crest width is

$$\frac{450}{8.32x5} = 10.8m \tag{11d}$$

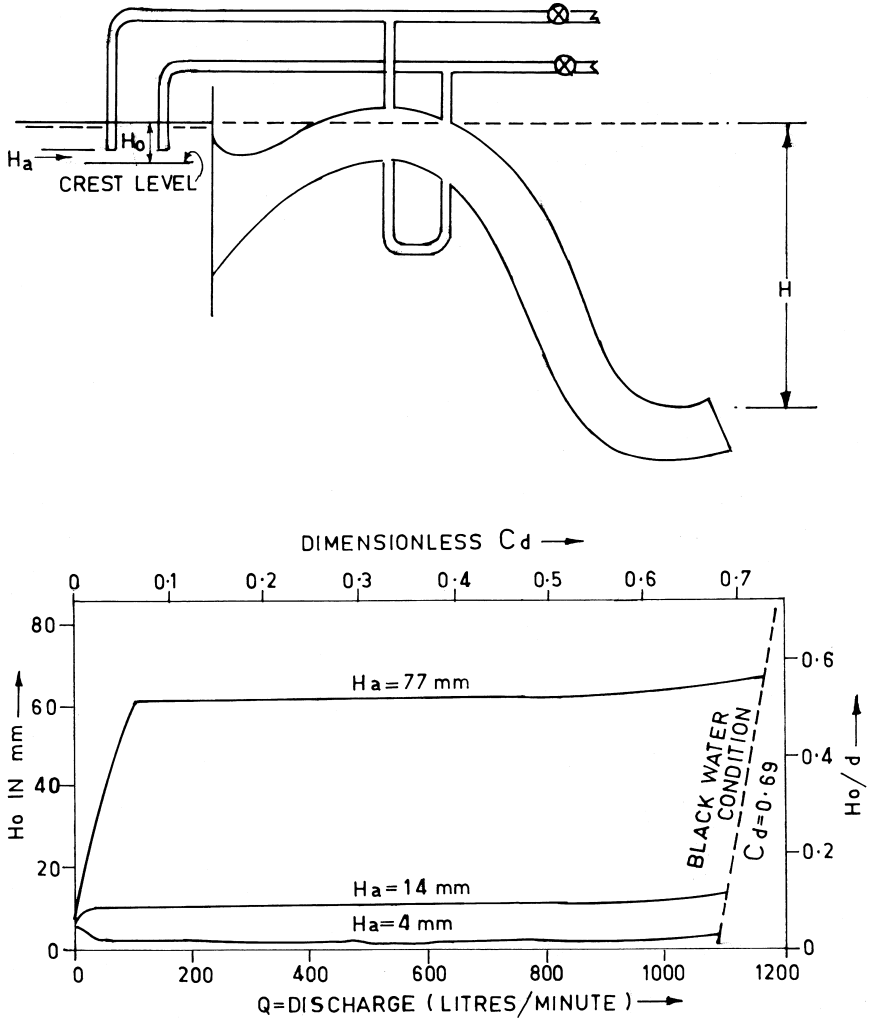

Figure 7 **Prettyjohn's experiments with novel arrangement of air regulated siphon: b = 64 mm, d = 27 mm, H = 522 mm, H_a = 4–77 mm, H_o = 0–80 mm.** (Ref. 11)

Thus, using a siphon spillway affects a reduction of width by about 40%.

c. Applying energy equation from the reservoir surface to the siphon outlet end, the operating head H will be

$$H = \frac{V_a^2}{2g} + H_L \Rightarrow H = \frac{8.32^2}{19.62} + 10 = 13.53m. \tag{11e}$$

The siphon outlet should be placed $(20 - 13.53) = 6.47$ m above the tail water elevation.

2. A siphon spillway of constant rectangular cross section 4 m wide $\times$ 2.5 m high has configuration as shown in Figure 8. The total length of the siphon is 80 m. Various loss coefficients are:

inlet 0.12
outlet 1.0
σ (bend loss coefficient) 0.75
friction factor 0.018

Determine (a) the maximum discharge, (b) whether cavitation would occur for that discharge, and if so, the safe discharge for avoiding cavitation, and (c) the required constriction of the outlet section to restrict that discharge.

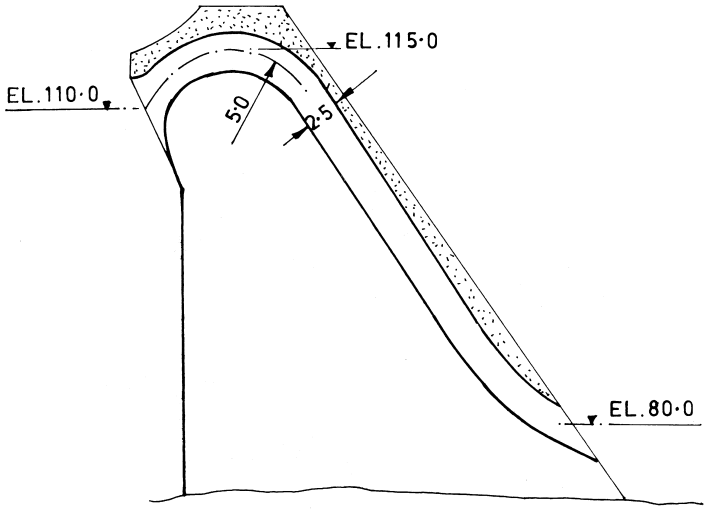

Figure 8 **Siphon spillway configuration—Illustrative example.**

a. The gross operating head = El 111.25 − El 81.25 = 30 m.

$$V_a = \mu\sqrt{2gH} \quad where\ \mu = \frac{1}{\sqrt{(1 + k_i + k_f + k_b)}} \tag{11f}$$

$$k_i = 0.12; \quad k_b = 0.75; \quad k_f = f\left(\frac{L}{4R}\right) where\ R = A / P$$
$$= \frac{4x2.5}{2(4+2.5)} = 0.769 \Rightarrow k_f = 0.018x\frac{80}{4x0.769} = 0.468 \tag{11g}$$

$$\mu = \frac{1}{\sqrt{k}} = \frac{1}{\sqrt{(1 + k_i + k_f + k_b + ...)}} = \frac{1}{\sqrt{(1 + 0.12 + 0.468 + 0.75)}} = 0.654$$

$$V_a = 0.654\sqrt{2gx\ 30} = 15.87 m/s. \tag{11h}$$

Max discharge equals 10 × 15.87 = 158.7 cumec

b. The average velocity should not exceed that given by Equation 5.

$$V_a = \frac{12R_1}{(R_2 - R_1)}\left[1n\frac{R_2}{R_1}\right]; and\ with\ R_1 = 3.75, R_2 = 6.25; V_a = 9.19 m/s \tag{11i}$$

Since the velocity in (a) of 15.87 m/s is considerably larger than 9.19 m/s, there would be danger of cavitation. The discharge should, therefore, not exceed 9.19 × 10 = 91.9 cumec.

c. Required outlet area to restrict the discharge to 91.9 cumec is given by Equation 9.

$$A_0 = \frac{Q}{V_0} = \frac{AV_a}{V_0} = \frac{A}{\sqrt{\frac{2gH}{V_a^2} - (k_i + k_f + k_b + ...)}} \tag{11j}$$

$$A_0 = \frac{10}{\sqrt{\frac{2x9.81x30}{84.4} - (0.12 + 0.468 + 0.75)}} = 4.28 sq.m \tag{11k}$$

If the width of the outlet section is retained the same, then the depth of the section should be reduced from 2.5 m to (4.28/4) = 1.07 m.

7.6 PRIMING DEPTH

The priming action of a siphon depends on the power of its air evacuation. On the inlet side, this is easily done by keeping the lip of the hood below the reservoir level. To prevent the entry of air from downstream and ensure smooth priming, it is necessary to provide a water seal in the downstream leg as shown

in Figure 1. In a saddle siphon, other factors that facilitate low priming are a narrow throat, a large radius at the crest, and a critical depth of submergence at the outlet exit. Ervine et al. (1975) express the entrainment of air by a falling nappe within the siphon barrel in terms of depth of free fall H_1, water velocity V, jet geometry (b), (p), (t), and water discharge Q_w.

$$\frac{Q_a}{Q_w} = 0.26\left(\frac{b}{p}\right)\left(\frac{H_1}{t}\right)^{0.446}\left(1-\frac{V_{\min}}{V}\right) \tag{12}$$

where

Q_a = Air discharge
Q_w = Water discharge
t = Thickness of the rectangular jet
b = Width of the rectangular jet
H_1 = Depth of fall of the rectangular jet
p = Perimeter of the jet exposed to atmosphere
V_{min} = Minimum velocity to entrain air (appx 1.1 m/s)

Equation 12 indicates the relative influence of various parameters on the rate of air entrainment within the siphon barrel and thus, on the rapidity of the priming.

Bollrich (1994) states that priming depth is approximately 0.16 to 0.20 times the vertical dimension of the waterway at the crest, i.e., $H_p \approx 0.16–0.20$ d.

In a volute siphon, priming depth decreases with the increase in the number and height of volutes, a decrease in the angle of their take-off from the lip, a decrease in the rise of the dome and in the slope of the funnel, and an increase in the height of the funnel.

However, it is observed that most of the factors that favor a low priming depth adversely affect the coefficient of discharge.

7.7 FLOW REGULATION

One of the prime disadvantages of the siphon spillway is the sudden release of discharge on priming and the sudden stoppage of this discharge on depriming, leaving any effort of flow regulation.

Air regulated siphons (similar to those proposed by Prettyjohns et al.) offer a relatively flatter discharge curve to ensure a wide range of discharge for small rise in upstream water level. However, discharge and water level in the downstream increase rapidly.

In the case of spillways with a battery of siphons, at least partial regulation of flow in the downstream is possible (i.e., adding or stopping discharge in steps) by manually closing or opening of air inlet valves of some siphons. However,

this must be done with due regard to inflow in the reservoir. Another method is to install siphons at different crest levels such that their priming/depriming occurs in stages, with increasing/decreasing upstream water levels, as described by Bollrich (1994) in the case of the Burgkhammer dam, Germany, having three pairs of siphons with their crest levels differing by 10 cm. Each siphon with inlet dimension of 3 m wide × 1.8 m deep, has been designed to pass a safe discharge of 42 cumec, with a priming depth in the range of 30–47 cm. Depriming is expected at a water level 5 cm above the relevant entrance lip (at the same level as the crest). Figure 9 shows the operating cycle of the siphon spillway.

Partial control of discharge through a siphon may also be possible by manipulating a valve-controlled air vent installed on the crown of the siphon. The necessary cross section of the air vent must be (Bollrich-1994),

$$A_{air} = 0.08xQ\sqrt{\frac{1+\Sigma\zeta_v}{(P_{amb}-P_0)/\gamma}} \tag{13}$$

where

$\Sigma\zeta_v$ = sum of hydraulic loss coefficients in the air vent
P_0 = pressure at the summit of the siphon
P_{amb} = Airbrent pressure

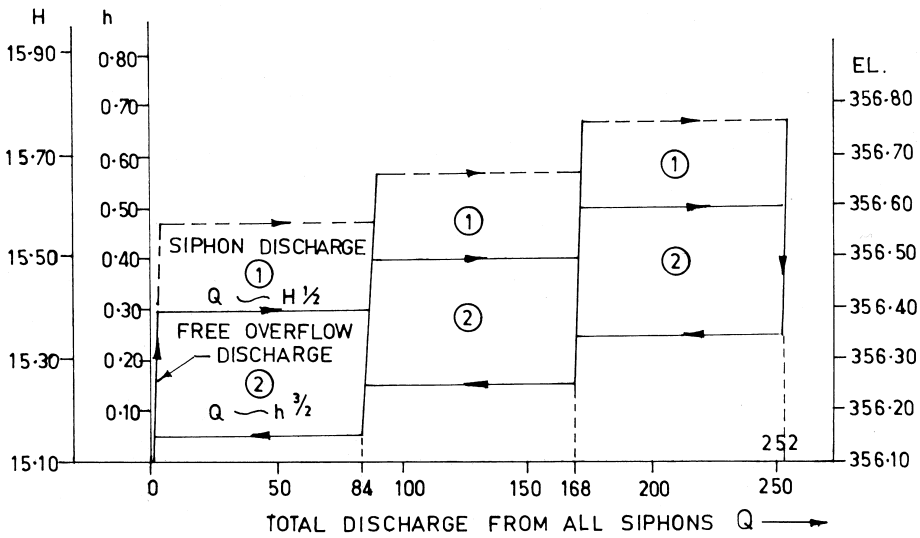

Figure 9 Operating cycle of Burgkhammer siphon spillway: ① Priming range and ②siphon breaking (after Bollrich 1994).

This is, however, seldom resorted to in actual practice because of apprehension about serious operational problems.

7.8 STABILITY OF FUNCTIONING

An examination of Figure 6 and Figure 7 will show that once the siphon primes, the increase in the discharge is substantial as compared to the increase in the upstream water level. A stage may be reached when the outflow through the siphon exceeds the inflow, at which time the upstream water level may start depleting leading to depriming. This results in reduction of discharge and increase in the upstream water level and priming again. This is called hunting or instability of siphonic action and is undesirable. Ackers et al (1975), however, noted that the indications of model tests on the control of upstream level by an air-regulated siphon could be misleading because in the full-scale situation the head pool area and the capacity are proportionately much greater.

The phenomenon of hunting of the siphon has been extensively studied on hydraulic models by Benfratello (1955), Boreli (1955), and Crump et al. (1961). The hunting of the siphon is influenced by the elevation of the lip of the siphon entry hood from the crest H_h, with reference to the priming depth H_p. For $H_h \leq H_p$, violent hunting was evident. It has been recommended by Crump et al.(1961) that

$$(H_h - H_p) = 0.48d \tag{14}$$

7.9 EFFECT OF WAVES

Perkins et al. (1975) have described model tests in which the performance of a siphon was effected by waves with amplitude up to 1.83 m and period varying from 3.5 to 7 seconds. Although, siphon did not deprime, the mean water levels were up to 0.46 m higher than they had been previously and the air was seen entering the siphon in bursts. In addition, the action of waves was cyclic. The arrangement suggested by them includes provision of a stilling box to suppress the effect of waves as shown in Figure 10.

7.10 CAVITATION

Siphons operating at high head may cavitate. This was evident from the experiments on the model of a saddle siphon as well as on a full-scale, 14 cumec siphon, having 1.5 m high barrel at the throat and operating under a head of 7.3 m. The

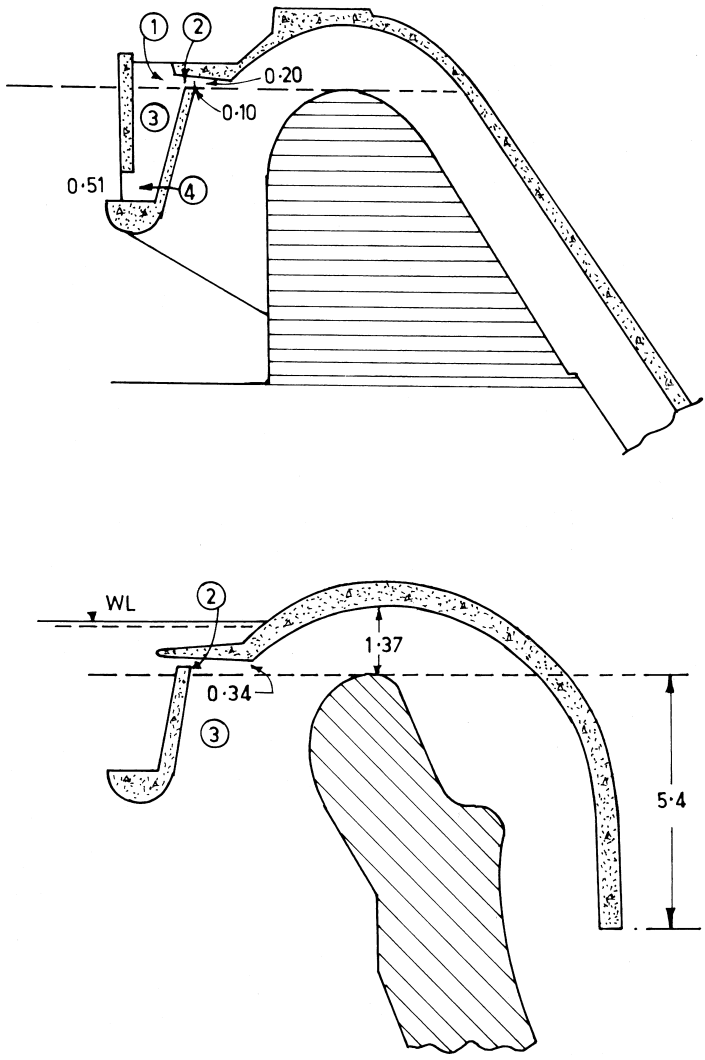

Figure 10 **Stilling box to suppress wave effects for hood siphons**: ① Air inlet valve, ②Air water slot, ③ Stilling box, and ④ Water slot. (Perkins et al. 1975)

pressures on the crest were about -7.5 m of water. However, by putting a flared outlet of 1:5 in the model, the negative pressure increased to -8.2 m and the discharge showed an increase of 31 percent. In the full-scale, the discharge increased by only 3% because of cavitation and separation. It was confirmed that the limiting negative pressure in a well-designed siphon corresponds to about -8.2 m of water.

Prototype investigations in regard to functioning of the Hirebhasgar volute siphons, such as one in India, brought out the limitations of volute siphons operating at heads in excess of 20 m. Cavitation damages were noticed on the vertical barrel just below the throat and on the bends.

Prediction of Cavitation

An approximate velocity in excess of about 12 m/s is a condition for the onset of cavitation. Bollrich (1994) has suggested a more precise method based on the vortex-core theory. According to this theory, the tension p_k inside the core of a single vortex rotating with a velocity V_i equal to the flow velocity can be expressed as

$$\frac{P_k}{\gamma} = -h_{vac} - \frac{V_i^2}{2g} \tag{15}$$

where

h_{vac} = vacuum pressure head, i.e., the difference between the atmospheric pressure (corresponding to the elevation of the structure with respect to msl), and the vapour pressure p_v

$$(p_v) = -\left[\frac{P_{atm}}{\gamma} - \frac{P_v}{\gamma}\right] \tag{15a}$$

The critical values of the pressure and the velocity are at the inner side (crest) of the siphon. Referring to Figure 1 and the general expression for discharge through siphon,

$$Q = b\, R_1 1n\left(1 + \frac{d}{R_1}\right)\sqrt{2g(H_p - h_l - h_{vac})} \tag{16}$$

Where h_l = head loss due to entrance, bend, friction etc, from the entrance up to the crest. Because of the proper bell-mouth entrance and the relatively shorter length involved, this loss of head is suggested to be only

$$h_l = 0.08\frac{V_i^2}{2g} = 0.08\frac{Q^2}{2gb^2d^2} \tag{17}$$

H_p is taken equal to zero as a worst case.

Thus, Equation 15 can be written as

$$Q = b\,R_1 \ln\left(1+\frac{d}{R_1}\right)\sqrt{2g\left(0-0.08\frac{Q^2}{2gb^2d^2}-h_{vac}\right)} \tag{17a}$$

$$\frac{Q^2}{\alpha^2} = 2g\left(-0.08\frac{Q^2}{2gb^2d^2}-h_{vac}\right) \tag{18}$$

Where

$$\alpha = bR_1 \ln\left(1+\frac{d}{R_1}\right) \tag{18a}$$

From which h_{vac} can be evaluated in terms of Q.

Also, $V_i = Q/\alpha$ and hence

$$\frac{V_i^2}{2g} = \frac{Q^2}{2g\alpha} \tag{19}$$

Thus $P_k/\gamma = -h_{vac} - V_i^2/2g$ can be expressed as a function of Q^2,

$$\frac{P_k}{\gamma} = \beta Q^2 \tag{20}$$

Assigning various values to P_k/γ gives corresponding values of discharge Q. Generally,

$P_k/\gamma = -10m$ corresponds to the beginning of local cavitation.

The entire procedure is explained next with reference to the siphon spillway of Illustrative Example 2.

Illustrative Examples

3. Determine the discharge through the siphon spillway of Example 2 corresponding to the condition of beginning of local cavitation.

$$h_l = 0.08\frac{V_l^2}{2g} = 0.08\frac{Q^2}{2gb^2d^2}$$
$$= 0.08\frac{Q^2}{2x9.81x100} = 0.0000408\,Q^2 \tag{20a}$$

$$\frac{Q^2}{\alpha^2} = 2g(-0.0000408\,Q^2 - h_{vac})\ and\quad \alpha = b\,R_1\ln\left(1+\frac{d}{R_1}\right) = 7.66 \tag{20b}$$

$$Q^2 = (7.66)^2\ x2x9.81[-0.0000408\ Q^2 - h_{vac}]$$
$$= 1151.93[-0.000048\ Q^2 - h_{vac}] \Rightarrow Q^2 = -0.047\ Q^2 - 11.51.93\ h_{vac}$$
$$\Rightarrow h_{vac} = -0.000909\ Q^2$$

$$V_i = \frac{Q}{\alpha} \Rightarrow \frac{V_i^2}{2g} = \frac{Q^2}{19.62x7.66^2} = 0.000868\,Q^2 \tag{20c}$$

$$\frac{P_k}{\gamma} = -h_{vac} - \frac{V_i^2}{2g} = -0.000909\,Q^2 - 0.000868\,Q^2 = -0.00178\,Q^2 \tag{20d}$$

$$Q = \sqrt{\frac{P_k/\gamma}{-0.00178}} \tag{20e}$$

For the limiting value of $P_k/\gamma = -10m$, $Q = 74.95 cumec$ from Equation (20e).

Thus, the maximum discharge should be restricted to about 75 cumec. With this, the velocity V_i at the crest would be $Q/\alpha = 75/7.66 = 9.8$ m/s and the average velocity $V_a = 75/10 = 7.5$ m/s.

7.11 VIBRATION

There may be a potential danger of vibration when a siphon operates with a large quantity of air that is gulped intermittently and then carried through the structure in discrete large pockets. Ackers et al. (1975) state that the intermittent admission of air and turbulent flow through the siphon mean that the structure of the hood must be capable of withstanding fluctuating suction pressures. There could be a dynamic interaction between the structure and the two-phase flow of air and water. However, any instance of severe vibrations on the saddle siphons has not come to the light. On the other hand, volute siphons have been subjected to severe vibrations (CBIP 1979). The tests conducted on volute siphons of Hirebhasgar dam revealed vibrations with the general level from 0.059 g to 0.15 g. It was also found that when the outlet of a siphon was tapered, though the discharge apparently dropped, the siphon ran smoothly.

Notations

A = Area of flow section
A_o = Area of outlet section
A_{air} = Area of the air vent
a = Area of annular space in volute siphon
b = Width of siphon throat section
C_d = Coefficient of discharge
d = Depth or height of throat section
f = Friction factor

H = Total operating head
H_L = Total head loss through the siphon
H_p = Priming depth
H_1 = Depth of free fall of the jet
h_1 = Head loss in the siphon from entrance up to crest
h_{vac} = Vacuum pressure head
k = Loss coefficients for inlet, friction, bend, outlet etc.
L = Width of the siphon
P_i = Critical value of pressure at crest
P_o = Pressure at crown
p = Perimeter of rectangular jet exposed to atmosphere
p_{amb} = Ambient pressure
p_{atm} = Atmospheric pressure
p_v = Vapour pressure of water
Q = Discharge through siphon
Q_a = Air discharge
Q_{max} = Maximum discharge through siphon
q = Discharge intensity
R = Radius of curvature
R_1 = Radius of curvature at crest of siphon
R_2 = Radius of curvature at crown of siphon
t = Thickness of the rectangular jet
V = Velocity of flow
V_a = Average velocity in the siphon
V_i = Critical value of velocity at crown
V_{min} = Minimum velocity to entrain air (appx 1.1 m/s)
V_o = Velocity at the outlet of the siphon
α = A factor
β = A factor
μ = Siphon coefficient
ζ = Hydraulic loss coefficients in the air vent

REFERENCES

1. Ackers, P.; Thomas, A. R. Design and operation of air-regulated siphons for reservoir and head-water control, Symp. on Design and operation of siphons & siphon spillways; BHRA, England, May 1975.
2. Benfratello, G. Experiments on transient of self-priming siphons; Proc. 6th IAHR Congress, C-20, Hague, 1955.
3. Bollrich, G. Hydraulic investigations of the high-head siphon spillway of Burgkhammer – 16th ICOLD paper Q 71-R2, Durban; 1994.

4. Boreli, M. Stability of aerated siphons – Proc. 6th IAHR Congress, C-12, Hague; 1955.
5. CBIP Water resources research in India, Publication No 78 (Revised), 1979.
6. Crump, E. S.; Ackers, P. An experimental investigation into the performance of spillway siphon – Report INT 22, HRS; Wallingford, England, 1961.
7. Ervine, D. A.; Elsawy, E. M. Some scale effects in modelling air-regulated siphon spillways, Symp. on Design and operation of siphons and siphon spillways; BHRA, England, May 1975.
8. Ganesh Iyer, V. Volute siphons, Jnl. of Irrigation and Power; CBIP, INDIA, 1950.
9. Govind Rao, N. S. Design of siphons; CBIP Publication No.59, 1956.
10. Perkins, J. A.; Charlton, F. G. The effect of waves on an air-regulated siphon, Symp. on Design and operation of siphons and siphon spillways; BHRA, England, May 1975.
11. Prettyjohns, R.C.; Markland, E. Air-regulated siphon with novel arrangement for air admission. Proc. Inst. of Civ. Engrs., Part 2, March 1989.

8
Shaft Spillways

8.1 INTRODUCTION

The shaft spillway is simply a closed conduit in which the flood flow is carried rapidly from a high to a low elevation. It is similar to a siphon spillway except for the absence of siphon action. Spillways of this general type are used not only for dams (where they are commonly known as morning glory spillways or glory holes), but also for erosion-control structures and as highway culverts (commonly known as drop-inlet spillways or drop-inlet culverts). This type of spillway can be used advantageously at dam sites in narrow canyons where the abutments rise steeply or where a diversion tunnel or conduit is available for use as the downstream leg. Another advantage of this type of spillway is that near-maximum capacity is attained at relatively low heads and this characteristic makes the spillway ideal for use where the maximum spillway outflow is to be limited. For this reason, they are most suited where temporary storage space in the reservoir is large enough to significantly attenuate the incoming flood.

Drop shafts also have the role of transferring water from a high elevation to a lower elevation, as part of a storm-sewer drainage system or as part of a water supply system (i.e., from intakes in mountainous catchments down to a collector tunnel system). In such cases, the shafts are provided with special types of intakes called vortex-flow intakes that impart an angular motion to the flow, which then continues as a swirling flow in the shaft.

8.2 TYPES OF SHAFT SPILLWAYS

Shaft spillways are classified according to hydraulic action.

I. Spillways with axial flow in the shaft as well as in the downstream leg or tunnel. Different combinations of flow conditions are possible:
   A. Free flow in the shaft as well as in the tunnel.
   B. Free flow in the shaft and pressure flow in the tunnel.

C. Pressure flow in the shaft and free flow in the tunnel.
D. Pressure flow in both, the shaft as well as in the tunnel.

II. Spillways with vortex or swirling flow in the shaft and axial flow in the tunnel.
III. Spillways with axial flow in the shaft and swirling flow in the tunnel.
IV. Siphon-shaft spillways.

8.3 SHAFT SPILLWAYS WITH AXIAL FLOW

The principal elements of a shaft spillway are an intake including spillway crest, transition from the crest to the shaft, the bend, and the downstream leg, and a tunnel and energy dissipator, as shown in Figure 1.

Although, most of the shaft spillways have their intakes with a crest of circular plan form and cylindrical shafts, rectangular plan forms are not uncommon. Shaft spillways with arrangement of double shafts, to increase the discharge capacity, have also been constructed. Damulevicius et al.(1999) cite examples of small shaft spillways of special shapes, constructed in Lithuania as shown schematically in Figure 2.

Elbow type shaft spillways, as shown in Figure 2, can be conveniently constructed, where topography does not permit radial inflow conditions, as in the case of left bank shaft spillway at Tehri dam. India.

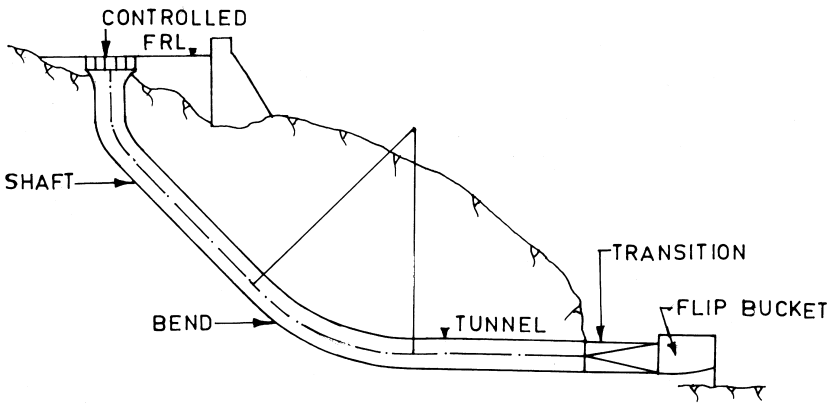

Figure 1 Elements of a shaft spillway.

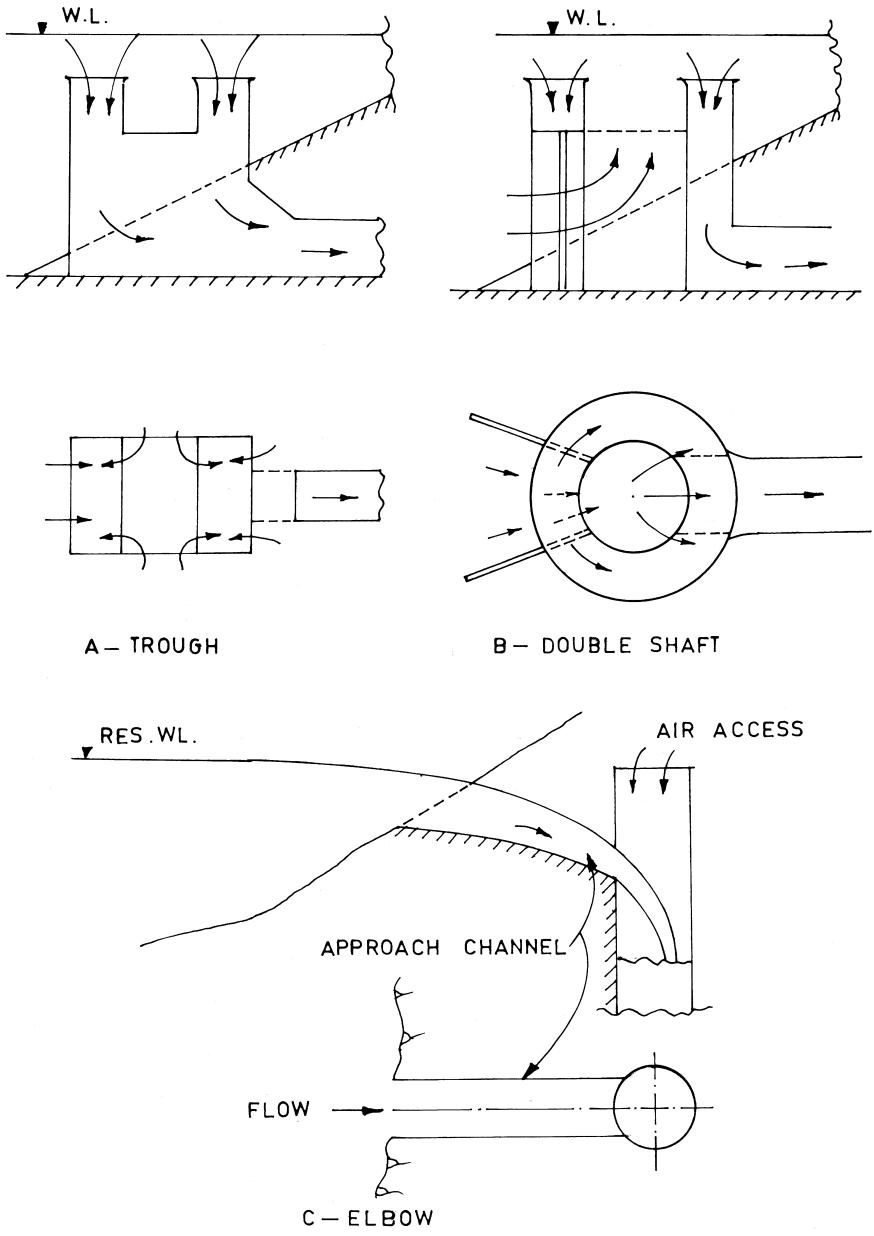

Figure 2 Shaft spillways of other shapes.

8.3.1 Hydraulic Action

Typical flow conditions and discharge characteristics for a shaft spillway with axial flow are depicted in Figure 3. (USBR-1973)

Generally, a free weir flow prevails over the crest for H_o/R_s up to about 0.45, partly submerged weir flow for H_o/R_s values between 0.45 and 1.0, and above this value the weir is completely submerged and the coefficient of discharge sharply falls.

Since it is impractical to construct a conduit with varying diameter, it is generally made a constant size beyond the inlet formation Thus, the conduit from the control point to the downstream end will have an excess area. If atmospheric pressure can be maintained along the portion of the conduit flowing partly full, it will continue to flow at that stage up to certain discharge.

As the discharge over the crest increases, the overflowing annular nappe becomes thicker and converges in to a solid vertical jet. The point where the annular nappe joins the solid jet is called the crotch. After the solid jet forms, a boil occupies the region above the crotch and both the crotch and the top of the boil rise progressively higher with an increase in the discharge. For high heads, the crotch and boil may almost fade out as a slight depression on the surface.

With the increase in the discharge, submergence of the crest begins and the control section moves gradually from the vertical bend to the throat, reaching finally a relationship. $Q = f(H_{of})^{1/2}$. The onset of this condition is unstable and often violent, marked by severe pressure fluctuations, as described by Fattor et al.(2001).

For a still higher discharge, if the condition of pipe flow is reached, both the inlet and outlet ends may be sealed and siphonic action may set in. The discharge function is then given by $Q = f(H_t - H_l)$. If air vents are not provided, or if aeration is inadequate, a make-or-break siphon action will accompany the flow with a range of discharges approaching full flow conditions. Erratic discharge vibrations and surges accompany this action. It is therefore necessary to ensure at the design stage what the expected hydraulic action is for the entire range of discharges and to provide for them. This becomes all the more obligatory when the existing diversion tunnels are utilized as downstream legs of the shaft spillway.

8.3.2 Analysis of Alternatives

As discussed earlier, shaft spillways with axial flow in the shaft, as well as in the tunnel, have four possible alternatives: free flowing shaft with tunnel flowing free or pressurized, and pressurized shaft with tunnel flowing free or pressurized. The decision whether the tunnel should be free flow or pressurized is crucial.

Filho et al. (1979) suggest that a decision whether to design the tunnel as free flow or pressure flow should be based on the influence of the parameters

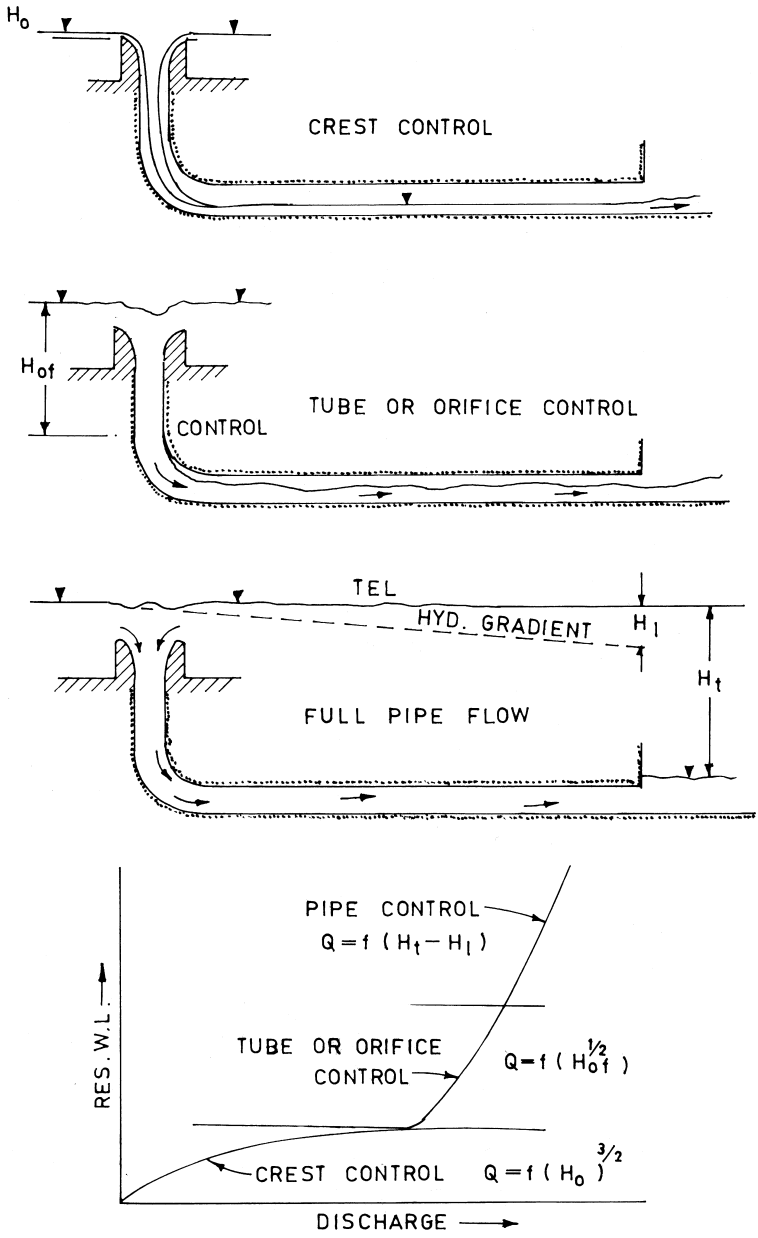

Figure 3 Flow conditions and discharge characteristics. (USBR-1973)

Table 1

Tunnel slope, i	Total head, H	Tunnel length, L	Remarks
Supercritical	High	Short	Conditions are favorable for free tunnel. Hydraulic jump, if formed, can be pushed down by increasing the cross-section. Due to high velocities, transitions have to be carefully designed together with air vents.
Supercritical	High	Long	Recommended solution is not so obvious. For free flow tunnel, hydraulic jump may occur and be difficult to eliminate or push out. For pressure tunnel, ensuring full flow conditions may entail greater head loss.
Supercritical	Low	Short	Pressure tunnel may be possible but devices are still required to maintain pressurized flow. For the free flow tunnel, hydraulic jump within the tunnel may occur unless tail water range is also very low and flat.
Supercritical	Low	Long	All conditions are favorable for a pressure tunnel with some device to ensure full-flow conditions. Due to the long tunnel length, hydraulic jump or full bore flow are more likely in the case of free flow tunnel.
Sub-critical	Low	Long	Pressure tunnel is more adaptable with appropriate device. Hydraulic jump is most likely to form in the tunnel eliminating the choice for a free flow tunnel.

such as total head (H), tunnel slope (i), and its length (L). For this analysis, H is greater than 13–15 m, slope *i* may be supercritical or sub-critical, and length L is considered to be long when hydraulic jump stays out for the tunnel for 30% design discharge and above. Generally, straight and short tunnels, steep slopes, existing large cross sections, and flat and low tail waters favor a free flow tunnel; whereas long and curved tunnels, existing small cross-sections, and high and sensitive tail waters lead to the selection of a pressure tunnel. Table 1 indicates preferences for various combinations of H, *i*, and L.

8.4 FREE SHAFT SPILLWAYS

Shaft spillways for flood disposal that have a relatively short length of the tunnel should preferably be designed as free shaft spillways. Commonly the free flow

condition in the shaft spillway comprises two reaches: the shaft itself and the tunnel. For low flows, weir control may exist and the shaft may run free, whereas for high flow the shaft may be pressurized while the tunnel remains in free flow condition for the entire range of discharges. Generally, the tunnel section is selected so that it will not flow more than 75 to 80% full at the downstream end for the maximum discharge. Under this condition, air will access from the downstream portal and prevent sub-atmospheric pressure in the tunnel. However, vertical or horizontal curvatures in the tunnel profile have to be designed so that sealing along any portion is avoided.

The shaft spillways where both the shaft and tunnel run free flow involve the following design considerations:

Crest profile
Transition from crest to shaft
Discharge characteristics
Air entrainment in shaft
Air entrainment in tunnel flowing partly full

8.4.1 Crest Profile

The crest profile of a morning glory intake conforms to the lower surface of a nappe flowing over an aerated sharp crested circular weir for various combinations of P/R_s and H_s/R_s as shown in Figure 4. R_s and H_s are with reference to the theoretical sharp crest. The head over the spillway crest H_o is considered for calculating discharging capacity. H_o is related to H_s, R_s, and P.

The converging flow over the crest is influenced by head H_s, radius R_s, and height of the crest P, and is so complex that a generalized mathematical

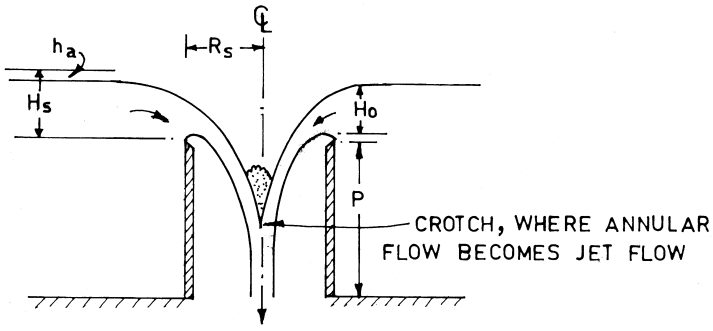

Figure 4 Crest profile of a morning glory spillway intake: P = Height of the crest above the bed, R_s = Radius of the crest circle, and H_s = Total head above the theoretical sharp crest.

equation defining the complete profile—as in the case of straight ogee spillway—has not been possible. USBR (1973) have compiled data in tabular form, in respect of coordinates of crest profiles for values of $P/R_s = 0.15$, 0.30, and 2.0, and H_s/R_s of 0.2 to 2.0 based on a study by Wagner (1956). Use of these tables requires relationship between H_o and H_s, as shown in Figure 4.

WES (1961) have defined the crest profile in terms of upstream and downstream quadrants for selected conditions of $P/R_s = 0.15$, 0.30 and 2.0, and $H_s/R_s = 0.2$, 0.3, and 0.4, similar to the crest profiles for straight ogee spillways. However, interpolation for other values is not possible.

In contrast to the crest profiles of straight spillways, where the profiles become flatter with increasing heads, the crest profiles for circular weirs become steeper as the head increases, as can be seen from Figure 5.

If the crest profile is designed for heads where H_s/R_s exceeds 0.25–0.30, sub-atmospheric pressures will occur on some portion of the profile for heads

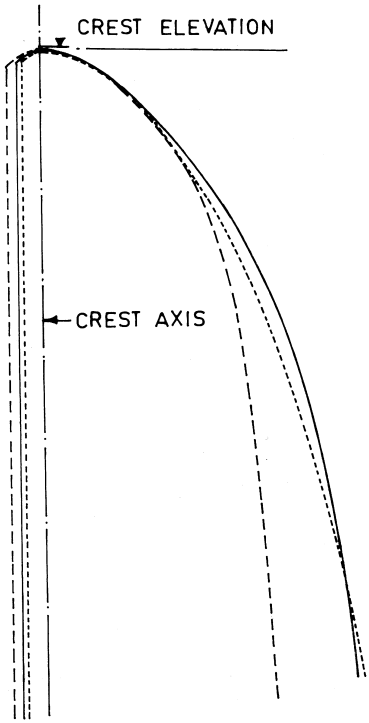

Figure 5 Comparison of crest profiles: $H_s = 2.0$, $R_s = 10.0$, and $P/R_s = 2.0$. ····· $H_s/R_s = 0.2$, ——— $H_s/R_s = 0.3$, – – – $H_s/R_s = 0.5$

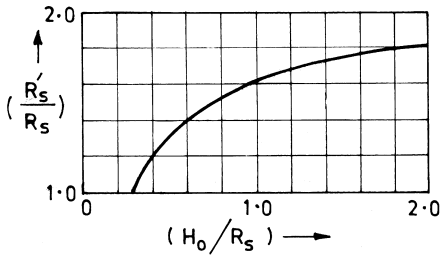

Figure 6 Increased crest radius needed to minimize sub atmospheric pressures. (USBR 1973)

less than design head. If this is to be avoided, crest profile should be designed corresponding to an increased radius R'_s as per the graph given in Figure 6 and with $H'_s/R'_s = 0.3$.

8.4.2 Transition from Crest to Shaft

The circular crest should converge to the shaft; the shaft's diameter would generally be the same as the diameter of the downstream leg or tunnel. USBR (1973) proposed a transition on the basis of continuity equation, considering the flow as a free falling, circular jet issuing from a horizontal orifice. Thus, Q = Area of the jet x Velocity of the jet, i.e., $Q = \pi R^2 x \sqrt{2gH_a}$, where H_a is the difference between the water surface and the elevation under consideration. Assuming losses to account for contraction, friction, etc. as 10% of the head

$$R = 0.275 \frac{Q^{1/2}}{H_a^{1/4}} \tag{1}$$

Lencastre (1955) proposed a similar criterion that the velocity head should be lower than the total available energy at a given point, to prevent separation and instability and hence

$U^2 / 2g < H_0$, and therefore

$$\frac{Q^2}{2\pi^2 R^4 g} \le H_a \quad OR \quad R \ge 0.268 \frac{Q^{1/2}}{H_a^{1/4}} \tag{2}$$

Which is nearly the same result as given by Equation 1.

The curve $R = f(H_a)$ for the design discharge is plotted along with the crest profile and the transition is adjusted for the shaft diameter.

Illustrative Examples

1. Design a shaft spillway to pass a design discharge of 410 cumec, without exceeding the depth of overflow of 2.35 m. Assume $P/R_s = 0.3$.

The design involves a trial method. The calculations begin with an assumed value of radius of the crest circle and finding the discharge corresponding to $H_o = 2.35$ m.

Starting with an assumed value of $R_s = 5$ m, $H_o/R_s = 0.47$ gives a coefficient of discharge of 1.96, corresponding to $P/R_s = 0.30$.

$Q = C_0 (2\pi R_s) H_0^{3/2} = 222$, which is much less. With $R_s = 10$ m, $H_o/R_s = 0.235$, $C_o = 2.16$ and $Q = 489$ cumec, indicating a larger than required radius.

Finally, $R_s = 8.5$ m gives $H_o/R_s = 0.276$, $C_o = 2.15$ and $q = 414$ cumec, which is acceptable.

For working out the coordinates of crest profile, the value of H_s/R_s is required. For $H_o/R_s = 0.276$ and $P/R_s = 0.3$, $H_s/H_o = 1.085$. Thus, $H_s = 2.55$ m and $H_s/R_s = 0.30$. Accordingly, the crest profile worked out is shown in Figure 7. The coordinates corresponding to $H_s/R_s = 0.20$ are also plotted therein for comparison.

The profile of the transition is given by Equation 1:

$$R = 0.275 \frac{Q^{1/2}}{H_a^{1/4}} = 5.568\, H_a^{-1/4}$$

A shaft diameter of 3 m is indicated as shown in Figure 7.

For the condition of $P = 0$ and fully submerged crest (orifice flow), Leskovec (1955) states that the shape of the jet flowing out of a sharp edged orifice is not dependent on the head above the orifice from the minimum head, approximately equal to six times the diameter of the orifice, $h \geq 6d$. For such a condition, he proposed the profile conforming to the equation

$$y = (0.683 - x)\sqrt{\frac{0.874 - x}{x - 0.492}} \tag{3}$$

As shown in Figure 8, the coordinates given by Equation 3 are for the shaft diameter $d = 1$. For other diameters, the coordinates are simply multiplied by that diameter. This equation also provides for a transition up to the required shaft diameter. For this shape, the coefficient of discharge C_d in the equation $Q = C_d \,.\, A \sqrt{2g\,H}$ was as high as 0.978.

8.4.3 Discharge Characteristics

The discharge characteristics of the crest (Fig. 4) is defined by the circular crest coefficient C_o as

$$Q = C_0 (2\pi R) H_0^{3/2} \tag{4}$$

C_0 depends on H_a/R_s and P/R_s. The experimental discharge coefficients for design head on spillway crest H_0 have been published by USBR (1973) on the basis of studies by Wagner (1956). These curves transformed in SI units are shown in

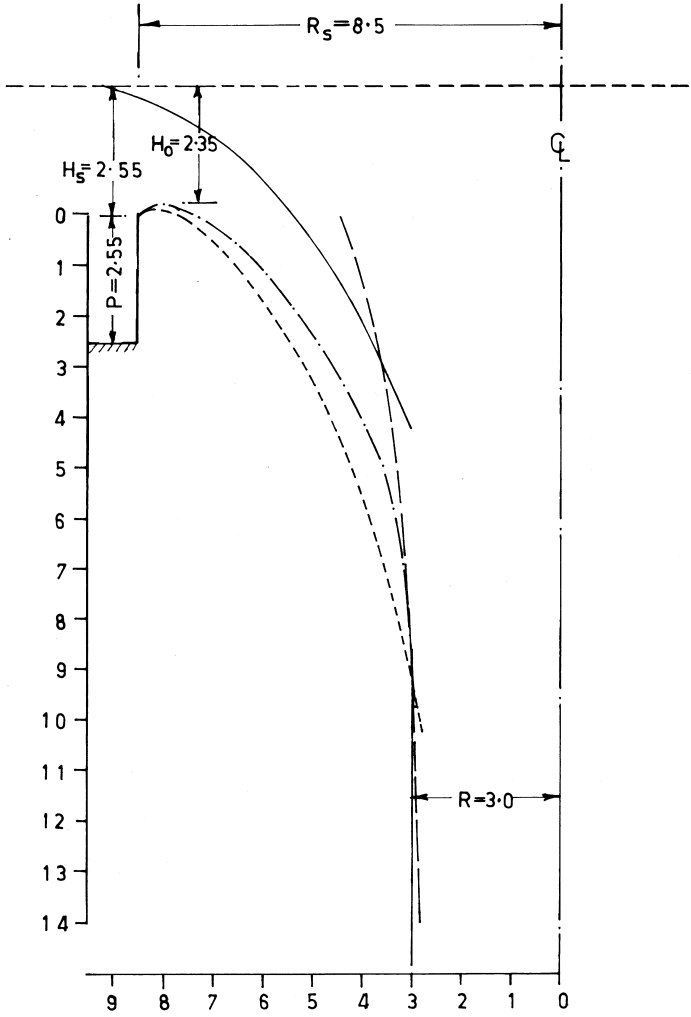

Figure 7 Illustrative example.

	Hs	Hs/R
–·–·–·–	2.55	0.3
- - - -- - - -	1.70	0.2
– – – –	$R = 0.275\ Q^{1/2}/H_a^{1/4} = 5.568\ H_a^{-1/4}$	

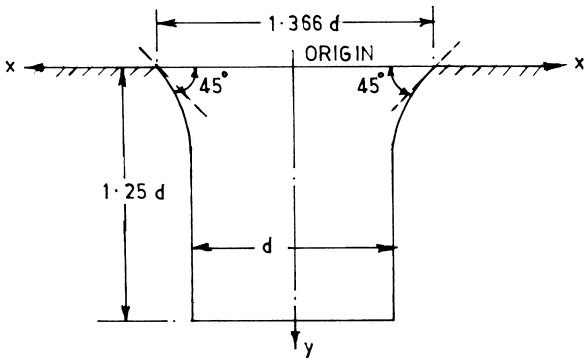

Figure 8 Liskovec profile for P = 0.

Figure 9(a). It will be seen that C_0 increases with reduction of approach depth P, in contrast to straight spillways.

Coefficient of discharge for heads other than the design head can be determined from Figure 9(b), for preparing the discharge-rating curve. However, this relationship is valid for the crest profiles free of sub-atmospheric pressures, i.e., for profiles designed based on radius according to Figure 6 and for $H_s / R_s = 0.3$. It is also not applicable for $H_e / R_s > 0.4$.

8.4.4 Air Entrainment in Drop Shafts

Air Entrainment

Air entrainment and air release in the axial flow shaft spillways and drop shafts are the most important, yet complicated, design problems. Air entrainment in drop shafts occurs when the flow strikes the water column in the lower portion of the shaft, regardless of the type of intake whether radial, elbow, or vortex. The air entrainment in vortex flow intakes has been described separately.

The air entrainment mechanism is closely related to the type of flow conditions in the shaft and has been schematically illustrated in Figure 10. At the beginning of overflow with low water levels, the discharge characteristics are similar to a weir control and the flow in the shaft clings to the walls as a relatively thin sheet. The volume flow rate of air is determined by the shear action of the air-water interface and by entrainment into the mass of water. This type of flow has been designated as Region I. The quantity of air entrained increases with discharge and with the increase in discharge, a point is reached when the sheet of water is sufficiently thick to completely seal the air passage at the lower end

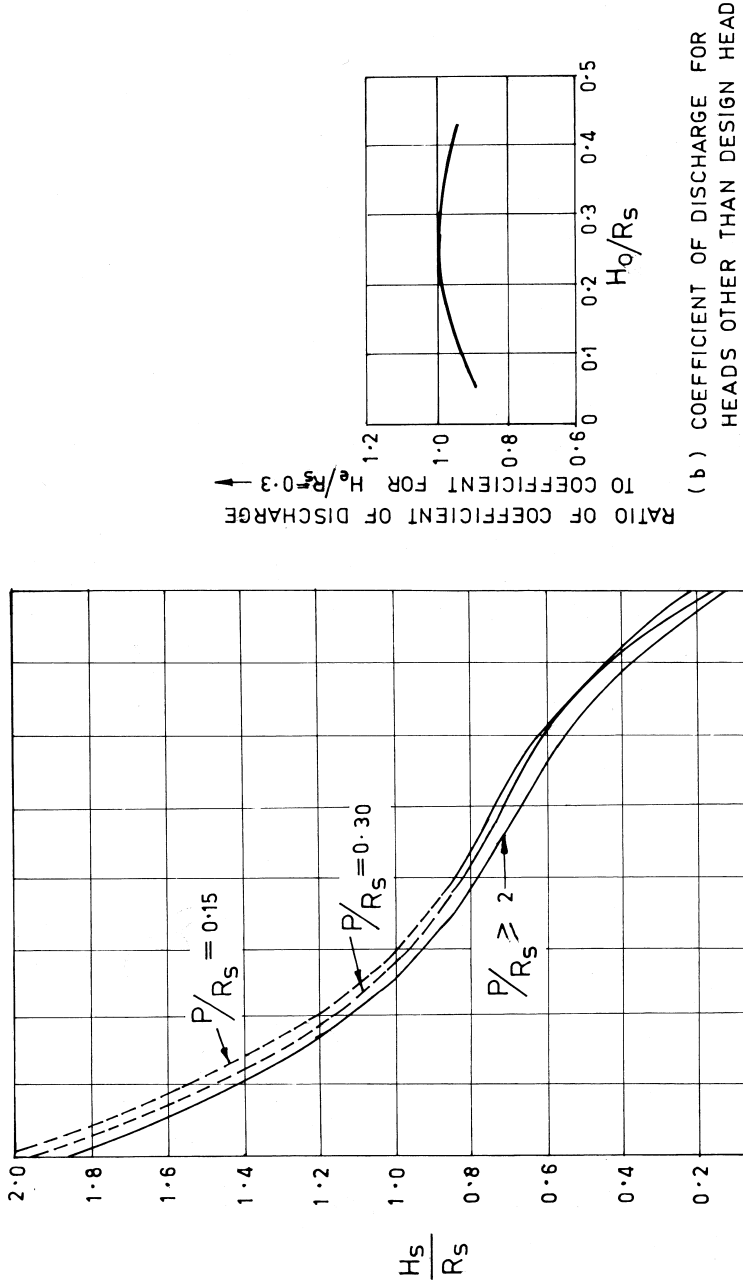

Figure 9 Discharge characteristics based on studies by Wagner (1956): Curves shown – – are extrapolated. (USBR-1973)

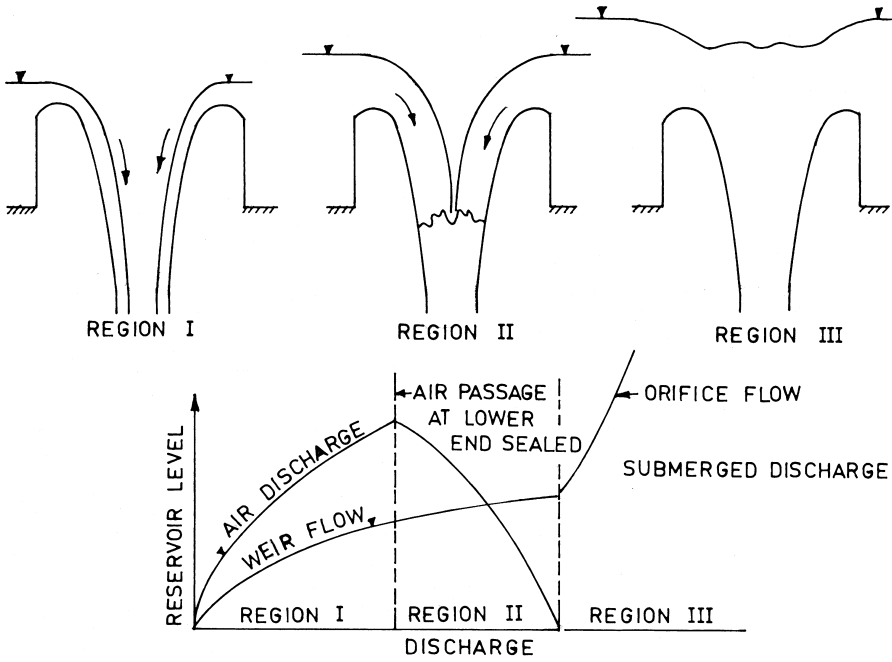

Figure 10 Flow conditions in the shaft.

of the shaft. This water discharge separates Region I from Region II. This type of flow is characterized by an annular hydraulic jump. Further increase in the discharge merely causes the location of the jump to move upward in the vertical shaft. The quantity of air entrained then decreases with discharge. When the jump reaches a point near the top of the shaft, the flow is said to become submerged. For reservoir elevations in excess of that required to produce the submerged water flow, inflow of air to the shaft ceases, if no air-entraining vortices occur. This is Region III where the discharge is similar to a pipe flow.

Region I: Air Flow Rates

The air flow rate for this region is calculated assuming that the water flow on the shaft walls is similar to open channel flow, and the lower end of the shaft is accessible to atmosphere.

Hack (1977) has derived the following relationships based on the study on a model of a drop shaft which ensured simulation of appropriate flow conditions of Region I.

$$Q_L = Q_{LK} + Q_{LE} \tag{5}$$

$$m = Q_{LE} / Q_w$$

$$C_L = \left[1 + \left(m_\lambda \left(1 - e^{k(F_0^{4/3} - F^{4/3})}\right)\right)^{-1}\right]^{-1} \tag{7}$$

$$\beta = 0.35 + 16.09\, C_L^{2.88} \tag{8}$$

where

Q_L = Total air entrained, consisting of,
Q_{LE} = Entrained air flow in annular layer
Q_{LK} = Entrained air flow in the central core in the shaft
Q_w = Water discharge
C_L = m/(1 + m) = mean air concentration.
m_λ = maximum possible air concentration – suggested value of $m_\lambda = 4$
$k = 1.8\, r_s + 0.0108$ where
r_s = relative roughness = e/d where
e = absolute roughness
d = diameter of drop shaft
F_o = Froude number at point where boundary layer intersects water surface.
F = Froude number of theoretical unaerated flow at the deepest point in the drop shaft
$\beta = Q_L / Q_w$

The point where the boundary layer intersects the water surface can be found on the lines of open channel flow as suggested by Falvey (1980), (Equations 27–30 therein).

Region II: Air Flow Rates

Flow characteristics of this region are similar to that of a ring jump. Falvey (1980) suggests application of a relationship evolved by Haindl (1971)

$$\beta = Q_a / Q_w = 0.02\,(F - 1)^{0.86} \tag{9}$$

Ervine and Ahmed (1982) investigated the aeration characteristics of a two-dimensional vertical drop shaft. They found that when a rough turbulent jet penetrated the slower moving water surface in the shaft, it carried air bubbles with it. This is defined as total air entrainment q_{at}. Due to discrete vortices, some of the air bubbles get released upwards; this rate is called recirculated air entrainment q_{ar}. Some bubbles get transported along the shaft, this being the net air transport q_{an}. They found that

$$q_a = 0.00045(U_1 - 0.8)^3 \tag{10}$$

Where U_i = jet velocity at the point of impact.

Also

$$\beta_{at} = q_{at} / q_w = 0.03 (F_r - 1) \quad (11)$$

and

$$\beta_{at} = 0.04 \sqrt{(H_e / d)} \quad (12)$$

where

F_r = Froude number at the point of impact.
$= U_1 / \sqrt{g d_j}$
d_j = Jet thickness normal to the shaft wall.
H_e = Drop length from entrance to the point of impact.

Ervine (1998) has described three mechanisms of plunge point aeration and types of relationships for air entrainment per unit width with jet velocity, conduit slope etc. These are as shown in Figure 11

1. Aeration due to surface disturbance in the upstream jet:

$$q_a = k_1 \left(\frac{U_1^3}{g} \right) (T_u)^2$$

Where k_1 is a constant and T_u is the turbulence intensity

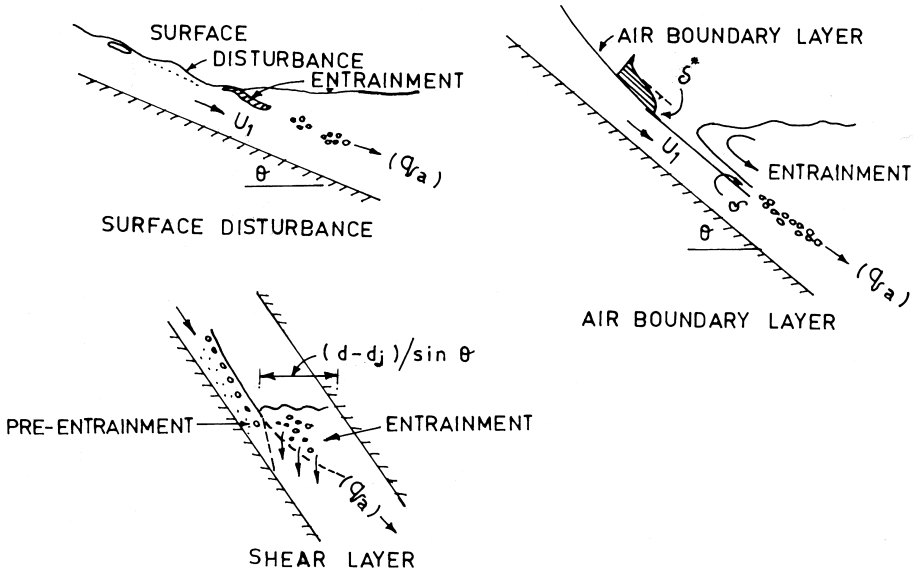

Figure 11 Mechanisms of plunge point aeration (shown in Ervine 1998).

2. Aeration due to air boundary layer: $q_a = 1.73\left(\frac{\upsilon}{2g}\right)^{1/2} U_1^{3/2}$

   Where ν is kinematic viscosity

3. Aeration due to free surface shear layer: $q_a = \frac{k_2(D-d_j)U_1}{Sin\theta}$

   Where k_2 is a constant and θ = angle of conduit with horizontal.

It is, however, difficult to apply the above relationships in practice. First because it is not certain which of the mechanism is relevant and secondly, some of the constants are not known in advance. Ervine (1998) analyzed results of model studies covering a range of hydraulic structures namely siphons, drop shafts, sloping conduits, and both wall jets and free-falling jets, with thickness greater than 20–30 mm. Data used were only with a Reynolds number greater than 10^5 and certainly greater than 5×10^4. In each case, the flow condition that gave the greatest measured rate of air entrainment was chosen and plotted against the upstream jet velocity at the plunge point. Figure 12 shows the maximum aeration rate per unit conduit width, as a function jet velocity. Although, various types of hydraulic structures are included, over a range of conduit slopes and model scales, the data is confined to a relatively narrow band.

A simple polynomial regression for all data sets analyzed revealed that the maximum rate of aeration per unit jet width could be given by

$$q_{at} = 0.0002U_1{}^3 - 0.00002U_1{}^2 - 0.0068U_1 - 0.0129 \quad (13)$$

where

q_{at} = Rate of air entrainment per unit jet width at the plunge point
U_1 = Jet velocity at plunge point

This relation is valid for the velocity range 1.5–15 m/s and for jet thickness greater than 30 mm. The accuracy of this expression is unknown but likely to be in the region of $+/-30\%$.

A measure of aeration scale effect can be incorporated by assuming that a minimum velocity of at least 1 m/s is required, so that

$$q_{at} = 0.00002(U_1 - 1)^3 + 0.0003(U_1 - 1)^2 + 0.0074(U_1 - 1) - 0.0058 \quad (14)$$

Region III: Air Flow Rates

In this region, the shaft is under submergence and the airflow down the shaft ceases. According to USBR (1973), this condition corresponds to $H_0 / R_s \geq 1$. No air entrainment will take place if an air-entraining vortex does not form. With

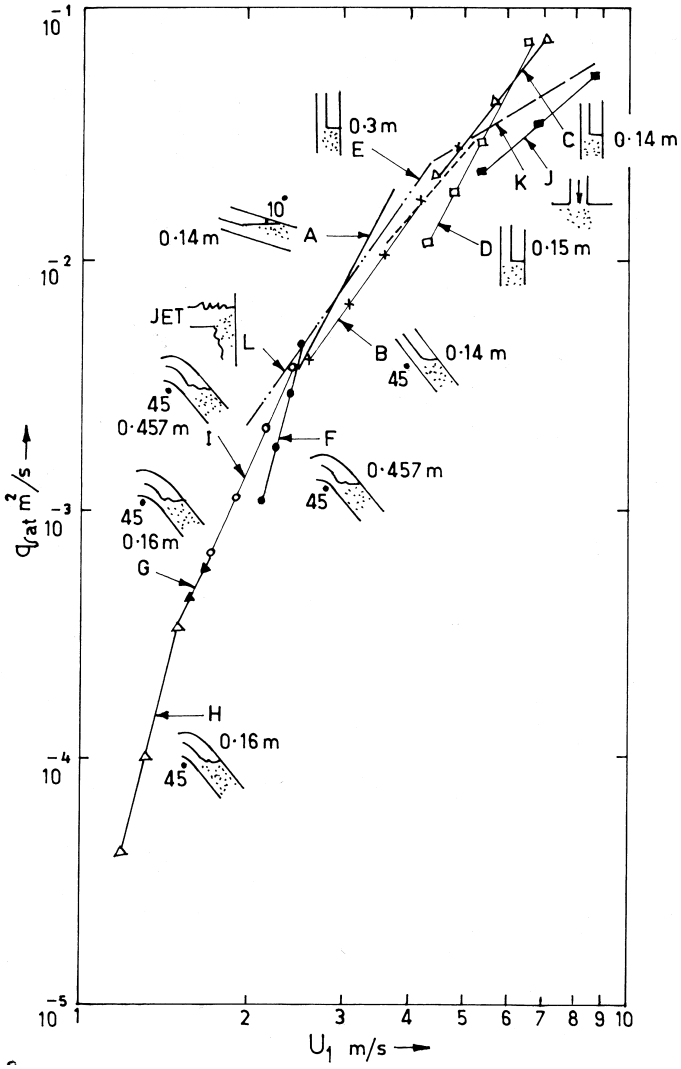

Figure 12 Maximum rate of aeration Vs jet velocity (shown in Ervine 1998):_—— A Ervine/Ahmed 10°–x–x–x–x B Ervine/Ahmed 45°△—△—△ C Ervine/Ahmed 90°□–□–□–□ D Whillock/Thorn 90°– – – – – E Whillock/Thorn 90°●–●–●–● F Delft 45° (1:7)▲–▲–▲–▲ G Delft 45° (1:20)△–△–△– △ H Delft 45° (1:20)○–○– ○– ○ I Delft 45° (1:7)■– ■– ■– ■ J Ervine jets >30 mm—— K Ervine jets >30 mm —··—··—·· L Renner impinging jet

the fully submerged condition, no air-entraining vortex will form so far as the approach flow is radial. However, for an approach flow having some circulation, a vortex may form with undesirable effects such as air entrainment, vibration, loss of performance, etc. A number of investigators have suggested the required submergence for ensuring absence of air entraining vortices. There is considerable variation in their results. The S/d values range from 0.20 to 4.0 for F varying from 0.1 to 0.8. The results are believed to be influenced by the approach configurations and scale effects.

Jain et al. (1978) have evolved the relationship, applicable only for radial flow,

$$S / d = 0.47 \sqrt{F} \tag{15}$$

where

S = Submergence depth at which air flow down the shaft ceases
F = Froude number given by U/ $\sqrt{gd}$
U = Mean water velocity in the shaft flowing full
d = Shaft diameter

Experiments with other models yield a similar relationship

$$S / d = 0.54 F^{0.51} \tag{16}$$

A reasonably conservative estimate of the submergence can be given by

$$S / d = 2.4 F^{0.25} \tag{17}$$

In order to ensure radial flow, at least in the vicinity of the crest, guide piers and vanes on the crest profile are usually provided, as shown in Figure 13.

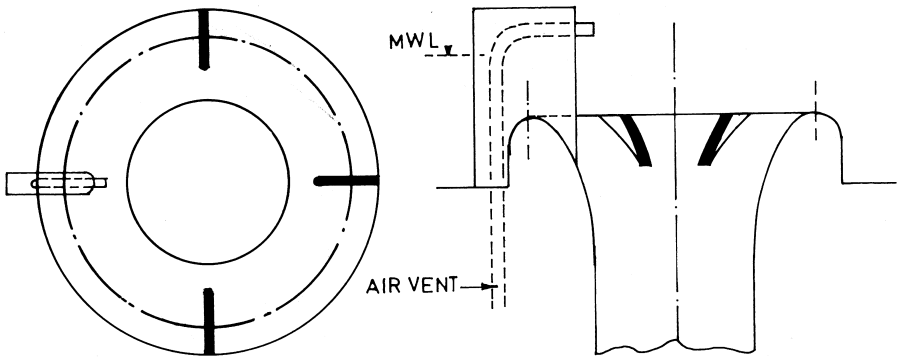

Figure 13 Guide piers to ensure radial flow.

Air Bubble Transport

The air entrained at the plunge point would either be detrained or transported downstream. It is possible to entrain significant air quantities at the plunge point and yet transport none further downstream. Ervine (1998) has described the mechanism of air bubble transport and relationships with reference to the classic works in this area by Thomas et al. (1983) and Sene et al. (1994). The forces involved in the process are: inertia (e.g., pressure gradient), buoyancy, drag, and lift forces due to shear layer vorticity between the two co-flowing streams with velocity difference. Based on a study of the probability of an air bubble escaping from a horizontal shear layer, it was found that a minimum value of velocity U_{min} of the main flow, of about 2.5 m/s, would be required to ensure transport downstream, at least for conduits on a horizontal or shallow slope.

Based on his experiments (Ervine and Ahmed 1984), Ervine (1998) evolved two important relationships: the threshold condition when entrained air would be transported along the closed conduit and the quantity of air transported. It was found that the threshold condition was dependent to some extent on the conduit slope. In this connection, the vortex trapping parameter (U_1 / u_{br}) and transport parameter U_1 $(d$ / $D)^{1/2}$ were significant. Here, U_1 is the jet velocity at plunge point, u_{br} is the air buble rise velocity, d is the shaft diameter and D, the tunnel diameter. For shallow slopes, a vortex trapping parameter (U_1 / u_{br}) $>$ 10–12 represented the threshold. For steep slopes or vertical conduits the transport parameter U_1 $(d$ / $D)^{1/2}$ is relevant and its value should exceed 0.8–0.9. Intermediate slopes will involve a combination of both parameters.

Reverse Airflow in a Shaft

The foregoing discussion indicates that a situation is possible where the rate of air entrainment is relatively larger than the water flow rate. This situation is described as the slug flow. Falvey (1980) has described the property of the slug flow with reference to a relationship developed by Martins (1973) that slug flow begins when the dimensionless airflow β exceeds 0.223 or so. These slugs move up the shaft for

$$Q^2 / g\ \mathrm{d}^5 < 0.3 \tag{18}$$

In addition, it is possible that blowback (a phenomenon of vertical air eruption out of shaft) will occur in the shaft.

Natural De-aeration

During the passage of the air-water mixture down the vertical shaft, there exists a flow velocity at which the zone of aerated water, with certain air concentration, reaches a limited length, and below the boundary of the aeration zone there is a

flow of water only. The air bubbles entering the upper layer of aeration zone are entrained by the local water velocity in the direction of the flow, but ultimately their descending motion is stopped due to bubble-rise velocity in the ascending direction with both of these velocities equal to each other and moving in opposite directions. Haindl et al. (1977) have studied this phenomenon, describing it as natural de-aeration. The relationship between the length of aerated zone and slip velocity V_g of air-water particles is

$$V_g = \frac{Q_w}{S(1-C_L)} \tag{19}$$

where

S = Area of shaft

V_g = Slip velocity

They found that the length L_s of de-aeration was dependent on slip velocity V_g and that after the nominal velocity of flow exceeded a critical value of V_g = 0.18 m/s, the length L_s increased substantially, indicating air transport in the flow further downstream.

8.4.5 Air Entrainment in Tunnels Flowing Partly Full

Flow in a partially-filled conduit can be thought of as open channel flow in a closed conduit. The major design parameter is the total air discharge in the tunnel. The provision should be made to admit the required flow of air into the tunnel through air vents or other means. The total volume flow of air, which enters at the upstream end of the air passage, equals the sum of the air that is insufflated into the flow and that which flows freely above the water surface as a result of the air-water shear forces. Thus,

$$Q_{air}^{total} = Q_{air}^{entrained} + Q_{air}^{free} \tag{20}$$

The quantity of air insufflated into the flow can be estimated using Equation 59 of Falvey (1980), but corrected by Bruschin (1982) as

$$\overline{C} = 0.055\ F - 0.3 \tag{21}$$

$$\overline{C} = \frac{\beta}{\beta+1} \qquad where\ \beta = \frac{Q_a}{Q_w} \tag{21a}$$

For the quantity of air that flows above the water surface, Falvey suggests several approaches. Typically, the maximum flow rate based on assumption of turbulent couette flow,

(22)

$$Q_m = \frac{A_a V_o}{2}$$

and

$$\left(\frac{Q_a}{Q_w}\right)_{\max} = \frac{A_d}{A} - 1 \tag{23}$$

where

A_a = Cross-sectional area of airflow passage
A_d = Cross-sectional area of conduit
A = Maximum cross-sectional area of water prism
V_o = Maximum water surface velocity in tunnel

Chanson (1997) analyzed data on self-aerated flows in partially filled circular pipes and suggested a procedure for estimating air-water flow properties such as C_{mean}, Y_{90}, Q_a, etc. for tunnels of circular cross-section. It is shown that the air-water flow properties are functions only of the centerline mean air concentration and of the filling ratio Y_{90} / D. For a tunnel of constant diameter, slope and roughness, and for a given discharge, the maximum airflow rate can be estimated for the uniform equilibrium condition (Chapter 27). At uniform equilibrium flow conditions the airflow Q_{air}^{free} is caused only by shear stress at the flow surface. The entrained air $Q_{air}^{entrained}$ can be estimated considering C_e corresponding to the tunnel slope, as in the case of open chute flow (Chapter 27) and filling ratio Y_{90} / D.

8.5 PRESSURE SHAFT SPILLWAYS

Designing shaft spillways, or drop shafts with long tunnels, or tunnels on curved alignment for free surface flow may be difficult and prove to be uneconomical. In such cases, alternatives of pressurized tunnel may prove to be advantageous.

In a pressure shaft spillway, the tunnel is permanently flowing full, the shaft itself may be or not pressurized. The advantages of such a condition are:

The flow conditions are less dependent on the tail water-rating curve, which is not the case with the free shaft spillway.

The flow conditions are more tranquil and average velocities are significantly lower than those for the free flow tunnel. For the free tunnel these may be as high as 35 to 40 m/s, in the pressure tunnel, the practical limit is in the range of 16 to 18 m/s and yet require smaller tunnel cross-section for the same discharge.

Some of the disadvantages are:

The main problem is to tackle air entrainment, or rather de-aeration, to avoid difficulties described in Section 8.3.1 earlier.

Tunnel cross-section has to be fully concrete lined and designed for pressure flow.

Energy dissipators tend to be more expensive.

8.5.1 Devices to Ensure Pressurized Flow in the Shaft

If the shaft is not flowing full, hydro-pneumatic phenomena may occur and disturb the flow at the tunnel. Filho et al (1979) have suggested special devices at various locations that force the formation of a stationary water column in the shaft, with the minimum height required, to significantly reduce the air discharges and mass oscillation. Some of these are:

1. Special shape of the bell-mouth entry.
2. Chute blocks on the shaft mouth.
3. Siphon at the base.
4. Short radius bend.
5. T-transition.
6. Nozzle.
7. Stilling basin with diving flow.

These are shown in Figure 14. It must, however, be noted that such devices cause additional head loss which may require further enlargement of cross-sections of shafts and tunnels to meet the design capacities. The optimum solution for a specific case must be obtained through hydraulic model studies.

If a pressurized shaft is to be connected to a free surface flow tunnel, it may become necessary to provide aeration at the beginning of the tunnel, as shown in Figure 15. In such a case, the discharge would be controlled by the contracted section C-C. Hajdin (1979) proposed the relationship

$$Q = C_Q A_0 \sqrt{2gH} \tag{24}$$

where

$$C_Q = \text{coefficient of discharge} = \frac{1}{\sqrt{1+K}}$$

K is the energy loss coefficient

A_0 = cross-sectional area of the contracted shaft

Based on the laboratory experiments with the parameters

$0 < d / R_e \leq 1$

$0 < t / d \leq 0.4$, *and*

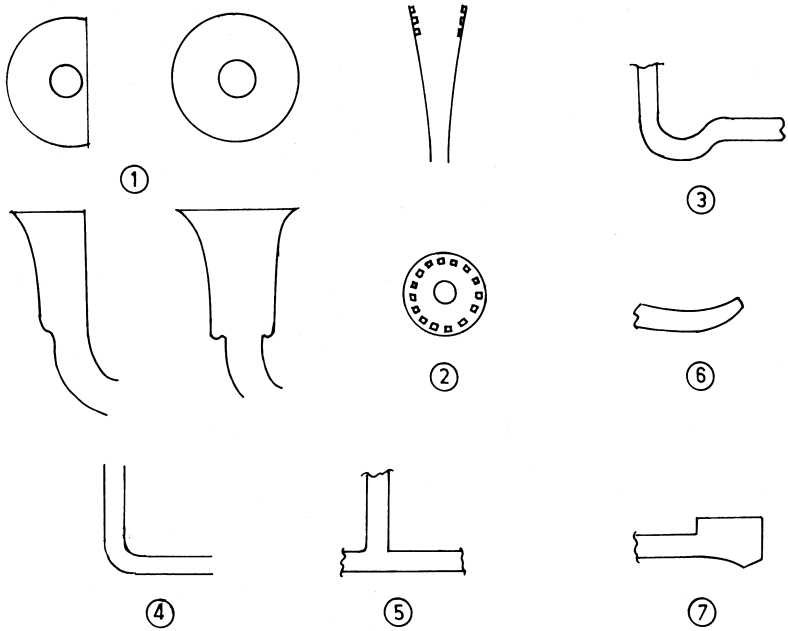

Figure 14 Devices to ensure pressurized flow in the shaft: ① Special shape of the bell mouth entry, ② Chute blocks on the shaft mouth, ③ Siphon at the base, ④ short radius bend, ⑤ T-transition, ⑥ Nozzle, and ⑦ Stilling basin with diving flow. (Filho, 1979)

$$0.1 \leq K \leq 0.2$$

Hajdin proposed the relationship

$$C_Q = 0.92 - 0.2\, d / R_e \tag{25}$$

8.5.2 Release of Air in Pressurized Tunnels

When the flow in the tunnel is full, any air drawn into it could effect conveyance capacity and cause unstable flow conditions and could possibly encourage algae growth with subsequent effect on lining friction. If the tunnel is horizontal or sloping upward in the direction of flow, then all the entrained air will move with the flow. However, if the conduit slopes downward, air bubbles can either move upstream or downstream relative to the pipe wall. If the air bubbles travel downstream in the sloping conduit, they tend to rise to the top of the conduit and form large pockets of air. The rise velocity of these pockets is greater in sloping con-

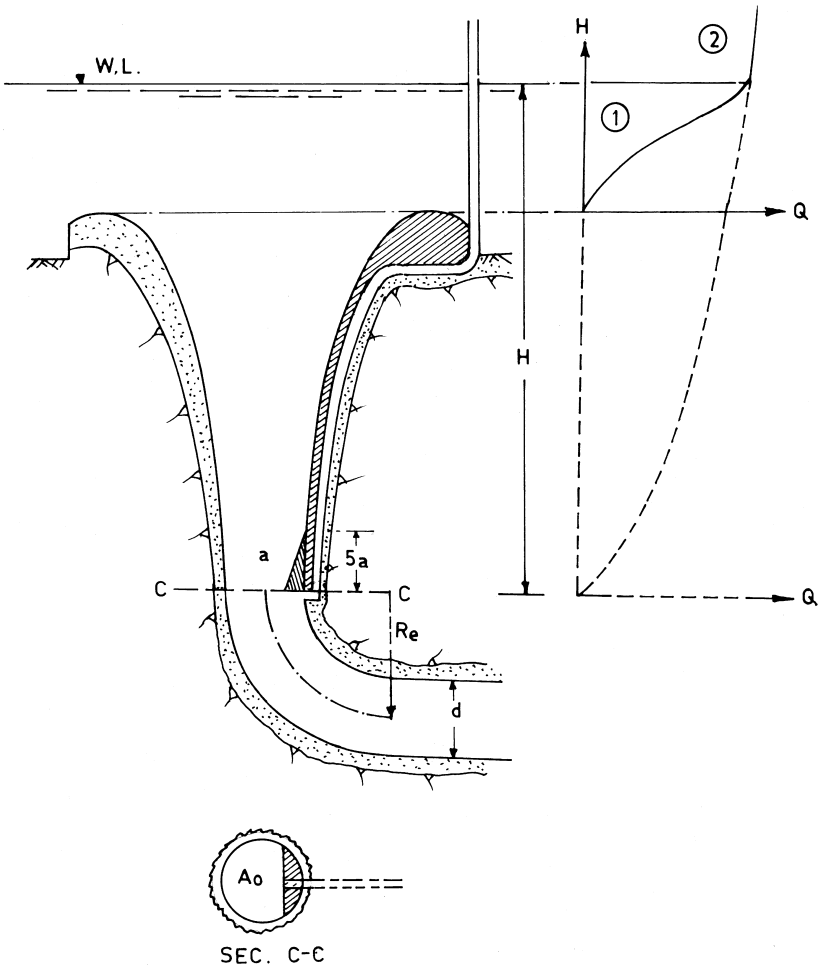

Figure 15 Discharge through pressurized shaft: ① $Q = C_0\ (2\pi\ R_s)H^{3/2}$ and ② $Q = C_0\ A_0\ (2\pi\ H)^{1/2}$. (Hajdin, 1979)

duits than it is in vertical conduits. For a specific range of discharge, a flow condition can exist whereby bubbles will move downstream and form into pockets that move against the flow in the upstream direction.

The quantity of air transported along a closed conduit depends not only on the rate of entrainment, but also on the flow conditions downstream in the shear layer. If the flow conditions have exceeded the threshold of air bubble transport,

the single most important parameter effecting transport is the length of the conduit downstream of the plunge point. Ervine (1998) classified them in terms of short, intermediate, and long conduits.

Short conduits have a length/diameter ratio less than 5. In this category, all the air entrained at the plunge point is transported downstream and out of conduit.

Intermediate length conduits have a ratio between 5 and 20. This length is sufficient for some transported air bubbles to have risen to the conduit roof due to buoyancy. The net transport rate of air bubbles to the exit of the conduit is given by

$$q_{an} = q_{at} [1 - e^{-2 (V - V_{0\min})/u_{br}}] \quad (26)$$

where

V = Mean water velocity in the closed conduit
V_{0min} = Minimum outlet velocity to commence air bubble transport ≅ 2–3 m/s
u_{br} = Air bubble rise velocity in still water (0.2–0.25 m/s)

Long conduits have a ratio of length/diameter that is greater than 20. In this case, the air bubbles collect on the conduit roof in the form of distinct pockets and will only be transported downstream when the flow has the capacity to remove or clear, large air pockets in a downward sloping conduit. If the flow does not have this capacity, the air pockets build up in size and eventually blow back upstream towards atmosphere and net transport is not achieved.

Sailer (1955) investigated prototype cases in which large air pockets moved against the flow with sufficient violence to destroy reinforced concrete platforms. It is therefore essential that proper air release devices be installed to prevent unstable hydraulic conditions such as blowback, surging, etc.

Typical devices are:

Air vent immediately downstream of the bend
Guide vanes in the bend
De-aeration chamber fitted with a baffle and an air release shaft
Diffuser with perforated roof

Figure 16 shows schematic detail of a diffuser system for release of air while transferring water to a lower reservoir. Stephenson (1991) has described the system of de-aeration chamber as adopted for the Muela drop shaft, (Figure 17).

Anderson et al. (1968) and Dahlin et al. (1982) have described some of the arrangements evolved from the hydraulic model studies conducted at the SAF*

* Saint Anthony Falls Hydraulics Laboratory, USA.

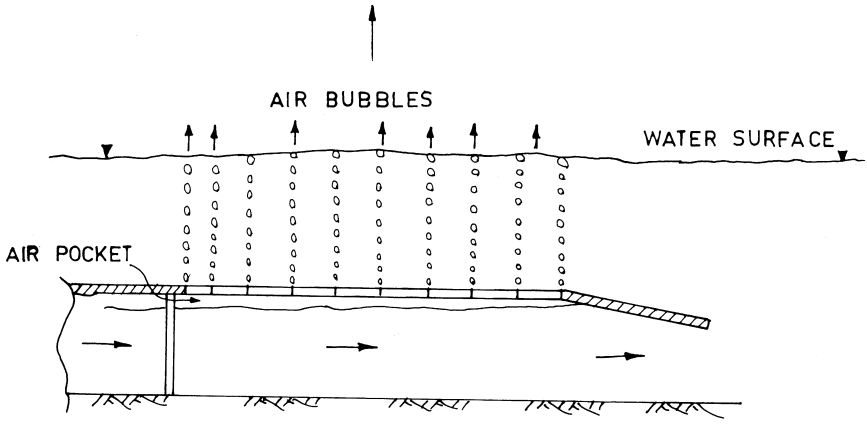

Figure 16 Air release with diffuser system.

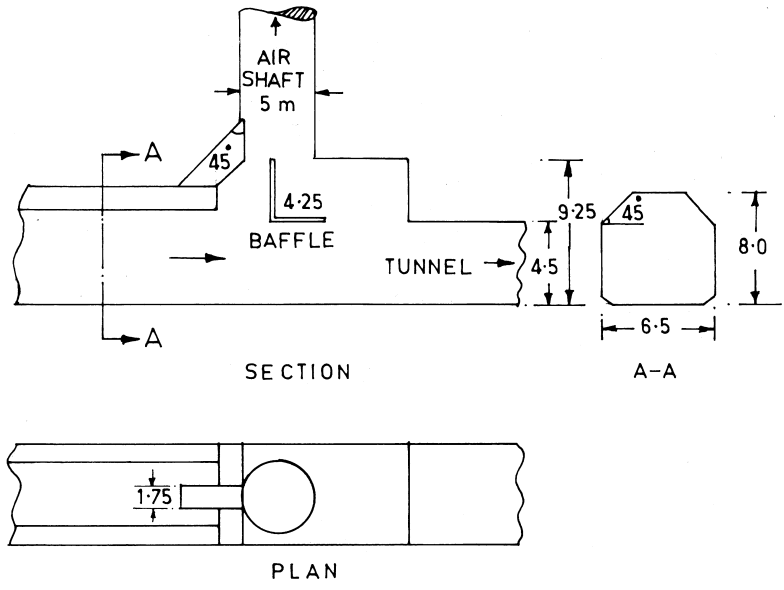

Figure 17 Muela drop shaft: De-aeration chamber. (Stephenson, 1991)

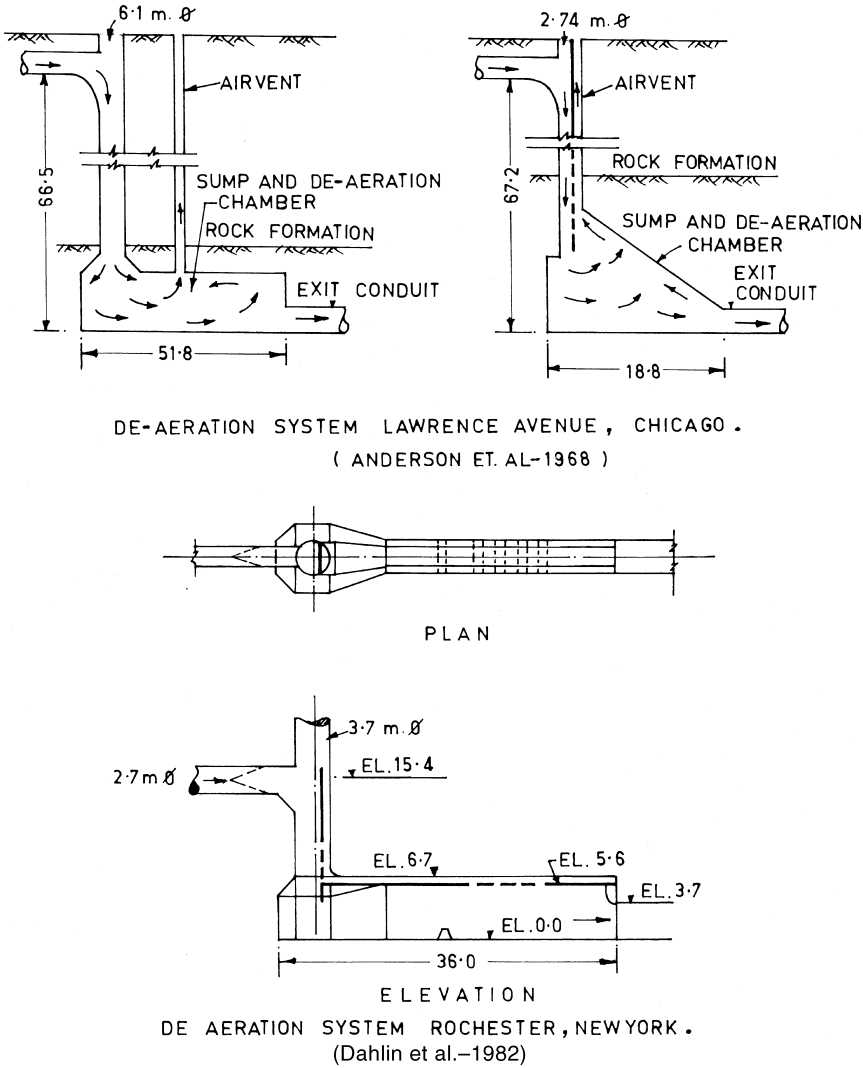

Figure 18 Air release methods: low height drop shafts.

Hyd.Lab. These arrangements are for low height drop shafts for conveying storm run-off/sewer (height up to 100 m; discharge up to 130 cumec) for the Lawrence Avenue Sewer System, Chicago, and Rochester, New York, US. The pertinent details are shown in Figure 18.

No general guidelines are available at present for determining size and dimensions of such devices and therefore hydraulic model study is the only means for their design.

8.6 THE VORTEX DROP

Vortices at intakes are generally considered to be undesirable, as they involve loss of performance, cause vibrations, and transport air bubbles, and are especially problematic for the hydraulic machinery. However, intakes involving the generation of an organized vortex perform efficiently without any undesirable effects. Such intakes are commonly adopted for schemes involving mass transfer of water from higher to lower elevation through vertical shaft. Such intakes could also be used as spillways for flood disposal; however, their discharging capacities are much less than that of conventional morning glory intakes.

The evolution of the design of vortex drops is largely due to the pioneering works by the Italian engineers M.Viparelli and C.Drioli in the 1940s and 1950s, which then continued in France, the former USSR, the US, and other countries.

In a vortex-flow intake, the flow enters a spiral chamber tangentially and a free vortex is generated as the flow spirals to the drop shaft. This imparts an angular motion to the flow and a swirling annular jet with an air core at the center of the shaft, thereby forming a throat. As the flow slides down the drop shaft, its vertical velocity increases, the swirl attenuates and the flow direction approaches the vertical. The flow, however, continues to hug the drop shaft wall. Figure 19 shows functioning of a typical vortex drop shaft.

The vortex-flow intakes offer the following advantages:

- Stable operation for all discharges.
- Significant dissipation of energy by friction in the shaft walls.
- Positive pressures on the shaft walls, thus minimizing the risk of cavitation.
- Air core through out the height of the shaft and yet air entrainment is minimized and release of air is much easier as compared to that with the conventional intake.
- Sinking and floating solids will have free passage through the system, making it suitable for sewerage and storm water transport.

The flow down a vortex shaft approaches a terminal velocity and, in theory, there is no limit to the height of the drop. In practice, the friction has a circumferential

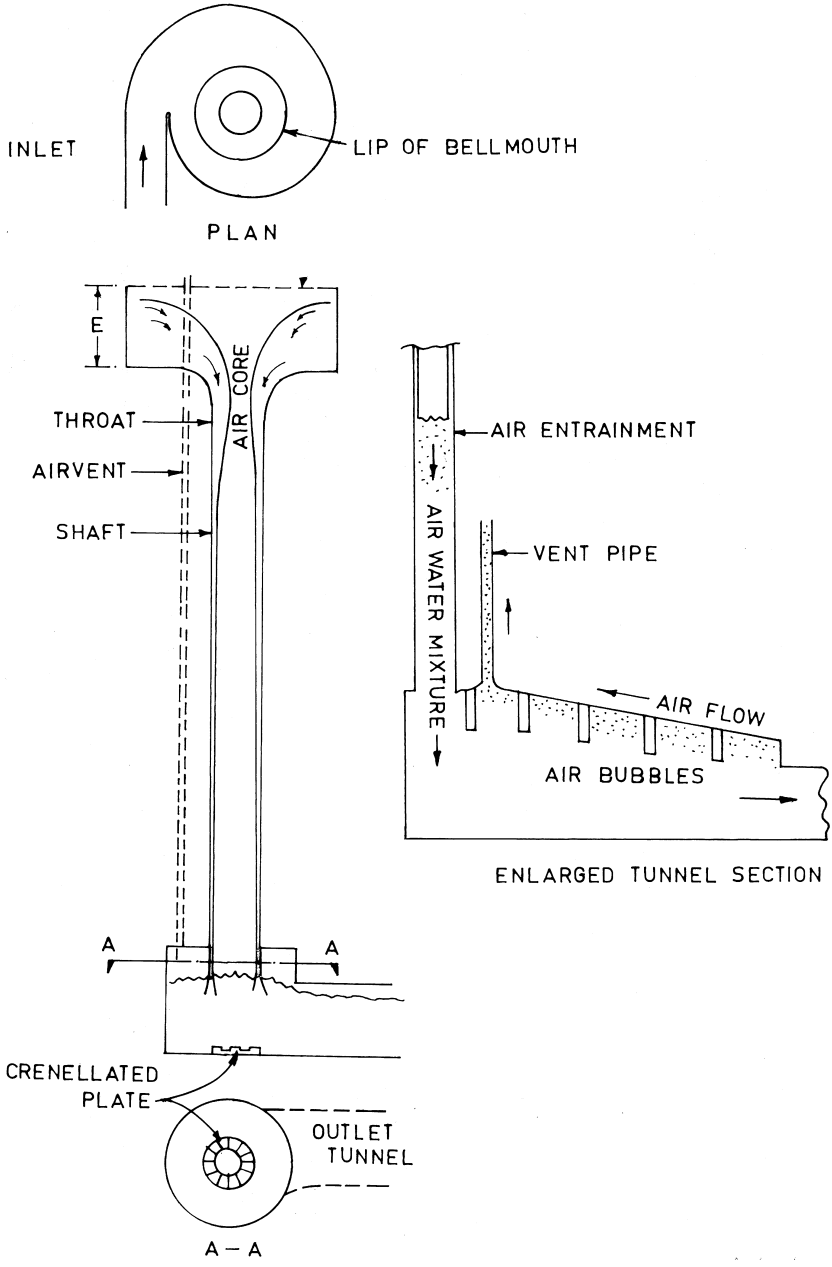

Figure 19 Typical vortex drop shaft.

component that causes the circulation to decay so the flow may break up into a spray in very deep shafts, especially if there is significant roughness.

If the conditions in the outlet tunnel submerge the shaft under any of the operating conditions, special attention has to be paid to the release of entrained air. An enlarged tunnel section forming a de-aeration chamber, as shown in Figure 19, would be suitable.

8.6.1 Configuration of Vortex-Flow Intakes

Several intake configurations are used to create swirling flows. These are broadly classified into five categories as shown in Figure 20.

1. Circular
2. Scroll
3. Spiral
4. Tangential
5. Siphonic

Circular intakes have become obsolete, mainly because they require unacceptably large depths of flow. Use of spiral intakes is limited to mountainous areas where the approach flow may be supercritical. Siphonic intakes are less commonly used because of the complex geometry and construction. The scroll configuration is widely used and has been studied extensively. However, the simpler and more compact tangential configuration is also popular. Further analysis is restricted only to the scroll and tangential intakes.

8.6.2 Standard Scroll Intake

Flow through vortex-flow intakes has been analyzed by several investigators. Two related hypotheses common to most analyses are that the throat (defined as the section where the air core area is a minimum) is a control section of the flow, and that the principle of maximum discharge is applicable at the throat. In the case of circular, spiral, and scroll intakes, the throat is assumed to coincide with the entrance to the drop shaft.

Ackers and Crump (1960) have analyzed the functioning of the standard scroll intake by applying the free vortex theory to determine the conditions at the inlet section and throat sections. A set of five equations has been proposed, which can be solved interactively to establish head-discharge characteristics for a given geometry of the intake, including the drop shaft diameter. The procedure, however, is not suitable for sizing an intake configuration—including the required diameter of the drop shaft—for a given approach flow condition, i.e., discharge and energy level.

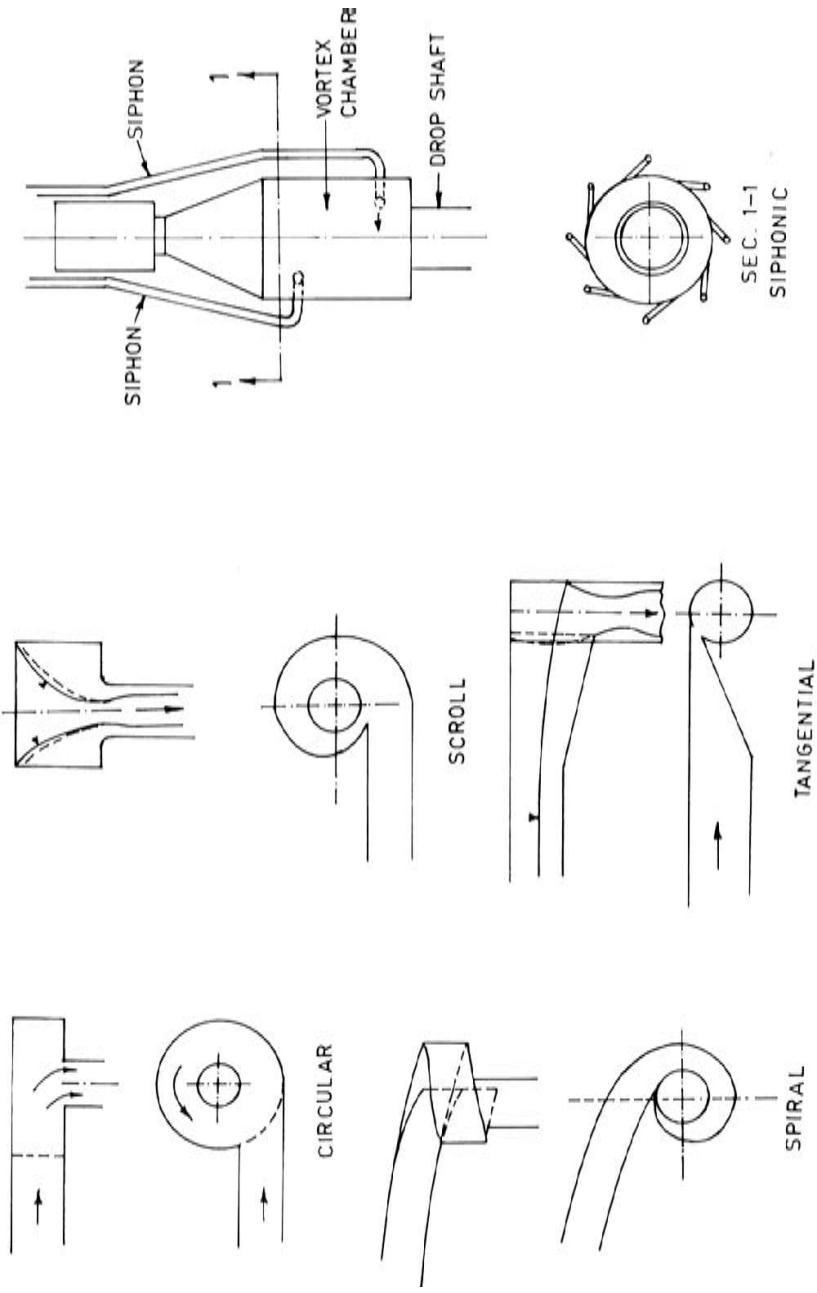

Figure 20 Vortex-flow intakes.

Jain et al. (1987) have extended the analysis of Pica and Viparelli for evolving relationships that help determining an intake geometry of a standard scroll intake.

The dimensions of a standard scroll intake are shown in Figure 21.

Their analysis is based on the following assumptions:

Energy head is constant within the vortex-flow intake, i.e., no loss of energy.
Pressure inside the air core is atmospheric.
The distribution of the tangential velocity component at the throat section is given by the free vortex theory.
Pressure at all points in the throat section is atmospheric.
Water depth and velocity along the approach channel section upstream from the intake remain practically constant.

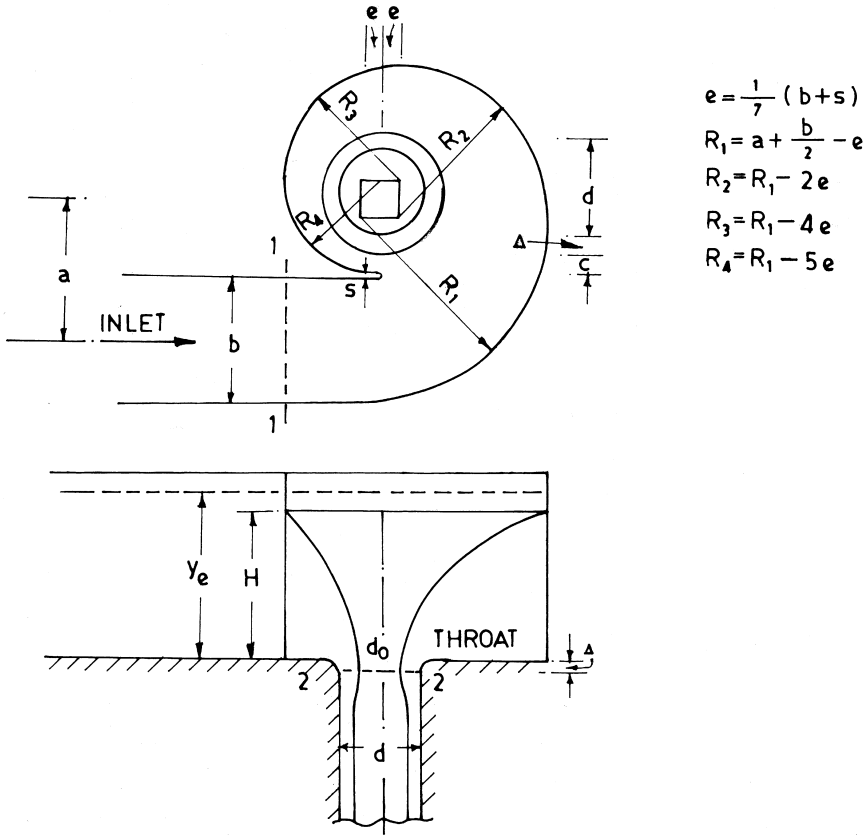

Figure 21 Standard scroll intake.

The relationships developed are:

$$\frac{Q}{\sqrt{gd^5}} = \frac{1}{2\sqrt{2}}\left[\frac{\frac{y_e}{d}+\frac{\Delta}{d}}{(\pi\, C_\lambda)^{-2} - \left(4\frac{b}{d}\frac{y_e}{d}\right)^{-2}}\right]^{1/2} \tag{27}$$

$$\frac{y_e}{d} = \frac{\pi}{2}\frac{a}{b}C_{\lambda o} \tag{28}$$

$$C_{\lambda 0} = \frac{3}{2}\frac{(1-\lambda^2)^2}{(1-\lambda^3)}\frac{C_\lambda}{\left[(1-\lambda^2)^2 - C_\lambda^2\right]^{1/2}} \tag{29}$$

$$C_\lambda = 0.95 - \lambda \tag{30}$$

(Viparelli recommended minimum $\lambda = 0.5$)

also

$$\frac{a}{b} - 0.5 > 0.65\frac{d}{b} \tag{31}$$

and

$$\frac{\Delta}{d} = 0.1\ to\ 0.2 \tag{32}$$

where

y_e = Depth of flow in the approach channel

λ = (d_o/d), d_o being air core diameter and other symbols as shown in Figure 21

Designing a Standard Scroll Intake

Principal dimensions of a standard scroll intake can be determined with the help of Equation 27 to 32. However, there is no set of rules or procedure for a straightforward calculation. For a given configuration of an approach flow (width, depth, and discharge), it is required to determine the diameter of the shaft and scroll dimensions. If the vertical shaft is already existing—this may be the case when a connection to be made to an existing tunnel, etc.—a suitable approach channel including the depth of flow, for a given discharge, has to be worked out. All these involve assumption of some parameters and trial procedure. Based on the analysis of some of the existing structures that are performing satisfactory, the following guidelines may be useful:

1. A suitable configuration of the approach channel is the one with the depth of flow slightly larger than the width. The ratio h/b usually varies from 1.1 to 1.5.

2. The Froude number of the flow in the approach channel is generally in the range of 0.35–0.45.
3. The distance between the centerlines of the approach channel and that of the vertical shaft, 'a', is generally 1.05 to 1.10 times the width of the approach channel.
4. The thickness of the dividing pier 's' and the chamfer at the inlet rib of the shaft 'Δ' have to be selected on the overall size of the structure and with regard to Equation 31–32.
5. A minimum value of 'λ' of 0.5 has been suggested to avoid choking of the throat. A larger value of λ would result in a larger diameter of the shaft.
6. From Equation 27, it would be seen that when $y_e = 0$, then $Q \neq 0$. Apparently, this relationship cannot be applied to evolve a discharge-rating curve. For lower discharges, relative air core diameter also increases, resulting in the increase in λ. The design worked out as above would require finalization through hydraulic model study.

Illustrative Examples

Determine the principal dimensions of a standard scroll intake to be connected to a 5 m wide rectangular channel, carrying a discharge of 105 cumec with a depth of flow of 6.5 m.

Assume s = 1 m, a = 7 m, and Δ = 0.7 m.

Also, adopt recommended minimum value of $\lambda = 0.5$, $C_\lambda = 0.95 - 0.5 = 0.45$

Shaft diameter. From Equation 27 the shaft diameter d can be worked out:

$$\frac{105}{\sqrt{9.81 d^{5/2}}} = \frac{1}{2\sqrt{2}} \left[\frac{(6.5 + 0.7)/d}{(\pi x 0.45)^{-2} - \left(4 x \frac{5}{4} x \frac{6.5}{d}\right)^{-2}} \right]^{1/2} \quad \text{reducing to}$$

$$\frac{8991}{d^5} = \left[\frac{7.2}{0.5d - \frac{d^5}{130^2}} \right] \Rightarrow d = 4.9\ m$$

Equation 31, $\frac{a}{b} - 0.5 > 0.65 \frac{d}{b}$ i.e., 0.9>0.64 is satisfied

Equation 32, $\frac{\Delta}{d} = 0.1\ to\ 0.2$ i.e., 0.143

The assumed values are therefore in order.

8.6.3 Tangential Vortex Intake

In a tangential intake, the flow from the approach channel enters the intake through a constricted section into the shaft along the wall. This oblique motion creates a swirl, which then forces the flow to cling to the walls of the shaft in the form of an annular jet with an air core in the center. The air core forms a throat. Figure 22 shows the geometry of a tangential intake and flow in it.

Several investigators have studied the hydraulic performance of tangential intakes. Although such structures are used preferably for storm-sewer and water transport applications, Slissky et al. (1979) mentions the successful operation of such an intake for a spillway for the Medeo dam, former USSR. Jain (1984) has conducted systematic studies on the hydraulic characteristics of tangential intakes.

There are three possible flow-control sections: one at the upstream end of the intake (section 1), the second at the downstream end of the intake (section 2), and the third at the throat (section 3). It is assumed that the flow control at the throat does not significantly affect the flow conditions at the second control section. The approach flow depth is then controlled by either section 1 or 2. For small flows, section 1 acts as the control so that flows in the approach channel and the tangential intake are critical and supercritical respectively. For larger discharges, the first control is drowned by the second control that now governs the flow depth, so that flows in both the approach channel and the tangential intake are subcritical. Jain (1984) proposes the following relations for calculating

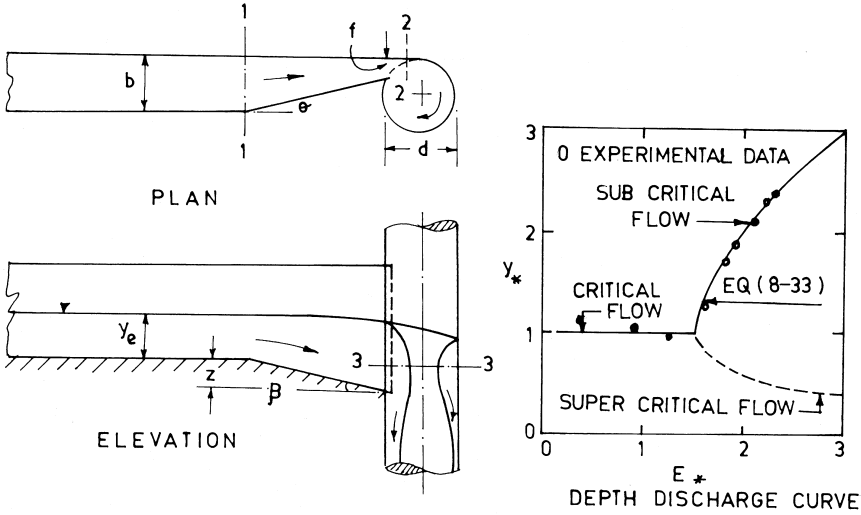

Figure 22 Tangential intake (shown in Jain 1984)

head-discharge characteristics, based on the consideration of specific energy at the entrance to the shaft and neglecting losses in the intake

$$y_* + \frac{1}{2y_*^2} = E_* \tag{33}$$

where

$y_* = y/y_c$

$E_* = \frac{3}{2}[b\,Cos\,\beta / f]^{2/3} - Z_*$

$Z_* = Z/y_c$

$y_c = [(Q / b)^2 / g]^{1/3}$

Z = drop in the transition floor at the mid point as shown in Figure 32

y = depth of uniform flow in the approach channel.

When $E_* > 3/2$, there are two physically real solutions. The solution with larger magnitude corresponds to sub-critical flow in the approach channel with section 2 as the control. For $E_* \leq 3 / 2$, section 1 acts as control with flow depth in the approach channel as critical, i.e.

$$y_* = 1 \quad for \quad E_* \leq \frac{3}{2} \tag{33a}$$

The relationship (Eq. 33) is also shown in Figure 22 along with the experimental data from Jain and Kennedy (1983). The agreement between the theory and experimental results has been satisfactory.

Drop Shaft Diameter

The drop shaft diameter is governed by the minimum permissible air–core area at the throat for the design discharge. The size of the air core at the throat is determined from the principle that the throat is another critical section and the velocity of streaming over the critical cross-section is equal to that of a small wave in the fluid. The minimum air–core area of 25% of the drop shaft area is commonly adopted. Based on experiments, the following relation for the drop shaft diameter has been recommended.

$$d = \left[\frac{Q_{max}^2}{g}\right]^{0.2} \tag{34}$$

This does not account for the effect of sidewall convergence in the approach transition and includes several tenuous assumptions. Therefore, additional analysis and experimental data are needed to further improve the relationships for designing tangential intakes.

8.6.4 Designs of Drop Shafts to Increase Discharge Capacity

The contraction of the air core at the inlet section of the vortex drop shaft limits the spillway discharge capacity. Akhmedov et al. (1998) have described designs where the upper part of the shaft was widened with a conical convergent nozzle, to increase the discharging capacity. Figure 23(a) shows the general arrangement and principal dimensions. It is claimed that this design can increase the discharging capacity by about 80% to 100%.

Another design shown in Figure 23(b) incorporates two intake channels and a conical transition chamber. This design is claimed to increase the discharge capacity almost three-fold that of ordinary vortex shaft spillway according to the standard design. Figure 24 shows comparison of the discharge capacity of different models of vortex shaft spillway. The magnitude of discharge and head are reported to be as obtained from hydraulic models.

8.6.5 Air Entrainment and Transport in Vortex Drops

Air entrainment in drop shafts occurs when the flow strikes the water column in the lower portion of the shaft, regardless of the type of intake, whether radial or vortex. However, the motion and transport of air bubbles downstream of the point of impact is different for the two flows. The swirling flow, caused by the vortex inlet, creates an inward pressure gradient to which the air bubbles respond in a

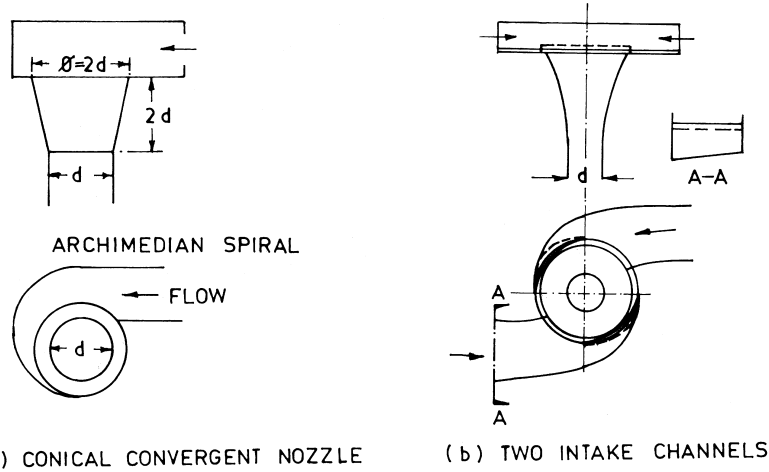

Figure 23 (a), (b). Designs of drop shafts to increase discharging capacity. (Shown in Akhmedov, 1998)

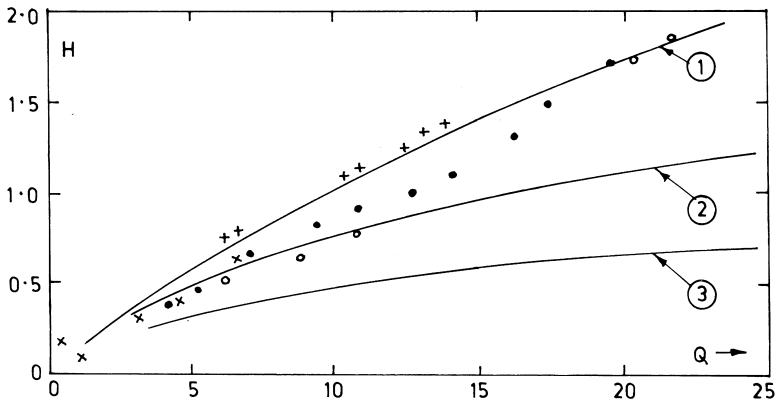

Figure 24 Comparison of discharging capacity of various designs (shown in Akhmedov 1998):

① Spiral chamber
② Spiral chamber with conical nozzle
③ Two intake channels
● Grotto Camponoro(Italy)
× Monte Maggiore (Italy)
+ Monte Argento (Italy)
○ Villa Santa-Maria (Italy)

different manner. The entrained air may be transported through the bottom of the shaft and further in to the water conductor system, for certain conditions. The transport of a significant quantity of air in to a pressurized tunnel may lead to the formation of high-pressure air pockets that grow large enough to release themselves by blowing back up the drop shaft.

Jain (1988) has developed an air-transport model based on theoretical analysis and laboratory experiments. It has been shown that most of the air is entrained in the annular hydraulic jump, formed when the annular jet flow changes to pipe-full flow.

A significant portion of the air bubbles converge due to an inward pressure gradient towards the center of the drop shaft and coalesce to form large bubbles, which then rise toward the surface. However, smaller bubbles may still be carried downstream for the flow conditions where the jump occurs at the location of low circulation. It was found that the air transport rate down the drop shaft was virtually zero if the jump formed in the strong circulation flow region corresponding to the value of the local swirl number, expressed as (Ω/U_0R), greater than 0.88.

where

Ω = Circulation
U_0 = Pipe full-flow velocity, and
R = drop shaft radius

8.7 SHAFT SPILLWAYS WITH SWIRLING FLOW IN OUTLET TUNNEL

Shaft spillways with axial flow in the tunnels for high head application involve risk of cavitation damage and an elaborate and expensive energy dissipation arrangement. Shaft spillways with the vortical water discharge (i.e., flow spinning or swirling flow) in the outlet tunnels were developed in the erstwhile Soviet Union with a view to solving both the problems. The flow in the tunnel spins round the longitudinal axis, along the inner periphery of the tunnel. Due to action of centrifugal forces and increased pressure on the tunnel walls, cavitation phenomenon is considerably reduced and increased dissipation of energy is accomp-

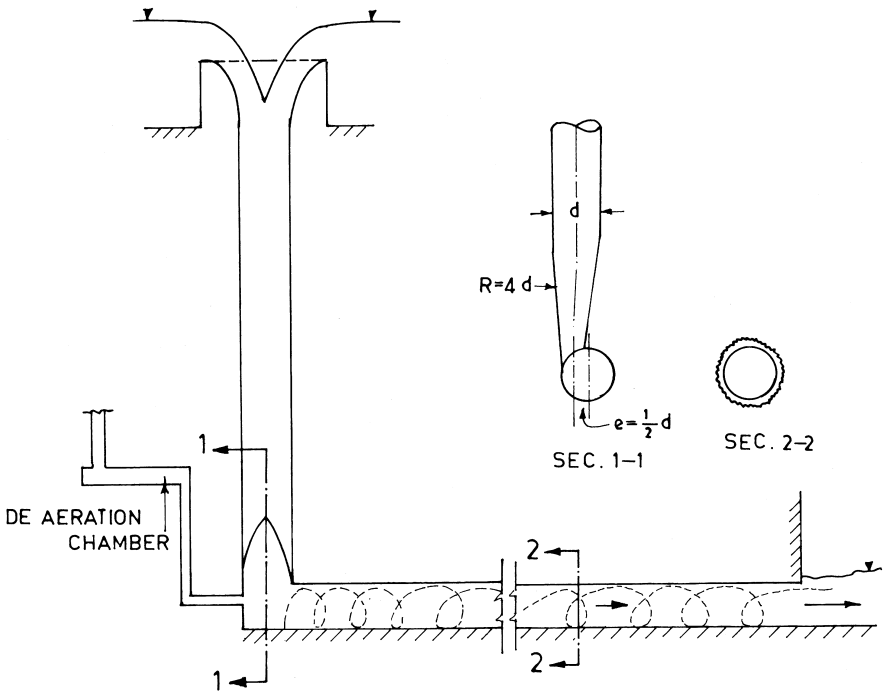

Figure 25 Typical shaft spillway with swirling device.

lished due to friction with the boundary. Although a number of small spillways were constructed in Italy, those for high head, large discharge applications were developed in the former USSR, notably for the dams of Medeo, Katun, Nurek, Rogun, etc. The spinning action of the flow in the tunnel is accomplished with a specially designed spinning device at the base.

Basically, there are two types of layouts: horizontal layout and vertical layout. In the vertical layout, the shaft may be vertical or inclined and may also have a control gate. In the horizontal layout, spinning of the flow is accomplished by angular deflection of the flow in the horizontal plane and without any special spinning device. In the inclined or vertical layout, a device called swirl chamber or swirling device is essential to accomplish flow spinning. Figure 25 shows typical shaft spillway with a swirling device.

Zuikov et al. (1989) have analyzed flow conditions in the outlet conduits and presented general guidelines for the hydraulic design. However, model study of each individual case would be necessary for finalizing the design.

De-aeration is a major problem in the shaft spillways with swirling flow in the outlet tunnel. It is generally observed that at low discharges the swirling flow along with air core does not persist up to the exit of the tunnel and hence, the entrapped air travels along tunnel ceiling and gets locked up depending on submergence at the exit. Arya et al. (1995) describe the de-aeration arrangement for the shaft spillways of Tehri HE project, India, evolved from hydraulic model studies. The arrangement consisted of de-aeration chamber at the blunt end of outlet tunnel, near the location of swivel device and de-aeration pipes near the exit end of the tunnel.

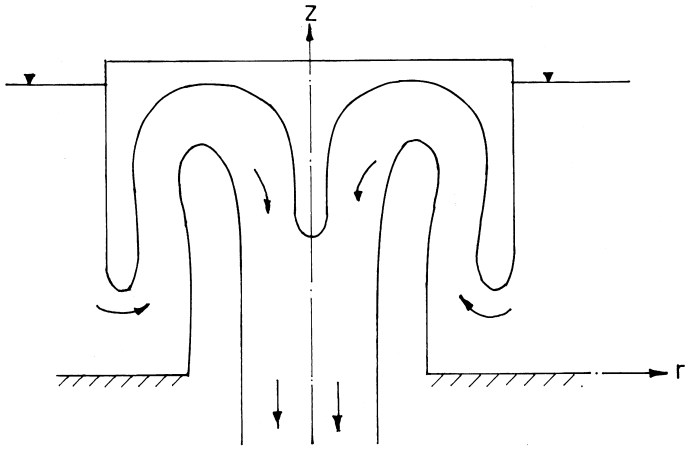

Figure 26 Typical siphon-shaft spillway (For coordinat*es, refer Agiralioglu et al. 1989*).

8.8 SIPHON-SHAFT SPILLWAY

A siphon-shaft spillway is essentially a shaft spillway with a hood that causes siphonic operation. The main advantage of a siphon-shaft over a shaft spillway is its capability to nearly reach its maximum discharge capacity under a small head sufficient to start siphonic action and to maintain nearly full capacity flow until reservoir level falls to the hood scirt edge elevation. It also enables the reservoir management authority to regulate the water level within the limits set by the crest and the skirt edge. Figure 26 shows details of a typical siphon-shaft spillway. Agiralioglu et al. (1989) have evolved hydraulic characteristics and guidelines for the design of siphon-shaft spillway based on laboratory experiments.

Notations

A = Maximum cross-sectional area of water prism
A_0 = Cross-sectional area of the contracted shaft
A_a = Cross-sectional area of airflow passage.
A_d = Cross-sectional area of conduit
a = Distance between the center line of approach channel and center of shaft (Fig. 21).
b = Width of approach channel
C_o = Coefficient of discharge: Circular crest
C_d = Coefficient of discharge: Orifice flow
C_L = Mean air concentration
C_Q = Coefficient of discharge
C_λ = A parameter in scroll intake design
$C_{\lambda 0}$ = A parameter in scroll intake design
$\overline{C}$ = Mean air concentration
D = Tunnel diameter
d = Shaft diameter
d_j = Jet thickness normal to shaft wall
d_0 = Air core diameter
e = Roughness
E = Specific energy in approach channel
E_* = Dimensionless specific energy
F = Froude number of flow in region II
F_o = Froude number at point where boundary layer intersects water surface
F_r = Froude number of flow at the point of impact
H = Operating head
H_o = Total head over the solid crest
H_e = Drop length from entrance to the point of impact

h_a = Head due to velocity of approach
h = Head above the orifice
H_a = Distance from the cross-section in question to the crest
H_l = Head loss
H_{of} = Head corresponding to orifice flow
H_s = Total head above the sharp crest
H_t = Head from reservoir to tail water
i = Slope of the tunnel
K = Energy loss coefficient
L = Length of the tunnel
L_s = Length of de-aeration zone
m_λ = Maximum possible air concentration
P = Height of the crest of shaft spillway from the bed
Q = Discharge (m^3/s)
Q_a = Discharge of air (m^3/s)
Q_w = Discharge of water (m^3/s)
Q_L = Total air flow
Q_{LE} = Entrained air flow in annular layer
Q_{LK} = Entrained air flow in the core region
q_{at} = Total air entrainment
q_{an} = Net air transport
R = Radius of shaft
R_e = Radius of shaft elbow
R_j = Thickness of annular jet
R_s = Radius of crest circle
S = Submergence depth above crest
Cross-sectional area of shaft
T_u = Turbulance intensity
t = Contraction of the shaft
U = Mean water velocity in the shaft flowing full
U_i = Jet velocity at the point of impact
Uo = Pipe full-flow velocity
U_1 = Jet velocity at plunge point
u_{br} = Air bubble rise velocity in still water
V_o = Maximum water surface velocity
V_{0min} = Minimum outlet velocity to commence air bubble transport
V_g = Slip velocity
x = Coordinate
y = Coordinate
y_c = Critical depth of flow in approach channel
y_e = Depth of flow in the approach channel
Z = Drop in the floor level

β = Q_a/Q_w
Δ = Throat section of scroll intake
Ω = Circulation
λ = Ratio of air core diameter to shaft diameter

REFERENCES

1. Ackers, P.; Crump, E. S. The Vortex drop, Paper No. 6430. Proc. Inst. of Civ. Engrs, Vol. 16 August 1960.
2. Agiralioglu, N.; Muftuoglu, R. F. Hood characteristics for siphon-shaft spillways. ASCE Jnl. of Hyd. Engg, May 1989; Vol. 115, No.5.
3. Akhmedov, T. Kh.; Dzhurumbayeva, T. Kh. Increase of capacity in a vortex shaft outlet, Proc. International conference on Modelling, Testing and Monitoring for hydropower plants. published by Intnl.Journal on Hydropower and Dams, France, October, 1998.
4. Anderson, A. G.; Dahlin, W. Q. Model studies-Lawrence Avenue Sewer System, City of Chicago, Project report No 100; University of Minnesota, USA, Oct, 1968.
5. Arya, R. S.; Verma, M. S.; Singh, K.; Singh, K. P. De-aeration of shaft spillways with swivel flow, Proc. Water and Energy (2001); Intnl. R&D Conference, CBIP, New Delhi, October 1995.
6. Bruschin, J. Air-water flow on spillways and in plugged bottom outlets; Intnl. Conf. Hydraulic modelling of civil engineering structures, BHRA, England, September 1982.
7. Chanson, H. Air-water flows in partially-filled conduits. IAHR Jnl of Hydraulic Research, 1997; Vol. 35, No 5.
8. Dahlin, W. Q.; Wetzel, J. M. Rochester Dropshafts model studies, Project report No 206; Saint Anthony Falls Hydraulic Laboratory, University of Minnesota, USA, March, 1982.
9. Damulevicius, V. D.; Ruplys, B. Drop inlet spillways in Lithuania, Proc. 28th I.A.H.R Congress, Graz, Austria, 1999.
10. Ervine, D. A.; Ahmed, A. A. A scaling relationship for a two-dimensional vertical dropshaft, ibid.
11. Ervine, D. A. Air entrainment in hydraulic structures: A review- Proc. Institution of Civil Engineers, Water, Maritime and Energy, September, 1998.
12. Falvey, H. T. Air water flow in hydraulic structures, USBR Engineering Monograph No.41, Dec. 1980.
13. Fattor, C. A.; Bacchiega, J. D. Analysis of instabilities in the change og regime in morning-glory spillways, 29th IAHR Congress, Beijing; 2001.
14. Filho, W. J.; Bandeira, M. S. Considerations on hydraulic design of free and pressure shaft spillways, C.3, 13th ICOLD, New Delhi, 1979.
15. Hack, H. P. Air entrainment in dropshafts with annular flow by turbulent diffusion, 17th IAHR Congress, Baden-Baden, Germany, August 1977; Vol. 1.
16. Haindl, K. Transfer of air by the ring jump of water, 14th IAHR Congress, France, 1971; Vol. I.

17. Haindl, K.; Ramesova, L. Modelling of zones of natural disaeration, 17th IAHR Congress, Baden-Baden, Germany, August 1977; Vol. 1.
18. Hajdin, G. Two contributions to spillway designing based on experimental studies, Q 50, R 45, 13th ICOLD, New Delhi, 1979.
19. Jain, A. K.; Raju, K. G. R.; Garde, R. J. Air entrainment in radial flow towards intakes. Proc. ASCE Jnl. of Hyd. Dn, Sept. 1978; Vol. 104, No.9.
20. Jain, S. C Tangential Vortex-Inlet. ASCE, Jnl. of Hyd. Engg, December 1984; Vol. 110, No.12.
21. Jain, S. C. Air transport in vortex-flow drop shafts. ASCE Jnl. of Hyd. Engg, Dec. 1988; Vol. 114, No.12.
22. Jain, S. C.; Ettema, R. Vortex flow intakes, Chapter 7 – Swirling flow problems at intakes. Edt. by J. Knauss. IAHR Hydraulic Structures Design Manual.
23. Jain, S. C.; Kennedy, J. F. Vortex-Flow Drop Structures for the Milwaukee Metropolitan Sewerage District Inline Storage System, Report No 264; The University of Iowa, 1983.
24. Lencastre, A. Shaft spillways, Theoretic experimental design, Proc 6th IAHR Congress, C-9, Hague; 1955; Vol. 3.
25. Leskovec, L. Suitable inlet form of pressure conduits, Paper C-14, ibid.
26. Martin, C. S. Characteristics fo an air-water mixture in a vertical shaft, Proc. Hyd. Div. Specialty Conference; ASCE, Montana, USA, Aug 1973.
27. Sailer, R. E. Air entrainment in siphon barrels. Civil Engineering, 1955; Vol. 25, No.5.
28. Sene, K. J.; Hunt, J. C. R.; Thomas, N. H. The role of coherent structures in bubble transport by turbulent shear flows. Journal of Fluid Mechanics, 1994; Vol. 259, 219–240.
29. Slissky, S. M.; Kuznetsova, E. V.; Akhmedov, T. K. Multy Storeyed Vortex shaft Outlets, 13th ICOLD, New Delhi, 1979; Vol. V.
30. Stephenson, D.; Metcalf, J. R Model studies of air entrainment in the Muela drop shaft. Proc. Instn. Civ. Engrs, Part 2, Sept. 1991.
31. Thomas, N. H. Entrapment and transport of bubbles by transient large eddies in multi-phase turbulent shear flows, International Conference on Physical Modelling of Multi-phase Flow; BHR Fluids, Coventry, UK, 1983.
32. USBR Design of small dams, 1973.
33. Wagner, W. E Determination of pressure controlled profiles. ASCE Trans, 1956; Vol. 121.
34. WES Morning glory spillways, HDC Chart 140-1/7, 1961.
35. Zuikov, A. L.; Chepaikin, G. A. Hydraulic calculation of free-flow eddy spillways, Hydro technical Construction. Original Russian Article, November 1988, 648–652.

9
Labyrinth and Duckbill Spillways

9.1 INTRODUCTION

An effective method to increase the spillway crest length without an associated increase in structure width is to use a labyrinth weir. The labyrinth weir consists of a series of relatively slender walls having a repetitive plan form, shaped generally triangular or trapezoidal, with a vertical upstream face. Labyrinth spillways are particularly suited to sites where the spillway width and upstream water surface are limited and larger discharging capacities are required. This may also provide additional storage capacity in lieu of a more costly gated structure. Labyrinth weirs can be particularly attractive for upgrading existing developments to satisfy more demanding design flood criteria in the limited waterway of an existing spillway. A special form of this type, the duckbill spillway, offers the advantage of an ungated spillway along with preserving most of the storage by virtue of a very small flood lift. Although their unusual shape and other complicated flow patterns have discouraged its use in the past, the recent development of design curves and continued operation of the projects should result in wider acceptance of these types of structures in future.

9.2 GENERAL CHARACTERISTICS OF LABYRINTH WEIRS

A labyrinth weir is, essentially, a uniform drop structure where the weir is constructed as a series of rectangles, triangles, or trapeziums in plan, as shown in Figure 1. This type of weir has many advantages and is particularly suited for use as a service or emergency spillway at a reservoir site where large discharges are to be handled at relatively narrower waterways. The disadvantage is that as the head increases, the relative performance decreases because of limited area in either the approach or receiving channels. The flow pattern in the labyrinth weir passes through four basic phases as the upstream head increases: fully aerated, partially aerated, transitional, and suppressed.

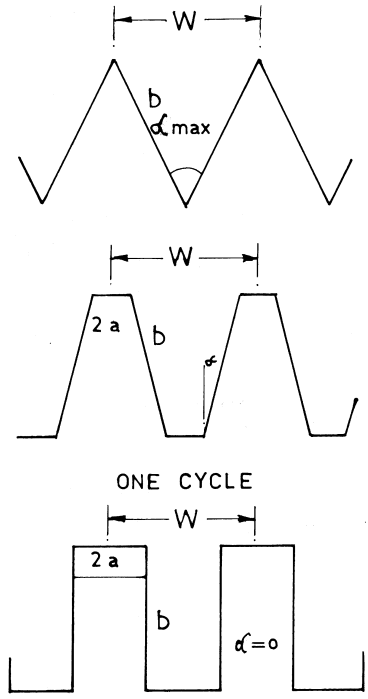

Figure 1 Labyrinth weir: configurations.

When the depth of overflow is small, the flow falls freely over the entire length of the weir and the air has an access from the downstream and from the corners. With an increase in the head, the flow over the upstream apex suffers interference from the flow over the sidewalls, and, as a result, air is drawn under the nappe at the downstream apron and a stable air pocket forms along each sidewall forming the downstream apex. By further increasing the head, the nappe becomes suppressed at various locations. The stable air pocket breaks up into smaller pockets which causes instability in the nappe. This stage is the beginning of the transitional phase. The main characteristics of this phase are discontinuity in the discharge coefficient curve. Finally, when the flow over the weir forms a solid and non-aerated nappe, the flow is in a suppressed phase and no air is drawn under the nappe. When the head is further increased, the efficiency decreases approaching that of a straight crest with a length equal to the chute width.

9.3 PARAMETERS AFFECTING PERFORMANCE

Labyrinth weirs can be constructed in different plan forms such as rectangular, triangular, trapezoidal, etc. A symmetric trapezoidal plan form is preferable because of its high efficiency and its easy construction.

The following terminology is applied to discuss the performance characteristics of labyrinth weir, as shown in Figure 2.

a = half length of weir apex
b = length of weir side wall
h = head over the weir crest
h_d = downstream water depth
l = developed length of one cycle = 4 a + 2b.
n = number of cycles in plan
w = width of one cycle of weir
W = total width of spillway = nw

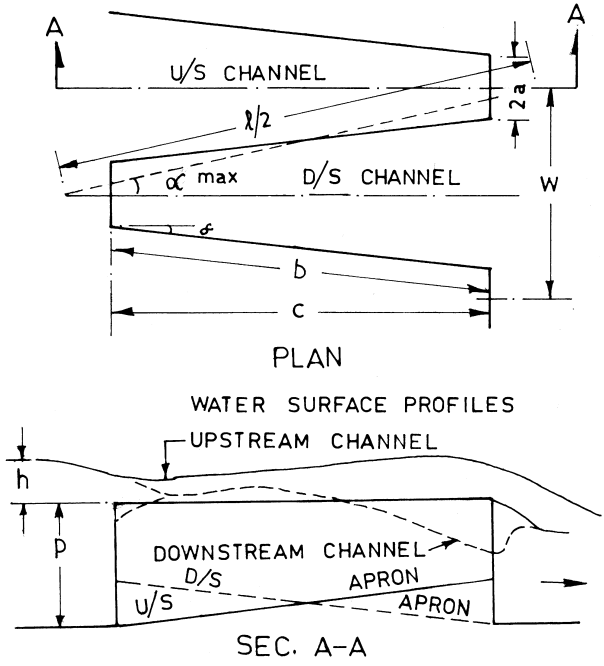

Figure 2 Labyrinth weir: Terminology.

l/w = length magnification
L = total length of weir = n l
p = weir height
w/p = vertical aspect ratio
h/p = head to weir height ratio
α = side wall angle
$\alpha_{max} = \sin^{-1}\left[\frac{w/2}{b + 2a}\right]$, which corresponds to triangular plan form.
Q_L = discharge over labyrinth weir.
Q_N = discharge over corresponding linear weir of same width, height and depth of overflow
Q_L/Q_N = flow magnification
E = effectiveness parameter

The shape of a plan form is completely defined by the length magnification factor *l*/w, the angle α of the sidewall, and number of cycles forming the weir, n. For a given length magnification, α varies from 0 for a rectangular plan form to a maximum for a triangular plan form. The parameters that influence the performance of the weir are:

Head to weir height ratio h/p
Length magnification l/w
Sidewall angle α
Vertical aspect ratio w/p
Number of cycles
Crest profile
Downstream interference
Drowning
Aprons

Head to Weir Height Ratio (h/p)

For small values of h/p, the discharge is small and the velocity head is neglible. Changes in depth due to contraction and expansion are small and the operating head is the same at every point along the length of the weir. The discharge per unit length of the weir is the same at every point and can be calculated from standard weir formula.

With increase in the head h (increase in h/p), the effect on the approach condition becomes visible in the form of water surface profiles along the upstream and downstream channels as shown in Figure 2. Thus, a large portion of the weir length operates under a head less than that in the approach channel. With further increase in the head, interference of the flows in the downstream channel increases and the performance is affected.

Length Magnification (l/w)

Increase in the length magnification l/w increases the flow magnification Q_L/Q_N only for a smaller value of h/p. Further increase in l/w increases Q_L/Q_N only marginally. It is found that there is no significant increase in flow magnification for values of l/w exceeding about 8.

Sidewall Angle (α)

As α increases, the length of weir tips decrease and the degree of flow contraction at entry to the upstream channel also decreases. Thus, head at each section of the weir is close to that in the approach channel. The performance improves until $\alpha = \alpha_{max}$, corresponding to the triangular plan form. However, the factor of nappe interference in the downstream channel—in the case of triangular plan form—may affect the performance.

Vertical Aspect Ratio (w/p)

For a given h/p, variation of w/p influences the size of the weir cycle in plan, relative to the operating head. As w/p decreases, the cycle size becomes small compared to the head. As w/p becomes still smaller, the plan form becomes a minute ripple in comparison to head and the weir performance approaches that of a normal weir. Loss of performance, with small w/p, arises from the impingement and interference between the nappes issuing from the facing sidewalls of the downstream channels. Thus, triangular plan form weirs are more prone to this effect than trapezoidal plan form weirs.

Number of Cycles

Labyrinth weir performance is found to be independent of the number of cycles n.

Crest Profile

It is found that the crest profiles formed of quarter-round top offered slightly higher coefficient of discharge than a sharp crested weir.

Downstream Interference

At high discharges, the exit sections of the downstream channels become choked and interference, in the form of localized drowning of the crest, may impair the

performance. A change in bed elevation equal to the operating head is sufficient to eliminate the loss of performance.

Drowning (h_d/p)

Drowning occurs by the downstream water depth h_d exceeding the height of weir p. This has the effect of reducing the discharging capacity.

Aprons

Both upstream and downstream aprons cause loss of performance by way of reducing flow magnification. However, aprons may be necessary in some cases from structural considerations. In such situations, a fall in the channel bed elevation beyond the downstream apron is provided.

9.4 DISCHARGE CHARACTERISTICS

The discharge over a labyrinth weir can be expressed in the most common form as

$$Q_L = C_L L h^{3/2} \tag{1}$$

Where C_L = Coefficient of discharge.

Dimensional analysis shows that $C_L = f\left(\frac{l}{w}, \frac{w}{p}, \frac{h}{p}\right)$ (2)

Hay and Taylor (1970) were the first investigators to systematically conduct studies in flume models, or the hydraulic performance of labyrinth weirs. They compared the discharge Q_L over the labyrinth weir of length l, with the discharge Q_N over a hypothetical linear weir of length equal to the total width of the labyrinth weir W. The flow magnification factor (Q_L/Q_N) was related to the parameters (h/p) and (l/w) and presented in the form of design charts (Fig. 3). With this method, the accuracy of the predicted discharge over the labyrinth weir depends on an accurate determination of the discharge Q_N over the linear weir. Q_N can be calculated from standard sharp crested weir formula:

$$Q_N = C_d W h^{1.5} \tag{3}$$

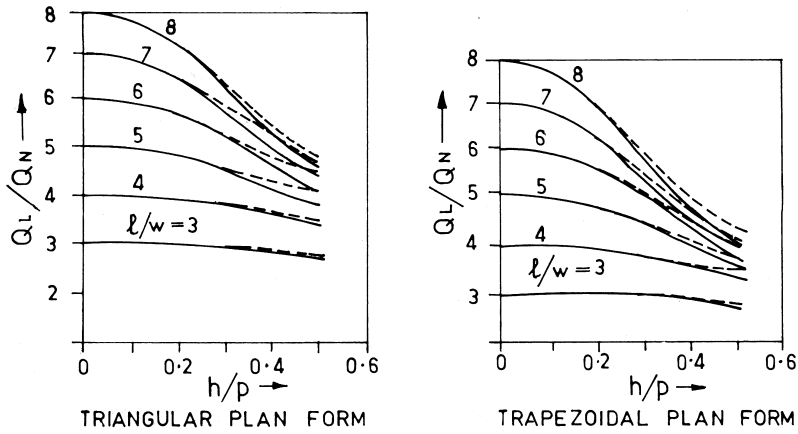

Figure 3 Design charts for labyrinth weir (shown in Hay and Taylor 1970):

———— No downstream interference
- - - - - - - - Downstream interference

where

$$C_d = 1.77 + 0.22\left(\frac{h}{p}\right) \tag{4}$$

Having obtained flow magnification factor with reference to h, p, and w, the required length and other details can be worked out as explained in the illustrative example.

Darvas (1971) commenting on the procedure suggested by Hay and Taylor observed that it was somewhat indirect because an imaginary sharp crested weir was brought into the calculations in a number of steps. Darvas introduced

$$Q_L = C_W W h^{1.5} \tag{5}$$

Where C_W = Coefficient of discharge referred to width of weir W and w/p $\leq$2, $\alpha \geq 0.8\alpha_{max}$.

Darvas presented a design chart giving C_W in terms of l/w and h/p, as shown in Figure 4. The values of C_W in the original chart being in ft units, SI equivalents have been indicated in the same figure. C_W generally varies from 6 to 26 (ft units) or from 3.3 to 14.3 (SI units).

It is also customary to express discharging capacity in terms of total length of labyrinth weir:

$$Q_L = C_L L h^{1.5} \tag{6}$$

Where C_L = coefficient of discharge referred to length L = n l.

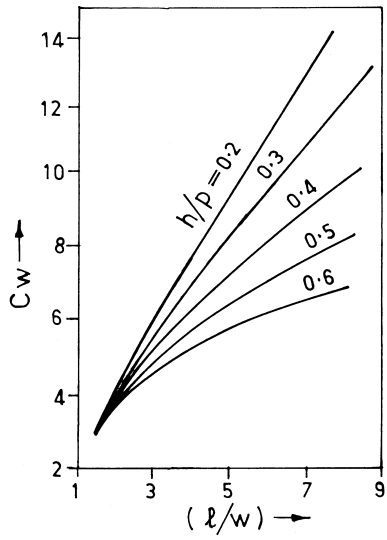

Figure 4 C_W Vs (l/w) (shown in Darvas 1971).

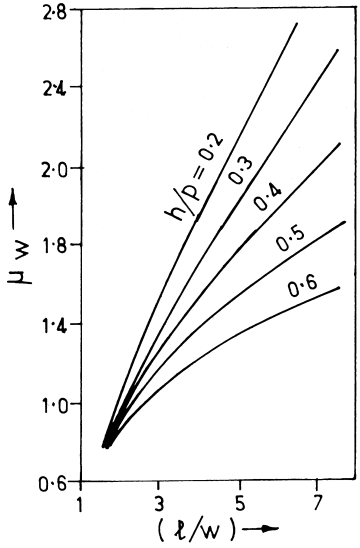

Figure 5 μ_w Vs (l/w) (shown in Magalhaes1985).

Equation 6 has been expressed in a different form by Magalhaes (1985) for a quarter-round crested trapezoidal labyrinth weir, as

$$Q_L = \mu_w W\sqrt{2g}\, h^{1.5} \tag{7}$$

Where μ_w = coefficient of discharge referred to width W and w/p≥2 and $\alpha/\alpha_{max} = 0.80$.

Figure 5 gives μ_w as a function of (l/w) and (h/p).

Lux and Hinchcliff (1985) proposed yet another alternative form of Equation 6 expressing the discharge per cycle as

$$Q = C_w\left(\frac{w/p}{w/p+k}\right)wh\sqrt{gh} \tag{8}$$

Where k = a constant equal to 0.10 for trapezoidal plan form and 0.18 for triangular plan form and

$2 \le l/w \le 8$
$2 = w/p \le 5$

Figure 6 shows variation of C_W with respect to parameters (h/p) and (l/w). It also marks different regimes of flow over the wier as aerated nappe, transitional stage, and suppressed nappe.

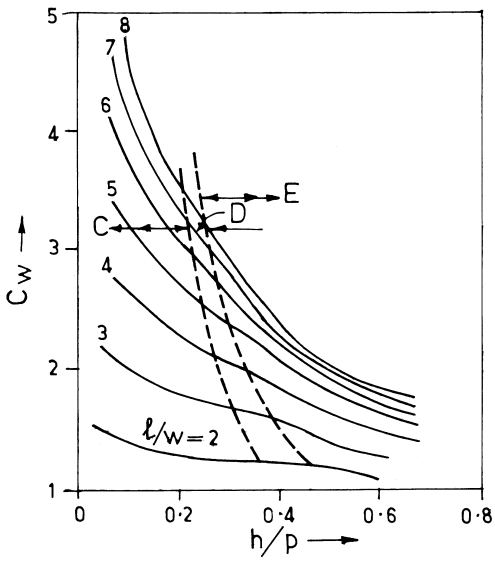

Figure 6 Cw Vs (l/w) (shown in Lux and Hinchcliff 1985): C = Aerated nappe, D = Transitional, and E = Suppressed.

Because the flow magnification (Q_L / Q_N) is somewhat less than the corresponding length magnification (l/w), the effectiveness parameter E is expressed as percentage:

$$E = \frac{(Q_L / Q_N)}{(l / w)} x100 \tag{9}$$

Zerrouk et al. (1995) transformed the coefficient of discharge μ_w in the form

$$\mu_w = \frac{Q_L}{W\sqrt{2g}\ h^{1.5}} \tag{10}$$

Zerrouk's equation compares the values obtained by the relationships of Hay and Taylor, Darvas, Magalhaes, and Lux and Hinchcliff. The comparison is shown in Figure 7.

As can be seen, there is a considerable variation among the values obtained from different relationships. This is because of the complexity of the flow pattern

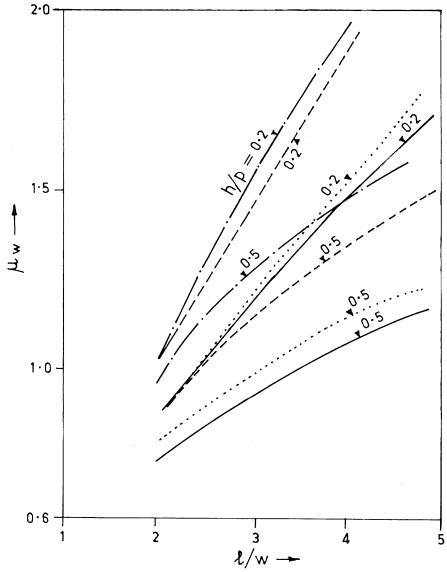

Figure 7 Comparison of discharge coefficient (shown in Zerrouk et al. 1995):

- · · · · · · · Hay and Taylor (1970)
- – – – – Darvas (1971)
- ..... Lux and Hinchliff (1985)
- ——— Magalhaes (1989)

resulting from involvement of a number of parameters. As such, these relationships can be used to prepare a preliminary design, and confirmatory tests on a hydraulic model would be necessary for a final design.

9.5 DESIGN OF LABYRINTH SPILLWAY

The hydraulic design of a labyrinth weir involves determination of geometric configuration including the plan form of triangular or trapezoidal, number of cycles, length magnification, etc., to suit the given discharge and reservoir water level. The design maximum discharge Q_L, depth of overflow h, height of the weir p, and width of the waterway W constitute the necessary input. These are governed by the site conditions and operational requirements. It may also be necessary to know the coefficient of discharge of the weir if it is intended to adopt a round crested weir. Triangular plan form weirs offer better hydraulic performance with as large a sidewall angle as possible. If trapezoidal plan form is to be used, the sidewall angle should not be smaller than 0.75 α_{max} corresponding to the triangular plan form. Decision regarding the number of cycles and determination of the lengths a and b depend solely on site conditions. The flow downstream of the weir, in the discharge channel, leading to the energy dissipator is characterized by criss-cross diamond pattern, and requires adequate free board for the sidewalls. The recommended values of the pertinent parameters are:

$0.2 < (h/p) < 0.6$
$\alpha/\alpha_{max} > 0.75$
$l/w = 3$ to 8
$w/p > 2$

Table 1 shows pertinent dimensions and parameters of some of the existing labyrinth weir installations, which can serve as a guideline in the design of labyrinth weirs.

Illustrative Examples

The case of South Heart dam (Canada) finalized from hydraulic model studies (Tacail et al.-1990) is discussed to illustrate the design procedure:

Design maximum discharge: $Q_L = 215$ cumec
Height of the weir: $p = 4$ m
Total width: $W = 24.5$ m
Max depth of overflow: $h = 1$ m
Weir with upstream rounded crest

Table 1 Parameters of some Labyrinth Weir Spillways

Name	Country	Q m^3/s	*l* (m)	w (m)	α (°)	p (m)	h (m)	*l* W	*w* P	*h* P	α … max	n	L* (m)	W* (m)	C L
Avon	Australia	1790	26.46	13.54	27.50	3.00	2.80	1.95	4.50	0.93	90	10	265.80	136.60	1.44
Avon (reconstructed)	Australia	1420	26.50	13.50	3.00	2.16	2.16	1.96	4.50	0.72		10			
Barletts Ferry Dam	U.S.A.	5920	70.30	18.30		3.43	2.19	3.84	5.34	0.64		20.5	1441.15		1.27
Belia	Zaire	400	31.00	18.00		3.0/2.0	2.00	1.72	6.00	0.67		2	76.60	40.80	1.85
Beni Behdel	Algeria	1000	62.50	4.00			0.50	15.63				20	1250.00	80.00	2.26
Boardman Spillway	U.S.A.	387	53.50	18.30	19.44	2.76	1.77	2.92	6.63	0.64		2	106.70	36.50	1.54
Carty	U.S.A.	387	54.60	18.30	19.40	2.8/4.3	1.80	2.98	5.18	0.50	100	2	109.20	36.60	1.47
Cimia Dam	Italy	1100	87.50	30.00		15.00	1.50	2.92	1.94	0.10		4	350.00		1.71
Dungo	Angola	576	28.56	9.73	15.20	3.5/4.3	2.40	2.94	2.78	0.69	72	4	115.50	40.10	1.34
Estancia	Venezuela	661	65.00	32.00	22.00		3.00	2.03				1	65.00	32.00	1.96
Harreza	Algeria	350	28.56	9.73	15.20	3.5/4.5	1.90	2.94	2.78	0.54	72	3	86.90	30.40	1.54
Hyrum	U.S.A.	256	45.72	9.14	9.60	3.66	1.68	5.00	2.50	0.46	84	2	91.40	18.30	1.29
Keddara	Algeria	250	26.30	8.92	14.90	3.5/4.2	2.46	2.95	2.55	0.70	75	2	53.80	19.00	1.20
Mercer Dam	U.S.A.	239	17.65	5.49		4.57	1.83	3.20	1.20	0.40		4	74.98		1.29
Nabet Pumped Storage	Trinidad	481	13.72	5.49		3.05	1.68	2.50	1.80	0.55		10	137.16	54.86	1.61
Ohau C Canal	New Zealand	540	37.50	6.25		2.50	1.08	6.00	2.50	0.43		12	450.00	77.10	1.07
Quincy Dam	U.S.A.	552	26.50	13.60		3.96	2.13	1.95	3.43	0.54		4	106.00	35.97	1.68
Santa Justa	Portugal	285	67.40	10.50	4.00	3.00	1.35	6.42	3.50	0.45	41	2	134.80	21.00	1.35
Samo Dam	Algeria	360	27.90			6.00	1.50			0.25		8	223.20		0.88
South Heart Dam	Canada	215	60.20	11.75	8.77	4.00	1.00	5.12	2.94	0.25	77	2	120.40	24.50	1.79
Ute Dam	U.S.A.	15574	73.15	18.29	12.90	9.14	5.79	4.00	2.00	0.63	84	14	1024.10	256.00	1.09
Ute Dam (Reconstructed)	U.S.A.	15600	73.70	18.30		9.14	5.79	4.00	2.00	0.63		14	1024.10	256.00	1.09
Woronora	Australia	1020	51.23	13.40	22.80	2.20	1.36	2.33	6.07	0.62	90	11	343.50	147.50	1.87

* L = n *l* and W = n w are sometimes not strictly correct because of the asymmetry of the weir cycles next to the lateral walls of the spillway.

Determine: $Q_N = C_d\ W\ h^{1.5}$ $C_d = 1.77 + 0.22\ (h/p) = 1.825$
$= 1.825 \times 24.5 \times 1 = 44.7$ cumec.
Flow magnification $= 215/44.7 = 4.8$

Determine Length Magnification

1. Hay and Taylor (Fig. 3)
2. With $Q_L/Q_N = 4.8$ and $h/p = 0.25$, $l/w = 5.1$
3. Darvas (Fig. 4)
4. $Q_L = C_W\ W\ h^{1.5}$
5. From which $C_W = 8.78$, which along with $h/p = 0.25$ gives $l/w = 4.8$.
6. Magalhaes (Fig. 5)
7. $\mu_w = \dfrac{Q_L}{W\sqrt{2g}\,h^{1.5}} =$ 1.98, with h/ p = 0.25 gives l/ w = 4.5.
8. Lux and Hinchcliff (Fig. 6)

$$C_w = \frac{Q}{\left(\dfrac{w/p}{w/p+k}\right)W\sqrt{g}h^{1.5}} = 2.85\ (k = 0.10)$$ with h/ p = 0.25 gives l/ w = 5.8

Since the total discharge—and not the discharge per cycle—is considered, w is replaced by W.

Adopt a length magnification factor of 5.

Determination of Geometric Configuration

Several alternative layouts are possible, however, the one with a two-cycle trapezoidal plan form appears to be more suitable.

Length: l per cycle $= 1/2 \times 24.5 \times 5 = 61.25$ m say 61 m $= 4a + 2b$

With $a = 2$, $b = 26.5$, $\alpha = \sin^{-1}[(w/2 - 2a)/b] = 4.6°$, and $\alpha_{max} = \sin^{-1}[(w/2)/2a + b] = -11.58°$.

The ratios $\alpha/\alpha_{max} = 0.40$, $w/p = 3.06$

$C_L = Q_L/(L\ h^{1.5}) = 1.76$

The final dimensions of the structure (from Table 1) are: $l = 6o.20$ m, $w = 11.75$ m, $\alpha = 8.77°$, $l/w = 5.12$, $w/p = 2.94$, $\alpha/\alpha_{max} = 0.77$, $n = 2$, $L = 120.4$ m, and $C_L = 1.79$.

Figure 8 shows the details of the spillway as finalized after extensive model studies.

9.6 DUCKBILL SPILLWAY

A duckbill spillway is a special form of labyrinth spillway that, as the name itself suggests, has usually curved segments in plan form; however, rectangular or

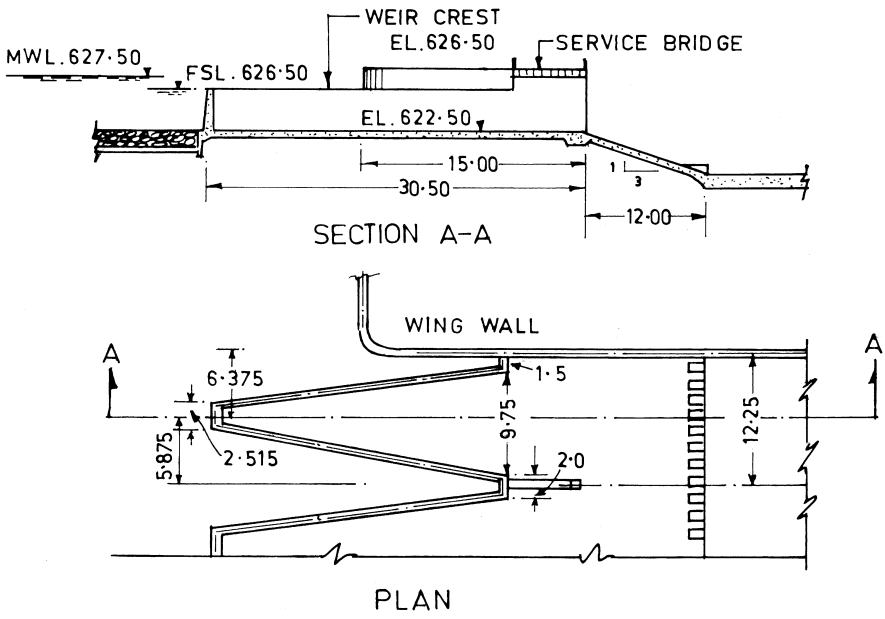

Figure 8 Labyrinth spillway of South Heart dam, Canada.

trapezoidal forms are not uncommon. This is suited at the sites where the spillway walls are to be constructed of masonry or concrete and where the plan form can be adjusted to the availability of foundation rock, etc. The surplussing water flows over the sides is collected in a trough and conveyed through a chute or discharge channel to the energy dissipator. Figure 9 shows layout of duckbill spillway on rectangular plan form.

Duckbill spillways are generally located on the flanks of earth or rock fill dams, as considerable reduction is achieved in excavation of the approach channel and tail channel. This type of spillway is advantageous where maximum allowable afflux is limited. It also increases storage capacity because the crest can be fixed at a higher elevation for the same maximum water level.

The discharge over a duckbill spillway would increase in direct proportion to an increase in the crest length only for low heads. With the increase in the overflow depth, the solid non-aerated nappe suppresses the flow thereby decreasing the efficiency of the spillway.

When a duckbill spillway is constructed with a rectangular or trapezoidal plan form, as shown in Figure 9, the upstream corners of the junction affect the overall coefficient of discharge. Thus, the discharge that can be passed over the

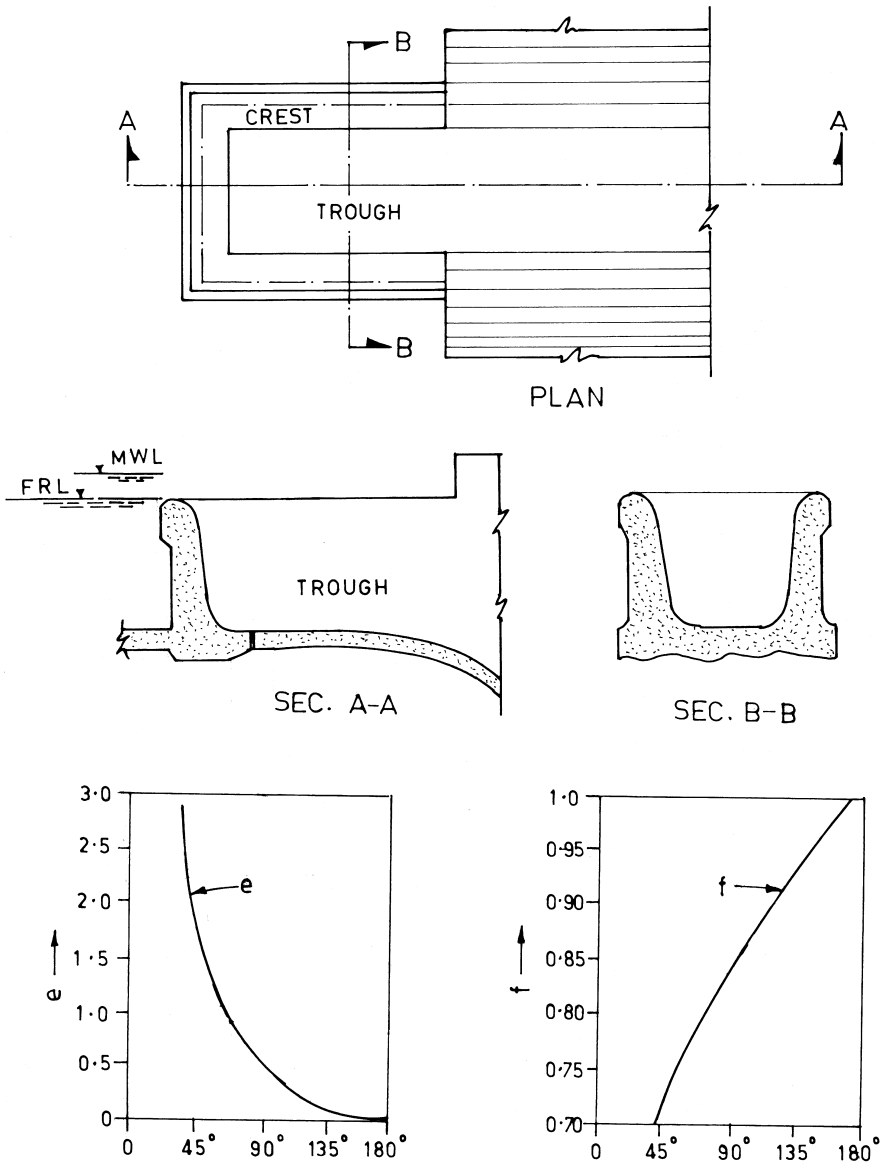

Figure 9 Duckbill spillway with rectangular plan form.

duckbill spillway would be less than that passed over an equivalent straight spillway having the same length as that of the three segments of the duckbill spillway. This is accounted by a reduced coefficient of discharge of the duckbill spillway due to corner effect as compared to that of the standard straight spillway having the same crest profile. The procedure is explained below:

1. For the given design maximum discharge Q_D, design head H_D and a spillway section with a known value of coefficient of discharge C_{ds}, determine the total length L_S of a spillway of a straight alignment:

$$L_s = \frac{Q_D}{C_{ds} H_D^{1.5}} \tag{11}$$

2. Determine the duckbill spillway configuration, rectangular or trapezoidal, such that its trial length L_{D1} is greater than L_S.
3. Work out corner effect ld = [e/(1-f)], where e and f are functions of corner angle Φ of the duckbill spillway as shown in Figure 9.
4. Work out reduction coefficient C_r as

$$C_r = 1 - \frac{2\ ld}{L_{D1}} \tag{12}$$

5. The discharge over the duckbill spillway with trial length L_{D1} is

$$Q_1 = C_r x C_{ds} x L_{D1} x H_D^{1.5} \tag{13}$$

6. If $Q_1 \neq Q_D$, repeat the trial with other length L_{D2} until the discharge calculated in (5) matches with the design discharge.
7. The total length of the duckbill spillway should be so adjusted as to

$$L_D = 2L_1 + L_2 \tag{14}$$

8. and

$$L_2 \rangle\ 2L_d \tag{15}$$

Illustrative Examples

Design a duckbill spillway with a trapezoidal plan form and corner angles of 120°. The spillway has a coefficient of discharge of 2.2 and the design maximum discharge will be 700 cumec without exceeding the depth of overflow of 4.5 m.

1. Determine the length L_S of an equivalent straight spillway

$$L_s = \frac{Q_D}{C_d H_D^{1.5}} = \frac{700}{2.2 x 4.5^{1.5}} = 33.3\ \text{m}$$

2. Assume $L_{D1} = 40$m
3. Read the values of e and f from Figure 9: $e = 0.21$ and $f = 0.9$ for $\phi = 120°$
4. Corner effect $ld = e/(1\text{-}f) = 0.21/(1-0.9) = 2.1$ m
5. $C_r = 1\text{-}[(2 \times 2.1)/40] = 0.895$
6. $Q_1 = 0.895 \times 2.2 \times 40 \times 4.5^{1.5} = 751$ cumec
7. With $L_{D2} = 37.5$; $C_r = 0.888$ and $Q_2 = 0.888 \times 2.2 \times 37.5 \times 4.5^{1.5} = 699.3$ cumec.

Therefore, the total length of the duckbill spillway should be 37.5 m and $37.5 = 2 \times L_1 + L_2$ with $L_2 > 2 \times 2.1$ or say 4.5 m.

Several combinations of L_1 and L_2 are possible and the one that fits best the site conditions can be adopted.

The other common plan form for a duckbill spillway is a semi-circular nose followed by chute with parallel sidewalls. This, however, was not found to be an efficient arrangement as born out by the model studies for Salauli dam spillway (India), Yasmos dam (Greece), etc. In the case of Salauli dam, a plan form consisting of compound circular arcs with a pointed nose at the most upstream end (Fig. 10) was found to be satisfactory in respect of flow conditions in the trough. The crest profile, also formed of a circular arc, gave a coefficient of discharge C_L as high as 2.165, and $\mu_w = 1.29$.

The trough of a duckbill spillway, particularly its invert profile, significantly influences the performance of the spillway. Considerable intermingling of the flow down the crest of the spillway takes place in the trough, dissipating a part of energy and ensuring a smooth water surface in the trough. A trough of an inadequate capacity results in an excessive boosting up of water levels, which may create drowning of the crest and an undulating water surface with reduction in discharge capacity. On the other hand, a deeper trough, or a trough with a steeper invert profile, results in a supercritical flow sweeping out the trough, creating cross-waves, and splashing. The trough for the duckbill spillway of rectangular plan form can be designed on the lines of the trough for the side channel spillways. Knight (1989) has described the procedure with reference to the design of the trough for a 10 m $\times$ 45 m duckbill spillway with rectangular plan form. For the spillways of other plan forms, hydraulic model study is the only means to finalize the design.

9.7 DESIGNS RELEVANT TO EXISTING AND NEW STRUCTURES

Replacement of an existing conventional spillway with a labyrinth or duckbill spillway alternative is fraught with numerous difficulties. Some of these are:

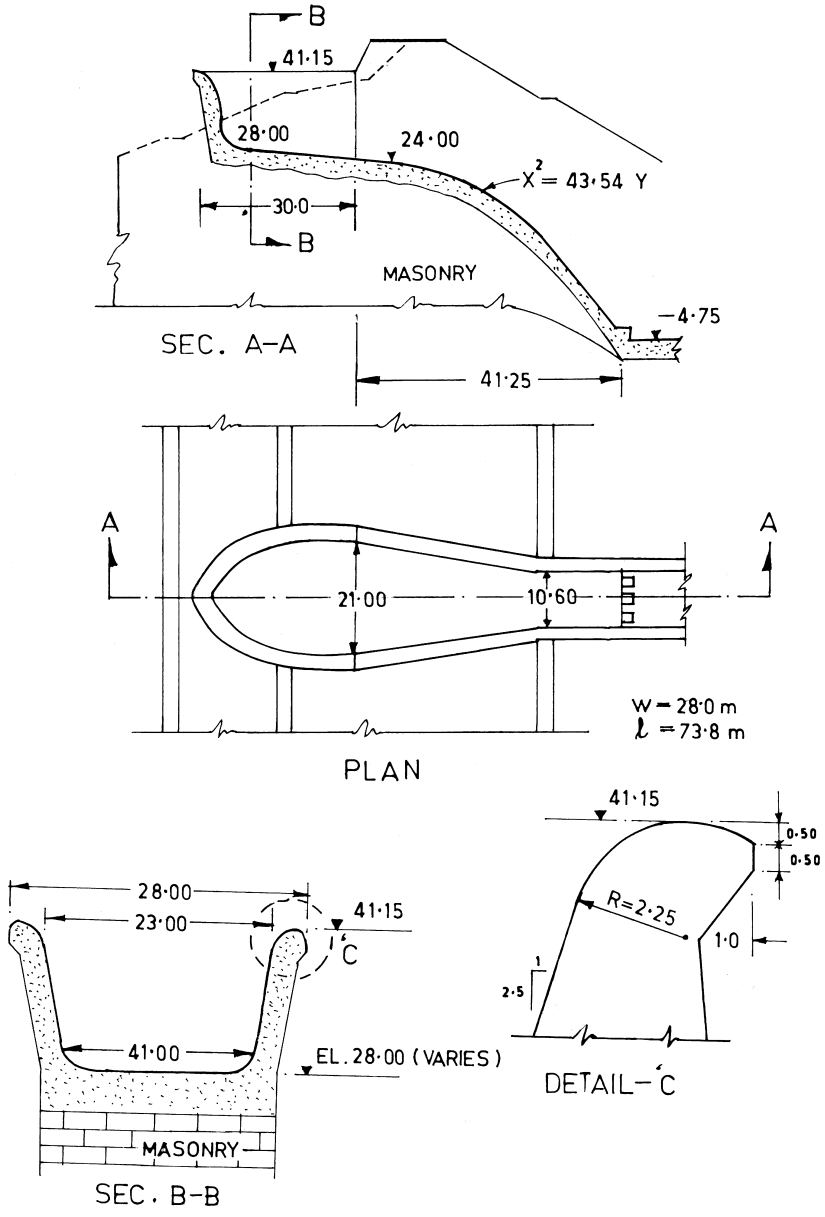

Figure 10 Duckbill spillway: Salauli dam, India. (Khanolkar et al. 1986)

1. Adequate length at the base of the proposed labyrinth/duckbill should be available. This may require truncating the existing spillway, resulting into extra height of the new weir for fixing its crest at the desired elevation.
2. Because of the increased discharge and cross-waves downstream of the crest and into the discharge carrier, higher sidewalls are required.
3. With the width of the new structure remaining almost the same and with increased discharge, the existing energy dissipation arrangement would prove to be inadequate. Often, major modifications may be required.
4. Similar problems may arise in regard to downstream protection works also.

In this connection, some of the case studies may be useful, as for example, the spillway of the Sainte Brigette-des-saults in Quebec, Canada and Salauli dam as reported by Khanolkar et al. (1986) and Khatsuria et al. (1988).

Designs for the proposed new structures permit a much wider range of choice than those available with the existing structures. Results of research and optimization studies can be fruitfully utilized to work out different alternatives. However, model studies play an important role in evolving a safe, efficient, and economic design. Some of the pertinent case studies are reported by Zerrouk et al. (1995) for Keddara dam, Algeria; Karya (1989) for Ciwadas, Indonesia; Tacail et al. (1990) for South Heart dam, Canada; and Darvas (1971) for Woronora and Avon dams, Australia.

Notation

a = Half length of weir apex
b = Length of weir side wall
C_d = Coefficient of discharge: Rehbock weir
C_{ds} = Coefficient of discharge of a spillway with straight alignment
C_L = Coefficient of discharge of labyrinth weir relevant to total length
C_r = Coefficient of reduction for a rectangular duckbill spillway
C_w = -do- relevant to width W
E = Effectiveness parameter in relation to flow magnification.
e = A factor (Fig. 10)
f = A factor (Fig. 10)
H_D = Head over straight spillway
h = Depth of overflow over the weir
h_d = Downstream water depth

k = A constant depending on the shape of the plan form (Eq. 6)
L = Total length of labyrinth weir
L_D = Length of duckbill spillway
L_S = Length of straight spillway
l = Developed length of one cycle of labyrinth = 4 a + 2b
l_d = Corner effect for duckbill spillway
n = Number of cycles
p = Height of the weir
Q_D = Discharge over straight spillway
Q_L = Discharge over labyrinth weir for total length L
Q_N = Discharge over corresponding linear weir of same width, height and depth of overflow
w = Width of one cycle of a labyrinth weir
W = Total width of a labyrinth weir- n x w
α = Sidewall angle
α_{max} = Maximum sidewall angle (corresponding to triangular plan form)
μ_w = Coefficient of discharge of labyrinth weir based on width W (Magalhaes formula)

REFERENCES

1. Darvas, L. A. Discussion on – Performance and Design of Labyrinth weirs, ASCE Jnl. Of Hyd. Dn. HY 8, Aug. 1971.
2. Hay, N.; Taylor, G. Performance and Design of Labyrinth weirs. ASCE, Jnl. of Hyd. Dn. HY 11, November 1970.
3. Karya, G.; Hutama, P. T. Laporan Akhir Rakyat (TIR); Ciwadas, Jakarta, Indonesia.
4. Khanolkar, B. V.; Dharwad, R. C.; Sayanak, S. D. An unconventional duckbill spillway which can be constructed on a limited width of foundation rock, Salauli Project, Goa – 53rd ARS; CBI&P (India), Bhubaneswar, 1986.
5. Khatsuria, R. M.; Deolalikar, P. B.; Bhosekar, V. V. Design of duckbill spillway and reversed sloping curved stilling basin – Salauli Project – 54th R&D Session; CBI&P (India), Ranchi, 1988.
6. Knight, A. C. E. Design of efficient side channel spillway. ASCE Jnl of Hyd Engg, Sept 1989; Vol. 115, No 9.
7. Lux, F.; Hinchliff, D. L. Design and construction of labyrinth spillway; 15th ICOLD, Lausanne, Switzerland, 1985.
8. Magalhaes, Pinto, A. Labyrinth weir spillways, ibid, 1985.
9. Tacail, F. G.; Evans, B.; Babb, A. Case study of a labyrinth weir spillway, 1990; Vol. 17.
10. Zerrouk, N. E.; Marche, C. Les evacuateurs de erues en labyrinthe – ibid, 1995; Vol. 22.

10
Tunnel and Culvert Spillways

10.1 INTRODUCTION

Tunnel spillways can be used advantageously at dam sites in narrow canyons with steep abutments or at sites where there is a danger to open channels from rockslides or snow. In many cases, a diversion tunnel already available can be used as the downstream leg of a tunnel spillway. The two basic parts of a tunnel spillway are: an upstream spillway crest, free or controlled, and a downstream tunnel, part of which is inclined and part is nearly horizontal, as shown in Figure 1.

When the closed channel is carried under a dam, it is known as a conduit spillway. These are generally suited to dams in wide valleys and in such cases the use of conduit spillway enables the spillway to be located under the dam near the downstream bed.

A culvert spillway is a special adaptation of the conduit or tunnel spillway. For drops not exceeding about 10 m, culvert spillways offer advantages over other types because of their adaptability for either part full or full-flow operation and because of their simplicity and economy in construction.

10.2 TUNNEL SPILLWAYS: DESIGN CONSIDERATIONS

10.2.1 Control Structure

The most common form of control structures is an ogee crest, either uncontrolled or equipped with radial gates. However, other forms of control structures such as vertical or inclined orifice entrances, drop inlet entrances, and side channel crests can also be used in conjunction with tunnel spillways as the topography may dictate. Figures 2 and 3 show control structures with multiple entry intakes for the Bolgenach and Polyphton dams, (Herbrand and Scheuerlien-1979). Figure 4 shows a control structure with side channel spillway.

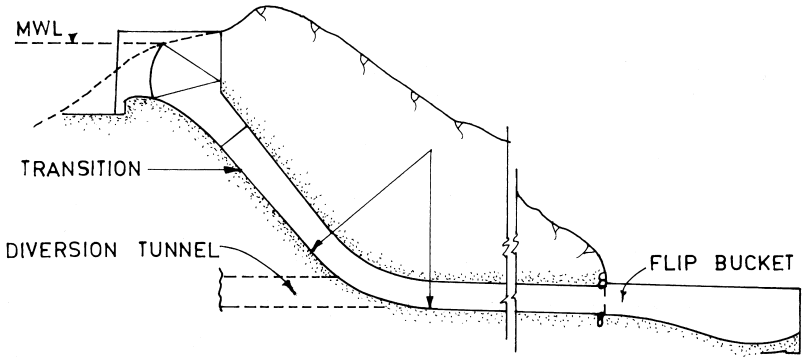

Figure 1 Typical tunnel spillway.

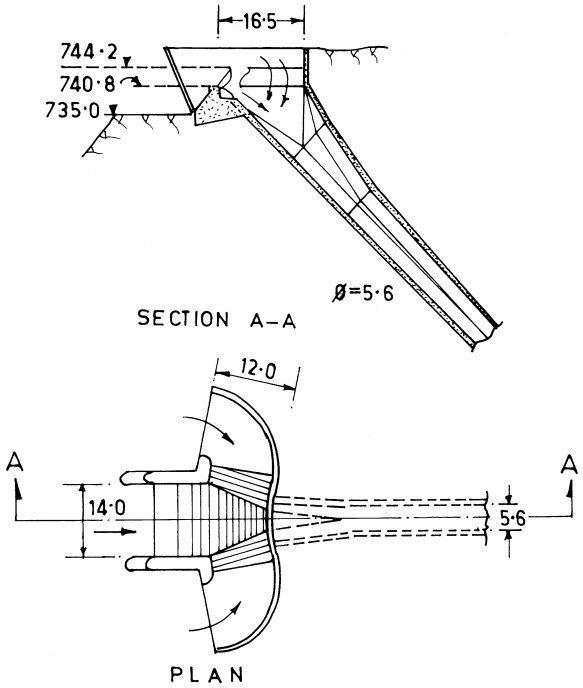

Figure 2 Control structure with three spillway sections; Bolgenach dam, Austria. (Herbrand et al.-1979)

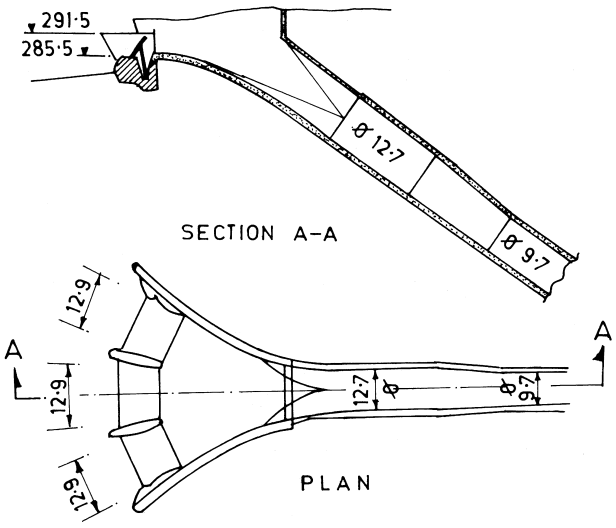

Figure 3 Control structure with three spillways converging: Polyphton dam, Greece. (Herbrand et al. 1979)

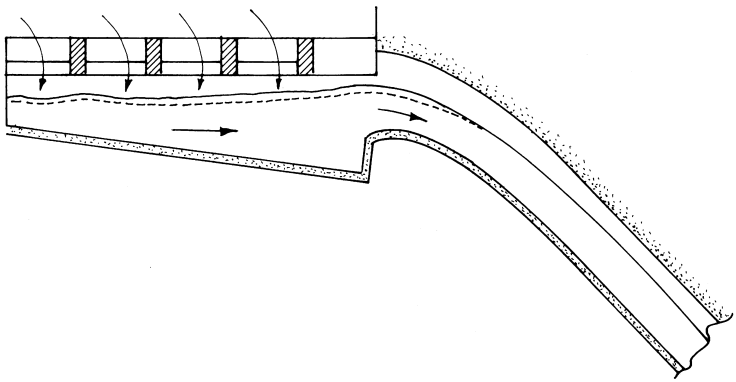

Figure 4 Control structure with side channel spillway.

10.2.2 Discharge Tunnel

In its most common form, the discharge tunnel consists of an inclined portion, a toe curve, and nearly horizontal or slightly sloping portion terminating into an energy dissipator. The following are the design considerations:

- The cross-section of the tunnel at the control section is rectangular because of the piers and gates. This section has to be transformed into a circular section or a horseshoe section for practical reasons. It is well known that these sections are most suitable for driving tunnels underground. A transition has to be provided for this, however it should begin only after the end of the ogee profile. The details of transition are finalized from hydraulic model studies.
- For economic considerations, the tunnel diameter may be kept to a minimum, but the tunnel is never allowed to flow full because of the possibility of siphonic action producing dangerous flow conditions. Spillway tunnels are usually designed to flow from 3/4 to 7/8 full at maximum discharge, so that a passage for air is available throughout its length, from the entrance up to the outlet portal.
- Similar to the flow in the open surface spillway, the flow in the tunnel spillway also is characterized by higher velocities and lower pressures. The flow therefore needs to be aerated to prevent cavitation damage. In this respect, it differs from the flow in a shaft spillway where release of entrained air is an important requirement.
- Calculations for a tunnel spillway can be carried out on similar lines as the free surface spillways, accounting for the boundary layer growth, point of inception, and aerated flow properties, as discussed in detail in Chapter 27: Air Entrainment and Forced Aeration. However, in the case of tunnel spillways, an additional parameter is involved, characterizing transition, due to the change in cross-section from rectangular to circular and vice versa. In this connection, the computer program written by Falvey (1990) giving the hydraulic and cavitation properties of free water surface flows is widely used in determining the point of inception, cavitation indices, and location of aerator. The details of aerators for tunnel spillways have been covered in Chapter 27.
- The toe curve joining the inclined and horizontal portions of the discharge tunnel is crucial in terms of performance of the tunnel spillway. Theoretically, this is the region where the flow would cling the spillway surface and the pressures would be highly positive, yet severe cavitation damage has taken place in the immediate vicinity of the toe curves of several tunnel spillways. Tunnel spillways of Sarrans, France, San Esteban, Spain, and Aldeadavila, Spain were damaged due to cavitation in these reaches. Falvey (1990) has discussed cavitation damage to

tunnel spillways of Blue Mesa, Flaming Gorge, Glen Canyon, Hoover, and Yellowtail dams of the US. Bribiesca (1979) has reported cavitation damage to the tunnel spillway of El Infiernillo dam, Mexico. In all these cases, misalignments and inadequate finishing of the concrete (resulting in surface irregularities) were the main causes of cavitation. This part of the structure is the most difficult from the standpoint of construction. It may be mentioned that the tunnel spillway of Fontana dam, US, has not suffered cavitation damage in spite of the flow velocities as high as 48 m/s, presumably due to the close tolerances in surface finishes and correct alignments.

- The radius of the toe curve should be as large as practicable. The flow conditions at the toe, in the case of tunnel spillways, differ significantly from those of the open surface spillways. In the latter, the width of the waterway is much larger than the depth of flow and hence the flow can be treated as two-dimensional. In the tunnel spillway, the depth and width of the flow are almost the same order of magnitude and hence the flow is essentially three-dimensional in nature. Consequently, a larger radius is required for the transition to be smooth and streamlined. A study of the existing installations reveal that the radius of the toe curve has varied from 2.5 to 10.5 times the diameter of the tunnel at the location of the beginning of the curvature. Too small of a radius may result in the detachment of the flow from the boundary and a possibility of intermittent sealing of the entire tunnel cross-section with a make-or-break siphonic action and surging. Too large of a radius would make the structure uneconomical. The radius of the toe curve should be finalized from model studies. As a rule of thumb, a conservative estimate of the radius for a preliminary design would be

$$R = 0.45\ H_t \tag{1}$$

Where H_t = Total head from MWL up to the inverted level of the tunnel at the end of the toe curve

- The downstream leg is horizontal or gently sloping in the downward direction. A transition from circular or horseshoe section to flat bottom rectangular section is required to provide an energy dissipater, generally a flip bucket or a stilling basin. However, the transition in the downstream leg of the tunnel, characterized by high velocity and large concentration of discharge has to be quite elaborate and may be very expensive. Several designs of energy dissipators have been developed that obviate the necessity of a transition.

High velocity flow in a partially filled conduit, such as in the downstream leg of a tunnel spillway, entrains air from the passage above the free water surface.

The quantity of air insufflated into the flow and air demand has been discussed in Chapter 8, paragraph 8.4.5, titled ''Air entrainment in tunnels flowing partly full.''

10.2.3 Other Forms of Discharge Tunnels

The construction of a tunnel profile conforming to an ogee profile at the top and a circular toe curve at the bottom requires extreme care in respect to alignment and surface finishing. When topography permits other, simpler forms of discharge tunnels are also possible. The ogee profile is constructed as a gravity section on the hill slope near the entrance. The tunnel then runs on a mild slope until its exit on the other side of the hill. An energy dissipator is provided here, either flip bucket or stilling basin, to suit the geological, topographical, and hydraulic conditions prevailing there. Tunnel spillways as shown in Figures 5 and 6 are, respectively, examples of such design.

A tunnel spillway of the aforementioned type could also be on a curved alignment in plan, provided the flow in the curved portion is pressurized. The pair of service spillways on the left abutment of El Cajon dam, Honduras, (Boesch et al. 1979) as shown in Figure 7 have been provided with pressurized flow up to the end of curvature and thereafter free surface flow leading to flip buckets.

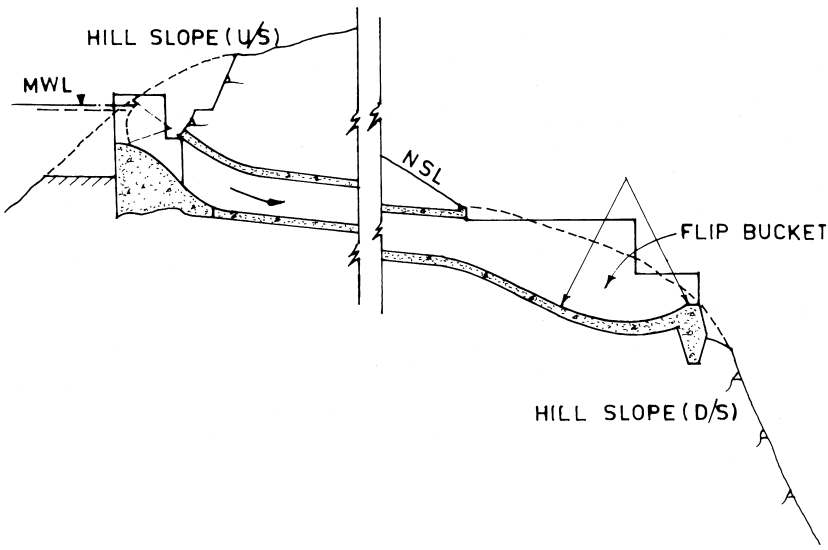

Figure 5 Tunnel spillway on mild slope terminating in flip bucket.

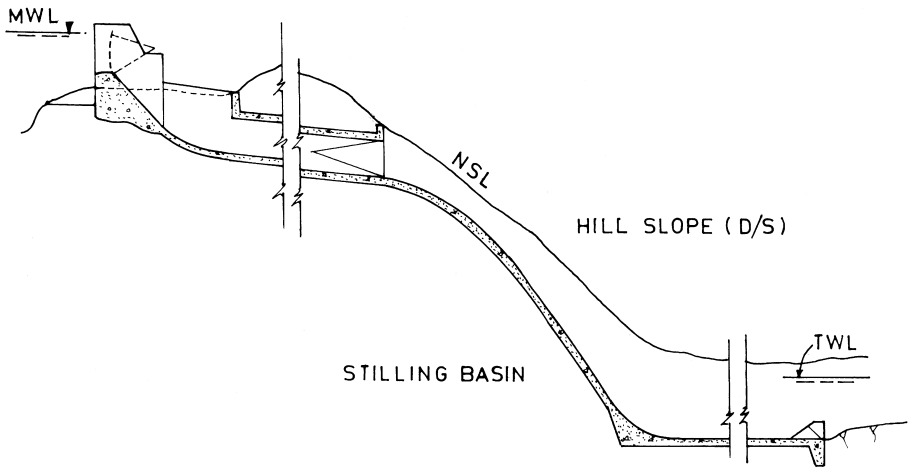

Figure 6 Tunnel spillway on mild slope terminating in stilling basin.

10.3 CULVERT SPILLWAY

A culvert spillway is a simple conduit, of any cross-section, placed through the dam, or along the abutment, generally on a uniform grade with its entrance placed vertically or inclined. Culverts can also be used for filling and emptying of lock chambers, outlet conduits for dams and tanks, turnout structures for irrigation canals, drainage opening below highways and railways, et cetera.

A great variety of flow phenomena can occur in a culvert spillway. It may flow full, partly full, with submerged or unsubmerged outlet, or on either mild or steep slopes. A number of parameters determine the flow condition in a culvert. However, when a culvert is intended to be used as a spillway, it is desirable to design it to flow full at design discharge, since a large discharge can be handled in a given section and a given inlet head.

A culvert will flow full when its outlet is submerged or when the outlet is not submerged, but the headwater is high and the barrel is long. Generally, when the head water H is equal or greater than 1.5 D, the culvert will run full, where D is the diameter of the culvert. If the culvert has a square edge at the top of the entrance, it will not flow full even if the entrance is below the headwater level and the outlet is not submerged. Such a culvert is considered hydraulically short. Carter (1957) has prepared charts that may be used to distinguish roughly between a hydraulically short and a hydraulically long culvert.

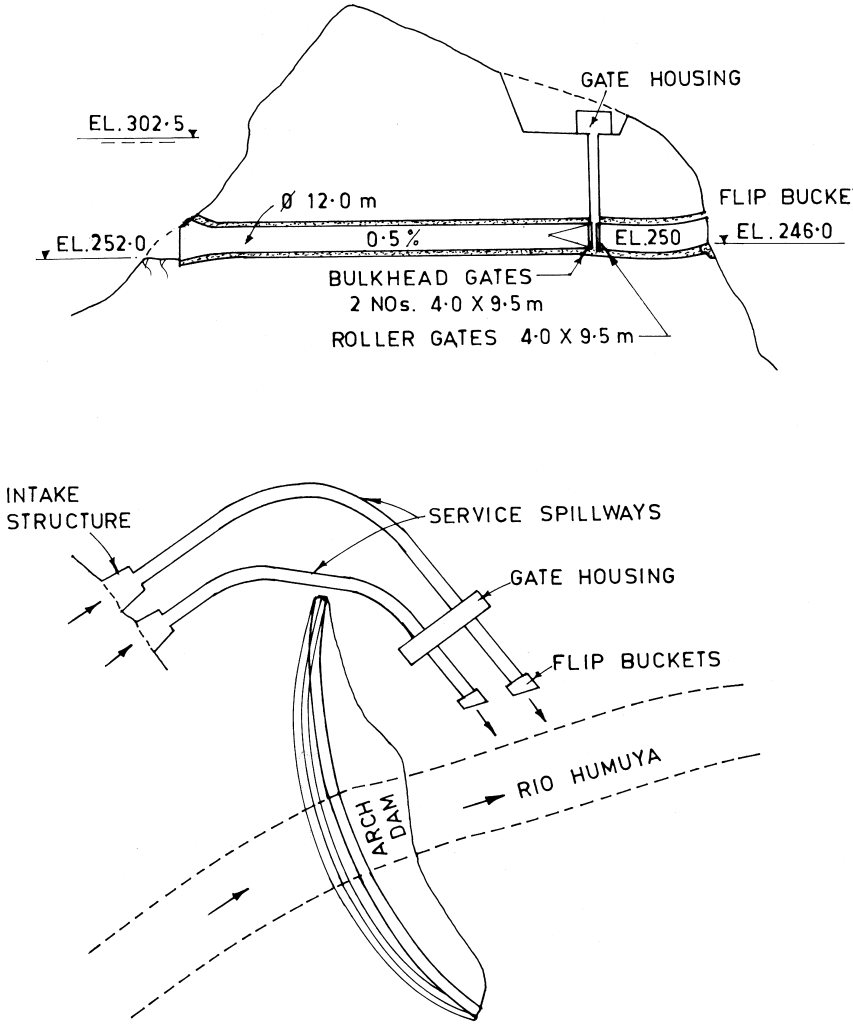

Figure 7 Service spillway tunnels: El Cajon dam, Honduras. (Boesch et al. 1979)

Two main considerations in the design of a culvert spillway are

- Ensuring full bore flow, at least for the design discharge, if the outlet is not submerged.
- Limiting the sub-atmospheric pressures at the inlet crown so as to prevent cavitation.

10.3.1 Full Bore Flow (Pipe culverts)

Preventing the inlet constriction, either by backwater produced by high tail water or by rounding the inlet, can inhibit part full flow. A radius of 1/7 pipe diameter or greater will theoretically eliminate all contractions. Model studies have shown that even on steep slopes with free outlets, the culvert with a rounded inlet will flow full if H/D exceeds unity. Subsequent prototype field tests, however, have not always confirmed the model results on the rounded inlets. Maintenance of full flow requires maintenance of siphon action near the inlet and this is easier to secure in a laboratory than in the field. Various devices have been developed to inhibit the formation of inlet vortices. Various forms of ''tapered inlets'' have been extensively tested by French (1964).

Blaisdell (1960) has shown that even a short steep culvert of circular section can be made to run full at low heads if the inlet is formed by cutting the culvert at an angle so that the soffit projects beyond the invert, as shown in Figure 8, and this is called hood inlet.

It is established that the optimum hood length, L_h, is equal to 3/4 D and for that value of hood length the culvert would prime and run full if H/D exceeds 1.25 for slopes S_0 up to $\tan\theta = 0.361$. A vortex inhibitor such as vertical splitter, also shown in Figure 8 is recommended.

A disadvantage of this type of inlet is that the combination of the anti-vortex plate and re-entrant inlet increases the inlet loss coefficient to almost 1.0,

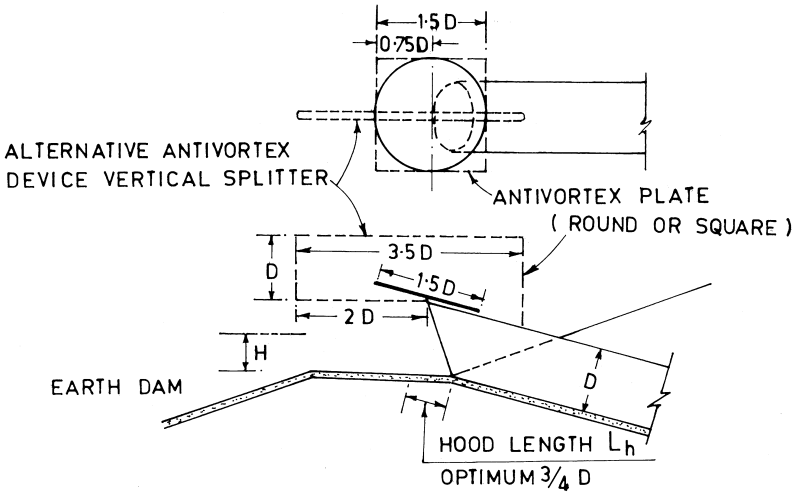

Figure 8 Circular culvert with hood inlet. (Blaisdell, 1960)

thus reducing the gain in flow energy due to the siphonic action. The following discharge relationships are available;

$$\frac{Q}{D^2\sqrt{gD}} = 0.48[S_0 / 0.4]^{0.05}[H / D]^{1.9}.. \quad (2)$$

For $0 < H/D < 0.8$

$$\frac{Q}{D^2\sqrt{gD}} = 0.44[S_0 / 0.4]^{0.05}[H / D]^{1.5}.. \quad (3)$$

For $0.8 < H/D < 1.2$

where

$Q =$ Discharge
$S_0 =$ Culvert slope

If the full bore flow is obtained without introducing the hood and without submerging the outlet, then

For a well rounded inlet,

$$Q = A\sqrt{\frac{2g(H + \frac{V_a^2}{2g} + S_0 L)}{1 + f\frac{L}{D}}}. \quad (4)$$

For a sharp edged inlet,

$$Q = A\sqrt{\frac{2g(H + \frac{V_a^2}{2g} + S_0 L)}{1.4 + f\frac{L}{D}}}.. \quad (5)$$

where

$V_a =$ Velocity of approach
$L =$ Length of culvert
$A =$ Cross sectional area of culvert
$F =$ Darcy resistance coefficient

10.3.2 Box and MEL Culverts

Culverts of square or rectangular section are known as box culverts. Presumably, the hood invert principle could be applied to this type as well to the circular culvert, but the relevant experimental results are not available. The following discharge relationships are available for short, steep box culverts that do not run full.

For H/D $<$ 1.2,

$$Q = 2 / 3\ C_b\ BH \sqrt{2/3gH} \tag{6}$$

For H/D $>$ 1.2,

$$Q = C_b\ BD \sqrt{2g[H - C_hD]} \tag{7}$$

where

C_b = Coefficient of width contraction
= 1 for rounded edges with radius = 0.1 B or more
= 0.9 for square edges

C_h = Coefficient of contraction in vertical plane
= 0.8 for rounded soffit and vertical edges
= 0.6 for square edges

B = Width of culvert

D = Height of the culvert

For further details on discharge characteristics of pipe and box culverts refer to the US Bureau of Public Roads Circular No. 10 (1965). A design example for a pipe culvert spillway flowing partly full has been given by USBR (1977).

In recent years, a special design of box culvert designated as the Minimum Energy Loss, or MEL. culvert has been popularized in Australia and New Zealand. Chanson (1999) has explained the concept of the design and given the design procedure for the MEL culverts. The culvert is designed such that there is practically no loss of energy or a minimum loss of energy.

10.4 CONDUIT PRESSURES

When the grade of a culvert spillway flowing full bore is greater than the friction slope, the pressure gradient will lie below the center of the pipe, as shown in Figure 9 The difference in head between this hydraulic gradient and any point on the pipe vertically above it will be the measure of the sub-atmospheric pressure existing at that point. Cavitation will occur when the sub-atmospheric pressure approaches one atmosphere, so that the residual absolute pressure is near vapor pressure. To avoid cavitation along the pipe surface, the minimum absolute pressure must be limited to some value greater than vapor pressure.

The pressure reduction will be greatest at the crown immediately downstream from the entrance. Any pressure drop caused by an inlet contraction such as sharp-edged or contracted opening can reduce it further. Generally, the residual pressure should not be less than about 3 m absolute to avoid cavitation.

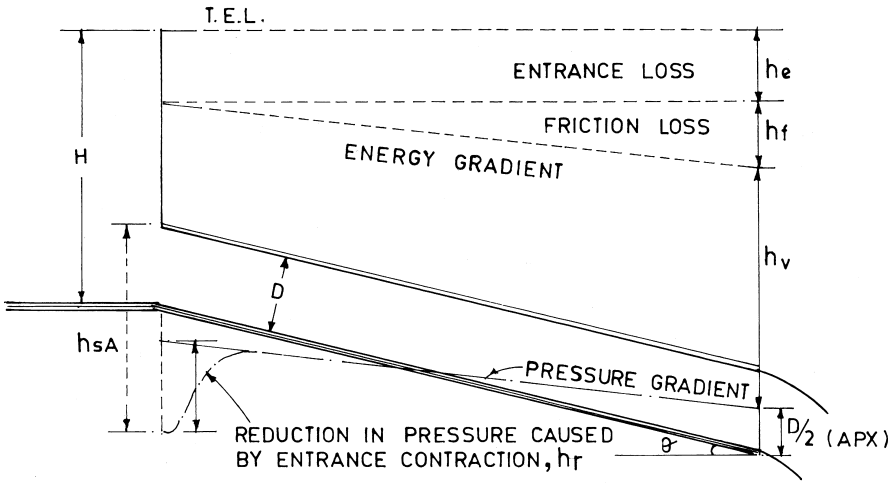

Figure 9 Pressure gradient for pipe culvert running full bore with outlet unsubmerged: h_{sA} = Sub -atmospheric pressure head on crown of inlet.

Notations

A = Cross sectional area of culvert
B = Width of culvert
C_b = Coefficient of width contraction
C_h = Coefficient of contraction in vertical plane
D = Diameter of pipe culvert
= Vertical height of box culvert
f = Darcy resistance coefficient
H = Depth of flow over the invert of culvert
H_t = Total head from MWL upto the invert level of the tunnel at the end of the toe Curve
h_e = Entrance loss
h_f = pipe friction loss
h_{sA} = sub-atmospheric pressure head on the crown
L = Length of the culvert
Q = Total discharge
R = Radius of the toe curve
S_0 = Slope of culvert = Tan θ

REFERENCES

1. Blaisdell, F. W. Hood Inlet for Closed Conduit Spillways. ASCE Jnl of Hyd Div, May 1960; Vol. 82, HY 5.
2. Boesch, A.; Aemmer, F. Spillways and outlet works for the El Cajon project, 13th ICOLD, Q50, R30. New Delhi, 1979.
3. Bribiesca, J. L. Transactions, Technical Sessions, Q 50, New Delhi, 1979; Vol. V, 528–532.
4. Carter, R. W. Computation of peak discharge at culverts, US Geological Survey Circular No. 376, 1957.
5. Chanson, H The Hydraulics of Open Channel Flow-An Introduction: Chapt 19 Arnold Publications. London, 1999.
6. Falvey, H. T. Cavitation in Chutes and Spillways, USBR Engineering Monograph No 42, April 1990.
7. French, J. L Tapered Inlets for Pipe culverts. ASCE Jnl of Hyd Div, March 1964.
8. Herbrand, K; Scheuerlien, H. C. Examples of model tests dealing with special problems and design criteria at large capacity spillways, 13th ICOLD, Q 50, R 10, 1979.
9. USBR Design of Small dams, 1977.
10. U.S. Bureau of Public Roads Capacity charts for the hydraulic design of highway culverts, Hydraulic engineering Circular No 10, March 1965.

11
Free Jet and Straight Drop Spillways

11.1 INTRODUCTION

Free jet spillways are most suitable for arch dams where the water jet leaves from either a short crested sill at the top of the dam, or a middle level or low level short length outlet with its exit shaped in the form of a deflector. Arch dams of height exceeding 200 m are not unusual and some dams while in planning or construction will be about 300 m in height. The main concern in the design of free jet spillways is either the deep scour just downstream of the dam (as in the case of a deflected jet) or impact forces on the stilling basin floor at the foot of the dam (with a free falling jet).

The straight drop spillway commonly installed in small drainage structures, also known as the box inlet drop spillway, is simply a rectangular box open at the top and at the downstream end from where a free jet falls freely at the base. Here, the emphasis is on ensuring maximum dissipation of energy by hydraulic jump or impact with the help of appurtenances.

11.2 FREE JET SPILLWAYS: DESIGN CONSIDERATIONS

The choice of the type of discharge structure—whether to have a free over-fall over a crest or a deep-seated bottom outlet—depends largely on the volume of flood to be disposed, width of the gorge, and the characteristics of the rock forming the gorge and riverbed. For large flood flows, longer crest length would be required which may not be available with narrow gorge and hence deep-seated bottom outlets may be suitable. However, a deep scour hole in the riverbed may pose problems of bank stability. With free over-fall over the top, the jet would fall very near the base of the dam where a concrete-lined stilling basin would be necessary to prevent undermining. Dissipating energy in the stilling basin is achieved through impact of the overflowing jet and its diffusion in the mass of

water. The bedrock there should be competent enough to withstand the impact load and hold the stilling basin floor anchored to it. With deep-seated outlets, the operation of control gates may be more problematic as compared to the free surface gates on overflow crests.

Sometimes, strategic considerations have dictated the choice of deep-seated outlets in preference to surface spillways; as for example, to protect the operating system against acts of sabotage or bombing, the submerged outlets have proved to be more reliable.

11.2.1 Overflow Crest

Overflow crest profiles on the top of arch dams have to be adjusted with overhangs either on the upstream, downstream, or on both the sides, since the width available at the top is seldom adequate to base an overflow profile. A standard ogee profile (WES type) or parabolic profile is suitable with the required overhang. Generally, three types of profiles are used:

- Profiles terminating such that the overflow jet is directed to fall on the concrete apron for the entire range of discharges. Typical examples are: the crest profiles of Devil's Gate spillway, Australia, Vouglans dam, France, and Beznar dam, Granada (Fig. 1)
- Profiles with nappe splitters to effect aeration of the jet and spreading over larger area as in the case of P.K.Le Roux dam, South Africa, Palawan dam, Rhodesia, Victoria dam, Sri Lanka, and Madupatty dam, India, etc. (Fig. 2)
- Profiles with ski jump buckets to deflect the jet far away, as in the case of Crystal dam, US and Inguri dam, Russia, as shown in Figure 3

11.2.2 Stilling Basin

The stilling basin design involves determining the elevation of the invert vis-à-vis water cushion, length, and other structural elements such as thickness of the concrete, reinforcement, and anchorage into the bedrock. However, there are no set rules or procedure for design of such stilling basins. The behavior of the water jet in air, in the mass of water, and pressures or forces exerted on the floor have to be taken into account, considering the prevailing standards adopted for such structures in different countries.

11.3 CHARACTERISTICS OF THE FREE FALLING JETS

Many investigators have studied the characteristics of the free falling, vertical jets of circular cross-section that issue from the nozzles or orifices, jets of rectan-

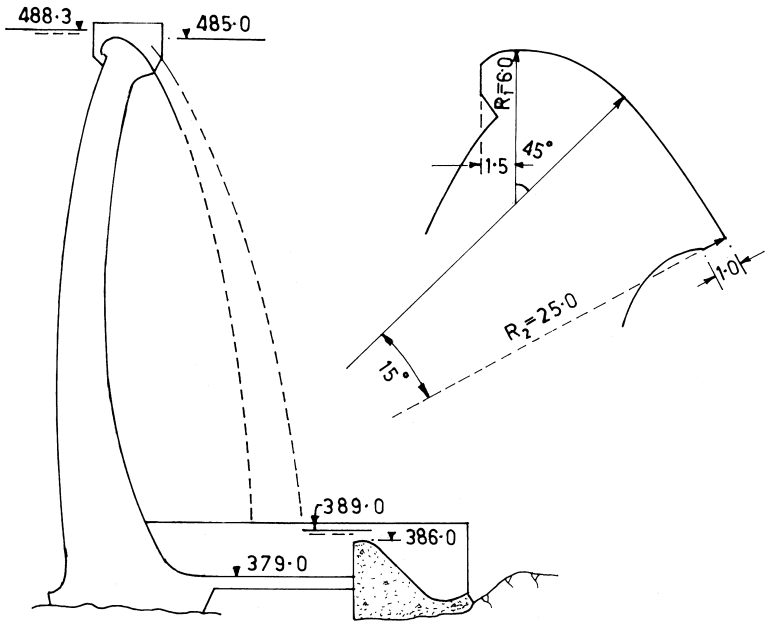

Figure 1 Overflow profile of Beznar dam.

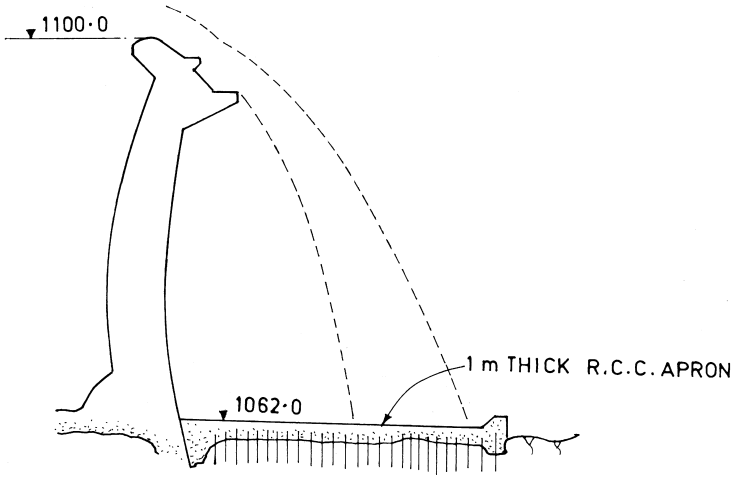

Figure 2 Overflow profile with nappe splitters, Palawan dam.

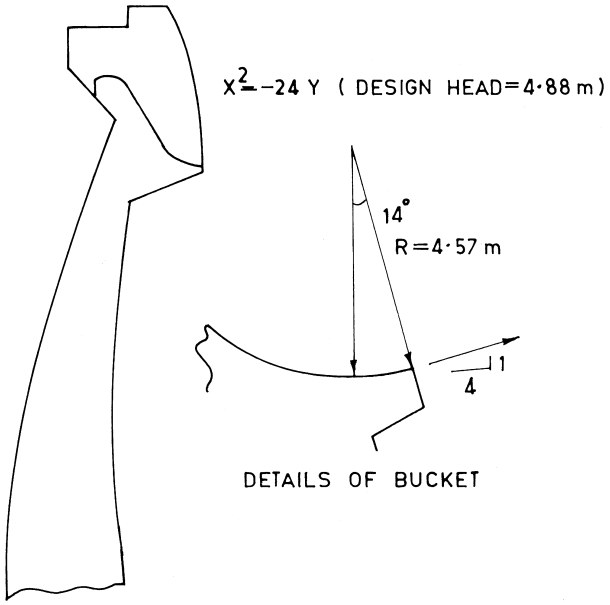

Figure 3 Overflow profile with ski jump bucket.

gular cross-section, and nappes. These included plunging jets and submerged jets. Plunging jets traverse some distance in the air before striking the water surface and may also break down due to turbulence if falling from a considerable height. Submerged jets are practically intact while penetrating the mass of water. Various characteristics studied include the spread and diffusion in the mass of water and energy and pressures imparted on the pool bottom. The volume of air present in the pool also influences these properties.

Although considerable work has been done on the above aspects, the results are predominantly empirical and have limited application to the design of the stilling basin for free jet spillways. The jets issuing from free jet spillways are either square or rectangular in cross-sections (jets issuing from bottom outlets or wide and thin nappes) falling down the overflow crests, and are often inclined while striking the water surface. In such cases, applying results of vertical circular jets requires careful consideration. The jets issuing from high dams may have been broken down while striking the water surface; however, very little information is available on the behavior of such jets in the pool. The design of the stilling basin, particularly the stability of the floor slab against uplift forces, warrants a specific model study. Nevertheless, the available information enables a preliminary design, in conjunction with some guidelines derived from a number of model studies.

Studies by Ervine et al. (1997) deal comprehensively with the circular water jet issuing from a nozzle, from its origin, and its travel in air up to its striking the water surface and further down in the mass of water up to the bottom. In these studies, the distance from the origin up to its striking the water surface—the jet drop length l—was less than half the length required for the jet to break down, and hence the jet was virtually intact at the point of impingement. The jet drop length l has been divided into three zones: A, B, and C as shown in Figure 4. Zone A is the region of growing instability characterized by waves and vortices. In zone B, the vortices break down into turbulence. The turbulence surface disturbances grow linearly with the square root of distance from origin of the jet. Air enters into the jet by flowing almost normal to the axis of the jet. The air motion parallel to the direction of the jet is negligible. Thus, shear between the jet and the surrounding air is small. In nature, mist forms around the falling jet. Instead of moving rapidly with the falling jet, the mist slowly flows towards the jet.

When the turbulence surface fluctuations are large enough to penetrate the core of the jet, flow begins to break down into individual clumps of water. This is beginning of the Zone C. The distance up to this point is called the jet break up length l_b. Since the jet is a continuous mass, up to the break up point, two conflicting effects determine the diameter of the jet. These are the spread of the

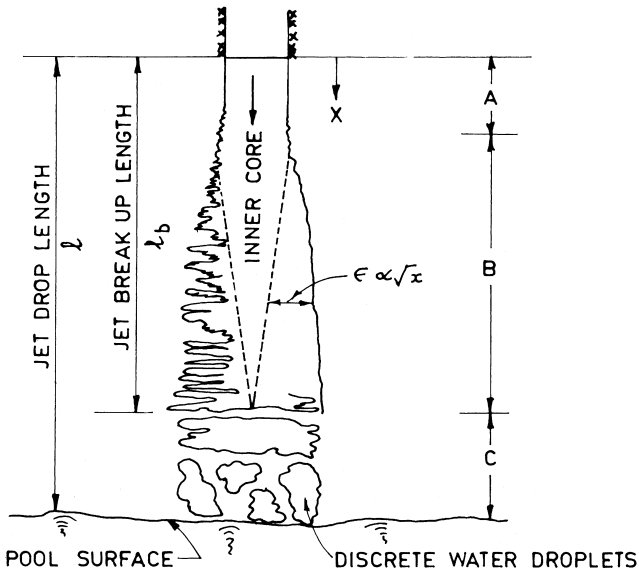

Figure 4 Structure of a free falling jet (shown in Ervine et al. 1997).

jet due to turbulence and the contraction of the jet due to gravitational acceleration. Ervine et al. (1997) give the following relationship:

The lateral spread ε (Fig. 4) is given by

$$\varepsilon = \frac{1.14 T_u U^2}{g}\left[\sqrt{\frac{2l_u}{D_o F_0^2}+1}-1\right] \tag{1}$$

where

T_u = Turbulence intensity defined as u'/U_0

U = Jet velocity at distance l_u measured from the origin

$= \sqrt{U_0^2 + 2gl_u}$

D_u = Jet diameter at the origin

$F_0 = U_0/\sqrt{g\, D_0}$

U_0 = Jet velocity at the origin

The turbulence intensity generally varies from 0 to about 5%.

The mean diameter of the jet core Dc, at any point during the plunge is given by

$$D_c = D_0\sqrt{\frac{U_0}{U}} \tag{2}$$

The jet break up length l_b is given implicitly as

$$C^2 = \frac{1}{\left(\frac{2l_b}{D_0 F_0^2}+1\right)\left(\sqrt{\frac{2l_b}{D_0 F_0^2}+1}-1\right)^2} \tag{3}$$

Where C is turbulence parameter defined as

$$C = 1.14 T_u F_0^2 \tag{4}$$

It has been shown that the theoretical relationship (Eq. 3) has been verified experimentally as

$$\frac{l_b}{D_0 F_0^2} = \frac{1.05}{C^{0.82}} \tag{5}$$

The air entrainment function $\beta = Q_a/.Q_w$ is given by

$$\beta = K_1\left[1-\frac{U_m}{U_j}\right]\sqrt{\frac{l}{D_j}} \tag{6}$$

where

U_m = Minimum velocity required to entrain air ≈1.1 m/s

U_j = Jet velocity at the entry to the pool surface

D_j = Jet diameter at the entry point
K_1 = A constant varying from 0.2 for smooth turbulent circular jets to 0.4 for very rough turbulent jets

For a jet of rectangular cross-section

$$\beta = 0.26 \frac{b_n}{p_n}\left[\frac{l}{d_n}\right]^{0.466}\left[1-\frac{U_m}{U_j}\right] \tag{7}$$

where

b_n = Nappe width
d_n = Nappe thickness
p_n = Nappe perimeter

The characteristics of circular jets that plunge into water have also been studied by Ervine et al. (1997). They have evolved parameters relating to the pressure distribution on the pool floor such as mean dynamic pressure, RMS fluctuation, maximum and minimum peak fluctuations, and their dominant frequencies, for $l/l_b<0.5$. The pertinent results are shown in Figure 5 The main conclusions are given below:

- The mean dynamic pressure coefficient $C_p = (P_m - y)/(U_j^2/2g)$ along the jet centerline is constant for $y/D_j < 4$. For $y/D_j > 20$, the dynamic head has decayed to zero. Here, D_j is the jet diameter at the entry point; P_m is the mean head on the transducer, and y is the pool depth.
- The RMS pressure fluctuation coefficient C_p reaches a value 0.2 in the plunge pool for depth equivalent of 6 jet diameters, increases with the jet break up parameter l/l_b until l/l_b reaches a value of 0.6. Thereafter, the coefficient decreases and becomes negligible for $l/l_b = 2$. Here, $C_p = P_{rms}/(U_j^2/2g)$, where P_{rms} is the RMS value of pressure head fluctuation, U_j is the jet entry velocity, l is the total drop of the jet and l_b is the jet break up length.
- The maximum pressure head coefficient $C_p^+ = (P_{max} - P_m)/(U_j^2/2g)$ reaches a value of 0.8 at a pool depth of y/Dj ≅ 10. The minimum pressure head coefficient $C_p^- = (P_m - P_{min})/(U_j^2/2g)$ reaches a value of 0.6 at $y/D_j \cong 5$.
- Pressure fluctuations in plunge pool exhibit two dominant frequencies corresponding to Strouhal number fy/U_j of 0.01 and 0.25, where f is the frequency of pressure fluctuations.

Although the experimental results have been presented for circular jets, the same can also be applied to jets of rectangular cross-section by calculating its equivalent diameter, if the aspect ratio is nearly equal to unity.

Hartung and Hausler (1973) have studied the behavior of submerged rectangular and circular jets plunging vertically into a mass of water. The jets were

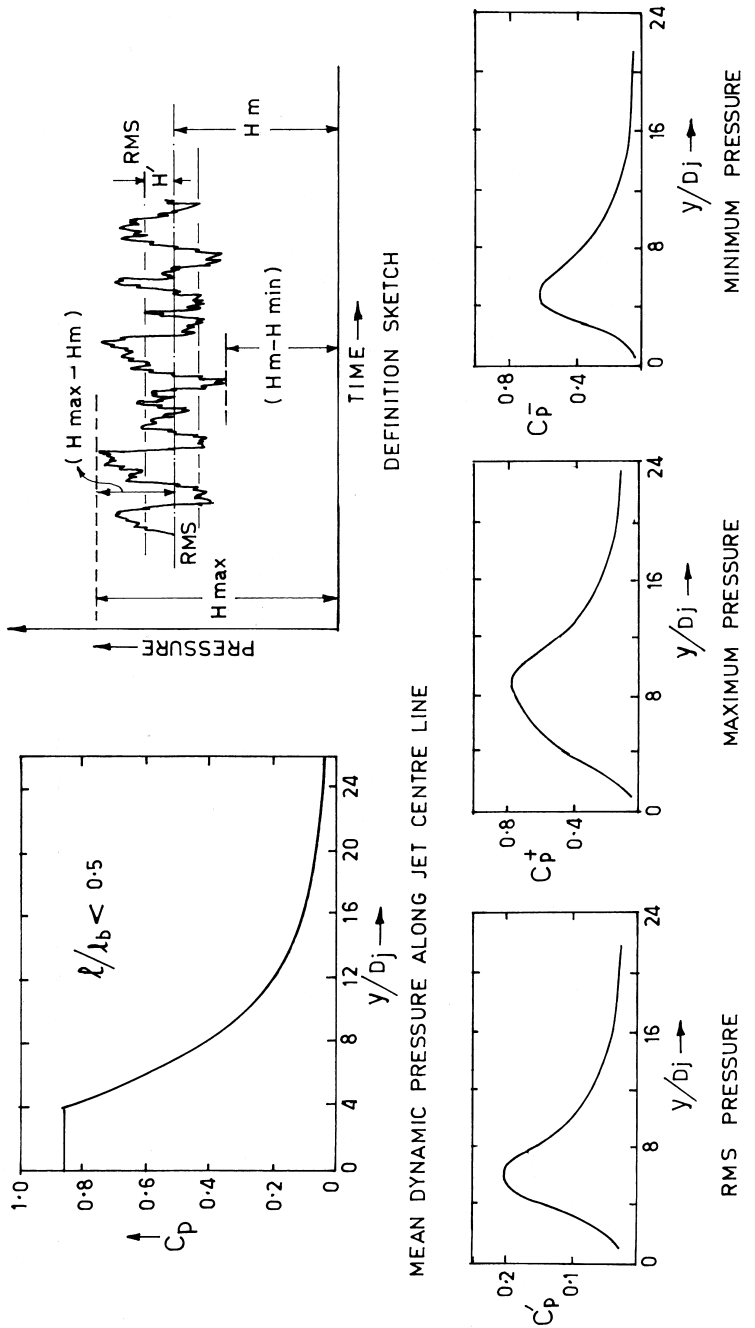

Figure 5 Characteristics of circular jets plunging into water (shown in Ervine et al.1997).

relatively intact while striking the pool surface. As the jet plunges into the pool it diffuses almost linearly. Water from the pool is entrained at the boundary of the jet. There are three regions in the pool defined by $y \leq y_k$ and $y > y_k$, as shown in Figure 6

1. $y < y_k$:
   In this region, $U_{max} = U_o$ in the entire core region where $U_0 =$ the jet velocity at the entrance into the pool
2. $y = y_k$: $y_k \approx 5$ width or 5 diameter
   A rectangular jet still retains about 80% of the initial energy, while a circular jet retains about 70% of the initial energy.
3. $y > y_k$:
   For practical purposes, the end of the jet may be defined as $y \approx 40$ width, with 30% of the initial energy still retained ≈ 20 diameter, with 15% of the initial energy still retained.

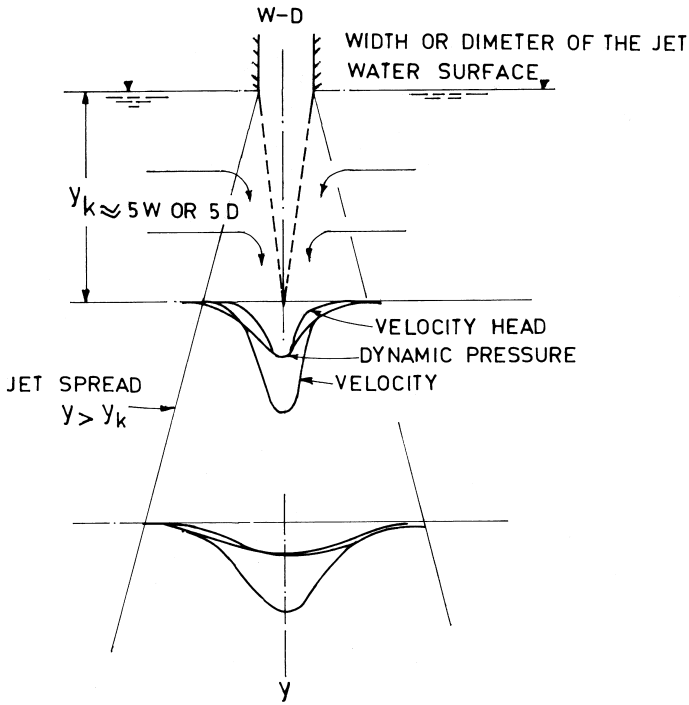

Figure 6 Submerged jet parameters (shown in Hartung et al. 1973).

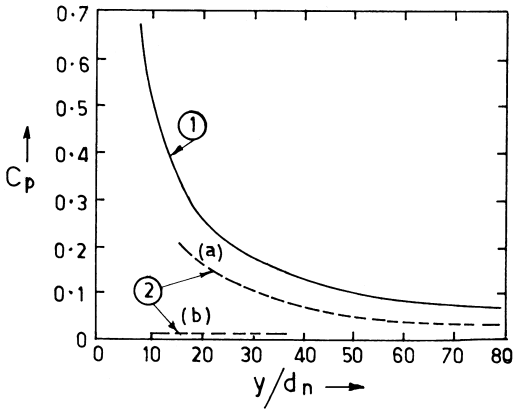

Figure 7 Rectangular jets: Variation of mean dynamic pressure (shown in Ervine et al. 1997):

① Hartung et al. (1973),
② Armengou (1991)
(a)$l/l_b = 0.9$
(b)$l/l_b = 2$

The analysis of the results of Hartung and Hausler (considering the jet entering the pool as intact), in respect of mean dynamic pressure, the coefficient Cp is shown in Figure 7. Superimposed on the same plot are the results of Armengou (1991) analyzed by Ervine et al. (1997) corresponding to the falling nappes with $l/l_b = 0.9$ and 2. It will be seen that the mean dynamic pressure decreases drastically when the fall length equals or exceeds the jet break-up length.

Martins and Viseu (1994) have presented some relationships concerning the design of slabs for plunge pools, which can also be applied for the stilling basin slabs:

1. Thickness of water cushion $y = 14\ d_n$ (8)
   Where d_n = jet thickness at the entrance to the water cushion. (This is considerably less than 40 d_n stated by Hartung et al. (1973)
   Alternatively

   $$y = 1.5\ y_c \quad (9)$$

2. Mean dynamic pressure

$$\overline{P_d} = 20\frac{q^{1.73}z^{0.395}}{g^{0.865}y^{1.99}} \text{.....} \quad (10)$$

where

q = Specific discharge

z = Fall from reservoir level to tail water level

Maximum value of pressure fluctuation P'_{max}

$$P'_{max} = 0.73(^{y/yc}) \quad (11)$$

3. Maximum dynamic pressure P_{max}

$$P_{max} = \overline{P}_d + P'_{max} = z \times 0.68(^{y/yc\ -1.5}) \quad (12)$$

It is also reported that the observed values of P'_{max} were close to three times standard deviation (σ) of the pressure fluctuations.

4. Pressures decrease extremely outside the point at which it was maximum, for instance, at a distance 0.3 y from this point, $\overline{P}_d$ was almost 10 times lower.
5. From the model studies conducted by Martins and Viseu for the plunge pool below the 51 m Viboras arch dam, Spain, it was found that the results were more or less conforming to Equation 11 and Equation 12 where as $\overline{P}_d$ (Eq. 10) were rather on lower side. The mean frequency of pressure fluctuations was 1.35 Hz and the mean uplift pressure on the slab at the instance of lifting was close to σ.

11.4 GUIDELINES FOR THE DESIGN OF A STILLING BASIN

Characteristics of the free falling jets can be applied to the design of various elements of the stilling basin. The design consists of determining geometrical elements such as length, width, and fixing the floor level with reference to the tail water elevation. The structural design involves consideration of the stability of the floor slab against fluctuating uplift forces. The design is usually finalized from hydraulic model studies. The following guidelines would be useful in preparing a preliminary design for purpose of further studies.

Length

The length of the basin should be adequate to contain the zone of impingement of the jet, and should include a length where the effect of impinging pressures is nullified or greatly reduced. This distance is approximately 1/3 y from the point of impingement.

Width

This may be equal to the width of the spillway, but often governed by the space available at the base of the spillway. In some cases orientation of the water jet is to be adjusted. This requires study of a hydraulic model.

Depth of the Water Cushion

The invert elevation of the stilling basin floor is generally set at or near the available bedrock. Deepening the basin to obtain larger depth of water cushion is generally avoided and instead artificial cushion by constructing a subsidiary dam or sill in the downstream, as in the case of Vouglans dam, France, [Ref-9], (Fig. 8) is preferred. However, there remains the question of dissipation of energy and protection downstream of the subsidiary dam.

Martins and Viseu (1994) have proposed Equations 8 and 9 for the water cushion.

Huang et al. (2001) suggest allowable upper limit of time average dynamic pressure (P_m-y), which indirectly gives the required value of y. The value of P_m should not exceed 30 m of water as per the practice in Japan, but restricted to 15 m according to the Chinese practice. When there are separate elements like surface spillway, middle outlet, bottom outlet, etc., the pressure resulting from the combined operation of all these, should also not exceed 15 m of water.

Finally, they suggest the volume-damping ratio

$$\eta = \frac{\gamma QZ}{V} \tag{13}$$

where

γ = Specific weight of water
Q = Total discharge

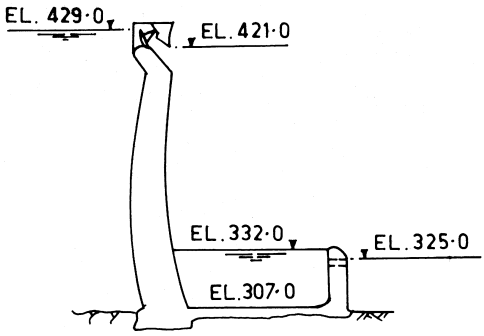

Figure 8 Vouglans dam, France (shown in 13th ICOLD 1979).

Z = Fall from MWL to TWL
V = Volume of water mass in the stilling basin

Equation 13 should be used in consonance with other criteria for the determination of the water cushion.

Stability of the Floor Slab

French National Committee on Large Dams (1979-a) have reported damages to the floor slabs of the 65 m Maury arch dam and 52 m Grangent arch dam, due to the impingement of the jet. An analysis revealed that damage was occurring whenever the jet power per unit area, P_u, imparted on the floor was exceeding 16 000 kW/sq.m. P_u is calculated as

$$P_u = \gamma \sqrt{2\, g\, H^3} \tag{14}$$

Where H = MWL- apron level.

However, the effect of other parameters such as the thickness of the slab, depth of water cushion, etc., is not reflected in the analysis. It is known that major damage can occur due to the dislodgement of the slab by dynamic uplift.

Dynamic uplift, responsible for lifting the floor slab monoliths, is caused by the transmission of fluctuating pressures beneath the slabs, through cracks, or unsealed joints between the monoliths. The zone, in the immediate vicinity of the jet impingement area, where the flow is reflected upward after striking the bed is characterized by intense pressure fluctuations—both above and below the mean pressure. It is in this zone, that pressure transmission is most likely, with fluctuating pressures acting on both the upper and lower faces of the slab. The uplift is caused when the instantaneous minimum pressure occurs on the upper face and the maximum pressure on the lower face, resulting in dislodgement of the slab from its joints. Even when all precautions are taken to ensure that the slabs are constructed as a surface of complete integrity, joints are sealed by effective water stops, and a comprehensive drainage system is provided beneath the floor to prevent generation of uplift, the required thickness is worked out assuming uplift resulting due to the pressure transmission as described before.

The uplift is resisted either by the submerged weight of the slab monolith alone or by the combined resistance offered by the submerged weight, anchorage force, and effective water stop between the joints. Usually, the latter alternative is selected.

Haung et al. (2001) suggest a basic relationship for the uplift as

$$\frac{P_1 + P_4 + P_s}{P_2 + P_3} \geq 1.3 \tag{15}$$

where

P_1 = Time average pressure
P_2 = Pulsating pressure
P_3 = Uplift
P_4 = Anchor rod tension, and
P_s = Submerged weight of the slab

Hydraulic model studies on a sufficiently large-scale model are necessary to assess these parameters. Model studies are also conducted simulating the slab monolith of various sizes, thicknesses, and weights to check the stability for various hydraulic conditions, as done by Anastasi et al. (1979).

11.5 NAPPE SPLITTERS AND DISPERSERS

If the free falling jet is aerated and spread, the forces on the basin slab or the depth of erosion downstream can be considerably reduced. Designs consisting of the combination of splitters and buckets with objectives of splitting the jets, aerating and colliding in the air, have been developed in South Africa and India.

Of particular interest is the profile equipped with nappe splitters, originally developed for dams in South Africa and later modified for Victoria dam, Sri Lanka. The splitter arrangement is shown in Figure 9. It consists of teeth projecting from the downstream face of the dam, immediately above a continuous projecting lip, also called cill. Correct proportioning of the arrangement can ensure that the two flows impact in the mid-air, break up the concentration of the jet, and cause it to fall as a disseminated spray. The teeth and cill are provided with aeration to protect them against possible cavitation.

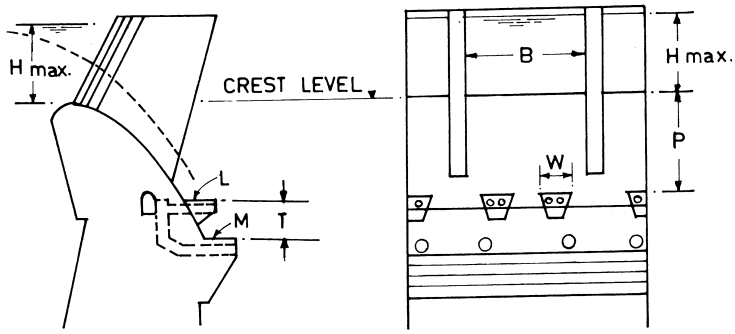

Figure 9 Details of nappe splitters. (Mason, 1983)

Based on the study and analysis of the performance of four dams equipped with splitters, Mason (1983) has modified the relationships between geometrical parameters, from those originally recommended by Roberts as early as 1936 for the Loksop and Vaalbank dams in South Africa. Referring to Figure 9, the recommended relationships are as follows;

$$P \cong H_{max} \tag{16}$$

$$M = L = T = 0.4\ P \tag{17}$$

$$W = 0.3\ P \tag{18}$$

$$\Sigma\ S = \Sigma\ W \text{ over the width of any one opening} \tag{19}$$

The effectiveness of the modified relationships has been demonstrated in the case of Victoria dam, Sri Lanka, where the mean dynamic pressure on the stilling basin floor, of 30 m and corresponding to the original geometry, was reduced to 18 m with the modified relationships, as reported by Back and Mee (1991) and shown in Figure 10

Pertinent details in respect of some of the spillways equipped with nappe splitters are given in Table 1.

Luthra (1950) evolved a design, termed bucket type splitters, while conducting model studies for the spillways with heights ranging from 40 m to 60 m and unit discharge from 20 to 30 cumec/m. In the nappe splitters, the jets interfere close to the spillway profile and fall at the toe or at a short distance downstream, while the bucket type splitter aims to throw the jet away from the dam. This

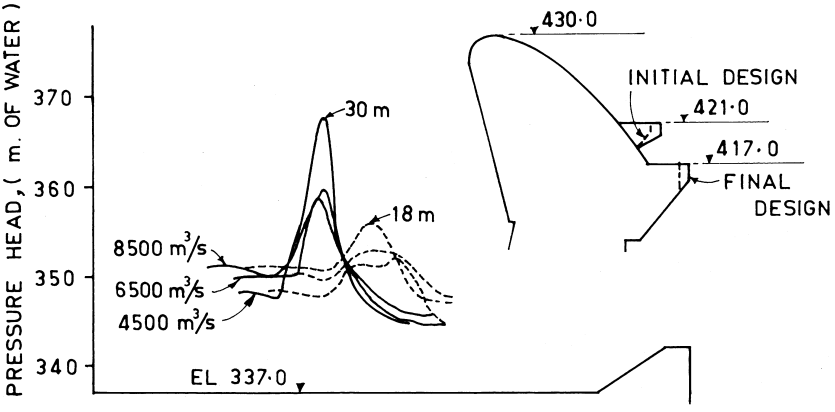

Figure 10 Victoria dam, Sri Lanka: Effect of splitter modification on impact pressures (shown in Back and Mee 1991). (Pressures on apren; —— Initial design, - - - - - Final design)

Table 1 Details of Spillways Provided with Nappe Splitters

Dam	Height, m*	q, m^2/s	TW cushion above floor, m	Thickness of Conc slab, m
Palawan	44	29	–	1.0
Hendrick Verwoerd	75	76	20	3.0
P K L Roux	98	57	30	3.0
Victoria	101	72.3	15.5	3.0

* From MWL to stilling basin floor elevation

design consists of a circular bucket in place of a level horizontal cill of the nappe splitter described earlier. The objective is to have the flow coming over the crest, split into two jets with one passing over the splitter blocks and the other passing over the bucket in such a way as to collide in the air. This serves two purposes: dissipation of part of the energy in the air and throwing away the air entrained mass of broken up jets at a safer distance off the toe of the dam. The suggested dimensions are:

H_{max}/P from 0.15 to 0.8
$W = S = L = 0.75\ T$
The clear drop of the jets from the splitters to the normal bed level downstream should not be less than 10–12 m.
The splitters and the bucket can be afforded protection against cavitation by artificial aeration on the sides or bottom.
The geometry of the splitters and the bucket can be calculated or finalized from model study to obtain the required throw of the jets.

The spillway of Madupatty dam, India, constructed in 1957, has been provided with bucket type splitters, as shown in Figure 11. It has been functioning satisfactory without any problem.

Singhal et al. (1978) have described a similar design consisting of bucket and splitters for the proposed 192 m Lakhwar dam, India. The 20 m deep stilling basin at the toe of the spillway will also serve for the reversible turbines of the power house and hence a flip bucket at the base of the spillway would not be suitable. An elevated bucket was therefore provided at about 33 m below the crest of the spillway, or about 127 m above the riverbed. Splitters were provided at a distance of 7.5 m above the bucket invert. Each span of 17 m width was provided with four splitters, 2 m wide each spaced at 1.5 m. The geometry of the bucket and splitters was finalized from model study. The splitters required artificial aeration through sides to minimize negative pressures. The air entrain-

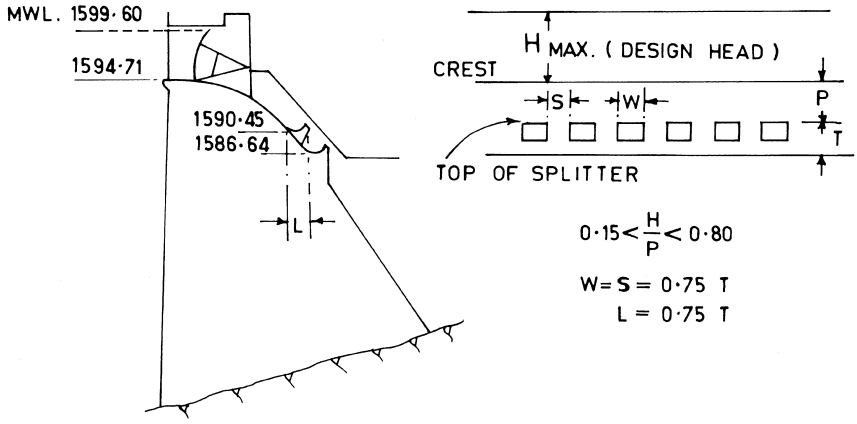

Figure 11 Bucket type of splitters—Madupatty dam (India), (Luthra-1950)

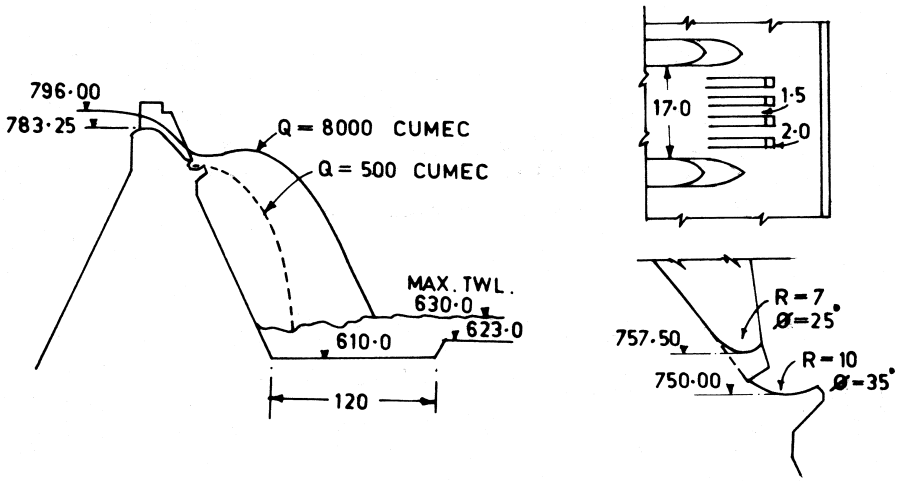

Figure 12 Bucket and splitters for Lakhwar dam, India (shown in Singhal et al. 1978).

ment and dispersion of the jets before penetration into the downstream water cushion resulted in reducing the impact pressures considerably and acceptable flow conditions in the stilling pool. Figure 12 shows the details of the spillway and buckets.

11.6 BOTTOM OUTLETS: DESIGN CONSIDERATIONS

Bottom outlets with their invert profiles shaped like upturned buckets or inclined towards downstream with dents, teeth, or splitters at the end are most suitable for arch dams located in narrow valleys. The objective is to have the jet issuing from the outlet impinge on the riverbed at as large of a distance as possible. It is desirable that the resulting scour hole is confined to the riverbed without endangering the stability of the banks or the main dam. The emphasis is therefore to affect maximum possible dissipation of energy of the jet before it strikes the riverbed. For this purpose, various means such as air entrainment, spreading of the jet, and collision of the jets issuing from two outlets, etc., are employed.

The number, size, and elevation of bottom outlets are governed by the discharge, the operating head, and the conditions to be obtained in the downstream. Often, the tendency is to provide multiple outlets (at the same elevation or at different elevations) of smaller size or capacity, rather than a single large sized one. At Cahora-Bassa, Mozambique, eight outlets, four on the left and four on the right side of the central axis, have been provided at the same elevation (Quintela et al.-1979). The operation sequence has been finalized from the model study to ensure that the jet impingement from the various outlets is spread over a length of about 300 m on the riverbed, as shown in 13, which also shows the profile of the bottom outlet of Cahora- Bassa dam.

Similar to the free surface flows down the crest, designs have also been developed for aerating and spreading the flows issuing from the bottom outlets. As for example, at La Barthe and Sainte-Croix dams, France, described in Reference 9, two outlets at the same elevation have been provided with dispersers and their orientation is such that the aerated jets issuing from outlets collide in the air before reaching the riverbed. The details of the dispersers provided at the outlet of Sainte-Croix dam, France, are shown in Figure 14. Jeanpierre (1979) has discussed its effectiveness in dispersing the jets in air.

Energy dissipation by collision of jets in air is also accomplished with outlets located at different elevations. The invert profiles are shaped so that the jets issuing from outlets collide in air during their flight, before impinging on the water surface. A common arrangement with multiple outlets with a stilling basin is shown in Figure 15a. Gao (1999) has analyzed existing structures in China and observed that stilling basins with this arrangement required rather excessive lengths: 1.67 to 2.04 times the difference in water levels upstream and downstream or 1.34 to 1.37 times the height of the dam. The reason for the excessive length is apparent from Fig. 15(a). It has to contain the farthest-

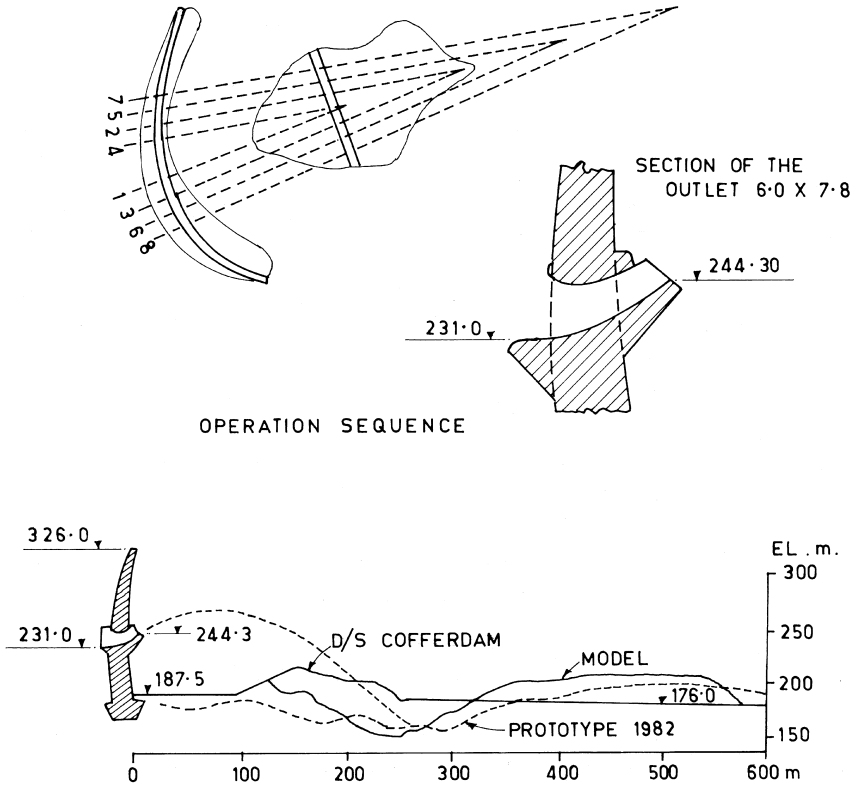

Figure 13 Cahora- Bassa dam bottom outlets, Mozambique (shown in Quintela et al. 1979).

reaching jet issuing from the middle level outlet. In order to achieve collision of the jet issuing from the middle level outlet with the jet issuing from the upper level outlet, the middle level jet is made to surpass the upper level jet. Gao points out yet another disadvantage with this arrangement, namely, that there is not a contribution of a sizeable volume of water contained in the pool, between the dam and the point of impingement of the upper level jet. In view of this, the arrangement as shown in Figure 11.15b is recommended. With this, the length of the basin is relatively shorter and the inactive water mass is reduced. Besides, the jet falling close to the dam tries to push the other jet on its downstream and provides a dynamic water cushion below this jet, flattening its angle of impingement, thereby decreasing the magnitude of pulsating pressures and increasing energy dissipation. This phenomenon has been studied on a numerical model employing the technique of large eddy simulation.

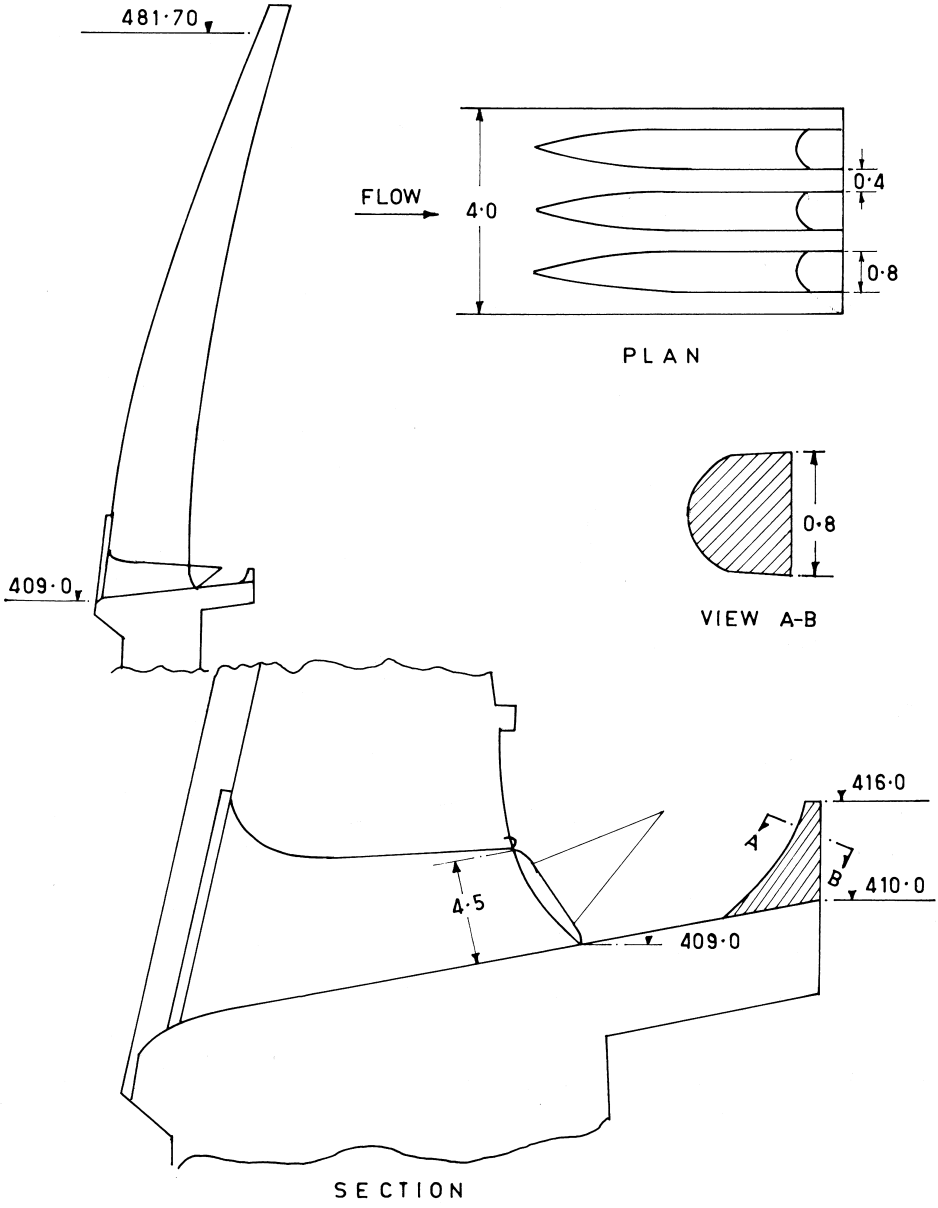

Figure 14 Sainte-Croix dam bottom: Outlet bucket with dispersers (shown in Jeanpierre 1979.

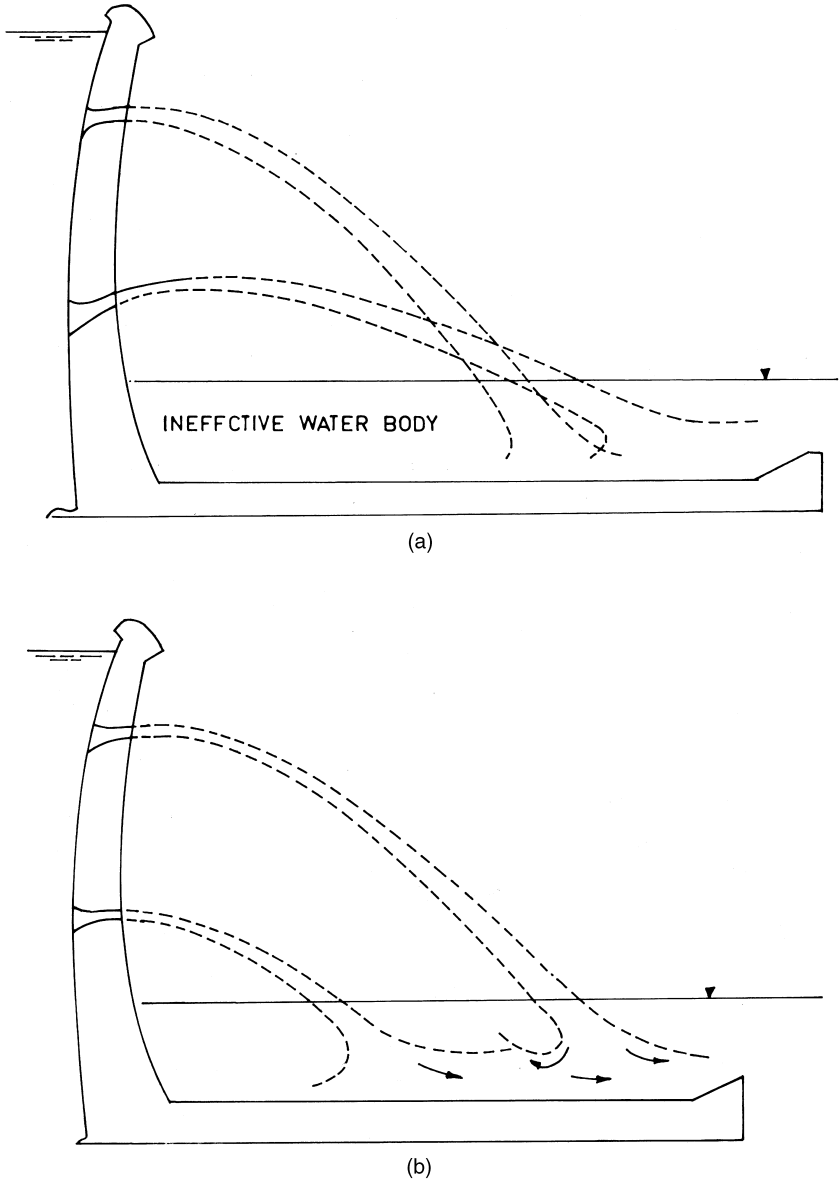

Figure 15 Comparative features of multiple level outlets (shown in Gao 1999).

Development of Scour

In regard to scour downstream of free jet spillways the following issues arise:

Prediction of scour
Reduction of scour
Protection against scour

A large number of relationships for depth of scour have been developed by various researchers. However, with the limited availability of information in respect of prototype structures, none of the formulas can be recommended. Quintela et al. (1982) have reported a prototype scour depth $d_s = 68$ m for Cahora-Bassa, corresponding to $q = 275$ m^2/s and $z = 101$ m. Relationships developed by Mason, Martins, Taraimovich give better predictions whereas the relationships for plunging jet scour overestimate the scour depth. For Kariba, the scour depth $d_s = 125$ m corresponds to $q = 155.6$ m^2/s, $z = 85$ m, $h_{ds} = 40$ m. The relationships of Mason (79 m) and Veronese (111 m) underestimate the scour, whereas the approach by Hartung and Hausler (1973), based on jet theory, gives $d_s = 138$ m which is fairly satisfactory. It would thus be seen that model study with semi-erodible bed, weakly aggregated with binding materials like aluminous cement, bantonite, gypsum, etc., would be the best means of predicting scour.

Dissipation of the energy of the jet before it strikes the riverbed is one of the alternatives of reducing the scour. Providing water cushions (plunge pools) at the location of jet impingement also controls the magnitude and extent of scour. Plunge pools in conjunction with air-entrained jet would be still more effective. If the jet is aerated 50% by volume, the depth of water cushion required for no scour is reduced to half of that required for the solid let without air entrainment, or in the absence of sufficient cushioning, the final scour depth could be reduced by 25% with total air entrainment and by 10% for partial air entrainment. It is believed that the presence of free air in the rock joints also influences the transient pressures generated due to impingement. The research on this topic is vigorously pursued in various laboratories (Ref- 23).

The most common reason for the protection is the scour taking place or approaching very near the base of the dam, threatening to undermine the base. It is therefore a common practice to provide a small concrete apron at the base of the dam. Such an apron should be laid in rock and properly anchored.

One of the measures of preventing the uncontrolled erosion at the foot of the dam is to dump concrete blocks in the scour hole as shown in Figure 16. The most effective shape of the blocks is the cube, giving optimum thickness for a given volume. Model studies are usually conducted for ascertaining the size of the cube and extent of the area to be covered.

In order to control the scour at Kariba dam, Hartung and Hausler (1973) have suggested providing a huge pre-stressed and anchored slab at the point of

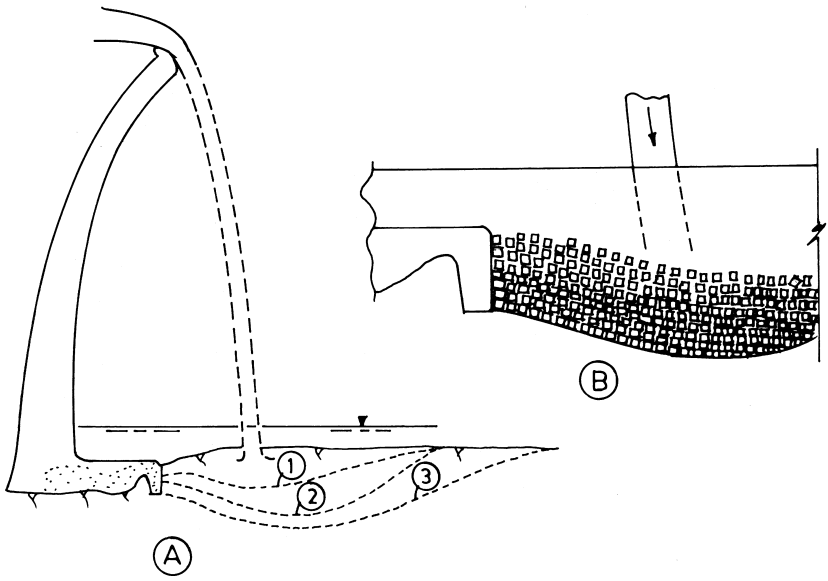

Figure 16 Protection with concrete blocks: one to three Development of scour.

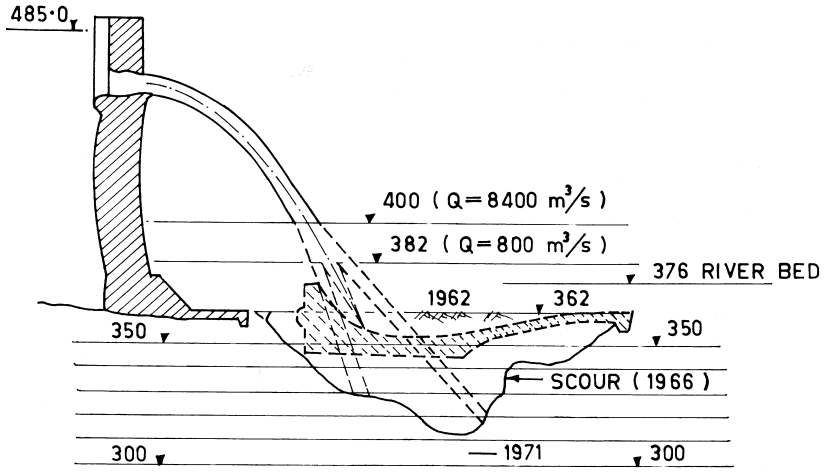

Figure 17 Protection suggested for Kariba dam (shown in Hartung et al. 1973).

impact as shown in Figure 17. The slab has to be of large enough extent to cover all points of impact for any spilling management policy and contain the hydraulic jump formed.

11.7 STRAIGHT DROP SPILLWAY

A straight drop spillway is one in which the flow drops freely from the crest. The underside of the nappe is ventilated sufficiently to prevent a pulsating, fluctuating jet. This type of spillway is most suitable for low earth-fill dams, for disposal structure for storm runoff schemes, and as canal falls.

The hydraulic conditions at the base of a straight drop spillway have been studied by Moore (1943), Bakhmeteff and Feodoroff (1943), and Rand (1955). As shown in Figure 18, the aerated free falling nappe will reverse its curvature and turn smoothly into supercritical flow on the apron.

The various parameters shown in Figure 18 can be described by functions of the drop number, defined as

$$D = \frac{q^2}{gh^3} \tag{20}$$

where

q = Discharge per unit width of the crest
H = Height of the drop

The relationships are

$$\frac{L_d}{h} = 4.30D^{0.27} \tag{21}$$

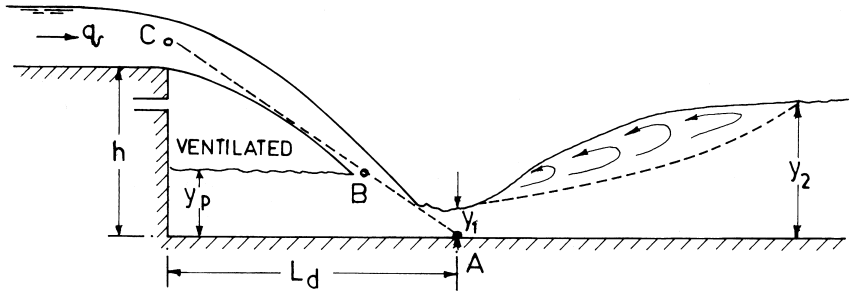

Figure 18 Flow geometry at the base of a straight drop spillway.

$$\frac{y_p}{h} = 1.0D^{0.22} \tag{22}$$

$$\frac{y_1}{h} = 0.54D^{0.425} \tag{23}$$

$$\frac{y_2}{h} = 1.66D^{0.27} \tag{24}$$

$$L_j = 6.9(y_2 - y_1) \tag{25}$$

where

L_d = Drop length i.e. the distance from the drop wall to the position of the depth y_1

y_p = Pool depth under the nappe

y_1 = Pre-jump depth at the toe of the nappe

y_2 = Tailwater depth sequent to y_1

The position of the depth y_1 can be approximately determined by the straight line ABC that joins the point A on the apron at the position of y_1, the point B on the axis of the nappe at the height of pool depth, and the point C on the axis of the nappe at the crest of the fall. The fact that these points lie on a straight line has been verified by experiments.

Utilizing the above characteristics, designs of straight drop spillways with energy dissipation achieved either by hydraulic jump or by impact have been developed by Donnely and Blaisdell (1954). The general dimensions are shown in Figure 19. These, along with the relationships in Equations 21 to Equations 25, would enable complete proportion of the simple drop structure.

Rajaratnam et al. (1995) have analyzed data of Moore (1943), Rand (1955), and their own data in respect to energy dissipation and proposed the following relationship:

$$\frac{E_1}{E} = 0.896\left(\frac{y_c}{h}\right)^{-0.766} \tag{26}$$

For the pool depth,

$$\frac{y_p}{h} = 1.107\left(\frac{y_c}{h}\right)^{0.719} \tag{27}$$

While all the studies were conducted with the sub-critical approach flow, Chamani and Beirami (2002) have included supercritical approach flow in their studies and presented generalized equations for calculating the relevant parameters. The procedure involves trial and error computations. An empirical relationship for energy loss is:

$$\frac{E_1}{E} = 0.0562\left(\frac{y_c}{h}\right)^{-1.032} F_1^{-0.559} \tag{28}$$

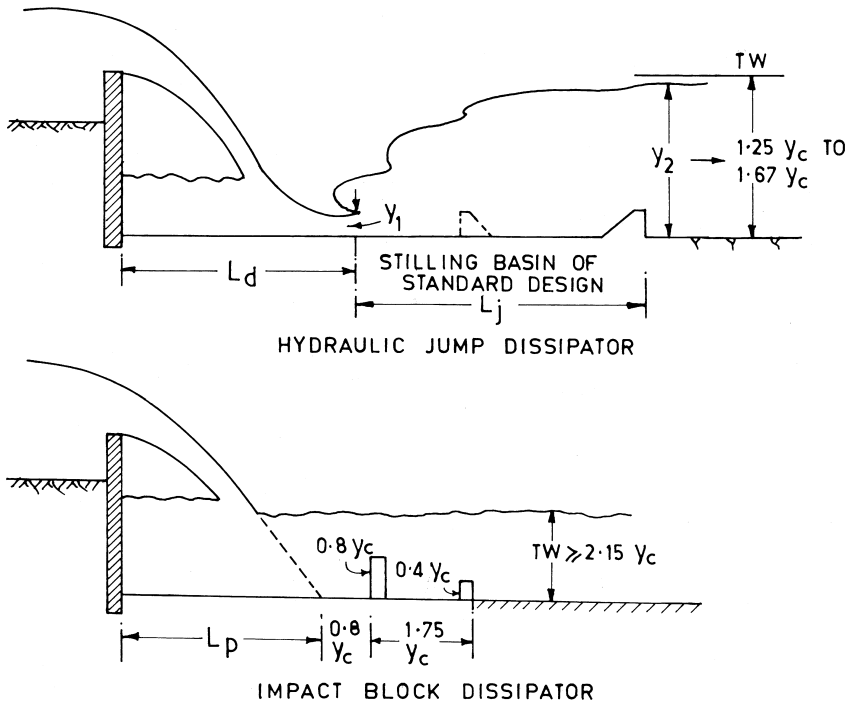

Figure 19 Energy dissipators for straight drop spillways.

Rajaratnam and Kwan (1996) have studied air entrainment characteristics of the drops. The results can contribute to the estimation of re-aeration of polluted streams below drops.

Notations

b_n = Nappe width
C = Turbulence parameter
C_p = RMS pressure fluctuation coefficient
C_p^+ = Maximum pressure head coefficient
C_p^- = Minimum pressure head coefficient
D = Drop number for straight- drop spillway
D_c = Mean diameter of the jet core
D_j = Jet diameter at entry point into the plunge pool
D_0 = Jet diameter at the origin

d_n = Nappe thickness
d_s = Depth of scour below tail water level
E = Initial energy at the free overfall
E_j = Energy loss due to formation of hydraulic jump
E_l = Energy loss at the base of a free over–fall
E_2 = Residual energy at the end of hydraulic jump
F_0 = Froude number given by $U_0/(2gD_0)^{1/2}$
f = Frequency of pressure fluctuations
H = MWL-Apron level
H_{max} = Maximum head of water over the crest of spillway
h = Height of drop for straight drop spillway
h_{ds} = Depth of tail water above original riverbed
K_1 = A constant defining turbulence
L = Length of splitter teeth
L_d = Drop length
l = Jet plunge length up to the pool water surface
l_b = Jet break up length
l_u = Distance of a point between the origin and jet break up point
M = Length of downstream lip of splitter
N = Number of teeth per gated opening
P = Distance between the spillway crest and top of the splitter
P_d = Mean dynamic pressure
P_{max} = Maximum dynamic pressure
P'_{max} = Maximum value of pressure fluctuation
P_{min} = Minimum instantaneous pressure
P_m = Mean pressure at the plunge pool floor
p_n = Nappe perimeter
Q = Total discharge
q = Discharge per unit width
S = spacing between splitter teeth
T = Level difference between splitter teeth and downstream lip
T_u = Turbulence intensity
U = Jet velocity at a distance l_u between the origin and pool surface
U_j = Jet velocity at entry to the pool surface
U_m = Minimum velocity required to entrain air $\approx$1.1 m/s
U_0 = Jet velocity at the origin
V = Volume of the stilling basin
W = Width of individual splitter tooth
y = Depth of water cushion
y_c = Critical depth
y_k = Core length of submerged jet
y_p = Pool depth under the nappe

y_0 = Depth of flow in the canal upstream of the fall
y_1 = Pre-jump depth/Depth at the toe of the nappe
y_2 = Tail water depth sequent to y_1
Z = Fall from MWL to tail water level
β = Air entrainment function- Q_a/Q_w
σ = Standard deviation of pressure fluctuation
η = Volume damping ratio
γ = Specific gravity of water

REFERENCES

1. Anastasi, G.; Bisaz, E.; Gerodetti, M.; Schaad, F.; Soubrier, G. Hydraulic and static dimensions of a stilling basin in respect to design and security of the floor slab for a high capacity spillway, 13 th ICOLD, Q 50, R 32. New Delhi, 1979.
2. Armengou, J. Disipacion de energia hidraulica a pie de presa en presas boveda, PhD thesis; Universitat Politechnica de Catalunya, Barcelona, Spain, 1991.
3. Back, P. A. A.; Mee, W. T. The Victoria Project, Sri Lanka: Project planning and design of Victoria dam, Proc. Instn Civ Engrs, Part I, 1991, 281–311.
4. Bakhmeteff, B. A.; Feodoroff, N. V. Discussion on the paper Energy loss at the base of free overfall by Moore. Trans ASCE, 1943; Vol. 108.
5. Chamani, M. R.; Beirami, M. K. Flow characteristics at drops. ASCE Jnl of Hyd Engg, Aug 2002; Vol. 128, No 8.
6. Donnely, C. A.; Blaisdell, F. W. Straight Drop Spillway Stilling Basin, SAF laboratory Technical Paper no. 15, Series B, Nov 1954.
7. Ervine, D. A.; Falvey, H. T.; Wither, W. Pressure fluctuations on plunge pool floors. IAHR Jnl of Hydraulic Research, 1997; Vol. 35, No 2.
8. French Committee on Large Dams Degradations observees dans la zone D'impact de la lame deversante, 13 th ICOLD, Q 50, R 38. New Delhi, 1979.
9. French Committee on Large Dams Ouvrages D'evacuation de Grande Capacite, 13 th ICOLD, Q 50, R 61. New Delhi, 1979.
10. Gao, J. High efficiency of energy dissipation by double layers of jets and super-short plunge pool, Proc. 28th IAHR Congress, Graz: Austria, 1999.
11. Hartung, F.; Hausler, E. Scours, Stilling Basins and Downstream Protection Under Free Overfall Jets at Dams, 11 th ICOLD, Madrid, 1973.
12. Haung, Guobing; Wang, Caihuan Analysis of energy dissipation effect of cushion pool and stress characteristics & stability of base slab, Proc 29th IAHR Congress, 2001.
13. Jeanpierre, D. Precesions sur le fonctionnement de l'evacuateur de crue du barrage de Sainte – Croix (Verdon), 13 th ICOLD, Technical Sessions, Q50. New Delhi, 1979, 563–66.
14. Luthra, S. D. L Dissipation of energy below overfall dams, Irrigation and Power, CBIP, Nov 1950.
15. Martins, R.; Viseu, T. Plunge pool slab design taking into account turbulent pressures, 9 th APD-IAHR Congress, August, 1994.

16. Mason, P. J. Energy dissipating crest splitters for concrete dams, Water Power and Dam Construction, November, 1983.
17. Moore, W. L. Energy loss at the base of a free overfall. Trans ASCE, 1943; Vol. 108.
18. Quintela, A. C.; Fernandes, J. S.; Cruz, A. A. Barrage de Cahora-Bassa Problemes poses par le passage des crues pendant et apres la construction, 13 th ICOLD, Q 50, R 41. New Delhi, 1979.
19. Quintela, A. C.; Cruz, A. A. Cahora-Bassa Dam Spillway Conception, Hydraulic model studies and Prototype Behaviour, Trans Intnl Symp on the Layout of Dams in Narrow Gorges, ICOLD. Brazil, 1982.
20. Rajaratnam, N.; Chamani, M. R. IAHR Energy loss at drpos. Jnl of Hyd Research, 1995; Vol. 33, No 3.
21. Rajaratnam, N.; Kwan, A. Y. P. Air entrainment at drops. Jnl of Hyd Research, IAHR, 1996; Vol. 34, No 5.
22. Rand, W. Flow geometry at straight drop soillways. Trans ASCE, Sept 1955; Vol. 81.
23. Schleiss, W., Bollaert, W., (Eds).; Rock Scour due to High-velocity Jets, ©; Swets & Zeitlinger, Lisse, ISBN 90 5809 518 5, 2002.
24. Singhal, M. K.; Mohan, M. K.; Jagdish, M. K.; Tiagi, S. S. Elevated trajectory bucket for Lakhwar spillway, 47th Annual Research Session; CBIP, Hubli-Dharwad: India, Nov 1978; Vol. II.
25. Taraimovich, I. I. Deformation of channels below high head spillways on rock foundation, Hydrotechnical construction, Sept. 1978.
26. USBR Design of Small Dams, 1977.
27. USBR Hydraulic design of Stilling Basins and Energy Dissipators, Engineering Monograph, 1978.
28. Veronese, A. Erosion of a bed dowsntream from an outlet: Colorado A & M College. Colorado, 1978.
29. WES Hydraulic Design Criteria, Sheets 623 to 624-1, Drop Structures, 1973.

12
Fuse Plugs and Fuse Gate Spillways

12.1 INTRODUCTION

Approximately one-third of dam failures can be attributed to inadequate spillway capacity. This means that all existing dams need to be critically analyzed in terms of spillway design flood to ensure that the available spillway capacity is adequate to meet the design flood or that the expected short fall is made up with other suitable means, such as increasing the depth of overflow, widening the existing spillway, or the provision of additional spillways. On existing dams, such measures may not be practical or may involve high investment costs, particularly because such additional capacity may be needed only for the floods of very low probability. It has been found that construction of a properly designed erodible fuse plug embankment is a safe and often economical alternative.

In recent years, a fuse gate alternative has also become available that has the advantages of an uncontrolled spillway while maximizing the storage capacity of the reservoir and providing adequate safety of the dam.

12.2 FUSE PLUG

Fuse plug, or a breaching section, is an erodible predetermined separate section of an earth dam designed to wash out when the inflow is in excess of the spillway capacity and the reservoir behind it reaches a specified level. The fuse plug collapses gradually over a reasonable time frame when overtopped, releasing surplus flood without endangering the safety of the main dam and lowering the reservoir level. An uncontrolled auxiliary spillway with a higher crest elevation would also serve the same purpose, however, the length of such a spillway would be very large in order to keep the depth of overflow as small as desired. A fuse plug can be provided in a shorter length by envisaging development of a deeper channel in downstream as the fuse plug embankment gets washed away.

12.2.1 Criteria for Selection of Fuse Plug

Whether a fuse plug embankment can be introduced in an existing or a proposed dam will depend upon a number of factors discussed next (Murthy et al. 1990).

Topography

It is necessary to have a saddle at a reasonable distance from the main dam along the rim of the reservoir for discharging the excess flood through a natural or artificial tail channel into the same river or a neighborhood valley.

Geology

A good quality rock should be available for the foundation of the fuse plug so as to withstand the erosive action of the flow when the fuse plug is washed out. If deep overburden exists in the saddle, it would be necessary to provide concrete cut-off walls beneath the fuse plug embankment to restrict the undermining of the foundation.

Downstream Condition

A suitable tail channel to lead the flow from the fuse plug into the main river should be available so that other adjacent structures are not endangered. The tail channel should be such that it would not be clogged by the eroded material from the fuse plug.

Optimization of Minimum Reservoir Operation Level

During optimization studies, the general level of the fuse plug saddle considerably influences the choice of the design for a normal reservoir level when the fuse plug is located on a non-erodible foundation at a level lower than FRL.

In the event of washing away of the fuse plug, certain storage will not be available for use in the ensuing season. Such loss, besides construction period for restoration of the fuse plug, should be taken into account in the economic analysis and optimization studies.

Maintenance and Operation Costs

The cost of rehabilitation measures for the fuse plug and repairs of damages to downstream facilities, if any, should be taken into account for economic analysis, even though it is infrequent and covers a short duration.

12.2.2 Design Considerations

Fuse plug embankments have been designed and constructed for mine tailing dams, levees, and for controlling the flow in auxiliary spillways. However, there are few documented cases of fuse plug spillways actually operating. There is, therefore, general reluctance on the part of the designers to accept this type of device with confidence. The fuse plug also tends to get stabilized and compacted

due to traffic, vegetal growth, and armoring over a long period. Doubts have been raised about the rate at which the fuse plug embankment would erode laterally or whether it would erode at all and pass the excess flood in time, so as to avoid overtopping of the main dam. As a result, fuse plugs have been adopted at a very few projects, say not exceeding about 20. Some of these are: Bartlett and Oxbow in the US, Victoria in Australia, Mnjoli in Swaziland, Gangapur and Muramsilli in India, etc. The upper limits of existing fuse plugs are: unit discharge up to 83 cumec/m, height up to 10 m, maximum head (from base elevation up to MWL) of 13.5 m, and breaching length up to 1200 m.

The principal features of a fuse plug spillway are

Pilot channel
Impervious core
Filters
Composition of sand and gravel
Slope protection

Pilot channel is a short length of the embankment crest to be overtopped when the reservoir reaches an elevation slightly lower than the crest. Embankment material below the pilot channel should consist of highly erodible nature to ensure effective washout of the fuse plug.

The impervious core is the key element in a fuse plug installation. It is a thin core inclined in the downstream direction. It prevents washout of the fuse plug for discharges smaller than the design flood and collapses under its own weight when the pilot channel is overtopped.

The impervious core could dry and crack because the reservoir level may seldom reach that elevation. Suitable filters covering the core to prevent piping and premature washout of the fuse plug should be provided.

Sand and gravel form the major portion of the fuse plug embankment. The size and gradation of the material forming the fuse plug embankment influence the rate of washout.

Slope protection consisting of riprap and coarse gravel is provided both on the upstream and downstream of the fuse plug embankment to protect it against the action of wind, waves, rainfall, and snowmelt.

The presently available design guidelines are based on empirical relationships derived from a few cases of hydraulic model studies and a field test on a 1:2 scale model of Oxbow project as described by Tinney et al. (1961) and Hsu (1963). Pugh (1985) has described hydraulic model studies for the performance of fuse plug embankment under breaching condition.

A fuse plug should be designed as a zoned earth and rock–fill dam and should washout in a predictable manner when overtopped. The washout of a fuse plug should begin at a pre-selected location and general overtopping of the entire fuse plug should not occur. The preferred method is to initiate breaching of the fuse plug with reservoir water. When the reservoir level reaches a predetermined

elevation, a low spot in the embankment called a pilot channel would be overtopped. By placing highly erodible materials in the pilot channel, breaching will occur rapidly and rest of the fuse plug embankment will washout laterally at a constant rate without overtopping. If the length of the fuse plug embankment is large, it can be sectionalized with rigid divide walls called splitter walls. By keeping the crest of the embankment at successively higher elevations along the length and providing pilot channel in each section, the washout process can be matched to cater to successive infrequent floods. The entire fuse plug would not washout unless the full capacity of the auxiliary spillway is exceeded.

The rate of lateral erosion is of primary importance in the design. The flood discharge through the auxiliary spillway is dependent on the rate of lateral erosion and is controlled by the elevation of the non-erodible foundation of the fuse plug.

General practice is to design the fuse plug to operate only for the inflow flood with a return period that is long enough in relation to the economic life of the project. Generally, fuse plugs are designed to operate for floods with a frequency of not less than 100 years. The flow velocity at the end of the breach should be such that the discharging water would carry the eroded material without clogging the tail channel.

In order to fulfill the requirements of the efficient performance of the fuse plug, appropriate zoning of the embankment is essential. The design section should have an impervious core inclined towards downstream, as shown in Figure 1. This is required so that when the material in the downstream zone is washed away, the overhanging impervious core breaks off under its own weight and the water load.

Selected core material should normally comprise silt and/or clay. Filter zones should be provided both on the upstream and downstream of the core to prevent piping through cracks that might develop in the core. The compacted sand and gravel zone in the main fuse plug embankment and compacted rock–fill zone in the pilot channel section as shown in Figure 2, should be non-cohesive and easily erodible so as to initiate washout.

In the model studies carried out at USBR (Ref 6 and 8), typical prototype fuse plug embankments varying in height from 3 to 9 m were tested on models

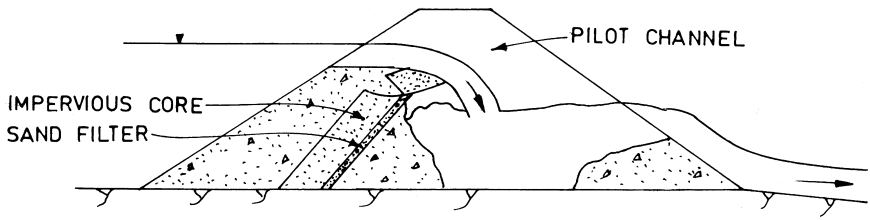

Figure 1 Typical section of a fuse plug with inclined impervious core.

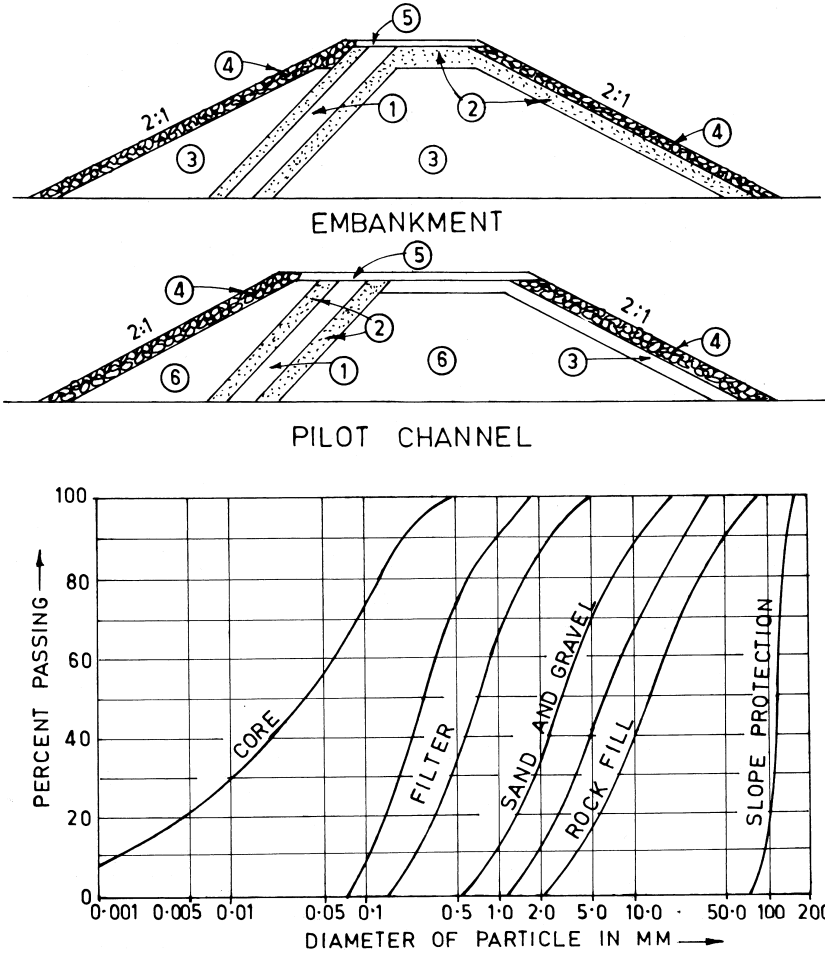

Figure 2 Zoning of materials and their gradation curves: (Pugh, 1985)

① Core
② Sand filter
③ Sand and gravel
④ Slope protection
⑤ Gravel surfacing
⑥ Compacted rock fill

to scales 1:10 and 1:25. From these studies, a series of gradation curves for embankment materials were derived and recommended for use in the prototype pilot channel and main section as shown in Figure 2. The gradation curves are shown in the same figure. Typical sections of the fuse plug of some of the dams are shown in Figure 3.

12.2.3 Providing a Fuse Plug in an Existing Dam

A fuse plug can be provided in an existing earth dam if a suitable location is available. Only locations where the emergency discharge would not endanger the main dam or other structures should be considered for fuse plug. Figure 4 shows a typical arrangement. The main emphasis is on segregating the non-overtopping portion from the fuse plug and embedding a rigid overflow structure in the body of the fuse plug so that erosion is limited to the extent required for the safety of the dam.

12.2.4 Hydraulics of Flood Discharge Through Fuse Plug Opening

The breaching of the fuse plug section and passing of flood discharge through the breached section is similar to the breaching of an earth dam but in a preconceived section. The flow through the opening is similar to a flow over a broad crested weir, as shown in Figure 5.

The broad crested weir flow depends on the depth of flow above the crest (H_0) and the length of the crest (J). In the range $0.08 < H_0/J < 0.5$, the flow over a horizontal crest is in the broad crested weir range, governed by

$$Q = C\,L\,H_0^{3/2} \tag{1}$$

Based on model studies conducted by USBR, the recommended values of coefficient of discharge C are:

During washout in one direction 1.51 m^2/s
During washout in both directions 1.71
After wash out is complete 1.44

The lateral erosion rate (after the initial breach) for a given embankment design and flow depth has also been evolved from the model studies. Typically

$$ER = 14.6 \quad H_f \quad + \quad 48 \tag{2}$$

where

ER = Lateral erosion rate in m/hour
H_f = Height of the fuse plug in metres.

If the configuration of the embankment or the flow condition is not changed with respect to that for the above equation, Pugh (1985) also explains procedure for adjustment in results.

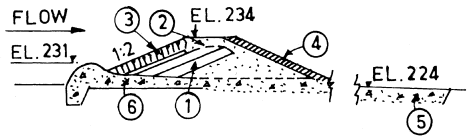

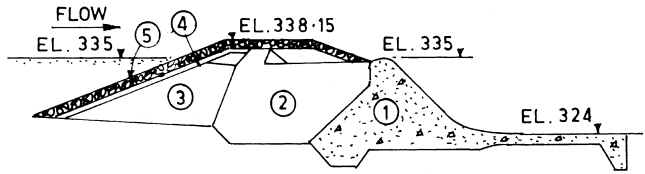

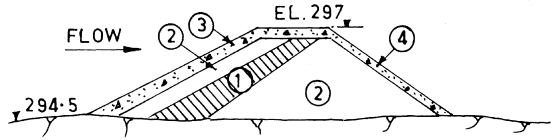

Figure 3 Typical sections of fuse plug. (Murthy et al. 1990)

A. Emergency spillway section of Mrica dam, Indonesia.

① Clay core
② Filter
③ Rip rap
④ Gravel fill
⑤ Oversize rock
⑥ Concrete weir

B. Fuse plug spillway: typical cross–section.

① Concrete dam
② Clay core
③ Sandy gravel
④ Gravel filter
⑤ Rip rap

C. Typical section of erodible bund: Mnjoli dam, Swaziland.

① Impervious core
② Filter sand
③ 500 mm blanket of concrete (aggregate size 40 mm)
④ ----DO-------(150 mm).

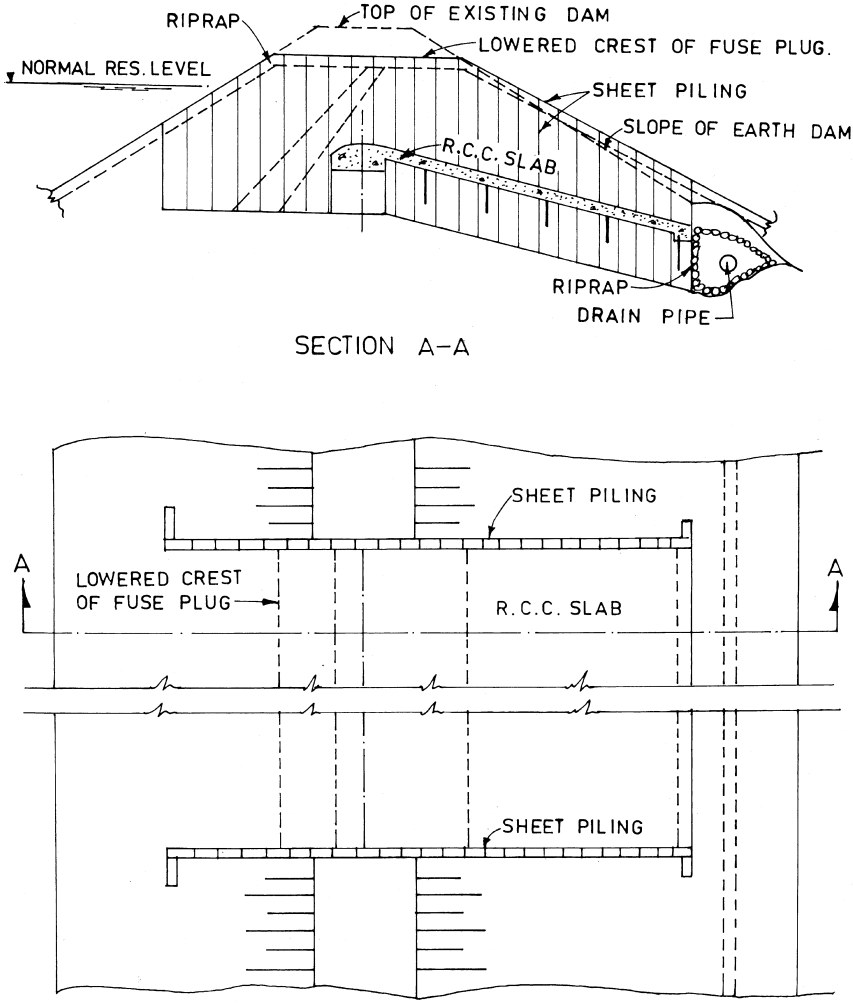

Figure 4 Fuse plug in an existing dam.

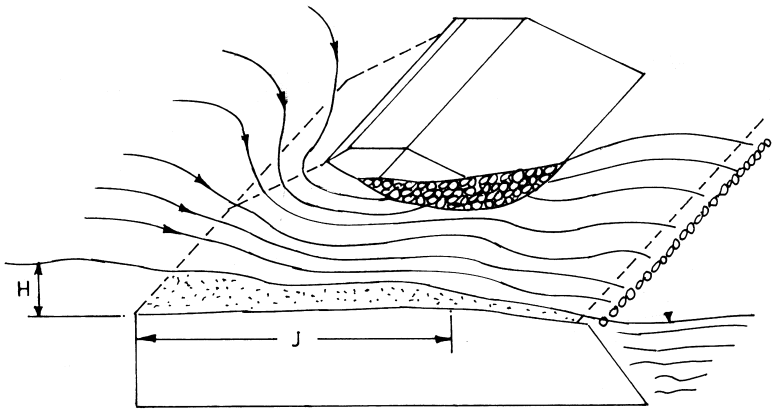

Figure 5 Flow through breached portion of a fuse plug. (Pugh, 1985)

12.3 FUSE GATES

Fuse gates can be described as the mechanical equivalent of fuse plugs. These are labyrinth weir type individual units placed side by side on an ungated and relatively flat crested spillway, designed to tilt and fall down automatically at a predetermined reservoir level. Thus, a fuse gated spillway combines the advantages of both: the storage offered by the gated spillway and flood control safety of the ungated spillway. In contrast to a fuse plug embankment, which when activated washes out entirely, fuse gates will become operational in a sequential manner, tilting one after the other in a predetermined mode. The system has been patented by Hydroplus International, France, in the US, Europe, and other countries.

Fuse gates can increase both spillway capacity and storage. If only the spillway capacity is to be increased, the crest of the fuse gates is set near the original crest elevation, thus increasing the depth of overflow substantially at the instance of fuse gate tilting. If the purpose is to increase the storage, the crest of the fuse gate is set above the original crest elevation. A number of fuse gates are installed side by side to occupy the entire width of the spillway. The existing fuse gates have allowed increase in the storage capacity up to a factor of 1.71 and increase in the spillway capacity up to a factor of 8.5. The maximum height a fuse gate has been installed is 6.5 m on Terminus dam, US, and Shongweni dam, South Africa.

12.3.1 Functioning of Fuse Gates

Each gate consists of three components as shown in Figure 6: a bucket made of metal or RCC, a base, and an intake well that is connected to a chamber in the base.

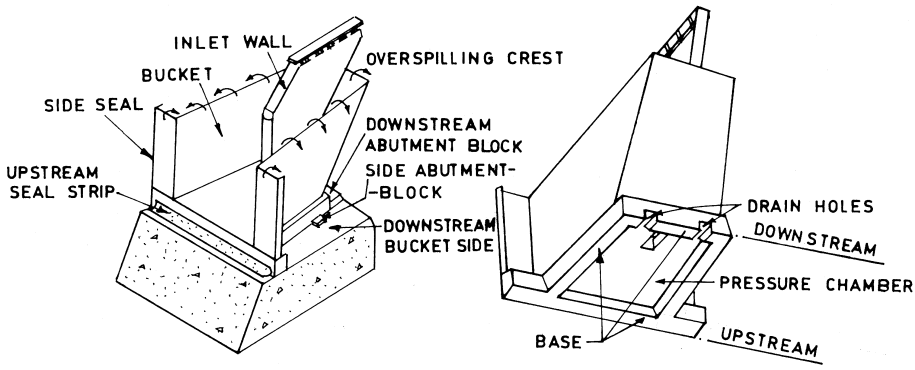

Figure 6 Components of a standard fuse gate. (Ait Alla, 1996)

Providing each chamber with two drains prevents accumulation of seepage water in the bottom chamber. The joint between the adjacent fuse gates is sealed with a flat rubber gasket.

The operation of the fuse gate is explained schematically in Figure 7. For discharges up to the design flow, the fuse gate functions like an aerated labyrinth

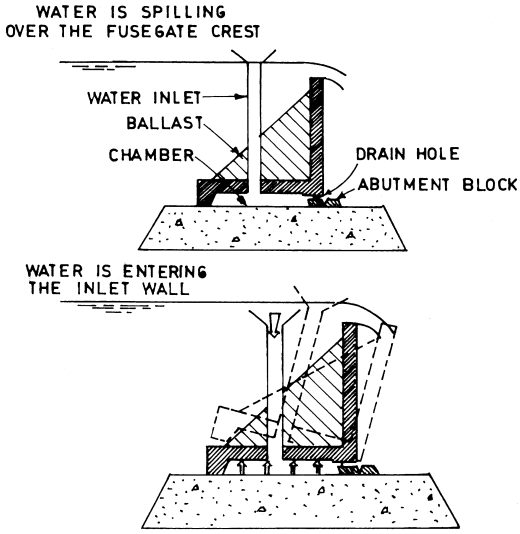

Figure 7 Operating sequence of a fuse gate. (Ait Alla, 1996)

weir. Typically, the design flow is chosen to be the discharge with a return period of about 100 years. The ratio of length to width of the fuse gate is approximately 3.

For discharges greater than the design flow, water begins to flow through the well and into the chamber located in the base of the gate. The opening into the top of the well is not horizontal, but matches with the water surface profile in the bucket. When the inflow into the well exceeds the flow out of the drain holes the water level in the well increases. This causes the pressure in the bottom chamber to increase. This exerts an uplift force on the gate decreasing its stability. For a specific depth of water in the well, the gate becomes unstable and tilts by rotating about its downstream edge. Due care must be taken so that the downstream channel is large enough to allow for tiling of the gates and their removal after they fall down.

Fuse gates are commercially available in three standard configurations and gate height as shown in Figure 8. These are designated by the width—W (wide) and N (narrow)—and tilting range as being low head (LH) or high head (HH). The standard heights are: 1.5, 1.8, 2.15, 2.60, 3.10, 3.75, 4.5, 5.4, and 6.5 meters. The three types are: WLH, NLH, and WHH.

12.3.2 Stability of Fuse Gates

Ait Alla (1996) has discussed the aspect of stability of fuse gate in terms of overturning and stabilizing moments with respect to rise in reservoir level.

The stability of a fuse gate against sliding is ensured by the downstream abutment blocks that are built into the spillway sill, as shown in Figure 6. The blocks are designed to withstand the horizontal load from the fuse gates.

The stability against overturning involves determining the moments about the downstream edge of the gate from all the forces acting on the fuse gate. Figure 9 shows various forces causing moments as follows.

Overturning Moments

1. Hydrostatic pressure from reservoir water acting on the upstream side of the fuse gate, F_{us}.
2. Uplift pressure in the chamber and under the fuse gate base, caused by the water entering through the inlet well for large floods, F_{up}.

Stabilizing Moments

1. Dead weight of the fuse gate, W_{fg}
2. Weight of the ballast (if any), W_{ba}
3. Weight of the water on the bucket floor, applying a downward pressure, W_{bu}
4. Back pressure from tail water against the downstream face of the fuse gate, F_{ds} caused by the water depth h_{ds}.

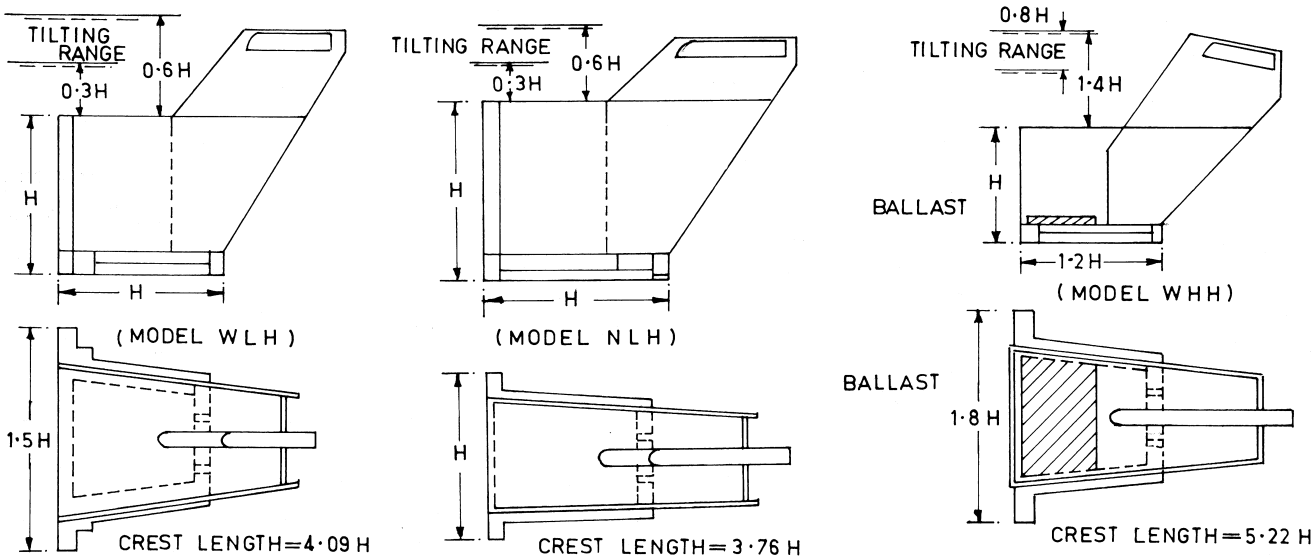

Figure 8 Standard configurations of fuse gates. (Falvey et al. 1995)

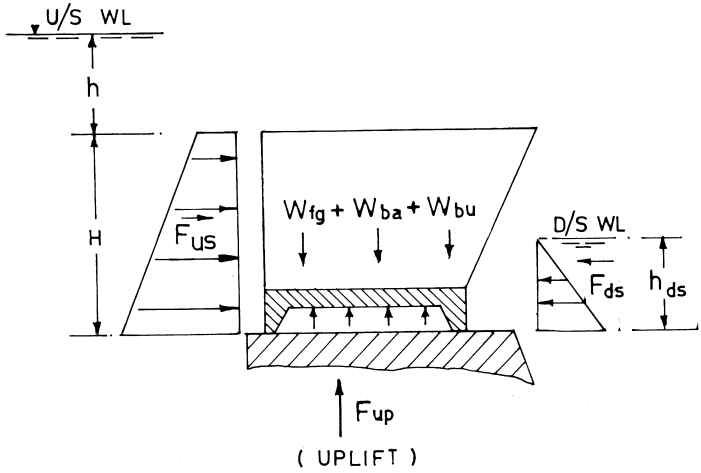

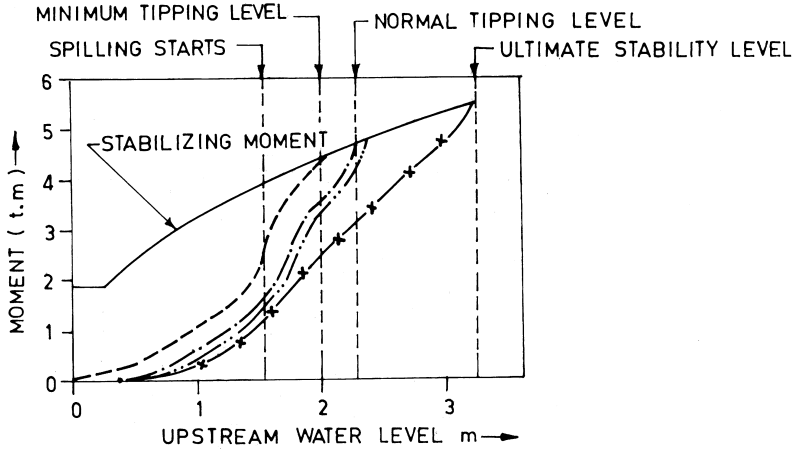

Figure 9 Forces acting on fuse gate and analysis of stability: (Ait Alla, 1996)

Overturning moment with
– – – – Maximum uplift pressure
–•–•–•– Upstream seal destroyed
—. —. —. Drain holes blocked
—x—x—x—x Natural uplift pressure

The fuse gates have a minimum tipping level below which they cannot overturn. As long as the headwater remains below the minimum overturning level, the fuse gate would return to its original stable position, even if water accidentally enters the chamber through the well or impact from a heavy body causes the upstream edge to lift off the sill for a moment. The minimum tipping level corresponds to a head on the fuse gate crest, of 60–80% of the normal overturning head. The rise in the reservoir level from the time the well first starts to discharge, to the time the fuse gate overturns is approximately 2–3% of the fuse gate height.

Extreme critical conditions such as blocked drain holes or upstream sill damage can cause uplift pressures and overturning moments; however, it is ensured that their magnitude is less than the uplift pressure needed to lift and rotate the fuse gate in normal conditions. Even in the event of no water entering the well, the overturning moment continues to increase and equals the stabilizing moment at an upstream water level H_u, called the ultimate stability level.

12.3.3 Design of Fuse Gates

The main design parameters for the selection of fuse gates are: spillway width and sill elevation, fuse gate height, number of fuse gates, and the reservoir levels at which different fuse gates overturn. Falvey et al. (1995) have described the design procedure covering all the aspects aforementioned.

The standard fuse gates are installed on a flat surface. For a retrofit on an existing spillway, a portion of the ogee crest is removed and provided with a flat surface as shown in Figure 10. For a new installation, a flat sill is constructed in the beginning. This amounts to a broad crested or long crested weir in place of a standard ogee profile, with different discharge characteristics. Rayssiguier

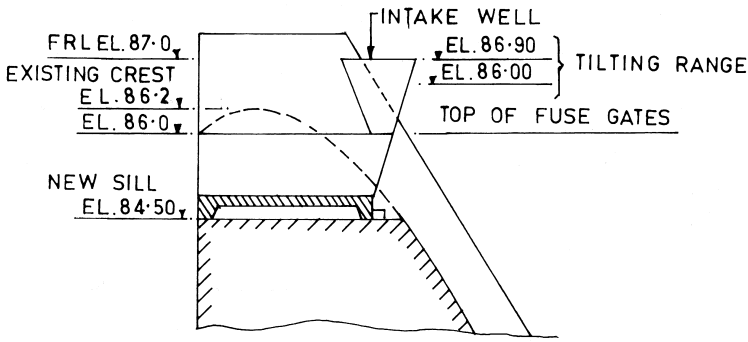

Figure 10 Installation of fuse gate on an existing spillway.

et al. (2000), Garrec (1998) and Gulati (1995) have presented case studies on installation and operation of fuse gates on existing spillways.

Discharge characteristics

Two types of discharge characteristics are considered in the design of a fuse gate system. These are the discharge over the sharp crested crest of the fuse gates and the discharge over the flat horizontal sill of the spillway structure, on which the fuse gates rest. The fuse gate discharge is given by

$$Q = \frac{2}{3}\sqrt{2g}C_d L_f h^{3/2} \tag{3}$$

where

C_d = Coefficient of discharge
L_f = Crest length of the fuse gate
h = Depth of overflow

The best-fit equation for C_d is

$$C_d = C_1\left[\left(\frac{h}{H}\right) - C_2\right]^{C_3} \tag{4}$$

H is the height of the fuse gate and C_1, C_2 and C_3 are experimentally determined constants for (h/H) greater than 0.1. Falvey et al. (1995) have summarized these values as shown in Table 1.

Discharge over the flat horizontal sill is dependent on the type of flow, namely the flow over the sharp crested, short crested, broad crested, or long crested weir, characterized by the ratio of head H_0 to the length W_c of the sill (in the direction of the flow). Based on the analysis of Hager, Falvey et al. (1995) have classified them as in Table 2.

Table 1 Empirical Discharge Coefficients for Fuse Gates

Model	C_1	C_2	C_3	R^2
WLH(NHL)	0.32 ±0.004	0.001	−0.292±0.006	1.00
WLH(TVA)	0.306±0.009	0.001	−0.360±0.013	0.98
NLH	0.254±0.012	0.0005	−0.319±0.018	0.94
WHH	0.315±0.009	0.0375	−0.258±0.005	0.99

NHL Experiments at National Hydraulic Laboratory, Chatou, France.
TVA Experiments at Tennessee Valley Authority Laboratory, US.
R = Correlation coefficient

Table 2 Classification of the Weir

Weir crest ratio	Type of crest	Equation number
$H_o/W_c \geqslant 1.5$	Sharp	(3) with Cd given by***
$0.4 \leqslant H_o/W_c \leqslant 1.5$	Short	*
$0.1 \leqslant H_o/W_c < 0.4$	Broad	(5)
$H_o/W_c \leqslant 0.1$	Long	**

* Interpolate discharge values between those given by Equation (3) and (5)
** Compute water surface profile to reservoir assuming critical depth at crest.
*** C_d=0.611+0.075(H_o/P) where P is the height of the weir above riverbed.

The discharge over a broad crested weir is given by the classical relationship of assuming critical flow and hydrostatic pressure distribution (Fig. 11).

$$\begin{aligned} Q &= \frac{2}{3} H_0 \sqrt{\frac{2}{3} g H_0}\, L_s \\ &= 1.705\, L_s\, H_0^{3/2}\ (SI\ units) \\ &= 3.09\, L_s\, H_0^{3/2}\ (ft\ units) \end{aligned} \tag{5}$$

Where Ls is the width of the flow passage.

In the long crested weir, the frictional resistance becomes appreciable and hence it is suggested to compute water surface profile assuming critical depth at crest. Alternatively, the discharge obtained by Equation 5 should be multiplied by a coefficient:

$$C = (1 - \delta^*/H_0)^{3/2} \tag{6}$$

Where δ* is the maximum displacement thickness of the boundary layer, as shown in Figure 11.

The relationship

$$(1 - C) = 0.069\ (W_c/H_0 - 1 + 2.84\ R_e^{0.25})^{0.8} - R_e^{-0.2} \tag{7}$$

can also be used, where Re = Reynolds number of flow relative to the theoretical velocity given by $v_1 = \sqrt{2gH_o/3}$.

When the flow over the horizontal sill occurs in the space vacated by a fallen fuse gate (with fuse gates on both the sides in position), side contractions should also be accounted for as

$$L_{se} = L_s - \left(\frac{nH_0}{10}\right) \tag{8}$$

Where L_{se} = Effective crest width for discharge calculations.

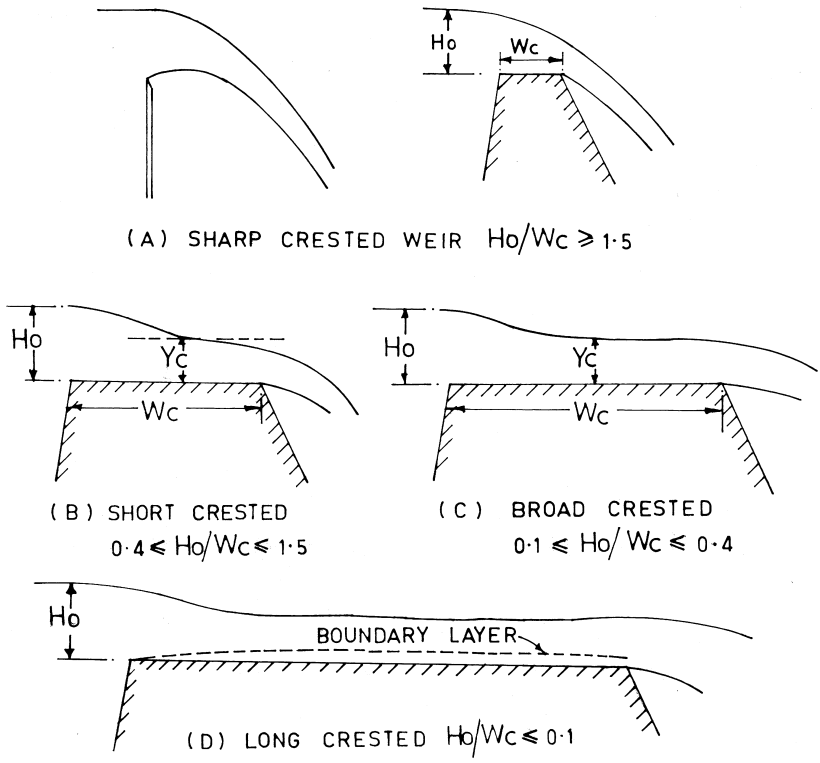

Figure 11 Broad crested weirs.

Spillway width and sill elevation

Usually the design maximum discharge (i.e. the routed outflow corresponding to the inflow design flood-PMF/SPF, etc.) and the maximum permissible reservoir level are given parameters. These parameters, together with the characteristics of the spillway sill, would decide the spillway width Ls and elevation of the sill, with consideration to the topography and other constraints at the site. The MWL, or a water level slightly lower than that, would correspond to the tilting of the last fuse gate, in a series of a number of fuse gates to be provided. The water level at which the first fuse gate should tilt would correspond to a predetermined discharge value; i.e., routed outflow corresponding to 100–year flood or so. Tilting of the intermediate fuse gates may be at, more or less, equal steps of discharge or water level between the two extreme values obtained. A number of trials may be necessary with fuse gates of different heights and widths, sill elevations, and flood routing for arriving at a final configuration.

Illustrative Examples

An existing ungated spillway shown in Figure 10 has been designed to pass a 100-year discharge of 25 cumec at a depth of overflow of 0.80 m. The width of the spillway is 15.75 m. It is decided to modify the spillway to cater to the outflow discharge of 100 cumec corresponding to PMF. Any increase in the reservoir level above FRL El 87.0 m, or increase the spillway width is not permissible. Discuss the principal elements of a fuse gate system that can be installed on the existing spillway.

It is assumed that the existing spillway crest would be lowered to install the required number of fuse gates, although, a new spillway with fuse gates may also be possible, keeping the existing spillway untouched.

The maximum depth of overflow corresponding to the discharge of 100 cumec with the spillway width of 15.75 m, is determined by trial method. First, treating this as a broad crested weir,

$$H_0 = \left[\frac{100}{1.705 \times 15.75}\right]^{2/3} = 2.4m \tag{8a}$$

which implies that the spillway sill should be at El 87-2.4 = El 84.6 m. The length of this sill, in the direction of flow, is about 2 m, which gives H_o/W_c = 2.4/2.0 = 1.2, corresponding to a short crested weir. It is suggested to determine the discharge capacity by interpolating between the sharp crested and broad crested weirs. A coefficient of 1.75 has been assumed for the purpose of calculations, although exact discharges should be ascertained from model studies, if warranted. Finally, a horizontal sill at El 84.5 m, sill length of 2.03 m and a depth of overflow of 2.5 m, (RWL El 87 m) satisfies the requirement of passing the discharge of 100 cumec.

Assume that the last fuse gate tilts at a reservoir level slightly lower than El 87 m, say El 86.9 m, or a depth of overflow of 2.4 m. It will be seen from Figure 8 that the upper limit of the tilting range of the model WLH is 1.6 H. Therefore, fuse gate of height 2.4/1.6 = 1.5 m would be suitable. With this, the width of each fuse gate will be 2.25 m and a crest length of (1.5 × 4.09) m. The number of fuse gates is 15.75/2.25 = 7. The base width of the fuse gate, of 1.5 m could be conveniently accommodated in a length of 2 m.

In order to determine the sequence of tilting of each fuse gate, the information in respect of RWL and discharges for various fuse gates in position is required. The head-discharge relationship according to Equation 3, 4, and Table 1,

$$Q = \frac{2}{3}\sqrt{2g}C_1\left(\frac{h}{H} - C_2\right)^{C_3} L_f h^{3/2} \tag{8b}$$

with $C_1 = 0.32$, $C_2 = 0.001$, $C_3 = -0.292$ and L_f = 1.5 × 4.09m reduces to Q = 6.526 $h^{1.208}$ neglecting $C_2 = 0.001$.

The discharge over the truncated spillway sill (El 84.5 m) is given by $Q_s = 1.75\ L_{se}\ H_0^{3/2}$, where L_{se} is the effective width of the spillway segment, vacated by fuse gate accounting for the end contractions.

The sequence of tilting of fuse gates is arranged so that no two adjacent fuse gates tilt one after another. The first fuse gate is made to tilt when the outflow has just reached 25 cumec, corresponding to a depth of overflow of 0.607 m over the crest of the fuse gate (RWL El 86.607 m). The last fuse gate would tilt at a discharge of about 90 cumec, corresponding to the depth of 0.90 m (RWL El 86.9 m). The intermediate fuse gates would tilt at nearly equal increments of depth over the crest, between 0.607 m and 0.9 m. All the calculations are shown in Table 3.

The provision of fuse gates obviates the necessity of locating a suitable site for the fuse plug. However, it requires large-scale modifications of the existing spillway. In the case of gated spillways, such modifications may prove to be very expensive. The advantage offered by the fuse gates is in the close regulation possible, linked either to the rise in water level or discharge. As such, only the required number of fuse gates would tilt depending upon the flood discharge.

There may be problems of operation also. The fuse gates falling down the crest may damage the spillway chute or energy dissipator and may need special

Table 3 Discharges Over Fuse Gates and Spillway

	Number of fuse gates in position Discharge in cumec							
Head on fuse gate h	0	1	2	3	4	5	6	7
(1)	(2)	(3)	(4)	(5)	(6)	(7)	(8)	(9)
0	50.63	42.43	34.24	27.0	18.81	12.54	6.27	0
0.2	61.08	51.96	42.86	35.06	25.96	19.48	13.08	6.54
0.4	72.18	62.29	52.42	44.23	34.34	27.92	21.51	15.10
0.6	83.87	73.17	62.47	54.01	43.33	37.10	30.87	24.65
0.8	96.14	84.58	73.02	64.28	52.72	46.78	40.83	34.90
1.0	108.95	96.46	83.95	74.92	62.42	56.84	51.27	45.68
Side contraction	0	2	4	4	6	4	2	0
Head at tilting	–	0.90	0.85	0.80	0.75	0.70	0.65	0.607
Discharge	100.0	90.5	75.8	64.3	50.4	41.9	33.4	25.0
Delta Q	9.5	14.7	11.5	13.9	8.5	8.5	8.4	0

(1) Discharges in Col (2) correspond to flow only over the spillway, with all the 7 fuse gates tilted.
(2) Discharges in Col (9) correspond to floe over the crest of all the 7 fuse gates in position.
(3) All other discharges comprise combination of discharges over the fuse gates and spillway segments.

arrangements to take them out of the downstream channel. Also, the recovered fuse gates may not be reusable. The energy dissipator of the existing spillway—designed for the original discharge—would be subjected to higher discharge and would require large-scale modifications.

The entire storage held behind the fuse gates is lost even if one fuse gate tilts. A replacement unit can only be installed when the overflow completely stops and the spillway sill is dry. The objective would therefore be to provide largest possible discharge capacity over the fuse gates, as possible.

12.3.4 Recoverable Fuse Gates

The standard fuse gates are usually not reusable because of the damage due to falling over a considerable height. Recently, a design of what is termed as Recoverable fuse gate has been evolved by the manufacturers. This is basically an improved version of the classical flashboard on spillway crest and stated to be less stable and less reliable than the standard fuse gates. Chevalier et al. (2003) have described functioning of recoverable fuse gates. Figure 12 shows schematic details of the fuse gate. The water is retained by a panel that can be overtopped

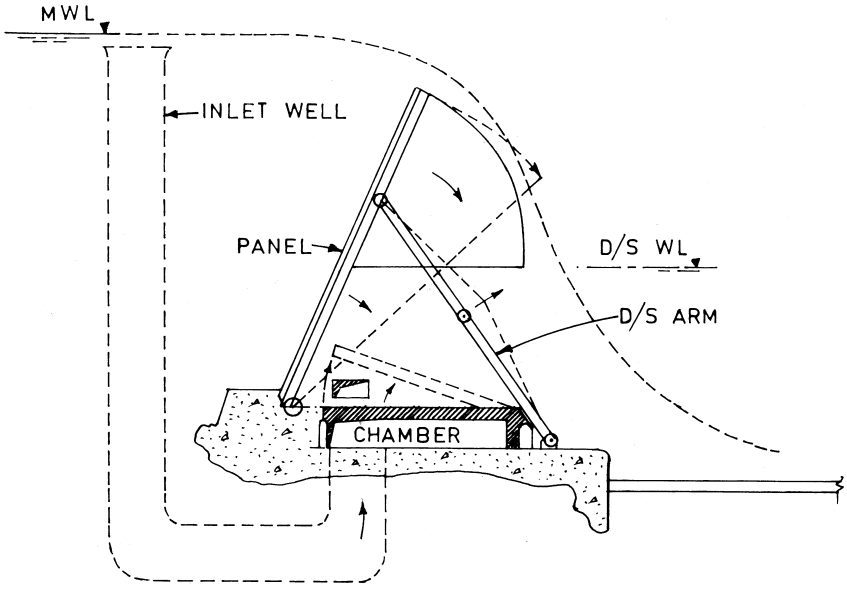

Figure 12 Schematic details and functioning of recoverable fuse gates. (Chevalier et al. 2003)

by moderate to medium floods. For higher floods, some water enters the inlet well and then moves to a mobile chamber located at the base, downstream of the panel. This chamber, under the uplift pressure rotates and causes a downstream arm to swing the panel downward. The panel can be reinstated after the floods.

Notations

C = Discharge coefficient of fuse plug
C_d = Discharge coefficient of fuse gate, spillway sill etc
C_1 = Constants
C_2
C_3
ER = Rate of erosion of the fuse plug
F_{ds} = Hydrostatic force on the downstream side of fuse gate due to tail water
F_{up} = Force due to uplift on the fuse gate
F_{us} = Hydrostatic force on the upstream side of the fuse gate
H = Height of fuse gate
H_0 = Head on the spillway sill
H_f = Height of fuse plug
h = Head on fuse gate crest
h_{ds} = Depth of tail water downstream of fuse gate
J = Length of eroded crest of fuse plug
L = Width of crest (water way)
L_f = Length of crest of one unit of fuse gate
L_s = Length of crest without accounting for end contraction
L_{se} = Length of crest with accounting for end contraction
P = Height of spillway crest from riverbed
Q = Discharge
R = Correlation coefficient
R_e = Reynolds number
W_{ba} = Weight of ballast
W_{bu} = Weight of water in the bucket portion of fuse gate
W_c = Length of spillway crest in the direction of flow
W_{fg} = Weight of fuse gate

REFERENCES

1. Ait Alla, A. The role of fuse gates in dam safety – Hydropower and Dams, Issue six, 1996.
2. Chevalier, S.; Sud, A. K. Hydroplus fuse gate system: An ideal solution for increasing water storage and dam safety – 4th International R&D Conference on Water and

Energy for 21st Century, Central Board of Irrigation and Power, Aurangabad: India, January, 2003.
3. Falvey, H. T; Treille, Philippe; Hydraulics and Design of Fuse gates – ASCE. Jnl. of Hyd. Engg, July 1995; Vol. 121, No.7.
4. Garrec, P. Fuse gates increase storage capacity at four dams in Gujarat, Hydropower and dams, Issue Five, 1998.
5. Gulati, O. T. Augmenting canal capacity through application of Hydroplus fuse gates at Mahi project of Gujarat, Water and Energy 2001, International R&D Conference, New Delhi, Oct 1995.
6. Hsu, H. Y. Design of fuse plug spillway – Indian Journal of Power and River Valley Development, Hydraulic Structures Special Number, 1963.
7. Muthy, Y. K.; Thatte, C. D.; Divatia, E Fuseplug for Auxiliary Spillway. Jnl. of Irrigation & Power, CBIP, July 1990.
8. Pugh, C. A. Hydraulic model studies of Fuse plug embankments, REC-ERC-85-7, USBR, USA, 1985.
9. Rayssiguier, J.; Lantheaume, P. How to optimise dam storage capacity without compromising safety: The Fuse gate Concept, CBIP Workshop on Role of Gates and their control in Water Resources Projects, Belgaum: India, 28–30 June 2000.
10. Tinney, E. R.; Hsu, H. Y Mechanics of washout of an erodible fuse plug – ASCE. Jnl. of Hyd. Div, 1961; Vol. 87, No. HY 3.

13
Spillways for Flood and Sediment Disposal

13.1 INTRODUCTION

The primary function of a spillway is to release the inflow of water that is in excess of the amount could be stored safely in the reservoir. In situations where large amounts of sediment enters the reservoir, the flood disposal capacity of the spillway can be utilized effectively to dispose sediment from the reservoir. This combination is possible, particularly in run-of-river schemes on mountainous streams with narrow and steep gorges. Although no design procedures are developed for such layouts, experience from the design, construction, and operation of a few spillways provide useful guidelines.

13.2 RESERVOIR SEDIMENTATION AND FLUSHING

Mountainous streams with dependable flows and considerable heads are ideally suited for run-of-river schemes with relatively small reservoirs and almost no possibility of long term storage. These streams also carry large amounts of sediment that could ultimately settle in the reservoir to reduce its capacity, which must be recouped periodically. Generally, provision of a facility in the dam-reservoir system to dispose of the deposited sediment at regular intervals is often more economical than having to provide very large reservoir capacity or to dredge out the sediment by external means.

The most efficient way of flushing out the sediment is to provide low-level bottom outlets or spillways and to affect draw down conditions by opening them fully during floods. When a single structure like a spillway, an under sluice, or a bottom outlet is contemplated to serve the combined function of head work, flood disposal, and sediment flushing, the choice of type is confined to a few alternatives and involves rather diverse requirements.

13.3 ALTERNATIVES AVAILABLE

Considerable work regarding reservoir flushing has been done in India and China. Several reservoirs had been silted up to the crest elevation of spillways and special measures such as reactivation of diversion tunnels or bottom outlets had to be resorted to for flushing out as much sediment as possible to operate the power plants as planned. White (2001) has delved in detail all aspects of reservoir flushing including hydrological, hydraulic, sedimentological, and topographical features.

The location, size, and dimensions and operating conditions for the device to serve the dual function are simultaneously governed by requirements, often contradicting. As for example, elevation, size, or dimension of the outlet or gate dictated by the requirement of flood disposal may not be favorable for sediment disposal or the choice of energy dissipator, based on the hydraulics of the system, may not be suited to the conditions imposed by sediment flushing.

Determination of spillway design flood is obviously governed according to the relevant code of practice and guidelines in various countries (Chapter 3). Combining the functions of the head work, flood disposal, and sediment disposal is, however, possible with only a few alternatives, such as:

Gated overflow spillway for simultaneous flood and sediment disposal for low dams.
Orifice spillways on high dams with large discharges.
Bottom outlets in the body of spillway or non-overflow dam for high heads.

In all the layouts, the powerhouse may be located by the side of the dam or elsewhere and fed through a water intake on the flank of the dam or reservoir.

13.4 FLUSHING DISCHARGE

In view of the small size of the reservoir and limited storage together with large sediment load, flushing has to be carried out almost every year. Thus, the flood discharge that can be expected to occur every year—average annual flood—is chosen as the design discharge for flushing operation. For the best efficiency of the flushing, all the gates of the spillway or bottom outlets are fully opened allowing the reservoir to be depleted, virtually inducing a flow similar to a river. Such a condition may prevail for a few hours up to a day or so, with considerable proportion of sediment passing down the spillway, energy dissipator, and finally into the downstream river. The resulting hydraulic conditions in the upstream as well as downstream need to be considered in the design of spillway and energy dissipator.

13.5 GATED OVERFLOW SPILLWAY

A low height spillway equipped with large size radial gates is the simplest device to accomplish both the functions. The power intakes must be located nearest to the spillway and preferably aligned normal to the spillway axis. During floods, the spillway gates are operated in such a way that swirling flows are generated in the upstream region with the result that deposited silt in the reservoir is agitated, brought into suspension, and carried downstream over the crest of the spillway. The gate operation pattern could be devised from model studies or from experience on the prototype itself. The spillway of Chukha dam in Bhutan is an ideal example of this system, as reported by Rao (1994). Figure 1 depicts the efficacy of the arrangement in respect of Chukha spillway during the past few years. It would be noticed that the power intake located farthest from the spillway is not effectively cleared of the deposition because it is inclined away from the main direction of the flow.

Although simplest, a gated overflow spillway is not the most efficient device considering the volume of water to be discharged in relation to the volume of sediment flushed out. Since the gates hold most of the water storage, the height of the gates is a crucial factor. For the spillway of Chamera II HE Project, India, highest radial gates adopted so far (21 m high) would be installed on a 3 m high spillway sill, with an objective to flush out deposited sediment from the reservoir every year.

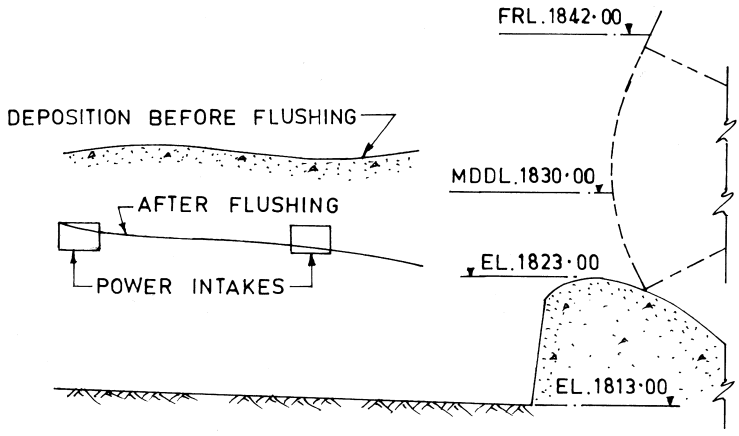

Figure 1 Gated overflow spillway Chukha spillway, Bhutan.

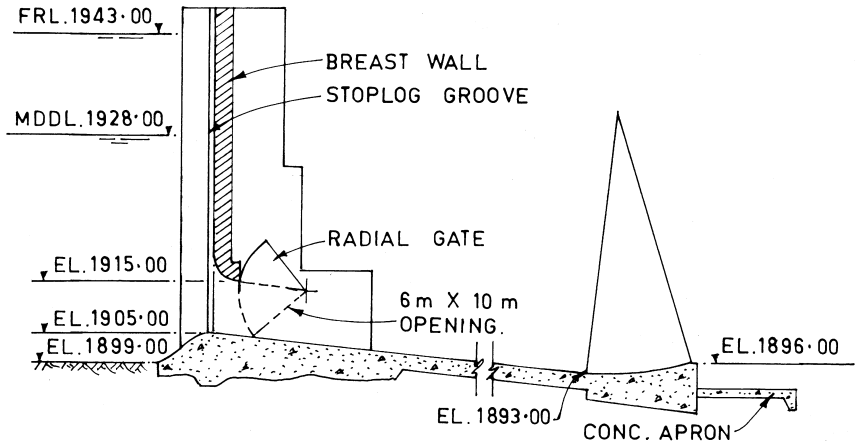

Figure 2 Orifice spillway with combination type energy dissipator.

13.6 ORIFICE SPILLWAYS

Since the efficiency of a gated overflow spillway is dependent on the depth of flow between the FRL and crest elevation of the spillway, its suitability is restricted to the gates of largest practicable size. Orifice spillways combine the advantages of greater depths of flow over the crest and moderately sized gates—an arrangement made possible by inclusion of a breast wall. An orifice spillway would allow the setting up of its crest at significantly lower elevation, yet retaining the choice of a high dam. A relatively smaller size of the radial gate results in overall economy. Greater depth of flow over the crest offers larger margin for setting the power intake and allowing larger submergence for vortex free operation, at the same time keeping it as high above the river bed as possible to keep it free of deposition. Figure 2 shows the details of a typical orifice spillway.

13.7 BOTTOM OUTLETS

When the dam height is high and the volume of flood to be handled is larger, crest gates cannot be relied upon for sediment disposal. Therefore, large size low-level bottom outlets embodied either in the spillway or non-overflow dam are a better choice for flood and sediment disposal. Because of higher heads, opening bottom outlet gates for passing small, non-monsoon flows is not practicable and often undesirable from an operational consideration. Generally a small overflow

spillway is provided separately from the bottom outlet to cater for the daily non-monsoon discharges. In addition, a provision is also required to bypass the discharge going to the powerhouse, from such a spillway, in the event of sudden closure of powerhouse for some reason. An automatic regulation of such discharges is preferred and made possible by any of the two alternatives:

1. Bottom outlets embodied in the spillway with its crest ungated so that flood and sediment disposal is carried out through the outlets. The daily discharges, as well as power generation discharge, is diverted over the ungated crest, not requiring operation of the gates.
2. Bottom outlets embodied in the non-overflow dam with a separate overflow spillway catering to the daily discharges and power generation discharges. Such a spillway could either be ungated or fitted with automatic counter weight gates.

Figures 3 and Figures 4, respectively, show the details of typical arrangements described in the previous paragraphs. Both the types have some advantages and disadvantages. The ungated spillway/bottom outlet combination eliminates the necessity of a separate arrangement for passing the daily discharges. It would, however, pose difficulty while carrying out inspection or repairs to the spillway,

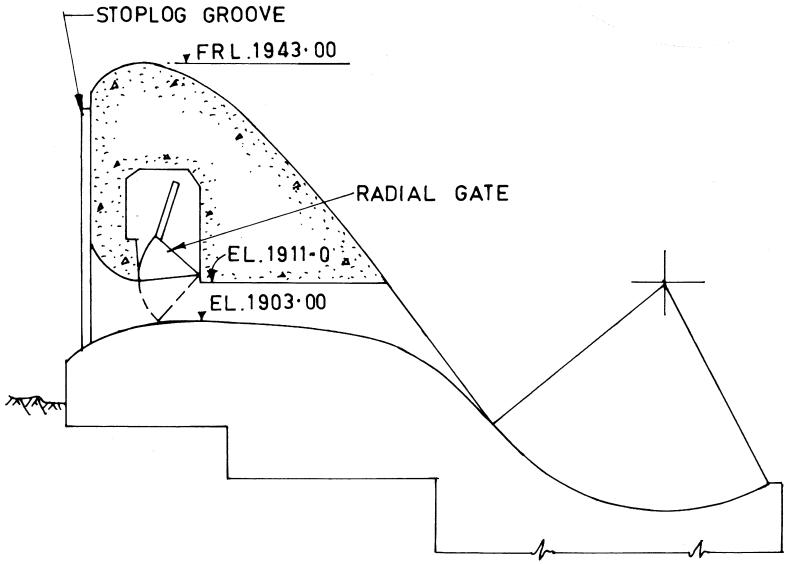

Figure 3 Bottom outlet embodied in spillway.

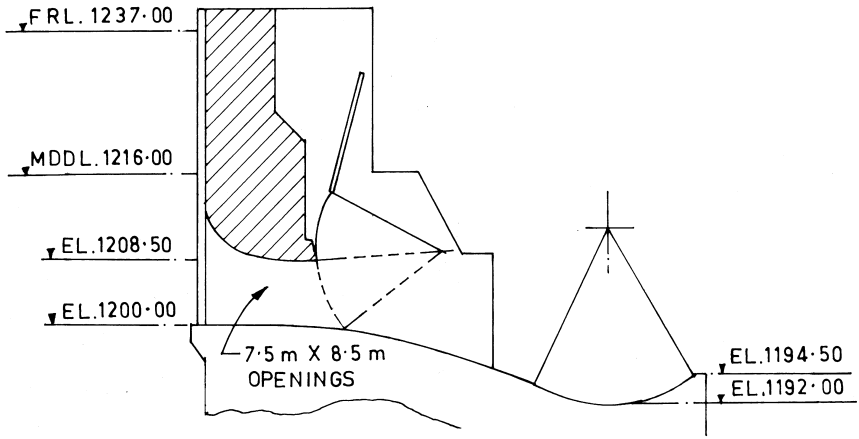

Figure 4 Bottom outlet embodied in non-overflow dam.

energy dissipator, or immediate vicinity downstream on account of continuous and uncontrolled flow over the ungated crest.

13.8 DESIGN CONSIDERATIONS

The following considerations arise while designing a system to serve the dual purpose of flood and sediment disposal:

Discharge characteristics of spillway as affected by sediment deposit on the upstream.
Waterway of the structure in relation to the width of the natural watercourse.
Size and dimensions of the structure.
Choice of energy dissipator.
Disposition of the power intake with reference to the structure.
Flow control and regulating devices.
Protection of flow surfaces to resist abrasion, etc.

13.8.1 Discharge Characteristics of Spillway

As discussed in Paragraph 4.3, siltation upstream of the spillway increases the afflux in the upper reach of the reservoir (Fig. 10, Chapter 4). Therefore, when spillways are designed to serve for sediment disposal, adequate allowance for the increased afflux should be made.

13.8.2 Waterway of the Structures

The design flood for the spillway is decided in accordance with the guidelines provided in relevant standard for considering the height of the dam, storage capacity, etc. The general tendency is often to keep the width of the spillway to the minimum possible from economic considerations. The preference is for larger depths of overflow rather than the wider ones so as to restrict the number of gates and to keep the cost of the energy dissipator to the minimum. However, efficient flushing requires that the waterway be as large as the width of the natural river. This is because the flushing action is more pronounced in front of the spillway or outlets during the reservoir draw down condition than with the flow, taking place parallel to it along the non-flowing sections.

13.8.3 Size and Dimensions of Structures

Orifice spillways and breast walls

Several large dams have been constructed with spillways having breast walls. The main advantages of having a breast wall are:

Reduction in height of spillway gates
Reduction in number of spillway spans
Ease of regulating flood discharge and storage
Reduction in cost of gates and operating mechanism

For the spillway performing the dual purpose of flood and sediment disposal, the one with a breast wall makes it possible to have a short crest with a relatively large depth of overflow and yet a small size gate—an ideal situation for flushing out sediment downstream of the spillway. The information available from the literature indicates that heads of the order of 30–40 m over the spillway crest are a common feature. The width of the span varies from 12 to 18 m and the height of the opening below the breast wall is of the order of 10 to 14 m for spillways with discharge intensities of the order of 100 cumec/m and above. Thus, the height of the breast wall above the opening is of the order of 18 to 25 m. In order to support such a high breast wall, the thickness of the pier also increases substantially.

Just as the standard ogee crest is derived from the flow over a ventilated sharp crest, the configuration of a breast wall spillway is derived from the flow through a rectangular orifice (whose length is much larger than the vertical dimension) as shown in Figure 5. Profile A results in the upstream face of the breast wall in line with the upstream vertical face of the spillway, whereas in Profile B, the breast wall has been shifted downstream. Although, hydraulically more efficient, Profile A does not leave any space for providing stop log groove. Either a separate cantilever structure for accommodating the groove has to be constructed

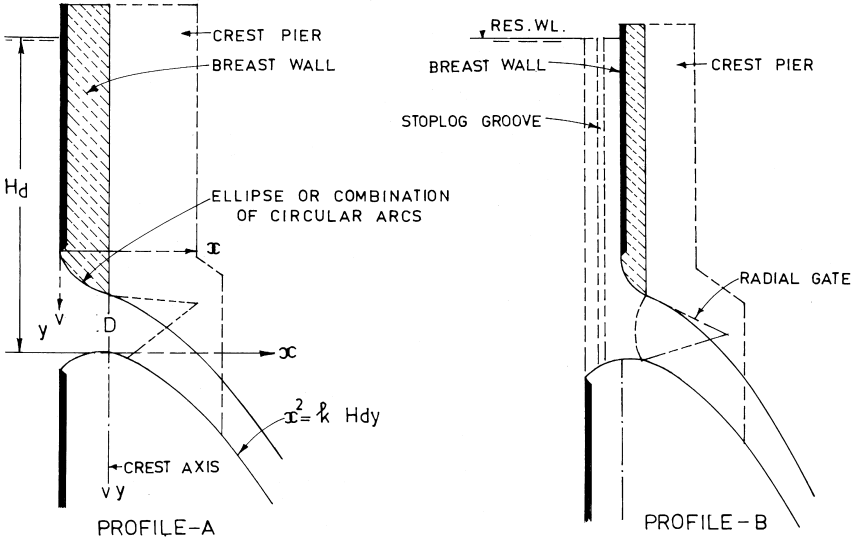

Figure 5 Evolution of breast wall profiles.

or a groove has to be provided through the body of the breast wall structure. Profile B eliminates this difficulty and is therefore generally preferred.

The bottom profile of the breast wall is an ellipse or a combination of circular arcs. The upstream quadrant of the spillway crest is generally a standard elliptical profile, where as the downstream profile is parabolic of the form of $x^2 = k\,H_d\,y$, where H_d is the design head and k is a factor, usually in the range of 3 to 4. This is necessary to prevent sub-atmospheric pressures on the spillway profile for small part gate opening.

The spillway operates as a free overflow spillway for low discharges and orifice flow for high discharges. Generally, the orifice flow condition sets in for heads over crest in excess of about 1.7 D, where D is the height of the orifice opening. Under this condition, the discharge is given by

$$Q = C_d n A \sqrt{2g\left(H_d - \frac{D}{2}\right)} \tag{1}$$

where

C_d = Coefficient of discharge
N = Number of spans
A = Area of orifice opening
H_d = Total head (Design head)
D = Height of the orifice opening

The coefficient of discharge is influenced by the entrance profile—composed by the roof profile and spillway crest profile and the inclination of the orifice barrel with reference to horizontal. The coefficient increases with increase in steepness of the barrel.

Unlike ogee spillways, the design of breast wall spillways has not been standardized. Table 1 gives pertinent details of spillway and breast wall profiles and coefficient of discharge for some of the existing structures.

Breast wall spillways necessitate some special structural design considerations. Breast walls resist water load with beams or slabs spanning between, and fixed with, the two piers. As such, the breast wall and both the piers have to be constructed as a single structural unit. The contraction joint is, therefore, provided at the center of each pier, except the end piers. Thus, a typical pier is virtually a combination of two full piers separated by a contraction joint, and a typical spillway monolith is composed of two piers and breast wall. In a standard overflow spillway without breast wall, contraction joints are provided at the center of the span, with only one pier at the center of the monolith.

Special care is also required in respect to the top seal of the radial gate in ensuring water tightness.

Bottom outlets

While the number and size of the bottom outlets are governed by the flood discharge they are supposed to handle, the following guidelines based on experience are available in the literature.

Paul and Dhillon (1988) reviewed sediment flushing techniques employed in various countries and also conducted model studies for a specific case by altering the size of bottom outlets. They suggested use of design curves for determining optimum area of the outlets for flushing purpose and recommended optimum height of the outlets from 1.5 m to 2.5 m, with the required area to be obtained by increasing the width.

Ke, Wu, and Huang (1994) observed that the velocity in the sluiceway should be high enough to flush the sediment and suggested that the required waterway be estimated by the following equation.

$$V_c = 1.5\ C\ d^{0.5} \tag{2}$$

where

V_c = Design velocity through the sluice way, m/s.
C = Shape factor of sediment, typically varying from 3.2 to 3.9.
d = d_{90} of the sediment, meters.

They also suggest that the width of the outlet should be large enough to allow the floating obstacles to pass. Typically, it should be 0.04 to 0.12 of the length of the dam.

Table 1 Details of Spillway and Breast Wall Profiles of Some Projects

Sr No	Name of project	Spillway profile Upstream	Spillway profile Downstream	Bottom profile of breast wall	D m	H m	Span width m	Discharge Intensity Cumec/m	Cd
1	Chamera HE Project, India	Combination of circular arcs of R=5.2 m and 13 m	$x^2 = 102\,y$	$\frac{x^2}{10^2}+\frac{y^2}{5^2}=1$	12.5	32.5	10.0	250	0.83
2	Ranganadi HE Project, India	Ellipse	$x^2 = 92\,y$	Circular arc R = 5 m	12.0	24.3	10.0	152	0.78
3	Kurichu HE Project, Bhutan	$\frac{x^2}{4.5^2}+\frac{y^2}{2.5^2}=1$	$x^2 = 80\,y$	$\frac{x^2}{5.5^2}+\frac{y^2}{2^2}=1$	14.0	28.0	10.5	232	0.83
4	Pandoh dam Spillway, India	Flat	$x^2 = 427.35\,y$	$\frac{x^2}{39.37^2}+\frac{y^2}{13.1^2}=1$	13.0	21.64	12.0	166	0.73
5	Mangala dam, Pakistan	Circular arc of radius 390.5 m	$x^2 = 1639\,y$	Circular arc R=26.22 m and sloping portion	10.67	41.15	11.0	250	0.95
6	Turnu Barrage, Romania	Flat		Circular arc and sloping Portion	4.5	23.65	15.0	96.67	0.82
7	Imperial dam, USA				2.10	8.53	4.88	20.25	0.80
8	Vogelgrun, France	Combination of circular arcs of R=2 m and 8 m	$x^2 = 16.67\,y$	Circular arc of R = 2 m and portion with 2 : 1 Slope	5.6	13.15	4.10	68.29	0.84

Experience shows that a number of conditions enter into the process while determining the size and dimensions of the structure because of site specific requirements. Various alternatives might be possible and studies on a physical model might prove to be helpful in selecting the best arrangement to serve the purpose.

Bottom outlets in the body of the spillway or non-overflow dam consist of

bellmouth entry
control gate
free flow conduit leading to energy dissipator

The most suitable type of control gate is obviously the radial gate, eliminating the need of gate grooves that are likely to pose problems while handling sediment-laden flows. Such gates, however, occupy considerable length of the outlet, resulting in a very short length of the pressurized entrance section. Because of this, the flow is detached from the roof profile and pressure flow does not take place for the condition of full gate opening. Sub-atmospheric pressures occur on the roof, which may result in cavitation. Huan-Wan (1979) suggest a downward constriction of the outlet barrel, in continuation of the roof bell-mouth, as shown in Figure 6. Although, their design involves a vertical lift gate with gate slots, the design as shown in Figure 6 would be suitable for the outlets to be used with radial gates.

The discharge relationship is

$$Q = C_d B h_2 \sqrt{2g (H - \varepsilon h_2)} \quad (3)$$

where

B = Width of the outlet
H = Total head
h_2 = Constricted height of the conduit
ε = Coefficient of contraction

The suggested values of C_d and ε (as functions of roof constriction slope S_2) are

S_2	C_d	ε
1 : 4	0.876	0.895
1 : 5	0.893	0.914
1 : 6	0.904	0.918

13.8.4 Energy Dissipator

The best form of an energy dissipator is the flip bucket because of its obvious advantage during flushing operation. The sediment passes down the spillway on

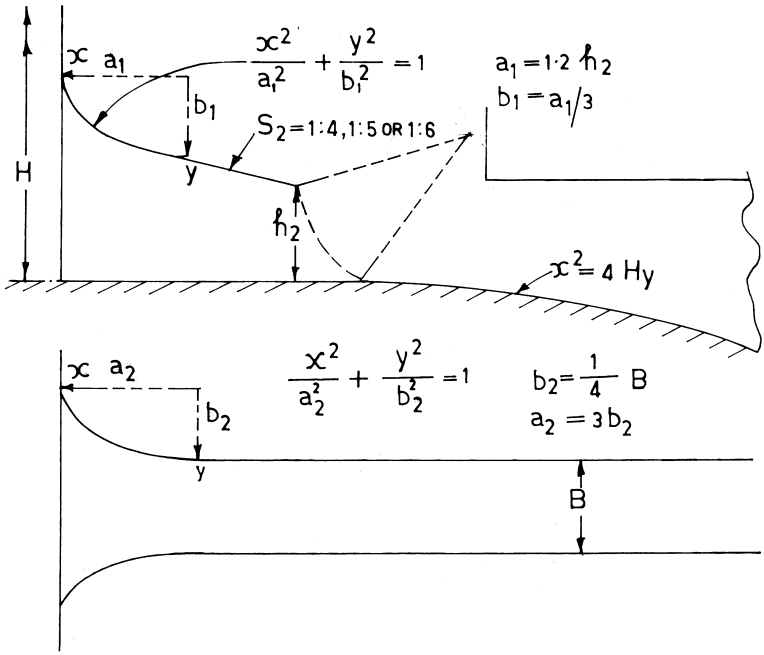

Figure 6 Bottom outlet profiles.

a relatively flatter bucket and supercritical flow, without deposition in the bucket. Fortunately, steep bed slopes of the rivers result in low tail water depths permitting the choice of such a device. If, however, geological conditions are not favorable, a hydraulic jump stilling basin may have to be adopted. The high unit discharge passing down a low head, results in a low Froude number condition. The stilling basins for the range of Froude numbers 2.5–4.5 are rather difficult to design to ensure satisfactory performance for the full range of discharge. Because of the requirement of passing silt-laden flows, use of energy dissipating appurtenances like chute blocks and baffle blocks is not advisable. The resulting basin is excessively long and often deep-seated below the general riverbed, making it vulnerable to deposition by silt during flushing operation. Experience shows that a trade-off is desirable between the hydraulic efficiency of energy dissipation and the self-cleansing potential of the stilling basin during flushing operation.

In some cases, head-discharge-tail water combinations for the full operating range of a structure do not result in a design, which is exclusively a flip bucket or hydraulic jump stilling basin. In such a situation, a combination type of energy dissipator with a horizontal apron terminating with a low circular upturned end

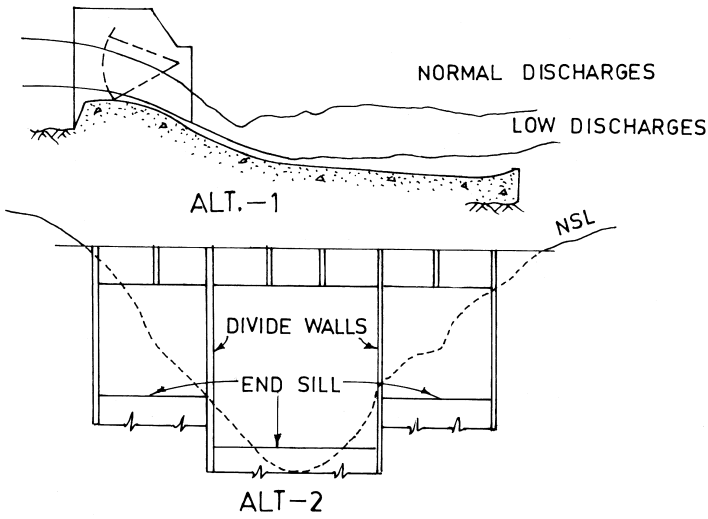

Figure 7 Suggested alternatives.

sill is found to be quite satisfactory. A concrete apron downstream of the end sill is required to protect the spillway against undermining due to scour during transition action from hydraulic jump to flip action and vice-versa (Fig. 2). Another alternative would be to isolate a few spans of the spillway on the flanks, providing with aprons at higher level for flushing out sediment, as shown in Figure 7. These spans would function with hydraulic jump under sweep out condition, for small discharges of the order of average annual flow, during flushing operation. The central spans would cater to the normal discharges.

13.8.5 Power Intakes

The disposition of the power intake with reference to the axis of the spillway or bottom outlets is yet another consideration of flushing. Various arrangements possible are shown in Figure 8. Experience shows that the best arrangement is the one in which the axis of the power intakes is normal to the axis of the spillway or bottom outlets and is located at one of the flanks without leaving any recess. With other arrangements, larger volumes of water must be let out or longer duration of flushing operation is required to recoup the capacity lost by deposition.

13.8.6 Gates

Looking to the requirement of large size or to handle flow containing large amount of sediment, radial gates are the most suitable devices for the control and regula-

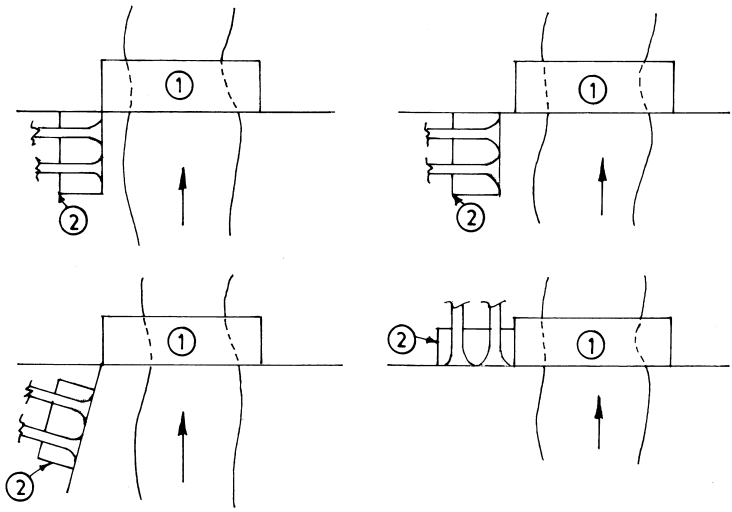

Figure 8 Various arrangements of power intake in relation to spillway/bottom outlets:

① Spillway/bottom outlet
② Powerhouse

tion of flow. These gates do not involve gate grooves susceptible to filling up with sediment during flow, and also offer trouble free operation even for very small openings.

13.8.7 Protection of Flow Surfaces

The flow surfaces of spillways, bottom outlets, and stilling basins suffer abrasion damage due to passing of sediment-laden flow. Rao (1995) has described the method of how to protect spillway surfaces against large boulders rolling over the spillway surface of Chukha project, Bhutan, during monsoon. At Chukha project, the spillway glacis has been protected against damage due to boulders, by embedding 50 pound rails at 30 cm centers. For the stilling basin, rich concrete of M 250 grade with 20 mm size aggregate has been provided for a thickness of 50 cm. It is reported that after the spillway came into operation in 1984, the above protection has stood very well without any damage. The proposal of protecting the flow surface by embedding rails has been a matter of debate recently. Questions are raised about the possibility of boulders reaching right up to the spillway, since these are likely to get deposited in the upper reaches of the reservoir itself. On the other hand, embedment of rails on the curved surfaces of spillway necessitates

bending the rails to the correct profile and elaborate arrangement of anchorage, etc., which often results in slowing down the speed of construction.

Similarly, flow surfaces of bottom outlets and breast walls are also provided with steel lining to protect them from abrasion damage. However, several instances have been reported where steel linings have been ripped off, the reasons attributed mostly to the imperfect joints from where high velocity flow penetrated below the lining, causing uplift.

New developments in concrete technology are being looked upon with expectations to overcome the above difficulties. Following successful application of silica fume concrete for repairs to Kinzua dam stilling basin, US, further research is pursued to use such concrete for wide applications. Also, a new product called Alag anti-abrasion concrete is being developed for velocity up to 100 m/s or so.

13.9 MATHEMATICAL AND PHYSICAL MODEL STUDIES

Mathematical and physical model studies are being successfully applied to solve problems pertaining to the efficient flushing of sediment vis-à-vis functioning of the spillway, outlet, and energy dissipator. One-dimensional numerical modeling is useful in predicting the rate and pattern of deposition in the reservoir. This constitutes an important input for the studies in a physical model to evolve suitable arrangement of spillway outlet in relation to the power intake and finalize the operating conditions for affecting the flushing of sediment. Recent examples of such studies conducted include projects of Nathpa Jhakri, India; Dhauliganga, India; Kurichu, Bhutan; and Tala, Bhutan.

Notation

A = Area of the outlet section
B = Width of the outlet
C = Shape factor of sediment
C_d = Coefficient of discharge
D = Height of the opening below breast wall
d = d_{90} of the sediment, meters
H = Head on the outlet
H_d = Design head
h_2 = Constricted height of the conduit
n = Number of spans
Q = Discharge
S_2 = Slope of the roof constriction
V_c = Design velocity through the sluice way
ε = Coefficient of contraction

REFERENCES

1. Huan-Wen, H.; Fu-Yi, C.; Sheng, C. Studies on the configuration of short intakes for free-flow spillway tunnels, 13th ICOLD, Q 50, R 57, New Delhi, 1979.
2. Wu-Sung, Ke; Sue-Jen, Wu; Che-Yoan, Huang An improved design of excluding sediment into river intake structures; 9th APD-IAHR Congress, Singapore, August 1994; Vol. 2, 208–214.
3. Paul, T. C.; Dhillon, G. S. Sluice dimensioning for desilting reservoirs; Water Power & Dam Construction, May 1988, 41–44.
4. Rao, G. N. Performance overview of the completed projects – Chukha Hydel Project, Bhutan, Proc. Fifth National Water Convention, Faridabad, India, Feb. 1994.
5. Rao, G. N. Method of protection of dam spillways of the projects in Himalayan region – Water & Energy International, 1995.
6. White, Rodney; Evacuation of sediments from Reservoirs; Thomas Telford Publishers, England, 2001, 280.

14
Unlined Spillways

14.1 INTRODUCTION

When a spillway is located in a saddle it is usually provided with a concrete lined chute (either straight or curved depending on the topography) terminating with an energy dissipator. The flow is then led to the main river through an excavated unlined channel called the tail channel. Several spillways the world over have been designed and constructed with this arrangement. Erosion in the tail channel takes place during initial years of operation, but stabilizes later. There is a considerable saving in cost due to such a design. This concept is further advanced in some countries to the evolution of what is termed as unlined rock spillways, unlined cascade spillways, and rock–fill spillways. Here, the design is optimized to combine the advantages of maximum use of rock excavation, saving in concrete, and eliminating or minimizing effort on energy dissipation.

14.2 UNLINED ROCK SPILLWAYS

For the gravity dam, the quality of the rock required for the dam makes spillway design straightforward. For the rock–fill dam, the optimum design involves consideration regarding maximum use of the excavated rock for construction. It is in this context that technical and economical considerations favor unlined rock spillways. An unlined chute is usually considered to be an excavated trench. It can terminate with discharge over a natural rock surface. The chute may have a short length of paving to ensure that any possible erosion is safe erosion. The general criteria are: unquestionable dam safety, minimum risk of erosion, and accepting some erosion with subsequent maintenance.

There are a number of successful cases of unlined rock spillways such as Ricobayo, Spain, Peixoto, Brazil, Pendari, Australia, Fortuna, Panama, etc. Van Schalkwyk (1994) has listed some 18 dams in South Africa with unlined chutes with discharge intensity varying from 3 to 206 cumec/m, head drop from 37 m to 52 m, and channel slope from 0.02 to 1.0.

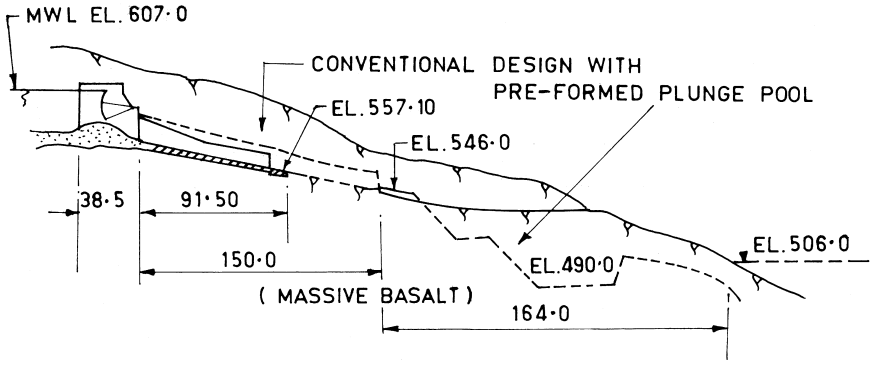

Figure 1 Unlined chute of a spillway.

Figure 1 shows an unlined chute spillway indicating how substantial economy could be achieved over conventional design without compromising safety.

14.3 UNLINED CASCADE SPILLWAYS

An unlined cascade spillway is appropriate when all or most of the rock–fill is to come from the spillway excavation. The cascade, with steps of 10–20 m height, provides more rock than a chute and is more efficient quarry excavation near the dam. Dissipation of energy is to be accomplished during the flow over the cascades and hence this type requires better rock. Some of the existing structures are:

Hell Hole, USA: A cascade of three 25 m steps with lower bench discharging into the natural slope 45 m above the river bed.

James Bay LG-2, Canada – 1.8 km long cascade negotiating a drop of about 110 m in several steps ranging in height from 10 m to 12 m.

Dartmouth, Australia:A total drop of about 180 m. The first 30 m drop is 3H:1V concrete lined slope from an ungated ogee to an unlined bench. The lips of the first two benches are leveled by rock bolted concrete. The bottom bench is below riverbed.

Paunglaung, Myanmar:A drop of about 140 m negotiated by four, 100 m long steps of approximately 35 m height.

14.4 GENERAL CONSIDERATIONS

The most important factors arising while considering a proposal for unlined spillway are:

Whether the rock is sufficiently resistant to erosion so that concrete lining and energy dissipator can be dispensed with

Whether the rock that is available from excavation is suitable for a rock–fill dam.

The answer to the first question requires assessment of the capacity of the flow to erode the bed material and the estimation of the strength of the material to resist erosion. It must be noted that in the phenomenon of scour downstream of flip buckets and free jet spillways, hydraulic forces outweigh the rock properties; however, for the flows parallel to the surface, evaluation of both these forces is necessary. The kinetic energy due to flow parallel to the bed causes loss of joint–fill material, allowing water to enter joints and cracks to cause pressures on the sides and base of rock blocks and shear along the surface. While the hydraulic forces can be assessed with a fair degree of precision and confidence, the property of rock mass to resist erosion is defined only on a macro scale. These features are specific to every site under consideration, and a detailed study of the geology of the site is necessary. However, a site to be considered for detailed studies should have a RQD (Rock Quality Designation) exceeding 75% and lowly stressed rock without erodible seams.

Similarly, the excavated rock for use in rock–fill dam is considered suitable only where UCS (Unconfined Compressive Strength) is exceeding 35 Mpa and water absorption is not more than 3%.

14.5 CONCEPTUAL FRAMEWORK

A conceptual model of the process of erosion is depicted in Figure 2 (Annandale 1995), which consists of three stages: jacking, dislodgement, and displacement. The most important force in the process is believed to be turbulence, causing pressure fluctuations that result in an action that progressively jacks out a material unit from its position of rest. Once jacked out, it is then dislodged by flow and finally displaced.

Since the rate of energy dissipation is indicative of turbulence and pressure fluctuations, and is easier to calculate, Annandale (1995) preferred it as the parameter representing the erosive power of the flow, as

$$P_{ed} = \gamma\, q\, \Delta E \tag{1}$$

where

P_{ed} = rate of energy dissipation

γ = unit weight of water

q = unit discharge

ΔE = energy loss

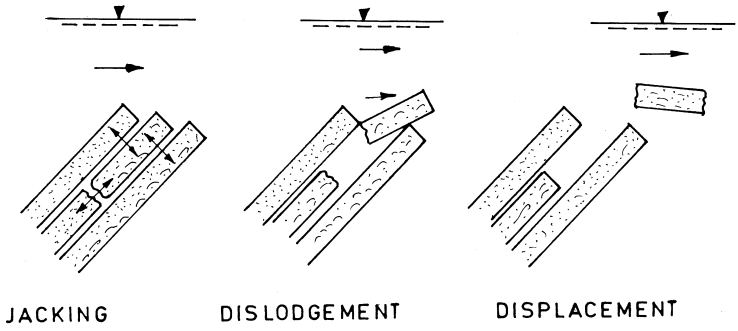

Figure 2 Conceptual model of rock erosion (shown in Annandale 1995).

The relationships giving rates of energy dissipation for different situations are given below:

1. Open channel flow
$$P_{ed} = \rho\ g\ q\ S\ L \quad (kW/m) \tag{2}$$
Where L = unit length.
2. Changes in the bed slope: the situation is depicted in Figure 3 along with notations.
$$P_{ed} = \rho.g\left[\frac{1-\cos(\theta-\alpha)V_g^2}{1+\cos(\theta+\alpha)2g} + S.L\right] \qquad (kW/m) \tag{3}$$

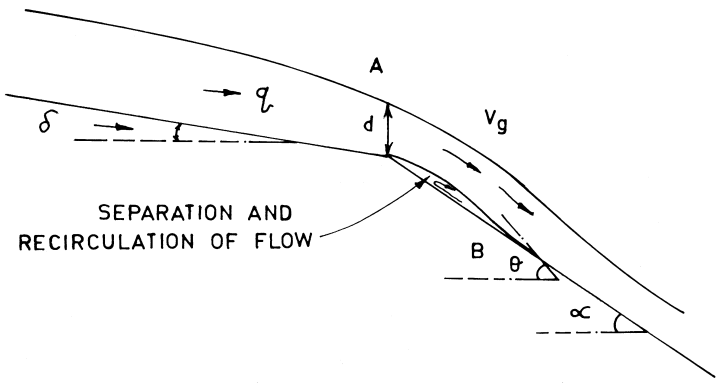

Figure 3 Discharge at a change in grade.

where
V_g = average flow velocity over the flow separation region
S = estimate of average energy slope of water discharging over the flow separation region

3. Drop structure: the situation is depicted in Figure 4 along with notations.

$$P_{ed} = \rho g q y_c \left[\lambda - \frac{y_1}{y_c} - \frac{\lambda}{4}\left(1 + \frac{1.06}{\sqrt{\lambda}}\right)^2 \right] \quad (kW/m) \tag{4}$$

where

$$\lambda = \frac{H}{y_c} + \frac{3}{2} \tag{4a}$$

y_c = critical depth
y_1 = downstream flow depth

4. Classical hydraulic jump forming on a flat portion downstream of steep slopes.

$$P_{ed} = \gamma g \left[y_1 + \frac{q^2}{2g y_1^2} - y_2 - \frac{q^2}{2g y_2^2} \right] \quad (kW/m) \tag{5}$$

Where y_2 is the conjugate depth.

Schalkwyk et al. (1994), however, prefer unit stream power as characterizing the erosive power of the flow. The unit stream power P_{st} is the total power T divided by the area A on which it is dissipated:

P_{st} = T/A and
$T = \rho\, g\, Q\, H$ (6)

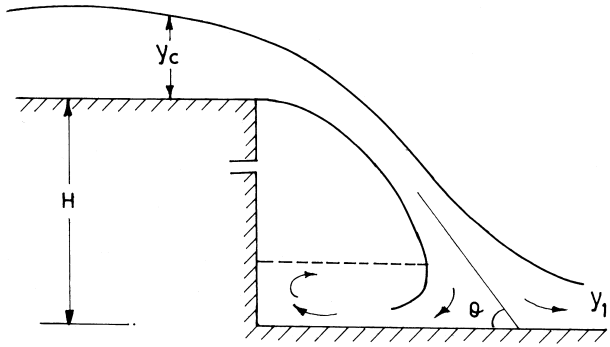

Figure 4 Discharge over the drop structure.

where

ρ = Density of water (1000 kg/m^3)
Q = Stream flow (m^3/s)
H = Total head (m).

For the situations involving open channel flow exerting shear stress, the unit stream power P_{st} is given by

$$P_{st} = \frac{\rho.g.q.S}{1000} \quad kW/m^2 \tag{7}$$

Where S = dH/dx, the slope of the energy gradient
For free fall drop structures, exerting impact force,

$$P_{st} = 3.g\ q\ kW/m^2 \tag{8}$$

The assessment of erosion potential has been based on the correlation of observed data on erosion characteristics with rock mass properties and hydraulic conditions involved. From the literature survey and field observations, it has been established that the erodibility of a rock mass is mainly influenced by the rock material strength, the properties of discontinuities, and the acting stress regime. A reasonable correlation exists between erosion depth, peak flow velocity, and the Kirsten erodibility index K_n that is calculated as follows:

$$K_n = M_s\ [RQD/J_n]\ J_s\ [J_r/J_a] \tag{9}$$

where

M_s = Material or mass strength number of the rock based on the uniaxial compressive strength (0.02 to 280).
RQD = Rock Quality Designation: a standard parameter in drill core logging.
J_n = Joint set number based on joint sets (1 to 5).
J_s = Joint Structure number or Relative ground structure number based on the orientation of the major joint sets with respect to water flow direction (0.37 to 1.5).
J_r = Joint roughness number based on wall roughness and wall contact (1 to 4).
J_a = Joint alteration number based on joint filling and wall separation (0.7 to 18).

Material or mass strength number M_s represents the strength of an intact representative sample without regard to geological heterogeneity within the mass. $\left[\frac{RQD}{J_n}\right]$, also called particle/block size number K_b refers to the mean size of blocks of intact rock material as determined by joint spacing within the rock mass. RQD is the Rock Quality Designation, a standard parameter in drill core logging and J_n is the joint set number, which is a function of the number of joint sets in a rock mass. K_b ranges between 1 and 100 for rock materials.

J_s is the relative ground structure number accounting for the structure of the ground with respect to the direction of the flow. It is a complex function expressed in terms of the orientation and shape of individual blocks determined by joint set spacing, dip angles and dip directions. $\left[\frac{J_r}{J_a}\right]$, also called K_d, is the discontinuity or inter particle bond shear strength number and represents the strength of joint interfaces in rock mass.

Schalkwyk et al. (1994) have indicated appropriate values for these parameters, slightly modified from the original reference (Kirsten 1982), for application in spillway channels, which are given in Appendix 1.

The above parameters have to be assessed from field investigations and should preferably be refined during construction after the overburden has been removed and rock surface is accessible.

Both the investigators have analyzed field data in respect of erosion of unlined spillway channels in the form

$$P = f(K_n) \tag{10}$$

Annandale (1995) has based his analysis on 137 field observations of spillway performance and other data, and correlated erosion characteristics with rate of energy dissipation per unit width of flow, i.e. P_{ed}, as shown in Figure 5.

Based on the observation of erosion characteristics of 18 spillway sites representing nine major rock types and floods ranging from 3 to 206 m^2/s with

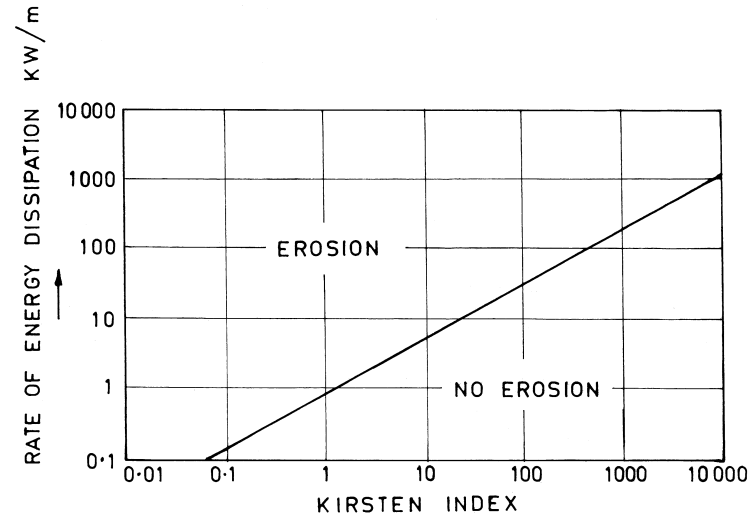

Figure 5 Scale of probable erosion (shown in Annandale 1995).

Appendix : 1 Tables for Assessment of Kirsten Index (From Ref-6)

1. Material or mass strength number Ms

Material description	Uniaxial strength	M_s
Very soft cohesive soil	0–80 k Pa	0.02
Soft cohesive soil	80–140 k Pa	0.04
Firm cohesive soil	140–210 k Pa	0.09
Stiff cohesive soil	210–350 k Pa	0.19
Very stiff cohesive soil	350–750 k Pa	0.41
Very soft rock	1–3 M Pa	1–2
Soft rock	3–13 M Pa	2–8
Hard rock	13–24 M Pa	8–35
Very hard rock	26–106 M Pa	35–70
Extremely hard rock	106–212 M Pa	70–280

2 Joint set number J_n

Description of joint set.	J_n
No Joints	1.0
1 Joint set	1.22
1 Joint set plus random	1.50
2 Joint sets	1.83
2 Joint sets plus random	2.24
3 Joint sets	2.73
3 Joint sets plus random	3.34
4 Joint sets	4.09
Multiple joint sets	5.00

3 Joint Structure number J_s

		J_s for block aspect ratio of			
Dip direction	Dip angle	1 : 1	1 : 2	1 : 4	1 : 8
–	90	1.0	1.0	1.0	1.0
Downstream	10	1.22	1.10	0.93	
	30	0.63	0.59	0.53	–
	60	0.49	0.44	0.37	
Upstream	10	0.63	0.70	0.81	
	30	0.49	0.53	0.59	–
	60	0.63	0.67	0.37	

4. Ratio of joint roughness to joint alteration (J_r/J_a).

Rock type	Friction angle (degree)	$J_r/J_a = \tan\theta$
Quartzite	65	2
Sandstone	40–55	1
Dolerite (sound)	40	0.8
Dolerite (decomposed)	25	0.5
Shale	20–22	0

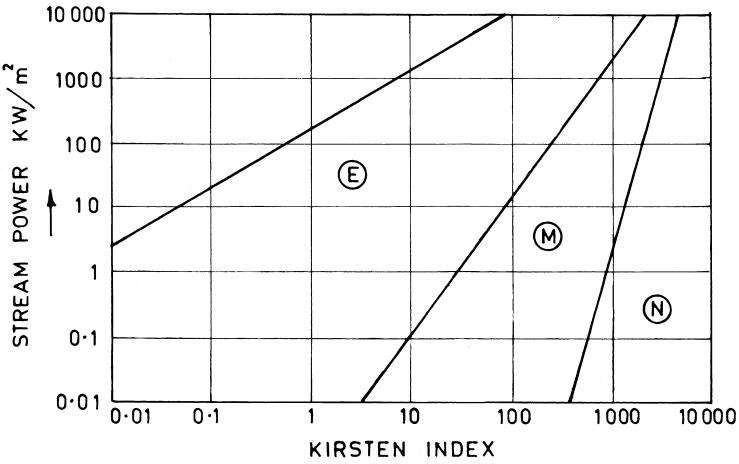

Figure 6 Scale of probable erosion. Extent of erosion: E: Excessive, M: Moderate, N: None. (shown in Schalkwyk et al.1994).

head drop from 37 m to 52 m, a diagram (Fig. 6) has been presented by Schalkwyk et al. (1994) giving scale of likely erosion with reference to Kirsten index K_n and unit stream power P_{st}.

Based on the analysis of the results, Schalkwyk et al. also make the following recommendations in Table 1.

Although, this method of erodibility assessment may not be representative for all geometrical, geomechanical, and hydraulic situations, it may be used as a first indication of erosion potential for rock in unlined spillways.

14.6 ROCK–FILL SPILLWAYS

In a rock–fill spillway, the discharge channel is paved with a layer of natural stones, overlying a filter layer. Increasing preference is given to rock–fill spill-

Table 1 Erosion Potential and Recommendations

Depth of erosion, m	Erosion potential	Rock quality	Recommended Action	Application
0–1	Low	Resistant	Leave unlined	Plunge pool Unlined channel
1–5	Medium	Moderate	Partly lined	Stilling basin
>5	High	Poor	Total lining	Apron lined channel

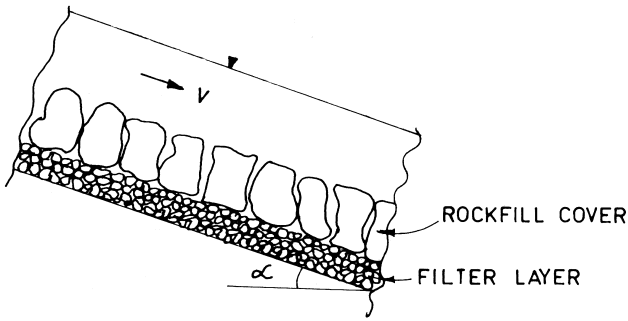

Figure 7 Typical rock–fill spillway channel.

ways for small earth dams with a height not exceeding 10 m or so. The spillway of this type is an attractive option because of its environmental friendly design and structural flexibility, in comparison with the conventional concrete lined structures, as well as good applicability as an auxiliary structure for increase in the spillway capacity of existing dams. Because of the loose cover of rock material, there is a strong interaction between flow and structure. Therefore, an interactive hydraulic and geotechnical design is necessary to meet the required safety standards for such spillways. Figure 7 shows details of a typical rock–fill spillway channel.

Design Considerations

The flow through and over a rock–fill layer has been investigated by Olivier, Linford and Saunders, and Hartung and Scheuerlein. Knauss (1979) has made a critical analysis of the results of various investigators and suggested the relationship for the size of the stone evolved by Hartung and Scheuerlein (1970), after modification as

$$\frac{q_{\max}}{\sqrt{g D_s^{3/2}}} = 1.9 + 0.8\Phi - 3Sin\alpha \tag{11}$$

where

q_{max} = Maximum unit discharge (m^2/s) corresponding to the threshold of the motion of individual stone in a rock fill layer

D_s = Equivalent diameter of the stone in the rock fill layer, being identical with the diameter of a sphere of the same volume as the average stone within the layer (m)

Φ = Packing factor of stones
= $0.0575\ G_s\ N^{3/2}$
Gs = Weight of the average stone (kN)
N = Number of stones per unit area (stones/m^2)
α = Angle of slope [°]

The factor $\frac{q_{\max}}{\sqrt{g D_s^{3/2}}}$ is generally termed as stone Froude number, although the term containing the density namely, $F_r = \frac{q}{\sqrt{\frac{\rho_s - \rho_w}{\rho_w} . g . D_s^3}}$ is more commonly used

Rathgeb (1999) has further investigated the aspect of the stability of the rock–fill layer. There was a large variation among the results obtained in respect of stone Froude number, applying various relationships: Hartung and Scheuerlein, Knauss, Larsen (unpublished), as well as his own studies. It was revealed that the shape of the stones and packing effect were also influencing the stability in addition to the weight of the stone and that similarity between the results obtained from the model and in nature in respect of these two parameters cannot be ensured.

The design of the rock–fill spillway consists of hydro–mechanical and geotechnical parts. The former deals with the equivalent stone diameter and its stability while the latter concerns with the stability of the rock–fill layer as a whole. Rathgeb conducted laboratory experiments on a large size model to analyze the pressures and forces that determine the stability of the individual stone and of the rock–fill layer. Tests were made on the natural stones as well as on concrete blocks of regular shapes that enabled measurement of turbulence pressure fluctuations.

Figure 8 shows various parameters involved in the process. The effect of the shape of the stones is represented by the offset Δh between the two adjacent stones, such as 2 and 3. The effect of packing is represented by the gap between the two adjacent stones such as 1 and 2. Both these parameters induce fluctuating pressures that act in the direction of the flow and perpendicular to it and influence the stability of the stone and the layer.

Following the terminology of Figure 8,

L_s = Length of the stone in the direction of the flow, m
D_s = Thickness of the stone, m
Δh = Offset, m
y = Flow depth, m
e_x = Lever arm for hydrodynamic force in X- direction, m
e_y = Lever arm for hydrodynamic force in Y- direction, m
v = Flow velocity, m/s
α = Slope angle

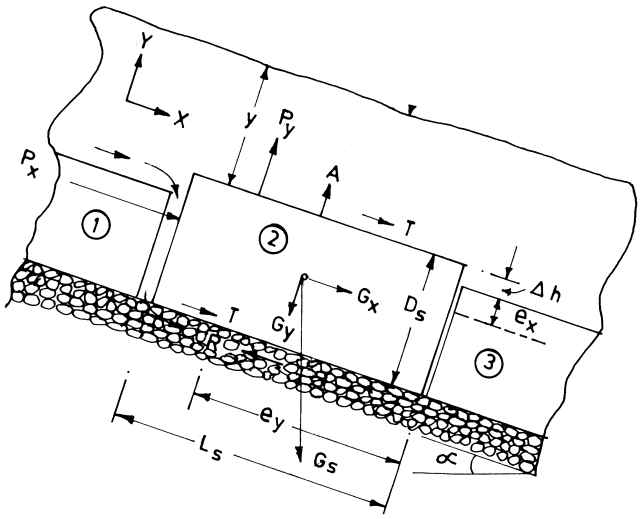

Figure 8 Stability of rock–fill layer (shown in Rathgeb 1999).

G_s = Weight of stone with its components G_x and G_y, N/m
A = Uplift force, N/m
P_x = Hydrodynamic force in X direction, N/m
P_y = Hydrodynamic force in Y direction, N/m
R = Friction force, N/m
T = Flow shear force, N/m

Hydrodynamic forces are given by

$$P_x = \frac{1}{2} C_{f,x} \rho_w v^2 D_s$$
$$P_y = \frac{1}{2} C_{f,y} \rho_w v^2 D_s \qquad (11a)$$

Where ρ_w is the mass density of water and C_f are the force coefficients obtained from pressure measurements.

The force R resisting sliding is

$R = (G_y - P_y - A)Tan\theta$ (θ is the angle of internal friction)

The force causing the layer to slide is $(P_x + G_x)$

Safety against sliding

$$\eta_{es} = \frac{R}{(P_x + G_x)} \qquad (12)$$

Similarly, safety against erosion or dislodgement of individual stone

$$\eta_{er} = \frac{\frac{G_y.L_s}{2} + G_x\left(\frac{D_s}{2} - \Delta h\right) + P_x.e_x}{P_y.e_y + \frac{A.L_s}{2}} \tag{13}$$

Rathgeb comments that the friction force R resisting the sliding may be rendered less effective due to the turbulence pressure fluctuations, and hence the sliding stability may be reduced for high discharges. It would, therefore, be necessary to introduce crossbars at appropriate intervals to withstand the tangential surplus forces.

Notations

A = Area (m^2)
= Uplift force, N/m
D_s = Thickness of the stone, m
e_x = Lever arm for hydrodynamic force in X- direction, m
e_y = Lever arm for hydrodynamic force in Y- direction, m
G_s = Weight of stone with its components G_x and G_y, N/m
g = Acceleration due to gravity (m/s^2)
H = Head drop (m)
J_a = Joint alteration number
J_n = Joint set number
J_r = Joint roughness number
J_s = Joint structure number
K_n = Kirsten's erodibility index.
L = Unit length
M_s = Material or mass strength number
P_x = Hydrodynamic force in X direction, N/m
P_y = Hydrodynamic force in Y direction, N/m
P_{ed} = Rate of energy dissipation per unit width of flow (kW/m)
P_{st} = Unit stream power (kW/m^2)
q = Unit discharge
R = Friction force, N/m
RQD = Rock Quality Designation
S = Slope of the hydraulic gradient.
T = Total stream power (kW)
= Flow shear force, N/m
v = Flow velocity, m/s
V_g = Average velocity over the flow separation regime.
y = Flow depth, m

y_1 = Pre-jump depth
y_2 = Conjugate depth
y_c = Critical depth
ΔE = Energy loss
Δh = Offset, m
γ = Unit weight of water
θ, = α Angles

REFERENCES

1. Annandale, G. W. Erodibility – Jnl. of Hydraulic Research, IAHR, 1995.
2. Hartung, F.; Scheuerlein, H. Design of overflow rockfill dams, 10th ICOLD, Q 36, R 35. Montreal, 1970.
3. Kirsten, H. A. D. A classification system for excavation in natural materials, The Civil Engr. In South Africa, July 1982, 293–308.
4. Knauss, J. Computation of maximum discharge at overflow rockfill dams (A comparison of different model test results), 13th ICOLD, Q 50, R 9, 1979.
5. Rathgeb, A. Design criteria for rock fill spillways, Proc. 28th IAHR Congress, TU-GRAZ, Austria, 1999.
6. Van Schalkwyk, A.; Jordaan, J. M.; Dooge, N. Erosion of rock in unlined spillways, Q 71, R-37, 18th ICOLD. Durban, 1994.

15
Inflatable Rubber Weirs

15.1 INTRODUCTION

Inflatable rubber dams are long tubular shaped fabrics placed across watercourses to impound or regulate storage behind them. On an ungated spillway crest or top of a dam, they serve to increase and regulate reservoir storage. Placed on the sill of a low-height diversion weir for an irrigation or power generation project, they function as gates to provide automatic flushing of sediment through deflation at the time of floods, thus eliminating the need for settling tanks. They also serve as the barrier between fresh and salt water or as a storm surge barrier protecting a delta. Rubber weirs are being increasingly used on several projects in Japan, USA, Australia, Hong Kong, the Netherlands, etc. Despite having peculiar problems of design and installation, rubber weirs offer significant advantages in respect of dependability, simplicity of operation, and maintenance.

15.2 PRINCIPAL ELEMENTS OF A RUBBER WEIR

A typical rubber weir installation consists of an upper structure (rubber tube), a lower structure (concrete sill or foundation), and an operating system. Figure 1 shows schematic details of a typical rubber weir installation.

A large tube is made of a thick rubberized fabric, anchored at the base and sides. This, obviously, is the most important element in the entire installation, as it has to resist the water load due to impounding, peripheral tension due to inflation, wear and abrasion due to passing of debris and other floating material during overflow, and fatigue caused due to alternate inflation and deflation. During certain conditions of overflow, it may also be subjected to vibrations. Rubberized fabrics are, therefore, composed of nylon fabric reinforcement for internal strength and coating with protective material like EPDM (Ethylene Propylene Diene Monomer) layers as also stainless steel meshes and ceramic chips. These materials

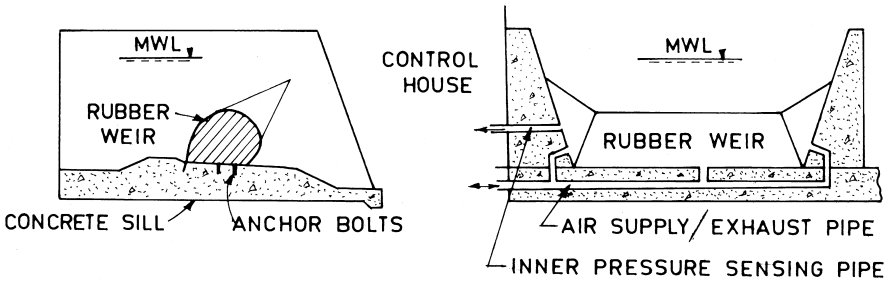

Figure 1 Schematic details of a typical rubber weir installation.

afford protection against ozone and ultraviolet light, abrasion, knife cutting, and fatigue. It is claimed that a coating with steel-mesh reinforcement will prevent fatigue failure until 1000 cycles of inflation and deflation.

The height of the rubber weir is normally up to 3 m. There is practically no restriction on the width. A single unit may have width up to 200 m and several such units can be placed side by side. The 8.2 m high rubber weir on river Ijssel, Netherlands, is perhaps the highest weir constructed so far.

The thickness of the rubber material is related to the height of the weir and varies from 8.6 mm for heights less than 1 m, to 22.5 mm for heights up to 6 m. Generally, the rubber fabric will have a life expectancy ranging from 25 to 40 years. Figure 2 shows cross–sections of a rubber dam fabric with different types of protective coating.

Ishimura (1995) has described a method of protecting the rubberized fabric from impact of boulders by placing a cushion inside the tube which, when deflated, helps absorb the impact as shown in Figure 3.

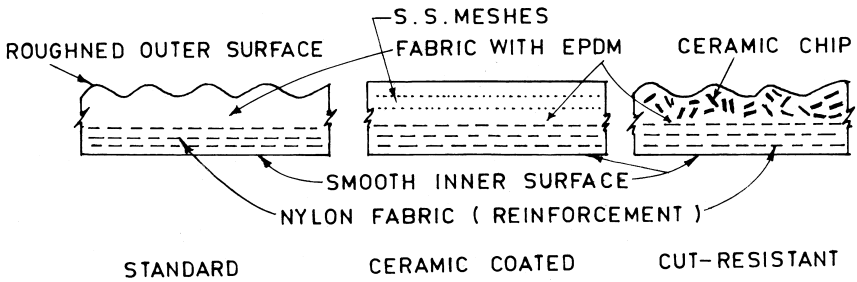

Figure 2 Cross–sections of rubber dam fabrics. (Tam et al. 1999)

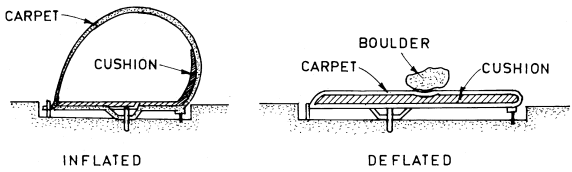

Figure 3 Cushion to absorb the impact loads (shown in Ishimura 1995).

The lower structure consists of concrete sill along with side walls that provide for anchorage of the rubber weir and is designed as per the standard procedure. Generally, the unfolded shape of the rubber membrane is rectangular across the width of the foundation with triangular ends, which represent the side slopes of the river channel. The membrane is anchored on its periphery with anchor lines on the upstream and downstream. These two lines meet at the vertex of the side slope.

Rubber weirs are filled either with air or water. The obvious advantages of filling with air are: speedy inflation/deflation, absence of freezing problems, and near circular shape of the cross–section that occupies comparatively lesser width at the foundation than water filled weir. However, overflow on the air filled rubber weirs is restricted to about 20% of its height, against about 50% height permissible with the water filled weirs. The pressure inside the weir is expressed as the pressure above the atmosphere.

The operating system provides for the inflation/deflation as per the water level upstream of the weir. Both water and air can be used to inflate the weir, but the air is preferred in view of the short time required for the process. Water filling is resorted to when stability of the weir against uplift due to ground water or waves is required. The 8.2 m high weir on river Ijssel in the Netherlands is partly filled with water and partly with air, to optimize the advantages of both. Inflation is generally done with a blower of the required capacity whereas deflation is through natural exhaust.

15.3 DESIGN CONSIDERATIONS

15.3.1 Hydraulic Design

The design in respect to the height and length of the weir, depth of overflow, etc. is finalized as per the standard procedure, taking into account the functions to be performed by the weir such as irrigation, flood control, power generation, etc. The special features of design in respect of rubber weirs are: sequence of inflation/deflation and measures for preventing vibrations.

Sequence of Inflation/deflation

In operating a rubber weir, its performance must be determined to secure the safety of the weir itself and the intake function and to assure the absence of adverse influences on both the upstream and downstream river channels. Since pumping/withdrawal of large volumes of air/water is involved in the process of inflation/deflation, the time taken in the process can be longer and may influence the rate of raising/lowering of the river water levels, which in turn affect the performance of the weir in accomplishing the objectives.

The design philosophy would be clear by the example of the inflatable rubber weir for the Kurotani power station, Japan, as described by Ishimura (1995). The 6 m high rubber weir will be subjected up to the design maximum discharge of 1120 cumec with a design flood water level of El 679.5 m, the top of the weir in inflated position being at El 678 m with the sill of the concrete structure at El 672 m. The weir is to divert a discharge of 12 cumec for generation of 19.6 MW of power. The weir is located in the mountainous reach where the river carries sediment load up to boulders of 60–70 cm in size. To prevent deposition upstream of the weir and in the vicinity of the power intake, the rubber weir has to be kept deflated as long as the flow rate is large enough to move the riverbed armor coat. The displacement limit flow rate, calculated from the armor coat grain size measured at the site in question, was about 35 cumec. Thus, the weir will be deflated as soon as the discharge exceeds 35 cumec. Just as the deflation begins, the water level in the downstream starts to rise. Since there is a statutory restriction on the maximum rate of rise, of 30–50 cm/30 min, the rate of deflation has to be in consonance with this. However, if the rate of deflation happens to be slower, it will result in a too fast rising of water level on the upstream because of continuous increase in the discharge. Thus, this calls for another threshold value of the discharge by when the deflation should be completed. In the present case, the deflation is to be completed before the discharge exceeds 150 cumec. The result of the analysis was:

Deflation

Upstream water level: El 678.80 m (overflow depth 0.8 m)
Discharge: 31.8 cumec and increasing
Duration: 120 min, speed 1.0–19 cm/min

Inflation

Upstream water level : El 672.44 m (overflow depth 0.44 m)
Discharge : 31.8 cumec and decreasing
Duration : 90 min, speed 1.5–9 cm/min

In the above example, the deposition of sediment upstream of the weir was a key parameter in determining the inflation/deflation cycle. Similar other parameters could be controlling the spread of pollutants, cooling water requirements of thermal power plants, water releases for fish, etc.

Flow induced vibrations

During overflow on the inflated rubber dams, vibrations might result from the fluid-structure interactions. Ogihara et al. (1985) have analyzed this in detail. The source of the fluid-structure interaction and resulting vibration of the structure is believed to be the Coanda effect. This effect happens when the overflowing nappe adheres to the downstream face of the weir which leads to the flow instability at the base of the nappe (i.e. next to the separation point.) and pressure fluctuations on the downstream face of the weir.

Model study is indispensable while ascertaining the suitability of a rubber weir installation in a situation where there is potential for fluid-structure interaction and problems of vibration. This necessitates dynamic similarity of elongation of the rubber fabric, which implies equality of Structural Merit law in addition to Froudian scaling law between the model and the prototype. The Structural Merit number is the ratio of inertial forces to elastic forces with reference to a characteristic length dimension and is expressed as $S = L\gamma/E$, where L represents thickness of the fabric, γ is the density, and E the elasticity of the rubberized fabric.

Jongeling et al. (1999) have described model study to determine the wave induced response of an inflatable barrier of 8.5 m height, placed across a river, and inflated when a severe storm occurs. Special attention was paid to a correct scaling of both the stiffness of the air in the dam and the over-pressure related to the atmospheric pressure. Both the over-pressure in the dam and the tension stiffness of the sheet appeared to be important parameters in the response of the dam.

Chanson (1998) conducted laboratory experiments to investigate nappe trajectory and wall pressure distribution on the downstream face of a circular shaped rubber dam, down the point of separation of the overflowing nappe with the weir surface. Following the notations in Figure 4a, the dimensionless wall pressure distribution at any position Φ, is given by

$$\frac{P_{atm} - P_s}{\rho_w g R} = \frac{d}{R}\left[F^2 - \cos\phi\left(1 + \frac{d}{2R}\right)\right] \quad (1)$$

where

d = Depth of flow

P_s = Absolute pressure at the wall

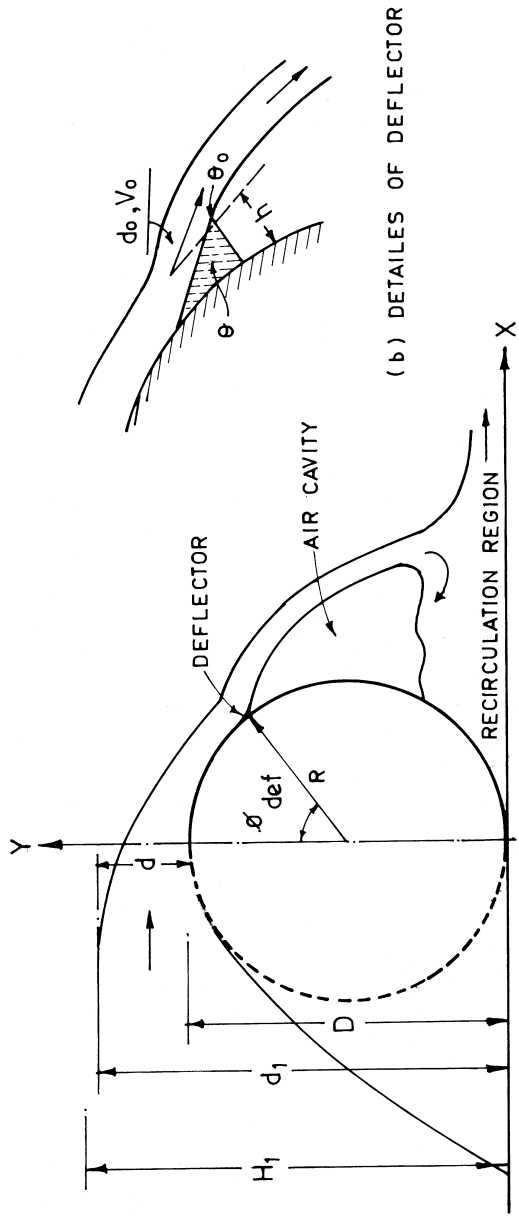

Figure 4 Rubber dam overflow: nappe trajectory (shown in Chanson 1998).

P_{atm} = Atmospheric pressure
ρ_w = Density of water

$$F = \text{Froude number} = \frac{V}{\sqrt{gR}}$$

It has been shown that Equation 1 predicts an increasing suction pressure (P_{atm}-P_s) down the surface as the flow is accelerated. This may cause the nappe to adhere to the wall surface and lead to flow instability and pressure fluctuation on the downstream face of the dam and vibrations of the flexible membrane. Nappe adherence instability can be eliminated by deflecting the nappe off the rubber wall. Chanson also suggests provision of a deflector at suitable location on the surface. Figure 4b shows a typical deflector with an angle θ and height h, defined by the position Φ_{def}. The deflected nappe angle θ_0 at take-off is smaller than the deflector angle θ, and is approximately given by

$$\frac{\theta_0}{\theta} = \sqrt{\tanh\left[\frac{h}{d_0\theta}\right]} \tag{2}$$

Where d_o and v_o are the values at the take-off point. The trajectory equations of a ventilated nappe are

$$\frac{x}{R} = \frac{V_0}{\sqrt{gR}}\cos(\phi_{def} - \theta_0)\sqrt{\frac{gt^2}{R}} + \frac{x_0}{R} \tag{3}$$

$$\frac{y}{R} = -\frac{1}{2}\frac{gt^2}{R} - \frac{V_0}{\sqrt{gR}}\sin(\phi_{def} - \theta_0)\sqrt{\frac{gt^2}{R}} + \frac{y_0}{R} \tag{4}$$

Where x is the horizontal direction, y is the vertical direction, t is the time, x_o and y_0 are the coordinates of the deflector edge, and Φ_{def} is the angular position of the deflector. It was also concluded that the optimum location of the deflector was $30° \leq \varphi_{def} \leq 60°$ to avoid reattachment of the flow.

A tentative deflector configuration namely Φ_{def}, h, and θ is the starting point of the calculations. Knowing the velocity and depth of flow at the crest, d_0 and V_0 are obtained from the energy equation, neglecting losses. The angle θ_0 is calculated from Equation 2. Inserting $y = R(1 + \cos\phi_{def})$ in Equation 4, the time t_0 is determined. Thereafter, x and y are determined for various time steps, $t \leq t_o$. This procedure is repeated until a suitable trajectory is obtained.

It is found that if the depth of overflow is less than 20% of the height of the weir, vibrations might not occur.

Methods to reduce vibrations are: increasing the rigidity of the structure by increasing stretching strength of the membrane per unit length and improving hydraulic conditions in the over-fall region.

Increasing the inner pressure of the dam, filling it with water instead of air, and decreasing the distance between the two anchoring lines at the base can increase rigidity of the structure.

15.3.2 Structural Design

The structural design comprises:

- Assessment of the impact force on the deflated rubber fabric due to rolling of the boulders and hence thickness of the cushion.
- Estimation of the peripheral tension in the fully inflated position and to arrive at the required tensile strength of the fabric and its thickness.
- Details of fasteners, anchor bolts, etc.
- Details of the lower structure, side walls, etc.

It is required to ascertain the size of the boulder that can be lifted by the flow and the energy imparted by that boulder on the membrane while impinging. Assuming that a typical boulder is of spherical shape, with a diameter a, the drag force exerted by the flow on river bed F is

$$F = C_D\left(\frac{\pi}{4}a^2\right)\rho\frac{v^2}{2} \tag{5}$$

where

a = Diameter of boulder assuming it as a sphere
C_D = Drag coefficient for sphere (appx C_D = 1)
ρ = Spcific gravity of river water
v = Flow velocity

The weight of the boulder in water is

$$W = (\rho_s - \rho)\frac{1}{6}\pi a^3 \tag{6}$$

Where ρ_s = Specific gravity of boulder ≈2.65.

The threshold of lifting of the boulder is represented by F = W. Thus,

$$\mathrm{a} = \frac{3}{4}C_D\frac{\rho V^2}{(\rho_s - \rho)} \tag{7}$$

The energy of such a boulder is given by

$$\mathrm{E} = \frac{W}{g}\frac{v^2}{2} \tag{8}$$

The above information is used to determine the suitable type of cushion and its thickness from the range of specifications of material commercially available.

The tension in the rubberized fabric is maximized in the peripheral direction, immediately before the process of deflation. A factor of safety of 8–10 is usually

adopted while deciding on the required breaking strength of the rubber material. For the 6 m high Kurotani weir with a maximum depth of overflow of 1.5 m, a 3-ply reinforced rubberized fabric 16 mm thick, having a breaking strength of 1600 kg/cm was used.

15.4 PROBLEMS ASSOCIATED WITH RUBBER WEIR INSTALLATION

Although rubberized fabrics can be made stiff and strong to withstand natural calamities, they could be damaged due to extraneous factors. Hakin et al. (2002) have reported a case of two uncontrolled deflations of 3.5 m high $\times$ 40 m long rubber weirs, used as control gates on the crest of Lyell dam, Australia. One of the failures was due to software malfunction in the gate operating system while in other it was due to manufacturing defects. Tam and Zhang (1999) have listed several problems associated with rubber weirs such as:

- Damage due to vandalism
- Damage due to flood-borne debris
- Damage due to deflation: during deflation, sharp objects lying on the base immediately downstream of the dam can puncture the body of the rubber weir
- Damage due to vibration
- Damage due to abrasion
- Fire damage
- Air loss: rubber itself is gas permeable. Therefore, no matter how well the dam installation has been done, some air loss is bound to occur. It would be necessary to reinflate it periodically to maintain inner pressure.
- Vulnerability to weathering
- Concentration of condensation water: frequent inflation and deflation cause changes of inner air pressure, resulting in accumulation of condensation water inside the dam body which can prolong deflation time. Regular opening of the discharge outlet is necessary to release the condensation water.

The above factors need to be taken into consideration while designing, constructing, and operating the structures.

Notations

a = Diameter of boulder
C_D = Drag coefficient of boulder, assumed spherical shape

d = Depth of flow
E = Energy of the boulder imparted on the rubberized fabric
F = Drag force exerted by the flow on the river bed
h = Height of deflector
P_{atm} = Atmospheric pressure
P_s = Absolute pressure at the wall
R = Radius of the weir cross section
t = Time
V_0 = Velocity of the nappe at the edge of the deflector
v = Velocity of flow in the river
W = Weight of the boulder
x = Coordinate of trajectory in horizontal direction
x_0 = x- coordinate of the deflector edge
y = Coordinate of trajectory in vertical direction
y_0 = y- Coordinate of the deflector edge
Φ = Angular position of a point on weir surface
Φ_{def} = Angular position of the deflector
θ = Angle of deflector
θ_0 = Deflected nappe angle at take-off from the deflector
ρ = Specific gravity of river water
ρ_s = Specific gravity of boulder

REFERENCES

1. Chanson, H. Hydraulics of rubber dam overflow: A simple design approach, 13th Australian Fluid Mechanics Conference; Monash University, Melbourne, Australia, 1998.
2. Hakin, W. D.; Siers, P.; Solomon, P. Defusing the situation, International Water power and Dam Construction, October, 2002.
3. Ishimura, Y. Design and installation of inflatable rubber weir, Water and Energy 2001; International R & D conference, CBIP, New Delhi: India, 1995.
4. Jongeling, T. H. G.; Rovekamp, N. H. Wave-induced response of inflatable barrier, 27th IAHR Biennial Congress, Graz, Austria, August 1999.
5. Ogihara, K.; Maramatsu, T. Rubber dam : Causes of oscillations of rubber dams and countermeasures, Proc 21st IAHR Congress, Melbourne, Australia, 1985.
6. Tam, P. W. M.; Zhang, X. Management of rubber dams in Hong Kong: Canadian Journal of Civil Engineering, 1999.

16
Overtopping Protection of Dams Used as Spillways

16.1 INTRODUCTION

Studies that assess the abilities of existing spillways to handle floods of various magnitudes have revealed that a large number of them were considered hydrologically deficient in that they were unable to contain or safely pass the current design flood or PMF without overtopping. They must be remodeled to handle floods larger than they were designed. Common remedial measures include raising the dam, adding parapet wall, addition of spillway capacity by modifying existing spillway or adding labyrinth/fuseplug/fusegate spillways, allowing overtopping of non-overflowing portions to let out part of flood discharge, etc. An analysis by Oswalt (1992) of some 140 projects that underwent such modifications, shown in Figure 1, indicates different alternatives adopted. It will be seen that overtopping protection was preferred for as many as 48 projects (i.e. about 35%). Obviously, overtopping protection remains a reasonable, safe, and the most economical solution. Both concrete and embankment dams can be provided with overtopping protection. Advances in technology, particularly roller compacted concrete (RCC) and precast concrete blocks, have made this approach more workable and reliable.

16.2 CONCRETE DAM OVERTOPPING PROTECTION

Concrete dams are often located in steep canyons where the topography does not allow construction of large auxiliary spillways. Overtopping of a non-overflow dam, for a small duration during PMF, is generally permitted, ensuring that the safety of the dam proper will not be jeopardized. Armoring of the downstream toe and abutments may permit overtopping of the dam as an acceptable feature and provide the cost-effective means of increasing reservoir release capacity for

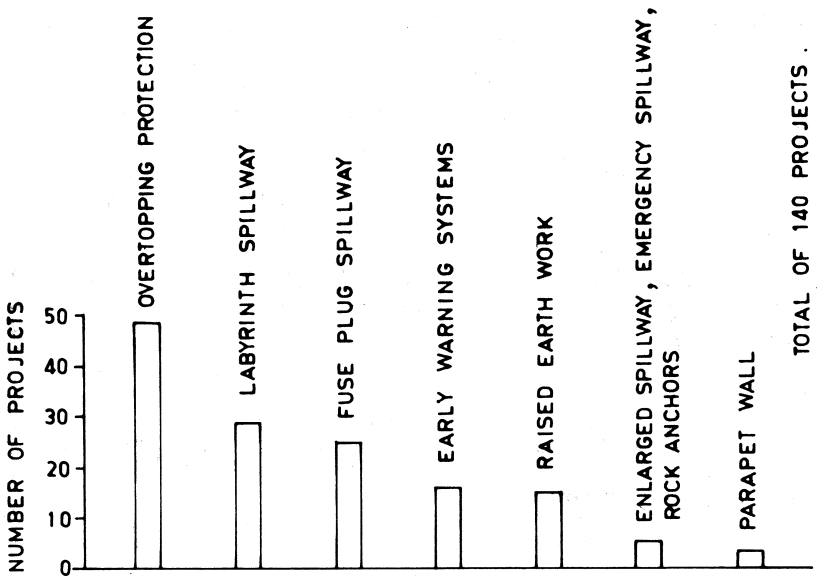

Figure 1 Type of modifications to accommodate larger floods (shown in Oswalt 1992).

higher floods. Overtopping protection must provide adequate energy dissipation of the flow and ensure stability of the dam. Since the overtopping flows will normally impinge on the downstream area in the form of free falling jets, the design of downstream foundation protection must adequately cover all potential failure modes and loading conditions. These are: scour, hydraulic jacking, hydrodynamic pressure fluctuations, abrasion, and increased pressures.

The most common method of protecting the downstream area for an overtopping concrete dam is to provide a protective slab made of cast-in-place concrete or roller compacted concrete (RCC). For the areas having exposed rock of good quality, rock bolting may be used to create a larger foundation acting as a single unit to resist scour or uplift. RCC normally has a significantly lower cost than conventional cast-in-place concrete and may be used to provide massive buttresses for protection of dam foundation. This larger mass may also be sufficient to resist uplift pressures without anchorage or reinforcement, although a drainage system is commonly provided. Santa Cruz dam in the United States is the first concrete arch dam with a RCC buttress. This dam, originally designed in 1929, was found to be capable of surplussing spillway floods only every 10 years without overtopping. The modification design consisting of a new outlet work, a new stepped

overflow spillway, and a RCC buttress is now adequate to ensure safety even up to PMF (Metcalf et al. 1992).

16.3 EMBANKMENT DAM OVERTOPPING PROTECTION

The earliest example of providing protection for a planned overtopping of an embankment dam is the Cottonwood Dam No. 5 (USA), where a flexible membrane called geomembrane was used.

Since 1983, extensive research and large scale field testing has been conducted in the USA, Great Britain, and the former Soviet Union to develop a more durable form of lining for overtopping protection of embankment dams. Protection systems include grass lining, geotextile membrane, riprap, gabions, in situ concrete, RCC concrete, and precast concrete mats, blocks, and slabs. Oswalt (1992) further analyzed the 48 cases of overtopping protection referred to earlier in terms of type of protection adopted, as shown in Figure 2. It will be seen that protection with RCC and concrete overlays accounted for approximately 60% of the cases, where as precast concrete blocks accounted for about 10%.

16.4 DESIGN CONSIDERATIONS

The design of any type of overtopping protection is intimately related to many site-specific issues such as the design flood, consequences of failure, downstream

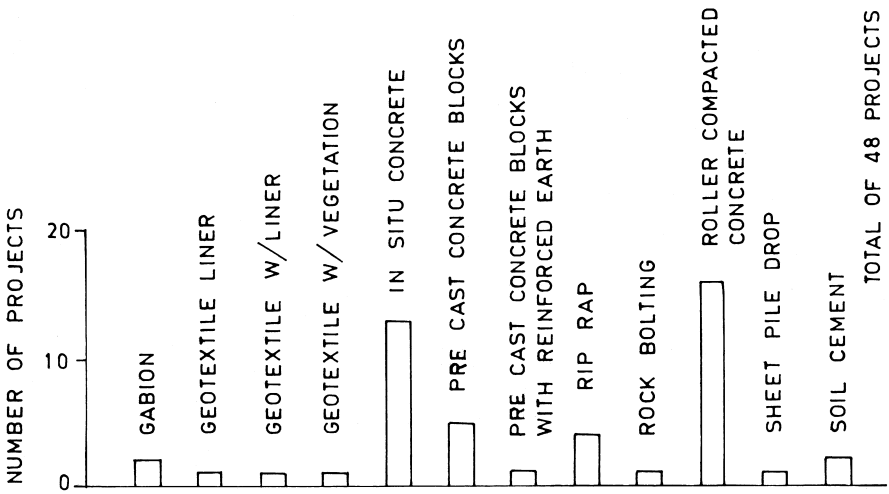

Figure 2 Types of overtopping protection (shown in Oswalt 1992).

impact, site topography, existing embankment design, and materials etc. An overtopping protection system for embankment dams greater than 30 m in height require detailed analyses to ensure stability for high unit discharge and velocity.

McLean et al. (1993) discuss various design needs in the case of embankment overtopping with reference to Figure 3 that helps visualizing various problems that may be encountered. As the flow lines from the upstream reach approach near crest, part of the upstream slope may be subjected to flow velocities, which otherwise would have been a stagnant zone. In most cases, the standard riprap protection already provided in this portion may be adequate to withstand these velocities.

The flow then becomes nearly parallel to the crest, and a transformation of the sub-critical flow to critical state occurs and flow velocities increase. Protection against erosion may be necessary in this portion. As the flow passes down the downstream corner, separation followed by negative pressures takes place over the edge and immediate downstream slope. Generally, RCC crests block with rounded shape, extending on the upstream slope and with a cutoff as shown in Figure 5 is provided. Special care is necessary to prevent seepage of the flow into the underlying material.

The flow on the slope remains in a supercritical state with velocities increasing as it descends further down. Any protective layer that is provided in this portion should be designed to resist the velocities and uplift forces, both hydrodynamic and due to seepage. Seepage flow may be influenced by the flow through the embankment and by infiltration into the downstream slope by the flow down the slope. Filters and pressure relief drains are provided to drain out the seepage flow.

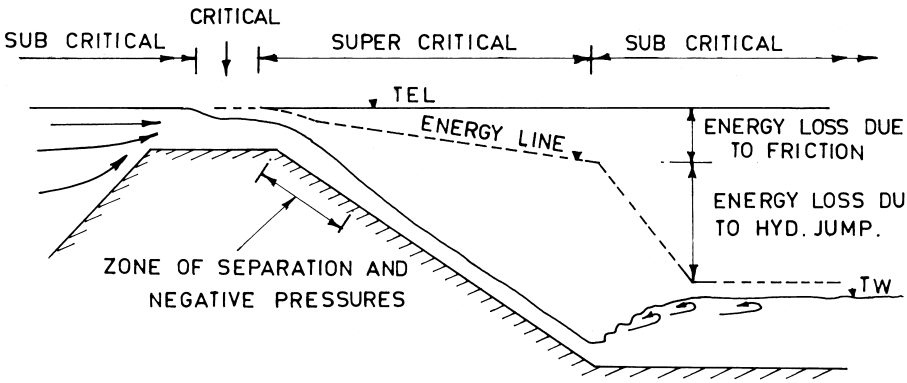

Figure 3 Schematic of embankment overtopping. (McLean et al. 1993)

The protective lining on the slope may be in the form of cast-in-place concrete slab, RCC lining, or precast concrete blocks. RCC or concrete blocks facilitate provision of steps as compared to the cast-in-place concrete lining, for which special formwork is needed.

Provision of an energy dissipator is required at the toe. In the case of protective lining composed of steps, a part of energy is dissipated on the slope itself and the energy dissipator could be designed for the residual energy leaving the toe (Chap. 6). The most common form of an energy dissipator for the embankment overflow is the hydraulic jump stilling basin.

16.5 SLOPE PROTECTION LINING

The most common form of protective lining for the embankment slope are: cast-in-place concrete slabs, RCC lining, and precast concrete blocks.

16.5.1 Cast-in-place Concrete

Cast-in-place concrete on the downstream face is preferred for dams of heights up to about 75 m and depths of overflow up to about 8 m. A continuous concrete slab, with or without reinforcement, is placed over the entire downstream face of the dam similar to the upstream facing currently used on concrete faced rock-fill dam. The continuous reinforcement provides monolithic behavior, controls cracks and creates a nearly impervious barrier without projections in the flow. Other design features include sub-surface drainage, an overflow crest, and accommodations for fluctuating pressures in the hydraulic jump region at the toe. A critical design requirement for continuous reinforcement concrete overtopping protection is tying in the perimeters of the slab as discussed by McGovern et al. (1992). Existing dams protected with cast-in-place concrete facing have heights up to 75 m, depth of overflow up to 8 m, and unit discharge up to 30 cumec/m.

16.5.2 Roller Compacted Concrete (RCC)

In recent years, the development of roller compacted concrete (RCC) technology has provided a method of erosion protection of embankment dams, which is proved to be cost-effective while affording a number of advantages. RCC protection is normally very rapid with minimal project disruption. In most cases construction is limited to the dam crest and downstream slope with no requirement of reservoir restrictions. The performance of the dams provided with RCC that have been subjected to overtopping flows has been excellent. There are at least 30 embankment dams in the USA, provided with such protection, ranging in height from 5–35 m.

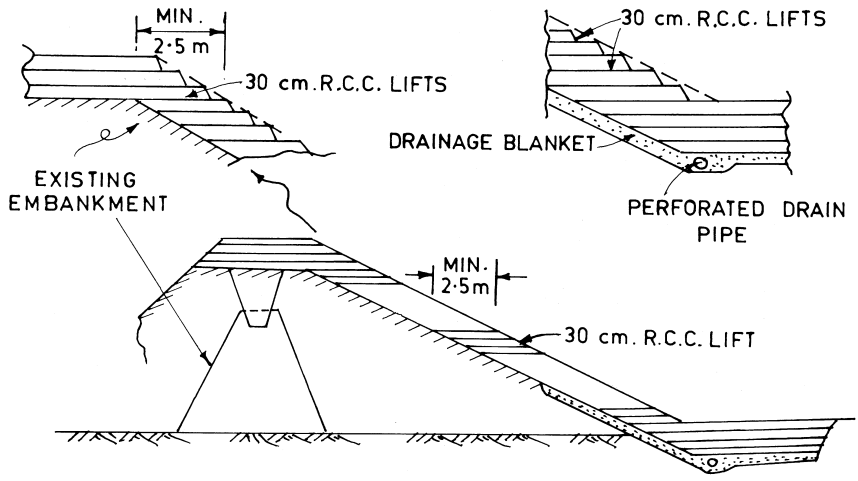

Figure 4 Stepped overlay of RCC on an existing embankment dam.

The entire crest of the embankment, the downstream face, and the area downstream of the toe are covered with roller compacted concrete placed in 30–60 cm thick horizontal lifts starting at the toe and proceeding up the slope of the embankment. The minimum width for the horizontal lift is specified as 2.5 m. Each lift could be made into a form of steps that may also help energy dissipation of the flow passing down the slope. A drainage system consisting of drainage blanket and filter along with perforated pipe drains is necessary. The existing dams provided with this type of protection have been designed for heights up to 45 m, depth of overflow up to 6 m, and unit discharge up to 30cumec/m. Figure 4 shows typical cross-section with relevant details. McLean et al. (1993) have described general guidelines for the hydraulic and structural designs.

16.5.3 Precast Concrete Block System

Perhaps the most innovative of alternatives to provide protection to the embankment dams during overtopping are precast concrete block systems. Such innovative systems require the greatest attention to avoid problems of possible failure. Based upon research and case history data during the past decade in the USA, Great Britain, and former Soviet Union, cost-effective methods for overflow protection for small to medium size embankment dams have been developed. There are two types of systems consisting of concrete blocks;

1. Cellular concrete mats
2. Wedge shaped concrete blocks

Cellular Concrete Mats

Originally designed for coastal protection against waves, cellular concrete mats provide a viable option for protecting embankment slopes from catastrophic erosion that could occur during overtopping. These are prefabricated mats of precast concrete blocks tied together by cables and anchored in place. Cellular concrete mats have been successfully adopted for dams up to 12 m in height, 1.2 m depth of overflow, and maximum flow velocity of up to 8m/s.

Wedge Shaped Concrete Blocks

The early experiments of covering embankment slopes with rectangular concrete revealed that the blocks were not stable against turbulent fluctuating pressures acting on their surfaces, which tend to lift up the blocks (Baker 1989). The development of wedge shaped blocks relies on prevention of uplift by overlapping part of the blocks. Flow over the steps separates from the block surface and reattaches some distance along the next step downstream. Within the separation zone, the flow rotates and forms a low or negative pressure zone. By providing drainage holes through each block in the low-pressure zone, it is possible to control the build up of seepage pressure and hold the block onto the underlying embankment. Figure 5 shows the details.

The blocks are inherently stable as the curved streamlines provide a stabilizing downthrust. Frizell (1993) has analyzed the stability of an individual block taking into account the various forces acting, as shown in Figure 6. Pravdivets et al. (1989) have described general guidelines for the design of wedge shaped blocks.

The roughness of the stepped surface provides additional energy dissipation and reduces the stilling basin requirement at the toe. The concrete crest is constructed as a broad crested or slightly curved overflow weir. The upstream portion

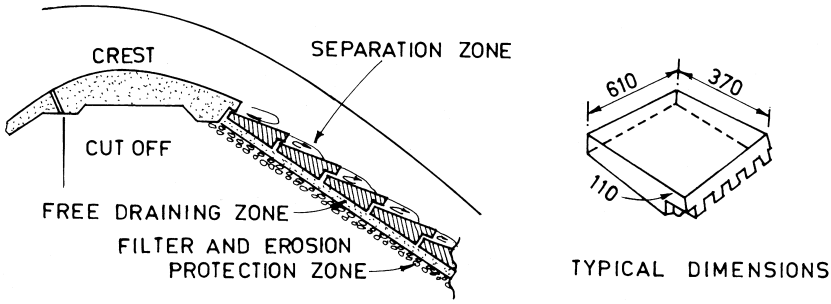

Figure 5 Wedge shaped concrete blocks.

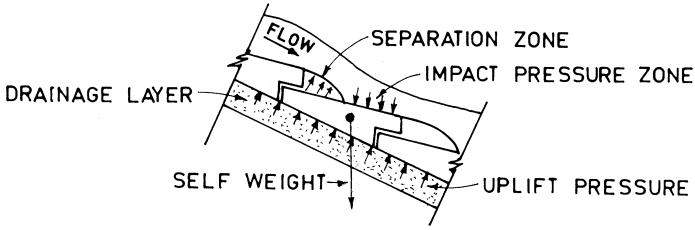

Figure 6 Stability of wedge shaped blocks (shown in Frizell et al. 1993).

of the concrete crest is terminated in a low velocity area to avoid erosion by the approach flow. The embankment dams, protected with wedge shaped blocks are up to 35 m in height, 12 m of overtopping depth, unit discharge up to 60 cumec/m, and flow velocity up to 25m/s.

Other Protection Devices

There are several examples of small embankment dams protected with riprap, gabions, reinforced rock-fill, and vegetation with geotextiles. These are for a very low unit discharge up to 3 cumec/m and flow velocity up to 5 m/s. Rock-fill spillways discussed in Chapter 14 have been investigated in greater detail and offer environment friendly option of protection.

Energy Dissipator

The spillway toe and tail water transition require careful design, particularly when precast concrete blocks are used. In order to ensure that the blocks remain free

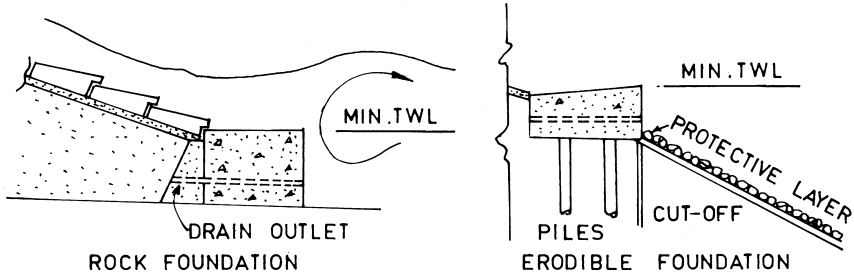

Figure 7 Details of toe blocks and protection of downstream bed (shown in Pravdivets et al. 1989).

of the effect of turbulence caused by the hydraulic jump, an arrangement with a surface-type hydraulic jump is made to form and blocks and the bed downstream of the toe block are protected. This is feasible when a rock foundation is available. In the case of erodible foundation, an arrangement as shown in Figure 7 is made to protect the downstream bed by flexible revetment.

REFERENCES

1. Baker, R. Pre-cast concrete blocks for dam spillways, International Water Power and Dam Construction, July, 1989.
2. Frizzel, K. H.; Ruff, J. F. Large scale embankment overtopping protection tests; ASCE Conf on Hydraulic Engineering, USA, 1993; Vol. 2.
3. McGovern, R. K.; Frizzel, K. H. Design of a continuously reinforced concrete slab to protect A. R. Bowman Dam during overtopping, 12th Annual USCOLD Lecture series. Fort Worth, 1992.
4. McLean, F. G.; Hansen, K. D. Geotechnical protection in Dam Rehabilitation, Proc ASCE Specialty Conference, April, 1993.
5. Metcalf, M.; Dolen, T. P.; Hendricks, P. A. Innovative aspects of the Santa Cruz dam modification, 12th Annual USCOLD Lecture series. Fort Worth, April 1992.
6. Oswalt, N. R. Overtopping protection-Alternatives for dams, Proc ASCE Conf on Hydraulic Engineering, Aug, 1992.
7. Pravdivets, Y. P.; Bramely, M. E. Stepped protection blocks for dam spillways, International water Power and dam Construction, July, 1989.

17
Spillway Crest Gates

17.1 INTRODUCTION

The debate of whether to have a spillway with crest gates or an ungated spillway is rather perpetual with arguments both in favor and against each. The decision must, however, be based on the consideration of factors such as dam safety, cost economics, operational problems, downstream conditions, etc. Experience from the operation of existing structures also helps appreciating the situation better.

The questions, thereafter, concern the most suitable type of gate, operational requirements, and design aspects. This is, indeed, an interdisciplinary topic involving structural, mechanical, electrical, and instrumental and control engineering in addition to hydraulic engineering. The emphasis is however, on the hydraulic aspects of control gates and stop logs.

A suitable pattern of gate operation is generally evolved from model studies based on the flow conditions in the downstream channel. Experience from model studies as well as prototype performance in this regard is now available to enable suggesting general guidelines

17.2 FACTORS INFLUENCING THE DECISION

The following factors influence the decision whether a spillway should be gated or ungated:

Safety of the dam
Cost economics
Operational problems
Downstream conditions
Special considerations

17.2.1 Safety of the Dam

Generally, gated spillways are incompatible with concept of the safety. An ungated spillway eliminates any possibility of operator error and is unaffected by the massive amounts of debris commonly accompanying high inflows.

The most well known argument against the gated spillways is that some of the gates may get jammed during the floods and may not open at all, or that electrical failure during the time of floods may render the gates inoperative resulting in the rise of reservoir level and consequent overtopping leading to failure of the dam. Kleivan et al. (1988) quote a few incidences of gate malfunctioning.

Schnitter (1979) has summarized ICOLD's analysis of failure of 216 dams according to which 34% of dams failed due to overtopping. Rate of failure of concrete dams was 29% whereas that of earth dams 35%. The analysis also revealed that modern earth and concrete dams are about equally safe, with approximately 0.4% probability of failure. With average rate of failure of 34% due to overtopping, it can be said that 1 out of 1000 earth dams stands the risk of overtopping. This is of particular concern because while a concrete dam can withstand overtopping for a considerable time, an earth dam will not stand up for more than a few hours to an overflow head of even a meter. Therefore, this is a prime consideration while deciding to have a gated spillway for earth dam projects

17.2.2 Cost Economics

The adoption of a gated spillway is likely to result in the lowering of the top elevation of a dam as compared to that with an ungated alternative. It can be shown that for a given volume of storage, an ungated spillway will result in a higher top elevation of the dam. The relative economy, increase in cost due to higher top elevation Vs that due to installation of crest gates, piers, and bridge and hoisting facilities, etc. should be considered.

Various codes for the safety of dams provide for stand-by gates against gate malfunctioning (of about 10% of the total number of gates) and provision of auxiliary spillway or breaching section (fuse plug, etc.), in the case of gated spillways. However, this is tantamount to the additional cost chargeable to gated spillways.

The maintenance of gates also adds to the cost; both capital and recurring. It is now a common practice to provide for stop logs upstream of the regulating gates on crests to stop the flow in a particular spillway span, such as where a gate has been jammed and can not be lowered during floods. This provision reflects in the addition to the capital cost for the stop logs, grooves, lifting devices, strengthening of the piers, and a road way. Periodic inspection, maintenance, and repairs contribute to the recurring expenditure.

17.2.3 Operational Problems

An ungated spillway would never fail to discharge even when unattended and under the most extreme conditions, such as earthquake damage together with power failure and broken communication lines or under panic conditions during large floods. With a gated spillway, very detailed and strict operating rules are required for safety. Any possible human or mechanical failure has to be anticipated and an emergency fuse plug is required. If a gated spillway is preferred in a region with severe earthquake conditions, it is obvious that an extra spillway with emergency fuse plug is required.

17.2.4 Downstream Conditions

Ungated spillways are best suited where it is to be ensured that the river flow pattern downstream of the dam is not materially affected (situation A of Fig. 1). On the other hand for a flood damage mitigation in the downstream reach, by reducing peak value of the flood (situation B of Fig. 1), a gated spillway would be the preference.

There are several instances where gated spillways have contributed to artificial or man-made floods, caused by panic or overreaction on the part of a gate operator. Often, selective operations of gates, intended mainly from consideration of least troublesome operation (without regard to conditions in the energy dissipator and downstream), have caused serious damages to stilling basins and roller buckets, etc. These could have been avoided with ungated spillways.

17.2.5 Special Considerations

Special considerations sometime compel the designer to adopt a particular type (gated or ungated) irrespective of other reasons. These may be hydraulic, operational, or even political.

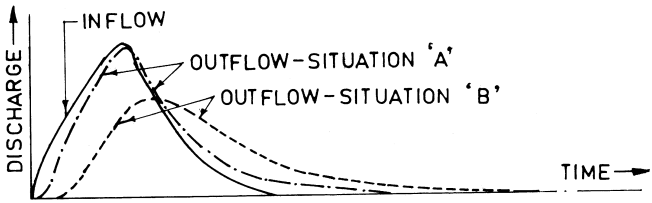

Figure 1 Gated Vs Ungated spillway.

For low height dams of run-off-river schemes in mountainous streams carrying large amount of sediment, the spillways are designed to serve the dual purpose of flood and sediment disposal. In such cases, reservoir flushing is to be carried out every year by full opening of gates at Minimum Draw Down Level (MDDL). These spillways are therefore equipped with the highest possible crest gates on low height spillways. For example, the spillway of Chamera II HE Project in India with 21 m high radial gates on 3 m high sill.

For dams situated at relatively high altitudes in Austria (Simmler 1979), spillways have not been provided with gates because of problems of accessibility and trouble-free operation, and also because of very small surcharge depths—not exceeding about 4 m—with ungated spillways.

On interstate and international rivers, construction of dams may be permitted provided natural river flows are not altered in the downstream reach. These dams have to be ungated regardless of other considerations.

Kleiven et al. (1988) suggest that where the consequences of dam failure or of faulty operation of the gates may become severe, costs alone should not be the deciding argument in the choice between a gated or ungated spillway. Where the latter alternative clearly provides a safer existence for the population in the downstream area it should be selected in any case. Gated spillways should be contemplated only when the consequences of a dam failure is less severe, the cost saving is significant, and the higher flood rise in the reservoir with an ungated alternative is not permissible.

17.3 TYPES OF GATES

From the standpoint of operation, the spillway crest gates can be divided into four groups:

Mechanical
Semi-mechanical
Automatic type fusible
Automatic type restoring

Mechanical gates open and close mechanically, require electrical power to operate and are not considered fully failsafe. The examples are radial gates, vertical lift gates, flap gates, etc.

Semi-mechanical gates open automatically but close mechanically and therefore they cause temporary loss of storage. Examples are drum gates, fish belly flap gates, inflatable rubber dam, etc.

Fusible type automatic gates open automatically; their main purpose is dam safety and entails loss of storage. Examples are fuse plugs, fuse gates, flash boards, etc.

Table 1 Types of Spillway Crest Gates

Type of Spillway	Ungated	Gated			
Features	Conventional raising	Mechanical	Semi-mechanical	Fusible	Fully automatic
Cost	X	X	T	T	T
Environment	O	O	T	T	T
Maintenance	T	X	X	O	O
Retain Storage after large floods	T	T	O	X	T
Time to Construct	X	O	O	T	T
Reliability	T	X	O	T	T
No Operator or External Power	T	X	X	T	T
Emergency Draw-down-Large Releases	X	T	T	X	T

X: Disadvantage, O: Possible advantage, and T: Advantage

Restoring type automatic gates open and close automatically, retain storage, and assure dam safety. Examples are moving fulcrum type tilting gates, TOPS, FDS gates, etc.

Townshend (2000) has prepared a matrix of these types of gates along with ungated alternative as shown in Table 1.

17.4 MECHANICAL GATES

The common types of mechanical gates include radial, vertical lift, and flap gates.

17.4.1 Radial Gates

Radial gates are the most common type of spillway gates. They do not require slots in piers for their support, which ensure least flow disturbances and a better coefficient of discharge. The construction of gates is simple and easy to maintain. The two types of radial gates that are in use are crest or surface type with a free water surface, and orifice type with breast wall. The crest type gates require less hoisting capacity than for a vertical lift gate. Except for very large size gates, rope drum hoisting arrangement is sufficient. The gate thrust is transmitted to two

bearings only. The circular shape of the skin plate provides favorable hydraulic condition. The orifice type gates require comparatively higher hoisting capacity and require hydraulic hoist. The main disadvantage is that it requires accurate construction of piers with required shape at trunnion level for movement of arms. The orifice type gates require effective sealing at both the bottom and top in addition to the sides. Figure 2 shows typical layout of a crest type radial gate and Figure 3 shows details of an orifice type radial gate.

Crest type radial gates have been constructed in very large sizes, with areas up to 560 sqm, widths up to 56.5 m, and heights up to 22.5 m. Orifice type radial gates have been constructed with areas up to 114 sqm, widths up to 12.8 m, heights up to 9.5 m, and heads up to 135 m.

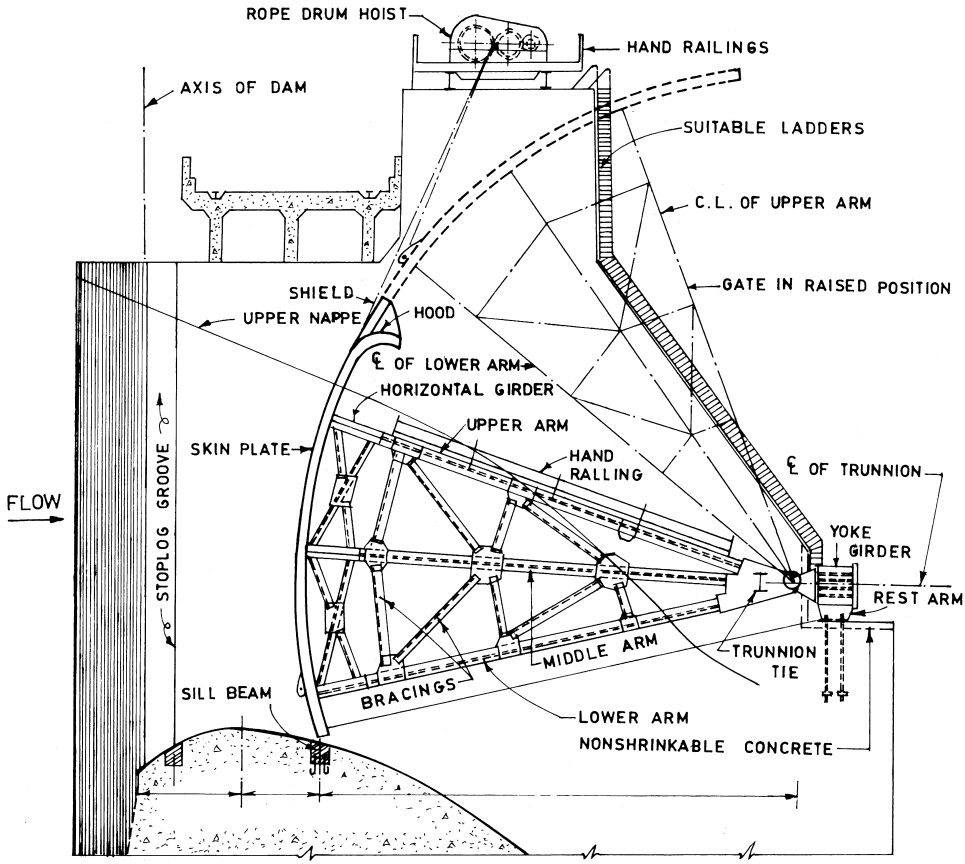

Figure 2 Crest type radial gate.

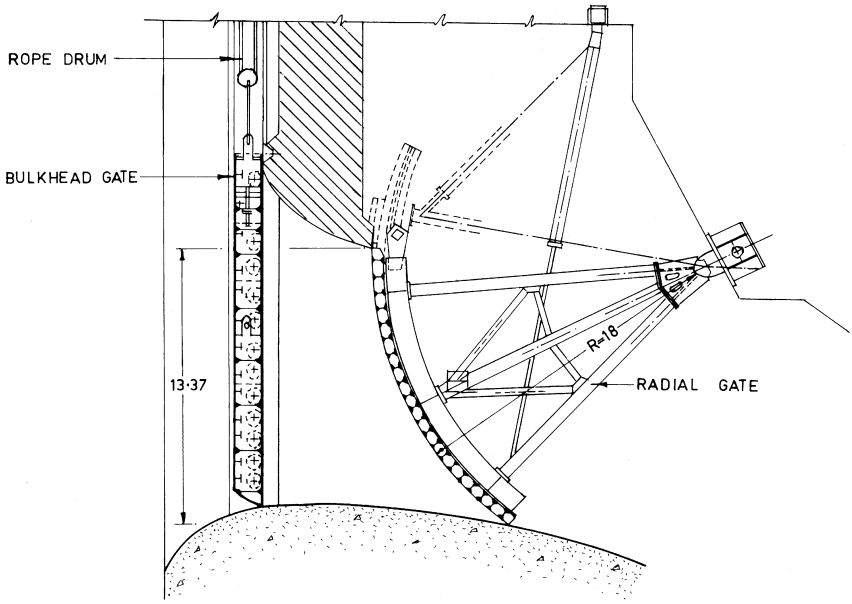

Figure 3 Orifice type radial gate.

The width to height ratio of a gate is not a critical design consideration. Sehgal (1996) states that gates have been successfully designed with width to height ratios that are less than, equal to, and greater than 1. For a given area of opening, however, gates with smaller width to height ratios are cheaper; the cost of the gate is given by the proportionality:

$$Cost \propto (width)^{1.28}\ x\ (height) \tag{1}$$

In addition, gates with smaller width to height proportion are less subject to choking and they provide better flow regulation because of greater height of opening for a given flow. The overall cost of a spillway, however, is smaller for wider gates because wider gates permit fewer and smaller height piers. Finally, the structural size is limited by the load transferred to the trunnion anchorage and hence to the piers, and by the maximum operating loads for which the operator and the support structures can be economically designed.

Gate trunnions of radial gates must be located usually 1–1.5 m above the maximum flow nappe to prevent damage to the trunnion by debris or ice. The radius of the gate is usually 1.25 times the vertical height of the gate above crest. The sill of the gate is usually located downstream of the crest at an elevation

0.3–0.5 m below the crest. Based on the statistical study of several gates, the center of gravity of most radial gates can be assumed to be located at about 0.75 times the gate skin plate radius and at a vertical distance from the gate sill of about 0.45 times the gate vertical height. For avoiding self-excited vibration, the position of the trunnion must be above the center of force acting due to the water pressure on the gate.

The radial gate and its operating system are divided into three groups:

1. Embedded parts: fixed in the concrete to transmit the load to civil construction
2. Gate leaf: curved plate and its supporting structures which transfer the water thrust to embedded parts.
3. Operating system: rope drum hoists/hydraulic hoists used for operating gate.

For a comprehensive discussion, guidelines, and detailed design procedures, refer to the excellent articles by Annigeri and Naidu (2000), Boro and Chauhan (2000), Central Water Commission (1999), Murti (1989), and Sehgal (1996). Lewin (2001) has comprehensively dealt with all design aspects.

Overtopping of Radial Gates

Radial gates may be overtopped accidentally sometimes or they might be designed for small overtopping for a specific purpose. Flow instability and vortices are the inherent problems of an overtopped gate. The overflowing nappe has to be prevented from impinging on gate arms so that the arms remain free of pulsating forces due to impingement. Strong suction forces develop in the space enclosed by the spillway profile, inside of the gate, and the overflowing nappe, which could result in nappe oscillations leading to vibration of the gate structure. The jet impinges on the spillway surface also, which requires special protection in view of the localized impact forces. The design, therefore, must include provision of non-overtopping side shields on both the ends of a gate and means of ventilating the nappe to prevent instability. Model studies were conducted for finalizing the design of the side shields, overflow hood, and flow breakers on the hood of the radial gates of Salal dam spillway in India, for a depth of overflow of 1.36 m (Fig. 4).

Discharge Characteristics of Radial Gates

Discharge through a partially open radial gate on a spillway crest can be estimated using the basic orifice equation:

$$Q_g = C_g A \sqrt{2gH} \tag{2}$$

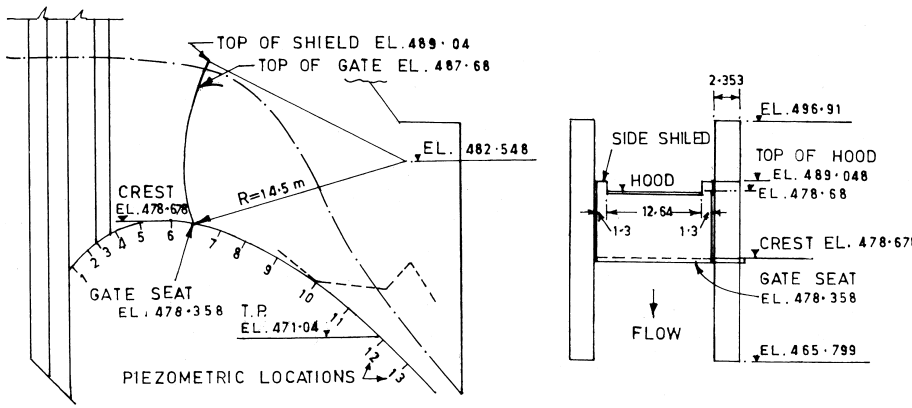

Figure 4 Overflow hood and side shields of radial gate: Salal dam spillway.

where

Q_g = Discharge passing through one spillway span
C_g = Coefficient of discharge
A = Area of orifice opening = $G_0 \times B$
B = Span width
G_o = Gate opening
H = Head to the center of the orifice

The coefficient of discharge C_g is primarily dependent on the characteristics of the flow lines approaching and leaving the orifice, which in turn, are dependent on the shape of the crest, radius of the gate, and location of the trunnion. WES (1977) in their Chart HDC 311 have presented a variation of C_g with respect to the angle β formed by the tangent to the gate lip and the tangent to the crest curve at the nearest point of the crest curve. The net gate opening G_o is considered to be the shortest distance from the gate lip to the crest curve, as shown in Figure 5. The coefficient Cg varies from 0.67 to 0.73. Computation of the angle β has also been explained in the charts.

Spillway Bay Surge

For certain combinations of spillway span width B, gate opening G_0, Pier length, (defined as the distance from the pier nose up to the upstream-most point on the gate face) P_L and head on the crest H_c, the surging of water surface upstream of the radial gates have been observed in model study. It was reported that water surface fluctuations as high as 3 m with periods less than 10 seconds occurred

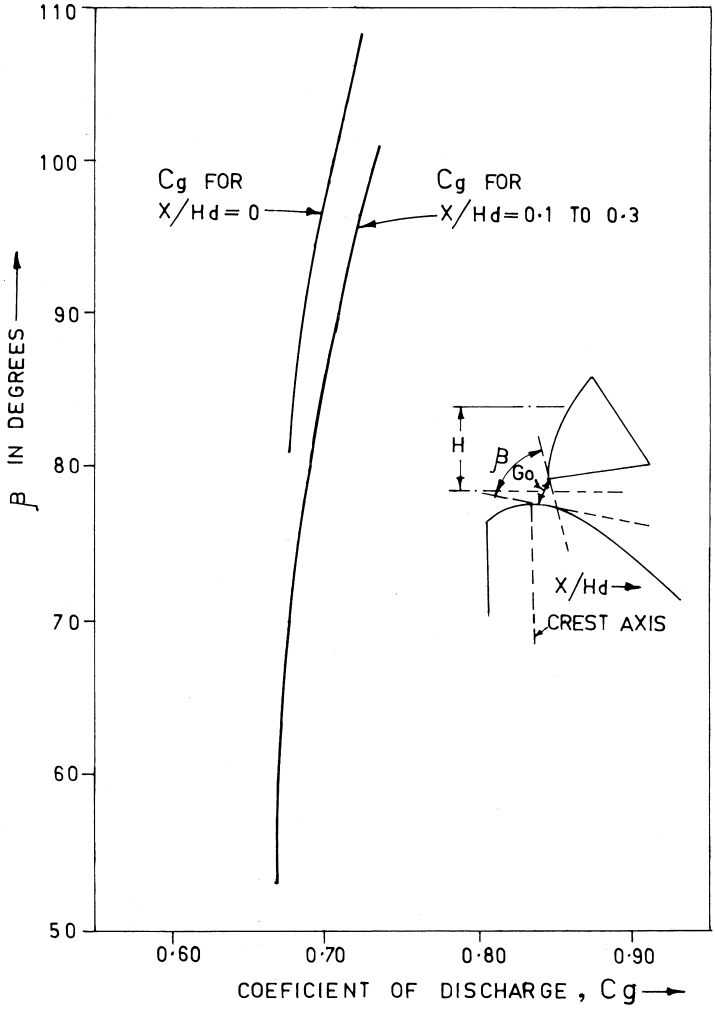

Figure 5 Coefficient of discharge for radial Gate (shown in WES-HDC 311).

in alternate spans. USACE (1990) recommends the following guidelines for preventing excessive surging:

1. Low head spillways ($P_L/H_c < 1$)
   $B \geq 1.1\ H_g$ for $P_L < 0.3\ B$
   $B \geq 1.25\ H_g$ for $0.3\ B < P_L < 0.4\ B$

2. High head spillways ($P_L/H_c > 1$)
   $B \geq 0.8\ H_g$ for $P_L < 0.3\ B$
   $B \geq 1.2\ H_g$ for $0.3B < P_L < 0.4\ B$

Where Hg is the maximum head on the crest where the gate controls the discharge. The maximum gate opening for which the radial gate will control the discharge can be taken as 0.625 times the head on the crest. By utilizing the spillway discharge curves for various gate openings, the maximum head on the crest for which the gates will control the discharge can be determined. These guidelines apply to all gated spillways regardless of the gate size. Where surging might be a severe problem, model study should be conducted for the specific case.

17.4.2 Vertical Lift Gates

Vertical lift gates are rectangular in shape and are supported by guides in which gates move vertically in their own plane. The closing member of the gate consists of a framework to which a skin plate is attached. The main load of water pressure is transmitted by the framework to the piers. These gates are usually designed as wheeled gates rather than slide gates to close by their own weight. The fixed wheeled gates are the most common. The seals and skin plates on the vertical lift gates are usually provided on the upstream side of the gate slot to minimize flow disruption by gate slots. The slots for downstream sealing gates are deeper in the direction perpendicular to the flow than those for upstream sealing gates because for downstream sealing gates the wheels and the seals are located on the same side, while for upstream sealing gates they are located on opposite sides. Figure 6 shows typical construction of a vertical lift gate with upstream skin plate and upstream seals. These gates require higher superstructure to accommodate the hoist and the gate in fully raised position.

Discharge Characteristics of Vertical Lift Gates

Discharge under high head vertical lift gates can be estimated using the standard orifice equation. WES (1977) in HDC Chart 312 relates the discharge corresponding to free overflow with gate-controlled discharge under the same head H as

$$\frac{Q_g}{Q} = \frac{C_g}{C_d}\left[\frac{H_2^{3/2} - H_1^{3/2}}{H_c^{3/2}}\right] \tag{3}$$

where

Q_g = Discharge through partially open gate Q = Discharge corresponding to free flow

Cd = Coefficient of discharge for free flow Cg = Coefficient of discharge for gated flow

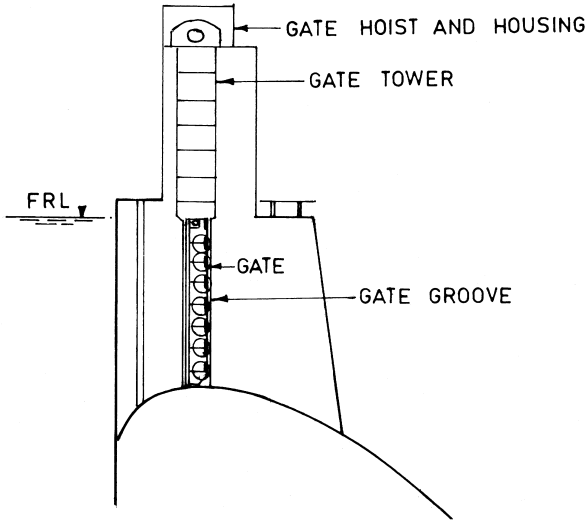

Figure 6 Vertical lift gate on spillway crest.

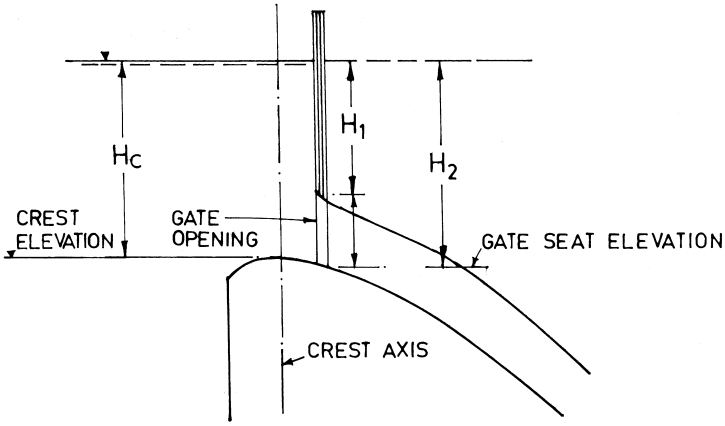

Figure 7 Definition sketch.

H_1, H_2 and H_c are defined in Figure 7

Analysis of the results of some of the studies also indicated that $C_g/C_d \cong 1$

17.4.3 Flap Gates

Flap gates are used when very close regulation of reservoir level is required or when floating debris or ice has to be skimmed. Flap gates can be built in very large width, up to 100 m, since the hydraulic operators to be fitted at regular intervals also support the gate throughout its width. Flap gates require very high hoisting forces to raise them from their fully open position because, besides the mass of the gate and friction, the mass of water flowing over the gate also has to be overcome. Flow breakers have to be provided at the downstream end of the skin plate to ventilate the space beneath the jet and prevent flow instability. Flap gates are usually inclined 20° to the vertical when in fully raised position. Figure 8 shows an installation of a typical flap gate of the size 11m × 4.5m.

One advantage of a flap gate is the high discharge coefficient, similar to ungated spillways, when the gate is fully lowered. Disadvantages include possible damage to hydraulic operators located downstream of the gate due to debris or ice falling over a partially open gate and difficulty in their maintenance due to problem of access.

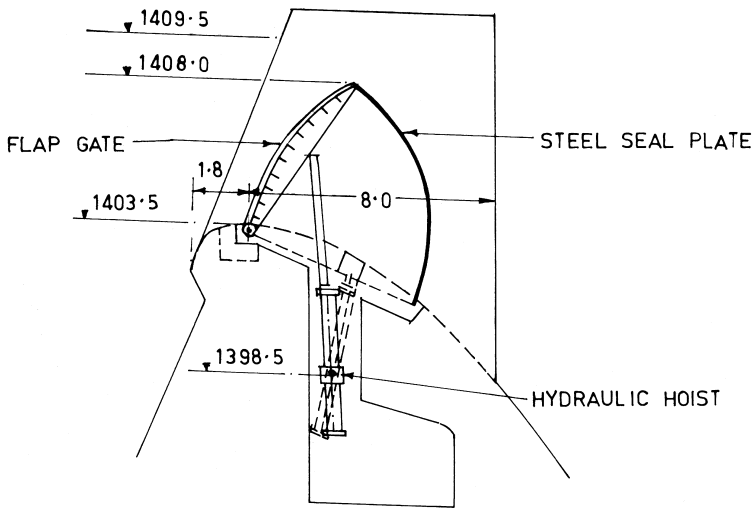

Figure 8 **Typical 11m × 4.5 m flap gate.**

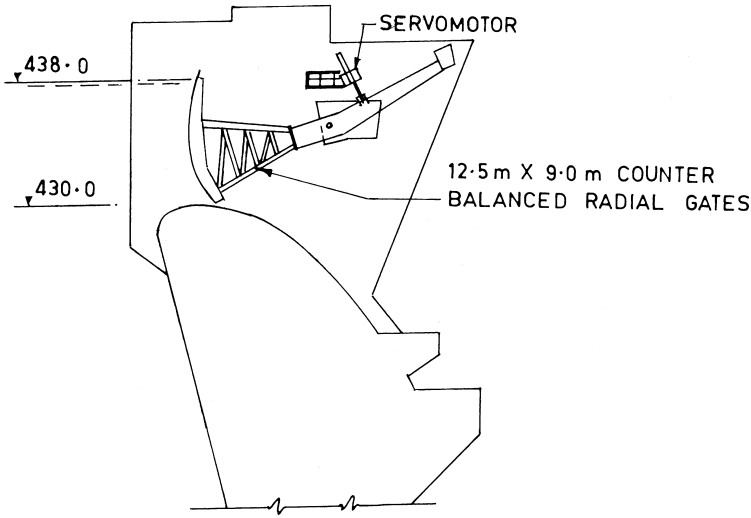

Figure 9 **Semi-automatic radial gate for** Victoria dam, Srilanka. (Back et al. 1991)

17.5 SEMI-MECHANICAL GATES

Semi-mechanical gates open automatically but they require external mechanical power to close them. An inflatable rubber dam is an example of this type of gate. A recent example of such an arrangement is the Gibb automatic crest gates installed at the Victoria dam, Sri Lanka, discussed by Back et al. (1991). The pertinent details are shown in Figure 9. The design adopted consists of eight 12.5 m wide by 9 m high counterbalanced crest radial gates. The gates are opened by an oil hydraulic circuit actuated by floats in a well connected to the reservoir. No operator or power is required to open the gate but power is required to close the gates when flood recedes. Some loss of storage is therefore inevitable.

17.6 AUTOMATIC TYPE: FUSIBLE

These are mainly fuse plugs and fuse gates that have been discussed in Chapter 12.

17.7 AUTOMATIC TYPE: RESTORING

These gates have fully automatic operation of closing and opening in consonance with the reservoir water surface elevation, and hence do not entail loss of storage.

At present, there are three types of such gates operating on different principles. These are:

1. Moving fulcrum type tilting gate functioning on hydrostatic load and moments created by it. It has been developed in India and named as Godbole gate after its inventor.
2. FDS gates working on buoyancy.
3. TOPS gates working with the aid of ballast tanks.

The FDS and TOPS gates have been developed in South Africa.

The functioning of Godbole gates has been described in detail by Godbole (1998). The gate comprises two basic components:

A pair of fulcrum assemblies fixed in the supporting structure.
A rotating gate leaf.

These components are shown in Figure 10, which is a diagrammatic representation of gate in sectional side elevation. The gate leaf rocks over the rolling surface of fulcrum assemblies and changes its angle of tilt whenever there is a change in the upstream or downstream water level. The operational behavior is also explained schematically in Figure 10.

It is claimed that more than 700 Godbole gates have been installed on different types of structures in India, in width up to 10 m and height up to 4 m.

Townshend (2000) has described the functioning of FDS and TOPS gates. The FDS gate consists of a buoyancy tank connected by ducted radial arms to an upstream axle. The buoyancy tank seals against the cill of the spillway and between vertically sided piers. An inlet weir on the upstream is connected to the hollow axle to allow water to flow into the buoyancy tank to the downstream

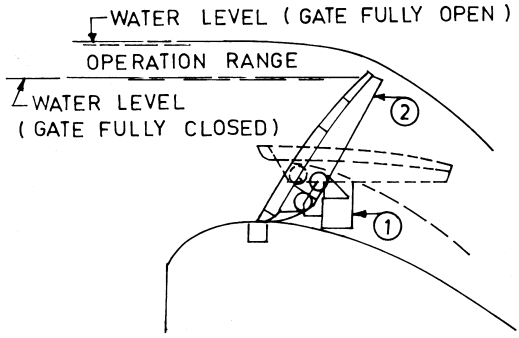

Figure 10 Moving fulcrum type tilting gate (Godbole gate):1 Pair of fulcrum assembly fixed on supporting structure 2 Rotating gate leaf. (Godbole, 1998)

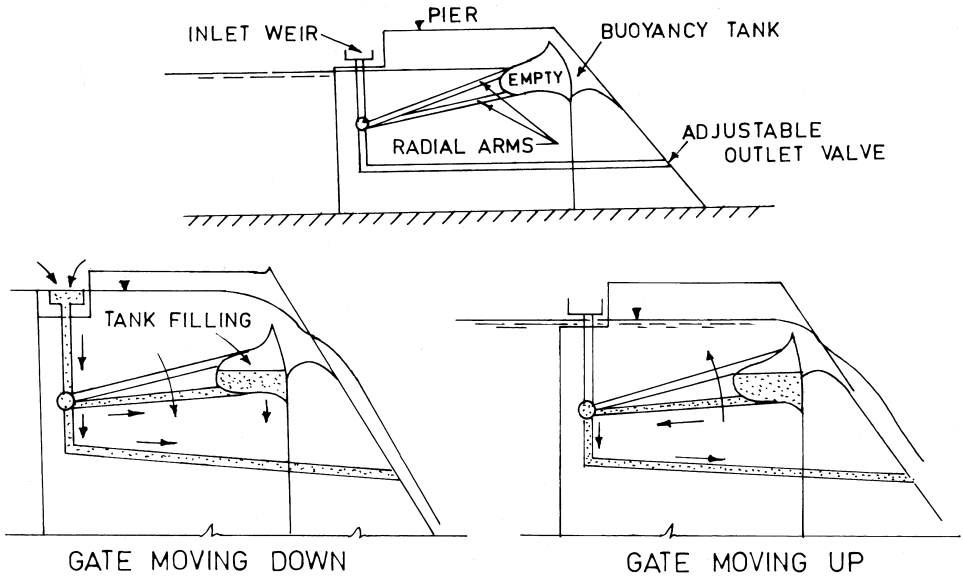

Figure 11 Operational behaviour of FDS gate. (Townshend, 2000)

side of the weir. The operational behaviour of the FDS gate is explained schematically in Figure 11.

The empty buoyancy tank floats on the water and seals against the spillway cill and sides to increase the water level above the spillway level. As the upstream water level rises due to a flood, water flows into the inlet weir and into the buoyancy tank at a rate greater than the discharge rate from the tank. The buoyancy tank fills and submerges. In the totally submerged position, the tank is full and the gate fully open to offer an unobstructed water way. As the flood level recedes, water ceases to flow into the inlet weir. The buoyancy tank drains until empty and the gate floats into its fully closed position.

The TOPS gate consists of a ballast tank attached to a closure plate that seals against the spillway cill and vertical sides of piers to retain the increased water level above the spillway. The gate is attached to two trunnions positioned above the water level. The operation of the TOPS gate is explained diagrammatically in Figure 12. The ballast tank is connected by conduits to the closure plate so that the water level in the reservoir and the ballast tank are in equilibrium. The mass of water in the ballast tank together with the gate's self weight create a closing moment about the axle, which is greater than the opening moment induced by the upstream water level, and hence the gate remains closed. With

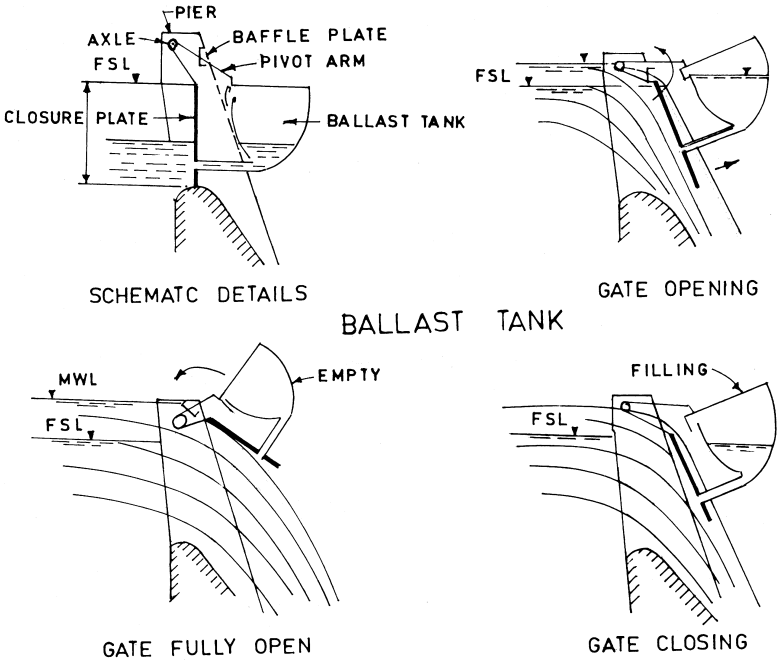

Figure 12 Operational behaviour of TOPS gate. (Townshend, 2000)

the rise in the upstream water level, the opening moment exceeds the closing moment. The gate then rotates upwards and outwards and by doing so, decants water from the ballast tank through the outlet thereby making the gate lighter. The gate then opens easily with increased upstream flood levels. In its fully open position, the ballast tank is empty and the gate rides on the water nappe almost tangentially with very little back up of upstream water level. The offset in the pivot arm causes the gate to rise as it rotates, thereby creating sufficient waterway to pass the design flood. When the flood water level recedes, the gate will rotate downwards and the ballast tank fills partially in order to balance the opening and closing moments. As the flood recedes the gate will close completely.

The FDS gates are installed at more than 10 sites in South Africa and have been working successfully for 10 years. The TOPS gate is a more recent development and has been installed on the Belfast dam in South Africa where the storage level has been increased by 2 m.

Leyland et al. (1986) have also described four automatically controlled gates installed and commissioned in New Zealand. The operating experience has generally been satisfactory.

17.8 VIBRATION OF GATES

The vibration of spillway crest gates is generally a rare incident and may be caused by extraneously induced excitation or instability induced excitation like vortices, sill seal leakage, or flow reattachment at lip and a hydraulic jump forming near the gate lip (for a low dam with high tail water level).

Vortices may form upstream of a partly open crest gate. In the case of radial gates with upstream suspension (i.e. hoist rope tied around the face of the gate), vibration of rope might be a problem. The main cause, namely formation of vortices, should be eliminated by suitable anti-vortex device evolved from model studies.

Certain designs of sill seals are reported to be the cause of vibrations. Continuous leakage from a damaged seal at the gate lip may cause vibration even when the gate is closed with a high pond level. Based on the operating experience at the USBR, Oswalt et al. (1979) distinguish between the unsuitable and suitable arrangements of sill seals for radial gates, as shown in Figure 13. For large gates, locating a seal downstream of the skin plate helps eliminate vibration. Bottom seals on orifice type radial gates may be a flat seal attached to the sill beam, as shown in Figure 13.

For low dams with high tail water levels, a hydraulic jump may form near the gate seat, for a partly open gate, causing pulsating flow conditions leading to vibrations. Either the formation of the jump should be avoided or the combinations of upstream water level/gate opening/discharge responsible for such a condition should be identified from model studies and be avoided as far as possible.

17.9 STOP LOG GATES

Spillway stop log gates are provided for the emergency closure of flow against the possibility of the regulating gate getting stuck up or failing to operate. The stop log gate may consist of one single unit—often called bulkhead gate—or a number of units of smaller height, spanning full width of the spillway, and lowered one above the other in the gate grooves of the spillway piers. A lifting beam operated by a gantry crane placed at the top of the dam is used for the purpose of emergency closure. Stop log units and lifting beam are fabricated from steel girders and plates and are provided with rollers on both sides for easy lowering over the spillway. A stop log gate may have its skin plate on the upstream or downstream side. Figure 14 shows details of a typical stop log unit for Salal dam spillway in India, having an upstream skin plate.

The stop log gate generally operates under balanced conditions, but as a precaution it is required to be designed for lowering in flowing water with flow over and under the stop log. As a result, it is subjected to horizontal thrust along

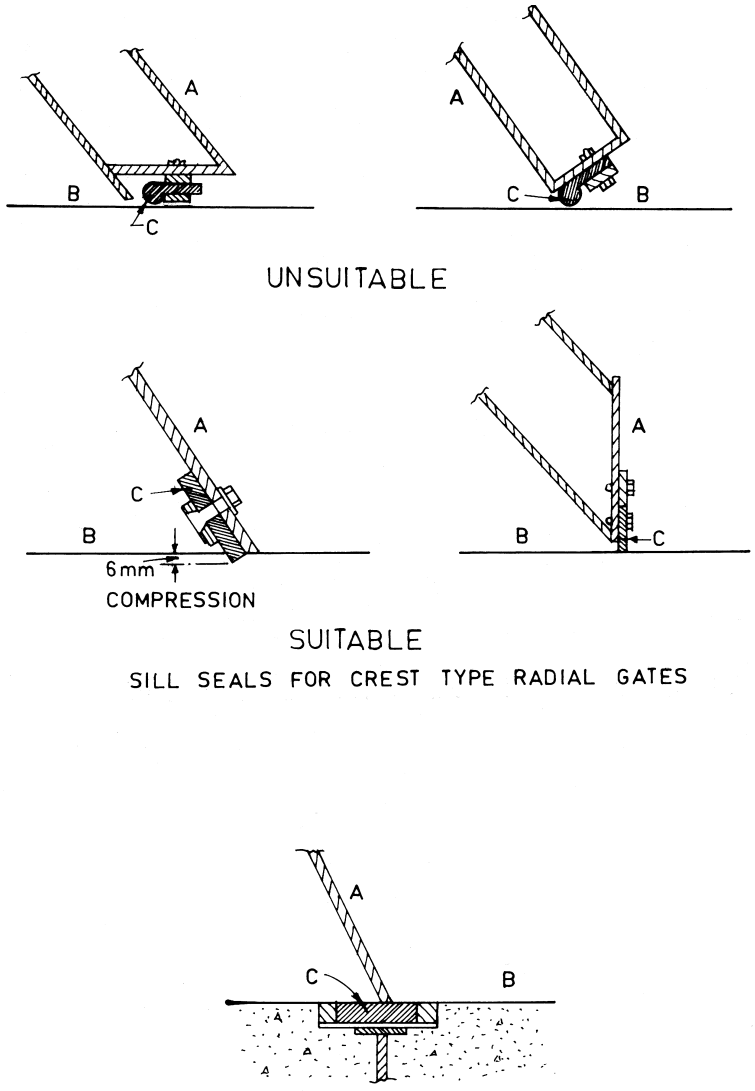

Figure 13 Details of sill seals for radial gates. A: Skin plate, B: Spillway surface, and C: Bottom seal. (Oswalt et al. 1979)

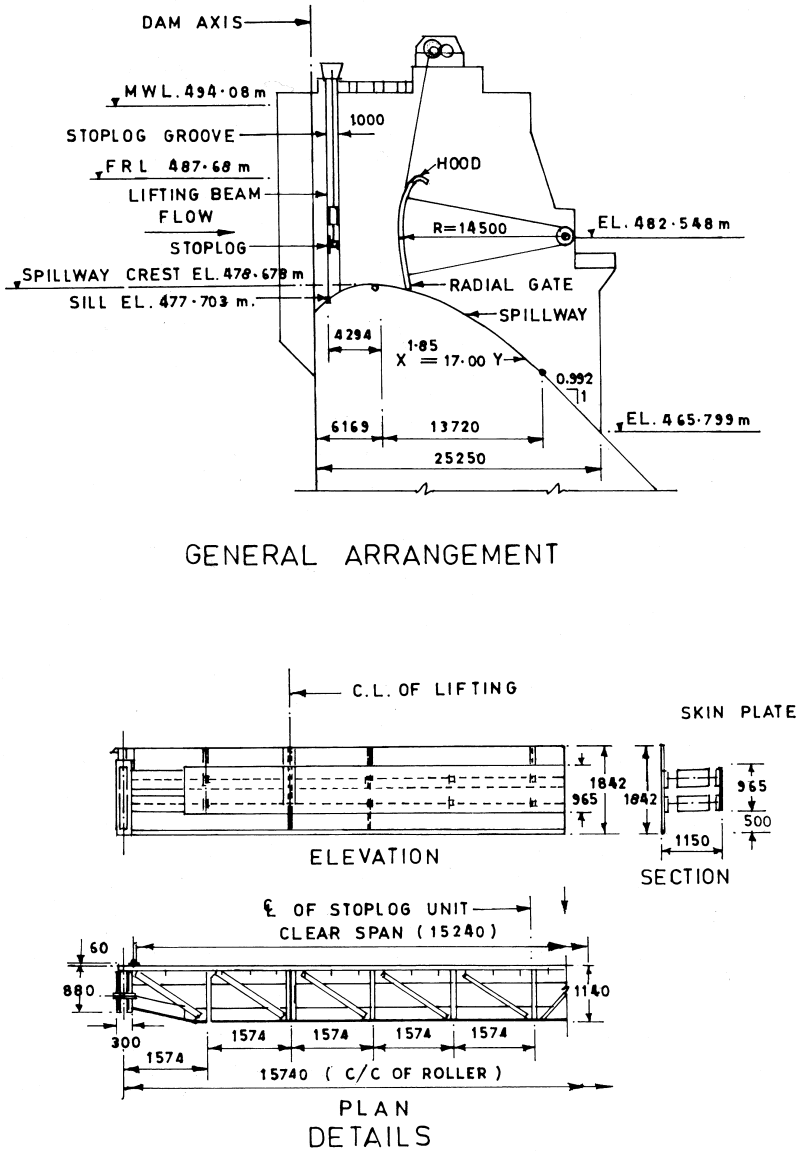

Figure 14 Salal dam spillway, India: stop log gates.

with down pull or uplift force, depending upon its position above the sill. The stop log gate at the bottom is generally designed for the maximum head and those above it for the reduced head.

Hydrodynamic Forces on Stop Logs

The determination of hydrodynamic forces, i.e. uplift and down pull, that stop log units experience is essential for deciding the self weight of the stop log element and the hoist capacity of the gantry crane for its safe operation. The hydrodynamic forces are influenced by the following parameters/factors:

- Location of the skin plate, whether on the upstream or downstream.
- Disposition of the stop log element with reference to spillway crest axis, i.e. on the steeper slope far upstream of the axis or on the flatter portion nearer to the crest axis.
- Area of girders of stop log element in plan.

A hydraulic model study is necessary for each specific case. However, as a result of a number of studies conducted by various laboratories, the following general guidelines can be given:

1. Although downstream skin plates offer a better sealing arrangement, they result in increased magnitudes of hydrodynamic forces as compared to the skin plates on the upstream. This is shown in Figure 15 with reference to the results of model studies for the stop log gates, with skin plate on upstream (Case A) and downstream (Case B).
2. Stop log grooves located towards upstream; such that the first stop log element rests on the upstream steeper portion of the spillway crest, result in larger uplift forces. As the groove moves towards downstream, nearer to the crest axis on the flatter surface, uplift force is reduced significantly. This holds good for both the stop log with their skin plates on the upstream as also on the downstream. In Case A, reduction of angle from 29° to 0° brought down the uplift force from 26 tons to 8 tons. For Case B, reduction from 35° to 10° brought down the uplift force from 50 tons to 29 tons.
3. It is observed that as the projected areas of the top and bottom of the stop log elements are reduced, hydrodynamic forces also reduce. Therefore, an open truss fabrication for the top and bottom sides ensures reduced forces. This also applies to stop log units with upstream or downstream skin plates.

Sinnarkar et al. (1995) and (2000) have described model studies for assessment of hydrodynamic forces on spillway stop log gates.

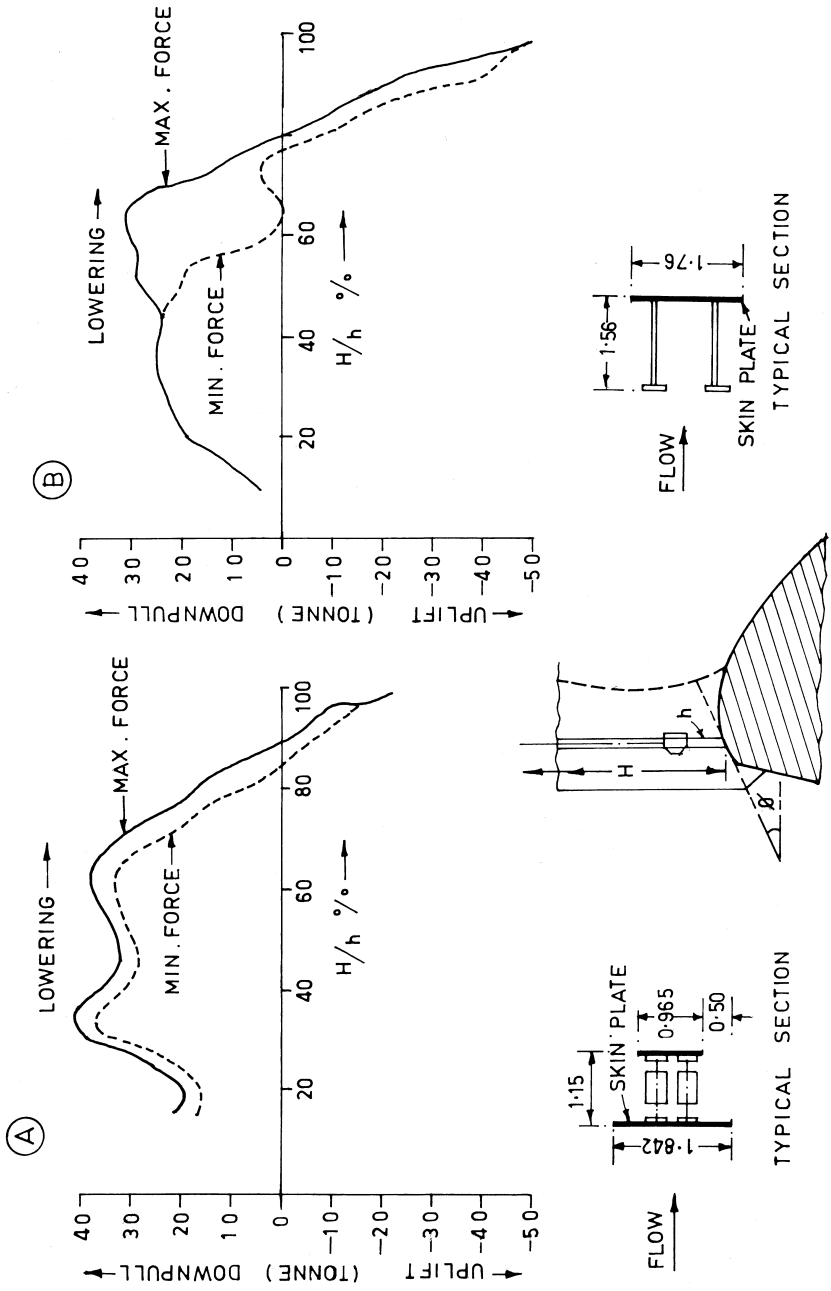
(A)
LOWERING
MAX. FORCE
MIN. FORCE
H/h %
40 30 20 10 0 10 20 30 40 50
DOWNPULL (TONNE) UPLIFT
0 20 40 60 80 100
(B)
LOWERING
MAX. FORCE
MIN. FORCE
H/h %
40 30 20 10 0 10 20 30 40 50
DOWNPULL (TONNE) UPLIFT
0 20 40 60 80 100
h
H
ø
FLOW
SKIN PLATE
1·15
0·965
0·50
1·842
TYPICAL SECTION
FLOW
1·56
1·76
SKIN PLATE
TYPICAL SECTION

17.10 SOME CONSIDERATIONS ON OPERATING PATTERN OF GATES

The pattern of operation of spillway crest gates becomes important when large discharges are to be passed down the spillway. Generally, operating all the gates equally and simultaneously for all discharges is the safest mode of operation since it ensures equitable distribution of discharge in the energy dissipator and in the river downstream. However, for spillways with large number of gates, opening all the gates to pass small discharges result in a very small gate opening which often proves to be difficult from the consideration of close regulation. There is a tendency on part of the operating staff to operate only a few gates with sizeable gate opening and add on other gates with increase in the inflow, with the sole consideration of maintaining a specified reservoir level. Sometimes failure of the gates or operating mechanism also compels such unequal operation. Many instances of damage caused to the energy dissipators or downstream channel as a result of such operations have been reported in literature. Some cases of damage have been discussed in Chapters 22 and 26. Improper operation of spillways results in damage to the structure in the case of stilling basins and roller buckets, whereas in the case of ski jump/flip buckets the damage is caused in the downstream. Experience from model studies and prototype performance enables suggesting general guidelines in this regard.

The pattern of gate operation should be decided on the consideration of the type of energy dissipator and downstream river topography, besides the objective of maintaining a specified reservoir level.

Stilling Basins and Roller Buckets

Hydraulic design of stilling basins and roller buckets imply equal and simultaneous opening of all the gates. It is therefore imperative to operate the gates accordingly. For spillways where FRL is to be maintained for all discharges, opening only a few gates will impair the performance of the energy dissipator. This is obvious since the energy level and unit discharge would correspond to the condi-

←

Figure 15 Hydrodynamic forces on stop logs (shown in Sinnarkar et al. 1995).

Case A: Upstream skin plate	Case B: Downstream skin plate
1. Projected area (in plan):12.25 sq.m	1. Projected area (in plan):6.30 sq.m
2. Total head (H): 9.98 m	2. Total head (H): 10.41 m
3. Angle (Φ): 29°	3. Angle (Φ): 35°
4. Radial gate fully open	4. Radial gate fully open

tion of the design discharge, but the available tail water depth would correspond to a smaller discharge. In addition, unequal distribution of discharge in the downstream channel would set up horizontal eddies that may bring loose material from downstream into the stilling basin or bucket and cause abrasion damage. It is therefore advisable to operate all the gates equally and simultaneously, as far as possible.

Sometimes, special conditions may compel a selective operation whereby some gates may not be operated for certain range of discharges. In such cases, a model study is essential. Kelkar et al. (1973) have described how a model study helped to evolve a suitable operating pattern for the spillway of Kadana dam, India. It is a 21 span spillway, designed as a solid roller bucket. The bucket invert in the three central spans is 3.05 m higher than the rest of the spans due to faults extending in the region of these three spans. The higher buckets would not function satisfactory and would result in flip action for low discharges, owing to inadequate tail water depth. Therefore, these spans were not operated up to about 50% discharge. For higher discharges, all the spans were functioning satisfactory. With the closure of three spans, return flows were created in the downstream channel, which traveled towards higher buckets and then turned sideways onto the lower buckets. The return flows with velocities as high as 8 m/s, carried loose material into the buckets. Low divide walls separating the higher and lower level buckets, and extending 30 m beyond the bucket were incorporated, which reduced the return velocities to less than 3 m/s.

Ski Jump and Flip Buckets

All of the spans of spillways with flip buckets in wide and shallow rivers should be operated equally as far as possible. Unequal operation, especially not opening a group of few spans, with inadequate tail water cushion, is conducive to localized scour and strong return flows towards closed spans. This may cause scour very near the bucket lip, threatening to undermine its foundation.

However, for the spillways located in narrow gorges with steep flanks, all the spans should not be operated simultaneously, except for the condition approaching the design maximum discharge. Prototype experience from several spillways with ski jump/flip buckets in the narrow and steep valleys indicate that opening all of the spans for all discharges with small gate openings results in a shorter throw of the trajectory, scour near the bucket and intense spray that saturates the flanks and causes slides. Opening gates in a sequence from the center towards the flanks as the discharge increases is found to be beneficial for restricting deeper scour in the center of the gorge and keeping it as far away from the dam as possible. The end spans are operated only when inevitable so that the flanks are not subjected to the spray hazard most of the time. A model study to evolve a pattern of gate operation for Srisailam dam spillway, on the above lines has been reported by Khatsuria et al. (1989).

Notations

A = Area of orifice opening $= B \times G_o$
B = Width of span
C_d = Coefficient of discharge for free flow
C_g = Coefficient of discharge for gated flow
G_o = Gate opening (Fig. 4)
H = Head to the center of the orifice (Fig. 4)
H_c = Head over crest (Fig. 6)
H_g = Maximum head on the gate where the gate controls the discharge
H_1 = Difference between RWL and bottom of vertical lift gate (Fig. 6)
H_2 = Difference between RWL and gate seat (Fig. 6)
P_L = Distance from the pier nose up to the upstream-most point on the gate face
Q = Discharge per span for free overflow over spillway
Q_g = Discharge per span for gated flow

REFERENCES

1. Annigeri, G. S.; Naidu, N. K. Radial gates- Some aspects for anchorage systems, gate leaf and hoisting system, CBIP Workshop on Role of Gates and their Control in Water Resources Projects. Belgaum, June, 1995.
2. Back, P. A. A.; Mee, W. T. The Victoria Project, Srilanka: Project planning and Design of Victoria dam, The Institution of Civil Engineers, Part I, April, 1991.
3. Boro, J. R.; Chauhan, G. Optimization of design of spillway gates, CBIP Workshop on Role of Gates and their Control in Water Resources Projects, Belgaum, June, 2000.
4. Central Water Commission-India Manual on Design of radial gates, April, 1999.
5. Godbole, P. Achieving automation in hydraulic gates without electricity by moving fulcrum type automatic tilting gate,CBIP Workshop on Hydraulic gates and their control in water resources projects. Nangal Township, October, 1998.
6. Kelkar, Y. S.; Khatsuria, R. M. Hydraulic forces on a submersible divide wall in a roller bucket, 43rd Annual Research Session, CBIP. Dehradun, June, 1973.
7. Khatsuria, R. M.; Ganesh Rao, H. C.; Deolalikar, P. B. Design of energy dissipator and downstream protection works- Srisailam dam spillway - CBIP, 54th R&D Session, Srinagar, Communication paper No 4, 1989.
8. Kleivan, E.; Torblaa, I. Opinions on ungated Vs gated spillway for embankment dams - 16th ICOLD, Q 63, R.9. San Francisco, 1988.
9. Lewin, J. Hydraulic gates and valves in free surface flow and submerged outlets; 2nd edition. Thomas Telford, London, 2001.
10. Leyland, B. W.; Jessup, G. R.; Berry, S. R. Automatic controls for spillway gates and outlets, International Water Power and Dam construction, January,1986.
11. Murti, N. G. K. Spillway and radial gates, CBIP Journal –Irrigation and Power, October, 1989.

12. Oswalt, N. R.; Pickering, G. A.; Hart, E. D. Problems and solutions associated with spillways and outlet works, 13th ICOLD, Q 50, R 15, 1979.
13. Schnitter, N. J. Discussion 52, Q 49, 13th ICOLD, Vol. V, 1979, 488-93.
14. Sehgal, C. K. Design guidelines for spillway gates, ASCE Jnl.of Hyd Div. March, 1996, 122(No 3).
15. Simmler, H. Spillway design principles in Austria - 13th ICOLD, Q 50, R 52, 1979.
16. Sinnarkar, R. M.; Diwanji, V. N.; Khatsuria, R. M. Hydraulic aspects concerning location of stop log groove for spillways and sluice outlets-Some case studies, CBIP Workshop on Hydraulic gates and hoists in water resources projects. Banglore, June, 1995.
17. Sinnarkar, R. M.; Diwanji, V. N.; Khatsuria, R. M. Operational problems in hydraulic gates and solutions-CWPRS experiences, Second Round Table Meet on Design Practices and Issues, Water Resources Development Sector, organized by the Central Water Commission, March, 2000.
18. Townshend, P. The use of fully automatic spillway gates to increase storage in existing dams, CBIP Workshop on Role of Gates and their Control in Water Resources Projects, Belgaum, June, 2000.
19. USACE Engineering and Design; Hydraulic Design of spillways, Engineer Manual EM 1110-2-1603, January, 1990.
20. WES Hydraulic Design Criteria, Chart 311- Tainter gates on spillway crests- Discharge coefficients, 1977.
21. WES Hydraulic Design Criteria, Chart 312- Vertical lift gates on spillways- Discharge coefficients, 1977.

18
Spillway Construction Stages

18.1 INTRODUCTION

The construction of major and medium multipurpose projects extends over several years. Construction schedules of large projects are governed by many factors such as volume of excavation, foundation treatment, earthwork or concreting that can be handled in a season, stage–wise building of irrigation/power potential, allocation of funds, etc. The construction phasing of spillways involves additional factors such as safe passage of floods during construction and the process of acquiring land under submergence and for the rehabilitation of the project affected population, and in general has to be commensurate with other activities of construction at the project site. Often, the spillway construction schedule is fraught with issues of conflicting natures. Experience gained from the construction of large projects enables the identification of the various issues involved and precautions required during planning and construction.

18.2 SPILLWAY CONSTRUCTION PROGRAM

Although the construction program of spillways is an integral part of the project construction, it involves considerations, some of which are exclusive to the spillway and some are linked with other components of the project.

1. Determining the construction flood.
2. Determining the reservoir levels during various stages of construction.
3. Phasing of spillway construction in accordance with the reservoir levels, as in (2) above.
4. Ensuring safety of the other elements of the project during passage of floods over the partly constructed spillway.

18.3 CONSTRUCTION FLOOD

The flood discharge to be handled during the period of construction is defined as the construction flood and is different than the diversion flood. While many countries have regulations laying down the flood return period for which the diversion works must be designed, there are no guidelines on the determination of construction flood. Selection of a construction flood is a complex process and is generally governed by an assessment of the risks involved due to the actual flood exceeding the design value. The criteria for selection vary between countries and among the projects of different magnitudes. The general practice is to adopt the magnitude of flood that has not been exceeded any time during the known history of the dam site. A flood of smaller magnitude may be adopted for concrete dams, where overtopping involves lesser risks than in the case of earth and rock–fill dams. Availability and capacity of the existing diversion tunnels may also influence the design value of the construction flood to be adopted. Another important consideration is the implementation of rehabilitation and resettlement for the project affected population in the submergence area upstream of the dams. This issue involves safety of human lives and property where the potential of risk must be kept to a minimum. Consequently, a flood of a larger return period is adopted.

The construction flood may not necessarily remain constant throughout the period of construction and up to the completion of the dam. At several projects, it was revised upwards, following floods of magnitude larger than the design construction flood during the progress of construction. A construction flood of gradually increasing magnitude may also be envisaged during the project planning itself. De Avila et al. (1979) have stated that during the five years of construction of the Itumbiara dam in Brazil, the magnitude of construction flood varied from 8500 cumec at the beginning to 16000 cumec (i.e. PMF) corresponding to the return periods varying from 25 to 2500 years. It is stated that the gradual increase in the return periods for various stages of the dam resulted from the necessity of taking smaller risks according to the higher possibility of damage, to both materials and human lives.

Finally, a strategy of absolutely no risk may dictate adoption of the routed probable maximum flood as the construction flood for the entire period of construction, as in the case of Guri dam, Venezuela. (Chavari et al. 1979)

18.4 RESERVOIR LEVELS DURING CONSTRUCTION STAGES

Reservoir levels to be reached during various stages of construction are determined with reference to the benefits to be accrued as a result of the development

of the irrigation/power potential and also various restraints that may be imposed by other factors. These may be levels of non-overtopping portions of the dam, progress of construction of the spillway, safety of other structures already constructed by that time, land acquisition in the submergence area, etc. If, however, utilization of the part potential were not envisaged, the objective would be to complete the project as early as possible. In such a situation, the spillway and the dam would be raised substantially each season and the reservoir level resulting from spillway stages would be determined for deciding temporary top levels of various elements of the project.

18.5 SPILLWAY CONSTRUCTION STAGES

The term ''Spillway construction stage'' means the level or levels a spillway or different monoliths of a spillway are brought at the end of a construction season. The spillway is raised in steps. The spillway may be raised uniformly over its entire width or different monoliths may be raised in steps of varying heights. This involves conflicting requirements. Ideally, raising the entire width (all monoliths) to a uniform elevation ensures satisfactory hydraulic conditions over the spillway, in the energy dissipater, and also downstream. However, in this scenario, spilling continues for prolonged periods over the entire width and further construction is possible only when the discharge completely stops. On the other hand, differential elevations of monoliths, similar to that shown in Figure 1, help confine the small flows to lower level monoliths only, keeping the rest of the width high and dry.

Model studies and prototype experience have established beyond doubt that the latter arrangement of monoliths has a potential for causing serious damage downstream through abrasion, erosion, and undermining. Notwithstanding this, practical considerations tilt the choice in favor of differential elevations, for obvious reasons. Studies on models and prototypes have indicated that a difference of up to 2 m can be permitted without causing undesirable flow conditions and damage. It would be preferable to have a symmetrical pattern of the monoliths as far as possible.

If development of the project in stages is not envisaged, concrete is placed on the spillway monoliths in horizontal layers, with the upstream and downstream profiles provided with final surface finishes, as shown in Figure 2. Various monoliths, in the form of truncated spillway profiles, operate for one season and are further raised in the next season and so on. Construction of the crest piers and erection of the gates are done during the last season.

When the project is to be completed in two or three stages, each stage resembles a small project itself catering to the needs of irrigation, power generation, etc., until in the next stage (which may be after a few years) further raising

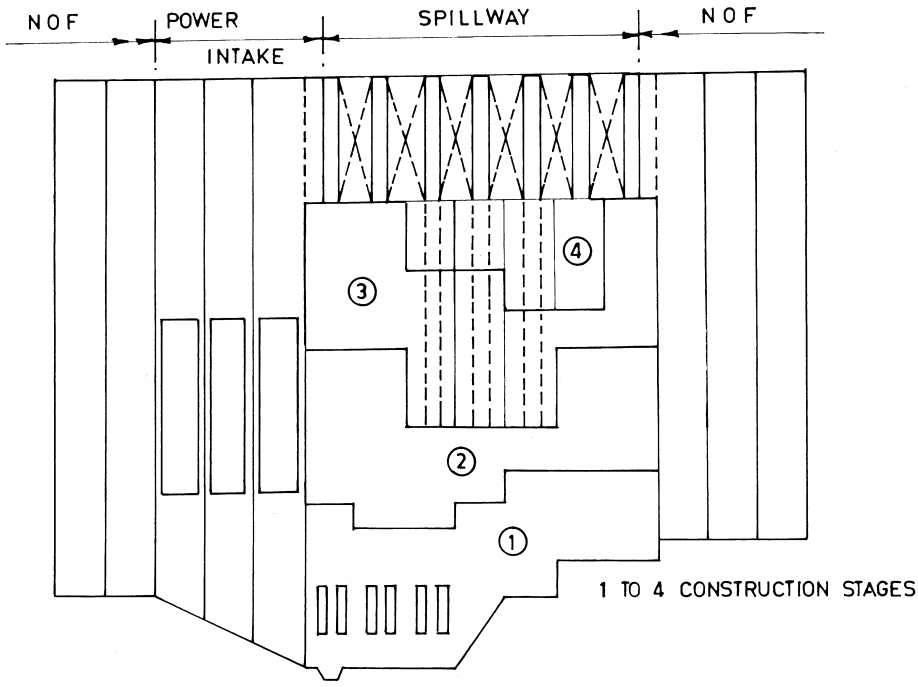

Figure 1 Typical construction stage of a spillway.

is done and potential increased. In such a development, an uncompleted spillway has to operate for a few years and must be provided with regular profiles for each stage, along with piers, gates, etc. The stage-wise raising of the Guri dam, (Carrera et al. 1979) shown in Figure 3 is an example of such a development. Figure 4 shows the pattern of raising spillway monoliths in 8 steps. A special feature of this pattern was the construction of all the ten crest piers, right from the stage I (El 195.20) up to the final top level (El 272.0). Such slender and freestanding piers necessitated steel stiffening trusses and steel struts for ensuring structural stability. Also, post-tensioned cable anchorages were required to be embedded at various stages of rising for installation of radial gates. However, these piers greatly facilitated the raising of the monoliths, providing crest gates at varying levels and enabling stop logs in the piers to temporarily close the flows from a part of the spillway. In the case of the raising of the spillway of Itumbiara dam in Brazil, three piers of 48 m height were constructed for similar purpose.

When crest piers are constructed in advance, a question arises in regard to proper bond between the piers and fresh concrete placed for raising the monoliths.

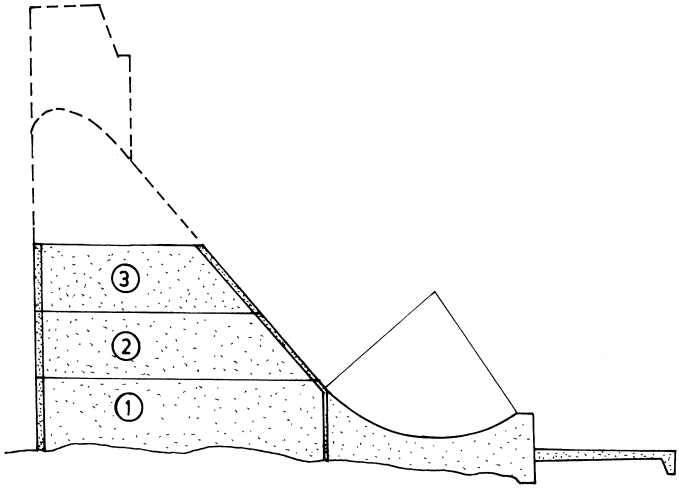

Figure 2 Raising of spillway in steps.

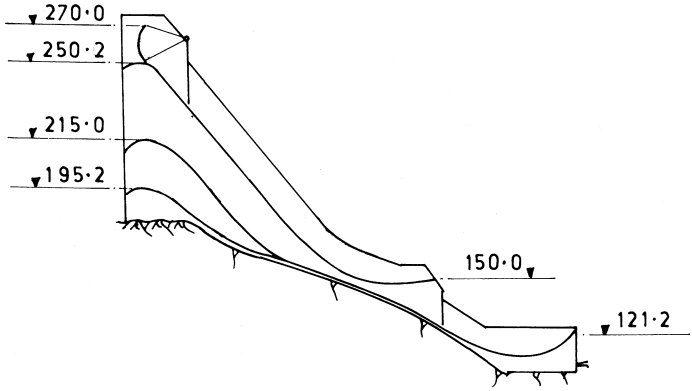

Figure 3 Stage-wise raising of Guri dam spillway. (Carrera et al. 1979)

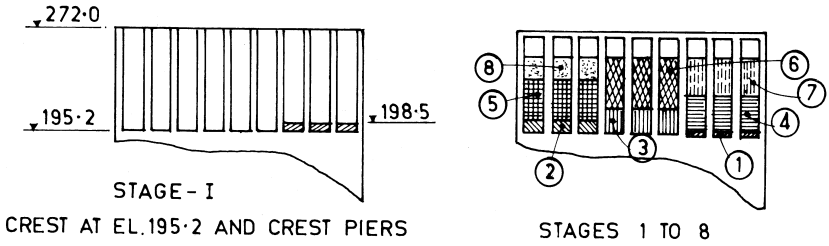

Figure 4 Pattern of raising spillway. (Carrera et al. 1979)

Of particular concern is the high overturning moment imposed by the water load retained by the crest gates. De Avila et al. (1979) have described provision of 10 cm deep horizontal keys, in the form of regular sinusoidal pattern, to be cast on the upstream of the piers for ensuring bondage. The keys would be grouted in the final stage.

18.5.1 Discharge Characteristics of Partly Constructed Spillways

The estimation of the discharge capacity of a partly constructed spillway is one of the most intricate problems in the design of spillways. A partly constructed spillway monolith could be idealized as a sharp crested, short crested, broad crested, or long crested weir as per the classification given in Table 2, (Chapter 12, Fig. 11). However, the involvement of other parameters such as varying heights of monoliths over the riverbed, varying widths and lengths, different elevations leading to varying depths of overflow, and variable submergence caused by the downstream water level, makes the phenomenon quite complex. Roughness of the unfinished concrete surface of the truncated monolith also affects the discharge capacity.

Experience from a number of model studies indicates that treating each individual monolith as a broad crested weir, calculating their discharge capacities separately and adding together, gives good results for the purpose of engineering decisions. The discharge over an individual monolith can be calculated either as per the WES (1977) HCD Chart 711, as reproduced in Figure 5, or as per the relationship given in Equation 1.

Khatsuria (1997) has reported a case study of the calculation of the discharge for a typical construction stage with monoliths at varying elevations, by applying Equation 1.

$$Q = \sum_{i=1}^{n} (2/3)^{3/2} \sqrt{g} C_i W_i H_i^{3/2} \tag{1}$$

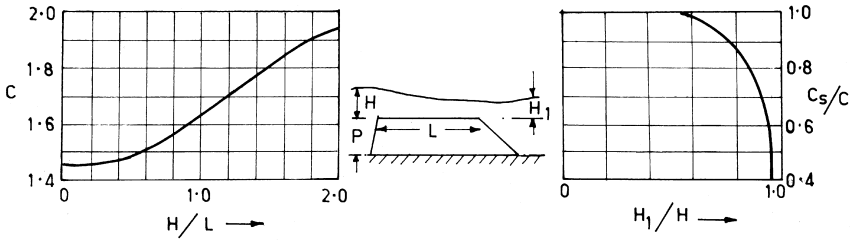

Figure 5 Coefficient of discharge of spillway monoliths (shown in WES HDC Chart 711).

where

C = Coefficient of discharge to be determined considering parameters H/P and H/L
H = Depth of overflow over a monolith (Fig. 5)
L = Length of monolith in flow direction
n = Number of monoliths
P = Height of monolith
Q = Discharge
W = Width of the monolith

The results were compared with those obtained from the model study and the agreement obtained was quite satisfactory.

While applying WES HDC Chart 711, the discharge equation is:

$$Q = \sum_{i=1}^{n} C_i (W_i - 2KH_i).H_i^{3/2} \tag{2}$$

Where K is the end contraction coefficient, in the case of monoliths adjacent to non-flowing blocks/abutments, etc. and the coefficient C has to be obtained from Figure 5.

The value of K is traditionally taken to be 0.10 for each contraction. Also, if the submergence over the crest due to downstream water level H_1 exceeds about 0.67 or so, the submerged crest coefficient C_s (Fig. 5), has to be considered.

Adequate information is not available regarding the effect of protrusion of unfinished concrete or masonry on the discharge characteristics. Equations 1 and 2 assume the crest surface to be smooth and even. In a particular case of model studies for the spillway, the roughness features, height and density (number per sq.m), were simulated for the purpose of comparing with smooth and even surfaced crest. Typically the protrusions varied from 75 mm to 230 mm and had an average density of 4.14 per square meter surface. It was indicated that the coeffi-

cient of discharge reduced by about 1.3% to 12.5% for H/L varying from about 0.3 to 0.05. More studies are, however, required to generalize this aspect.

18.6 FLOW DOWNSTREAM OF PARTLY CONSTRUCTED SPILLWAYS

Flow conditions downstream of partly constructed spillways are often unsatisfactory and conducive to damage. When different monoliths are kept at varying elevations instead of at a uniform level for the entire spillway, unequal discharge distribution results downstream of the spillway in the energy dissipator and in the river channel. Floors of hydraulic jump stilling basins are particularly vulnerable to damage due to the horizontal eddies forming in the downstream. Such eddies pick up loose material from the downstream, bring it inside the basin, and cause abrasion damage to the concrete floor, commonly known as roll-mill action. The damage sometimes is so extensive as to expose even the reinforcement steel of the apron floor. Figure 6 shows a view of the damage to the stilling basin floor of a dam as a result of the abrasion caused due to material that was brought in by the return eddies during a construction stage. This, perhaps, cannot be prevented in ordinary situations. A remedy adopted at the Sardar Sarovar dam, India, was to provide a number of low height divide walls in the basin. The divide

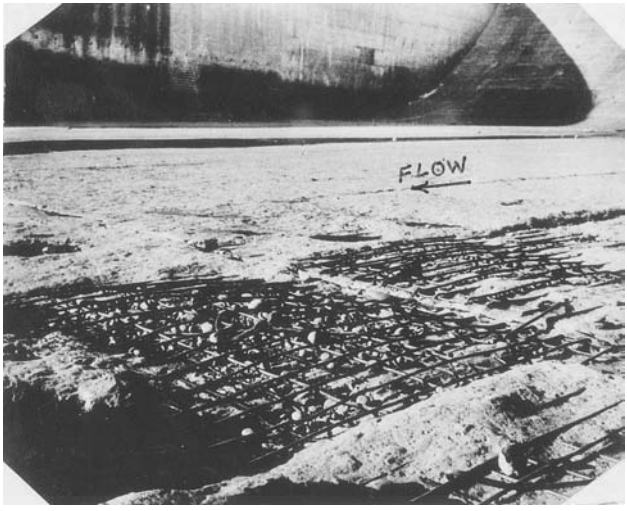

Figure 6 Damage to stilling basin floor.

walls help confining the extent of such eddies, restricting only to the downstream of the basin, eliminating or reducing the possibility of the transport of loose material from the downstream into the basin. Eventually, the divide walls perform the duty for the finally completed spillway in the event of unequal operation of the crest gates. Khatsuria et al. (1987) have described model studies for the design of divide walls for Sardar Sarovar dam spillway.

Impingement of the flow leaving the uncompleted truncated surface of a monolith on the apron floor and causing damage is yet another concern for the spillways with stilling basins. This is schematically shown in Figure 7. Except for small discharges, the flow has a tendency to spring clear at the downstream end of the monolith, similar to the jet of a free over-fall spillway. Its impingement on the apron floor results in fluctuating pressures with a definite frequency. Basically, the apron floor of a hydraulic jump stilling basin is not designed for such a loading. The fluctuating pressures may cause vibration of the floor panels, disrupt the joints and water stops, and may cause uplift of the slabs. It is experienced that if the energy of the falling nappe is greater than about 16,000kW/sq. meter, damage to concrete surface is likely. The remedy lies in ensuring that the flow leaving the monolith adheres to the spillway profile similar to ogee profile, for all discharges.

Since shaping the monoliths to the profiles similar to ogee profile during each year of the construction stage is not possible, rounding of the downstream corner or adding a hump with a rounded crest, as shown in Figure 8, may be a solution.

However, with this, there remains a problem of the so-called feather edge at the joint of old and new concrete. In order to avoid dismantling of a part of the old concrete for providing proper bonding with the new concrete, slots were

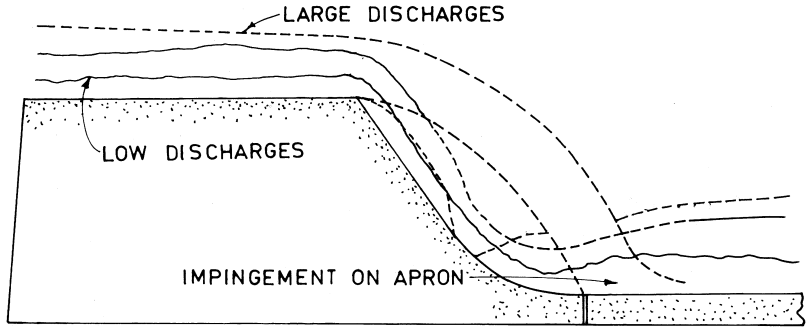

Figure 7 Separation of flow at the downstream corner of the monolith and impingement on the apron.

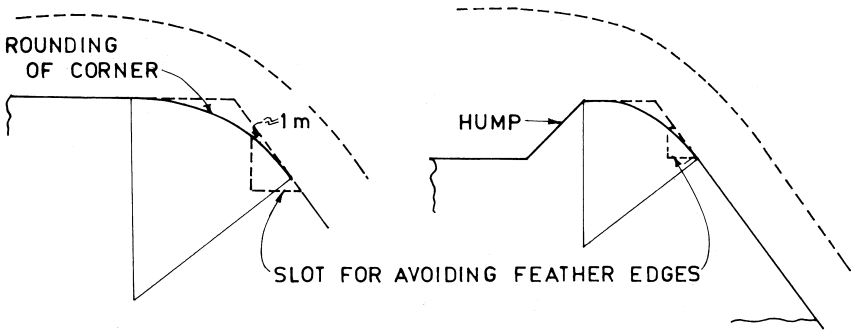

Figure 8 Rounding of corners and humps to avoid separation.

introduced in the humps on the spillway monoliths of Sardar Sarovar project as shown in Figure 8. Humps are preferable over the rounding of corners, because of improved coefficient of discharge and the additional factor of safety against sliding offered by the humps.

It may be mentioned that the effectiveness of a hump in ensuring streamlined flow on the spillway glacis depends on its height. In other words, the hump of a given height will offer acceptable conditions up to a certain discharge only, beyond which the flow again tends to separation. This can be finalized only on a hydraulic model. Humps of 3 m heights were provided on the spillway monoliths of Sardar Sarovar dam spillway, which catered to approximately 40% of the construction flood discharge.

When the spillway is raised substantially, the ratio of the depth of flow to the length of the monolith increases, the magnitude of discharge for the streamlined flow increases, and the severity of the problem is reduced.

Spillways with bucket type energy dissipators face a different type of problem during construction. Large flows passing down the low level monoliths result in thick jets that are unable to turn along the bucket curvature and hence a cascading flow over the bucket surface takes place. This causes deep scour very near the bucket, threatening to undermine the foundation. Concrete aprons are laid in continuation of the buckets to prevent it from scouring action. Such aprons should be laid on fresh rock and properly anchored. At Srisailam dam, India, construction stage (1978) had resulted in a flow condition that damaged even the concrete apron laid during earlier stages, as shown in Figure 9.

In addition to the safety of the spillway, energy dissipator, and the river channel in the immediate downstream vicinity, safety of other structures such as partly constructed earth dams, power intakes, etc. may also be of concern. These

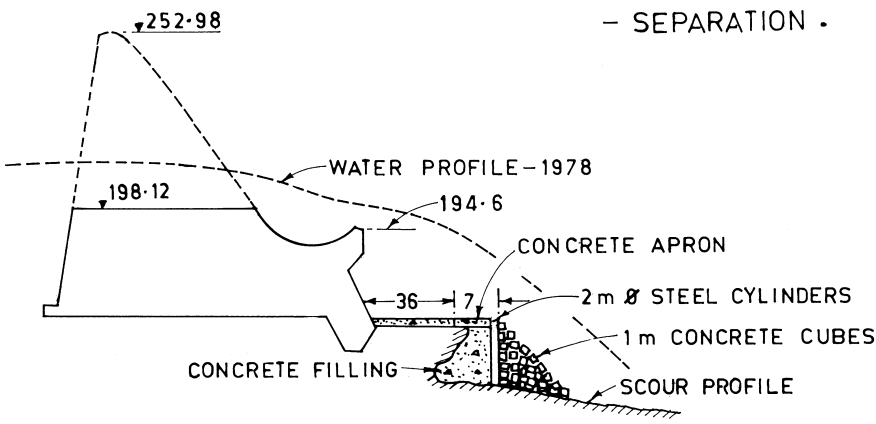

Figure 9 Srisailam dam spillway, India: 1978 construction stage.

could be identified and resolved only through hydraulic model study in each specific case.

Notations

B Width of the monolith perpendicular to flow direction
C Coefficient of discharge
C_s Coefficient of discharge for submerged crest
H Depth of flow over the monolith
H_1 Submergence over the crest due to downstream water level
K End contraction coefficient
L Length of the monolith in the direction of flow
n Number of monoliths under flow
P Height of monolith above riverbed
Q Discharge
W Width of monolith

REFERENCES

1. Carrera, E.; Roddy, R.; Hasen, H. Raising Guri dam. Safe construction to meet load growth in Venezuela, 13th ICOLD, Q 48, R 14, 1979.
2. Chavari, G.; Louie, D.; Castillejo, N.; Coleman, H.W. Spillway and tailrace design for revising of Guri dam using large scale hydraulic model, idbi, Q 50, R 12.
3. De Avila, L.; De Barros, P.; Tavares, G.; Ferreira, W. Itumbiara Project River Diversion. Interface problems during spillway construction, ibid, Q 48, R 44, 1979.

4. Khatsuria, R. M.; Deolalikar, P. B.; Bhosekar, V. V. Recent studies concerning design of divide walls in spillways and energy dissipators, Supplement to the Proceedings of the International Symposium on Design of Hydraulic Structures; Colorado State University, USA, August 1987.
5. Khatsuria, R. M. Staying high and dry- flood prediction and control, International Water Power and Dam Construction, April 1997.
6. WES Hydraulic Design Criteria- Low monolith diversion, Discharge Coefficients, Chart 711, 1977.

19
Energy Dissipators for Spillways

19.1 INTRODUCTION

Dissipation of the kinetic energy generated at the base of a spillway is essential for bringing the flow into the downstream river to the normal—almost pre-dam—condition in as short of a distance as possible. This is necessary, not only to protect the riverbed and banks from erosion, but also to ensure that the dam itself and adjoining structures like powerhouse, canal, etc. are not undermined by the high velocity turbulent flow.

Although a variety of devices are used for energy dissipation at the base of spillways, the dissipation of energy is through internal friction and turbulence or impact and diffusion of the high velocity flow in the mass of water. Devices and appurtenances which aid the process of energy dissipation may also create peculiar problems that need to be identified and solved.

19.2 CLASSIFICATION OF ENERGY DISSIPATORS

Energy dissipators for the spillways can be classified in several ways:

1. Based on hydraulic action: turbulence and internal friction as in hydraulic jump stilling basins, roller buckets, and impact and pool diffusion as with ski jump buckets and plunge pools.
2. Based on the mode of dissipation: horizontal as in the hydraulic jump, vertical as with ski jump buckets/free jets, and oblique as with spatial and cross flows. The vertical dissipation may be in the downward direction as with free jets and plunge pools and in upward direction as with roller buckets.
3. Based on geometry or form of the main flow: situations involving sudden expansion, contraction, counter acting flows, impact, etc.

4. Based on the geometry or form of the structure: stilling basin employs hydraulic jump with or without appurtenances like chute blocks, baffle piers, etc. Buckets (ski jump or flip buckets) include special shapes like serrated, dentated buckets, and roller buckets that are either solid roller bucket or slotted buckets.

It is found that the most practical way of classifying the energy dissipators is to adopt the classification based on the structural form such as stilling basin apron, bucket, etc.

19.3 PRINICIPAL TYPES OF ENERGY DISSIPATORS

The energy dissipators for spillways can be grouped under the following five categories:

1. Hydraulic jump stilling basins
2. Free jets and trajectory buckets
3. Roller buckets
4. Dissipation by spatial hydraulic jump
5. Impact type energy dissipators

Hydraulic jump stilling basins include horizontal and sloping aprons and basins equipped with energy dissipating appurtenances such as chute blocks, baffle piers, and dentated end sills. This is the most common type of energy dissipator for the spillways and outlets and effects up to 60% dissipation of the energy entering the basin, depending on the Froude number of the flow. For heads exceeding about 100 m, hydraulic jump stilling basins are not recommended because of the problems associated with turbulence like intermittent cavitation, vibration, uplift, and hydrodynamic loading (Chapter 20).

Free jets and trajectory buckets are not dissipators of energy in real sense. The bucket deflects the high velocity jet into the air and is made to strike the riverbed at a considerable distance from the structure. Any scour that may occur in the impingement zone remains away from the structure and hence does not endanger the stability of the structure. Nappe splitters and dispersers contribute to the dissipation of energy by spreading and aerating the jet (Chapter 11). Nevertheless, at some projects, problems of spray and retrogression of the scour hole towards the structure threatened the stability. Coupled with the plunge pools, part of energy of the deflected jet can be dissipated by pool diffusion. (Chapter 21)

Roller buckets can be conceptualized as hydraulic jump on a curved floor, as its performance is closely related to the Froude number of the incoming flow

and tail water depth. It can also be seen as an economical alternative to the elaborate sloping aprons. Solid roller bucket is a simple device that gives satisfactory performance provided it is operated symmetrically. Asymmetrical operation results in a horizontal eddy downstream of the bucket that can carry loose material into the bucket causing abrasion damage. The slotted bucket, claimed to be an improvement over the solid bucket, has a self-cleansing potential by way of slots and teeth in the bucket. In spite of this, as many slotted buckets as solid roller buckets have been damaged due to abrasion and cavitation. The performance of the slotted bucket is more sensitive to tail water variation than that of the solid roller bucket (Chapter 22).

The most common form of energy dissipator at the outlets of shaft/tunnel spillways is a flip bucket. However, when topographical or geological conditions are not favorable, a hydraulic jump stilling basin is the only choice regardless of concentration of discharge and energy at the entrance to the energy dissipator. The standard design of stilling basin would normally not be suitable. In such situations, dissipation of energy by spatial hydraulic jump has been accomplished successfully in some cases (Chapter 23).

Impact induced by an obstacle placed against the high velocity flow is also applied to accomplish energy dissipation in small chutes and spillways. Since the successful performance of such structures is dependent on the stability of the impact-inducing obstacle against fluctuating drag force and cavitation damage, these designs have found limited application for low heads and small discharges (Chapter 24).

Besides, there are quite a few designs of unconventional types of energy dissipators suited to the site-specific conditions. No generalized procedures are developed for such structures and imagination, experience, and judgment on the part of the designer play an important role in their selection (Chapter 25). Recently stepped spillways that combine the features of both the spillway and energy dissipator have become popular. These are suitable for dams being constructed with roller compacted concrete (RCC) because of the obvious advantage of steps being formed with placement of concrete in lifts of required thickness. It offers dissipation of part of the energy on the spillway chute itself and enables reduction in the size of the stilling basin; however, their use is limited up to the unit discharge of 30 cumec/m in view of the apprehension about cavitation damage.

19.4 SELECTION OF THE TYPE OF ENERGY DISSIPATOR

The factors that govern the choice of the type are: hydraulic considerations, topography, geology, type of the dam, layout of other associated structures, eco-

nomic comparison, frequency of usage, as well as special and environmental considerations. When a number of alternatives are possible, personal preference of the designer may also govern the selection. However, it is not likely that all the factors unanimously point to a unique choice. In most cases, a choice so obviously apparent as favored by a majority of factors could still be a subject of rejection as dictated by some other factors. Therefore, all the factors involved in the process have to be applied comprehensively rather than on their individual merits.

Topography influences the type of the dissipator in the same way as it influences the type of the dam or the spillway. The topography that favors the selection of a shaft spillway or a tunnel spillway will most likely be an ideal site for a flip bucket, as discussed in Chapter 10. Even for the gravity or arch dams in steep and narrow canyons, ski jump buckets or flip buckets would be more suitable, provided the problems of spray and resulting bank erosion and land slides can be tackled. Ski jump buckets are found to be most suitable for dams to be constructed in steep and narrow valleys where a power house would be accommodated at the foot of the dam, with the roof of the power house, in the form of an inverted circular arc, also serving as the ski jump bucket. On the other hand, hydraulic jump stilling basin would prove to be more problematic, not only from consideration of deficient tail water depth and longer training walls, but also due to the concern arising from the falling of debris from the steep slopes into the stilling basin.

Flip buckets would be preferable also for the chute spillways located on flanks but in the vicinity of the main river channel. While a hydraulic jump stilling basin along with the river joining works would be inefficient and expensive, flip bucket with a deflector to divert the jet towards the main river channel would result in a compact structure.

Hydraulic jump stilling basins and slotted buckets would be less preferable for the spillways whose construction may continue for several years and where seasonal floods have to be passed down the partly constructed spillways. Stilling basins for such spillways are prone to be filled up intermittently and damaged due to impinging concentrated flows, abrasion, etc. Similarly, for the spillways that serve dual functions, such as flood and sediment disposal, stilling basins or roller buckets should be avoided as far as possible, due to the possibility of abrasion damage caused by sediments passing down the spillways during flushing operation.

Sometimes environmental factors play a decisive role in determining the type of the energy dissipator. As for example, deep seated stilling basins with highly aerated flows inducing nitrogen supersaturation would not be permissible where fish life is an important consideration. (Chapter 22). Erosion due to plunging jets and spray caused by the flows from ski jump buckets adversely affect

the river water quality by turbidity, harmful for the fish population. In the cold regions where ice floes have to be passed down the spillway crest, hydraulic jump stilling basins are not desirable as the floes are likely to be trapped in the return roller, hinder the movement of the floes coming from the top, and cause damage to the floor of the basin. Flip buckets are obviously the most suited types of energy dissipator in such situation. When the tail water levels were too high to hinder the formation of a clear flip action, a submerged hydraulic jump on a step followed by an apron was found to perform satisfactory. Thus, the type or design of the energy dissipator has to be adapted as demanded by the prevailing environment.

While a wide range of energy dissipators has been developed to suit different conditions, the limit on their use is vaguely defined. Guidelines vary for the ranges of head and discharge over which the various types of energy dissipators can be used and in some cases are not given at all. As Mason (1982) has noted, ''That the design of prototype hydraulic energy dissipators is not the exact science that design charts sometimes suggest is confirmed by the problems that continue to be reported with all types of dissipator.'' In an attempt to broadly establish the ranges of head and discharges over which the main types of dissipators are most commonly used, Mason carried out a literature survey of 370 prototype dissipators from dams in 61 countries. The energy dissipators were grouped in: rock basins, simple hydraulic jump basins, baffle basins, simple over-falls, ski jumps, and flip buckets. The hydraulic parameters considered were: total discharge Q and total head drop H from reservoir level to tail water. Use of the parameter total discharge Q—in place of the unit discharge q—however, limits the utility of the analysis for application. It can be shown that for a given Q, H and all other conditions, a wide spillway—smaller q—would operate quite different than a narrow spillway—larger q.

19.5 ANALYSIS OF PARAMETERS

The problem of dissipation of energy at the base of a spillway can be visualized with reference to the situation illustrated in Figure 1 (Rudavsky 1976). This clearly shows the key parameters: the height of the spillway (P), the unit discharge (q), the headwater representing the initial energy (E_0), and the tail water representing the energy level downstream (E_t). Also,

$$E_0 = y_0 + \frac{V_0^2}{2g} \tag{1}$$

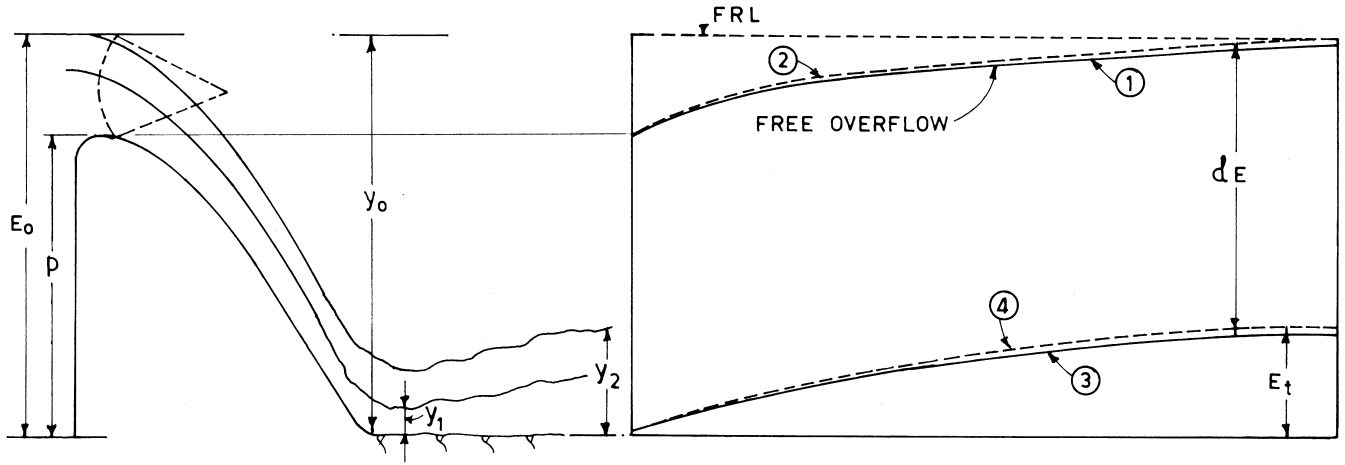

Figure 1 Key parameters in energy dissipation. (Rudavsky, 1976)

① Headwater rating curve
② Energy line for head water
③ Tail water rating curve
④ Energy line for tail water

$$E_t = y_t + \frac{V_t^2}{2g} \tag{2}$$

where

y_0 = Approach depth
y_t = Tail water depth
V_0 = Approach velocity, and
V_t = Downstream velocity

It would be seen that the difference between the upstream and downstream energies (dE) is the energy that must be dissipated by the energy dissipator. A combination of the four parameters would determine the type of flow condition at the base of the spillway, namely an effective hydraulic jump, a sweeping or deficient jump, a submerged jump, a diving jet, or a floating jet. As several combinations of parameters exist, a variety of flow conditions at the base are possible. The latitude of the changes in parameters is limited; only the headwater rating curve can be changed by altering the depth of overflow or width of the spillway, resulting in the change of unit discharge q. The tail water rating curve is imposed by nature and cannot be changed except with an artificial control in the river downstream.

A preliminary indication as to the expected flow condition for the entire range of discharge can be obtained by superimposing the jump-height curve on the tail water rating curve. A jump-height curve is formed by adding the conjugate depth of hydraulic jump, y_2, to the assumed elevation of the apron (that can be constructed economically on the bedrock available at the site) corresponding to various discharges. The procedure of calculating the jump-height curve is discussed in Appendix. A

Figure 2 shows four possible cases of relationships between the jump-height and tail water rating curves.

The general guidelines are indicated in Table 1.

Based on the dimensional analysis of the parameters involved in the process, Rudavsky (1976) evolved a relationship

$$\frac{y_t}{E_0} = f\left[\frac{q}{\sqrt{g}E_0^{3/2}}\right] \tag{3}$$

Which, in combination with the theoretical relationship for the hydraulic jump on a horizontal floor

$$\sqrt{\frac{y_1^2 y_2}{2E_0^3} + \frac{y_1 y_2^2}{2E_0^3}} = \left[\frac{q}{\sqrt{g}E_0^{3/2}}\right] \tag{4}$$

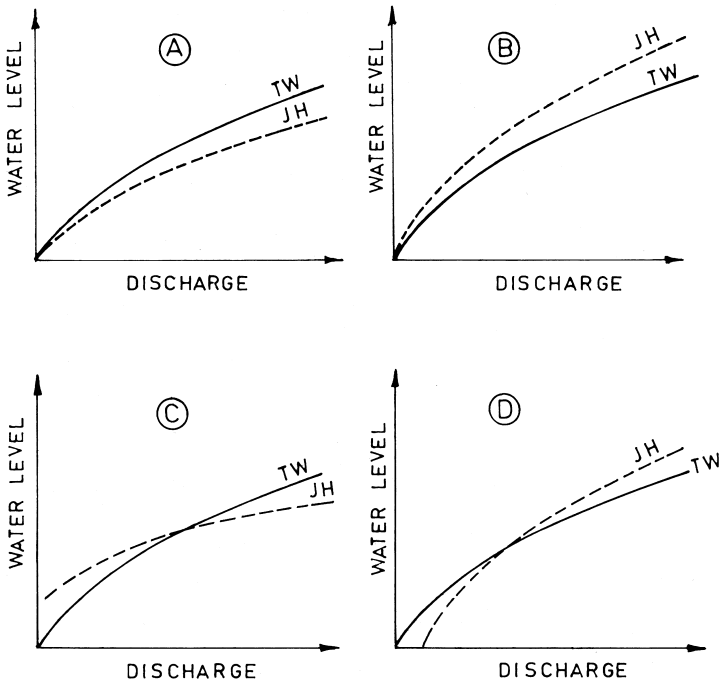

Figure 2 Jump height and tail water rating curves.

Table 1 Choice of Energy Dissipator Based on Analysis of JH and TW Rating Curves

Case	Situation	Suggested arrangement
A	TW curve is above the JH curve for all the discharges	Horizontal apron if $1 < y_t/y_2 < 1.1$ and sloping apron/roller bucket if $y_t/y_2 > 1.1$
B	TW curve is below the JH curve for all the discharges	Flip bucket
C	TW curve is below the JH curve for lower discharges and above the JH curve for higher discharges	Sloping-cum-horizontal apron such that the jump forms on the horizontal portion for low discharges and on the sloping portion for high discharges
D	TW curve is above the JH curve for lower discharges and below the JH curve for higher discharges	A combination energy dissipator performing as a hydraulic jump apron for low discharges and flip bucket for high discharges

can be used to perform similar analysis as in Figure 2. The curve representing Equation 3 is also called the characteristic curve, since this curve combines the characteristics of both the headwater and tail water rating curves. The diagram superimposing the characteristics curve on the theoretical curve (Eq. 4) is called the fence diagram. Rudavsky analyzed results of several model studies in respect of different types of energy dissipators and prepared fence diagrams that define the range of applicability of various types of energy dissipators such as (a) hydraulic jump stilling basin without baffle piers, (b) hydraulic jump stilling basins with baffle piers, (c) solid roller buckets, (d) slotted bucket, and (e) deep-seated excavated stilling basin called Smetana's basin. The diagrams are shown in Figure 3. The curve (1) is the theoretical relationship for hydraulic jump as given by Equation 4. The characteristics curve for the specific spillway structure under consideration, given by Equation 3 should be plotted on the same diagram. If the curve is contained within the shaded region called application range, for a given type of energy dissipator [(a) to (e)], that type of energy dissipator is adopted. As discussed earlier, small adjustment in the position of the characteristics curve relative to the theoretical curve (1) is possible by changing the depth of overflow/width of the spillway and hence q.

It must, however, be noted that diagrams such as Figure 2 and Figure 3 are not the design charts. These may be used only as design aids in visualizing the possible flow conditions at the toe of a spillway, as a result of the interaction between the relevant parameters involved in the process of energy dissipation. A final selection would aptly depend on the experience and judgment on the part of the designer, as discussed in the illustrative example.

Illustrative Examples

Discuss the available alternatives of energy dissipation arrangement for a spillway with the following details:

FRL El 677 m, crest El 662 m, width at toe 52 m, maximum Q 5160 cumec, unit discharge q 99.2 cumec/m, and acceptable apron elevation El 605 m.

The spillway will be operated with reservoir at FRL, passing discharges lower than the maximum discharge with partial opening of crest gates. The tail water rating curve is defined as curve B in Figure 4.

Calculation of jump-height curve:

Conjugate depth y_2 has been calculated as follows;

$q = 99.2$cumec/m; $E_0 = 72$ m $= y_0$ (Head water maintained by gate operation)

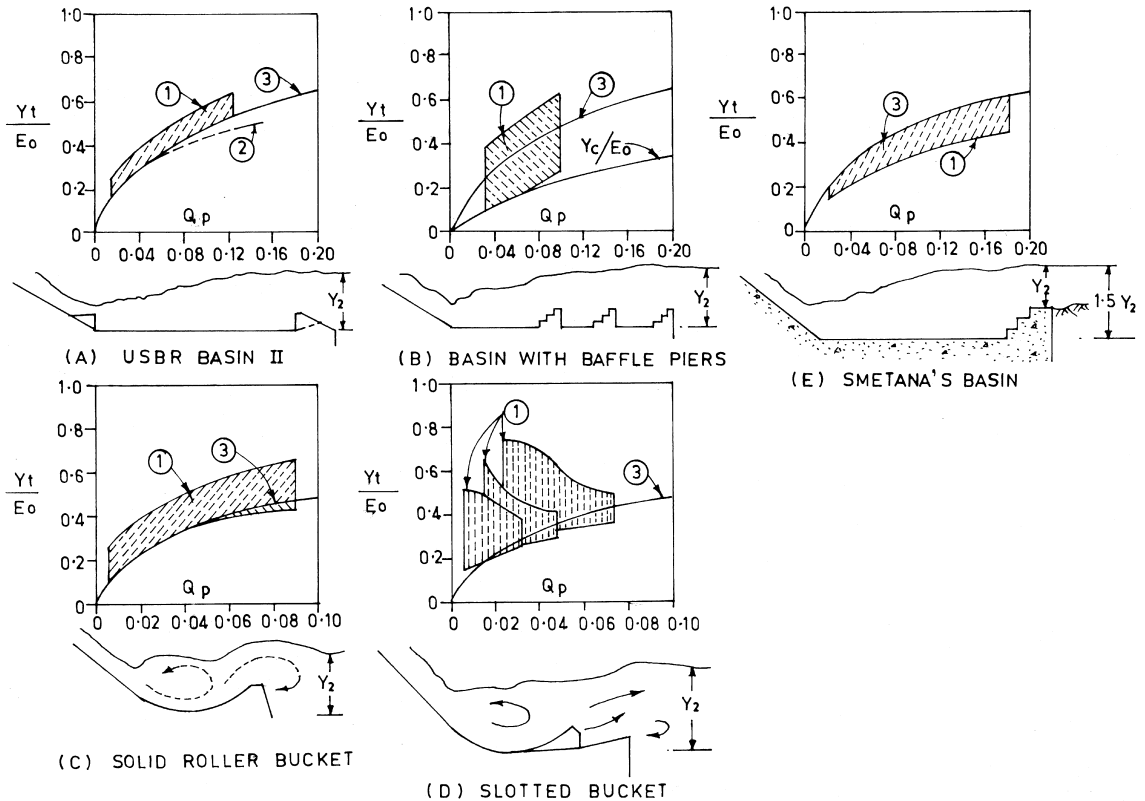

Figure 3 Application ranges of various energy dissipators (shown in Rudavsky 1976): $Q_p = q/\sqrt{g}\,E_0^{3/2}$ 1 Application range, 2 Sweep out begins, 3 Theoretical curve.

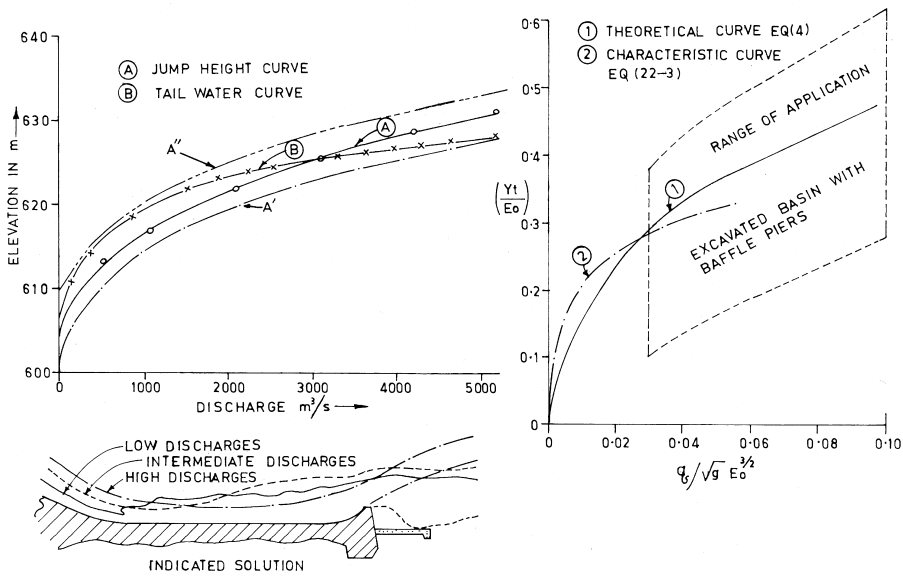

Figure 4 Illustrative example: Alternatives of energy dissipator.

$V_1 = \sqrt{2gx72} = 37.58m/s \Rightarrow y_1 = 2.64m$ Corrected $y_0 = 72 - 2.64; \Rightarrow$
$V_1 = 36.89m/s$
$y_1 = 2.69m \quad y_0 = 72 - 2.69; \Rightarrow V_1 = 36.88m/s$
$y_1 = 2.69m\ V_1 = 36.88m/s; F_1 = V_1/\sqrt{g\,x\,y_1} = 7.18$

$$y_2 = \frac{y_1}{2}\left[\sqrt{1+8F_1^2} - 1\right] = 26.0m$$

Similarly, values for other discharges have been calculated and shown in Table 2.

Figure 4 shows the jump-height curve (A) plotted superimposed on the tail water rating curve (B). It also shows the fence diagram with the theoretical curve for hydraulic jump on horizontal floor, curve (1) plotted superimposed on the characteristic curve (2). From the series of application curves (Fig. 3), the one that fits in, at least partly, namely excavated basin with baffle piers (case B), is also plotted there in. Analysis of the above indicates that:

1. Hydraulic jump will form on the apron proposed at El 605 m, for the discharges smaller than 3000 cumec. For higher discharges, a deficient jump may form or sweep out condition may take place.

Table 2 Calculation of Jump Height Curve

Discharge Q, cumec	Unit discharge, q, cumec/m	V_1, m/s	y_1, m	F_1	y_2, m	JH,El m	E_0, m	y_t, m	Y_t/E_0	Q_p*
5160	99.2	36.88	2.69	7.18	26.0	631	72	23.2	0.32	0.052
4160	80	37.01	2.16	8.04	23.5	628.5	72	22.0	0.30	0.042
3120	60	37.16	1.61	9.35	20.5	625.5	72	20.5	0.29	0.031
2080	40	37.30	1.07	11.5	16.9	621.9	72	18.5	0.26	0.021
1040	20	37.44	0.53	16.3	12.1	617.1	72	15.0	0.21	0.010
520	10	37.52	0.27	23.2	8.6	613.6	72	11.0	0.15	0.005

* $Q_p = \dfrac{q}{\sqrt{g}E_0^{3/2}}$

2. From the series of fence diagrams indicating range of application of various types of energy dissipators (Fig. 3), the one pertaining to the alternative of the excavated basin with baffle piers is partly applicable and suggests a stilling basin with baffle piers for higher discharges. The lower discharges (up to about 60% of the maximum discharge) however, are not covered by the application range.
3. Incorporating baffle piers in flow velocities as high as 37 m/s, is not advisable from apprehension of cavitation. This alternative, therefore, cannot be pursued further.
4. One may also consider altering the vertical position of the stilling basin, indicated by the vertically shifted JH curves, A′ and A″. The position A′ represents the stilling basin lowered by about 5 m, making the entire JH curve below the TW curve, so that hydraulic jump forms for all discharges. The curve A″ is above the TW curve for all discharges and corresponds to a flip bucket placed about 5 m higher than the elevation 605 m under consideration. Besides ascertaining the suitability of submerged hydraulic jump for low discharges and competence of rock in the downstream for a flip bucket proposal, increased cost due to excavation or concreting also should be considered.
5. A design combining the features of hydraulic jump and flip bucket, i.e. a combination type energy dissipator, functioning as hydraulic jump stilling basin for low discharges and flip bucket for high discharges, as shown in Figure 4, may also be suitable.

A provisional decision in regard to the type of the energy dissipator should be based on considerations of hydraulic performance, site conditions, and cost economics. The final design could be evolved from model studies.

Notations

E_0 = Total energy level upstream of the spillway
E_t = Total energy level downstream of the spillway
F_1 = Pre-jump Froude number
P = Height of the spillway crest from riverbed
Q = Discharge
q = Unit discharge
V_0 = Approach velocity upstream of the spillway
V_1 = Velocity of supercritical flow at the toe of the spillway
V_t = Velocity of flow downstream of the spillway
y_0 = Depth of flow upstream of the spillway
y_1 = Depth of supercritical flow at the toe of the spillway
y_2 = Conjugate depth of hydraulic jump
y_t = Depth of tail water above the apron

APPENDIX: A

Jump-height Curve, Characteristics Curve, and Fence Diagram

A jump-height curve requires calculation of conjugate depth, y_2, of hydraulic jump for different discharges, relative to the assumed elevation of apron. Following the notation shown in Figure 1,

$$y_2 = \frac{y_1}{2}\left[\sqrt{1+8F_1^2} - 1\right] \tag{5}$$

where

y_1 = Supercritical pre-jump depth
F_1 = Supercritical Froude number = $V_1/\sqrt{g\ y_1}$
y_1 is related to E_0 and q, such that

$$E_0 = y_1 + \frac{V_1^2}{2g} + losses \tag{6}$$

y_1 and V_1 are related as

$$y_1 = \frac{q}{V_1} \tag{7}$$

Neglecting losses and combining Equations (6) and (7) gives

$$y_1^3 - E_0 y_1^2 + \frac{q^2}{g} = 0 \tag{8}$$

This is a cubic equation, which can be solved by trial method or can be easily programmed on a hand-held programmable calculator.

A quick manual method is to start with Equation (6), assuming $y_1 = 0$, thus obtaining the first approximation of V_1 as $V_1 = \sqrt{2gE_0}$ and thus $y_1 = q/V_1$. A revised value of V_1 can then be worked out as $V_1 = \sqrt{2\ g\ (E_0 - y_1)}$ from which the corrected values of y_1 and V_1 can be obtained until the differences in the values are negligible.

It is found that the procedure converges rapidly with 3 to 4 steps. The jump-height elevation for the given discharge is then

JH = Apron level + y_2

For calculating the characteristic curve, y_t is used, where

y_t = Tail water elevation – apron level for the given discharge

The theoretical curve (1) can also be calculated with the values of y_1 and y_2 for different discharges.

In the calculations for y_2, head loss from the crest up to the toe of the spillway has been neglected. This is reasonable in the case of a steep gravity spillway. However, for chute spillways of longer lengths on flat slopes, 10% to 20% energy loss may be assumed for the purpose of calculations.

REFERENCES

1. Mason, P. J. The choice of hydraulic energy dissipator for dam outlet works based on a survey of prototype usage. Proc. Instn. Civ Engrs, Part I. May 1982, 72.
2. Rudavsky, A. B. Selection of spillways and energy dissipators in preliminary planning of dam developments, 12th ICOLD, Q 46, R 9 Mexico, 1976.

20
Hydraulic Jump Stilling Basins

20.1 INTRODUCTION

One of the most extensively investigated phenomena in hydraulic engineering—both theoretically as well as experimentally—is the hydraulic jump. Numerous investigators have studied it over the past century. It remains the most favorite choice of designers for energy dissipation below spillways and outlets, because of its extensively studied and well-documented characteristics. A properly designed hydraulic jump stilling basin can ensure 60–70% dissipation of energy in the basin itself. Supported by laboratory investigations and prototype experience, a suitable stilling basin that caters to a variety of conditions covering discharge intensity, head, tail water variation, and topographical conditions can be designed with confidence. The most serious problem with the hydraulic jump dissipator, however, is more of structural strength rather than hydraulic efficiency. Experience in recent years gives many examples of stilling basins suffering serious damages due to uplift, vibration, cavitation, and abrasion, all having their origin in the internal structure of hydraulic jump. Although the studies in this regard are of recent origin, their results are useful in evolving some guidelines for designing hydraulically efficient and structurally safe stilling basins, particularly for high heads.

20.2 HYDRAULIC JUMP CHARACTERISTICS

Hydraulic jump characteristics relevant to its application to the energy dissipation are only discussed here. These are:

Classification of jump
Length, including length of the roller
Conjugate depth and energy loss
Turbulence characteristics
Air entrainment by hydraulic jump

The discussion would then cover the relevance of these five characteristics to the design.

20.2.1 Classification of Hydraulic Jump

Hydraulic jumps can be classified according to the geometrical form, pre-jump Froude number of the flow relating it to the energy dissipation efficiency, or as a free, forced, or submerged jump.

In the first category, the jump is designated as classical jump, A-type, B-type, C-type, or D-type. A classical hydraulic jump is the transition from super-critical to sub-critical flow in a horizontal prismatic channel. An A-jump is the hydraulic jump formed at the junction of a sloping channel with the horizontal floor as shown in Figure 1. If the jump forms at a location on the slope but ends on the horizontal floor, it is termed B-jump. The C-jump occurs in sloping channels with a horizontal channel portion when the end of the jump is located at the junction. In a D-jump, the entire jump is formed on the sloping portion.

Hydraulic jumps have also been classified according to the pre-jump Froude number (F_1). For values of F_1 up to about 1.7, a slight ruffle on the water surface is the only apparent feature for such a jump, often termed as undular jump. For the higher range of F_1, the classification is

1.7 to 2.5 (pre-jump): low energy loss.
2.5 to 4.5 (transition or oscillatory jump): energy loss 25 to 50%.
4.5 to 9.0 (steady or good jump): energy loss 50 to 70%.
Greater than 9 (effective but rough jump): energy loss $>$ 70%.

These are illustrated in Figure 2.

The jumps have also been classified as

1. Free jump: when the tail water depth (y_t) available at the end of the jump is equal to the conjugate depth y_2.

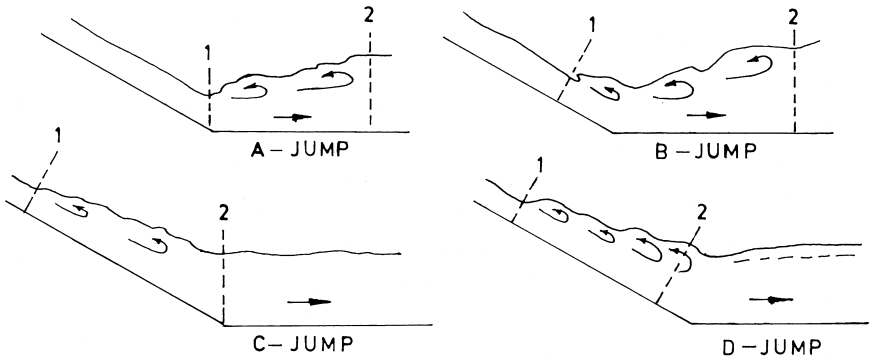

Figure 1 Types of hydraulic jump: 1 Beginning of jump and 2 End of jump.

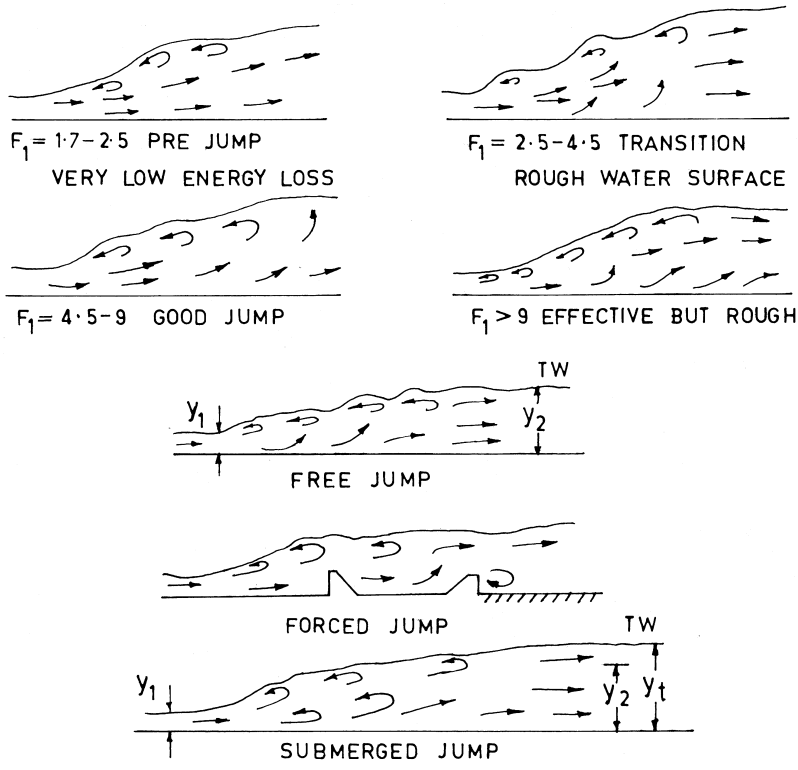

Figure 2 Classification of hydraulic jump.

2. Forced jump: the formation of jump is aided by use of appurtenances such as chute blocks, baffle piers or high end sills. These help reduction in the length of the basin or tail water depths required for an otherwise free jump.
3. Submerged jump: the available tail water depth y_t is greater than the conjugate depth y_2.

These are also shown in Figure 2.

Yet another category of classification that can be made is based on the form of channel in which the jump occurs: channels of rectangular, circular, trapezoidal, parabolic, or triangular cross-sections. Characteristics of jumps have also been investigated in channels of non-prismatic form such as expanding or contracting. Ead and Rajaratnam (2001) have studied characteristics of jumps on corrugated beds.

20.2.2 Length of the Jump

The length of the jump is rather difficult to measure or determine precisely. Various propositions have been forwarded such as:

- L_j: measured from the toe or front of the jump up to the section of the maximum depth.
- L_r: length of surface roller ending at the surface stagnation point and indicating the limit between the backward and forward flow.
- L_e: ending at a section where no bottom erosion appears and bottom shear forces have greatly reduced.

A number of formulae (about 40) have been suggested defining L_j in terms of y_2 or y_1, ranging from 5 to 6 y_2 or 35 to 60 y_1. Based on experiments conducted at USBR and other research laboratories, Peterka (1978) has presented a graph relating the length L_j to F_1, which can be summarized as

Range of F_1	L_j
2.5–4.5	5–6
5–14	6–6.1
14–20	6–5.5

Based on experiments in a flume model, Hager et al. (1990) proposed following relations for the length of the roller L_r

$$\frac{L_r}{y_1} = -12 + 160 \tanh (F_1 / 20) \text{ for } \frac{Y_1}{b} < 0.10 \quad (1)$$

$$\frac{L_r}{y_1} = -12 + 100 \tanh (F_1 / 12.5) \text{ for } 0.10 < \frac{Y_1}{b} < 0.7 \quad (2)$$

where

F_1 = Pre-jump Froude number
y_1 = Pre-jump depth of flow
b = Width of the channel

20.2.3 Conjugate Depth and Energy Loss

The flow depths y_1 and y_2 at the extremities of a classical hydraulic jump are conventionally related by the classical Belanger's equation based on force-momentum balance in a rectangular channel, which neglects bottom shear forces.

$$y_2 / y_1 = \frac{1}{2}\left[\sqrt{1 + 8F_1^2} - 1\right] \quad (3)$$

Hager et al. (1989) conducted a series of experiments to correlate parameters representing bottom shear forces to propose the following equations

$$(y_2 / y_1)_s = Y_o\left[1 - 3.25\left(\frac{y_1}{b}\right).\exp(F_1 / 7).\log(R_1)^{-3}\right] \quad (4)$$

$$\text{Where } Y_o = \left(\frac{y_2}{y_1}\right)_o\left[1 - 0.7(\log R_1)^{-2.5}.\exp(F_1 / 8)\right] \quad (5)$$

Where $\left(\frac{y_2}{y_1}\right)_s$ = conjugate depth ratio accounting for shear force

$\left(\frac{y_2}{y_1}\right)_o$ = conjugate depth ratio without accounting shear force, i.e. Equation 3.

where R_1 = Inflow Reynolds number = $Q/b\,\nu$
Q = Discharge
ν = Kinematic viscosity of water

It was found that provided $F_1 < 10$ and $\left(\frac{y_1}{b}\right) < 0.1$, variation between conjugate depths calculated by Equations 3 and 5 were insignificant when the discharge per unit width was larger than 0.1 cumec/m.

Zirong et al. (1987) incorporated the coefficient C_f to estimate the shear force F_s as $F_s = 0.5\, C_f\, \rho\, g\, (y_2 - y_1)^2$ in the momentum equation to obtain the relationship

$$y_2 / y_1 = \frac{1}{2}\left[\sqrt{0.72 + 7.4F_1^2} - 0.85\right] \quad (6)$$

It was shown that the difference in the magnitudes of (y_2/y_1) obtained by using Equations 3 and 6 was about 4% for $F_1 = 9$ and for lower values of F_1, the difference was still smaller.

Peterka (1978) analyzed the measurements of energy loss in hydraulic jumps at USBR laboratory and developed a graph showing the loss of energy E_l/E_1 with reference to pre-jump F_1. The results are summarized in Paragraph 20.2.2.

As for the similar relationships in respect of B, C, and D jumps, notable contributions have been made by Bakhmeteff et al. (1936), Bradely et al. (1957), Kindsvater (1944), Rajaratnam et al. (1974), Kawagashi et al. (1990), Hager (1988), Ohtsu et al. (1991), Husain et al. (1994), and Negm (1996). The experimental results of Peterka (USBR Engineering Monograph No.25) have been extensively used for designing hydraulic jump stilling basin on sloping floors. Ohtsu's results are a composite of theory, experiment, and dimensional analysis for B and D jumps and are summarized below:

B Jumps

$0° < \theta < 19°$ $19° < \theta < 60°$

$$\frac{L_j}{y_2} = 5.75 \tan\theta + 5.70 \qquad \frac{L_j}{y_2} = 4.6\,(y_1 / y_2 - 1) + 5.7$$

$(4 \le F_1 \le 14)$ $(4 \le F_1 \le 14)$

$$\frac{l / y_2}{\left[2.3 / (\tan\theta)^{0.73} - 0.8\right]} = \left(\frac{y_1}{y_2} - 1\right)^{0.75}$$

$6 \le F_1 \le 14$

$1.1 \le (y_1 / y_2) \le 3.0$

D Jumps

$0° < \theta < 19°$ $19° < \theta$

$$\frac{L_j}{y_2} = 5.75 \tan\theta + 5.70$$ Formation of jump is not recognized

$$\frac{y_t}{y_1} = (0.077\,\theta^{1.27} + 1.41)(F_1 - 1) + 1$$

$\theta\ in\ \mathrm{deg}\,rees, \quad 4 \le F_1 \le 1.4$

Ead and Rajaratnam (2002) studied the characteristics of hydraulic jump on corrugated bed defined by constant wavelength and wave amplitude. Their studies covered Froude numbers ranging from 4 to 10 and three values of relative roughness t/y_i from 0.25 to 0.50, where t is the amplitude of wave in corrugation. It was found that the ratio y_2/y_1 was noticeably smaller than on the jump over smooth bed. The dimensionless depth deficit factor D, defined as $(y_2\text{-}y_{2c})/y_2$ was fairly constant and equal to 0.25, where y_{2c} is the conjugate depth on corrugated bed. This implies that the conjugate depth on corrugated bed would be around 75% of the depth on a smooth bed. The length of the jump on the corrugated bed was about half as long as on smooth bed and the integrated shear stress was about 10 times that for a smooth bed.

20.2.4 Turbulence Characteristics of Hydraulic Jump

The study of turbulence structure of hydraulic jump is important in understanding the origin and mechanism of damaging forces such as uplift, vibration, cavitation, and other forms of hydrodynamic loading. Till recently, the research on this topic was predominantly experimental, starting perhaps with the classical work

of Rouse et al. (1959) followed by Schroder, Rajaratnam, Hinze and many others. Until recently, the studies have been confined to the level horizontal floor.

The most commonly used parameters for expressing turbulence are the fluctuations of velocity, pressure and force.

Fluctuations of Velocity

Khatsuria (1994) has described results of measurements carried out on a hydraulic model of a high head spillway using temperature compensated hot film anemometer. Figure 3 shows variation of maximum fluctuation of velocity U'_{max} normalized with respect to the time averaged mean velocity $\bar{U}$. The maximum fluctuations are 2.5 to 5 times the mean velocity in the jump at sections 1, 2, and 3, as compared to the plain open channel flow, at a section about 20 y_2 from the front of the jump, where it was 1.75 to 2 times the mean velocity. The variation of the kinetic energy of turbulence shows that the corresponding magnitudes in the case of hydraulic jump range from 10 to 100 times larger than those of plain open channel flow.

Zirong et al. (1987) indicated that intensity of turbulence, expressed as $U_{rms}/\bar{U}$, was decaying to a near constant value of about 10% at a distance of about 18 to 20 (y_2 -y_1) downstream of the front of the jump. They also found that instantaneous maximum velocity at bottom U'_b

$$U'_b = \bar{U} + 3.2\sqrt{\sigma} \tag{7}$$

Where σ = standard deviation of fluctuating components. Also, the bottom instantaneous maximum energy of turbulence h_{ib} was

$$h_{ib} = C_i U^{-2} / 2g \tag{8}$$

Where C_i = a coefficient varying from 1.7 to 4.5 at the end of the jump for F_1 varying from 2.35 to 6.20.

These results explain as to how the natural bed is protected against scour by lifting up the flow with the end sills of the stilling basins.

Pressure Fluctuations

The hydraulic jump in the stilling basin can be considered macroscopically as a time-averaged steady, abruptly varied flow characterized by a free surface discontinuity and the formation of strong vortex that generates macro turbulent fluctuations, air entrainment, and energy dissipation. The fluctuating pressures may cause vibration, uplift, excessive hydrodynamic load, and intermittent cavitation.

Because of highly random nature of fluctuations, the analysis is based predominantly on statistical methods. A brief review of the parameters involved in the analysis is presented here. Figure 4 shows a typical time series record of pressure fluctuation phenomenon.

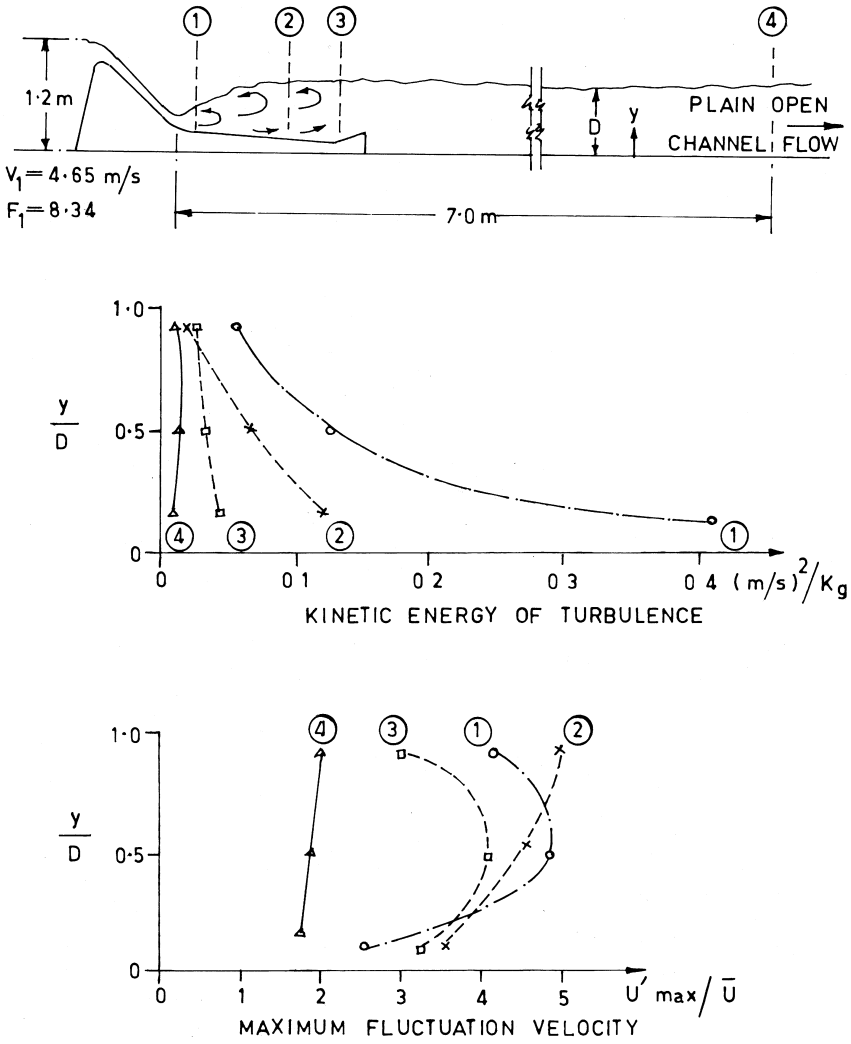

Figure 3 Turbulence characteristics of hydraulic jump. ① to ④: locations of measurement. (Khatsuria, 1994)

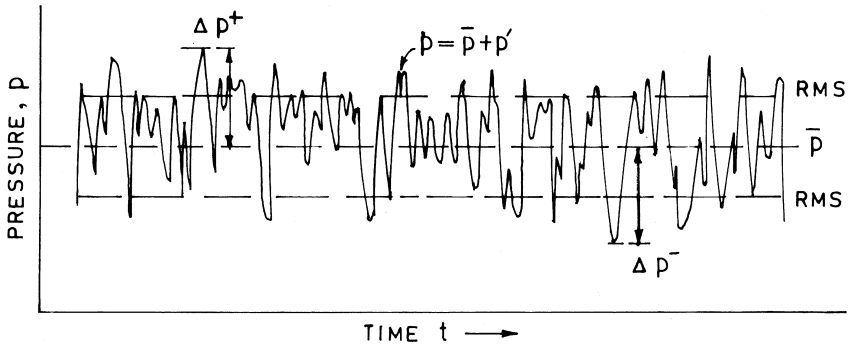

Figure 4 Typical time series record of pressure fluctuations.

The relevant parameters are:

Total pressure at a given instant: p

Time averaged mean pressure $\bar{P} = \frac{1}{T}\int_o^T p\,dt.$

Fluctuating component $p' = p - \bar{P}$

RMS of fluctuation $= \sqrt{\overline{(p')^2}} = \frac{1}{T}\int_o^T (p')^2\,dt.$

There are three types of dimensionless pressure coefficients:

1. Based on RMS pressure fluctuations.

   $C'_p = \sqrt{\overline{(p')^2}} \,/\, \frac{1}{2}PV_1^2$ *or* $\sqrt{\overline{(p')^2}} \,/\, \frac{V_1^2}{2g}$

   Where the pressure may be expressed in Pa or height of water column and V_1 is the reference velocity.

2. Based on pressure deviation from mean pressure.

   $C_p^+ = \Delta\, p^+ \,/\, \frac{V_1^2}{2g}$ Δp^+ and Δp^- are the maximum positive and negative pressure deviation from the mean pressure.

   $C_p^- = \Delta\, p^- \,/\, \frac{V_1^2}{2g}$

3. Pressure coefficient corresponding to the mean pressure.

   $\bar{C}_p = \bar{P} \,/\, \frac{V_1^2}{2g}$

Numerous investigators have conducted general studies of pressure fluctuations under free and submerged hydraulic jumps on a level horizontal floor. The fluctuating pressures were characterized as the maximum pressure differential as a function of kinetic head entering the dissipation structure regardless of Froude number. One of the first studies on the extent of turbulent fluctuations was carried out by Bowers and Tsai (1969). Related work was also published by Vasiliev and Bukreyev (1967) concerning the statistical characteristics of pressures in the region of hydraulic jump. Abdul Khader and Elango (1974) provided statistical data on pressure measurements for hydraulic jumps with Froude numbers 3 to 6. Results in respect of turbulence characteristics of hydraulic jump can be found in the papers of Locher (1971), Suzuki (1973), Narasimhan and Bhargava (1976), Bribiesca et. al. (1979), Akbari et. al. (1982), Lopardo et. al. (1982), Spoljaric et al. (1982), Tullis and Rahmeyer (1982), Lopardo and Henning (1985), Gaikwad et. al. (1987), Toso and Bowers (1988), Fiorotto and Rinaldo (1992 a & b), and Khatsuria et al. (1992).

Results of some of the above studies for free and submerged hydraulic jumps are shown in Figure 5 to Figure 7. The following general conclusions had been derived:

- Magnitude of C'_p depended on whether the flow was fully developed or the flow had a thin boundary layer.
- The maximum value of C'_p reached about 0.07 for fully developed flow and 0.08 for undeveloped flow and occurred at about 0.20 L_r or 10 to 15 times y_1 sharply decreasing thereafter.
- Decrease in the magnitude of C'_p was more conspicuous and rapid for free hydraulic jump in comparison to submerged jump.
- Correlation in the longitudinal direction was shorter (of the order of 2 to 4 y_1) than in the transverse direction (of the order of 8 to 10 y_1).
- Dominant frequency of pressure fluctuations ranged from 2 to 5 Hz.
- Cp^+ and Cp^- were of the order of 10 to 20 times the RMS value C'_p.
- With the toe of the jump located upstream from the base of the inclined chute, the maximum values of Cp^+ and Cp^- were found to be substantially larger than those with the toe of the jump at the base of the chute.
- Addition of chute blocks, baffle piers, and end sill did not change the extreme values significantly.
- Areal extent of extreme pressure pulses in the longitudinal and transverse directions were of the order of 8 y_1 and 13 y_1, respectively.
- Magnitude of fluctuating pressure depressions in the initial region of hydraulic jump ($P'_{0.1}$), reaching the value of vapor pressure had 0.1% probability of occurrence.

These results can be applied to assess cavitation tendency.

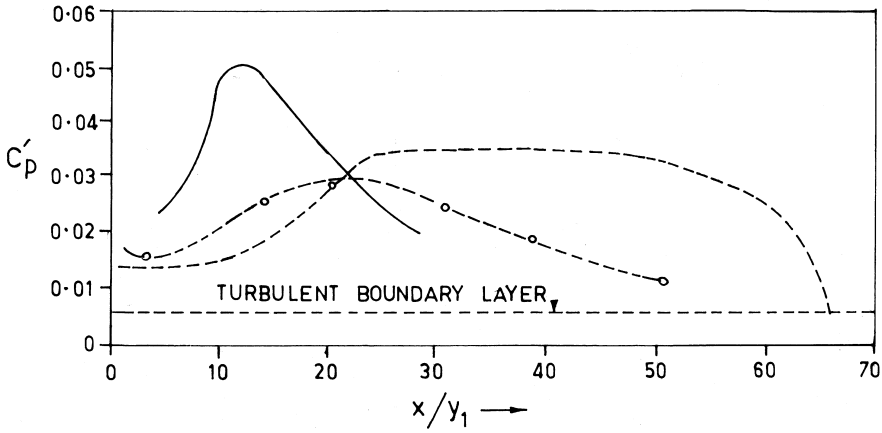

Figure 5 Pressure fluctuations beneath hydraulic jump (shown in Narasimhan et al. 1976).

Legend	F_1	Type of jump	(y_t/y_1)
—	4–5	Free	—
°	5	Submerged	9.1
--	5	Submerged	12.3

Recently, the studies on pressure fluctuations have been extended to cover the effect of a negative step at or near the front of the jump, vide Armenio et al. (2000). They have defined the configuration of jump combined with a negative step into three categories: A-jump, B-jump, and W-jump, as shown in Figure 8. It was indicated that in the case of B-jump, maximum pressure fluctuations were larger than in the classical jump. The magnitude of Cp reaches values even higher than unity, and the probability density and the probability density function was not Gaussian. With W-jump, the pressure fluctuations were smaller than in the classical jump, the magnitude of Cp being confined within 20% of the values corresponding to the classical jump and the probability density function was reasonably Gaussian.

Fluctuating Forces

Assessment of hydrodynamic loads on elements of hydraulic jump stilling basins, based on analysis of fluctuating pressures, involves simultaneous measurements at several locations and computational efforts. As such, many investigators pre-

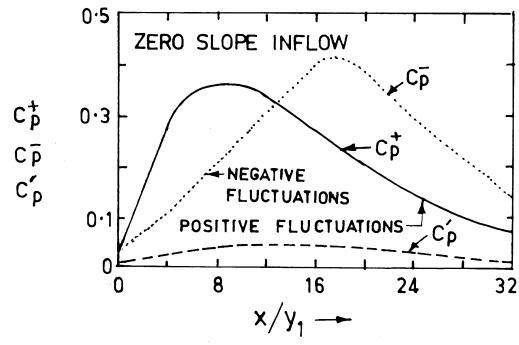

A – ENVELOPE OF MAXIMUM PRESSURE DEVIATION FROM MEAN; ZERO SLOPE, F= 5·7; 10 MIN RUN, DEVELOPED FLOW

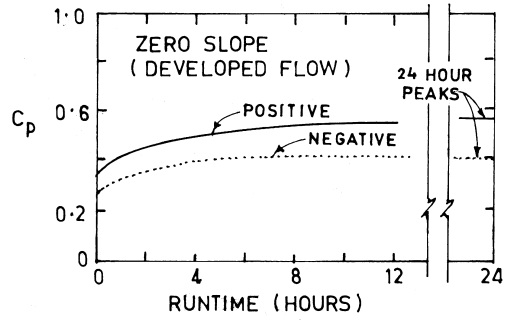

B EFFECT OF RUN TIME ON PEAK DEVIATION FROM MEAN: AVERAGE MAXIMUM PRESSURE FLUCTUATION VERSUS RUN TIME (F=5·7· V_1=11 86 tps; X/Y_1=11)

Figure 6 Extreme pressure fluctuations (shown in Toso et al.1988).

ferred to measure directly the fluctuating forces with the help of suitable force transducers. Notables among these are

1. Uplift forces on stilling basin: Spoljaric (1982), Hajdin (1982), Farhoudi et al. (1991), Bellin and Fiorotto (1995), and Fiorotto et al. (2000).
2. Pullout forces on anchored walls: Khatsuria et al. (1992).
3. Forces on baffle piers, sills, etc.: Basco (1970), Basco et al. (1971), Pennino et al. (1977), Gomasta et al. (1977), Narayanan et al. (1980 a & b), Ranga Raju et al. (1980), Cassidy et al. (1994), and Nakato (2000).
4. Bending moments on divide walls: Gaikwad et al. (1987) and Khatsuria et al. (1989), (1994), (1995).

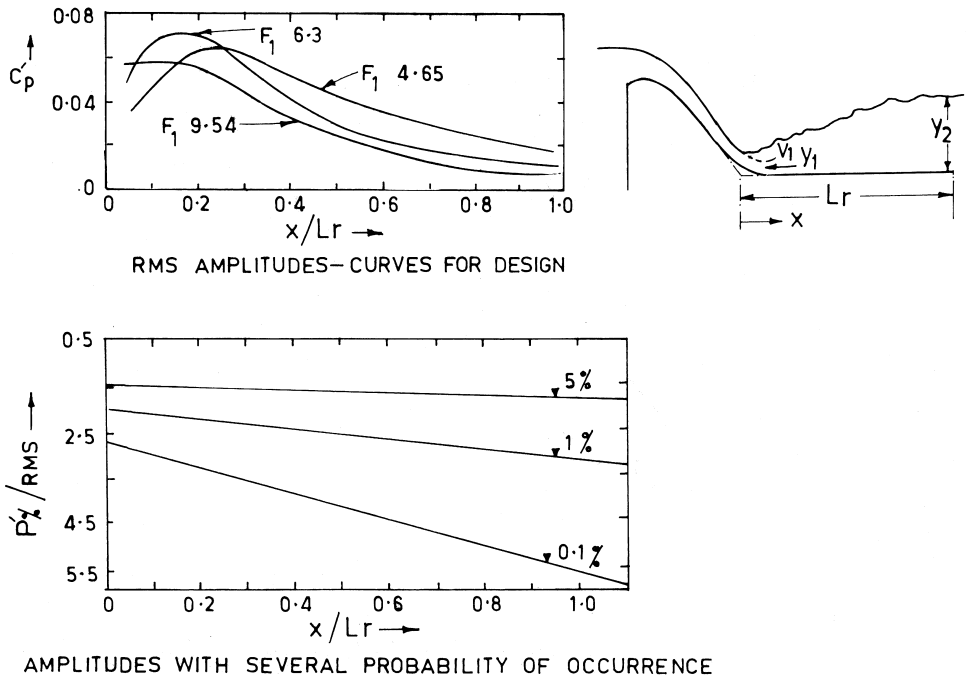

Figure 7 Pressure fluctuations beneath hydraulic jump (shown inLopardo et al. 1985).

$$C_p' = \frac{\sqrt{\overline{p'^2}}}{\gamma} \Big/ \frac{V_1^2}{2g}, \quad \overline{C_p} = \frac{2}{F_1^2} + \frac{x/L_r}{F_1^2}\left(\sqrt{1+8F_1^2} - 3\right)$$

$$\overline{p} = \overline{C_p}(V_1^2/2g)$$

It may be mentioned that in some cases, assessment of the forces were attempted by both the approaches, namely pressure as well as force measurements and the results were in good agreement.

20.2.5 Air Entrainment by Hydraulic Jump

Large quantities of air are entrained at the front of the jump into the free shear layer, characterized by intensive turbulence production and large vortices with horizontal axis perpendicular to the flow direction. The quantity of air entrained, i.e. the parameter Qair / Qw, is relevant in estimating the bulking of the flow and determining the free board requirement of sidewalls in a stilling basin. The other parameter concerning air concentration across the depth of flow or particu-

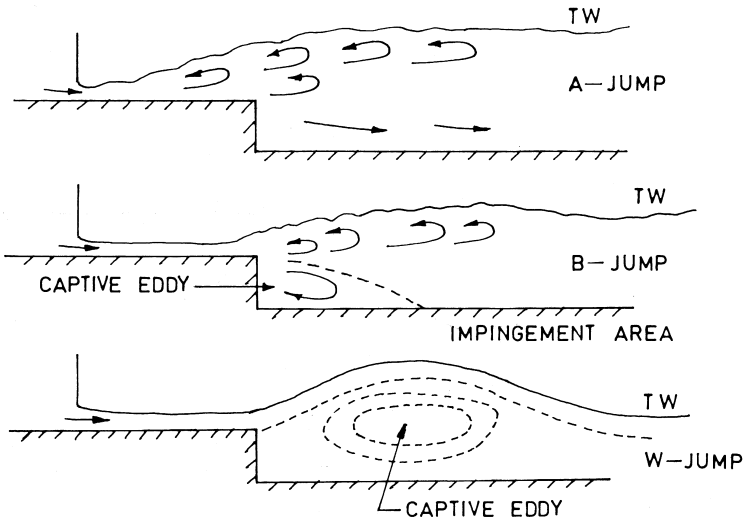

Figure 8 Hydraulic jump on a negative step (shown in Armenio et al. 2000).

larly the air concentration in the bottom layers C_b is relevant to the mitigation of cavitation damage to the basin floor and appurtenances like chute blocks and baffle piers, against fluctuating pressure depressions.

Dimensional analysis suggests that the quantity of air entrained can be expressed as

$$\frac{Qair}{Qw} = K_1 \frac{(V_1 - V_e)^2}{g \quad y_1} \tag{9}$$

where

Qair = Quantity of air entrained
Qw = Water discharge
K_1 = Constant
V_1 = Upstream flow velocity
y_1 = Upstream flow depth
V_e = Onset velocity of air entrainment for hydraulic jump

The parameter on the right side of Equation 9 is a form of Froude number. The equation implies that air entrainment should increase with increase in the Froude number.

A number of investigators, starting with Kalinske and Robertson (1943) have studied the phenomenon of air entrainment by hydraulic jump and evolved

relationships of the general form $\beta = a(F_1 - 1)^b$, where the factors a and b differ only marginally among the various relationships.

One of the first studies on air concentration distribution was conducted by Rajaratnam (1960) and (1962) for F_1 in the range 2.4 – 8.7. The characteristics studied by him were:

Air entrainment function β
Maximum air concentration
Aerated length of the hydraulic jump, and
Air concentration distribution in a vertical section

The air entrainment function

$$\beta = \frac{q_a}{q_w} = 0.018(F_1 - 1)^{1.245} \tag{10}$$

is valid in the range $2.5 < F_1 < 9$, where $F_1 = V_1/(g\ y_1)^{0.5}$

The maximum air concentration is

$$\overline{C}_{max}\ (\%) = 2.55\ (F_1 - 1.5) \tag{11}$$

The aeration length of the jump can be estimated as

$$\frac{L_a}{y_2} = 3.5\sqrt{F_1 - 1.5} \tag{12}$$

In general, $L_a > L_r$

The analysis of his results in respect of air concentration close to bed C_b is shown in Figure 9, which shows that jumps with Froude number higher than 6 or so entrain large quantity of air with high concentration close to the bed and that the concentration drops rapidly downstream from the front of the jump.

The process of aeration and air bubble redistribution depends upon the inflow conditions: partially developed jump, fully developed jump, and pre-entrained jump. Generally, for hydraulic jumps with fully developed inflow conditions, the quantity of air entrained is comparatively larger than with the partially developed jumps. However, the partially developed jumps exhibit larger concentration of air in the bottom layers. With the pre-entrained jumps also, the distribution appears to be distributed more uniformly over the depth than with fully developed jumps. For detailed discussion on this topic, reference may be made to Resch and Leutheusser (1972), Thandaveswara (1974), Chanson and Brattberg (2000), and Chanson and Toombes (2001).

20.3 HYDRAULIC JUMP STILLING BASINS

20.3.1 Basins with Horizontal Aprons

The most widely used standard designs of stilling basins with horizontal aprons have been evolved by USBR. The designs can be classified accordingly:

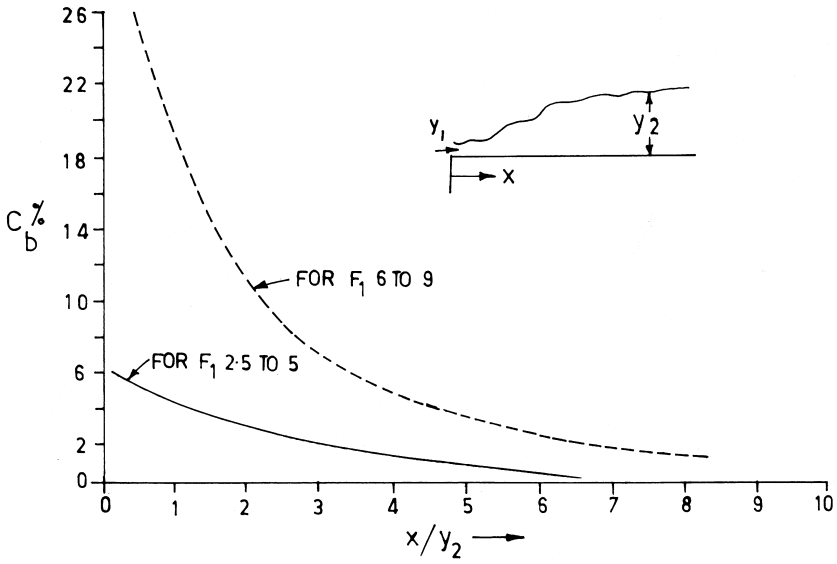

Figure 9 Air concentration close to bed in a hydraulic jump. (Analyzed from Rajaratnam, 1960)

I. According to the velocity of the flow entering the stilling basin.
   A. Velocity up to about 15 m/s, for which appurtenances like baffle piers can be used.
   B. Velocity higher than 15 m/s, where such appurtenances are not recommended from apprehension of cavitation.

II. According to the Froude number of the flow entering the stilling basin.
   A. Low Froude number 2.5-4.5.
   B. High Froude number, i.e. above 5.

In all the designs involving horizontal aprons, it is recommended to place the basin floor at a depth corresponding to y_2 below the available tail water elevation. Sometimes this may result in a basin deeply placed below the average river bed and may also involve excessive rock excavation. There may then be a temptation to provide the basin invert at a higher elevation resulting in deficiency of tail water depth, with an attempt to compensate the same by inclusion of chute blocks and baffle piers and increase in the apron length. Peterka (1978) has specified that there is no simple remedy for a deficiency in tail water depth and that measures like chute blocks, baffle piers, or increased apron length are only partly successful in substituting for the tail water depth. Similarly, a shorter than the required apron length cannot be compensated by an extra tail water depth.

Basin II (Fig. 10) can be used for Froude number greater than about 5, heads up to 60 m and discharge intensity up to 46 cumec/m without recourse to a model study. For higher heads and discharges, model study has been recommended. Similarly, Basin III (Fig. 10) can be used safely for velocity entering the basin up to about 18 m/s and discharge intensity up to about 19 cumec/m without recourse to model study. Inclusion of baffle piers permits a reduction of apron length by about 1.5 y_2 and prevents sweep-out of hydraulic jump until the tail water depth of 0.85 y_2. However, for higher velocities, model studies are required to determine the location of the baffle piers so that their efficiency in reducing the apron length is preserved yet ensuring that pressures at critical locations are still safe from consideration of cavitation. Harkauli (1979) has reported the case of Ramganga dam spillway, India, where the velocity of flow entering the stilling basin worked out to about 42 m/s, which according to USBR design practice, did not permit the use of baffle piers. However, while conducting the hydraulic model studies, it was revealed that the velocity of flow at the location of baffle piers—at approximately 2.48 y_2 form the toe of the apron—was less than 15 m/s. This spillway has been operating for many years and no damage to baffle piers has been reported. The relative efficiency of this arrangement in comparison to the standard design with baffle piers or a design without baffle piers is, however, not indicated.

USACE (1990) suggest a slightly different version of Basin III for application for low Froude number (2.5–4.5) as well as for the higher range up to $F_1 = 9$. The baffle piers are suggested to be located from the toe of the spillway at 1.5 y_2 for $F_1 < 4.6$ and 2 y_2 for $F_1 = 9$; this distance to be interpolated linearly between $F_1 = 4.6$ and 9. Similarly, height of baffle piers is 1.0 y_1 for $F_1 < 4.6$ and 1.6 y_1 (or $y_2/6$) for $F_1 = 9$, interpolated in the same manner.

Baffle piers of special shapes to avoid cavitation damage have been evolved. This aspect has been discussed in more detail in Chapter 26.

Special designs have been evolved for F_1 in the range of 2.5-4.5 where the efficiency of hydraulic jump in dissipating energy is less and the high velocity jet entering the basin is oscillating, generating a wave in the downstream which is difficult to dampen. For such a condition, USBR has proposed a stilling Basin IV incorporating large chute blocks, apron length corresponding to the natural length of the jump, i.e. about 6 y_2, and a triangular solid end sill as per Basin III. (Fig. 10) It has been recommended that the basin invert be placed at a depth corresponding to 1.1 y_2 below the tail water.

USACE (1990) basin for application in the range $2.5 < F_1 < 4.5$ has a configuration similar to the USBR Basin III, but the location of the baffle piers at a distance of 0.75 y_2 from the toe and height of chute blocks, baffle piers, and end sill as 1 y_1.

An alternative design called SAF (Saint Anthony Falls) stilling basin was developed by Blaisdell (1948) covering the range of Froude numbers 2–17 for

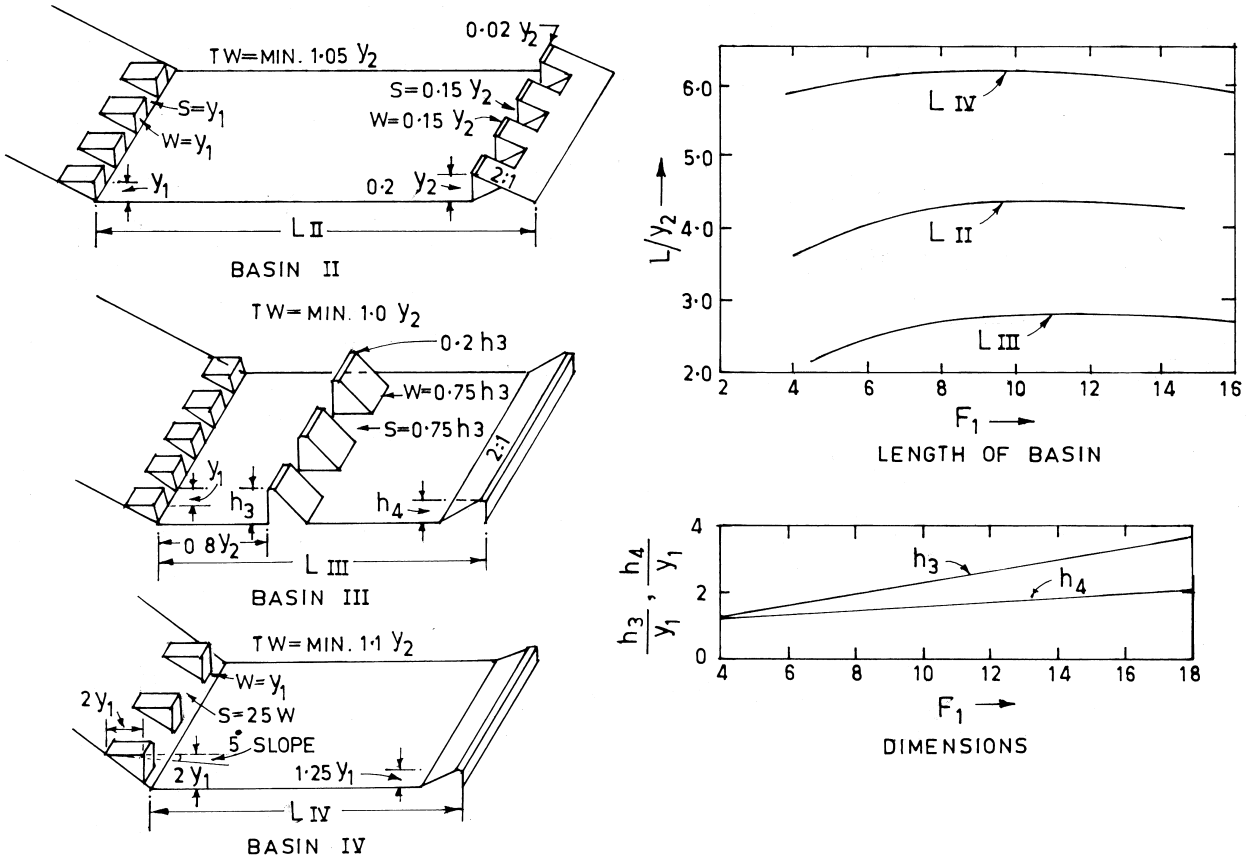

Figure 10 USBR stilling Basins II, III, and IV.

small structures in canals and diversion works involving smaller discharges and heads. This is similar to USBR Basin III with a much shorter length ($L = 2\ y_2$) of the apron. This length is considered to be so short that a significant amount of energy dissipation must occur downstream from the end sill. As a result, some scour in the downstream has to be accepted. Rice et al. (1993) have presented the following relationships to determine the minimum size and length of riprap to be placed in the downstream to ensure basin integrity against undermining. The design is shown in Figure 11

$$\frac{L_s}{y_1} = 4.5\ F_1 \tag{13}$$

$$\frac{D_{50}}{y_1} > \left[\frac{F_1 + 2.2}{10.2}\right]^2 \tag{14}$$

For protection laid at basin floor elevation.

$$\frac{D_{50}}{y_1} > \left[\frac{F_1 + 4.0}{10.2}\right]^{3.33} \tag{15}$$

For protection laid at end sill elevation.

A number of designs have been proposed for the low Froude number (2.5–4.5) applications. Sharma et al. (1973) have presented design procedures

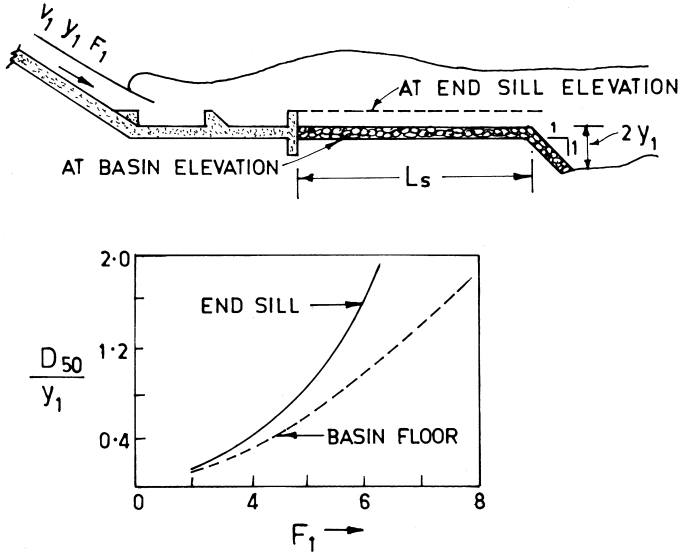

Figure 11 Riprap protection for SAF stilling basin (shown in Rice et al. 1993).

for a stilling basin consisting of a row of baffle piers and a dentated end sill with apron length varying from 5 to 6 y_2 as shown in Figure 12. The design is based on studies on a large number of low head structures such as weirs, barrages, and canal falls at UPIRI, Roorkee. Various parameters such as height and location of the baffle pier, length of the apron, and height of the end sill have been optimized from a series of experiments.

$$\frac{h_3}{y_1}.\frac{y_2}{y_t} = 0.7\,(F_1 - 1)^{0.65} \tag{16}$$

$$\frac{X}{y_1}.\frac{y_2}{y_t} = 2\,(F_1 - 1)^{0.75} \tag{17}$$

$$\frac{h_3 + h_4}{y_1} = 1.15\left[F_1^{0.25}.\left(\frac{y_t}{y_2}\right)^{0.5}\right]^{0.32} \tag{18}$$

Bhowmik (1975) evolved a design termed basin L consisting of an apron of length varying from 4.5 to 3.5 y_2, special shapes of baffle piers and a triangular end sill, as shown in Figure 13.

Another USBR design developed by George (1978) is similar to Basin III with slight variation in the location of baffle piers, inclusion of dentated end sill and an extended apron downstream of the end sill as shown in Figure 14

Pillai et. al. (1989) have proposed a design similar to Basin III with the exception that the standard baffle piers have been replaced by wedge-shaped

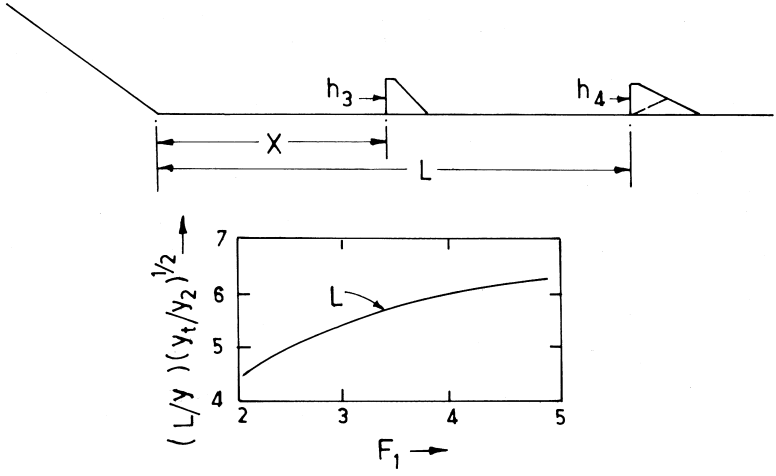

Figure 12 Low Froude number stilling basin (shown in Sharma 1973).

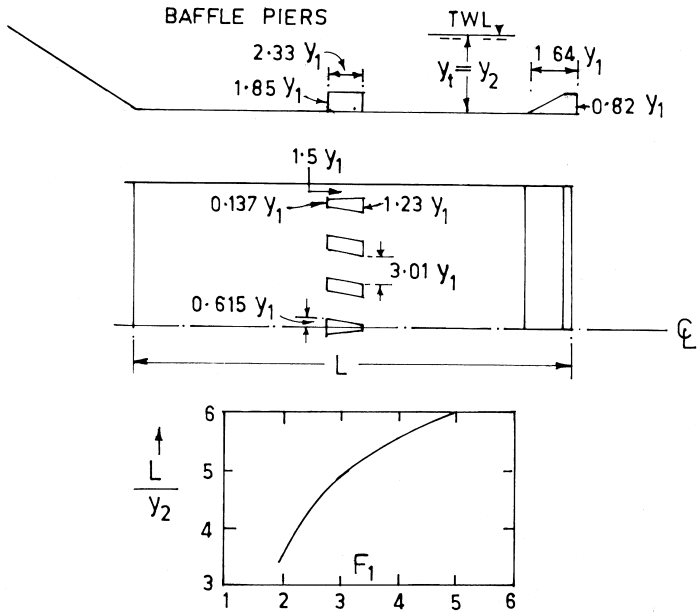

Figure 13 Low Froude number stilling basin (shown in Bhowmik 1975).

baffle piers of vertex angle 150° and cut back at 90° on the sides. The peculiar shape has been evolved to offer greater resistance to the flow and avoid reattachment of the separated eddy on the sides, to prevent cavitation. The pertinent details are shown in Figure 9, Chapter 26.

In all the above designs, baffle piers of different shapes have been relied upon for significant dissipation of energy. However, there are no guidelines available in respect of upper limit of velocity or other condition leading to cavitation, except for Basin III. It is therefore necessary to conduct specific model study for assessing cavitation potential of a particular design, whenever velocity entering the basin V_1 exceeds about 18 m/s. Khatsuria et al. (2000) describe a model study for a spillway where V_1 was of the order of 22 m/s. Measurement of hydrodynamic pressure fluctuations on the chute blocks and baffle piers revealed that they would be largely free of cavitation damage.

Often, a design evolved on the basis of maximum discharge condition results in a basin with excessive tail water depth for lower discharges with submerged hydraulic jumps. Besides being uneconomical, this design results in reduced efficiency for small discharges. Could then, a design be evolved which ensures a jump height curve matching the available tail water curve for most of

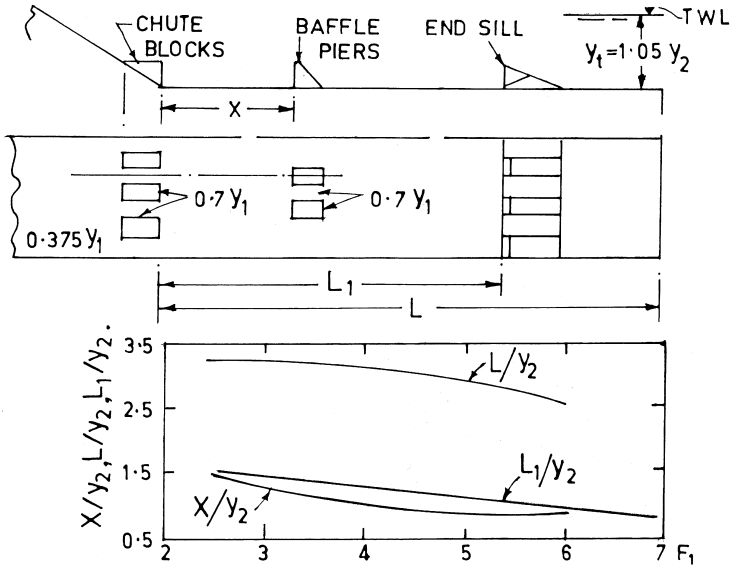

Figure 14 Low Froude number stilling basin (shown in George 1978).

the discharges? Vittal et al. (1992) have presented a procedure for modified Basin III (consisting of two rows of baffle piers) introducing a dimensionless semi-theoretical relationship for forced jump height curve matching the dimensionless tail water curve with certain limitations. The original article may be referred for further details.

In the case of stilling basins for very high head spillways, sometimes foundation conditions such as high ground water table or the cost of excavation, make it impossible to obtain the required tail water depth for an apron near about the riverbed level. Deep seated aprons with stagnant water pools also pose difficulties in dewatering for periodical inspection and maintenance repairs. In such situations, the provision of two-stage energy dissipators or double basins could be advantageous. Such designs rely upon creation of the required tail water depth for the principal basin with a higher apron elevation by an end sill in the form of a weir or subsidiary dam, which in turn will have a secondary energy dissipator at or near the riverbed. Such designs are highly site-specific and no general guidelines are available. Model studies have to be conducted in each case for evolving the best possible arrangement. Notable examples are:

Mangla dam, Pakistan: two hydraulic jump stilling basin.
Sidi Saad, Algeria: two flip buckets.

Ranjitsagar, India): principal basin a hydraulic jump stilling basin followed by a subsidiary dam with a solid roller bucket.
Tehri dam, India: two hydraulic jump stilling basins.

20.3.2 Basins with Sloping Aprons

When the available tail water depth is larger than the conjugate depth of the jump y_2, a sloping apron is one of the alternatives for energy dissipation. However, the decision to adopt a sloping apron should be based on site conditions that would permit construction of a purely sloping or sloping-cum-horizontal apron, requiring minimum amount of excavation and concrete, for the maximum discharge condition. For this condition, the jump should form at the upstream end of the slope and preferably be contained within the length of the apron to be provided. The procedure for designing the sloping apron has not been standardized, as in the case of horizontal aprons, and hence a greater individual judgment is required. The guidelines generally adopted in the design have been summarized as follows:

- The slope itself has little effect on the performance of the basin and as such, it should be based on the site conditions as discussed earlier.
- The theoretical length of the jump for the maximum discharge is obtained from the relevant design chart or relationship. The position of the jump to be confined on the apron is a decision for the designer. Analysis of the existing structures in operation over the years shows that the length of the apron ranges from 39–83% of the length of the jump, the average being about 60%. The apron may be lengthened or shortened, depending on the quality of the rock in the riverbed and other site conditions.
- The jump height and other characteristics are then checked for intermediate and lower discharges. It is not necessary that the front of the jump form at the upstream end of the slope for these discharges, provided that tail water depth and length of basin available for energy dissipation are adequate. If the tail water depth be insufficient for intermediate discharges, it may be necessary to increase the depth by increasing the slope or reverting to a horizontal apron.
- In the case of sloping-cum-horizontal aprons, i.e. B jumps, the proportion of the length of horizontal portion to the length of the sloping portion or the total length is also designer's choice with due consideration to site conditions. Generally, the length of the horizontal portion is shorter than that of the sloping portion.

D Jump Aprons (Figure 1)

The first step in the design of sloping aprons, i.e. D jump aprons, is to tentatively decide a profile including slope and length. Then y_1, V_1 and F_1 for the design

maximum discharge are calculated at the upstream end of the slope assuming a horizontal apron extending at that elevation. The length L_j and the required tail water depth y_t are determined, either referring to (Peterka 1978) or Ohtsu's equations (paragraph 20.2.3.):

$$\frac{L_j}{y_2} = 5.75 \tan\theta + 5.7 \tag{19}$$

$$\frac{y_t}{y_1} = (0.077\,\theta^{1.27} + 1.41)\,[F_1 - 1] + 1 \tag{20}$$

$4 < F_1 < 14$ and θ in degrees.

With the assumed configuration and length, y_t is compared with the available tail water depth at the end of the apron. Several trials may be required before the slope and location of the apron are compatible with the hydraulic requirement. It may be necessary to raise or lower the apron, or change the original slope entirely. With the apron designed for the design maximum discharge, it is checked for the intermediate discharges. If the tail water depth is adequate or in excess of the jump height for these discharges, the design is acceptable. If the tail water is deficient, it may be necessary to try a different slope or reposition the sloping portion of the apron. It is not necessary that the front of the jump form at the upstream end of the slope for intermediate discharges. The front of the jump may move upstream or downstream from the point, provided the tail water depth and length of apron are considered adequate for these flows. A final design is thus evolved which satisfies the requirements for all the discharges.

B Jump Aprons (Figure 1)

A tentative configuration is the starting point. The length L_j can be calculated using Equation 19 for the D jump, at least up to a slope of about 0.25, i.e. $\theta \leq 14°$. *For* $14° < \theta < 19°$, the error may be negligible. In some cases, the calculation of length of the jump may not be of particular concern, since the basin may not be designed to confine the entire jump. The conjugate depth is given by

$$\left[\frac{y_t}{y_2} - 1\right]^{0.75} = \frac{\ell / y_2}{\left[\dfrac{2.3}{(\tan\theta)^{0.73}} - 0.8\right]} \tag{21}$$

Where l = length of the sloping portion of the apron and y_t/y_2 can be assessed from Equation 20.

The rest of the procedure is the similar as for D jumps.

These guidelines would be useful in preparing a preliminary design, which would require model study to finalize. Designs of sloping aprons for a number

of spillways have been finalized by USBR (1978) from model studies. It is noteworthy that dimensions in the finalized designs (emphasizing on the riverbed conditions and economy in construction) differed considerably from that in the preliminary designs worked out from the design charts. The lengths of the aprons were 39–83 % of the calculated length and the deepest levels of the aprons were set, not corresponding to the depth TW but higher; the ratio TW/y_2 reduced by as much as 50%–90%.

20.4 OPTIMIZATION OF DESIGNS

As discussed in Paragraph 20.2.4, fluctuating velocities in the jump and in the downstream region play a significant part in dissipation of the energy. The characteristics of fluctuating velocities are influenced by the geometrical and hydraulic parameters of stilling basin such as length of the apron, height of end sill, tail water depth, etc. It would, therefore, be interesting to know if the turbulence characteristic could be related to these parameters to optimize the design of the stilling basin. Studies in this regard are indicative of how the turbulence measurements helped optimizing the length of the stilling basin, height of the end sill, and elevation of the apron floor for a horizontal apron of a high head spillway, with $F_1 = 8$. Figure 15 gives relevant measurements which led to the optimization as $L = 5\ y_2$ and end sill height as $0.25\ y_2$.

20.5 STRUCTURAL DESIGN PROBLEMS

The most serious problem with the hydraulic jump dissipator is more of structural strength rather than hydraulic efficiency. Experience in recent years gives many examples of stilling basins suffering serious damages arising from uplift, vibration, cavitation, abrasion, and hydrodynamic loading. A brief review of the present state of knowledge in each of the aspects has been presented here. The reader is referred to the pertinent articles listed for detailed information.

20.5.1 Uplift

Many instances of damage to the apron lining of hydraulic jump stilling basins of high and medium head spillways have come to the light in recent years. The most frequent type of damage recorded is a complete floor slab being torn up, which may or may not be followed by erosion of the foundation. Lifting up and throwing out of the stilling basin slabs of size 12 m $\times$ 12 m $\times$ 2 m, weighing about 700 tons, at the Netzahuacoyotl dam, Mexico, during a flood which was only 37% of the design maximum magnitude, revealed for the first time the

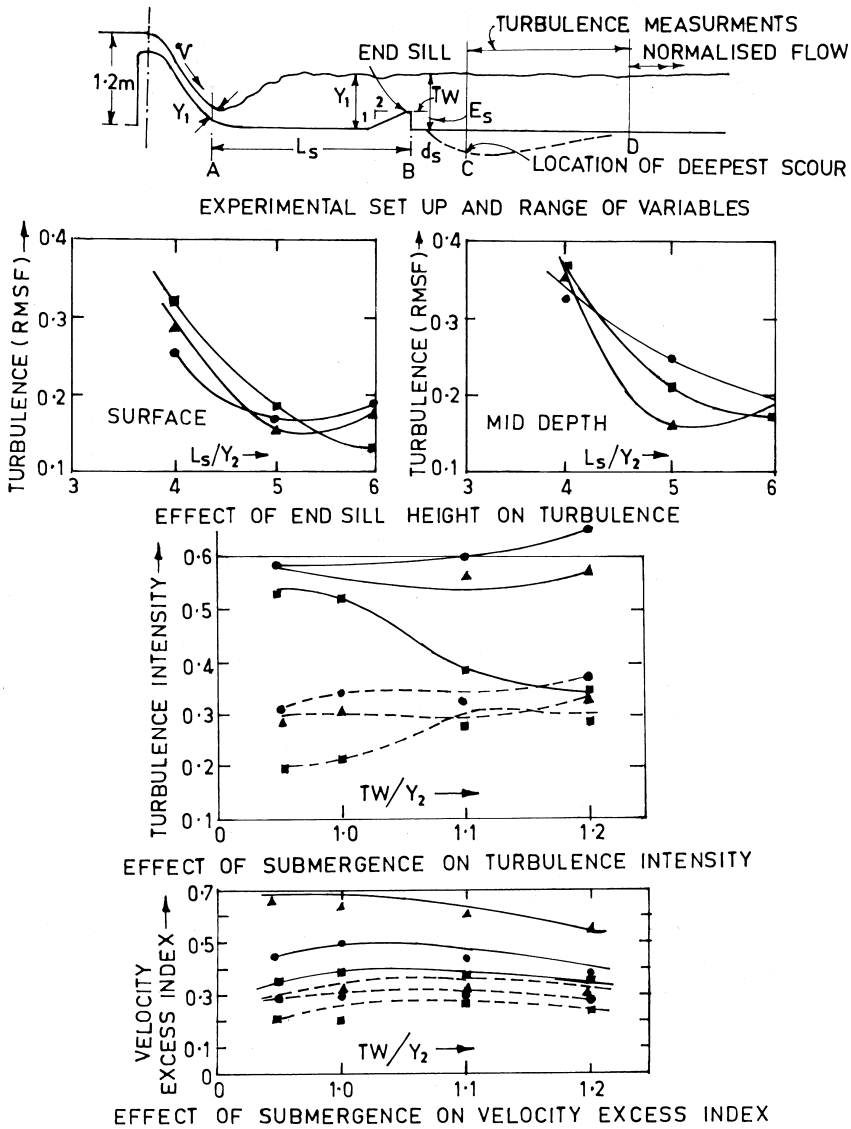

Figure 15 Optimization of stilling basin design for $F_1 = 8$:

▲ $L_s = 4\ y_2$, $E_s = 0.4\ y_2$
■ $L_s = 5\ y_2$, $E_s = 0.25\ y_2$
● $L_s = 6\ y_2$, $E_s = 0.125\ y_2$
———— Measurements at bed
– – – – – Measurements at surface

damage potential of the hydrodynamic uplift caused by the macro turbulent pressure fluctuations.

The spillway chute lining of the Karnafuli H.E. Project, Bangladesh, was damaged by flows, which were about 20% of the design discharge. The spillway, with a total head of about 37 m has a hydraulic jump stilling basin with chute blocks. The spillway chute lining (thickness from 0.5–1.5 m) had an under drainage system consisting of graded sand and gravel and pipe drain of 0.3 m diameter with open joints and discharging through the chute blocks. Bowers et al. (1988) have described the hydraulic model studies conducted at SAF Laboratory, US, to ascertain the causes of damage. The main cause of the damage was found to be the transmission of the fluctuating pressures in the hydraulic jump—occurring at the toe of the spillway—to the underside of the chute slab through the drainpipes. Figure 16 shows schematic of the chute block and drainage system. In the design of the hydraulic jump apron, the jump is assumed to form at the toe of the spillway, with the jump profile as per Curve (1). However, consideration of future retrogression in the tail water levels, factor of safety, etc. adds some allowance, with the result that the jump actually moves upstream of the toe, as shown by the Curve (2). With this, the chute blocks come under the intense turbulence and fluctuating pressures. The model studies indicated that pressure pulses traveled upstream through the drainpipes and open joints right up to the underside of the chute slabs. Simultaneous measurement of fluctuating pressures at the chute blocks and typical locations on the top surface of the spillway chute revealed that high pressure pulses at the chute blocks coincided with low pressures on the chute surface, to cause pressure differentials that were large enough to lift the slab and damage it. A typical result of analysis showing occurrence of a pressure differential of about 3.35 m is shown in Figure 16. A maximum value of about 4.9 m occurred during the tests.

The uplift of the apron slab could be caused due to one or a combination of the following:

- Hydrostatic uplift caused by the seepage gradient below the stilling basin.
- Intermittent pressure depressions due to turbulence, especially in the initial reach of the jump. Such pressures may cause suction effect on the upper face of the slab, trying to lift it from its position.
- Difference between the fluctuating pressures on the upper and lower faces of the slab monolith. Such a difference can result due to the transmission of pressure peaks from the upper to the lower face of the slab, through exposed construction joints, cracks, etc. on the slab.

The uplift pressures tending to lift the slab are caused by the intermittent conversion of kinetic energy into pressure energy, transmitted through any opening, joint, or crack that may be in the apron floor. This mechanism poses a threat

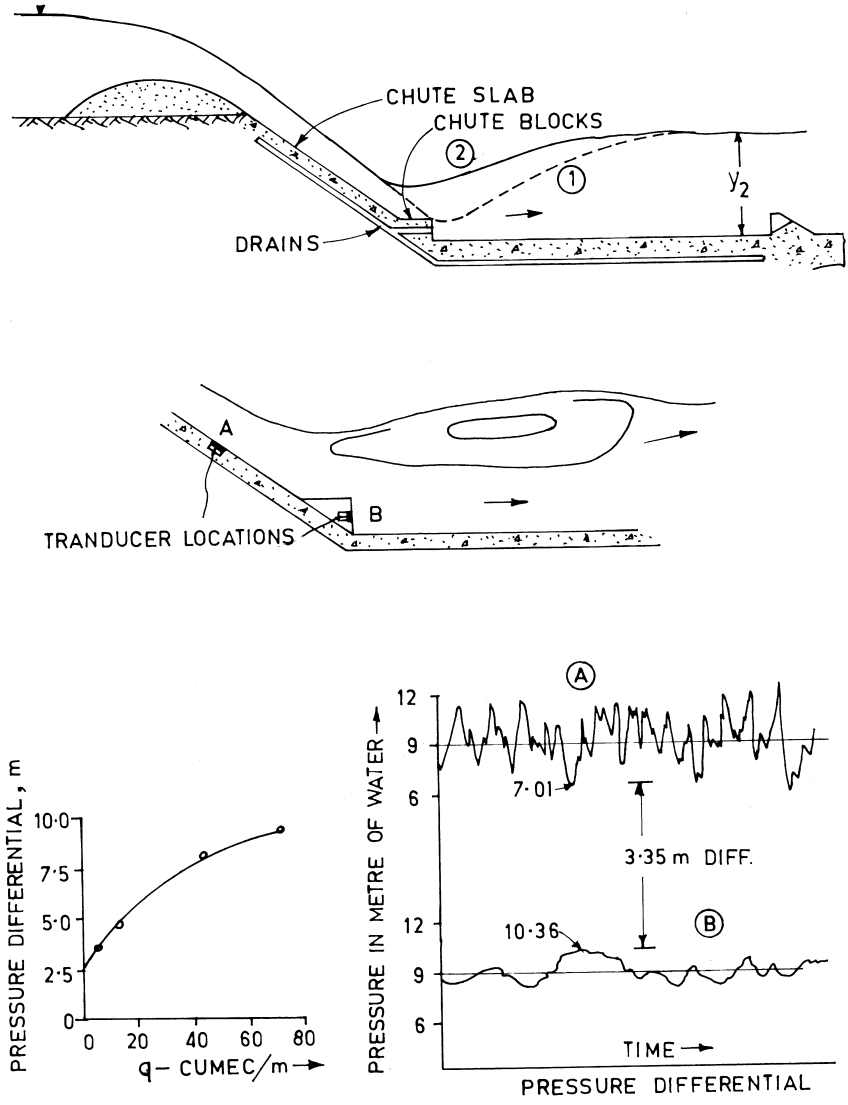

Figure 16 Analysis of the pressure differential below the spillway chute (Karnafuli Dam, Bangladesh, shown in Bowers et al. 1988).

especially at high Froude numbers and is accentuated by incoming turbulence by which the energy is dissipated in the hydraulic jump. When the pressure becomes negative at a point on the apron, there may be a short local instability if there is a steady uplift pressure at the concrete-rock contact or at any other interface within the thickness of the slab. When this uplift is greater than the submerged weight of the concrete plus the water load, the floor slab is lifted up. Damage to many stilling basins indicated that the probability of occurrence of this unfavorable combination is far from being negligible.

Hydrostatic Uplift

Hydrostatic uplift is caused by the difference between the upward force due to the saturated foundation below the slab and reduced pressure on the slab because of the slope of the jump profile during operation of the spillway. The procedure for estimating the uplift caused by the hydrostatic seepage gradient below the stilling basin has been fairly standardized. USBR (1977) considers the design profile of the jump with normal tail water level to calculate the uplift force. However, the present practice is to consider other conditions as well and to account for the reduction in the uplift force due to effective drainage system below the slab. Generally, a reduction of 50% is allowed for an effective under drainage system that is not likely to be clogged. The following conditions are considered as shown in Figure 17:

1. Stilling basin operating under design flood with the corresponding tail water level, water surface profile as per the hydraulic jump on the apron with unbalanced force as shown in Figure 17

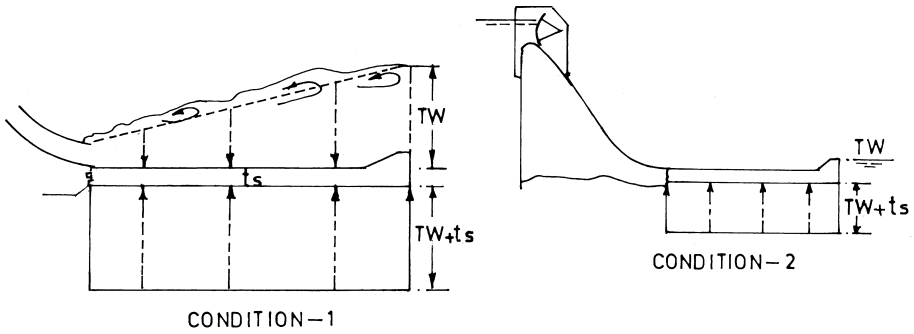

Figure 17 Hydrostatic uplift on the apron.

2. FRL with gates closed and stilling basin dewatered for inspection or repairs, with tail water level corresponding to flow from powerhouse or other outlet etc., as shown in Figure 17.

Usually, condition (1) gives the maximum uplift force. This force is to be jointly resisted by the weight of the slab as well as anchorage in to the bedrock. A combination of the thickness of the slab and the number and the diameter and depth of anchor rods is so chosen as to satisfy the following requirements:

No tension in the rock
The anchor depth satisfying both the permissible stresses between steel and grout and between grout and rock.
No dislodgement of rock mass anchored, against uplift force.

Theory of Hydrodynamic Uplift: A brief Introduction

Consider a stilling basin floor slab monolith L × B in the region of hydraulic jump. Each point on the slab is subjected to instantaneous pressure p', fluctuating between magnitudes below and above mean pressure $\overline{P}$. At a given instance of time, pressures of different magnitudes and signs would occur. If the monolith area A = L × B is subdivided into N elements having equal areas a_1, a_2 etc, the force F(t) on the slab can be expressed as

$$F(t) = \sum_{1}^{N} a_i p_i(t) \tag{22}$$

This can also be expressed as the sum of the mean and fluctuating parts as

$$F(t) = \overline{F} \pm F' = \sum_{1}^{N} A.\overline{P} \pm \sum_{1}^{N} a_i . p_i \tag{23}$$

Since magnitudes of pressures fluctuate between the minimum and maximum on different elements in varying fashion, the mean square value representative of the entire area of the monolith is considered

$$\left(\overline{F'}\right)^2 = \frac{1}{t}\int_0^t \left[\sum_{i=1}^{N} a_i p_i'(t)\right]^2 dt = \frac{1}{t}\int_0^t \left[\sum_{i=1}^{N}\sum_{j=1}^{N} a_i p_i'(t) p_j'(t) a_j\right] dt \tag{24}$$

$$= \sum_{i=1}^{N}\sum_{j=1}^{N} a_i C_{ij} a_j$$

Where C_{ij} is covariance of pressures at points (i) and (j). When i = j, it is the variance of pressure at point (i).

When F' relevant to the entire area has a negative sign, the monolith can be lifted up if its submerged weight together with anchorage force is less than F'.

Various investigators have sought to evolve expression for F', based on the theory of correlation, which can be applied, if it is assumed that distribution of fluctuating pressures at various locations is Gaussian.

There are two methods of assessing hydrodynamic uplift, one based on measurement of fluctuating pressures with their spatial correlation and another based on direct measurement of fluctuating force. Contributions by Bribiesca et al. (1979), Spoljaric et al. (1982), Hajdin (1982), Lopardo et al. (1985), Toso et al. (1988), and Fiorotto et al. (1992) involved pressure measurements. In all these studies, propagation of fluctuating pressures below the apron was not considered. Studies by Peiqing et al. (1996) considered this aspect. The other method involves direct measurement of uplift force using force transducer. Farhoudi et al. (1991) were the first to conduct such a study, but without simulating propagation of fluctuating pressures below the apron. Studies conducted by Bellin et al. (1995) have included such propagation and presented a method of calculating uplift force and thickness of concrete lining.

Hajdin et al.(1982) have derived

$$F' = \frac{1}{2}\rho_w V_1^2 A\, k\, C'_p\, \phi_L\, \phi_B \tag{25}$$

where

k = A factor defining the probability of occurrence of the force: generally k = 3.09 corresponding to 99.8 % probability of occurrence.

C'_p = Pressure fluctuation coefficient.

ϕ_L = Coefficient of correlation along length L.

ϕ_B = Coefficient of correlation along width B.

The equivalent thickness of the monolith t_s is then

$$F' = A.t_s\,(\gamma_c - \gamma_w) \tag{26}$$

Various parameters of Equation 25 can be obtained from Figure 18.

Bribiesca et al. (1979) obtained an expression for the time average of the square of the total vertical force acting on the slab, $\overline{S_p^2}$ as

$$\overline{S_p^2} = f_p^2\, S_p^2\, A^2 \tag{27}$$

$$\text{with } f_p = \frac{2}{(\alpha L + \beta B)}\sqrt{[e^{-\alpha L} + (\alpha L - 1)]\,[e^{-\beta B} + (\beta B - 1)]} \tag{28}$$

where

S_p^2 = Variance of the total pressure acting on the upper face of the slab

f_p = Coefficient of distribution of pressure

The thickness is given by

$$t_s = \frac{\gamma_w}{\gamma_c - \gamma_w} f_p S_h \sqrt{2 \ln (\tau\, f_m)} \tag{29}$$

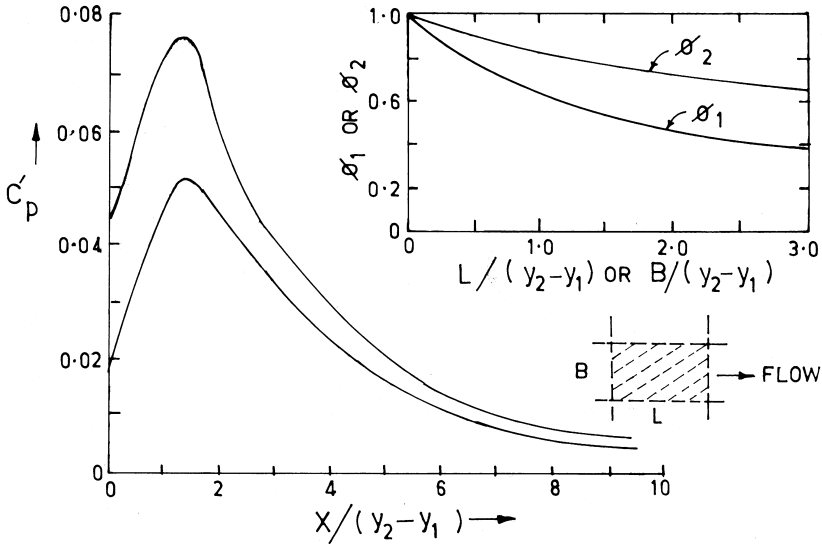

Figure 18 Estimation of hydrodynamic uplift (shown in Hajdin 1982).

where

S_h = Standard deviation of the depth of flow at the center of gravity of the area A, m

τ = Useful life of concrete lining of the slab, in seconds

f_m = Main frequency of pressure fluctuations,hz

Authors have presented a number of design charts (not reproduced here) and explained the procedure of calculation, for which the original paper may be referred.

Toso et al. (1988) state that for practical purposes, the pressure fluctuations tend to approach a definite limit, of the order of 80–100% of the head. Table 1 lists nominal limits of maximum pressure fluctuations for different flow situations. The longitudinal scale of extreme pressure pulses in the flow direction is of the order of eight times the incident flow depth, where as lateral scale is about thirteen times the flow depth. With selecting an appropriate value of C_p from Table 1, the maximum deviation from the mean pressure is worked out as

$$\Delta_p = C_p \frac{V_1^2}{2g} \tag{30}$$

This deviation pressure Δp is assumed to act on the center of an area 8 y_1 × 13 y_1. Moving out from the center of the area, the pressure would drop off to the

Table 1 Nominal Limit of Maximum Pressure Fluctuations within Hydraulic Jump

Jump Condition	Froude Number	10 min Cp^+	10 min Cp^-	24hr Cp	Suggested maximum Cp
0° slope, undeveloped inflow	3.0	0.3	0.27	-	0.6
	4.2	0.5	-	-	1.0
	5.0	0.55	-	-	1.2
	5.5	0.50	0.38	-	1.0
	7.7	0.44	0.23	-	0.9
	10.0	0.43	0.28	-	0.9
0° slope, developed inflow	3.0	0.48	0.43	-	1.0
	4.2	0.55	0.51	-	1.2
	5.0	0.53	0.47	-	1.1
	5.7	0.39	0.41	0.6	0.9
30° slope, toe of jump at base of chute	3.8	0.33	0.35	-	0.7
	4.5	0.40	0.36	-	0.8
	5.1	0.40	0.32	0.8	0.8
	8.4	0.46	0.30	-	0.9
30° slope, toe of jump on chute	3.3	0.42	0.37	-	0.8[a]
	4.5	0.55	0.59	-	1.0[a]
	5.2	0.59	0.54	0.6[a]	0.9[a]
	6.8	0.70	0.58	-	1.3[a]
15° slope, toe of jump at	5.0	0.40	0.40	0.6	0.8
45° base of chute	5.0	0.45	0.36	1.0	0.9
45° slope, toe of jump on 458 chute	5.0	0.56	0.43	0.9[a]	1.0[a]
	5.0	0.72	0.56	0.9[a]	1.0[a]
30° slope, with Type II basin	5.0	0.35	0.33	0.6	0.7
30° slope, with Type III basin	5.0	0.38	0.52	0.9	1.0
On the sidewall	5.0			1.7[b]	1.7[b]

NOTE:
a-Cp with velocity head increased by elevation difference between toe of jump and basin floor.
b-Possible error in incident velocity; further study desirable.

mean pressure. Choose the smaller area between the actual slab area and the area 8 $y_1 \times 13\ y_1$. The uplift force would then be

$$F' = \Delta_p . \frac{1}{3} . L_c . B_c . \gamma_w \tag{31}$$

Farhoudi et al. (1991) performed direct measurements of uplift force using a force transducer in a model set up. Slabs of various lengths and widths were used

at Froude numbers varying from 4 to 10. Since dynamic force reduces as the area of the slab increases, authors have measured the force on strips of slab, with $L/y_1 = 1$ and B/y_1 varying from 2.0 to 14.4 and then with $B/y_1 = 1$ with L/y_1 varying from 3.75 to 22.5. The results have been presented in terms of RMS force coefficient C'_f defined as

$$C'_f = \frac{\sqrt{\overline{(F')^2}}}{\frac{1}{2}\rho_w V_1^2} \tag{32}$$

The values of C'_f for different values of L/y_1 and B/y_1 for various Froude numbers for the position of the upstream end of the slab at $15y_1$ from the toe of the jump are shown in Figure 19.

The procedure of calculations is as follows:

1. From Figure 19, obtain $C'_f = C'_{fL}$ for slab length ratio L/y_1 with $B/y_1 = 1$
2. Similarly obtain $C'_f = C'_{fB}$ for slab width ratio B/y_1 with $L/y_1 = 1$

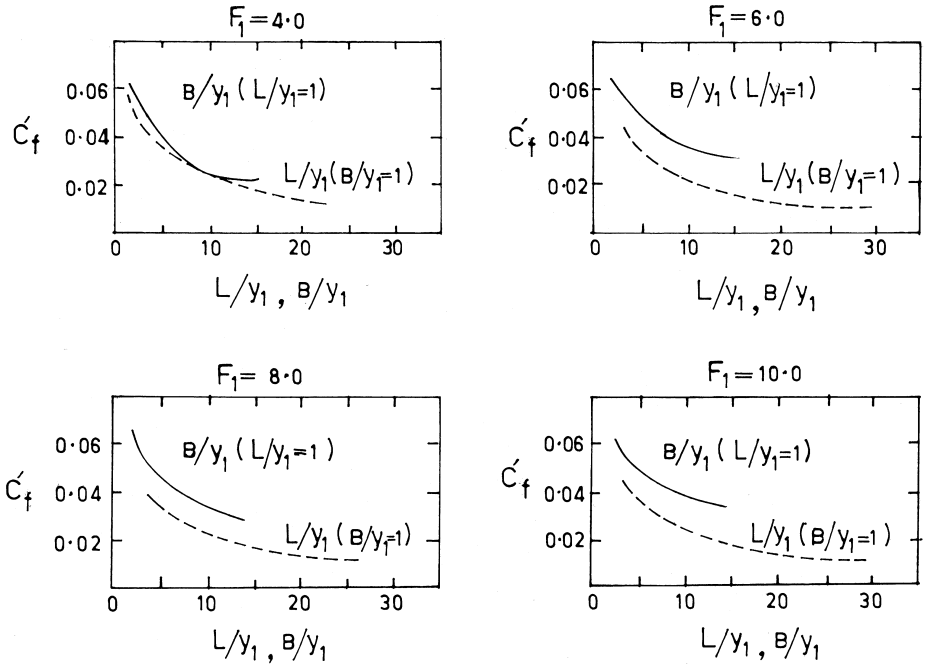

Figure 19 Variation of C'_f with length and width ratios (shown in Farhoudi et al. 1991).

3. $(C'_f)^2 = C'_{fL}.C'_{fB}$ and hence evaluate C'_f
4. Obtain F' from Equation 32
5. Experimental measurements have shown that peak instantaneous value of force fluctuation could be as much as 3.5 times the RMS value. Therefore

$$F'_{\max} = 3.5\, C'_f \frac{1}{2}\rho_w V_1^2 A \text{ and the thickness of the slab}$$

$$t_s = \frac{F'_{\max}}{A(\gamma_c - \gamma_w)} \tag{33}$$

Estimating the uplift considering fluctuating forces on the upper surface of the slab as well as seepage forces below is similar to that applied in the case of Karnafuli spillway chute lining. However, in the case of seepage below the slab under a hydraulic jump, it is assumed that for practical purposes, underpressures propagate instantaneously and undamped. Bellin et al. (1995) conducted laboratory studies simulating this phenomenon with a direct force measurement system. The maximum uplift force $F'_{\max}$, just exceeding the submerged weight of the slab was measured and related to the dimensionless pressure coefficients and C_p^+ *and* C_p^- and uplift coefficient Ω_s considering standard deviation of fluctuating force and pressure. The relationship is

$$F'_{\max} = \Omega_s \left(C_p^+ + C_p^-\right)\gamma_w \frac{V_1^2}{2g} LB \tag{34}$$

The experiments also indicated:

1. The probability density functions of the force show negligible skewness and kurtosis close to the value characteristics of the Gaussian distribution.
2. The maximum values of C_p^+ *and* C_p^- were approximately 0.9, but may be assumed to be equal to unity.
3. The most suitable form of slabs (for a given area) is rectangular, with width kept to the technical minimum.

Figure 20 shows values of uplift coefficients Ωs for different values of the ratios L/y_1 and B/y_1.

Illustrative Examples

Uplift force and equivalent thickness have been calculated applying various relationships given above for a hydraulic jump stilling basin with the following details:

Size of panel monolith: 11.5 m wide $\times$ 25 m long.
$V_1 = 48.3$ m/s; $y_1 = 2.56$ m, $F_1 = 9.63$; $y_2 = 33.7$ m.

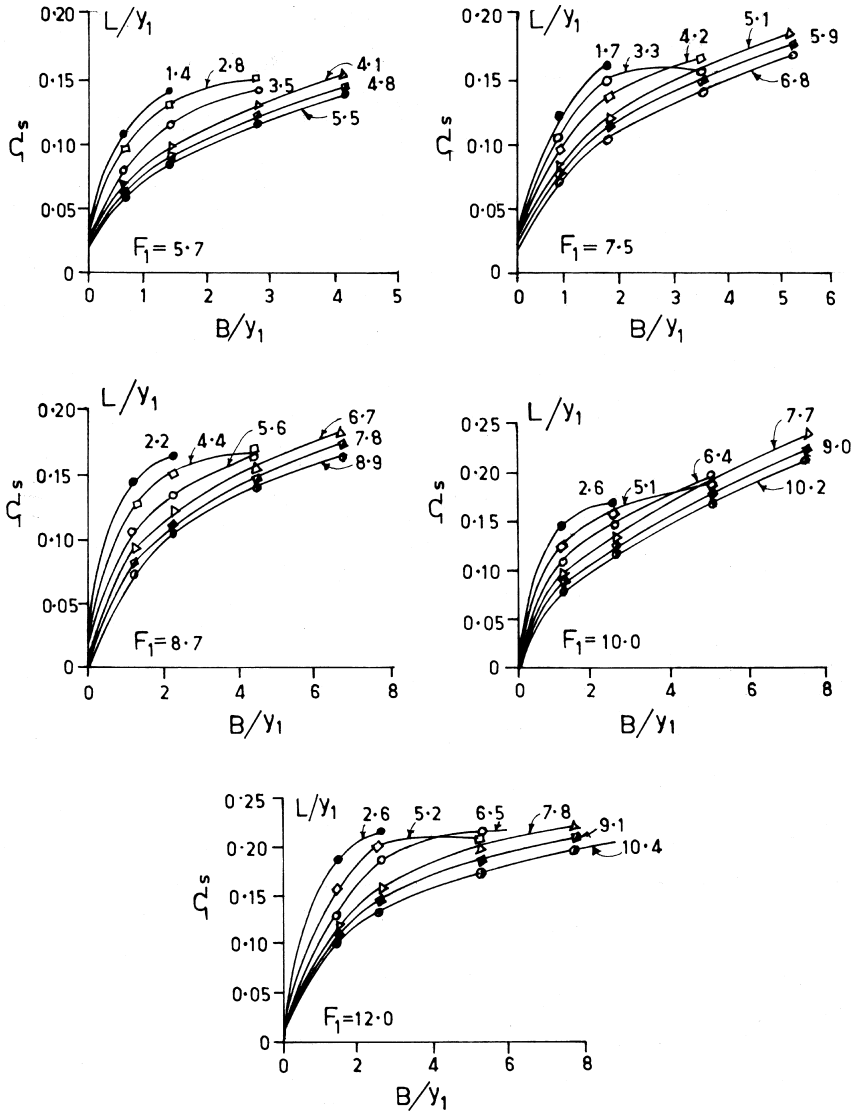

Figure 20 Values of Ω_s for L/y_1 and B/y_1 (shown in Bellin et al. 1991).

Submerged weight of concrete: 1.6 tons/cum.
Equivalent thickness means that if the lining is anchored to underlying rock, the failure strength of the anchors is included in the total weight.
No factor of safety included in the calculations.

The results of calculations are summarized in Table 2. The vast variation in the results obtained points out to the fact that this science is still in an evolutionary stage and it would be desirable to conduct specific studies on a model to determine the uplift force.

The similarity in the results obtained by the methods of Hajdin (Pressure measurement) and Farhoudi (Force measurement) is striking.

It must be noted, however, that the applicability of the equivalent thickness criterion, based on the balance of the forces acting on the slabs in static condition, is considered to be unsafe for the anchored slab. Analysis by Fiorotto et al. (2000) lead to the recommendation to double the area of anchor steel as computed by the equivalent thickness criterion described above.

20.5.2 Hydrodynamic Forces

The turbulence in a hydraulic jump imposes forces against divide walls, sidewalls, and appurtenances, particularly baffle piers. The magnitude, frequency, and distribution of these dynamic loads are of interest to the structural design of these elements.

Gravity Walls

Past practice consisted of designing side walls in a hydraulic jump stilling basin to withstand the loads resulting from maximum anticipated heads due to water and/or soil loading plus an additional unknown but estimated dynamic load. The inclusion of earthquake force is also suggested under severe loading condition. Previous laboratory measurements with pressure transducers have indicated that pressure near the base of a wall may fluctuate from the static pressure to as much as 1.5 times the velocity head entering the basin. Although dynamic loading equivalent to such pressure fluctuations has been used in the design of sidewall monoliths, this practice appears to be too conservative. A general procedure for calculating dynamic load and bending moment has been evolved by Fletcher et al. (1988), using a specially devised force transducer. Maximum, minimum and average forces and bending moment on the sidewall can be estimated with the generalized design chart in Figure 21.

The average maximum unit force R_m (in N/m) is given by

$$R_m = 1.077 H_D^{1.05} \rho_w \, q \, V_1 \, F_1^{-1.42} \tag{35}$$

Where H_D = Height of spillway from apron level to crest level.

Table 2. Comparison of Uplift Force and Thickness of Concrete Lining as Calculated from Various Approaches

Method	Assumptions/conditions	Area of panel considered m xm	Uplift force on a full size panel (tons)	Peak Value of uplift pressure in meter of water	Equivalent thickness of lining, m
(1)	(2)	(3)	(4)	(5)	(6)
Hydrostatic	– Drainage system inoperative	1 m × 1 m	6411	22.3	14
	– Drainage system operative	1 m × 1 m	3205	11.15	7
Bribiesca (1979)	– Drainage system not considered – No seepage under the lining.	11.5 × 25	4312	15.0	9.4
Hajdin (1982)	-do-	-do-	3142	10.9	6.8
Toso (1988)	– $C^{+}_{p}, C^{-}_{p} = 1.0$	-do-(a)	11413	39.7	24.8
	– $C^{+}_{p} = 0.45$ – $C^{-}_{p} = 0.36$	-do-	4108	14.3	8.9
Farhoudi (1992) (Direct measurement of force)	– Drainage system not considered – No seepage under the lining.	11.5 × 25	3260	11.3	7.0
Bellin (1995) (Direct measurement of force)	–$C^{+}_{p}, C^{-}_{p} = 1.0$ – Drainage system not considered –Seepage under the lining.	11.5 × 25	10957	38.1	23.8
Experimental (Direct measurement force)	–Seepage under the lining – Drainage system not considered – Peak value of uplift scanned from a test duration of 30 minutes in the model.	11.5 × 25	10224	35.6	22.3

(a) Actual area of the panel being smaller than $8Y_1 \times 13\ Y_1$.

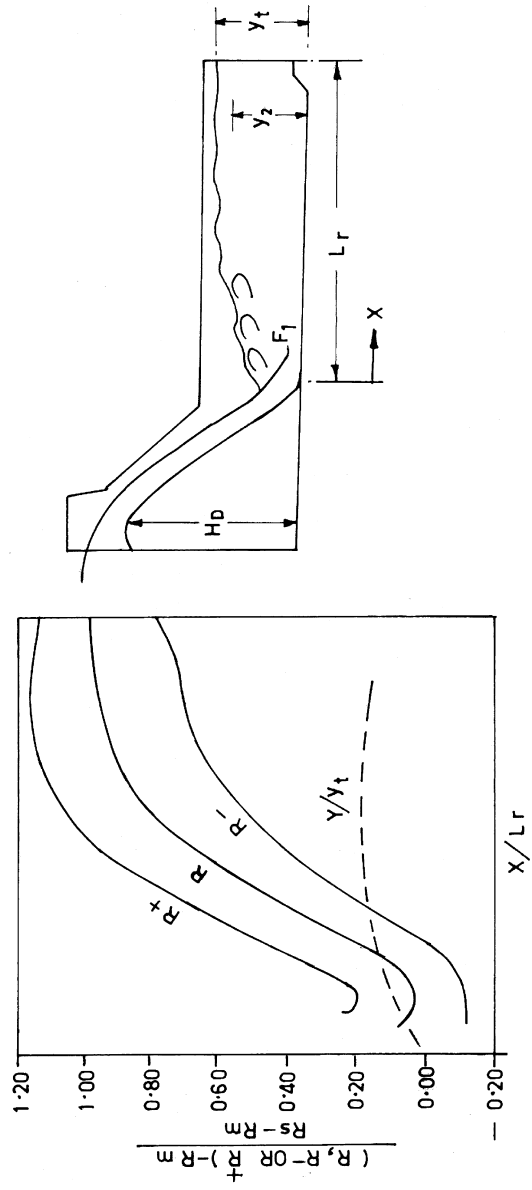

Figure 21 Hydrodynamic loads on sidewall in a stilling basin (shown in Fletcher et al. 1988).

Static unit force R_s due to theoretical conjugate depth y_2 is

$$R_s = \frac{1}{2}\gamma_w y_2^2 \tag{36}$$

The average, maximum and minimum unit forces(R, R^+, R^-) corresponding to the distance x from the toe of the jump can be obtained from Figure 21. Here L_r is the length of the jump. The moment arm Y corresponding to x can also be obtained from the chart, where y_t is the actual tail water depth. The maximum bending moment M (in Nm/m) is then

$$M = R^+ Y \tag{37}$$

If the actual tail water depth y_t is greater than y_2, then R, R+ and R− may be increased by the factor $\frac{\gamma_w}{2}\left(y_t^2 - y_2^2\right)$.

Anchor Walls

Sometimes the sidewalls of stilling basins are in the form of anchor walls, i.e. concrete cladding on dressed rock surface. The lining secured to the rock with anchors may be subjected to hydrodynamic pull out force in a way similar to the concrete lining of the stilling basin. The anchors for such lining have to be designed considering the magnitude of pull out force and strength of the rock. As there is no generalized procedure available, evaluation of forces has to be made on a hydraulic model. Khatsuria et al. (1992) have described studies conducted on a model to determine magnitude of pull out forces on the right training wall of Sardar Sarovar spillway, India. Experiments were conducted using both, the pressure and force measurement and the results obtained agreed quite well, as shown in Figure 22.

Divide Walls

Submersible divide walls are sometimes incorporated in the stilling basins for various considerations. Conventionally, the structural design of a submersible divide wall is based on the bending moment caused by the hydrostatic force, which results from the condition of the water level retained up to its top on one side, with no water on the other side. However, hind casting studies on the failure of divide walls in the hollow jet valve stilling basins of Navajo and Trinity dams, US, indicated that the above practice was not safe.

A generalized method for evaluating such forces has not been developed so far and hence model study for each specific case is necessary. Khatsuria (1995) reported model studies for assessing dynamic bending moments from studies on the 1:55 model of divide wall of Sardar Sarovar stilling basin. It was revealed

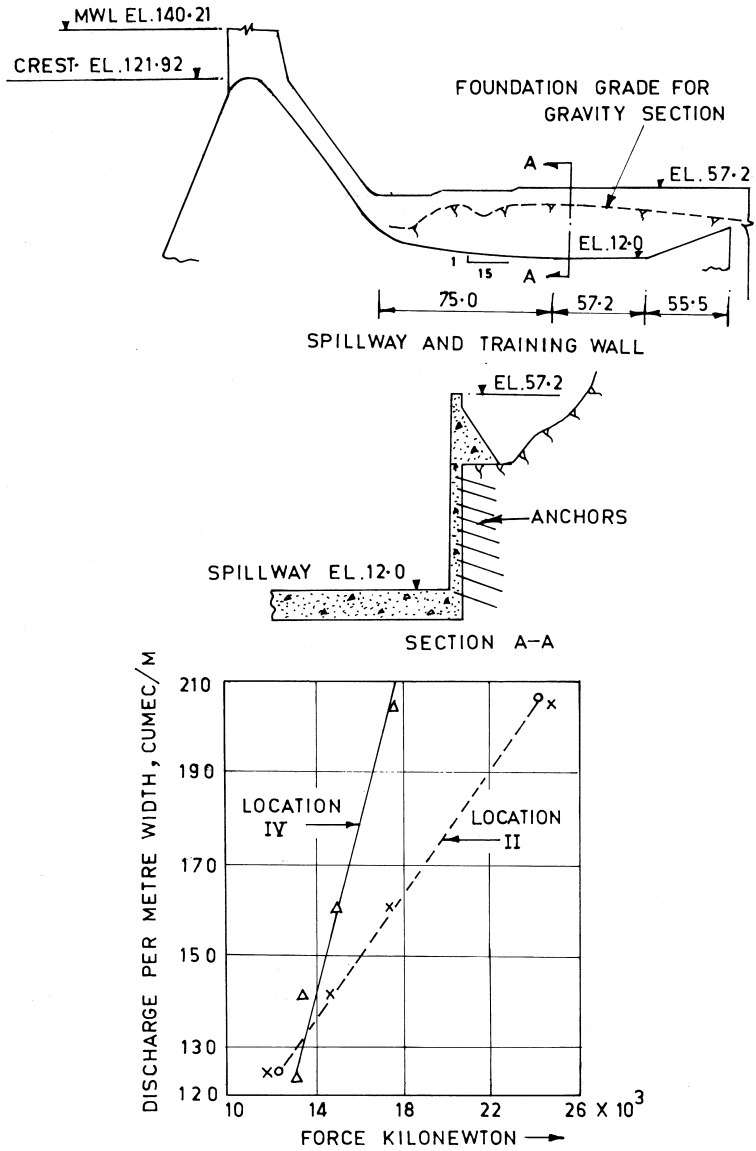

Figure 22 Concrete lined training wall: Sardar Sarovar spillway, India. (Shown in Khatsuria, 1992)

○, △ Force Measurement
x Pressure Measurement

that measured values of bending moments in the region of intense turbulence were about 1.8 to 2.7 times those obtained from the hydrostatic distribution. Typical results are shown in Figure 23. Khatsuria et al. (1994) have described general procedure for designing special BM transducer for such studies.

Baffle Piers

The repeated damages caused to the baffle piers of Pit 6 dam stilling basin, US, is an ideal example of the nature of hydrodynamic forces involved. The hydraulic efficiency of the stilling basins incorporating baffle piers depends largely on the resistance offered by the baffle piers, secured in position against the drag force exerted by the flow. This is influenced by the factors such as: shape, velocity entering the basin, the distance of the upstream face of the baffle from the toe of the jump, Froude number of the flow, and tail water depth, etc. In the past, baffle piers used to be designed on the basis of the theoretical maximum force derived either from momentum theory ($\rho_w\ q\ V_1$) or drag force consideration ($2\gamma_w[y_1 + V_1^2/2g]$), neglecting the stabilizing force offered by the downstream water pressure. Studies for generalizing the procedure for calculating drag force were first conducted by Basco (1969, 1970,1971) and Basco et al. (1971). The design charts presented by Basco (1970) enable determination of optimum geometry and force ratio in longitudinal direction on standard USBR baffle piers. Ranga Raju et al. (1980) reanalyzed Basco and Adam's (1971) data and other data with a view to simplifying their use and eliminating the errors due to interpolation. The design charts presented by them are shown in Figure 24. The factors Ψ_1 *and* Ψ_2 are determined with reference to the ratio (h_3/y_1), where h_3 is the height of baffle pier, and $\eta = W/(W + S)$, where W is the width of the baffle pier, and S is the spacing between the piers. The average (F_a) and maximum (F_{max}) drag forces per unit width of the channel have been related to the hydrostatic force $\frac{1}{2}\gamma_w y_2^2$.

However, the fluctuating lateral forces on the baffle piers are of more concern, as has been reported by Nakato (2000). Model studies conducted for assessment of longitudinal and lateral forces on the special types of baffle piers revealed that extremely large fluctuating loads on the baffle piers in the lateral direction were the primary cause of the repeated failure. As a result of studies, triangular hollow blocks that substantially reduced the lateral loads were developed as shown in Figure 25.

20.5.3 Cavitation

Discussion on cavitation in stilling basin and appurtenances is covered in Chapter 26.

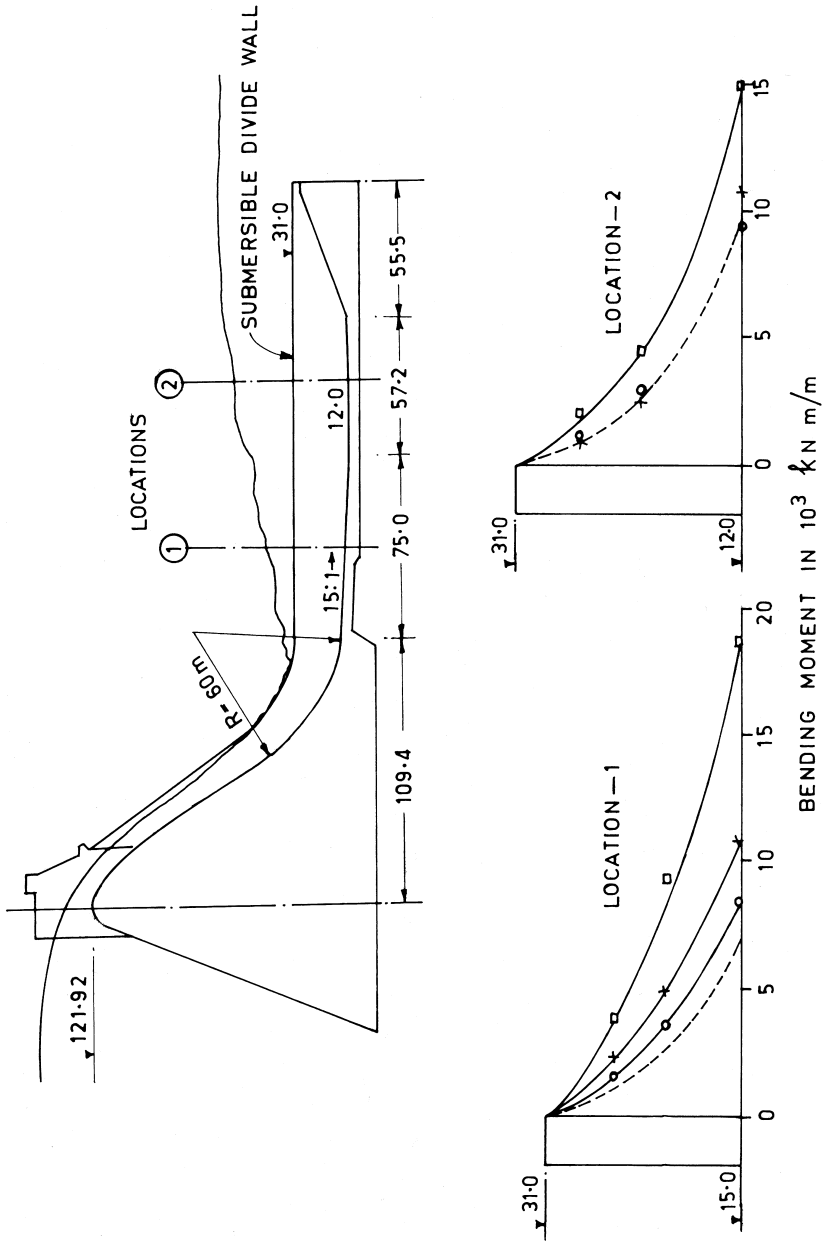

Figure 23 Sardar Sarovar stilling basin: bending moments on divide wall (shown in Khatsuria, 1995).

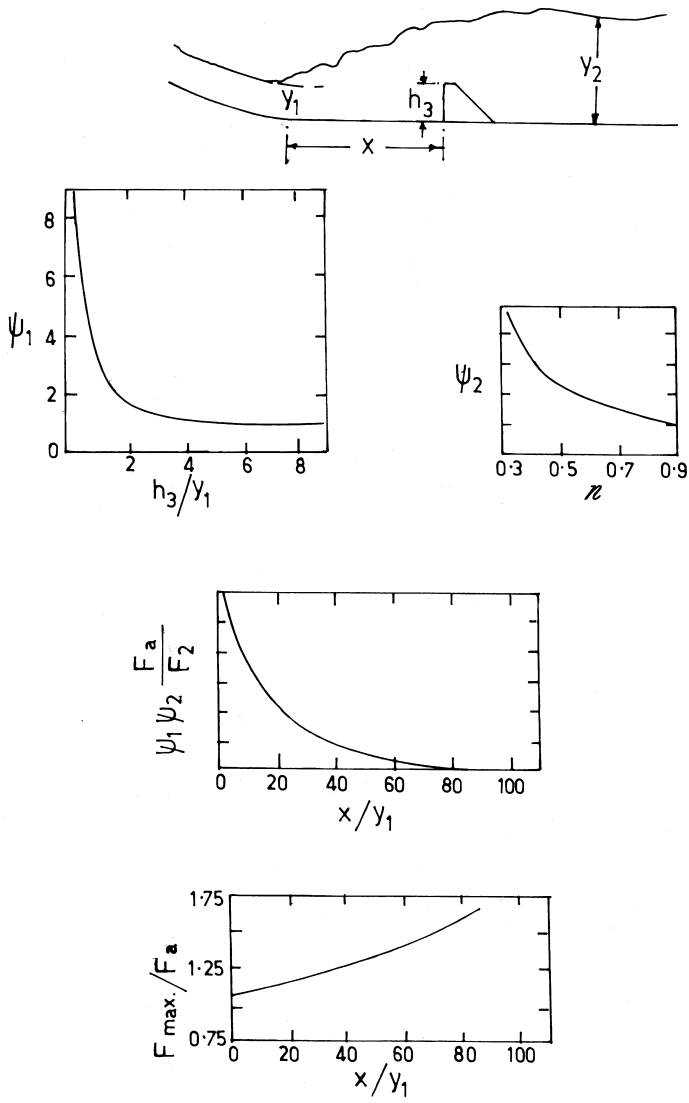

Figure 24 Hydrodynamic forces on baffle piers (shown in Ranga Raju et al. 1980).

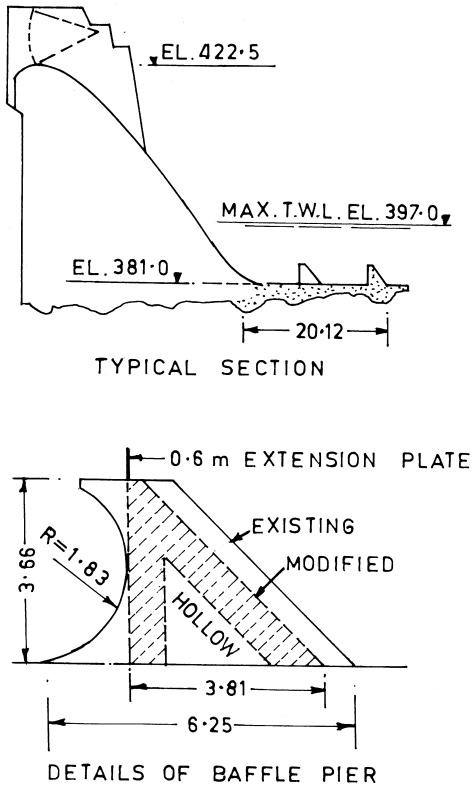

Figure 25 Pit 6 dam stilling basin and baffle piers (shown in Nakato 2000).

20.5.4 Vibrations

In the energy dissipation through macro turbulence, the dominant pulsating components of pressure fluctuations have frequency between 0 and 10 Hz. This means that cantilevered divide walls and sidewalls, slabs and deflectors, etc. are in danger of resonant vibration. The divide wall of Navajo hollow jet valve stilling basin had been damaged due to fatigue caused by vibrations. It was revealed that the natural frequency of the divide wall was nearly coinciding with the forcing frequency. A divide wall should preferably have a natural frequency greater than 5. Providing braces at the top of the divide walls or covering the basin with a concrete slab are ways to accomplish this.

Vibrational movement of the slab opens up joints between monoliths and interfaces in depth and throws up the corners of the joints, encouraging the fluc-

tuating pressures to be transmitted leading to dynamic uplift and lifting. Also, the pressure fluctuations could produce fatigue in some structures, especially rock anchors, which is difficult to estimate.

20.5.5 Abrasion

A number of stilling basins have suffered severe abrasion damage due to transporting loose material from the riverbed into the stilling basin. During the spillway construction stages, unequal distribution of discharge, due to differential levels of spillway monoliths, results in horizontal eddies that pick up loose material from the riverbed and transport into the basin. In the case of completed spillways, eddies were created due to unequal operation of bottom outlets or spillway gates. A simple remedy would be to keep the top level of the end sill sufficiently higher than the riverbed, if it does not impair the hydraulic performance. The best method is to ensure symmetrical flow by equal and simultaneous operation of gates. For basins with a large number of gates, this may be difficult. In such cases, provision of adequate number of low height divide walls in the stilling basins would be effective in reducing the strength and extent of eddy thereby preventing transport of material into the stilling basins, as shown schematically in Figure 26. Divide walls in the stilling basins of Canyon Ferry, USA, and Sardar Sarovar dam, India, are some of the examples. It must, however, be ensured that the structural design of the divide walls is based on the hydrodynamic forces/bending moments, as illustrated in Figure 23.

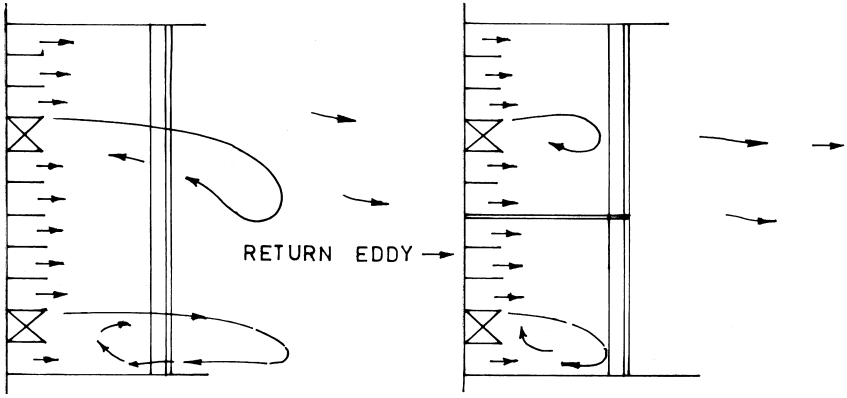

Figure 26 Effectiveness of the low height divide walls in a stilling basin.

20.6 ENVIRONMENTAL CONSIDERATIONS

Environmental considerations sometimes govern the choice of energy dissipator or necessitate its adaptability to meet the requirement. When highly aerated flows plunge or diffuse into deep-seated stilling basins, a process known as nitrogen supersaturation occurs. It is expressed as Total Dissolved Gases (TDG). Water with nitrogen supersaturation is harmful for the fish population because the dissolved gas coming out of solution in their respiratory system or tissues and proves to be fatal. This problem had been studied in greater detail in the United States as a result of fish mortality in the Columbia and Snake River basins.

The most primary demand made on the spillways and energy dissipators in this situation is to prevent highly aerated flows from plunging deep in to the stilling basins and water bodies. This requirement is rather conflicting with the need to have aerated flows close to the flow boundaries to mitigate cavitation damage. The most commonly used device is some form of deflector on the spillway surface that would cause the aerated layers of the flow to remain on the surface and reduce its penetration into the pool. Such deflectors have been installed on a number of spillways: Lower Granite, Bonneville, John Day, Lower Monumental dam in the United States, Ana-Cua spillway, Yacyreta dam, Argentina, etc. Generally, the deflectors are designed for normal flows and become ineffective for large flows and may even be damaged.

Bacchiega et al. (1999) have studied comparative performanced of a typical stilling basin with and without deflector in respect of general flow conditions in the stilling basin, downstream of the stilling basin, and characteristics of pressure fluctuations on the stilling basin floor. The characteristic dimensions of the deflector were: length equal to 0.216 H_d and location 0.351 H_d below the crest. It was found that the presence of deflector significantly altered the flow conditions in the stilling basin. The hydraulic jump had a tendency to move towards downstream for discharges exceeding about 35% of the maximum discharge, as shown in Figure 27. The extent of recirculating flow in the stilling basin increased which could adversely effect the self-cleansing potential of the stilling basin. It also increased the scour in the downstream channel. Pressure coefficients C'_p and $P'_{0.1}$ along the basin floor were also modified. These studies indicate the need to optimize the configurations of the deflector and the stilling basin to achieve the desired objectives. An alternative would be to consider the formation of a surface hydraulic jump such as that designated W-jump in Figure 8 (Armenio 2000). This would confine the hydraulic jump on the surface and at the same time offer favorable pressure distribution on the floor of the stilling basin.

The design of the baffle developed by the USACE (1990) during the model study of the proposed Libby Reregulating dam, US, shown in Figure 2 is also claimed to be effective, not only in energy dissipation, but also in aerating the

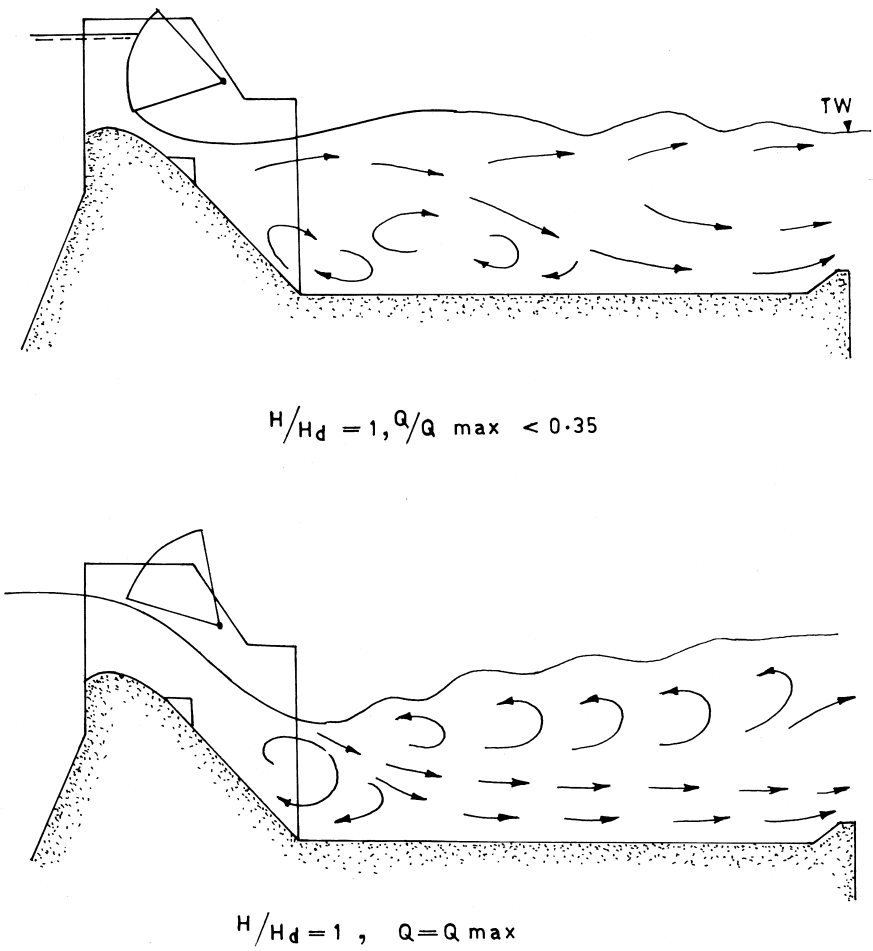

Figure 27 Performance of a typical flow deflector and stilling basin (shown in Bacchiega et al. 1999).

flow and reducing nitrogen supersaturation. The baffles could function effectively for unit discharges as large as 80 cumec/m.

20.7 IMPLICATIONS OF VARIOUS FACTORS

The severity of the problems discussed in this chapter increase with the increase in the head. Pinto (1994) has therefore rightly concluded that for heads in excess

of about 120 m, other alternatives for energy dissipation in place of hydraulic jump stilling basins should be considered.

Notations

A = Area of the slab monolith
a_i = Element of area
B = Width of the slab monolith
b = Width of the channel
C_b = Air concentration close to bed
C_i = Coefficient relating maximum energy of turbulence to the mean velocity head
C_f = Coefficient of shear drag
$\overline{C_p}$ = Pressure coefficient corresponding to mean pressure
C'_p = Pressure coefficient corresponding to fluctuating part of pressure
C_p^+ = Pressure coefficient corresponding to maximum value of positive pressure deviation from mean pressure
C_p^- = -do- for the maximum value of negative pressure
C_{ij} = Variance between two adjacent fluctuating pressures, forces, etc.
D = Dimensionless depth deficit factor
E_1 = Energy entering the stilling basin
E_l = Energy loss in the stilling basin
F_a = Average force on baffle pier
F_1 = Froude number entering the stilling basin
F' = Fluctuating force
$F(t)$ = Force on the slab monolith
f_p = Coefficient of distribution of pressure
H_d = Height of spillway from apron level to crest level
h_{ib} = Maximum energy of turbulence
h_3 = Height of baffle pier
L = Length of apron
L_a = Aeration length of the jump
L_e = Length of jump measured upto a section where no bottom erosion appears and bottom shear forces have greatly reduced
L_j = Length of jump measured upto the section of maximum depth
L_r = Length of jump indicating the limit between the backward and forward flow
$\underline{l}$ = Horizontal projection of the length of sloping apron in 'B' jump type basins
M = Bending moment on the sidewall
$P'_{0.1}$ = Pressure depression corresponding to 0.1% probability
p = Total pressure = $\bar{P} + p'$

$\bar{P}$ = Mean pressure
p' = Fluctuating pressure
Q = Discharge
Q_a = Air discharge
Q_w = Water discharge
q = Unit discharge
R_m = Average maximum unit force on the sidewall
R_s = Static unit force on the sidewall due to conjugate depth
R^+ = Maximum unit force on the sidewall
R^- = Minimum unit force on the sidewall
R_1 = Reynolds number of the flow entering the stilling basin
S = Spacing between the baffle piers
S_h = Standard deviation of depth of flow on the center of gravity of the slab monolith
S_p^2 = Variance of the total pressure acting on the upper face of the slab
T = Time
T = Amplitude of wave on a corrugated bed
t_s = Thickness of the slab monolith
$\bar{U}$ = Mean velocity
U'_{max} = Maximum value of fluctuating velocity
U'_b = Instantaneous maximum velocity at bottom
V_1 = Velocity of flow entering stilling basin
V_e = Minimum velocity for air entrainment
W = Width of baffle pier
Y = Lever arm for the bending moment on sidewall
y_1 = Pre-jump depth
y_2 = Conjugate depth
y_{2c} = Conjugate depth on a corrugated bed
y_t = Tail water depth
β = Ratio Q_a/Q_w
θ = Angle of sloping apron with horizontal
σ = Standard deviation of fluctuating components
ϕ_1 = Coefficient of correlation along length L of the slab monolith
ϕ_2 = Coefficient of correlation along width B of the salb monolith
γ_c = Density of concrete
γ_w = Density of water
η = Blockage ratio of baffle piers
ν = Kinematic viscosity
Δ_p^+) = Maximum positive and negative pressure deviations
Δ_p^-) from the mean pressure.
Ω_s = Uplift coefficient
Ψ_1 = Factors in calculation of drag force on baffle piers
Ψ_2

REFERENCES

1. Abdul Khader, M. H.; Elango, K. Turbulent pressure field beneath a hydraulic jump. IAHR Jnl. of Hyd. Res, 1974, 12(4).
2. Akbari, M. E.; Mittal, M. K.; Pande, P. K. Pressure fluctuations on the floor of free and forced hydraulic jumps, Proc. Int. Conf. on Hydraulic Modelling of Civil Engg. Structures, 1982.
3. Armenio, V.; Toscano, P.; Fiorotto, V. On the effect of a negative step in pressure fluctuations at the bottom of a hydraulic jump. IAHR Jnl of Hydraulic Research. 2000, 38(No 5).
4. Bacchiega, J. D.; Fattor, C. A.; Barrionuevo, H. D. Environmental considerations in the design of spillways: Analysis of hydrodynamic behavior, 28th IHHR Congress. TUGRAZ, 1999.
5. Bakhmeteff, B. A.; Matzke, A. E. The hydraulic jump in terms of dynamic similarity, Trans. ASCE, 1936.
6. Basco, D. R. Trends in baffled hydraulic jump stilling basin designs of the Corps of Engineers since 1947, Misc. Paper H-69-1, USWES, 1969.
7. Basco, D. R. An experimental study of drag forces and other performance criteria of baffle blocks in hydraulic jumps, Paper H-70-4, USWES, 1970.
8. Basco, D. R. Optimized geometry for baffle blocks in hydraulic jump, IAHR, 1971.
9. Basco, D. R.; Adams, J. R. Drag forces on baffle blocks in hydraulic jump. ASCE, Jnl. of Hyd. Div, Dec. 1971, 97.
10. Bellin, A.; Fiorotto, V. Direct dynamic force measurement on slabs in spillway stilling basins. ASCE, Jnl. of Hyd. Div, Oct. 1995, 121(No.10).
11. Bhowmik, N. G. Stilling basin design for low Froude number. ASCE, Jnl. of Hyd. Div, July 1975, 101(HY 7).
12. Blaisdell, F. W. Development and hydraulic design, Saint Anthony Falls stilling basin, Trans. ASCE, 1948; Vol. 113, 483–520.
13. Bowers, C. E.; Tsai, F. Y. Fluctuating pressures in spillway stilling basins. ASCE, Jnl. of Hyd. Dn, 1969, 95(6).
14. Bowers, E. C.; Toso, J. Karnafuli project, Model studies of spillway damage. ASCE, Jnl. of Hyd. Dn, May 1988, 114(No.5).
15. Bradely, J. N.; Peterka, A. J. The hydraulic design of stilling basins. ASCE, Jnl. of Hyd. Dn, Oct. 1957, 83(No.5).
16. Bribiesca, J. L. S.; Mariles, O. A. F. Experimental analysis of Macroturbulence effects on the lining of stilling basins, Q50, R6 13th ICOLD, 1979.
17. Cassidy, J. J.; Locher, F. A.; Lee, W.; Nakato, T. Hydraulic design for replacement of floor blocks of Pit 6 stilling basin – 18th ICOLD. Durban, 1994.
18. Chanson, H.; Brattberg, T. Experimental study of the air-water shear flow in a hydraulic jump. Intl. Jnl. of Multiphase Flow, 2000, 26.
19. Chanson, H.; Toombes, L. Experimental investigations of air entrainment in transition and skimming flows down a stepped chute, Research Report No. CE 158, The University of Queensland, July 200l.
20. Ead, S. H.; Rajaratnam, N. Hydraulic Jump on Corrugated Beds. ASCE Jnl of Hyd Engg, 2002, 128(7).

21. Farhaudi, J.; Narayanan, R. Force on slab beneath hydraulic jump. ASCE, Jnl. of Hyd. Engg, 1991, 117(1).
22. Fiorotto, V.; Rinaldo, A. Fluctuating uplift and lining design in spillway stilling basins. ASCE, Jnl. of Hyd. Engg, 1992-a, 118(4).
23. Fiorotto, V.; Rinaldo, A. Turbulent pressure fluctuations under hydraulic jumps. IAHR, Jnl. of Hyd. Rs, 1992-b, 30(4).
24. Fiorotto, V.; Salandin, P. Design of anchored slabs in spillway stilling basins. ASCE, Jnl. of Hyd. Engg, July 2000, 126(7).
25. Fletcher, B. P.; Saunders, P. E. Dynamic loading on sidewall monoliths of spillway stilling basins, Tech. Report HL-88-10, USWES, 1988.
26. Gaikwad, S. R.; Kumthekar, M. J.; Khatsuria, R. M.; Khurjekar, M. J.; Deolalikar, P. B.; Bhosekar, V.V. Consideration of macro-turbulent pressure fluctuations in design of divide walls of stilling basins – Intnl. Symp. on New Techniques in model testing in hydraulic research, CBIP, held at CWPRS. Pune, 1987.
27. George, R. L. Low Froude number stilling basin design, Tech. Report No. REC-ERC-78-8, USBR, August 1978.
28. Gomasta, S. K.; Mittal, M. K.; Pande, P. K. Hydrodynamic forces on baffle blocks in hydraulic jump, 17th Congress, IAHR. Baden-Baden, 1977.
29. Hager, W. H. B-jump in sloping channel. IAHR, Jnl. of Hyd. Res, 1988, 26(No.5).
30. Hager, W. H.; Bremen, R. Classical hydraulic jump: Sequent depths. IAHR, Jnl. of Hyd. Res, 1989, 21(No.4).
31. Hager, W. H.; Bremen, R.; Kawagoshi, N. Classical hydraulic jump: Length of roller. IAHR Jnl. of Hyd. Res, 1990, 28(No.5).
32. Hajdin, Georgije Contribution to the evaluation of fluctuation pressure on fluid currents limit areas- based on the pressures recorded at several points of the area, VIII Conference of Yugoslav Hydraulics Association. Portoroz, 1982.
33. Harkauli, A. N. General Comments on Q 50, 13th ICOLD, 1979, 513.
34. Husain, D.; Alhamid, A. A.; Negm, A. M. Length and depth of hydraulic jump on sloping floors. IAHR Jnl. of Hyd. Res, 1994, 32(No.6).
35. Kalinske, A. A.; Robertson, J. M. Closed conduit flow, Trans. ASCE, 1943.
36. Kawagashi, N.; Hager, W. H. B-jump in sloping channels-II. IAHR Jnl. of Hyd. Research, 1990, 28(No.4).
37. Khatsuria, R. M.; Balkrishnan, V. K. Two stage energy dissipator and appurtenant works – Ranjitsagar dam spillway, Punjab, 55th R&D Session, CBIP. Srinagar, 1989.
38. Khatsuria, R. M.; Deolalikar, P. B.; Bhosekar, V. V. Pull out forces on a concrete lined training wall in a stilling basin, 8th APD-IAHR Congress. Pune, 1992.
39. Khatsuria, R. M. State-of-art on role of turbulence in the design of spillway appurtenant structures, Technical Memorandum Published by Central Water&Power Research Station. Pune, 1994.
40. Khatsuria, R. M. Hydraulic and Structural Design Problems of High Head Stilling Basins, Intnl. R & D Conference—Water and Energy 2001, CBIP, New Delhi, Oct. 1995.
41. Khatsuria, R. M.; Deolalikar, P. B. Considerations on measurement of hydrodynamic bending moments on models of hydraulic structures, Proc. Ninth APD-IAHR Congress. Singapore, August 1994.

42. Khatsuria, R. M.; Deolalikar, P. B.; Bhosekar, V. V.; Sridevi, M. I. Energy dissipator for a low head high discharge intensity spillway, 3rd Intnl. R&D Conference, CBIP. Jabalpur, March 2000.
43. Kindsvater, C. E. The hydraulic jump in sloping channel, Trans. ASCE, 1943.
44. Locher, F. A. Some characteristics of pressure fluctuations on low-ogee crest spillways relevant to flow-induced structural vibrations, USWES, Report No. H-71-1, 1971.
45. Lopardo, R. A.; DeLio, J. C.; Vernet, G. F. Physical modelling of cavitation tendency for macroturbulence of hydraulic jump, Proc. Intnl. Conf. on Hyd. Modelling of Civil Engg. Structures, BHRA, 1982.
46. Lopardo, R. A.; Henning, R. E. Experimental advances on pressure fluctuation beneath hydraulic jump – Proc. 21st IAHR Congress. Melbourne, 1985.
47. Nakato, T. Model tests of hydraulic performance of Pit 6 dam stilling basin. ASCE Jnl. of Hyd. Engg, Sept. 2000, 126(No.9).
48. Narasimhan, S.; Bhargava, V. P. Pressure fluctuations in submerged jump. ASCE Jnl. of Hyd. Dn, 1976, 102(HY 3).
49. Narayanan, R.; Schizas, L. S. Force fluctuations on sill of hydraulic jump. ASCE Jnl. of Hyd. Div, 1980-a, 196m(HY4).
50. Narayanan, R.; Schizas, L. S. Force on sill of forced jump, ASCE. Jnl. of Hyd. Div, 1980-b, 106(HY 7).
51. Negm, A. M. Hydraulic jumps at positive and negative steps on sloping floors. IAHR Jnl. of Hyd. Res, 1996, 34(No.3).
52. Ohtsu, I.; Yasuda, Y. Hydraulic jump in sloping channels. ASCE, Jnl. of Hyd. Engg, 1991, 117(No. HY. 7).
53. Pennino, B. J.; Larsen, J. Measurement of flow induced forces on floor blocks, Pit 6 dam model studies, Alden Res. Lab Report No. 109-77/M 303 CF, July 1977.
54. Peterka, A. J. Hydraulic design of stilling basins and energy dissipators, Engineering Monograph No.25, USBR, 1978.
55. Peiqing, L.; Cheingui, L.; Dong, J. R. Using two dimensional instant fluctuation flow equation to analyse the transmision law of fluctuating pressure in the rock crack surface layers, Irrigation/Water Conservancy Journal, April 1996 (in Chinese).
56. Pillai, N. N.; Goel, A.; Dubey, A. K. Hydraulic jump type stilling basin for low Froude numbers. ASCE, Jnl. of Hyd. Engg, July 1989, 115(No.7).
57. Pinto, N. General Report on Q-71, Deterioration of spillways and outlet works, 18th ICOLD. Durban, 1994.
58. Rajaratnam, N. An experimental study of the air entrainment characteristics of hydraulic jump, Publication No.14/1960, I.I.Sc, 1960.
59. Rajaratnam, N. An experimental study of air entrainment characteristics of the hydraulic jump, Jnl of the Institution of Engineers (India), March 1962.
60. Rajaratnam, N.; Murahari, V. Flow characteristics of sloping channel jumps. Proc. ASCE Jnl. of Hyd. Div, 1974, 100(No.HY6).
61. Ranga Raju, K. G.; Mitall, M. K.; Verma, M. S. Analysis of flow over baffle blocks and end sills. IAHR Jnl. of Hyd. Res, 1980, 18(No.3).
62. Resch, F. J.; Leutheusser, H. J. The hydraulic jump – turbulence measurements in the two phase flow region – La Houille Blanche (4) –, 1972.

63. Rice, C. E.; Kadavy, K. C. Protection against scour at SAF stilling basins. ASCE Jnl. of Hyd. Engg, Jan.1993, 119(No.1).
64. Rouse, H.; Siao, T. T.; Nagaratnam, S. Turbulence characteristics of the hydraulic jump, Trans, ASCE, 1959.
65. Sharma, H. D.; Varshney, D. V. Stilling basins for hydraulic structures with low Froude numbers, Proc. 42, ARS, CBIP. Dehradun, June 1973.
66. Spoljaric, A.; Maskimovic, C.; Hajdin, G. Unsteady dynamic force due to pressure fluctuations on the bottom of an energy dissipator – An example, Proc. Intnl. Conf. on Hyd. Modelling of Civ. Engg. Structures, BHRA, 1982.
67. Suzuki, Y.; Sakurai, A.; Kakumoto, N. A design of a chute spillway jointly serving as a roof slab of a hydropower station, 11th ICOLD, Q 41 – R 21. Madrid, 1973.
68. Thandaveswara, B. S. Self aerated flow characteristics in developing zones and in hydraulic jumps. I.I.Sc, Bangalore, 1974, PH.D Thesis.
69. Toso, J. W.; Bowers, C. E. Extreme pressures in hydraulic jump stilling basins. ASCE, Jnl. of Hyd. Engg, 1988, 114(8).
70. Tullis, J. P.; Rahmeyer, W. J. Spillway models, Proc. Intnl. Conf. on Hyd. Modelling of Civil. Engg. Structures, BHRA, 1982.
71. USACE Hydraulic design of spillways- Engineer Manual 1110-2-1603, January 1990.
72. USBR Design of Small Dams, US Government Printing Office, 1977.
73. USBR Hydraulic design of stilling basins and energy dissipators, Engg Monograph No 25, 1978.
74. Vasiliev, O. F.; Bukreyev, V. I. Statistical characteristics of pressure fluctuations in the region of hydraulic jump, Proc 12th IAHR Congress. Fort Collins, 1967.
75. Vittal, N.; Al-Gaini, A. M. Modified type III stilling basin new method of design. IAHR, Jnl. of Hyd. Res, 1992, 30(No.4).
76. Zirong, Liu; Yuchunan, Xin Turbulence characteristics downstream of hydraulic jump, 22nd IAHR Congress Lausanne, September 1987.

21
Trajectory Buckets

21.1 INTRODUCTION

In the early twentieth century, engineers in France were considering various layouts of high head hydropower installations in the deep and narrow river valleys. The available waterways were often too narrow to accommodate spillway and power plant structures side by side. It was solely due to the imagination of Andre Coyne that a novel layout with a compact arrangement of the power plant and spillway, located one above the other, was evolved. The power plant was located at the base of the dam with the spillway above the power plant. The roof of the power plant was given the shape of an upturned circular arc that served to deflect the high velocity flow from the spillway above in the form of a jet trajectory. The scour hole formed due to the impingement of high velocity jet far away on the riverbed—composed of hard and sound rock—was of little concern, since it was at a considerable distance away from the structure and chances of retrogression towards the structure were remote. This arrangement, later to be named ''Saut de ski'' became very popular in France, Spain, and Portugal for the dams to be constructed on deep, narrow, and rocky gorges with limited waterways. The first series of dams so constructed were Mareges in 1931, L′ Aigle and Saint Etienne Cantales in 1938, and Chastang in 1943.

21.2 TYPES AND CLASSIFICATION

Different names are used by authors and designers in various countries to describe structures that employ hydraulic action of jet trajectory to accomplish energy dissipation; ski jump bucket, flip bucket, trajectory bucket, free jet spillways, and free over-falls. Mason (1982) defines ski jumps as jets issuing from the lower part of the main body of a dam and flip buckets as structures situated at the end of spillway chutes away from the main body of the dam, widely used in conjunc-

tion with earth and rock-fill dams where discharge directly through or over the dam is not possible. Rudavsky (1976) classifies ski jump energy dissipators into four arrangements.

However, in the opinion of the author, the term trajectory bucket covers all these structures, which could be further classified as ski jump buckets, flip buckets, and free jet spillways. In line with the original version of the saut de ski structures, the ski jump buckets are those located considerably above the river bed, with or without the power house below the bucket as shown in Figure 1. Flip buckets are based at the foot of the spillway or at the exit of a tunnel, at or near the riverbed as shown in Figure 2.

In a free jet spillway, the high velocity jet leaves from either a short crested spillway at the top of an arch dam or a deep seated short length bottom outlet, with its exit shaped in the form of a deflector, as shown in Figure 3.

This classification is meaningful as it seeks to highlight the differences in the shape and form of the trajectory as also the mechanism of energy dissipation. In a free jet spillway, the jet is subjected to air resistance and air entrainment whereby a significant portion of its energy is dissipated before it plunges into the tail water. Further dissipation of energy takes place by pool diffusion and impact. In a ski jump bucket, although the jet is subjected to air resistance and entrainment, the objective is to have it impinge at as large a distance as attainable so that the main dam is not endangered by the scour caused by the jet. In a flip

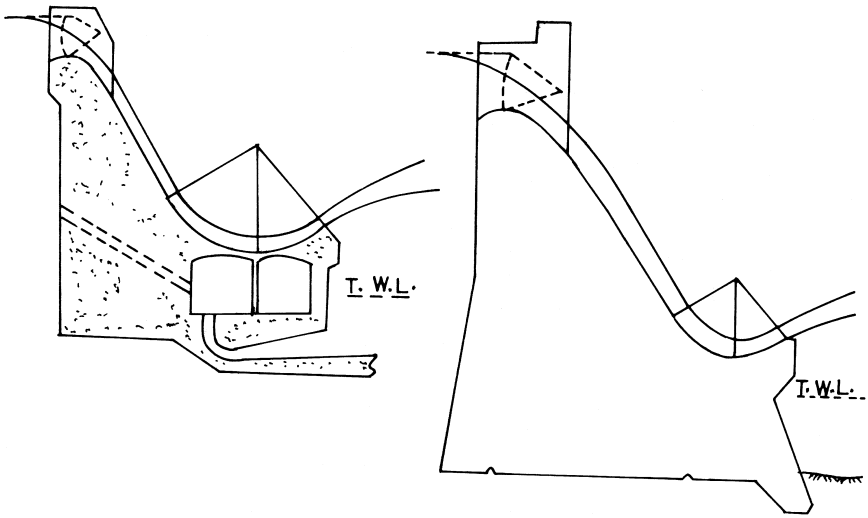

Figure 1 Ski jump buckets.

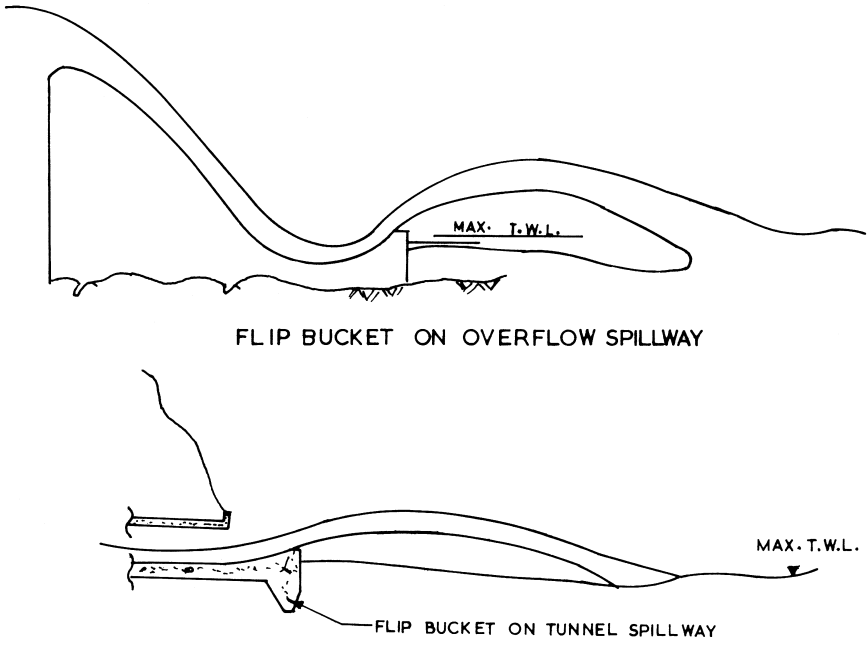

Figure 2 Flip buckets.

bucket, dissipation of energy is mainly through pool diffusion and impact as the jet being very close to the riverbed, air resistance and entrainment is limited to its top surface. In fact, in many flip bucket installations, the tail water levels are higher than the elevation of the bucket lip as a result of which the jet issuing from the bucket is submerged. The behavior of the jet in the free jet spillways and ski jump buckets is more akin to a three dimensional jet, that in the flip buckets the resemblance is more to a two dimensional jet.

21.3 DESIGN OF BUCKET COMPONENTS

The main components of bucket for which design guidelines are available include:

Shape of the bucket
Invert elevation
Bucket radius
Lip angle or exit angle

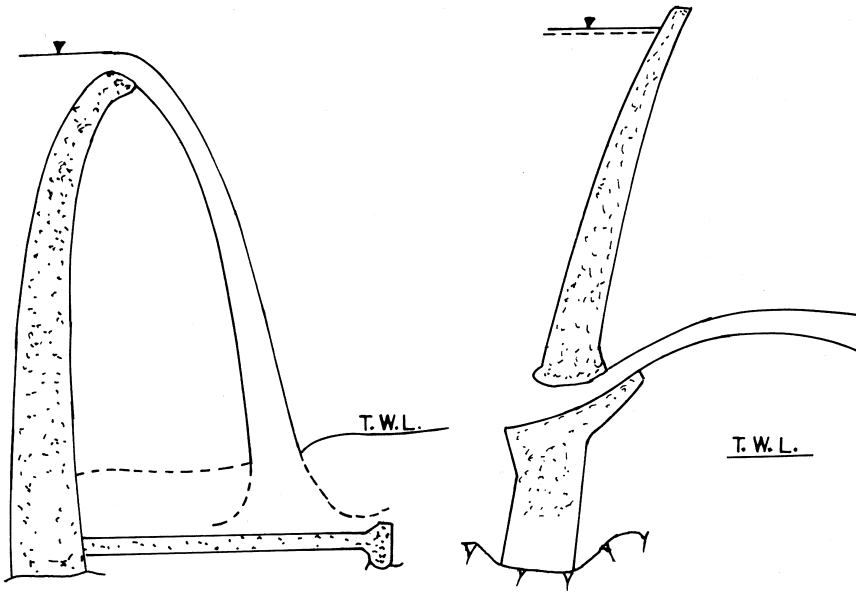

Figure 3 Free jet spillways.

Many of the guidelines emerge from practical experiences from the operation of the existing structures and a few from theoretical analysis and generally apply to both the ski jump and flip buckets. It may also be pointed out that although the above components have been grouped separately for ease of reference, many of these are interrelated.

21.3.1 Shape of the Bucket

Although it is claimed that a parabolic shape of the bucket results in a smoother water surface without increasing the size of the structure, as in the case of Anchor dam, US, the shape generally preferred is the circular one. Buckets made out of intersecting planes, warped, or compound surfaces have been used for special applications, but as Mason (1993) states ''few designers would have confidence in a bucket invert for high velocity flow formed by anything other than smooth curves'' tends to lean in favor for a circular arc. Even where the entrance to the bucket is parabolic, the portion downstream of the bucket invert is circular arc as in Amaluza, Equador, and Baishan, China.

21.3.2 Invert Elevation

Except in the case of ski jump buckets placed above the powerhouse, the invert level of the bucket is generally governed by the rock level available for the foundation. A designer would prefer this to avoid placing large quantity of concrete for keeping the invert at a higher elevation. The combination of invert elevation, bucket radius, and lip angle then decides the lip elevation, in conjunction with the tail water level, particularly if the latter is higher than the lip level. The cascading of the flow over the bucket lip and impinging at the base of the bucket, especially of small discharges in the case of low and medium head spillways, is yet another consideration while deciding the invert elevation.

21.3.3 Bucket Radius

A proper hydraulic action in the bucket is ensured if the flow in the bucket is concentric and there is no tendency of springing away, which could result in reduction of the contact pressure on the bucket surface. This tends to indicate that the radius R of the bucket is governed by the supercritical flow depth y_1 entering the bucket. Since y_1 is a function of the total head, the depth of overflow, and the discharge intensity, all these parameters influence the radius of the bucket. Recommended values vary from 3 y_1 to 7 y_1. Model tests for the bucket located immediately downstream of the gates of bottom outlet for Victoria dam in Sri Lanka with $R = 2.5\ y_1$ and for the Kettle Project, Canada with $R = 3\ y_1$ revealed that the flow did not smoothly follow the bucket profile and that the trajectory impinged on the river bed was too close to the bucket. For the flip bucket of the Guri Expansion Project, the radius of 3.33 y_1 was evolved as a result of model studies.

Various other formulae for bucket radius have been quoted from time to time, using factors such as depth of flow over the crest, total head, discharge intensity, Froude number, etc. Some of these are given here:

1. Varshney and Bajaj (1970) analyzed dimensions of the existing installations and derived the relationship

$$F^{0.5} = 0.06\frac{R}{y_1} + 1.96\ (\textit{in metric units}) \tag{1}$$

where

F = the Froude number of the flow entering the bucket.
y_1 = the depth of flow entering the bucket.

2. The radius expressed as the geometric mean of the depth of overflow and height of the spillway

$$R = \sqrt{h_d\, H} \tag{2}$$

where

h_d = depth of overflow.

H = Fall from crest to bucket invert.

3. KNS Rao (1978) on the basis of analysis of existing structures.

$$\frac{R}{y_1} = 11.534\, F^{0.5} - 9.113\, F^{0.25} \quad for\ 3 < F < 5.5 \tag{3}$$

$$\frac{R}{y_1} = 4.037\,(F - 3.7627) \quad for\ 5.5 < F < 10 \tag{4}$$

21.3.4 Lip Angle

The choice of lip angle is dictated by the requirement of the throw distance and the angle of impingement of the jet into the tail water. Theoretically, the maximum throw is achieved when the jet leaves the bucket at an angle of 45° and if the tail water level is at the same elevation as that of the lip level, the impingement angle is the same as lip angle. For tail water levels lower than the lip level, the impingement angle increases. In the case of ski jump buckets set high above the riverbed, such as L' Aigle dam, the lip angle may be much smaller, even horizontal and still a reasonable impingement angle would be attainable. Preferably, the height of the lip above invert may be 0.1 R for high dams and 0.125 R for low dams, which means that an angle of 26° to 29° would be preferable. In most of the installations, lip angles varying from 20° to 40° have been preferred. Based on the analysis of existing structures, Varshney and Bajaj (1970) have developed the following relationship for the lip angle θ;

$$F = 7.8 - 0.000091\ R\ \theta^3/h_1 \tag{5}$$

where

F = Froude number of the jet entering the bucket.

R = Radius of the bucket.

h_1 = Total head from pool to invert.

It must be noted that the flow exit angle generally is somewhat less than the bucket angle, because the bucket radius may be too small to turn the jet completely. Quadri et al. (1977) observed in the models that the effective jet angle θ_1 was related to the bucket angle θ, y_1, and R. They have presented the relationship in the form of curves as shown in Figure 4.

Yildiz et al. (1994-a) have presented a relationship between the bucket angle θ and jet impact angle to tail water, θ_2 as

$$\tan\theta_2 = \sqrt{\frac{\sin^2\theta + y_3 / h_o}{\cos\theta}} \tag{6}$$

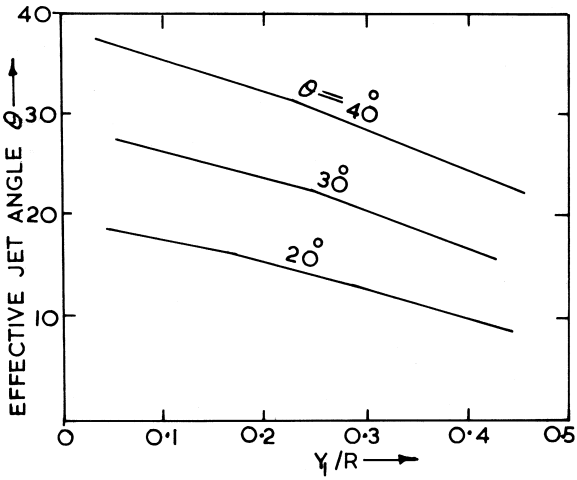

Figure 4 Effective jet angle.

where

y_3 = Difference between downstream water level and bucket lip.
h_o = Difference between upstream water level and bucket lip.

This relationship can be applied only when the tail water does not submerge the bucket lip.

Too small of a lip angle results in the so-called skimming flow at the tail water level causing waves and bank erosion whereas higher angles produce the jet penetrating deep into the tail water causing excessive scour. This is best illustrated by the example of model study for a high head spillway constructed in a deep and narrow gorge.

The bucket has been set about 25 m above the riverbed due to foundation problems. The trajectory issuing from the bucket would plunge into a 24 m deep tail water pool for the design discharge of about 38000 cumec. The lip angle (and consequently the angle of jet penetration) was to be such that would minimize scour on the flanks, return flow velocity at the flanks and water level fluctuations near the power house, situated on the right bank at about 450 m downstream of the bucket. Lip angles of 35°, 40°, 45°, and 60° were tested on an erodible bed model to observe the above parameters. Figure 5 gives summary of the results. It was seen that with increase in the lip angle, return flow velocity and water level fluctuations decreased, depth of scour increased but the area affected by the scour decreased. A 45° bucket was chosen as a result of the studies.

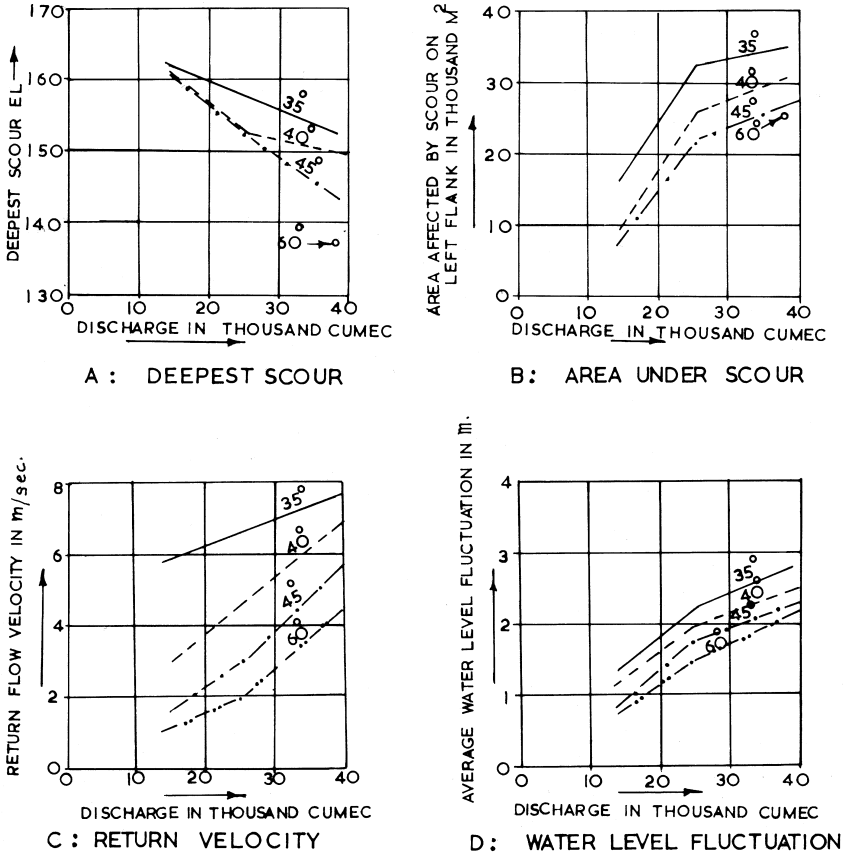

Figure 5 Determination of lip angle from model study.

21.4 HYDRAULIC CHARACTERISTICS OF TRAJECTORY BUCKETS

The hydraulic characteristics that are of interest in the design are:

Pressures on the bucket surface and side walls
Free jet trajectory and throw
Effect of submergence by tail water
Erosion of the riverbed

21.4.1 Pressures on Bucket and Sidewall

Investigations concerning pressures on the trajectory buckets were aimed mainly for the structural design of the bucket sidewalls. During the 1950s, the structural design of sidewalls often ignored the high centrifugal pressures caused by the flow in the curved buckets, and the walls of buckets often remained standing in a condition of near failure.

Studies for the estimation of bucket pressures can be grouped under the following four categories:

1. Inclusion of centrifugal pressure along with hydrostatic pressure.
2. Application of free vortex theory.
3. Complex analytical solutions based on mathematical modeling of flow in the bucket treating it as irrotational and incompressible.
4. Correlation based on results from model and prototype investigations.

Generally, the total pressure is the summation of hydrostatic and centrifugal pressures

$$P = y_1 + \frac{y_1 V_1^2}{g\,R} \tag{7}$$

Balloffet (1961) assumed that velocity distribution in the bucket was as in an irrotational vortex, i.e. VR = constant. His relationship for the pressure at the invert of the bucket is

$$P_{\max} = y_1 + V_1^2/2g\,(1 - ((R - y_1)/R)^2) \tag{8}$$

Chen and Yu (1965) considered a steady two dimensional potential flow and neglected the effect of gravity. Lenau and Cassidy (1969) assuming the flow to be irrotational and incompressible, obtained integral equations, the numerical solutions of which would yield velocity and pressure distribution. A simplified method based on perturbation solution neglects the effect of gravity, whose results are given in the form of relationship between the parameters $\frac{R\,C_p}{2y_1}$ and S/y_1 up to 9. Prasad (1984) has extended this relationship up to 32. A comparison of computed and observed pressure distributions in the case of a spillway bucket; (Fig. 6) shows that it is the best available analytical method.

Design charts based on correlation from model and prototype investigations have been developed by USBR and WES. While USBR charts have been derived from the data on flip buckets at the base of tunnel spillways, WES charts utilize data from the model and prototype observations on Pine Flat and Hartwell dams. These charts are reproduced in Figures 7 and 8, respectively.

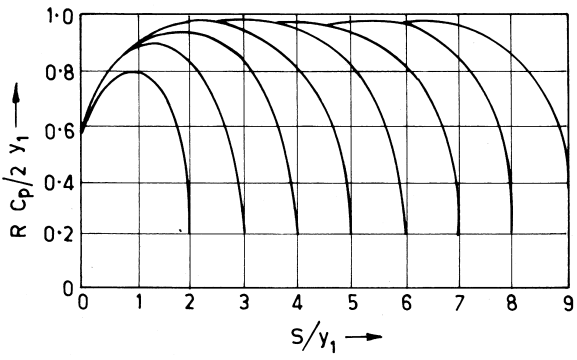

LENAU AND CASSIDY S' PRESSURE FUNCTION.

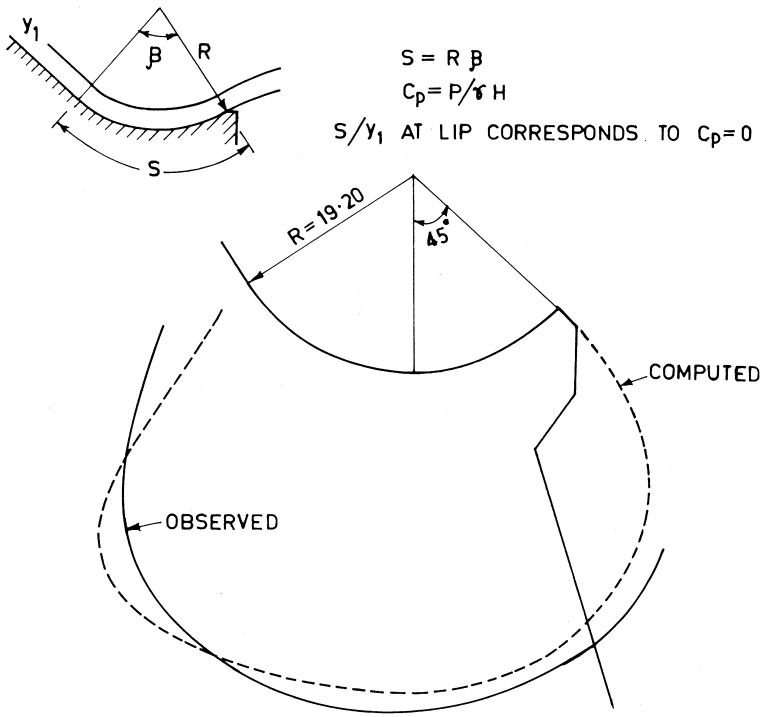

Figure 6 Pressures on bucket: comparison between the computed and observed values.

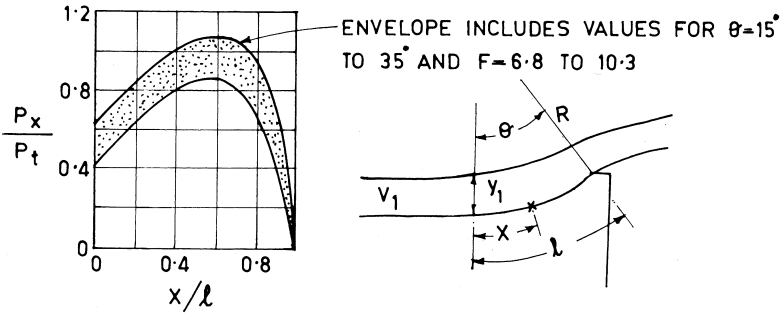

Figure 7 Pressures on flip buckets (shown in USBR 1978).

P_x = Pressure at point X

P_t = Theoretical pressure $\left(y_1 + \frac{y_1 V_1^2}{gR} \right)$

Balloffet's equation gives the value of maximum pressure to a reasonable accuracy. An alternative form of this equation

$$P = H_x - (H_x - y_1 \cos \phi) \left(\frac{R - y_1}{R} \right)^2 \tag{9}$$

can be used to obtain pressure distribution along the bucket curvature.

where

H_x = Head from reservoir upto any point x on the bucket

ϕ = Angle formed by the radii passing through x and the invert

However, this equation fails to predict the drop in the pressure over the downstream part of the bucket, particularly the lip. It can be obtained by means of simple flow net sketching. Analytical solutions by Chen and Yu and Lenau and Cassidy provide complete details. Design charts by WES and USBR also give indications about the variation that can be expected. For major works, hydraulic model studies are the best means of obtaining reliable results.

Pressures at the bucket lip can also be affected by the angle of the downstream portion of the bucket lip as shown in Figure 9. The curve in this figure shows the relation between pressure and the angle β. It can be seen that this angle should not be less than about 40°. This may, however, pose some problem in connection with inspection of lip and bucket as in such a case, the lip cannot be used as a walkway.

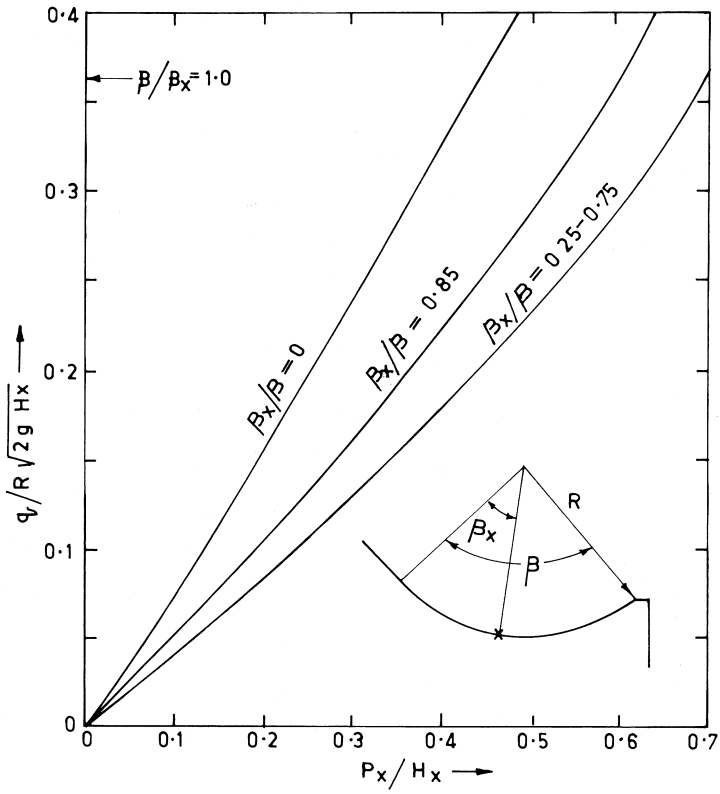

Figure 8 Pressures on flip buckets (shown in WES-HDC 112-7).

The curves of Figure 10 indicate the pressures to be expected on the sidewalls. It can be seen that for a lip angle of 35°, the maximum pressure is about eleven times as great as hydrostatic and occurs near the base of the wall at about x/l = 0.75, whereas near the lip x/l = 0.99, it is only four times as great as hydrostatic. The curves also show the effect of radius, lip angle, and location on the bucket surface on pressures. The variation of pressure on a vertical on the sidewall is nonlinear because of variation in fluid density with air entrainment.

Mason (1993) suggests that sidewall design loading can be based either on solid water or on a greater air entrained depth with a lower effective water density. Shear forces on the walls will be the same in both cases, but bending moments will be higher in the latter case. It is recommended that the latter case be adopted for the design. Roose et al. (1973) have reported that the depth of air water mixture may be as high as 2.5 times the clean water depth. Since the height of

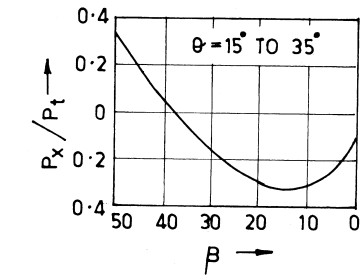

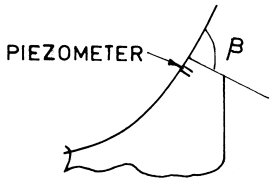

P_x = MEASURED PRESSURE
P_t = THEORETICAL PRESSURE

Figure 9 Pressures at the end of bucket. (Shown in USBR, 1978)

the side walls have to be adequate to include the effect of air entrainment, surface waves and sprays, it is advisable to provide a height of about 3 times the depth observed in the model or calculated based on clean water.

21.4.2 Free Trajectory and Throw

The profile of the trajectory leaving a bucket depends on the velocity at the bucket lip and lip angle. The jet trajectory can be computed on the basis of projectile theory, resulting in the following expression by WES -HDC 112-8,

$$X / H_v = Sin\ 2\theta + 2 \cos \theta (\sin^2 \theta + y / H_v)^{0.5} \quad (10)$$

where

X = Throw distance at the point the jet strikes the tail water
y = Vertical drop from lip to tail water level
H_v = Velocity head of jet at bucket lip
θ = Lip angle, degree

Various parameters are shown in Figure 11.

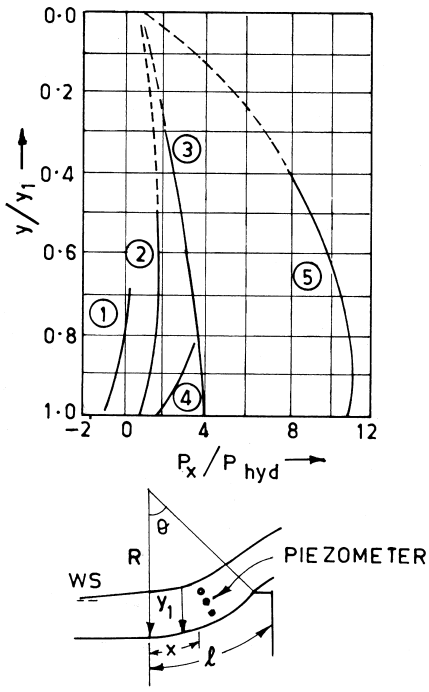

Figure 10 Pressures on side wall. (Shown in USBR, 1978)

① $\theta = 15°$, $x/l = 0.99$, $R/l = 3.73$
② $\theta = 15°$, $x/l = 0.99$, $R/l = 3.82$
③ $\theta = 15°$, $x/l = 0.26$ to 0.80, $R/l = 3.82$
④ $\theta = 35°$, $x/l = 0.99$, $R/l = 1.62$
⑤ $\theta = 35°$, $x/l = 0.75$, $R/l = 1.62$

y_1 = Vert. Dist. from WS to floor
y = Vert. Dist. from WS to piezometer
P_x = Measured pressure
P_{hyd} = Hydrostatic pressure

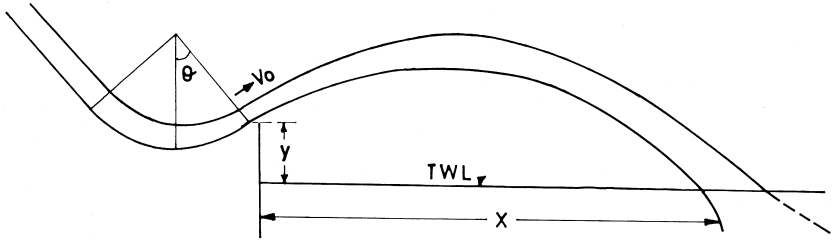

Figure 11 Throw distance of jet.

The factor H_v is to be accounted allowing for the head loss up to the bucket lip. Peterka (1978) has presented charts for throw distances for the flip buckets at the base of tunnel spillways, where a horizontal length of tunnel portion is preceded by the bucket.

It is found that air resistance, particularly for velocities exceeding 20 m/s, affects the throw distance in a prototype. Kawakami (1973) presented results of some field investigations of trajectories affected due to air resistance and introduced a coefficient k for the following equations

$$y = (1 / gk^2) \ln (\cos v + \tan \alpha \sin v) \quad (11)$$

$$L_1 = (1 / gk^2) \ln (1 + 2k \alpha V_o \cos \theta) \quad (12)$$

Where

$$\alpha = \tan^{-1} (k V_o \sin \theta) \quad (13)$$

$$v = (\exp (g k^2 x) - 1)/k V_o \cos \theta \quad (14)$$

where

x and y are cartesian co-ordinates
V_o = velocity at the lip
θ = lip angle
L_1 = throw distance considering air resistance
k = Constant related to air resistance

Figure 12 shows empirical relationship between V_o and k and also L_1/L_o corresponding to various values of V_o, where L_o is the throw distance without considering air resistance.

It would be seen that the effect of air resistance is small whenever V_o is less than about 20 m/s but it reduces the throw distance by about 30% when the velocity is about 40 m/s.

Rae et al. (1994) estimated, indirectly, the throw distances of some trajectories in prototypes from the distances of deepest scours and compared with those calculated using Equations 12 and 15. The pertinent details are given in Table 1.

It was found that the distances calculated by using Kawakami Equation 12 agreed well with the measured distances, whereas the values obtained using the theoretical equations were about 1.15 to 1.25 times the measured values.

21.4.3 Effect of Submergence by Tail Water

The bucket lip should normally be placed above the tail water level for all flow conditions. This is particularly desirable for high head dams where high velocity flow meeting relatively still water could lead to cavitation and damage. However, for dams on wide and flat rivers, as in India, placing the bucket lip above the tail water may involve placing large quantity of concrete or masonry.

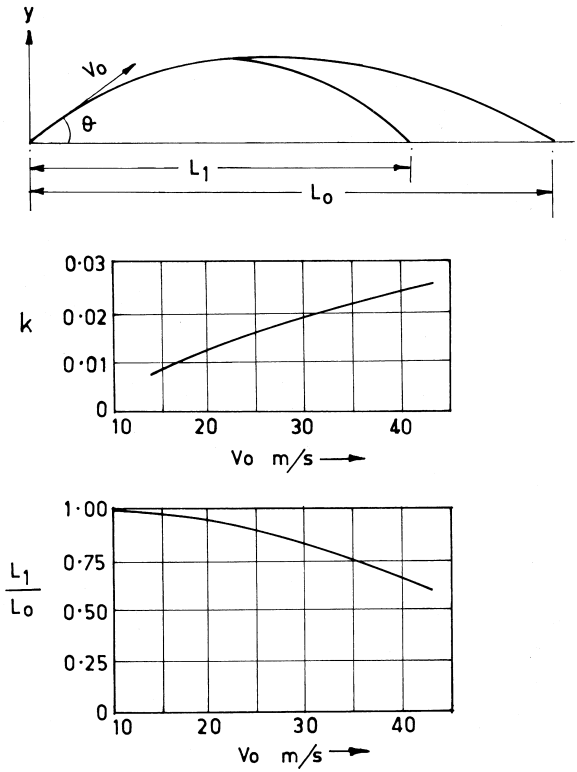

Figure 12 Effect of air resistance on jet trajectory. (Shown in Kawakami, 1973)

Submergence of lip has the following implications:

- Flow instability at bucket lip followed by reduction in pressure down to sub-atmospheric with increase in submergence. Beyond certain depth of submergence, the pressures become highly positive.
- Reduction in the throw of the trajectory.
- Reduction in the scour.
- Fall-back of the trajectory into the bucket and functioning as a submerged roller bucket for very high submergence.

Figure 13 depicts various stages of performance of a typical jet leaving the bucket as affected by submergence of the lip by tail water. It can be seen that tail water depth above the lip exerts a force in the upstream direction, as though trying to push the jet swing towards upstream. Initially, this results in loss of contact of

Table 1 Estimation of Trajectory Dimensions (shown in Rae et al. 1994)

			Trajectory height, m			Trajectory throw, m		
Lip Angle	Head m	Velocity m/s	Theoretical	Kawakami	Measured	Theoretical	Kawakami	Measured
20°	98.5	34.9	10	7.5	7.0	114	67	57.9
20°	70.4	29.5	7.5	5.0	5.2	77	50	48.2
30°	98.5	34.9	22.0	15.0	14.3	155	83.3	53.3
30°	70.4	29.5	16.3	10.0	13.1	111	63.9	45.7

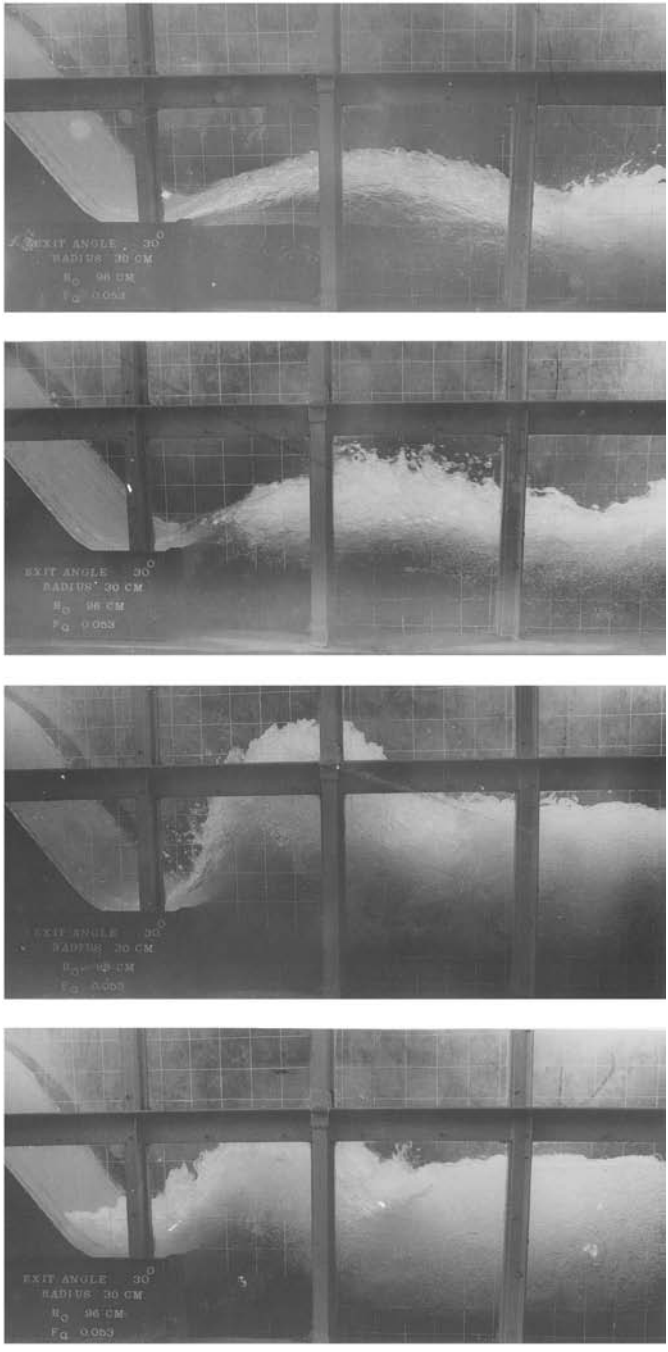

Figure 13 Various stages of transformation of ski action into roller action.

the jet with bucket surface just near the lip, resulting in negative pressures in that region. With the increase in the submergence, the separation can no longer be sustained and high positive pressures result. The most visible effect of submergence is the virtual increase (α) in the lip angle. The resultant angle ($\theta + \alpha$) up to about 45° would increase both the height and the throw of the trajectory, beyond which the trajectory would tend to be compressed and finally fall back into the bucket - the initiation of roller action.

Chavarri et al. (1979) have described cavitation damage that resulted due to negative pressures on the bucket lip of Guri dam spillway in Venezuela, in the initial stage of the project, when the bucket lip was placed below the tail water level. The remedial measures included addition of a small wedge 0.75 m long to the lip as shown in Figure 14, to maintain positive pressures on the lip. Based on this experience, a similar wedge was provided on the bucket lip of Itaipu spillway also. In the final stage of Guri project, the bucket was raised 4 m above the tail water level.

Virtual increase in the lip angle would cause the depth of scour to increase (because of increase in the angle of penetration of the jet) but would also provide

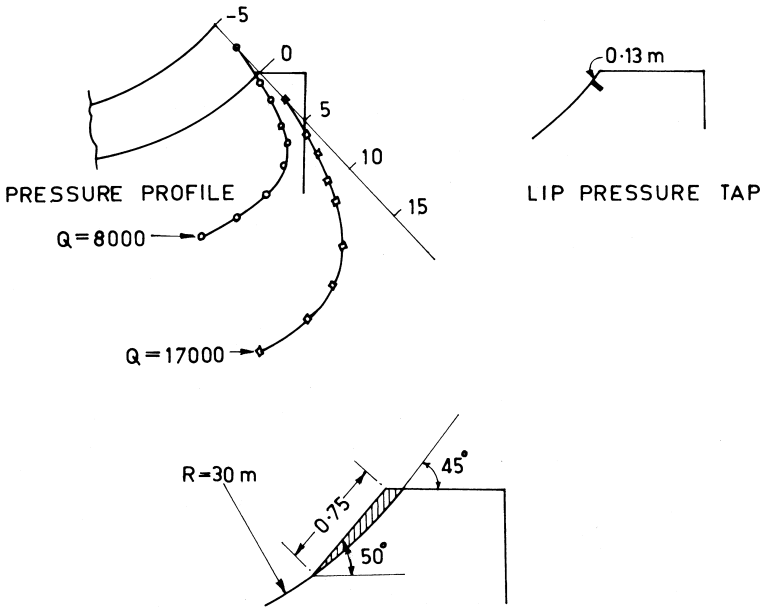

Figure 14 Addition of wedge to the bucket lip of Guri dam spillway (shown in Chavarri et al.1979).

larger tail water depth increasing dissipation of energy by pool diffusion. Varshney (1975) has presented a graph showing relationship between the apparent increase in the lip angle α with TW/y_1, ignoring other parameters like q , V_1, R, etc. A more refined analysis can be made applying momentum theory to a control volume (a b c d e a), as shown in Figure 15. It must be noted that the high velocity jet leaving the bucket lip would entrain some discharge from the tail water pool so that q_2, V_2, and y_2 are different from q_1 , V_1, and y_1. However, estimation of q_3 is difficult and can be assumed negligible for the purpose of preliminary analysis.

The analysis involves resolving all forces in the x and y directions and correcting for the error due to assuming $q_3 = 0$. Finally,

$$\tan\alpha = \frac{0.5\, y_3^2 \sin\theta}{\frac{q_1 V_1}{g} + 0.5\, y_1^2 - 0.5\, y_3^2 \cos\theta - \frac{y_3 \sin\theta}{\sin(\theta+\alpha)}\left[y_1 + \frac{y_3 \cos(\alpha+\theta)}{2}\right]} \quad (15)$$

Equation 15 can be solved, first by assuming $\alpha = 0$ on the right hand side and then inserting the value of α obtained thus until the desired convergence.

Evaluation of α would also be necessary for computing the profile of the trajectory under the effect of submergence, with the bucket lip angle replaced by $(\theta + \alpha)$. It is, however, imperative to account for the spillway energy losses up to the bucket lip in the values of V_1 and y_1.

A limited amount of experimental data, as shown in Figure 16, shows that the depth of maximum scour would decrease with the increase in the submerg-

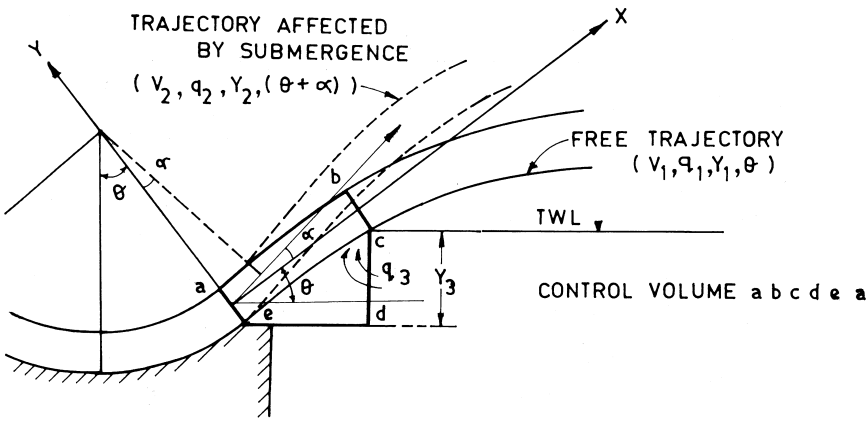

Figure 15 Apparent increase in lip angle due to submergence.

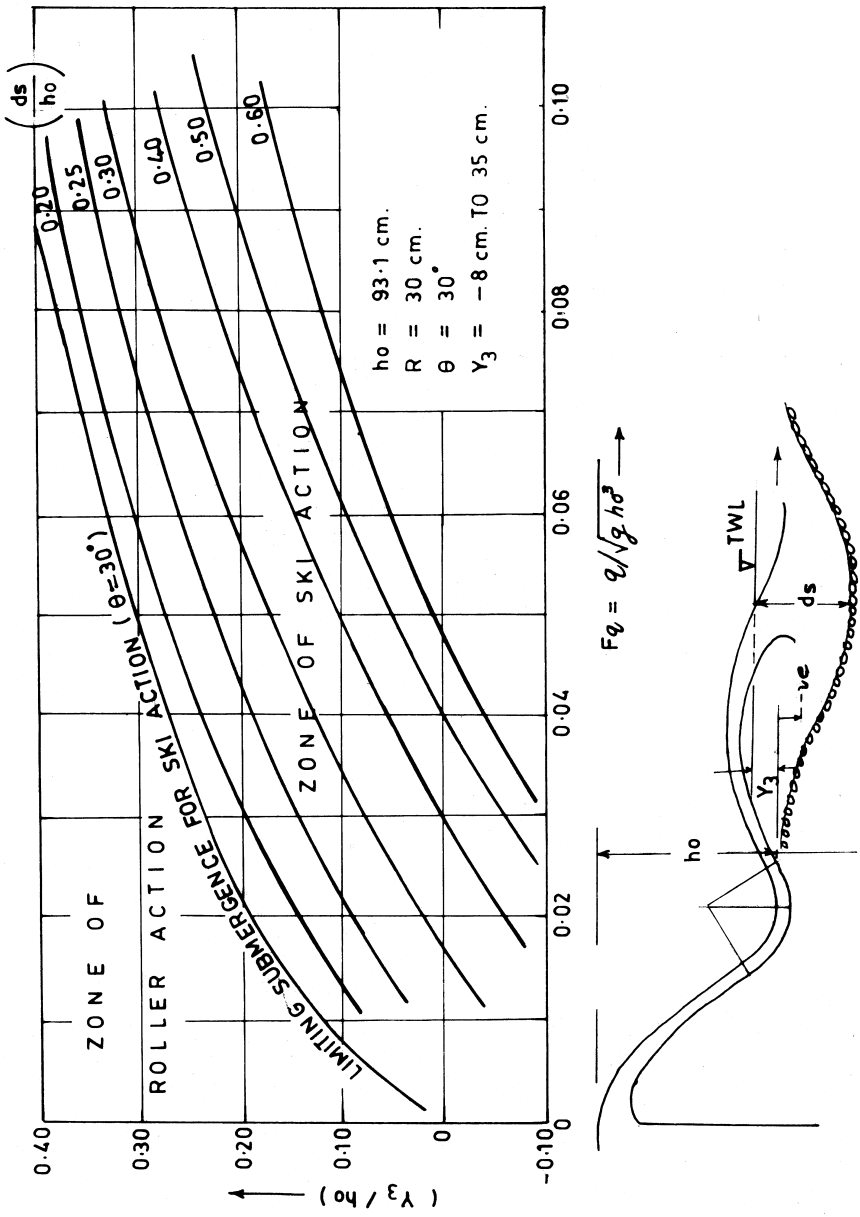

Figure 16 Effect of submergence on scour.

ence of the lip, until the roller action sets in, causing a radical change in the flow conditions.

Transformation of ski action into roller action can also be analyzed applying momentum equation at the bucket lip. Kelkar and Khatsuria (1975) obtained

$$Cos\theta\left[C\sqrt{2}F_q + \frac{F_q^2}{4C^2}\right]\left(\frac{y_3}{h_o}\right) = F_q^2 + \frac{1}{2}\left(\frac{y_3}{h_o}\right)^3 \tag{16}$$

where

C = a coefficient to account for the losses along the spillway surface and curvature effect of the bucket.

F_q = discharge parameter = $q / \sqrt{g\, h_o^3}$

y_3 = depth of submergence causing transformation of ski-action into roller action.

h_o = head from reservoir level to bucket lip level.

Figure 17 shows the above relationship assuming value of C as unity. Experimental results for lip angles of 30°, 35° and 40° are also plotted which indicate that C would be less than unity. The authors suggest that

$$C = C_1 \times C_2 \tag{17}$$

Where C_1 is the coefficient of velocity reduction due to losses along the spillway surface due to friction and C_2 is the coefficient of velocity reduction due to curvature effect of the bucket. C_1 can be assessed from the data presented by

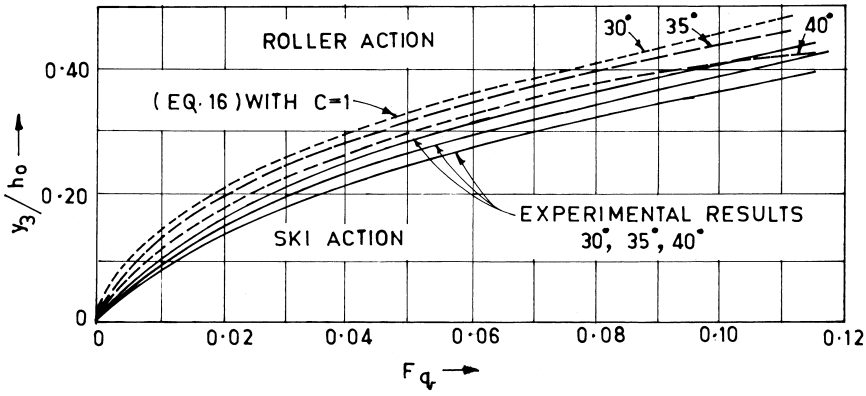

Figure 17 Transformation of ski action into roller action. (From Kelkar et al. 1975)

Peterka (1978) and Cabelka (1955). The coefficient C_2 representing reduction of velocity due to bucket curvature effect can be estimated, assuming the flow in the bucket as an irrotational vortex

$$\frac{y_1}{R} = \frac{R_1}{R}.\ln\frac{R}{R_1} \tag{18}$$

Where R_1 is the radius of the free surface of the flow in the bucket. Thus, $(R\text{-}R_1)$ is the depth of flow in the bucket, from which the velocity and hence C_2 can be assessed.

Equation 15 can also be used to estimate y_3 corresponding to the transformation of ski-action into roller action with the application of classical hydraulic jump equation at lip level

$$\frac{y_3}{y_1\cos(\theta+\alpha)} = \frac{1}{2}\left(\sqrt{1+8F_s^2}-1\right) \tag{19}$$

$$\text{Where } F_s = \frac{V_1 Cos(\theta+\alpha)}{\sqrt{g y_1\cos(\theta+\alpha)}}$$

This is solved by trial and error for assumed values of y_3 until Equation 19 is satisfied.

Some designers consider the tail water depth equal to the critical depth y_c as the threshold of transformation. This criterion appears to be based on a simple assumption that when the depth of submergence exceeds the critical depth of flow over the bucket lip, a phenomenon similar to a hydraulic jump would occur over the bucket lip, resulting in transformation of ski action into roller action. This approach, neglects the equally important parameter of the energy head. It is possible to express Equation 16 to obtain ratio $\left(\frac{y_c}{h_0}\right)$ in terms of F_q and $\left(\frac{y_3}{h_0}\right)$.

$$\left(\frac{y_3}{h_0}\right)\left[\frac{2\sqrt{2}C}{F_q}+\frac{1}{2C^2}\right]Cos\theta - 2 = \left(\frac{y_c}{y_3}\right)^3 \tag{20}$$

From this equation, for the range of discharge parameters 0.03 to 0.10, commonly encountered in practice, the ratio $\left(\frac{y_c}{h_0}\right)$ for a lip angle of 40°, assuming C as unity, works out to be between 2.5 and 1.9. It is also seen from the data on the existing flip buckets that this ratio could be as high as 1.93.

Laxmanswami et al. (1972) have reported that in the case of low Froude number buckets (F_1 up to about 4.5), a satisfactory trajectory action with a clear throw may not occur even though the tail water is below the bucket lip level. Their results are shown in Figure 18

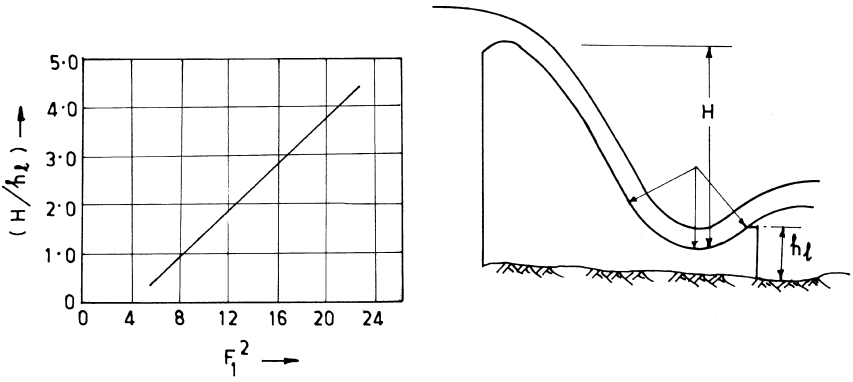

Figure 18 Low Froude number buckets. (Shown in Laxmanswami, 1972)

where

H = height of the spillway from crest to invert
h_l = difference between lip level and river bed
F_1 = Froude number at the bucket invert

For values below the line shown, the bucket is expected to function as a trajectory bucket with a clear throw and aeration beneath it.

Illustrative Examples

For the flip bucket with the following characteristics, determine the tail water depth at which the ski action would turn into roller action.

Unit discharge q = 50 cumec/m: Head from RWL to bucket lip level = 60 m
Velocity at lip level = 33.9m/s: Depth of flow y_3 = 1.476 m: Lip angle = 30°

1. Equations 15 and 19:
   Starting with an assumed depth y_3 of, say 10 m, and $\alpha = 0°$, the first estimation of α is 19.04°. Then, with $(\alpha + \theta) = 49.04°$, the revised estimation is $\alpha = 14.17°$. Successive trials converge to $\alpha = 14.75°$. With $(\alpha + \theta) = 44.75°$, the Froude number F_s = 7.5. The right hand side of Equation 19 is then 10.6. $y_1 = 1.476$ m and y_3 = 10 m yield the left hand side at 9.45. Hence, another trial with a revised value of y_3 is necessary. Finally, $y_3 = 10.5$ gives $\alpha = 17°$, $F_s = 7.35$, the right hand side of Equation 19 as 10 and the left hand side as 10.4, which is considered acceptable.

2. Equation 16 and Figure 17

   Discharge parameter $F_q = 0.034$ and $\theta = 30°$ gives $\left(\frac{y_3}{h_0}\right) = 0.22$. Hence, $y_3 = 13.2$m.

   The difference between the two values is considerable. This can be explained as follows: In the derivation of Equation 15, the depth y_3 is considered to be just downstream of the bucket lip. This depth is lower than the actual tail water depth measured downstream of the trajectory, due to the tail water drawdown effect, observed on many projects. On the other hand, the curves shown in Figure 17 are based on observations on models that were made sufficiently down stream of the trajectory.

21.5 SCOUR DOWNSTREAM OF TRAJECTORY BUCKETS

Although the choice of trajectory buckets is restricted to sites where generally sound rock is available in the river bed, occurrence of scour downstream of the spillway is, however, a major consideration in the design of such spillways. Not only the safety of the main structure but also that of the adjacent structures, together with ancillary works such as training walls, guide bunds, power outlets, etc. have to be considered.

Mason (1984) reports from the prototype experience on several projects that unacceptable scour is by no means limited to soft rocks and that in many of the cases such scour has occurred in conjunction with hard igneous rocks also. Often rocks weighing several hundred tons have been displaced by the flow. There are also indications as though the scour has a tendency to approach towards the structure—a phenomenon that was never considered to be likely in the original concept. This is indeed a potential threat to the stability of the structure and special protection works are necessary to avert this danger.

The designer is concerned with the following aspects:

Computation or prediction of scour under various operating conditions.
Analysis to assess the likely effects of scour vis-à-vis the stability of the structure.
Scour control and remedial measures.

21.5.1 Computation and Prediction

The different approaches for estimation of depth of scour can be classified under four general groups:

Theoretical analyses coupled with laboratory investigations.
Theoretical analyses coupled with prototype observations.
Empirical relationships based on prototype observations.
Laboratory experiments for specific project

Relationships developed vary from those extensive involving a host of parameters such as discharge, head, bucket geometry, downstream water depth, and rock mechanic characteristics including jointing pattern, compressive strength, and block size to those simple relationships containing only the parameters of discharge, head, and downstream depth regardless of rock characteristics. It may, however, be pointed out that application of scour depth formulae is limited to the estimation of the maximum depth of scour likely to occur during the operation of the spillway over the years. This information in itself does not serve the purpose because other aspects such as areal extent of scour, pattern of scour adjacent to the structure, and variation of scour as related to the minor changes in the structure geometry are far more important for the designer. The use of complex relationships is often fraught with the difficulty of ascertaining rock mechanic characteristics (requiring in-depth investigations) and which after all, offer almost the same result as could be obtained by using very simple relationships. Based on the experience, Damle's relationship

$$d_s = A\ (g\ h_o)^{0.5} \tag{21}$$

evolved in 1966, from the results of model studies, substantiated with the limited data from six prototype structures, gives reliable information on depth of scour.

where

d_s = Depth of scour below tail water level, meter
q = Discharge intensity cumec/meter
h_o = Head from reservoir level upto the bucket lip level, meter
A = Coefficient indicating status of scour:

0.65: Ultimate maximum scour
0.54: Probable scour under sustained operation
0.36: Minimum expected scour

The author re-evaluated the constant A, when more information from prototypes became available. Accordingly, the value of A is 0.90 instead of 0.65 corresponding to the ultimate state of scour. Figure 19 shows the relationships evolved.

Mason and Arumugam's (1985) analysis of scour development at Kariba dam, in terms of jet power per unit area and the volume of material scoured, indicated that the depth of scour was a function of $(q\ h_o)^{0.5}$, which agrees with the proposition of Damle. In fact, Damle's is the only formula that relates the jet energy to the depth of scour, ignoring the effect of other parameters. This

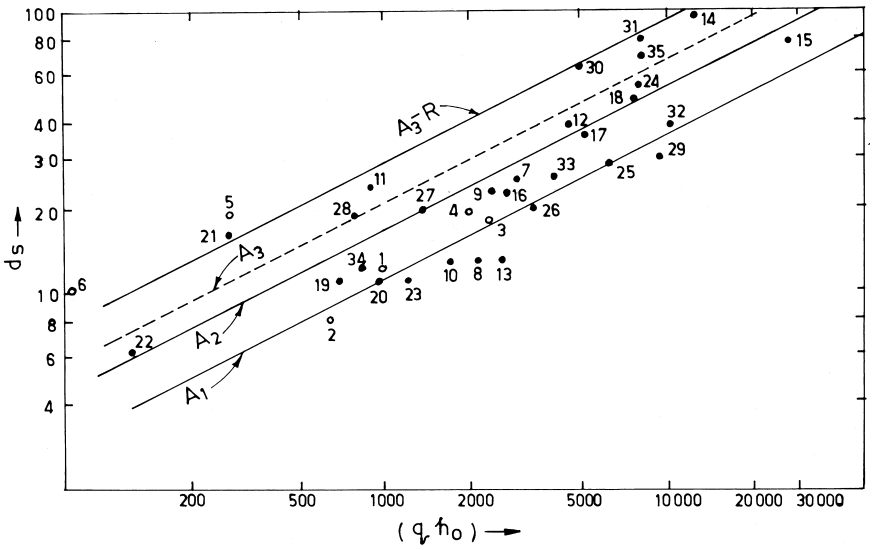

Figure 19 Modified Damle formula based on data from prototype.

$A_1\ d_s = 0.36\sqrt{g\ h_o}$ (Minimum)
$A_2\ d_s = 0.54\sqrt{g\ h_o}$ (Probable)
$A_3\ d_s = 0.65\sqrt{g\ h_o}$ (Ultimate)
A_3-R $d_s = 0.90\sqrt{g\ h_o}$ (Ultimate-Modified)

Original data (1966) ○ and New data ●

1 Maithon
2 Panchet Hill
3 Hirakud
4 Gandhisagar (1962)
5 Mandira
6 Tilaiya
7 Gandhisagar (1973)
8 Ukai (1973)
9 Ukai (1976)
10 Dantiwada
11 R.P.Sagar
12 Srisailam (1983)
13 Pandoh
14 Kariba
15 Cahora Bassa
16 Tarbela
17 Tarbela
18 Tarbela
19 Conowingo
20 Elmali
21 Farkhad
22 Kondopoga
23 Getalsud
24 Picote
25 Kukuan
26 Wuchien
27 Tienlung
28 Houling
29 Shihman
30 Srisailam (1993)
31 Srisailam (1998)
32 Karkaya
33 Keban
34 Kilickaya
35 Itaipu (1983)

form of equation is, however, not dimensionally homogeneous. Dimensional considerations require that the equation have the form

$$d_s = \text{constant x } (q\ h_o / \sqrt{g}\ )^{0.4} \tag{22}$$

The value of constants worked out from 37 sets of data indicated that the constants would have the values as

0.9–1.3: minimum
1.4–2.3: probable
2.4–4.5: ultimate

A relationship evolved by Mason et al. (1985) has the form

$$d_s = 3.27 \frac{q^{0.6} H_t^{0.05} h_{ds}^{0.15}}{g^{0.3} d_m^{0.06}} \tag{23}$$

where

H_t = head from reservoir upto tail water
h_{ds} = tail water depth above original river bead
g = acceleration due to gravity
d_m = bed material mean particle size

Mason (1993) has recommended that in the absence of any other data, the mean bed particle size d_m can be taken as 0.25 m.

Mason (1989) demonstrated that the head drop H_t may not directly affect the scour depth, other than by varying the amount of air entrained in the plunge pool. This is in turn affects the force on particles of bed material. An alternative expression that better described the scour process was therefore proposed.

$$d_s = 3.39 \frac{q^{0.6} (1+\beta)^{0.3} h_{ds}^{0.16}}{g^{0.3} d_m^{0.06}} \tag{24}$$

For free jet spillways such as those on the crests of arch dams, Veronese formula is generally applied in which the volumetric air to water ratio β in the plunge pool is as defined by Ervine (1976).

$$d_s = 1.90\ q^{0.54}\ H_t^{0.225} \tag{25}$$

Attempts have been made to generalize this formula as

$$d_s = K_r\ q^{0.54}\ H_t^{0.225} \tag{26}$$

Where K_r is related to the rock mass characteristics and takes values between 0.25 and 2.5.

Yildiz et al (1994-b) suggest that for applying this formula to spillways with flip buckets etc, it should be modified to

$$d_s = 1.90\ q^{0.54}\ H_t^{0.225} \sin\ \theta_2 \tag{27}$$

Where θ_2 is the jet impact angle at tail water surface (Eq. 6).

Since scour depth estimation by empirical relationships has limited utility, a hydraulic model is usually tested to examine the potential scour and, perhaps more importantly, any interaction of scour with structure geometry and hydraulic conditions. However, a physical model has its limitations too in simulating the entire process of rock scouring. The process of rock scouring with trajectory buckets has three distinct phases: fracturing of rock into blocks of various sizes as a result of dynamic pressures in the fissures and discontinuities in the rock mass, pulling out, and disintegration and transport of rock blocks by the flow forces to outside the zone of fracturing, thus producing a scour hole and a downstream mound. It is almost impossible in a model to simulate the entire process of fracturing, pulling out, and disintegration and transport of rock blocks. Therefore, most model tests employ a downstream bed simulated with cohesionless fractured material that could atleast be transported by the flow, out of scour hole. This approach of fully erodible bed results in what is usually considered as established or ultimate scour. The erodible material is a mixture of sand and pea-size gravels. In the case of narrow and steep valleys, flaky material consisting of stone metal is an obvious choice for molding steep slopes. The difficulty with cohesionless bed is that the resulting dish-shaped scour hole in the model overestimates the areal extent and is unable to predict steep sides and secondary scour patterns near the structures, so important from designers' view point. In a few cases, semi-erodible material composed of some weakly binding additive like gypsum, bentonite, etc. has been used to obtain steep side slopes of scour holes and secondary scour patterns. Several compositions of the semi-erodible material are tested in the model and the one that gives the maximum depth of scour in the model, as indicated by any of the scour equations of the choice, is selected for detailed investigations.

21.5.2 Analysis

The interpretation and application of model results require a good deal of experience and judgement on the part of a designer. The problems often arising in a design are:

1. What is the extent of scouring that should be expected to occur in the prototype in respect to its depth, location, and shape, against that indicated by the model?
2. Whether there is any possibility of scour working back towards upstream endangering the stability of the structure?
3. To what depth, foundation of bucket lip, training wall, etc. be taken considering the scour depths along such structures obtained from a fully erodible bed model?

The first question is concerning the model-prototype conformity in respect of magnitude and location of scour. The scour profiles observed in the model and prototype on the spillways of several dams in India and elsewhere tend to indicate

that the depth of scour in the prototype may eventually approach that indicated by the model with an erodible bed.

Prototype experience from a number of projects also tends to indicate as though the scour has a tendency to approach towards the structure, threatening the stability. In an idealized situation, the scour is expected to be confined to the impact area of the jet on the riverbed. However, with a possibility of its progression towards the upstream, elaborate and expensive protection works had to be undertaken on a number of dams to protect the buckets against undermining due to scour approaching very near the structure. Indiscriminate operation of the spillway, such as those involving passing the discharges through a limited number of spans at design head with lower tail water depths and those passing large discharges through sluices opening out in the buckets or unsymmetrical opening of spillway spans, generally cause lateral spreading of the jet with shorter throw, resulting in scouring very near the bucket. These aspects can be studied on a model to devise a pattern of spillway operation to avoid such situations.

Application of the model results for determining foundation levels of the buckets and adjacent structures require consideration of several factors and calls for the experience and judgement on the part of the designers.

Other related issues that are often debated in connection with scour are the influence of geology, air entrainment, and time on scour.

It has been observed that major scour holes have developed in massive hard rocks such as granite and gneiss as with weaker sedimentary rocks. The process of scouring is also observed to be rapid. In general, it has been concluded that it is the characteristics of the rock mass (represented by macro-structure with jointing pattern, fissures, cracks, etc.) and not of the rock material, which is relevant to the scouring process and the shape of the scour holes tends to depend more on hydraulic factors than on geological ones.

Experimental investigations suggest that small amounts of entrained air were found to significantly reduce scour depth and to increase the minimum jet velocity required to initiate motion of the bed material.

As for the influence of time, it is seen that scour progresses remarkably rapidly and hence, time can be ignored as a parameter, and thus, the concept of a maximum ultimate scour depth can be accepted for all practical purposes.

21.5.3 Scour Control and Remedial Measures

Complete elimination of scour is hardly practical since it requires prior treatment of bed rock which may involve filling of fissures and joints with concrete, laying of concrete raft, creation of water pool by a subsidiary check dam in the downstream, etc.

The extent and location of scour hole can be controlled either by the creation of a pre-excavated plunge pool or incorporating structural modifications in the bucket shape and geometry.

The principle of pre-excavated plunge pool is to control the progression of scour by excavating in advance the area downstream of the bucket corresponding to the configuration and dimensions of a stabilized scour hole obtained in a model. If a plunge pool is considered to be the total replacement of scour, the depth of excavation would be governed by Hartung and Hausler's (1973) analysis of diffusion of water jets within a stagnant infinite mass of water. The jet behavior is continued at least for a depth equal to about 40 times the jet thickness with about 30% residual energy still imparted at that depth. Taraimovich (1978) has presented guidelines for the shape and dimensions of the plunge pool. Recommendations for the design of concrete-lined plunge pools have been given by Ramos (1982) and Martins et al. (1994).

In the case of free jet spillways of the arch dams, deep scour may occur very near the base of the dam due to impingement of the jet, as in the case of Kariba, Zimbabwe and Cahora Bassa, Mozambique. This can be avoided by provision of a concrete slab or apron to withstand the highly turbulent impact load. For the design of the slab, the guidelines offered by Martins (1994) are useful.

21.5.4 Protection Against Scour

The most common cause for protection is the scour taking place, or approaching very near the structure, threatening to undermine it. The reasons for the scour to occur very near the bucket are often the low flows cascading down the bucket lip (in absence of flip action) or discharges passed down the spillway with unsymmetrical gate openings or through sluices opening out in the buckets, causing spread of the jet or return flows. In such cases, a concrete apron of about 15 m width, just downstream of the bucket, as shown in Figure 20, would provide adequate protection. Such an apron should be laid on rock and properly anchored.

Other protection measures include dumping concrete cubes in the scour hole, filling cavities eith concrete, covering with mass concrete with anchor bars,

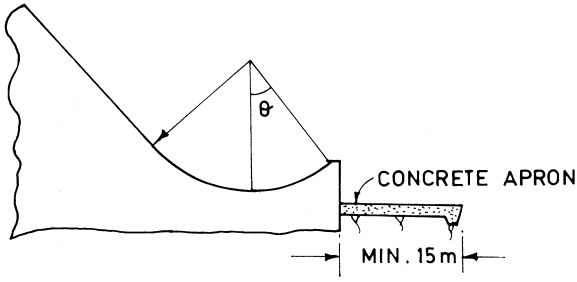

Figure 20 Concrete apron downstream of the bucket.

and guniting treatment to exposed rock joints, as has been done for Ukai dam, India. Extensive protection works provided for the Keban and Karakaya dams in Turkey have been reported by Yildiz et al. (1994-b).

21.6 SPECIAL FORMS OF BUCKETS

Special forms of buckets are sometimes provided to deflect the jet issuing from the bucket towards the main river course when the spillway is located on the flank. Buckets consisting of jet splitters are specially designed to affect lateral spreading of the jet in order to entrain air and dissipation of part of the energy before it strikes the riverbed. The shape of the deflectors depends on the slope of the spillway chute, namely spillway chutes on flat slopes and those on steep slopes. The arrangements also differ according to whether the chutes are narrow or wide.

For the flip buckets at the end of the narrow chute spillways, simple deflector on one of the sides of the bucket, as shown in Figure 21, serves to deflect the flow to a desired location. Juon and Hager (2000) have studied such a deflector in detail and made recommendations.

If the spillway chute is wide or the amount of deflection required is too large to be accomplished by deflectors, the entire chute has to be curved in plan. This also necessitates the provision of super elevation to ensure equal distribution of discharge across the width. Khatsuria et.al. (1989) have described studies for a number of alternatives on a model to finalize an alignment of the chute on a curve for the spillway of Baira dam, India. Figure 22 shows details of the spillway. With this design, the difference between the flow depths on the left and right sidewalls of the spillway was restricted to about 0.4 m and pressures to about 1 m.

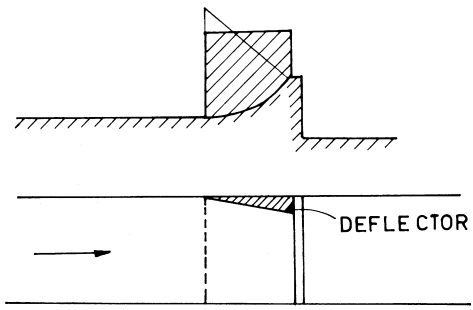

Figure 21 Deflector on flip bucket (shown in Hager 2000).

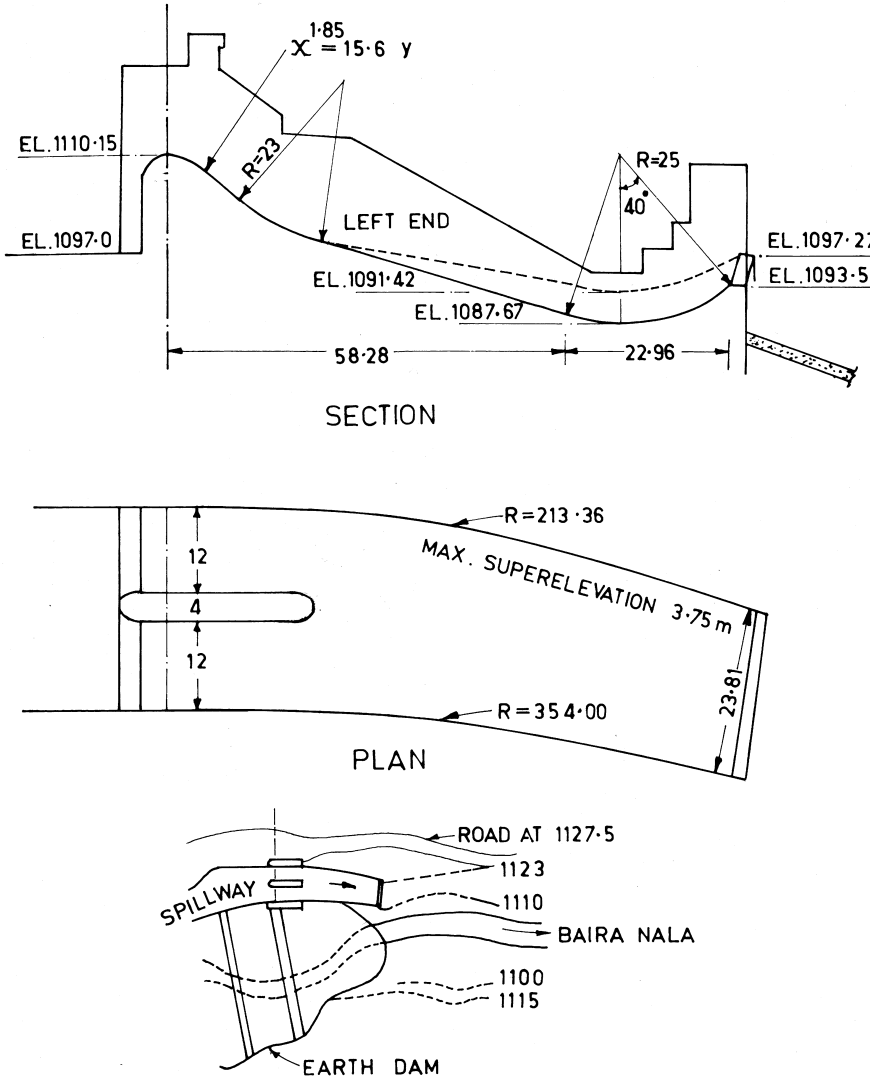

Figure 22 Flip bucket on a curved chute: Baira dam spillway, India. (Shown in Khatsuria et al.–1989)

Special forms of buckets have been evolved to deflect the flow for buckets with steep entrance slopes, though of relatively narrow width. For the spillway of Umium-Barapani dam, India, super elevated bucket, with lip angles varying from 23^0 at left end to 40° at the right hand, resulting in a difference in elevations of about 3.1 m was developed from model tests as shown in Figure 23.

However, for wide and steep gravity spillways, deflection of the flow requires elaborate arrangements. On a number of projects, this has been eliminated by suitable realignment of the spillway axis so as to direct the jet in line with the main river course. When this was not possible, flow from each span was turned in the desired direction right from the crest up to the bucket lip, by provision of sidewalls and intermediate divide walls, appropriately curved in plan. Two alternative arrangements are possible:

1. Providing the required curvature to the divide walls between the crest and bucket keeping the portion of the divide wall in the bucket straight without curvature.

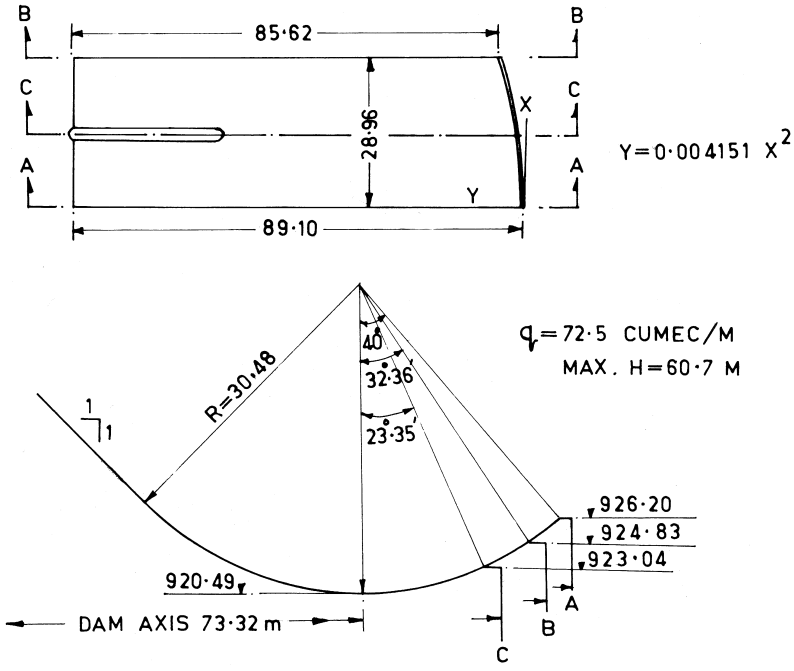

Figure 23 Super-elevated bucket: Umium-Barapani dam, India.

2. Divide walls up to the bucket on a straight alignment with the required curvature in the bucket portion.

In both the alternatives, risk of flow separation and consequent cavitation damage to the divide walls and spillway surface, particularly on the convex side, is imminent. Curving the divide walls on the spillway chute may have the advantage of relatively low velocities, whose performance would, however, be marred by the low mean pressures due to convex curvature of the chute and formation of the cross-waves. The curved divide wall in the bucket portion, although subjected to the high velocities, would have the advantage of higher mean pressures, reducing the susceptibility of cavitation. The cross-waves in such a case could be eliminated by providing super elevation to the bucket surface. Divide walls in the ski jump bucket of the Karun dam, Iran, were curved in the bucket portion. Cavitation damage to the spillway surface was reported for small discharges.

In the case of spillway of Chamera Project, Stage I, India, all of the eight spans were separated by divide walls curved in plan, in addition to providing buckets of alternative spans with 15° and 35° lip angles, and super elevation to deflect the flow towards right and spread over a large area. Khatsuria et al. (1991) have described model studies for both the alternatives indicated from the consideration of the hydraulic performance and cavitation susceptibility. The details of the alternatives studied are shown in Figure 24. It was concluded from the model studies that alternative 2 layout, with curved divide walls in the bucket portion, was better in respect of flow conditions, pressures on the spillway surface, and along the divide walls, signified in terms of cavitation indices based on mean and fluctuating pressures.

Since the curved surfaces create the problems of flow separation and cavitation, a bucket made of only plain surfaces had been considered. The corners formed by intersection of plain surfaces would be the regions of flow stagnation, thus eliminating possibility of separation. A schematic of such a configuration is shown in Figure 25. This must be finalized from model studies.

Special forms of buckets that increase dispersion and air entrainment can be classified as: interacting jet dissipators, dentated buckets, serrated buckets, and nappe splitters.

The simplest arrangement to affect spreading of the flow and dispersion is to construct the bucket with dispersion blocks in the portion downstream of the invert, in a fashion similar to that in a slotted bucket. Model tests conducted for the spillway of Itaipu dam, with such a bucket, indicated reduction in depth of scour as compared to that with the conventional plain bucket. It was however, concluded that the reduction was not to an appreciable degree and that a highly elaborated and complex design of the blocks would be required to ensure absence of cavitation. A design employing jet splitters in an expanding bucket is shown in Figure 26.

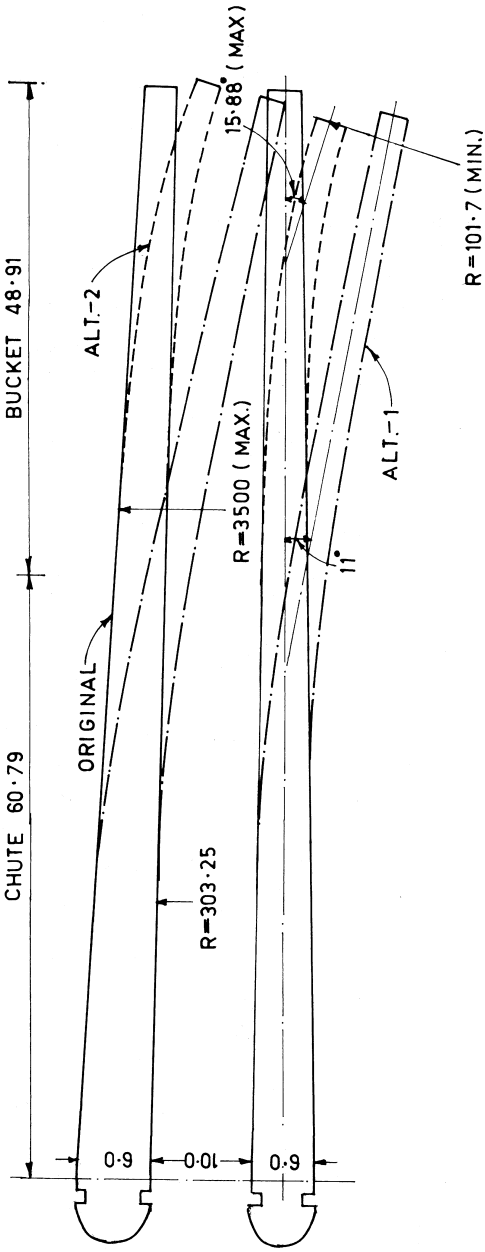

Figure 24 Curved divide walls for ski jump spillway of Camera dam, India. (Shown in Khatsuria et al.–1991)

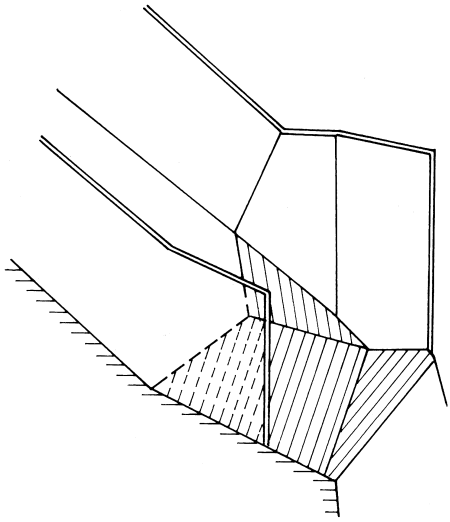

Figure 25 Schematic of a bucket made of plain surfaces.

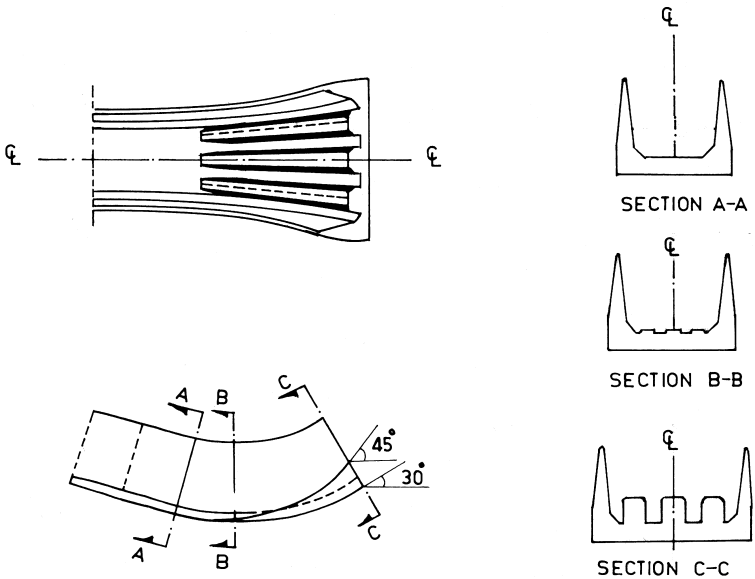

Figure 26 Bucket with flow splitters.

A special shape of flip bucket, called serrated bucket, ensures considerably larger areal distribution of the jet input and entrainment of abundant air. Typical details are shown in Figure 27. A bucket of this shape was provided on the spillway of Magat dam in Philippines.

Nappe splitters as shown in Figure 9 (Chapter 11) are ideally suited to the overflow spillways located on the arch dams, as for example P.K. Le Roux dam in South Africa and Victoria dam in Sri Lanka. A similar arrangement is provided for the deep seated outlet of St. Croix dam in France, as shown in Figure 14 (Chapter 11). These devices ensure large amounts of air entrainment and disintegration of jet so that residual energy imparted at the base of the dam is minimum.

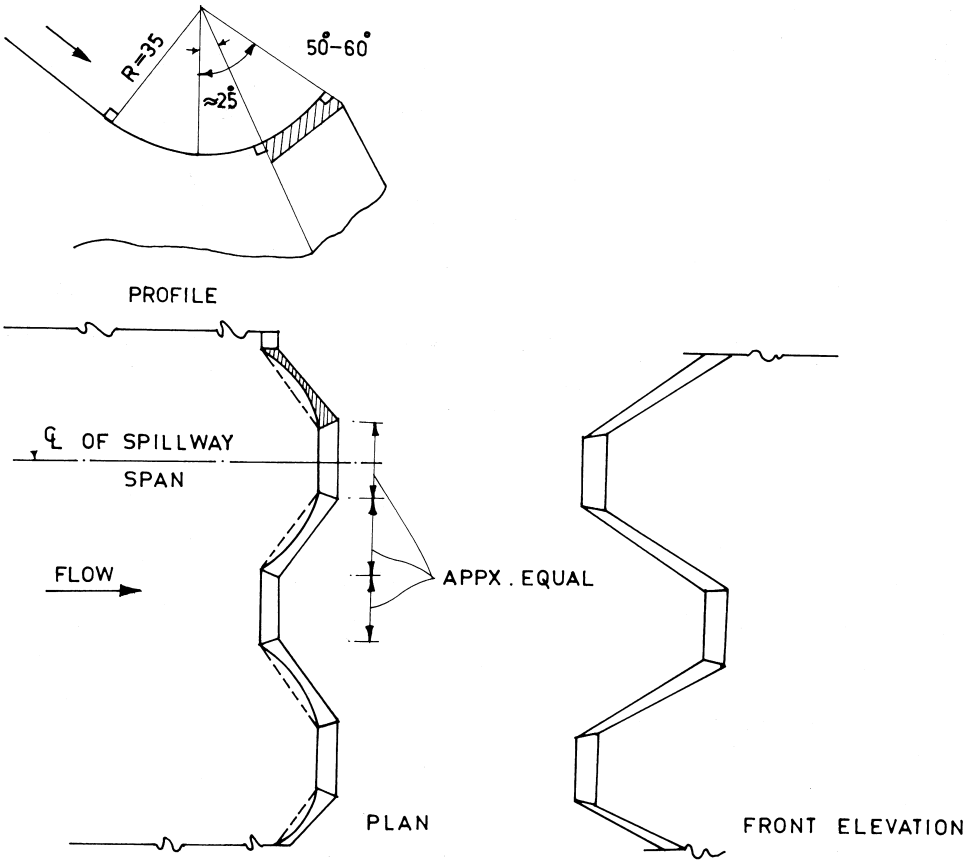

Figure 27 Serrated bucket configurations.

Although several shapes and arrangements of buckets have been evolved to cater to the specific needs, no generalized procedure for designs has been developed. Consequently, model studies for specific case are required to finalize a design. Again, such buckets function as anticipated only for a narrow range of discharges of design and model studies are required to ensure that their performance for other discharges is not unacceptable. Further more, it must be ensured that such designs are free from flow separation and cavitation.

Notations

A = Constant in scour equation
C = Coefficient to account for losses along spillway surface
C_1 = Coefficient for velocity reduction due to friction
C_2 = Coefficient for velocity reduction due to curvature effect
C_p = Pressure coefficient
d_m = Mean bed material size
d_s = Depth of scour below tail water level
F = Froude number at bucket invert
F_1 = Froude number at bucket lip.
F_q = Discharge parameter = $q / \sqrt{g\ h_o^3}$
g = Acceleration due to gravity
H = Fall from crest to bucket invert
H_s = Fall from upstream pool level to the jet surface in the bucket
H_t = Fall from reservoir up to tail water level
H_v = Velocity head of jet at bucket lip
H_x = Head from reservoir up to any point x on the bucket
h_o = Fall from reservoir level to bucket lip level
h_1 = Fall from reservoir level to bucket invert
h_d = Depth of overflow over the crest
h_{ds} = Tail water depth above original river bed
h_l = Difference between bucket lip and river bed
K_r = Constant related to rock mass characterisitcs
k = Constant related to air resistance
L_1 = Throw distance considering air resistance
l = Length of the bucket along curvature
P = Pressure at a point on the bucket
P_{max} = Pressure at the invert of the bucket
q = Discharge per unit width
R = Radius of the bucket
R_1 = Radius of the free surface of the flow in the bucket

S = Total length of the bucket along curvature
V_o = Velocity at the bucket lip
V_1 = Velocity at the toe of the spillway or at the bucket invert
X = Throw distance at the point the jet strikes the tail water
x = Cartesion co-ordinate
y = Cartesion co-ordinate; Drop from lip to tail water level
y_1 = Depth of flow at bucket invert
y_2 = Thickness of jet
y_3 = Submergence of lip by tail water
Z = Head between reservoir and bucket invert
α = A coefficient
= Apparent increase in lip angle
β = Angle indicating slope of lip in the downstream direction
= Volumetric air to water ratio
= Total deflection angle of the bucket
ϕ = Angle formed by the radii passing through a point x on bucket surface and the invert
θ = Bucket lip angle (Geometrical)
θ_1 = Bucket lip angle or Effective jet angle
θ_2 = Angle of jet impact on tail water surface

REFERENCES

1. Balloffet, A. Pressures on spillway flip buckets - ASCE. Jnl. of Hyd. Dn. Sept. 1961.
2. Cabelka, J. The Losses of Mechanical Energy of the Overfall Jet on the Spillway Sections of Dams - IAHR 6th Congress, The Hague, 1955.
3. Chavarri, D.; Louie, S.; Castillejo, N.; Coleman, H. W. Spillway and tailrace design for raising of Guri dam using large scale hydraulic model, 13th ICOLD, Q 50, R 12. New Delhi, 1979.
4. Chen, T. C.; Yu, Y. S Pressure Distribution on Spillway Flip Buckets – ASCE, March 1965.
5. Ervine, D. A. The entrainment of air in Water - Water Power and Dam Construction, 1976, 28(12).
6. Hartung, F.; Hausler, E. Scour, stilling basins and downstream protection under overfall, 11th ICOLD. Madrid, 1973.
7. Juon, R.; Hager, W. H. Flip bucket without and with deflectors, Jnl. of Hyd. Engg ASCE, November 2000.
8. Kawakami, K. A study on the computation of horizontal distance of jet issued from a ski-jump spillway; Trans Japan Society of Civil Engineers. 1973; Vol. 5.
9. Kelker, Y. S.; Khatsuria, R. M. Hydraulic characteristics of ski-jump buckets subjected to submergence by tail water, CBIP 44th Annual Research Session. Chandigarh, 1975.
10. KNS, Rao ME, WRD Thesis: University of Roorkee, 1978.

11. Khatsuria, R. M.; Ganesh Rao, H. C.; Deolalikar, P. B. Design of a ski-jump spillway governed by downstream channel configuration - CBIP, 54th R&D Session, Srinagar, Tech. Session IV, Paper 3, 1989.
12. Khatsuria, R. M.; Deolalikar, P. B.; Pethe, P. C. Prediction of cavitation potential for alternative designs of spillway, Chamera H.E. Project - A case study, First International Conference on Research needs in Dam Safety, CBIP. New Delhi, 1991.
13. Laxmanswami, A. Performance of Trajectory Buckets at Low Froude Numbers, CBIP, Proc. 42 ARS, 1972.
14. Lenau, C. W.; Cassidy, J. J. Flow through spillway flip buckets. ASCE Jnl. of Hyd. Dn. May 1969.
15. Martins, R.; Viseu, T. Plunge pool slab design taking into account turbulent pressures, 9th APD - IAHR, Singapore 1994.
16. Mason, P. J. The choice of hydraulic energy dissipator for dam outlet works based on a survey of prototype usage. Proc. Instn. Civ Engrs, Part I. May 1982, 72.
17. Mason, P. J. Erosion of plunge pools downstream of dams due to the action of free-trajectory jets. Proc. Inst. Civ. Engrs. Part I. May 1984.
18. Mason, P. J.; Arumugam, K Free jet scour below dams and flip buckets. Proc. ASCE, Hyd. Dn. February 1985.
19. Mason, P. J.; Armugam, K. A review of 20 years of scour development at Kariba dam, 2nd Intl. Conf. on The Hydraulics of flood and flood control, BHRA, September 1985.
20. Mason, P. J. Effect of air entrainment on plunge pool scour. ASCE Jnl. of Hyd. Engg. March 1989.
21. Mason, P. J. Practical guide lines for the design of flip buckets and plunge pools, Water Power and Dam Construction, Sept./Oct. 1993.
22. Peterka, A. J. Hydraulic design of stilling basins and energy dissipators, USBR, Engg. Monograph, No.25, 1978.
23. Prasad, R. K. Pressure distribution on ski-jump buckets, Irrigation and Power, CBIP, 41(3), July 1984.
24. Quadri, S. A. W.; Jilani, A. K. M.; Fakhri, A. I. Some aspects on the design of trajectory buckets, Vol. II. Proc. 46th Research Session, CBIP. Trivandrum, Nov. 1977.
25. Rae, P. J.; Castro, D. H. Estimation of spillway free jet trajectory length, ASCE conference Hydraulic Engineering, 1994.
26. Roose, K.; Gilg, B. Comparison of the hydraulic model tests carried out for the ski-jump shaped spillways of the Smokovo and Paliodherli dams, 11th ICOLD. Madrid, 1973.
27. Rudavsky, A. B. Selection of spillways and energy dissipators in preliminary planning of dam developments, 12th Congress ICOLD, Q 46, R-9. Mexico, 1976.
28. Taraimovich, I. I. Deformation of channels below high head spillways on rock foundation, Hydrotechnical Construction, Sept. 1978.
29. USBR Hydraulic design of stilling bsins and energy dissipators, Engg Monograph No 25, 1978.
30. Varshney, R. S.; Bajaj, M. L. Ski-jump buckets on Indian dams, Irrigation & Power, CBIP, October 1970.

31. Varshney, R. S. Pressure variation in mixed bucket type of energy dissipators, Irrigation and Power, CBIP, October 1975.
32. WES Hydraulic Design Criteria, Chart No 112-7 and 112-8, 1962.
33. Yildiz, D.; Uzucek, E. Prediction of scour depth from free falling flip bucket jets, Water Power and Dam Construction. Nov. 1994-a.
34. Yildiz, D.; Uzucek, E. Experience gained in Turkey on scours occurred downstream of the spillways of high dams and protective measures, 18th ICOLD, Q 71, R 9. Durban, 1994-b.

22
Solid and Slotted Roller Buckets

22.1 INTRODUCTION

When the tail water depth is too great for the formation of a good hydraulic jump, submerged roller buckets are suitable for energy dissipation. The hydraulic behavior in this type of dissipator is manifested primarily by the formation of two rollers: a bucket roller moving counter clockwise and a ground roller downstream of the bucket moving clockwise. The intermingling of the flows in the form of rollers effects energy dissipation. Solid roller buckets were developed in 1933, following their first application on the 85 m high Grand Coulee dam, USA. Slotted buckets, developed and first used on the 36 m high Angostura dam in 1945, is claimed to be an improvement over the solid bucket. This design was so popular at that time that the USBR (1977) recommended that a solid bucket should not be used wherever the tail water limitations of the slotted bucket can be met. The range of application for both the buckets is depicted in Figure 3 – Chapter 19. Figure 1 shows comparison of hydraulic actions in solid and slotted buckets. Prototype experience on the performance of both the types of bucket is available enabling a critical reappraisal.

22.2 SOLID ROLLER BUCKET

The hydraulic action in a solid roller bucket is that of a hydraulic jump on a curved invert under excessive submergence by tail water. McPherson and Karr (1957) have studied various characteristics of the solid bucket. The bucket is circular in shape and lip angle is usually 45°, although smaller angles up to 30° have been favored by many researchers. The principal elements of the design of solid roller buckets are: fixing invert elevation, lip angle, and radius of the bucket. Important hydraulic characteristics include: determination of depth of water in the bucket h_b, surge height h_s, maximum scour depth d_s and its distance from the lip, and pressures on the bucket surface and side walls. Figure 2 shows various parameters involved.

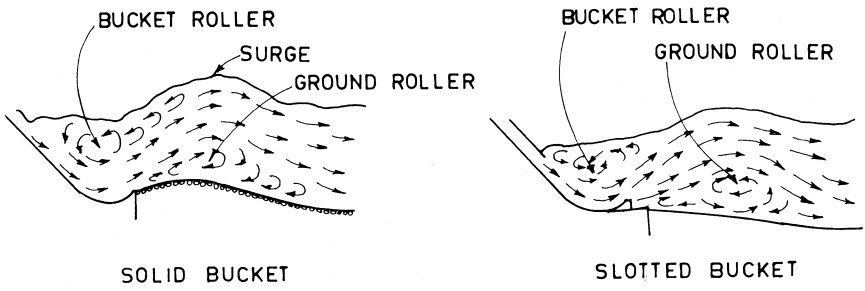

Figure 1 Hydraulic actions in solid and slotted buckets.

Invert Elevation

Fixing invert elevation involves a major decision governed both by geological conditions and tail water depths available. It is necessary to fix the invert level such that the roller action is ensured for the entire range of discharges expected. Various investigators have mode recommendations, either in terms $\frac{y_2}{h_2}$ *or* $\frac{h_b}{h_2}$, notably

1. WES(1966): $0.75 < \frac{h_b}{h_2} < 0.90$
2. Govind Rao et al. (1963): Assuming roller action as submerged hydraulic jump, 1.1 y_2 below TWL for $F_1 > 7$

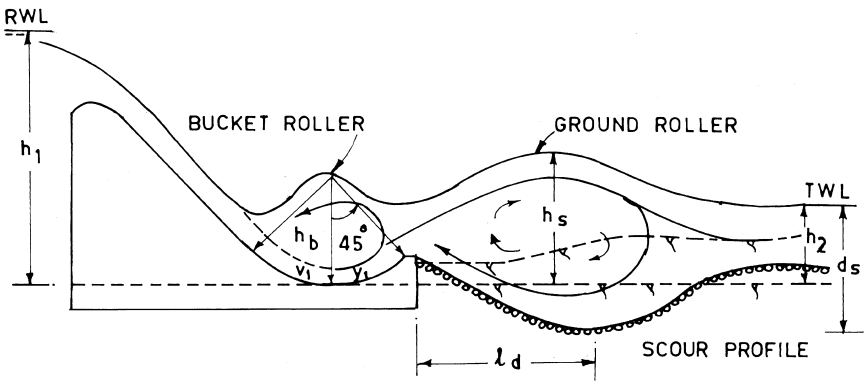

Figure 2 Solid roller bucket: relevant parameters.

3. Varshney (1968): 1.3 − 1.4 y_2 below TWL
4. Doddaiah (1960): $h_2 \approx 0.7\ h_1$
5. Khatsuria (1975): 1.1 − 1.2 y_2 below TWL

Figure 3 summarizes various relationships as in the list.

Khatsuria (1975) conducted studies on an erodible bed model of a typical solid roller bucket with lip angle of 45°, in respect of depth of scour, surge height, and distance of scour with h_2/y_2 varying from 1.1 to 1.8, up to the Froude number of 9, and observed that with increase in submergence, the depth of scour d_s decreased and distance of deepest scour l_d increased sharply up to $h_2/y_2 = 1.3$ whereas surge height increased steadily for all submergence. It was concluded that the bucket invert should be placed such that h_2/y_2 is between 1.1 and 1.2

Sometimes this requirement results in a deep seated bucket, namely a bucket invert considerably below the river bed and consequently, the bucket lip has to be joined to the ground level by a recovery slope as shown in Figure 2. In such a case, special care in the operation of the spillway is required to prevent damage by entry of material into the bucket.

Lip Angle

A 45° lip angle is the most widely investigated and recommended lip angle. However, Hiranandani et. al. (1962) and Doddiah (1960) favor smaller lip angles, of the order of 30° to 40°, esspecially for the advantage of lesser scour. Varshney et al. (1974) conducted studies for hydraulic characteristics of a 30° lip angle roller bucket. It was indicated that the free jet action (transformation of roller action into ski action) occurred for $h_b/y_2 = 0.25$ as against $h_b/y_2 = 0.20$ for a 45° bucket. It was also found that the depth of tail water required for a good roller action for a 30° bucket was more than that required for a 45° bucket. Comparison of a limited amount of data in respect of scour downstream indicated that while the magnitude of scour remained the same order as that with a 45° bucket, the deepest scour occurred nearer to the bucket lip with the 30° bucket. Based on an analysis of prototype data of existing dams, KNS Rao (1978) concluded that for the values of discharge parameter F_q from 0.03 to 0.08, i.e. F_1 from 9.7 to 5.9, a 45° lip angle would be the best and for lesser values of F_q, i.e. Froude numbers higher than about 10, a smaller exit angle would be beneficial.

Radius

The radius of a solid roller bucket is directly proportional to the Froude number of the flow entering the bucket. Generally, for the Froude numbers commonly encountered in practice—5 to 8—the ratio (h_1/R) in the range of 3 to 5 is recommended. It is found that too small of a radius makes the flow unsatisfactory due

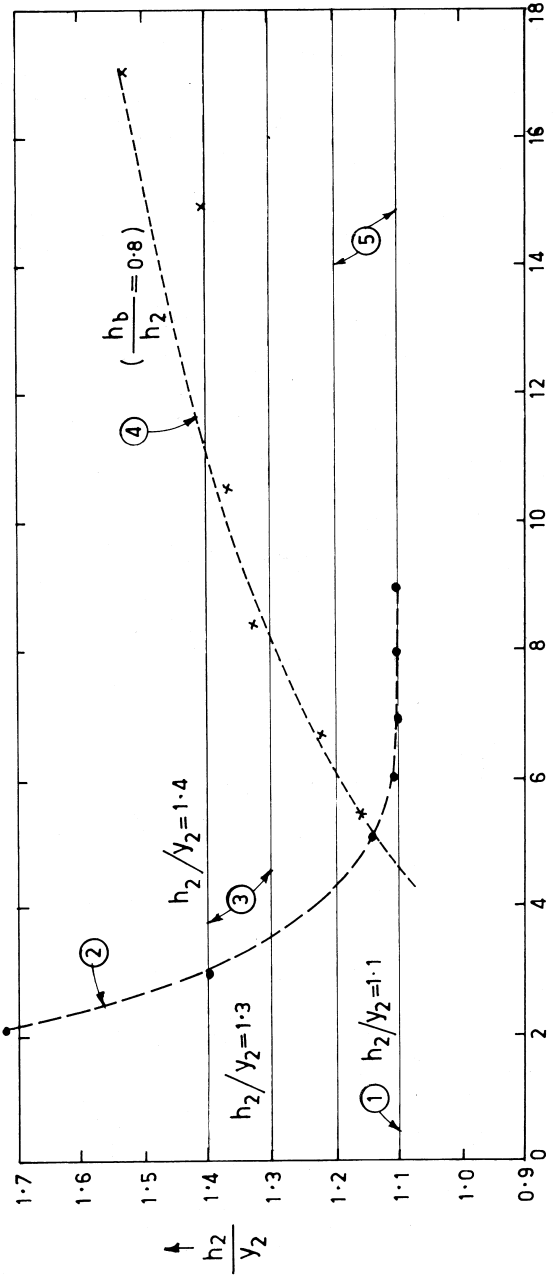

Figure 3 Optimum submergence for solid roller bucket: ① Hydraulic jump, ② Govind Rao (1964), ③ Varshney (1968), ④ WES (1966), and ⑤ Khatsuria (1975).

to pulsating surges while too large of a radius would increase the cost with only a marginal improvement.

USACE (1990) suggest a minimum radius given by

$$R = \frac{5.19(y_1 + V_1^2 / 2g)}{F_1^{1.64}} \text{(ft units)} \tag{1}$$

KNS Rao (1978) based on study of prototype data for 45° bucket found that the radius of the bucket can be calculated as

$$\frac{R}{h_1} = 0.0826 + 2.07\, F_q + 14\, F_q^2 \tag{2}$$

Pressures on the Bucket

After comparing various methods available for computing the pressures in the roller buckets, KNS Rao (1978) suggest that pressure at any point x on the bucket can be calculated as

$$P_x = H_x - \frac{1}{2g}\left[\frac{q}{R \log (R / r_1)}\right]^2 \tag{3}$$

where

H_x = Head from reservoir up to point x on the bucket
R = Radius of the bucket
q = Intensity of discharge
r_1 is calculated from

$$r_1 \log\left(\frac{R}{r_1}\right) = \frac{q}{\sqrt{2g}\, h_1} \tag{4}$$

Kelkar and Khatsuria (1973) studied pressure distribution on sidewalls and divide walls in the roller bucket. They found that the maximum pressures on the side walls were on a vertical section passing through the invert of the bucket and can be approximated by superimposing centrifugal pressure over the depth Y_1, on hydrostatic pressure corresponding to the total depth of flow in the bucket, as shown in Figure 4.

Surge Height and Scour Downstream of the Bucket

Khatsuria (1975) conducted studies for the surge height, depth of maximum scour, and distance of maximum scour from the bucket lip for a typical solid roller bucket

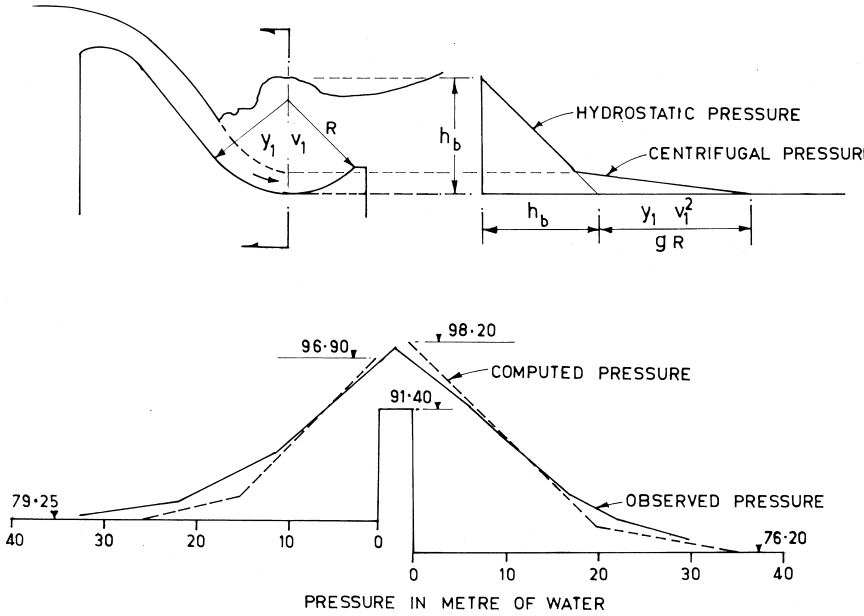

Figure 4 Pressure distribution on side wall (shown in Kelkar et al. 1973).

with 45° lip angle for $6 < F_1 < 18, 2.7 < \frac{h_1}{R} < 3.0$ *and* $1.0 < \frac{h_2}{y_2} < 2.3$. The results are shown in Figures 5 and 6.

It is seen that for a given submergence over the bucket invert, increase in the Froude number decreases the depth of scour and reduces the height of the surge, but the location of the deepest scour approaches nearer to the bucket lip. Whereas, for a given Froude number, an increase in the submergence reduces the depth of scour, increases the surge height and increases the distance of the deepest scour. However, for the Froude number exceeding about 13, the scour depth is virtually insensitive to the increase in the tail water depth. Also, the rate of variation of scour depth, its distance and the surge height is much more pronounced for Froude number up to about 9.

Range of Tail Water Depths

Solid roller buckets have a comparatively larger range of tail water depths as compared to the slotted buckets. The minimum tail water depth required for ensuring satisfactory roller action is of the order of 1.1 to 1.3 y_2. The upper limit

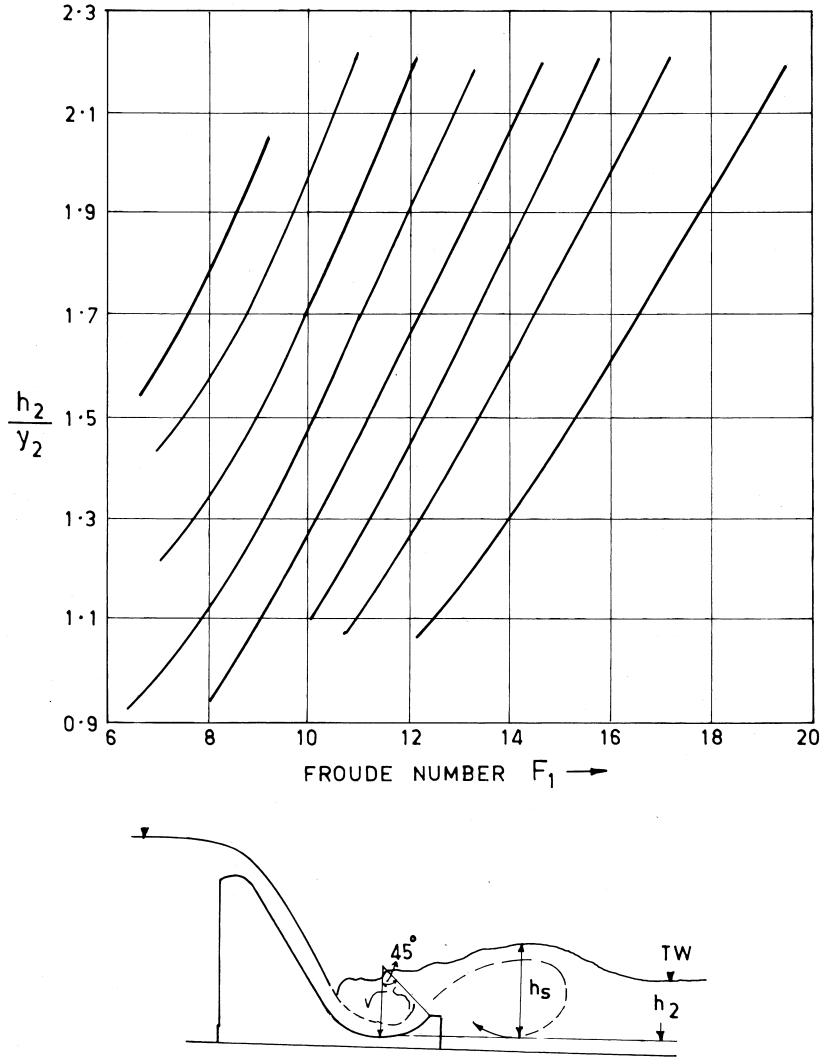

Figure 5 Surge height downstream of solid roller buckets.

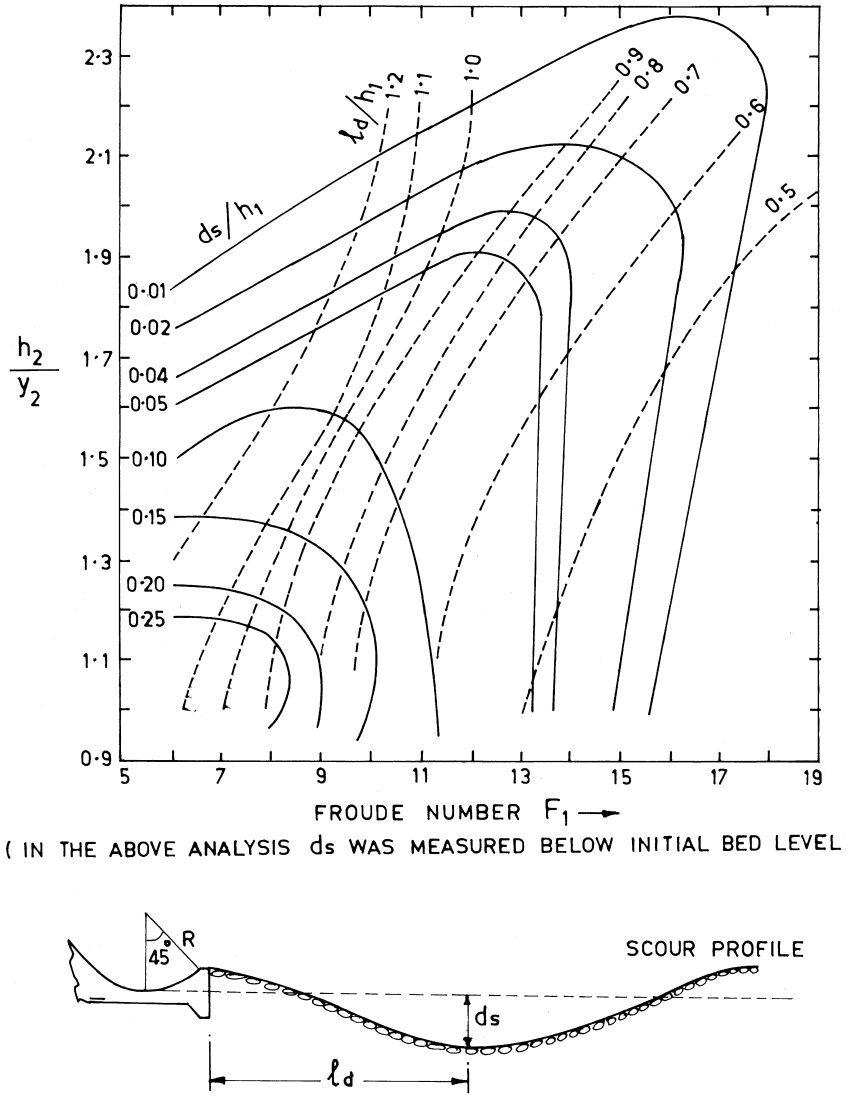

Figure 6 Scour downstream of solid roller buckets.

of the tail water depth has not been defined clearly; however, observations in some specific cases of model studies indicated such limit to be as high as 3 y_2.

22.3 SLOTTED ROLLER BUCKET

The slotted bucket has been claimed to be an improvement over the solid bucket (USBR- 1978). Figure 1 shows comparison of hydraulic action of both types of bucket. In a solid bucket, all the flow is directed upward by the bucket lip to create a boil on the water surface and a violent ground roller on the riverbed. The ground roller has a tendency to move bed material towards the bucket lip where it could be picked up and carried inside the bucket. The slotted bucket aims at minimizing this tendency with the help of a bucket design combined with teeth and apron, as shown in Figure 7. In this bucket, part of flow passes through slots, spreads laterally, and is lifted away from the channel bottom by an apron. Thus, the flow is dispersed and distributed over a greater area, providing less violent flow concentration than that occurring with a solid bucket. Bed material is neither deposited nor carried away from the bucket lip. The slots of the bucket, not only keep the bucket lip free of loose material, but also provide exit for the material that might find its way into the bucket because of unsymmetrical operation of the spillway. This action also adds to the energy dissipation efficiency of the slotted bucket.

Many of the claims in favor of a slotted bucket over a conventional solid bucket were confirmed in a model study. The performance of both the buckets was studied on a two dimensional model of a typical medium height spillway with the same invert elevation and tail water conditions. The results are given in Figure 8. It would be seen that a slotted bucket ensures less scour, less violent rollers, and better velocity distribution downstream.

Unlike solid buckets, the hydraulic design of slotted buckets has been fairly standardized based on the generalized studies conducted at USBR (1978). The principal elements of the design are: fixing bucket invert elevation and radius of the bucket, bucket and apron dimensions, as well as teeth and slot sizes standardized in terms of bucket radius, as shown in Figure 7. The first step in the design is to calculate the Froude number of the flow on the spillway slope, F_t, at the elevation of the tail water corresponding to the discharge considered. The head loss up to that elevation is also taken into account. The minimum allowable radius R is then worked out from the relationship F_t Vs $(R/(d_t + V_t{}^2/2g))$. After choosing an appropriate radius, the range of tail water limits, T_{max} and T_{min} are determined from the relevant relationships, shown in Figure 9. These ranges are determined for all the discharges and finally the bucket invert is set so that the available tail water elevation is between the T_{max} and T_{min}. Tail water sweep out depth T_s (the depth at which the roller action would covert into a free jet action called sweep

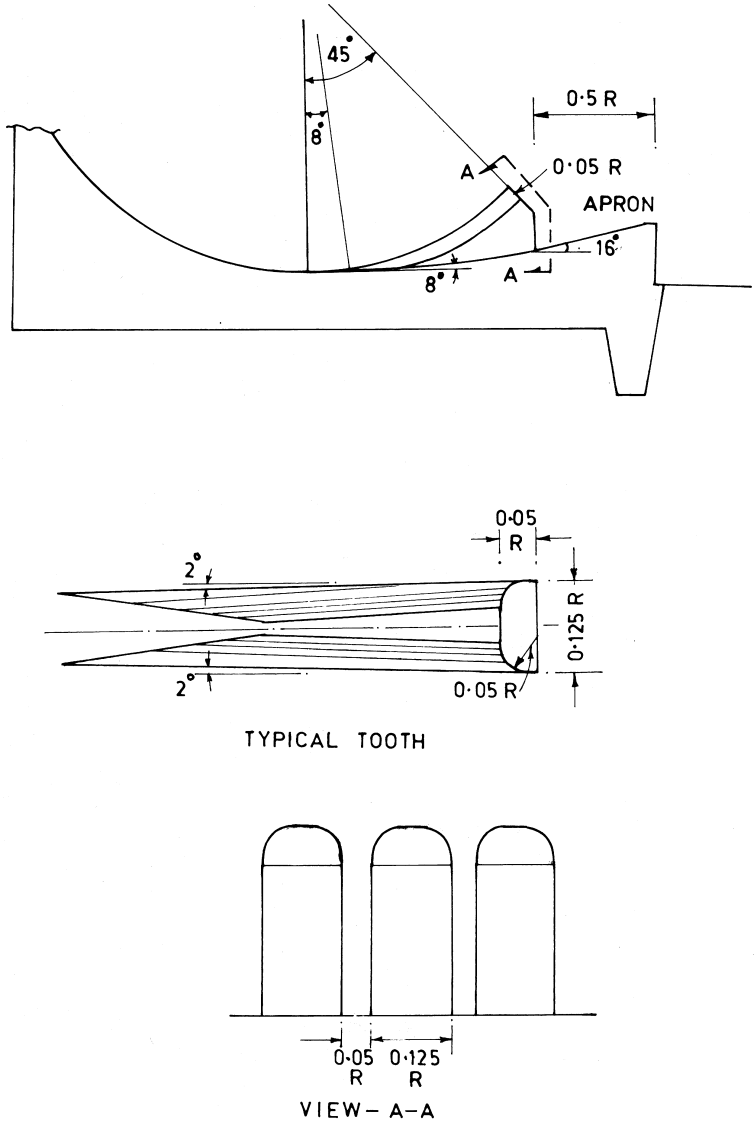

Figure 7 Slotted bucket configuration (shown in USBR 1978).

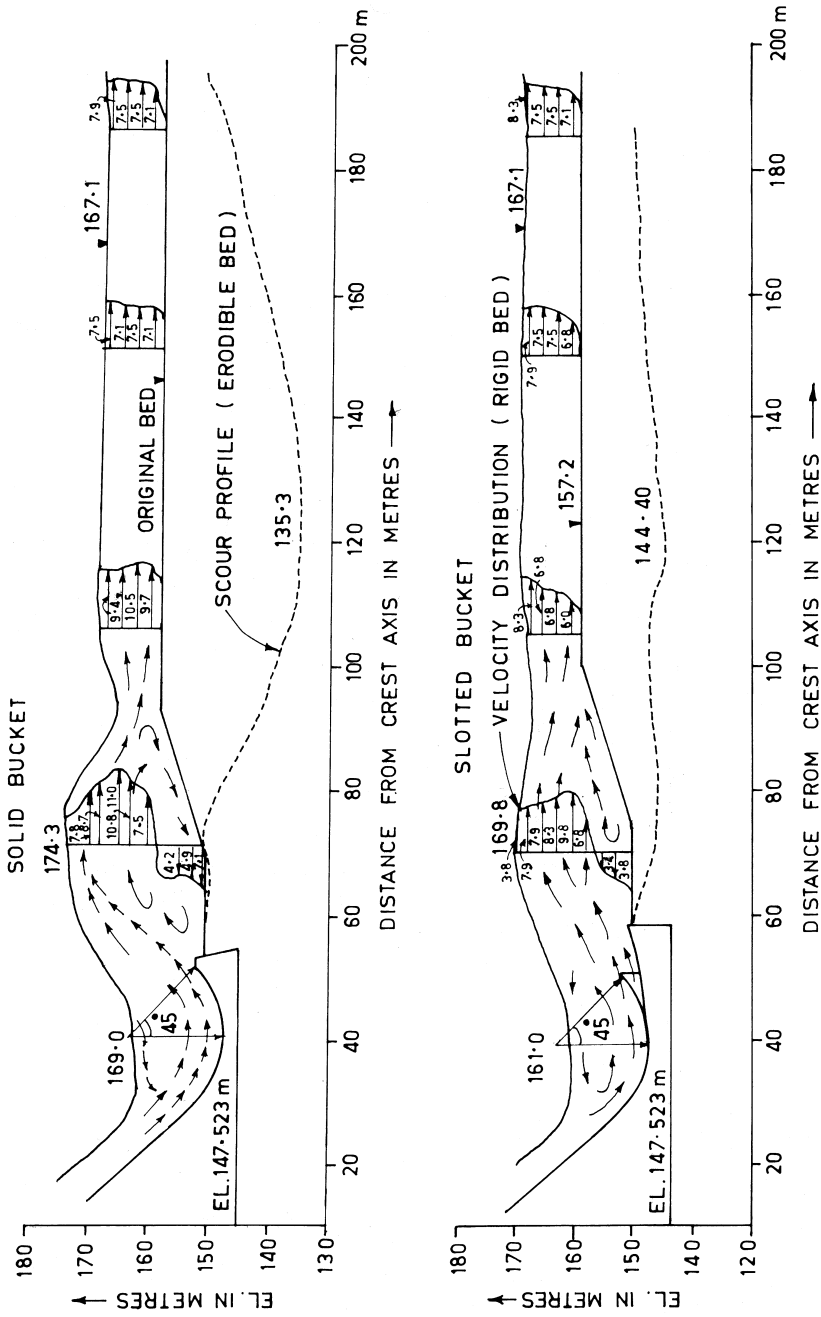

Figure 8 Comparative performance of solid and slotted buckets.

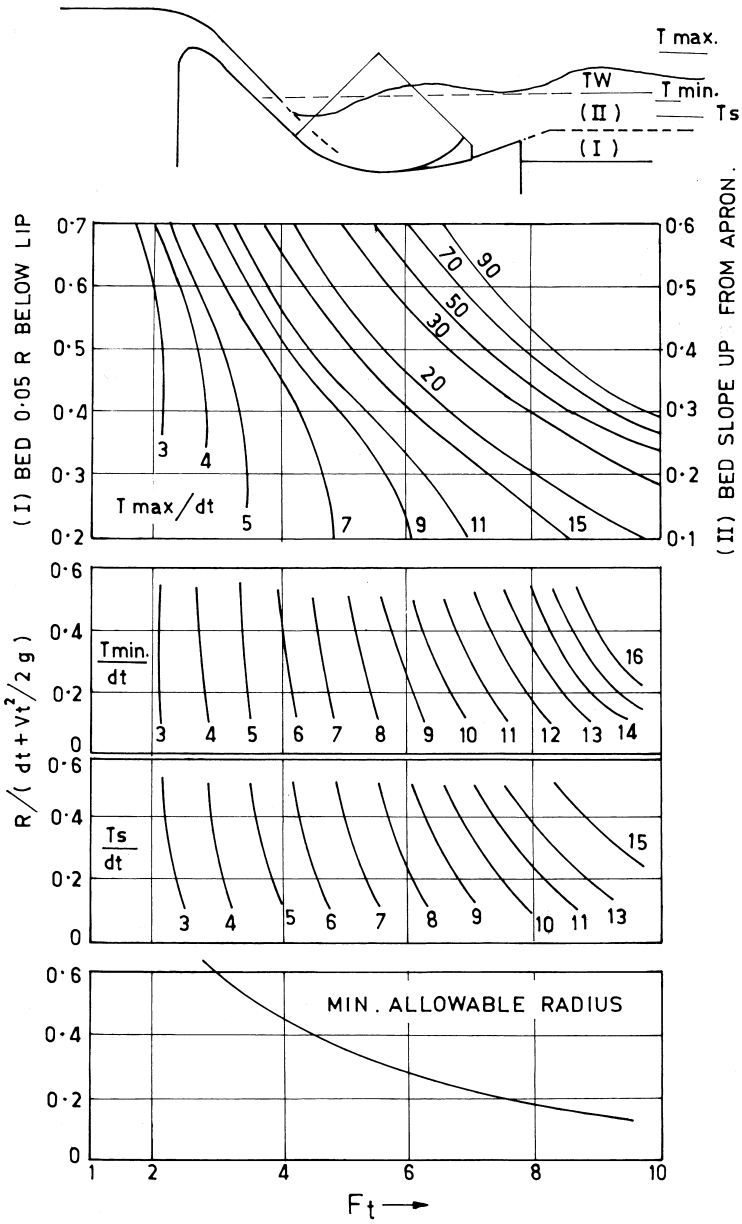

Figure 9 Slotted buckets: relevant relationships (shown in USBR 1978).

out) is also determined to verify the invert elevation considering uncertainty in the establishment of tail water rating curve. The dimensions of the bucket, teeth and slots are then worked out as per Figure 7.

During the development studies, conducted at USBR, (Peterka 1978) subatmospheric pressures were found to occur on the downward sloping face and downstream vertical face of tooth. It was concluded that significant cavitation should not occur for velocities up to about 25 m/s, based on the difference between the head water and tail water elevations. Reducing the tooth spacing from 0.05 R to 0.035 R further improved the pressures. In general, it has been recommended that confirmatory hydraulic model tests be made whenever velocities entering the bucket are over 25 m/s.

22.4 COMPARATIVE PERFORMANCE BASED ON PROTOTYPE EXPERIENCE

Roller buckets have been less favored in comparison to stilling basins and trajectory buckets due partly to the requirement of large tail water depths in general and due to the sensitivity of the slotted buckets to tail water variation in particular. Even then, many spillways have been provided with either solid or slotted buckets. In India, such buckets have been provided on several dams constructed on wide and flat rivers with large overburden.

The earliest example of damage in the case of solid roller bucket is that of Grand Coulee dam where abrasion had taken place in the bucket due to the entry of material into the bucket and subsequent roll-mill action. Similar damages have occurred on the solid roller buckets of Indian dams also. As for the slotted buckets, instances of damages—both due to abrasion and cavitation—have also been reported on India dams. Tables 1 and 2 give details of projects and damages occurred. Khatsuria (1999) has studied comparative performance of both the buckets in the light of their susceptibility to damage and effectiveness of repairs.

Thatte et al. (1991) have reported damages caused to solid roller buckets of Kadana, Dharoi, Damanganga, and Hiran-II dams of India and subsequent repairs. Thatte et al. concluded that the damages were mainly caused by abrasion due to entry of material into the bucket when the spillways were operated unsymmetrically. It was also found that sometimes gates were suddenly closed resulting in reverse flow of water from downstream into the bucket, which was responsible for carrying material into the bucket. However, no cavitation damage was observed in such type of buckets.

Dange et al. (1989) have described damages caused to the slotted buckets of Ujjani, Kamtikhedi and Itiadoh spillways, India. Repeated damages have also been found to occur on the slotted bucket of Jawaharsagar dam. The damages included are both due to abrasion and cavitation. The abrasion damage was caused

Table 1 Slotted Roller Buckets: Prototype Data

Sr. No.	Project	No. of spans	Discharge intensity m^2/s	Head from MWL to bucket invert m	Velocity at bucket invert m/s	Tail water depth above bucket invert m	Prototype performance
1	Majalgaon		62.92	31.3	23.71	17.87	Not reported
2	Jayakwadi	27	43.4	32.5	24.56	16.8	No damage reported so far
3	Itiadoh	Ungated	7.02	33.22	25.42	12.2	Negligible damage –Ungated spillway
4	Manheri		78.1	33.5	25.6	18.0	Not reported
5	Pochampad	20	59.2	35.97	25.7	18.3	First flood (55%) passed in 1983 – No damage reported
6	Pench (Kamtikhedi)	16	50.63	37.0	26.23	21.6	Repeated damage to teeth and apron
7	Karanjawan	5	21.24	40.57	27.95	12.30	Not reported.
8	Barna	8	50.5	41.41	27.97	19.06	Damage to top concrete layer in the apron up to 20 cm
9	Ichari		222	42.5	26.77	25.0	Minor abrasion damage.
10	Ujjani	41	29.92	43.74	28.94	20.35	Repeated damages to bucket, teeth and apron
11	Jawaharsagar	12	95.2	45.4	28.74	22.30	Repeated damages to teeth and apron
12	Angostura (USA)	5	83.74	48.2	29.71	22.6	No damage reported.
13	Rajghat	18	99.1	48.82	29.88	26.95	Not reported.
14	Bargi	26	109.4	57.78	32.68	25.62	Abrasion damage
15	Bansagar	18	106.92	68.93	35.97	28.1	Under construction.
16	Narmadasagar	20	163.66	72.18	36.44	34.43	Under construction
17	Hasdeo Bango	11	108.3	82.2	39.49	37.28	Abrasion damage.
18	Kallada	3	73.33	64.92	35.11	19.51	Not reported.

Table 2 Solid Roller Buckets: Prototype Data

Sr. No.	Project	No. of Spans	Discharge Intensity m^2/s	Head from MWL to Bucket Invert m	Velocity at Bucket Invert m/s	Tail Water Depth above Bucket Invert m	Prototype Performance
1	Banas	6	40.4	45.7	29.5	16.8	Minor abrasion damage reported.
2	Damanganga	10	115.37	50.0	30.0	24.0	44% of the bucket surface area damaged
3	Dharoi	12	74.0	44.7	28.7	18.3	64% of bucket surface area damaged upto 0.30 m due to small floods.
4	Kadana	18	84.5	57.0	32.7	26.5	2% bucket surface damaged due to 50% of flood in 1981.
5	Yeldari	10	53.6	40.5	27.5	19.2	No damage reported.
6	Sidheswar	14	26.6	31.9	24.6	15.7	No damage reported
7	Hiran - II	7	36.27	–	–	–	41% surface area of bucket damaged, maximum depth of 1 m, 97% flood in 1982.
8	Hatnur	41	56.07	26.5	22.5	17.0	Not reported.
9	Manjra	18	32.9	29.5	23.5	17.65	Not reported.

by the material entering into the bucket due to horizontal eddies formed by unequal operation of the spillway. Although the slotted bucket is effective in flushing out material entering into the bucket by action of teeth and slots, the rolling action during wash out of material had been causing abrasion damage. In projects like Jawaharsagar and Ujjani, there have been instances of abrupt operation of spillway such as sudden opening or closing of gates and disturbing the normal relationship between the discharge and corresponding tail water level. When the gates were suddenly opened, the buckets performed as flip buckets in the absence of adequate tail water depths. Detailed studies have indicated that during such operation, cavitation damage to teeth could have taken place. When the gates were suddenly closed, excessive tail water in the downstream caused reverse flow that brought material inside the bucket resulting in abrasion damage.

While there are many instances of material entering into the bucket from downstream, Harkauli (1979) has reported the case of Ichari dam spillway, India, where boulders were expected to pass down the spillway crest and enter the bucket. The 53 m high Ichari diversion dam has a very high unit discharge: 222 cumec/m. The sediment studies indicated that the dam would get silted up to the crest within a couple of years and boulders of size up to 1 m may roll over the spillway. To enable the boulders to pass smoothly through the slots of the bucket, the width of the slots was kept 1.2 m, i.e. 0.1 R in place of the standard spacing of 0.05 R, the bucket radius being 12 m. The reservoir was silted up to the crest in about 5 years and there after boulders were seen rolling over the spillway, the maximum size being of the order of 20 cm. No significant damage was caused to the spillway face or to the bucket except some abrasion damage to the side faces of the teeth.

It is rather surprising to notice the occurrence of cavitation on teeth and apron on the slotted bucket of Jawaharsagar dam, which was almost identical (in respect of head, discharge intensity, and TW depth) to Angostura dam, based on the studies of which, the design of slotted bucket had been evolved. (Table 1). The aspect of cavitation damage to the slotted bucket has been discussed in Chapter 26.

Prototype experience on Indian dams has brought out that under transient and unsymmetrical flow conditions, both the solid and slotted buckets are vulnerable to damage. The slotted buckets have more damage potential than solid buckets, as the teeth and apron involves greater uncertainty of hydraulic action and increased cost of repairs. In the case of solid buckets, the damage is confined to the bucket surface only and that does not impair its hydraulic action. Although model studies invariably advocate equal and symmetrical opening of spillway gates, practical difficulties on spillways with a large number of gates often compel unsymmetrical operation. As such, slotted buckets would be advantageous only for the spillways with few spans or ungated spillways where symmetry of operation could be ensured.

22.5 ALTERNATIVE DESIGNS FOR IMPROVEMENTS

Alternative designs aiming at eliminating adverse effects and yet retaining beneficial features in both the solid and slotted buckets have been proposed.

In a solid bucket, the violent ground roller is the cause of entry of material into the bucket and the resulting abrasion damage. A design designated as dentated bucket, introducing alternative slot and dent in the lip of the bucket to counter the ground roller has been provided for a 35 m high dam in India. The details are shown in Figure 10. As expected, the performance of the design was found to be superior when compared with the conventional design. This bucket has been performing satisfactory in the prototype also.

The teeth in the slotted bucket, involving curved and warped surfaces are difficult to construct and may also be subjected to cavitation damage, as seen from the experience of operation of various structures. An alternative design incorporating teeth constructed of simple plain surfaces was developed by USWES, vide Johnson et al. (1975), for the bucket of Little Goose dam, USA. Figure 11 shows the details. It is reported that the design retained the benefits of the teeth and also exhibited favorable pressures than with the original design.

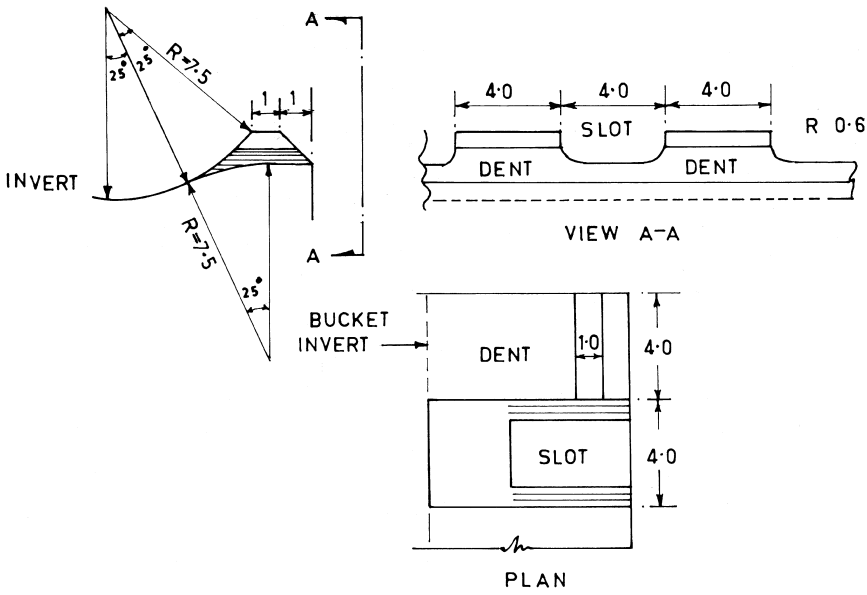

Figure 10 Dentated bucket configurations.

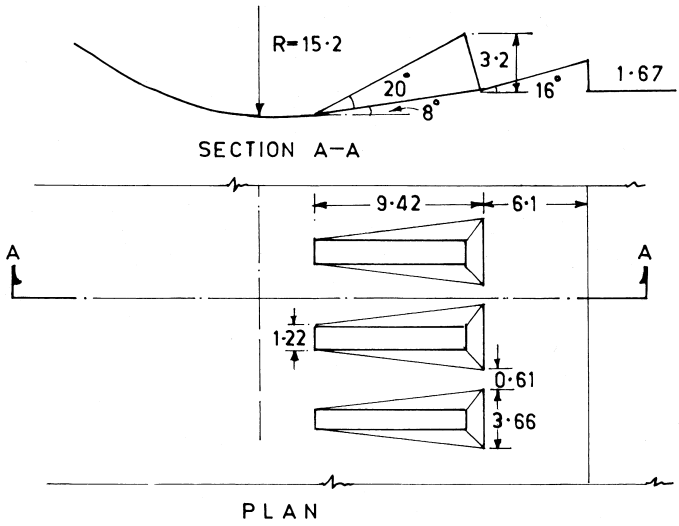

Figure 11 Alternative slotted bucket design for the Little Goose dam, US. (Shown in Johnson et al. 1975)

Although the alternative designs described have performed satisfactory in the model, the prototype experience is limited. It is hoped that it would be possible to adopt these designs when more experience is available.

Notations

d_s = Depth of scour below tail water level.
d_t = Depth of flow on spillway slope at the elevation of tail water.
F_1 = Froude number of flow at bucket invert
F_q = Discharge parameter = $q/\sqrt{g/h_1^3}$
F_t = Froude number of flow on the spillway slope at the elevation of tail water.
h_1 = Head from reservoir W.L. upto bucket invert
h_2 = Depth of tail water above bucket invert
h_b = Depth of flow in a solid roller bucket i.e. height of roller above bucket invert
h_s = Height of surge above bucket invert
H_x = Head from reservoir upto any point x on the bucket.
l_d = Distance of deepest scour from the bucket lip.
P_x = Pressure at any point x on the bucket curvature

q = Discharge intensity
R = Radius of the bucket
r_1 = Radius of streamline of jet in the bucket.
T_{max} = Maximum TW depth for good performance – slotted bucket
T_{min} = Minimum TW depth for good performance – slotted bucket
T_s = TW depth corresponding to sweep out – slotted bucket
V_1 = Velocity of the flow entering the solid roller bucket
V_t = Velocity of flow on spillway slope at the elevation of tail water
y_2 = Conjugate depth of hydraulic jump corresponding to the bucket invert elevation

REFERENCES

1. Dange, N. M.; Waghmare, D. S.; Ghodke, C. V.; Joshi, V. L. Prototype Behaviour of Slotted Roller Bucket - Proc. Intl. Workshop on Research Needs in Dam Safety; CBIP, New Delhi, 1989.
2. Doddiah, D. Study of bucket type energy dissipators with special reference to surge characteristics, Irrigation and Power; CBIP(India), July, 1960.
3. Govind Rao, N. S.; Rajaratnam, N. The submerged hydraulic jump. Jnl. of Hyd. Dn., ASCE, January 1963, 89(No.HY1).
4. Harkauli, A. N. General Comments on Q 50, 13th ICOLD, 1979, 513.
5. Hiranandani, M. G.; Wadekar, G. T. Spillways and Energy Dissipators - Hydraulic Model Investigations, CWPRS Tech. Memo. Hyd 1, April, 1962.
6. Johnson, R. L.; Perkins, L. Z. Spillway for Little Goose dam, Snake River, Washington, TR No 114-1, US WES, North Pacific Bonneville Lab, 1975.
7. Rao, K. N. S. Some studies on hydraulic energy dissipators, Thesis submitted to the University of Roorkee, April, 1978.
8. Kelkar, Y. S.; Khatsuria, R. M. Hydraulic forces on a submersible divide wall in a roller bucket, 43rd Annual Research Session; CBIP, Dehradun, June, 1973.
9. Khatsuria, R. M. Performance of solid roller buckets with special reference to submergence by tail water - Dissertation submitted to the University of Poona, for the degree of ME (Civil), March, 1975.
10. Khatsuria, R. M. Comparative performance of solid and slotted bucket energy dissipators for spillways - Indian Experience, National Conference HYDRO-99; Indian Society for Hydraulics, Nagpur, March, 1999.
11. McPherson, M. B.; Karr, M. H. A study of bucket type energy dissipator characteristics - ASCE Jnl. of Hyd. Dn, June 1957, Corrections, August, 1957.
12. Peterka, A. J. Hydraulic design of stilling basins and energy dissipators, USBR Eng. Monograph. 1978.
13. Thatte, C. D.; Patel, J. K.; Rana, J. C.- Repairs of energy dissipators of dams in Gujarat damaged due to spillway overflows - Proc. First Intnl. Conference in Research Needs in Dam Safety; CBIP, New Delhi, 1991.
14. USACE Hydraulic design of spillways- Engineer Manual 1110-2-1603, January, 1990.

15. USBR Design of Small Dams. (1977).
16. USBR Hydraulic design of stilling basins and energy dissipators, Engg Monograph No 25, 1978.
17. Vaeshney, R. S. Effect of bucket parameters on pressures and energy dissipation characteristics, Vishwakarma, April, 1968.
18. Varshney, R. S.; Dass, R. K. Roller action in bucket type energy dissipator - Irrigation and Power, CBIP, January, 1974.
19. WES Hydraulic Design Criteria, Chart 112-6, 1966.

23
Energy Dissipators for Shaft and Tunnel Spillways

23.1 INTRODUCTION

Shaft and tunnel spillways pose peculiar problems for energy dissipation which necessitate special considerations when being design. A number of problems arise because of the dissimilarities between the factors that influence the choice of energy dissipator for the open gravity/chute spillways and shaft/tunnel spillways. Some of these are:

- Full-bore pressurized flow in part of the downstream leg of the tunnel spillways in contrast with free-surface flow in the gravity/chute spillways.
- A three-dimensional nature of the flow in the tunnel spillways in contrast with a wide chute flow that is two-dimensional in nature.
- Tunnel exit portals, in general, that are located on the flanks, which result in the outlet flow being obliquely oriented with reference to the general direction of the river flow. This also results in deficient tail water depths, restricting the choice of energy dissipators to flip buckets.

Obviously, there is no standard procedure for the design of an energy dissipator. Designs that have been developed to cater to the various factors imposed by the hydraulic, topographic, and geologic conditions at the site, would serve as the guideline.

23.2 FULL-BORE PRESSURIZED FLOW

For pressurized flow tunnels with significant length, dissipation of part of the energy within the tunnel would be possible by introducing devices that cause head loss. The following devices are generally employed:

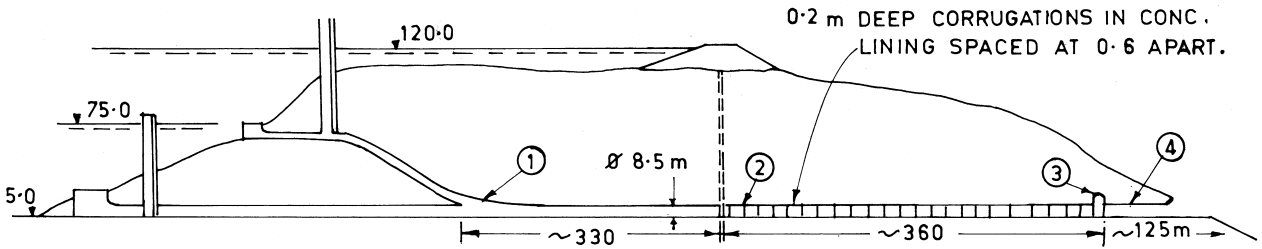

Figure 1 Dissipation of energy by friction

① Tunnel with non-reinforced corrugated concrete lining, flow velocity 15 m/s
② –do– but with reinforcement
③ Outlet with reducer
④ Free flow tunnel

1. Providing tunnel lining with frictional elements such as slots, rounded forms, etc.
2. Introducing orifice plates at specified intervals along the tunnel length
3. Swirling devices

23.2.1 Dissipation By Friction

In an article prepared (see 13th ICOLD) in 1979 by the French National Committee on Large Dams, details of pressurized spillway tunnels utilizing hydraulic friction for dissipation of energy have been provided, as shown in Figure 1. Four tunnels with an approximate length of 700 m and diameter of 8.5 m were used for diversion and later converted into permanent bottom outlets. A total discharge of 3000 cumec is passed through the tunnels with a velocity of about 15 m/s. The tunnel lining is formed using corrugations with 0.2-m depth rounded edges and 0.6-m spaced centers. Such a lining, in the author's opinion, permits dissipation of about 83% of flow energy, thereby lightening the terminal structure for dissipating the residual energy. The flow approaching the outlet end is converted to free flow.

23.2.2 Dissipation By Head Loss

Significant energy dissipation can be achieved by creating head loss by introducing orifice plates at specified intervals. A schematic of the arrangement is shown in Figure 2. The main concern is the cavitation. Model studies are required to determine the diameter of the orifice opening with reference to the tunnel diameter, shape of the orifice edge, and number and spacing between the orifices. The flow downstream of the orifice section is converted to free flow. This concept is becoming popular in China.

23.2.3 Swirling Devices

A general description of the swirling device for the downstream leg of a shaft spillway was given in Chapter 8. This device is suitable for a shaft spillway

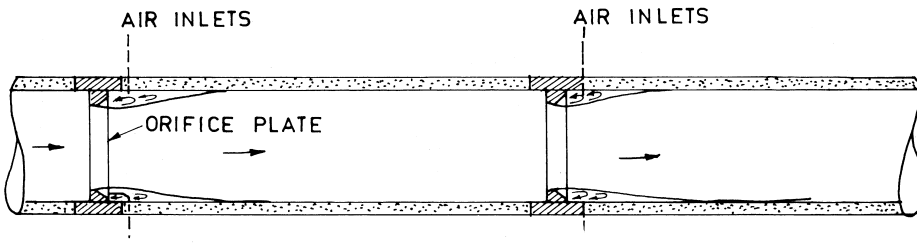

Figure 2 Schematic of dissipation by head loss with orifice plates

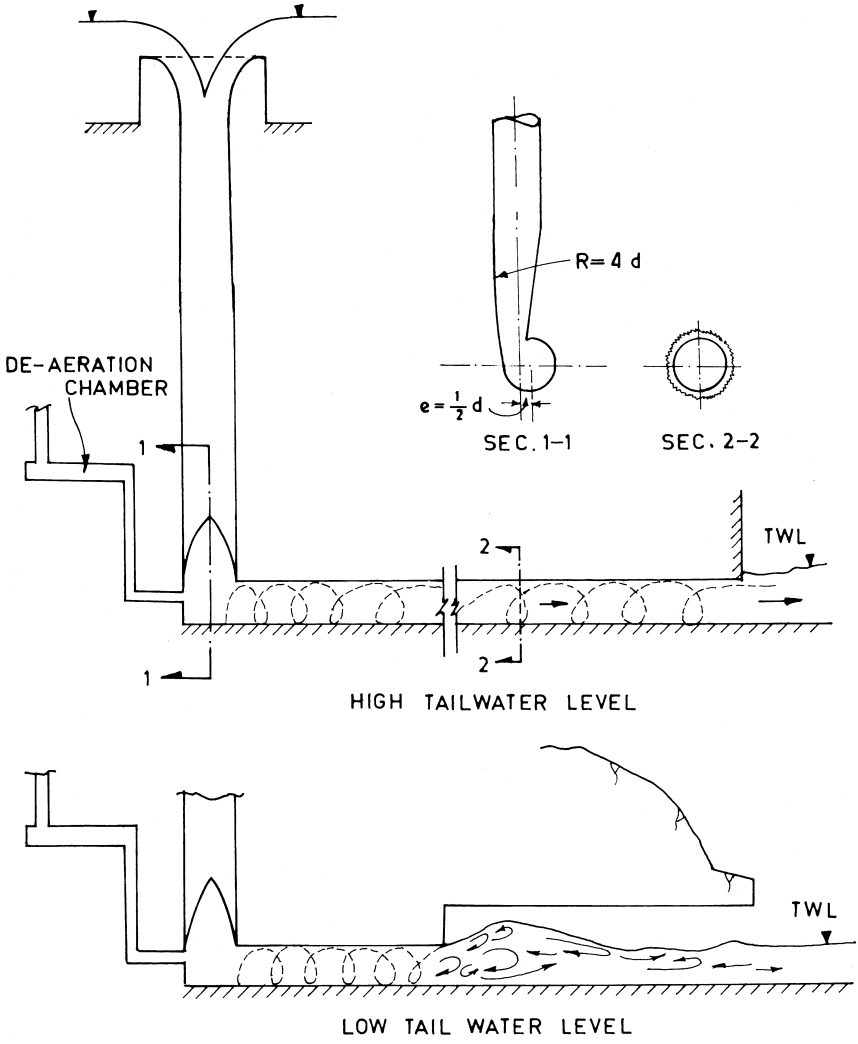

Figure 3 Energy dissipation by swirling flow

where the flow descends down a vertical shaft and joins a horizontal tunnel. The flow in the tunnel must be pressurized irrespective of the tail water level. Two arrangements are possible as shown in Figure 3. Energy dissipation occurs due to friction between the spinning water flow and the tunnel boundary. The intensity of spinning gradually reduces as the flow moves away from the spinning device. Significant amount of air is entrained by the spinning flow, which needs to be released by an air vent provided at the upstream end of the tunnel. The possibility of cavitation is reduced due to the high positive pressures along the tunnel walls and the presence of air. It is estimated that about 70% of the energy is dissipated in the shaft, swirling device, and tunnel.

23.3 FREE SURFACE FLOW

23.3.1 Flip Buckets

The flow at the outlet end of the tunnel is always a free-surface flow. Generally, the tunnel exit portals are located on the flanks and, hence, flip buckets are the most commonly used energy dissipators. Earlier designs involved transitions from circular or horseshoe sections to flat-bottom rectangular sections in order to provide buckets and side walls—with or without deflectors—so as to guide the flow from the bucket toward the main river course. Later, in 1978, the USBR developed designs that either combined the transition and flip bucket into a single structure or eliminated the need for a transition altogether.

A flip bucket developed for the Fontana Dam spillway tunnel was meant to direct the jet issuing from the bucket toward right. Its configuration evolved from the model studies to such an extent that it could not be defined by ordinary dimensioning or mathematical equations. A dispersion flip bucket for the Trinity Dam, as shown in Figure 4, is another unusual design.

For the spillway tunnels of the Glen Canyon and Flaming Gorge Dams, transition flip buckets, shown schematically in Figure 5, were meant to combine the transition and the bucket into a single structure. These buckets cause a planned dispersion of the jet, which contributes to air entrainment and energy dissipation. The sidewalls of the bucket can also be provided with deflectors to guide the flow in a desired direction.

For the Whiskeytown Dam spillway, a transition flip bucket was not suitable because of its divergence in a rather narrow waterway. A design called Tube Elbow Flip Bucket, as shown in Figure 6, was developed for this situation. The semicircular invert of the tunnel is curved upward radially, as a turned up tube or elbow. The sidewalls above the spring line of the invert are vertical. Also, a 3° wedge turning inward along both the sidewalls was introduced to converge the jet and reduce the spreading.

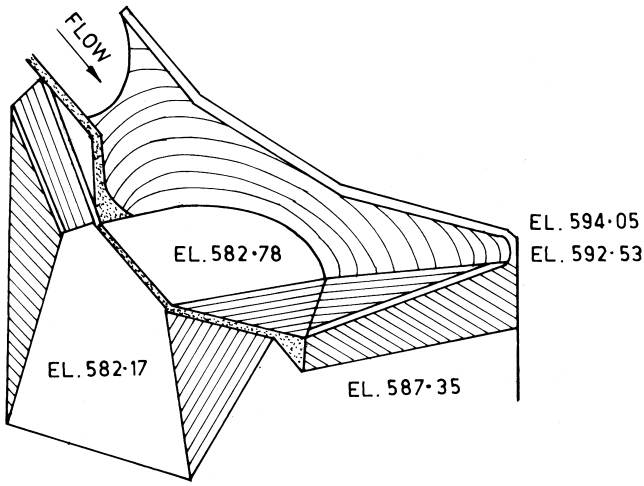

Figure 4 Dispersion flip bucket – Trinity dam, (Shown in USBR, 1978)

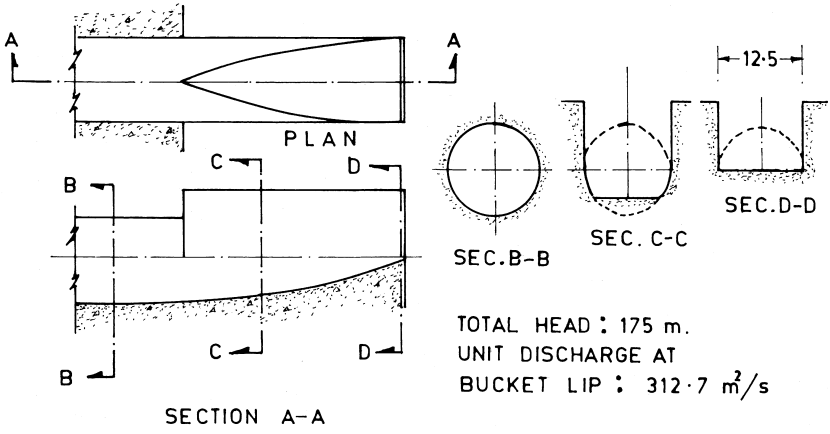

Figure 5 Transition flip bucket – Glen Canyon dam (Shown in USBR, 1978)

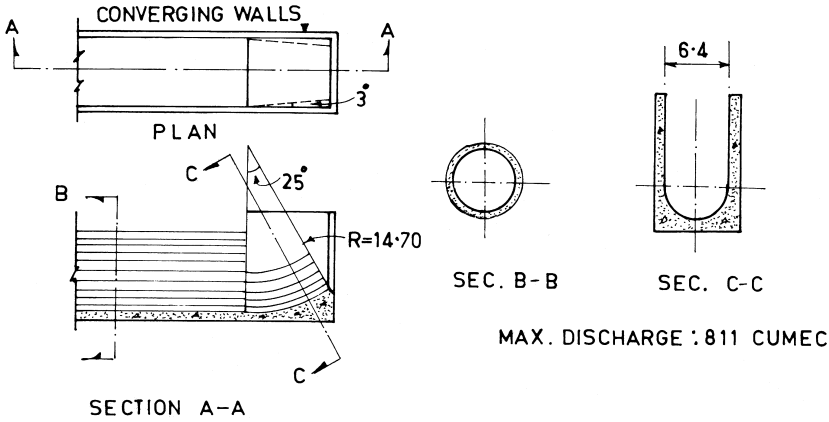

Figure 6 Tube elbow flip bucket, Whiskey town dam (Shown in USBR, 1978)

If the goal is dispersion of the flow—and not simultaneous deflection—an expanding bucket with flow splitters, as shown in Fig 26 – Chapter 21, would work efficiently.

Combination stilling basin flip bucket

Sometimes the tail-water conditions at the tunnel exit are such that a hydraulic jump may form for lower discharges, yet the tail-water depths corresponding to higher discharges are inadequate for the formation of a hydraulic jump. Also, it may not be feasible or economical for the stilling basin to be set at a deeper elevation to make it function as a hydraulic jump basin for the entire range of discharges. In such cases, a dissipator in the form of combination stilling basin flip bucket would be suitable. For example, the energy dissipator for the Yellowtail Dam tunnel spillway, U.S.A., as shown in Figure 7, functions as a stilling basin for low discharges, up to about 12% of the maximum design discharge, and as a flip bucket for higher discharges (USBR, 1978). While designing such structures, it is necessary to depress the invert of the stilling basin below the tunnel exit elevation and join it with a suitable glacis profile so that the hydraulic jump does not move upstream and inside the tunnel. It is also necessary to ensure that low flows cascading down from the lip of the bucket do not undermine the bucket foundation.

23.3.2 Hydraulic Jump Stilling Basin

Either tail-water conditions or geological characteristics of the area at the tunnel exit necessitate provision of a hydraulic jump stilling basin. Hydraulically, this al-

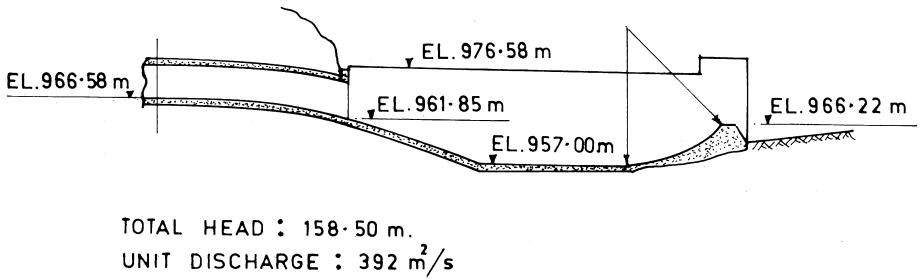

Figure 7 Combination stilling basin flip bucket for Yellowtail dam tunnel spillway (Shown in USBR, 1978)

ternative may pose serious difficulties due to the high velocities and large discharge concentration in a narrow width. For example, a hydraulic jump stilling basin in place of a compact transition flip bucket for the Glen Canyon Dam tunnel spillway would have required a basin elevation some 52 m below the tail-water elevation and a length of about 230 m. (USBR, 1978) This would be necessary particularly in view of the fact that stilling basin appurtenances such as baffle piers cannot be used for velocities as high as 50 m/s. Under the specified circumstances, a spatial hydraulic jump is an effective and efficient means of energy dissipation.

Spatial hydraulic jump

A spatial hydraulic jump occurs when supercritical stream confined between parallel boundaries meets a wider channel, either through a sudden or gradual expansion. The main advantage of a spatial hydraulic jump is that it requires a smaller conjugate depth than a conventional jump that forms in a channel of constant width. The basic structure of a spatial hydraulic jump is shown in Figure 8. The most effective jump is the one that forms at or near the location of the expansion. A jump forming downstream of this section—due to a tail-water depth smaller than the conjugate depth—is called a repelled jump (R-jump). When the jump forms farther upstream than the location of expansion—due to a higher tail-water level—so that it lies partly in a narrower channel and partly in a wider channel, it is called a broken jump (B-jump).

Herbrand et al. have derived some important characteristics of the spatial hydraulic jump that are relevant to its application for energy dissipation at the outlets of shaft/tunnel spillways, where discharge and energy are concentrated in a relatively narrow width. Starting from the momentum equation applied to the control volume enclosed between sections (1) and (2) and following the terminology as shown in Figure 9,

$$\rho Q(V_1 - V_2) = \frac{\gamma}{2}\left[B y_{2B}^2 - b y_{1b}^2 - (B-b) y_e^2\right] \tag{1}$$

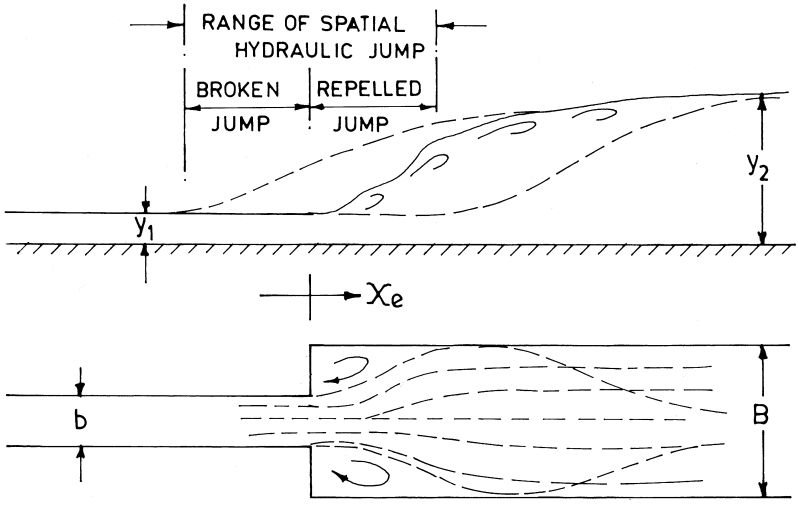

Figure 8 Spatial hydraulic jump.

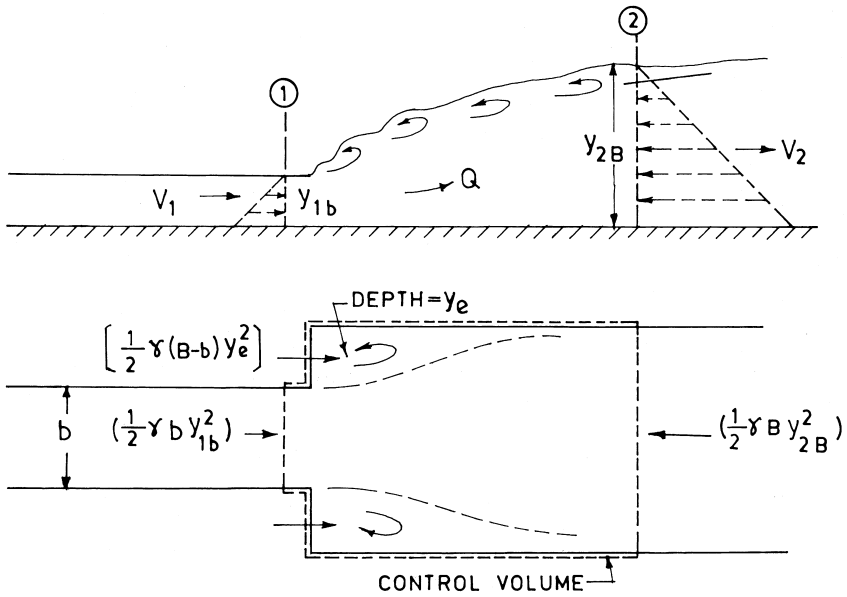

Figure 9 Momentum equation as applied to spatial hydraulic jump (Shown in Herbrand et al, 1973)

This, together with the continuity equation $Q = bV_1\, y_{1b} = BV_2\, y_{2B}$ and dimensionless parameters $n_B = \frac{y_{2B}}{y_{1b}}$, $\beta = \frac{b}{B}$, and $F_1 = V_1/\sqrt{g\, y_{1b}}$, simplifies to

$$n_B^3 - n_B\left[\beta - \beta\left(\frac{y_e}{y_{1b}}\right)^2 + \left(\frac{y_e}{y_{1b}}\right)^2 + 2\beta F_1^2\right] + 2\beta^2 F_1^2 = 0 \tag{2}$$

In order to evaluate y_{2B}, y_e must be known. Herbrand made simple assumptions, $y_e = 0$ and $y_e = y_{1b}$, to get an identical solution as

$$n_B = F_1\sqrt{2\beta} - \frac{\beta}{2} \tag{3}$$

In a similar manner, the relationship between y_{1b} and y_{2b} for a conventional hydraulic jump in a channel of constant width b,

$$n_b = \frac{y_{2b}}{y_{1b}} = \frac{1}{2}\left(\sqrt{1 + 8F_1^2} - 1\right) \tag{4}$$

can be simplified (treating $\sqrt{1 + 8F_1^2} \approx \sqrt{8F_1^2}$) as

$$n_b = F_1\sqrt{2} - \frac{1}{2} \tag{5}$$

and hence,

$$\frac{n_B}{n_b} = \sqrt{\beta} + \frac{\left(1 - \sqrt{F_1}\right)}{2n_b} \tag{6}$$

For large values of F_1, the second term $\frac{\left(1 - \sqrt{F_1}\right)}{2n_b}$ is considered to be small and can be neglected, so that

$$n_B = \sqrt{\beta}\, n_b \; OR \; \beta = (n_B/n_b)^2 \tag{7}$$

Eq (7) is of primary concern in the design of spatial-jump energy dissipator, because the equation relates the conjugate depth to the amount of expansion. It states that the stilling basin must be widened by the second power of the factor by which the depth is reduced.

Laboratory experiments conducted by Herbrand et al. and others, with expansion ratio β varying from 0.288 to 1.0 and with expansion in the form of symmetrical and unsymmetrical sudden enlargement as well as gradual enlargement (which also included an S-curve), gave the following relation

$$n_B = n_b\, \beta^{3/8} \tag{8}$$

Herbrand, however, suggests application of Eq (7) for design purposes.

The length of the spatial hydraulic jump can be expressed approximately as

$$L_B = 0.8\, L_b \approx 4\,(y_{2b} - y_{1b}) \tag{9}$$

For mild expansions ($\beta = 1$ to 0.64)

$$L_B = L_b \sqrt{\beta} \tag{10}$$

When the front of the jump is located upstream of the section of expansion (B-jump), the flow pattern is hydraulically satisfactory, but the required conjugate depth is only partially reduced (as compared to that of a conventional jump)

$$n_{br} = n_B \left(\sqrt{\beta} + \frac{x_e - x_e \sqrt{\beta}}{L_b} \right) \tag{11}$$

Where

x_e = Distance from the point of expansion to the front of broken jump

The length of this jump is $L_{br} \approx 5\,(y_{2b} - y_{1b})$.

Practical design considerations

A number of stilling basins employing spatial hydraulic jump have been developed based on model studies at the Oskar V. Miller Institute, in Germany. Herbrand and Knauss (1973) and Herbrand and Scheuerlein (1979) have reported typical case studies. In these studies, the unit discharge varied from 10 to 140 cumec/m, with a head from 14 m to 103 m, a Froude number of the flow entering the stilling basin from 3 to 13.8, a β from 0.20 to 0.50, and the ratio $\frac{n_B}{n_b}$ from 0.54 to 0.86. The following guidelines can be suggested:

- The shape of expansion (sudden, gradual, curved, etc.) does not significantly influence the relationship discussed earlier if the flow is evenly distributed across the width, B, at the end of the jump. Since spatial hydraulic jump has a tendency to oscillate across the width, gradual or curved expansion would minimize the disturbance caused by oscillations. However, appurtenances like sills, baffles, deflector hoods, and adverse slope, etc., are essential to ensure a stable jump. This is even more necessary when the Froude number of the incoming flow is in the range of 2.5–4.5.
- An expansion normally should not exceed four times the width of the entering jet. The hydraulic limitation of the expansion is met when critical flow occurs in the tail-water cross-section.
- The chute width, generally, is expanded and its bottom profile depressed by a transition curve to join a short horizontal apron, which then rises as a reverse slope to meet the original ground level, as shown in

Figure 10 and Figure 11. Appurtenances like deflector hoods, baffle piers, etc., may also be required to stabilize the jump. In many cases, a secondary stilling basin continuing from the main stilling basin may also be necessary.

- The type, size and position of the appurtenances are highly variable for the spatial-jump stilling basin and can only be determined by studying the hydraulic model.
- The expanded portion is generally narrowed down due to economic considerations and is joined to the natural watercourse through a smooth curve wherever necessary.

Herbrand and Scheuerlein (1979) have described the design of stilling basins for the tunnel spillways of Bolgenach Dam, Austria, and Polyphyton Dam, Greece.

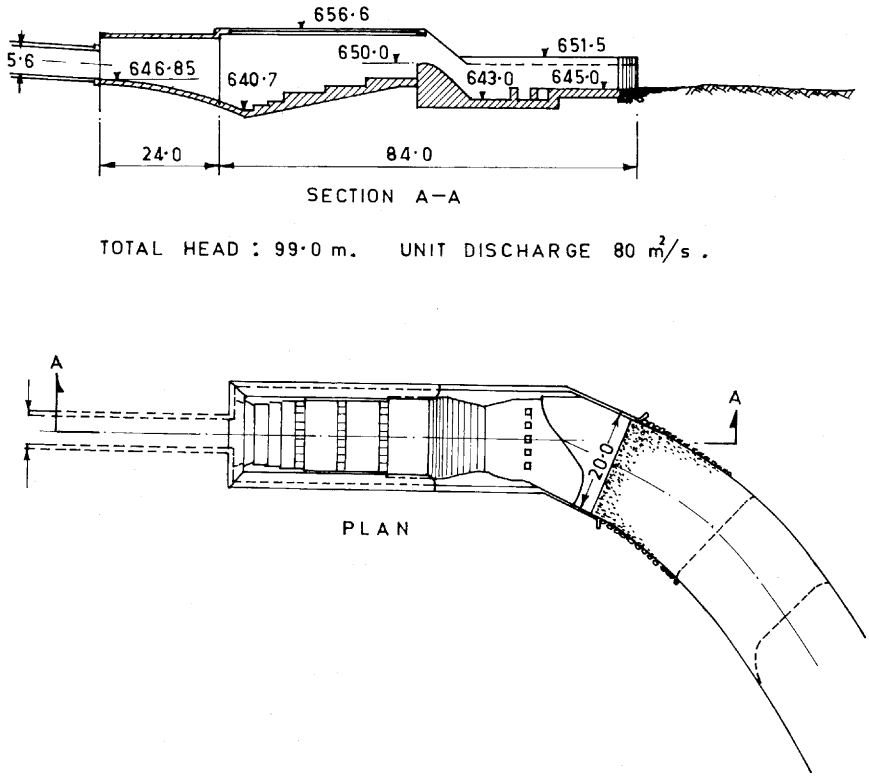

Figure 10 Bolgenach dam stilling basin (Shown in Herbrand et al, 1979)

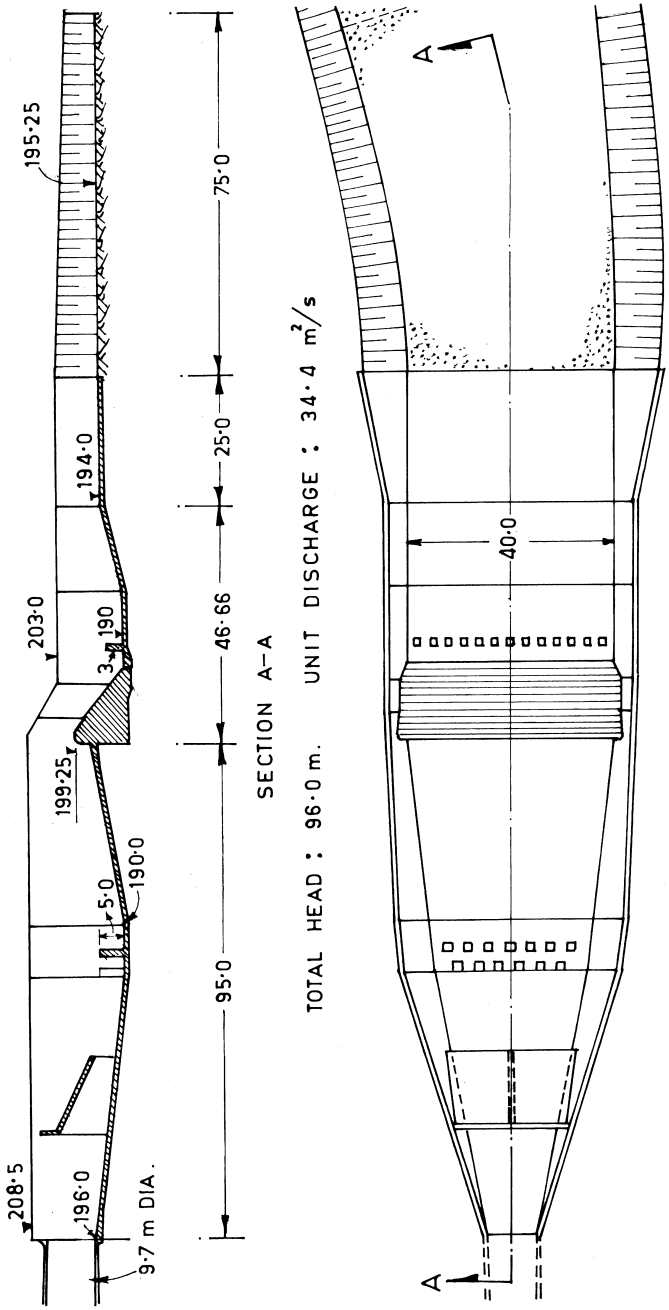

Figure 11 Polyphyton dam stilling basin, (Shown in Herbrand et al, 1979)

These designs amply demonstrate the nature of the problems faced in dissipating the energy and guiding the flow from the energy dissipator to the main river course.

The details of the stilling basin for Bolgenach Dam are shown in Fig 10. The flow entering the stilling basin had a unit discharge as high as 80 cumec/m and a velocity of 31 m/s. The flow leaving the stilling basin had to be turned almost 45° to join the main river course. An abrupt, expanding spatial stilling basin was developed from model studies. An adversely sloped stepped apron helped dissipate significant amounts of energy before the flow passed over a low-height spillway containing a secondary stilling basin with baffle piers and a curved end sill connecting to the channel leading to the main river.

Fig 11 shows details of the Polyphyton Dam stilling basin. With the velocity of flow entering the stilling basin as high as 40 m/s, the Froude number of the flow was about 4.4. This signifies an unstable and oscillating hydraulic jump, which is difficult to handle. As can be seen, adequate energy dissapation could only be obtained by employing a two-stage stilling basin, by flaring the basin, by employing a provision of steps and baffles, by using wave suppressors, etc.

Notations

B = Width of the channel after expansion
b = Width of the channel before expansion
F_1 = Froude number of the flow entering the stilling basin
L_B = Length of spatial hydraulic jump with expansion B
L_b = Length of conventional hydraulic jump in a channel of constant width b
L_{br} = Length of broken hydraulic jump
n_B = Ratio of sequent depths for spatial hydraulic jump $n_B = \frac{y_{2B}}{y_{1b}}$
n_b = Ratio of sequent depths for conventional jump $n_b = \frac{y_{2b}}{y_{1b}}$
Q = Discharge
V_1 = Velocity of flow entering the stilling basin
V_2 = Velocity of flow leaving the stilling basin
x_e = Distance measured from the location of expanded section
y_{1b} = Depth of supercritical flow in the channel of width b
y_{2B} = Conjugate depth of spatial hydraulic jump in expanded channel B
y_e = Depth of flow in horizontal roller in the expanded channel (Fig 9)
β = Ratio of channel widths = b/B
γ = Unit weight of water
ρ = Mass density of water

REFERENCES

1. French National Committee on Large Dams. Ouvrages D'evacuation de Grande Capacite, 13th ICOLD. Q50, R61. New Delhi, 1979.
2. Herbrand, K.; Knauss, J. Computation and design of stilling basins with abruptly or gradually enlarged boundaries, 11th ICOLD, Q41, R 4. Madrid, 1973.
3. Herbrand, K.; Scheuerlien, H. C. Examples of model tests dealing with special problems and design criteria at large capacity spillways, 13 th ICOLD, Q 50, R 10. New Delhi, 1979.
4. USBR Hydraulic design of stilling Basins and Energy Dissipators, Engineering Monograph No25, 1978.

24
Impact-Type Energy Dissipators

24.1 INTRODUCTION

The phenomenon of impact by placing an obstacle in the high velocity flow is widely utilized for dissipation of energy in the stilling basins for low-head spillways and outlets. The objective has been to economize the design by reducing its length and ensuring formation of the hydraulic jump, even for a deficient tail-water depth, up to about 0.85 y_2. Examples are: USBR basin III, USACE impact basin, etc. However, the term ''Impact-type energy dissipator'' will be applied only to those structures that rely solely on the phenomenon of impact for dissipation of energy, even without tail-water build up. Dissipators of this type involve impacting a high velocity jet on a solid object, separating the flow through contorted shapes to create additional rollers or shear planes, or directing jets through a winding conveyance to strike each other. Due to their compact shape and short length, such structures have proved to be attractive alternatives in place of standard designs. However, their application is limited to relatively low velocities from the apprehension of cavitation or excessive drag force on the elements creating impact force.

24.2 CLASSIFICATION OF IMPACT-TYPE ENERGY DISSIPATORS

Impact-type energy dissipators can be classified into two categories. In the first category are those structures that seek to prevent acceleration of the flow during its passage itself so that the flow velocity remains essentially constant and the size of the energy dissipator is smaller. This is generally applied to flows on flat chutes carrying small discharges. This type is specially suited to small structures like highway drainage chutes, culverts, drops, and canal waste ways. In the other category, turbulence is created by obstructing the flow at the base of spillways

and outlets to effect dissipation of energy. The special feature of these structures is that no tail water is required for their functioning.

24.3 BAFFLED CHUTES

Providing stilling basins of standard designs at the base of structures like high way drainage chutes, canal drops, etc, which carry small discharges, may prove to be uneconomical. One way of economizing the size of the stilling basin or eliminating it all together is to dissipate part of the energy on the chute itself. Different designs of stepped chutes (as discussed in Ch. 6) can be considered as one of the alternatives. Here, the principal forces contributing to the energy dissipation are shear and turbulence. Dissipation of energy by impact requires inclusion of devices like friction elements and baffles. The objective is to prevent undue acceleration of the flow, thus limiting the velocity to a magnitude that can be handled easily.

24.3.1 Energy Dissipation by Induced Tumbling Flow

One of the ways to limit velocity is to use simple roughness elements on the bed of the chute, utilizing size and spacing to induce what is termed as the tumbling-flow regime in the channel. Tumbling flow consists of a series of hydraulic jumps in which the flow oscillates from subcritical to supercritical and then, through the jump, back to subcritical as it passes each roughness element. This phenomenon is shown in Figure 1.

Tumbling flow is a quasi-critical flow condition where the specific energy is maintained at its minimum level for a given discharge. The velocity at the outlet of the channel is nearly equal to the critical velocity ($\sqrt[3]{gq}$), which can be handled safely by a stilling basin of smaller size. The efficiency of this device is dependent on the height and spacing of the elements that ensure succession of hydraulic jumps as described earlier.

Morris (1968) conducted extensive studies at the Virginia Polytechnic Institute, USA. It was shown that the optimum spacing of elements was related to the critical spacing for maximum friction factor for flow in closed conduits or tranquil flow in open channels. Such spacing marks the boundary between wake-interference flow and isolated-roughness flow. The elements thus should be separated just sufficiently so that each jump is fully developed without interfering with the adjacent jumps. Morris suggested that, for practical design purposes, the spacing-height ratio λ / h should be between 7.5 and 12.0 with a recommended value of 10. For this spacing, the empirical design equations for roughness elements are:

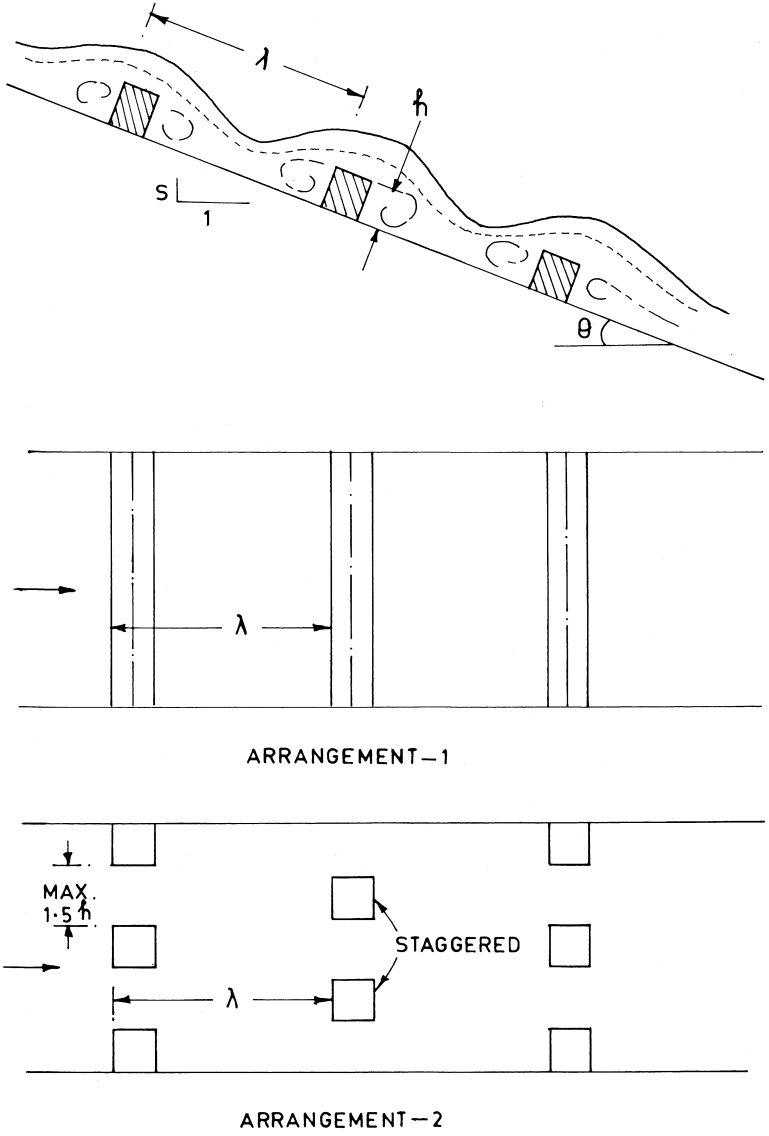

Figure 1 Energy dissipation by induced tumbling flow. (Shown in Morris 1968.)

-For roughness elements of square cross-section (Arrangement 1, Figure 1)

$$h = \frac{1}{(3-3.7S)^{2/3}} y_c \quad (1)$$

Where

S = Slope of the chute, S = Tan θ

y_c = Critical depth

-For cubical roughness elements, with cubes staggered in adjacent rows and with a maximum transverse element spacing of 1.5 h (Arrangement 2, Figure 1)

$$h = 0.7\ y_c \quad (2)$$

The height of the element, h, obtained from the above equations is the minimum size to ensure tumbling flow. The equations apply specifically to rectangular channels but can be also used for trapezoidal channels where y_c must be calculated based on the bottom width alone. The roughness elements should also be beveled on their ends to fit against the sloping sides of the channel.

As Equation 1 suggests, the bed slope of the chute can not be steeper than say 39°. Generally, a slope of 2H:1V is preferred.

The elements should normally be used throughout the entire length of the chute. However, if economy dictates, an alternate method is to use only five rows of elements at the downstream end of the chute, preceded by a single large leading element. The large element establishes one large hydraulic jump and the five following elements are then adequate to establish uniform tumbling flow for the given discharge from the leading element's overfall. The size, h_1, of the leading element is given by

$$h_1 = \left[\sqrt{\frac{2}{(1-S)^2}\left(\frac{y_c}{y_0}\right) - (1-S)^2} \right] y_c \quad (3)$$

where y_0 is the supercritical depth just upstream from the leading element. This depth can be determined by flow profile calculations.

Since there is no restriction on the height of the chute—as the velocity all along the chute is practically constant—the limit of application of this device is governed by the unit discharge, with consideration of the absolute size of the elements and factors such as cavitation and drag. Knowing the size of the element and the flow velocity, the tendency of cavitation and drag force (using standard coefficients) can be assessed.

24.3.2 Baffled Apron Drops

Baffled apron drops or chutes consist of a sloping channel, usually on a 2:1 or flatter slope with multiple rows of baffles equally spaced along the chute. The

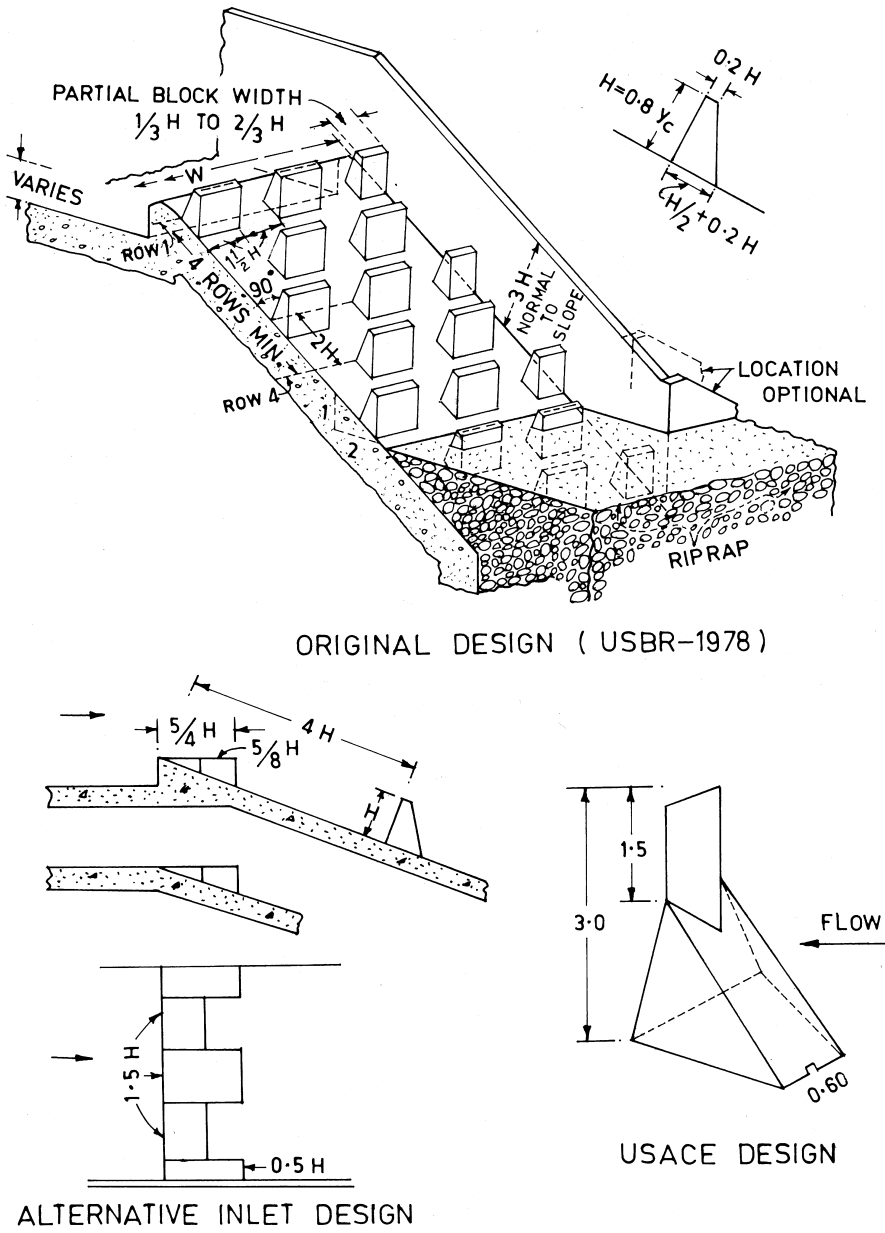

Figure 2 Baffled-apron drop. (Shown in USBR 1978.)

flow passes over, between, and around the baffles. The resistance offered by the baffles prevents excessive acceleration of the flow and provides a reasonable terminal velocity, regardless of the height of the drop. A number of baffled chutes have been constructed and tested by USBR. A standard design developed by USBR (1978) is shown in Figure 2.

The design is suitable for unit discharge not exceeding 30 cumec/m and approach velocity less than critical velocity $\left[V_c = \sqrt[3]{gq}\right]$. If the velocity is higher, an entrance sill should be placed whose height can be worked out considering it as a weir, to ensure subcritical flow in the approach channel. The baffled apron is also extended below the channel bottom. Backfill is placed over one or more rows of baffles to restore the original streambed elevation. When scour or downstream channel degradation occurs, successive rows of baffles are exposed to prevent excessive acceleration of the flow. If degradation does not occur, the scour creates a stilling pool at the downstream end of the chute, stabilizing the scour pattern. If excessive degradation occurs, it may be necessary to extend the chute further.

The design of the baffle developed by the USACE (1990) during the model study of the proposed Libby Reregulating Dam, USA, has also been shown in Figure 2. The 3-m high baffles were spaced about 5.5 m in the flow direction on a 25-m high spillway chute at about 1.5 m in the transverse direction. It is claimed that these baffles were effective, not only in energy dissipation, but also in aerating the flow and reducing nitrogen supersaturation. The baffles could function effectively for unit discharges as large as 80 cumec/m.

24.4 ENERGY DISSIPATORS FOR SPILLWAYS AND OUTLETS

Impact type energy dissipators at the base of spillways and outlets do not require initial tail-water for their functioning. However, their size and the range of application is restricted by the apprehension of cavitation damage and excessive drag.

24.4.1 USBR basin VI

The most commonly used stilling basin VI developed by USBR for pipe outlets is a small, rectangular box-like structure equipped with vertical hanging baffle. This is shown in Figure 3. Energy dissipation in the stilling basin is initiated by the flow striking the baffle and being turned upstream by the horizontal portion of the baffle and by the floor, which creates vertical eddies and turbulence. The structure requires no specific tail water for energy dissipation: however, tail water as high as (E + T/2) as shown in Figure 3 improves the performance by reducing outlet velocities and smoother water surface profiles. The energy dissipation effi-

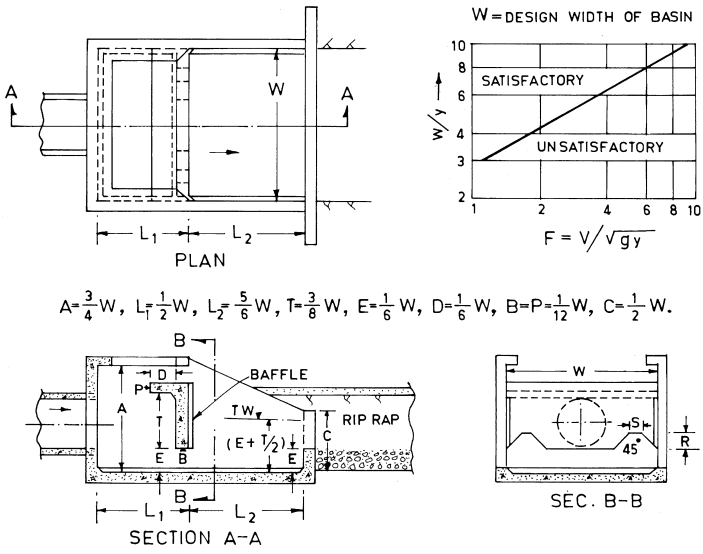

Figure 3 Basin IV for pipe or open channel outlet. (Shown in USBR 1978.)

ciency of this basin is about 10% more than the conventional hydraulic jump basin.

The basin operates as well, whether a small pipe flowing full or a larger pipe flowing partially full, is used. The basin would work equally well for an open channel, in which case its entrance to the basin should be narrower than the basin width and be placed with invert elevation, the same as the pipe.

Various dimensions of the structure in terms of basin width, w, are suggested, as in Figure 3. The width of the basin has been related to the Froude number of the flow entering the basin

$$F = \frac{V}{\sqrt{g\,y}} \tag{4}$$

Where

V = Velocity of the incoming flow

y = Depth of the flow entering the basin, which is taken as the square root of the cross-sectional flow area.

Based on the performance of the existing structures, the graph in Figure 3 suggests the width of the basin for ensuring satisfactory performance.

The capacity of such a basin is limited to the feasibility of the structural design and to an incoming velocity of about 15 m/s and Froude number 1 to 9,

in view of the large dynamic forces, turbulence, and vibration. An individual unit can handle a discharge up to about 11 cumec. Greater discharges can be handled by constructing multiple units side by side. Adequate protection should also be made for the downstream bed and banks against scour, by riprap.

24.4.2 Bhavani-Type Stilling Basin

Bhavani-type stilling basin is one among the few designs of energy dissipators for spillways relying largely on the phenomenon of impact for its functioning. Kuttiammu and Rao (1951) have described the development of this design for the 35 m high spillway of the Lower Bhavani Dam in India. The stilling basin consists of a short, depressed apron equipped with T-shaped floor blocks. Its special features are that (1) a hydraulic jump is ensured inside the basin for all conditions of flow; (2) the dissipation of energy is fairly complete as indicated by the absence of any boil in the jump profile and minimum scour; (3) the T-shaped blocks are strong and stable and free from cavitation; and (4) the design is economical on account of the short length of the apron provided.

The design was developed from extensive studies on a model. The principal objective was to finalize a design of the stilling basin that would cater to the head of about 35 m and unit discharge of the order of 20 cumec/m (velocity of about 27 m/s), under a deficient tail-water depth. Model studies included some 18 shapes of floor blocks whose performance was judged based on the profile of the jump as well as the magnitude and distance of the maximum scour from the structure. The design of the T-shaped blocks finally adopted was in the form of rectangular blocks 0.9 m $\times$ 1.22 m $\times$ 1.83 m spaced at 7.32 m centers, at a distance of 1.83 m from the entrance to the stilling basin. Each of these blocks was buttressed against the end sill of the stilling basin by a strut 1.22 m wide and 1.52 m high. A 3.05 m high vertical end sill was provided whose top level was set at the average riverbed. The length of the apron required was only 9.15 m, which was hardly one y_2 or so. The details of the design are shown in Figure 4.

The T blocks contributed to the efficiency of energy dissipation in several ways, namely (1) by direct impact, (2) by friction on all the sides, (3) by splitting up the jet, and (4) by interaction among the jets. The buttresses were helpful in preventing lateral flows caused by uneven opening of crest gates.

The T blocks finalized from the model studies were tested for pressure distribution under different operating conditions. Being fully submerged, the pressures on the blocks were highly positive, except for the condition of the shooting flow created by lowering the bed downstream. The cavitation tendency was assessed based on the cavitation indices calculated from pressure measurements with reference to the critical cavitation of 0.68. The blocks were considered safe in this regard.

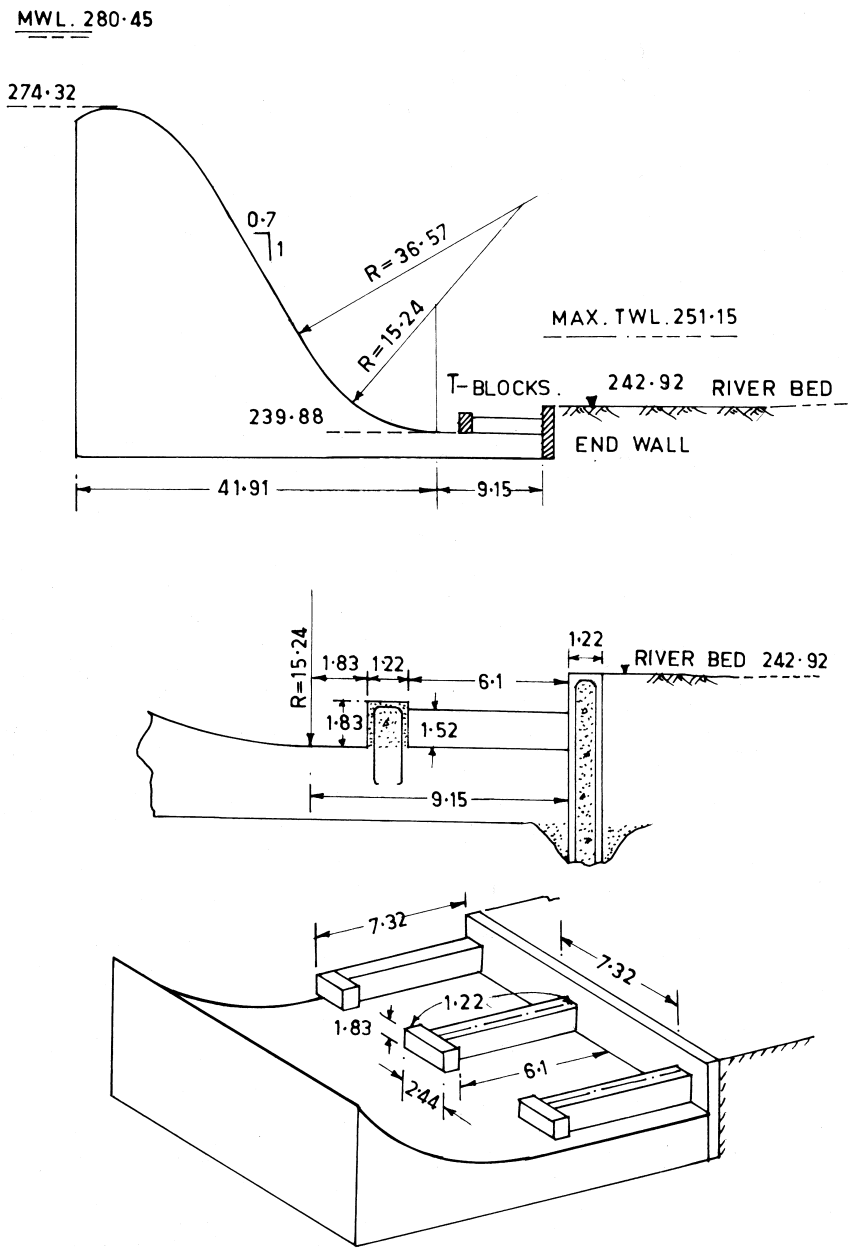

Figure 4 Lower Bhavani stilling basin with T blocks. (Shown in Kuttiammu et al. 1951.)

The authors claim that the design would perform satisfactory for spillways of 25 m to 35 m height, with overflow ranging from nothing to 6 m, and tail-water depth from nothing to 12 m over the riverbed. The stilling basin has been performing satisfactory without any problems for the past four decades, though the design has not been generalized.

However, the experience of installing T blocks of similar shape on the apron floor of the stilling basin of Matatila Dam, India, was not encouraging as reported by Gupta (1979). The 27 m high spillway with 4 m depth of overflow has a unit discharge of about 35 cumec/m. Initially, a 30.50-m long apron, about 2.45 times y_2, without any appurtenances was constructed. The stilling basin was operated with a deficient tail-water depth, and hence the hydraulic jump swept out causing considerable scour in the granite rock downstream. Subsequently, T blocks of similar design as in Lower-Bhavani spillway, of size 4.88 m $\times$ 2.44 m $\times$ 2.44 m with 7.2 m long buttresses of section 2.44 m $\times$ 2.44 m, were installed on the apron, anchoring up to 0.91 m depth. The blocks were dislodged and thrown out. The failure of the T blocks could be attributed to the inadequate bond between the old concrete of the apron and the new concrete of the T blocks, with a short length of anchors. The size of the T blocks was almost twice that of the blocks used at the Lower-Bhavani spillway, though the velocity entering the basin was almost the same order.

Notations

E = Height of baffle from the apron floor (Figure 3)
F = Froude number of the flow entering stilling basin
H = Height of baffle block (Figure 2)
h = Height of roughness element
h_1 = Height of roughness element
q = Unit discharge
S = Slope of the chute, S = Tan θ
T = Vertical dimension of the baffle (Figure 3)
V_c = Critical velocity
y = Depth of flow entering basin VI (= discharge/cross sectional area of flow)
y_c = Critical depth
y_0 = Supercritical depth upstream of the leading element (Equation 3)
λ = Spacing between the roughness elements (Equation 1)

REFERENCES

1. Gupta, B. N. Operational experience of the spillway and energy dissipation devices of Matatila dam located in south-west Uttarpradesh (India), Technical session, Q 50; 13th ICOLD, New Delhi, 1979; Vol. V, 533–536.

2. Kuttiammu, T. P.; Rao, J. V. Bhavani type stilling basin for spillways of large dams, Q 12, R 44; 4th ICOLD, New Delhi, 1951.
3. Morris, H. M. Hydraulics of energy dissipation in steep, rough channels, Bulletin 19, Research division; Virginia Polytechnic Institute, USA, Nov 1968.
4. USACE Hydraulic design of spillways- Engineer Manual 1110-2-1603, January 1990.
5. USBR Hydraulic design of stilling Basins and Energy Dissipators, Engineering Monograph No25, 1978.

25
Unconventional Designs

25.1 INTRODUCTION

Although, a large number of designs of energy dissipators that meet the standard requirements are available, site specific conditions, economy in construction, and urge for innovation have often led to the evolution of unconventional designs of energy dissipators. These designs have been developed from hydraulic model studies, although, in a majority of cases, generalized design procedures have not been established.

As stated above, site-specific conditions, in most cases, have led to departure from the conventional practice. Standard designs either would not fit in or would result in inefficient, elaborate, or expensive design. The decision, therefore, was to bring in additional forces that contribute to increased dissipation of energy, thus resulting in a compact structure, that still performed satisfactorily. These additional forces/devices brought in may be: an abrupt change of direction, additional friction, interaction, dispersion, diffusion, etc.

A survey of literature indicates that such designs can be broadly categorized under the following groups:

Dissipating part of the energy on the spillway slope
Interaction within the region of flow, and
Bifurcation/by pass of flow

25.2 DISSIPATING PART OF THE ENERGY ON A SPILLWAY SLOPE

Dissipation of energy along the spillway slope itself helps economizing the size of the structure, if a hydraulic-jump stilling basin or roller bucket is adopted. To this end, design of stepped spillways (see Ch. 6) has been advanced considerably. Another well-known design employing the principle of impact is that of the tumbling flow and baffled-apron drops (see Ch. 24). However, these designs are

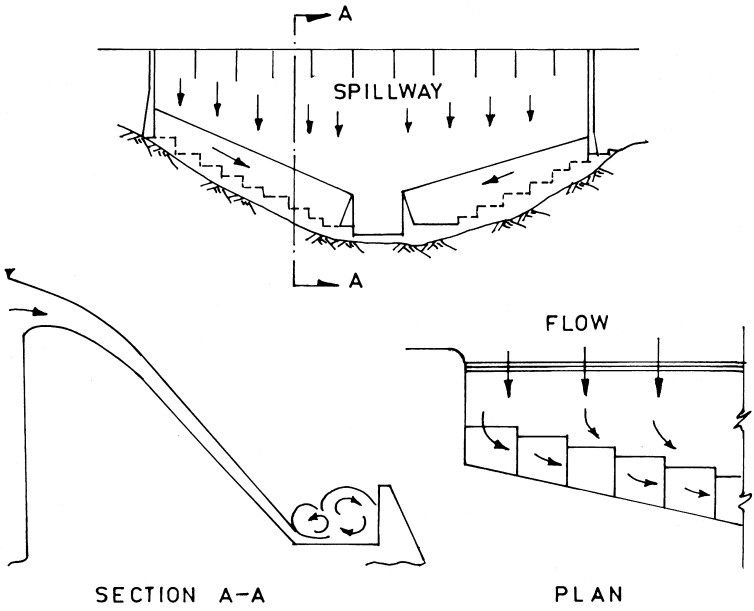

Figure 1 Layout and details of dam-foot training channel. (Shown in Kashiwai et al. 1997).

not applicable for unit discharges exceeding, say 30 cumec/m or so. Kashiwai et al. (1997) have described layouts of spillways and training walls where an abrupt change of direction and steps have been introduced to affect dissipation of the energy before the flow enters the energy dissipator. A layout designated as ''Dam-foot training channel'' is shown in Figure 1. This is particularly suitable for the spillways located in narrow V-shaped valleys with limited width available at the base for the energy dissipator. The design has been evolved from model studies and no information about its application to prototype is available.

25.3 INTERACTION WITHIN THE REGION OF FLOW

Interaction within the region of flow is induced by means such as counter currents, obstacles, or solid boundaries that bifurcate the flow and direct it to collide to dissipate the energy.

Khalifa (1993) has suggested a method of diverting part of the spillway flow at a lower elevation on the same slope and merging again to counter the

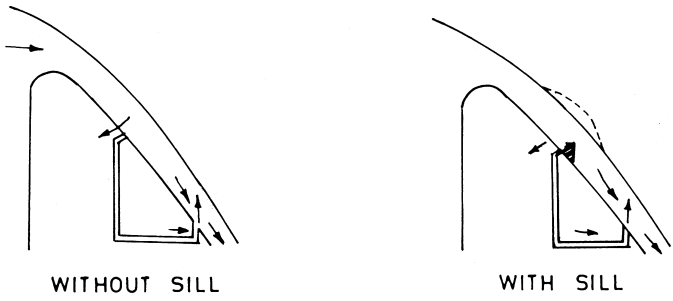

Figure 2 Compacted spillways (CSW). (Shown in Khalifa 1993.)

main flow, in what has been termed a ''Compacted Spillway (CSW).'' Figure 2 shows schematic details. Although, this design has a potential for application on small- and medium-head spillways, there is no information about its implementation in a prototype.

Rajaratnam et al. (2000) conducted laboratory experiments to show that screens or porous baffles with a porosity of about 40% could be used in place of solid baffles as effective energy dissipators below small hydraulic structures. When a supercritical stream (Froude number F_1) passes through such a screen, the resistance forces a hydraulic jump to form upstream of the screen, as shown in Figure 3. The flow downstream of the screen is also supercritical, but with a Froude number in the neighborhood of 1.65. It was also found that the tail water depth, y_t, required to form a jump for this situation was about 0.5 times the

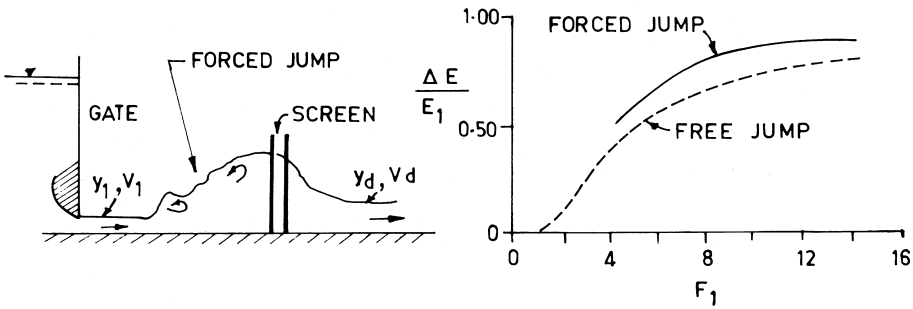

Figure 3 Screen-type energy dissipater. (Shown in Rajaratnam et al. 2000.)

subcritical sequent depth corresponding to the flow with Froude number F_1. The energy loss, ΔE, caused by the screen is

$$\frac{\Delta E}{E_1} = \frac{\left[y_1 + \left(V_1^2/2g\right)\right] - \left[y_d + \left(V_d^2/2g\right)\right]}{\left[y_1 + \left(V_1^2/2g\right)\right]} \tag{1}$$

In their experiments using different arrangements of screens, such as single, double, triangular, etc., they found that the relative energy loss produced by these screens was appreciably greater than that produced by the classic hydraulic jump, as shown in Figure 3.

The above phenomenon has the potential of application of being an energy dissipator below small hydraulic structures like drops, chutes, and erosion-control structures used in storm-water ponds in urban areas, etc. The screens would have to be constructed of concrete with uniformly distributed holes and could be placed at about 2 y_2 from the structure, producing a supercritical stream. A further length of apron of about 0.7 y_2 would be required beyond this, similar to the USBR basin III, but it would need only 50% of the tail-water depth otherwise required (without screens) and would appreciably affect greater dissipation of energy.

Devices that affect dissipation of energy through interacting or colliding jets include interacting jet dissipators and interacting parabolic buckets. In the former, the supercritical flow at the base of a spillway is bifurcated into jets with the splitters in such a way that these jets collide in the air. Although this design, as shown in Figure 4, has been adopted in the Koilsagar and Bendsura spillways in India, it has not become popular because of the damage likely to take place at the pointed tip of the splitters hit by the floating debris.

Gandolfo et al. (1955) have developed a design of interacting parabolic buckets as shown in Figure 5. This consists of alternate buckets, formed by parabolic surfaces, shaped into a circular arch in continuation of a portion of the rear slope of the spillway. The radius of the arc, the parameters defining the bucket surfaces

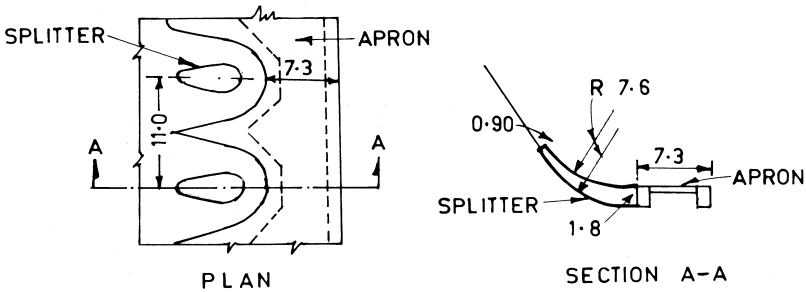

Figure 4 Interacting jet dissipater.

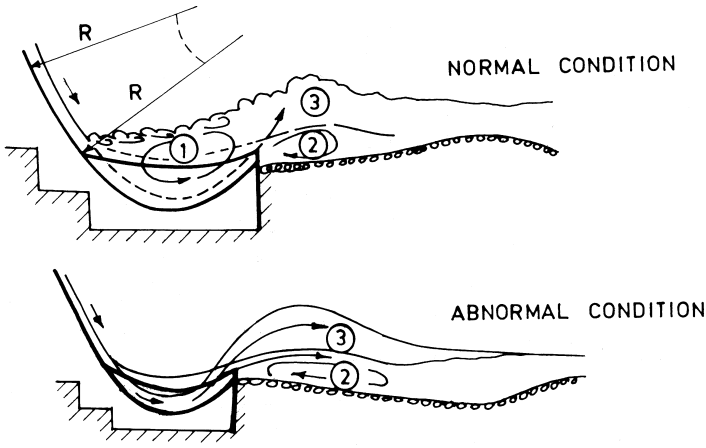

Figure 5 Interacting parabolic buckets. (Shown in Gandolfo et al., 1955.)
① Hydraulic jump ② Ground roller and ③ Surge

and widths of the individual buckets, has been specified in terms of unit discharge, q, and hydraulic head, $\Delta H = (H_2 - H_1)$, where H_1 is the tail-water depth above the average river bed and H_2 is the total energy referred at the same datum.

When a bucket functions within q and ΔH for which it has been designed, it is said to be operating under normal condition. Under this condition, a hydraulic jump forms in the lower bucket with a surge in the downstream and a high velocity stream passes along the higher bucket with a ground roller in the immediate vicinity downstream of the bucket. The intermingling of all these results in intense turbulence and energy dissipation. The efficiency of the design is indicated by a small depth of scour.

The bucket operates under abnormal condition when q and ΔH are outside the range of design values. In this condition, no hydraulic jump forms but the efficiency of the energy dissipation is ensured.

Pressure measurements carried out on the bucket surfaces and sides for the normal, as well as abnormal, conditions indicated high positive pressures so that fear of cavitation damage was remote. The authors claim that this device can be safely used for heads up to 30 m and unit discharge up to 20 cumec/m.

Gandolfo et al. (1957) have also developed similar design for a gated outlet, suitable for heads up to 20 m and unit discharges up to 20 cumec/m.

25.4 BIFURCATION/BYPASS OF FLOW

Sometimes, in a given situation, standard design energy dissipators would be quite feasible, but only within a limited range of discharge. Outside this range,

the structure would either not perform satisfactory or result in an elaborate and expensive design. Designers have evolved innovative devices for such cases, which function in combination with bifurcation or bypass the part of the flow to be handled separately, without additional structure.

Yang (1994) has developed what is termed, ''Dispersive-flow energy dissipator.'' This design evolved from model studies for the Shanzi Dam spillway, China, aims at combining the features of three conventional designs—hydraulic-jump apron, slotted bucket, and ski-jump bucket. As shown in Figure 6, dispersive-flow energy dissipators consist of three main parts: dispersive flow boards (basically ski-jump buckets with deflectors to disperse the flow horizontally and vertically), chute blocks, and adverse-current end sill.

The flow is divided into three parts: flow over the boards, Q_1, flow passing over the top of the chute blocks, Q_2, and flow between chute blocks, Q_3. Small discharges follow the spillway profile with no flow passing over the flow boards. The Q_2 flow forms a surface current in the stilling basin similar to a bucket type with lip angle $= 0°$. The Q_3 flow forms a contracted hydraulic jump. The discharges Q_2 and Q_3 are dispersed and redistributed by the flaring chute blocks, which require less tail-water depth and a shorter apron. It is claimed that reducing

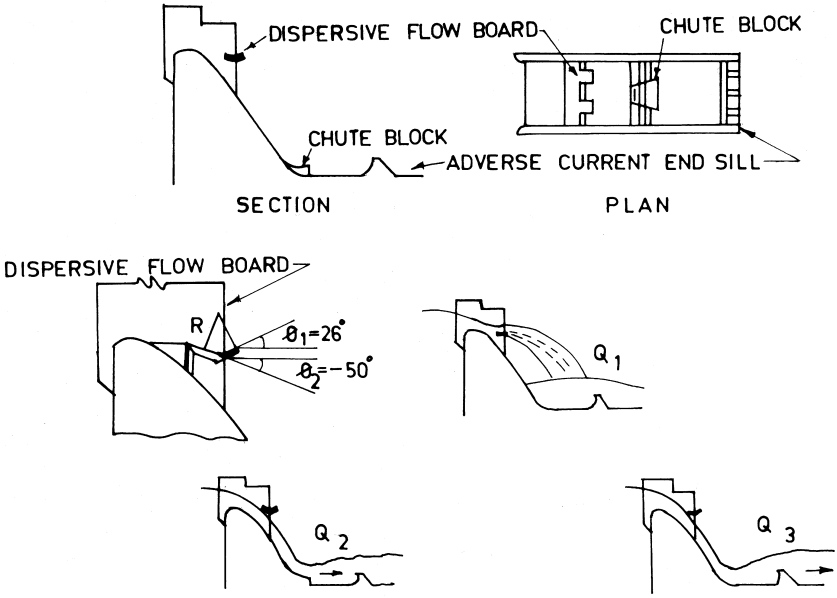

Figure 6 Dispersive-flow energy dissipater. (Shown in Yang 1994.)

the length of the stilling basin by about 50–66% and decreasing the stilling basin depth by 20–40% would be possible compared to the conventional design of the stilling basin to cater to the entire discharge. It is suggested that about 50–70% of the total discharge should be passed under the boards. The new dissipator is suited to heads ranging from 50 to 80 m and for Froude number of the entering flow between 5.2 and 7.2. The design has not been generalized and prototype experience is not available. Khatsuria (1996) has pointed out the possibility of spray, cavitation, and vibration, particularly with regard to the flow board and chute blocks.

The spillway of Asprokremmos Dam in Cyprus has been designed as an ungated side-channel spillway with its discharge channel leading to a flip bucket. A low-level diversion tunnel runs underneath the spillway and opens out with a hydraulic jump stilling basin below the spillway flip bucket, as shown in Figure 7. The spillway design flood of 660 cumec, which is about 50% of the PMF, is to be passed with full hydraulic and structural safety factors. Taylor (1979) has described the model studies for the design of the spillway and flip bucket. It was observed that when the overflow commenced over the spillway, flip action over the bucket was not established until the discharge exceeded about 100 cumec. A hydraulic jump was forming in the bucket with an overflow over the bucket lip, cascading down the river bed situated about 17 m below. This may cause a deep scour very near the end sill of the stilling basin and undermine its foundations. Advantage was taken of the availability of the stilling basin just below the flip bucket to divert such low flows into the stilling basin. The discharges were passed

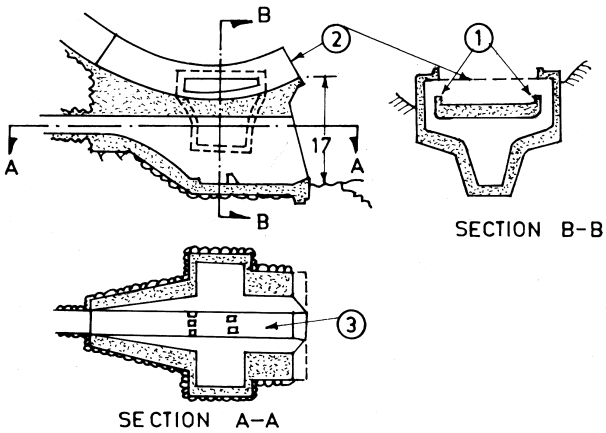

Figure 7 Flip bucket of Asprokremmos Dam, Cyprus. (Shown in Taylor, 1979.)
① Side weirs on the flip bucket ② Bucket lip and ③ Stilling basin

down from the specially constructed slots in the sidewalls of the flip bucket, as shown in Figure 7. The profile of the slots forming the side weirs was developed from the model studies in such a way as to be above the water surface in the bucket corresponding to the flip action so that flows corresponding to only the hydraulic jump would fall into the stilling basin.

The efficiency of the above arrangement was evident from the analysis of the events with a 25-year outflow hydrograph. It was indicated that flow was cascading down the bucket lip only for an hour, compared to a simple flip bucket, which would have taken over 25 hours. Floods with a frequency greater than once in five years will be discharged entirely by the side weirs without cascading.

25.5 HYDRAULIC MODEL STUDIES

From the functioning and performance of the unconventional designs described earlier, it is seen that such designs would have to be tailor-made to fit into the conditions at the site. These designs have been model tested, and some broadly investigated, to define the application range. In a few cases, sufficient data enables planners to design a preliminary layout. However, the decision to adopt a particular design would be governed by considerations of hydraulic and structural safety consistent with the economy. To this end, model study would be inevitable to evaluate possible alternatives available.

Notations

E_1 = Energy of the supercritical flow leaving the gate
F_1 = Froude number of the supercritical flow leaving the gate
H_1 = Tail-water depth above the mean riverbed
H_2 = Energy head measured from the mean riverbed
Q_1 = Flow over the dispersive flow board
Q_2 = Flow passing over the chute blocks
Q_3 = Flow passing between the chute blocks
q = Unit discharge
V_1 = Velocity of the supercritical flow leaving the gate
V_d = Mean velocity just downstream of the screen
y_1 = Depth of the supercritical flow leaving the gate
y_2 = Subcritical sequent depth of free jump corresponding to F_1 and y_1
y_d = Depth of flow downstream of the screen
ΔE = Energy loss through the screen
$\Delta H = (H_2\text{-}H_1)$

REFERENCES

1. Gandolfo, J. S.; Cotta, R. D. Dissipateur D'Energie, 6th Congress. IAHR, C-23. The Hague, 1955.
2. Gandolfo, J. S.; Cotta, R. D. Kinetic energy dissipation on apron for gate dams, 7th Congress. IAHR, D-22. Lisbon, 1957.
3. Kashiwai, J.; Yakushiji, K.; Miyawaki, C. Hydraulic characteristics and design of spillways and outlets for flood control of uncontrolled discharge dams, 19th ICOLD, Paper C.8. Florence, 1997.
4. Khalifa, C.; Abdelkawi, C. Compacted spillways, ASCE Conf on Hydraulic Engineering, 1993.
5. Khatsuria, R. M. Discussion on the paper by Yang (1994)-Sr No 7 below. ASCE Jnl of Hyd Engg, June 1996, 122(No 6).
6. Rajaratnam, N.; Hurtig, K. I. Screen- type energy dissipator for hydraulic structures. ASCE Jnl of Hyd Engg, April 2000, 126(No 4).
7. Taylor, E. H. Asprokremmos dam spillway, 13th ICOLD, Q 50, R 18, 1979.
8. Yang, S. L. Dispersive–Flow energy dissipator. ASCE Jnl of Hyd Engg, Dec. 1994, 120(No 12).

26
Cavitation in Spillways and Energy Dissipators

26.1 INTRODUCTION

This chapter is not intended to discuss the theory of cavitation or aspects related to cavitation. A number of classic books on cavitation have been published that comprehensively cover the subject in greater details. Emphasis here will be on exposing the reader to the understanding required concerning the causes of cavitation in spillways and energy dissipators; the precautions that should be heeded while designing, constructing, and operating these structures, and any remedial measures that should be prepared. A general description of the process of cavitation is, however, necessary as a starting point for the discussion of these topics.

26.2 CAVITATION

The phenomenon of cavitation is often compared to boiling water at local atmospheric pressure. When water is heated, its vapor pressure increases with the temperature (from 0.61 kpa at 0° C to 101.3 kpa at 100° C). At the temperature for which the vapor pressure equals the local atmospheric pressure, boiling will occur. Conversely, if the atmospheric pressure can be reduced, boiling would occur at a lower temperature. At high enough elevations, boiling would occur at room temperature. In flowing water, if the pressure can be reduced locally (because of flow separation or by other means) down to the vapor pressure corresponding to the ambient temperature, a process similar to boiling could occur, whereby bubbles or cavities would form locally in the body of flow, which is defined as cavitation. This is vaporous cavitation.

Another example of cavitation is seen when bubbles form in a glass from a freshly poured carbonated drink. In a sealed bottle, the carbon dioxide is kept in solution under a high pressure. When the bottle is opened, the pressure is decreased and the carbon dioxide begins to diffuse out and form voids. This is called gaseous cavitation. It should be noted here that voids are formed although

vapor pressure in the liquid is not reached. Gaseous cavitation is observed in flowing water with low-flow velocities and high-gas contents. In hydraulic structures, vaporous cavitation is normally the most important parameter. As velocities increase, the effect of gas contents decreases. Generally, water that passes through hydraulic structures is frequently drawn from the lower strata of the reservoir, where the air content is low. In model studies, velocities are low, so some problems can be expected when scaling model results to prototype values.

In addition to considering the contents of the void (vapor or gas), one could also describe cavitation by its occurrence. For instance, with flow in a venturi, a region of low pressure is formed in the throat of the venturi. As the flow rate is increased, the pressure is reduced. At some critical value of the flow, the water in the throat begins to vaporize. This vaporization takes place first at local weaknesses in the liquid, which are called cavitation nuclei. This onset of vaporization is called incipient cavitation. If the flow rate is further increased, the volume of voids, which appear as small bubbles, also increases. At some other critical value of the flow rate, the many small bubbles suddenly form one large void. The developed void is known as a cavity flow, developed cavitation, or supercavitation. Once supercavitation forms in venturi or downstream from an inline orifice, the flow rate cannot be increased. This is called choking of the flow. Decreasing the flow rate will result in the elimination of the cavitation. This point is called desinent cavitation. These two flow rates may not be identical, with the latter usually occurring at a higher pressure.

26.3 CAVITATION INDEX

The cavitation index is a dimensionless measure used to characterize the susceptibility of a system to cavitate. Fig 1 illustrates the concept of cavitation index. In such a system, the critical location for cavitation is at point C.

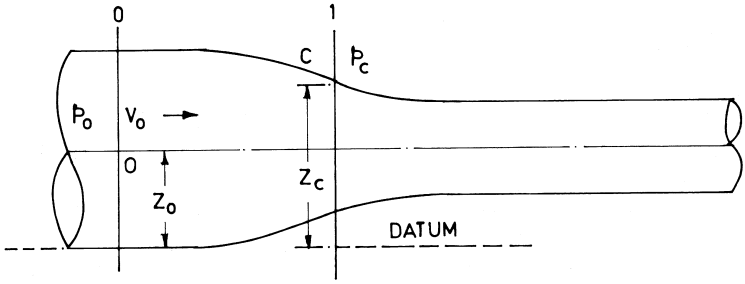

Figure 1 Concept of cavitation index.

The static fluid pressure at location O is p_0. At location 1, it will be

$$p_c + \gamma(Z_c - Z_0) \tag{1}$$

Where

p_c = Static pressure at point C
γ = Specific weight of fluid
Z_c and Z_0 are the elevations at points C and 0

The pressure drop in the fluid as it moves along a stream line from location 0 to location 1 will be

$$p_0 - [p_c + \gamma (Z_c - Z_0)] \tag{2}$$

The cavitation index σ normalizes this pressure drop to the dynamic pressure $\frac{1}{2}\rho V_0^2$, where ρ is the mass density of the fluid and V_0 is velocity at 0. Thus,

$$\sigma = \frac{p_0 - [p_c + \gamma(Z_c - Z_0)]}{1/2\rho V_0^2} \tag{3}$$

If cavitation is just beginning and there is a bubble of vapor at point C, the pressure in the fluid adjacent to bubble is approximately the pressure in the bubble, which is vapor pressure, p_v, of the fluid at the fluid's temperature. Therefore, the pressure drop along the streamline from 0 to 1 required to produce cavitation at the crown C is

$$p_0 - [p_v + \gamma (Z_c - Z_0)]$$

and the cavitation index at the condition of incipient cavitation is

$$\sigma_i = \frac{p_0 - [p_v + \gamma(Z_c - Z_0)]}{1/2\rho V_0^2} \tag{4}$$

For large velocities, the elevation terms can be ignored; hence, $\sigma_i = \dfrac{p_0 - p_v}{1/2\rho V_0^2}$

The pressures are usually expressed in absolute units, i.e., local barometric pressures are added to gauge pressures. The general expression for cavitation index on a spillway surface is

$$\sigma = \frac{y.Cos\theta \pm \dfrac{yV^2}{gR_c} + p_b - p_v}{\dfrac{V^2}{2g}} \tag{5}$$

Where

y = Depth of flow
θ = Angle of chute with horizontal

R_c = Radius of curvature of chute, if any
P_b = Barometric pressure in m of water, usually 10.3 m
P_v = Vapor pressure in m of water, usually 0.233 m
V = Velocity of flow m/s

The radius of curvature R_c can be worked out as

$$R_c = \frac{\left[1+(dy/dx)^2\right]^{1/2}}{d^2y/dx^2} \tag{5a}$$

The term $\frac{yV^2}{gR_c}$ has +ve sign for a concave slope and −ve sign for a convex slope.

The values of σ_I for different systems differ markedly depending upon the shape of the flow passages, the shape of objects fixed in the flow, and the locations where reference pressure and velocity are measured. If a system operates at a σ above σ_I, it will not cavitate. If σ is below σ_I, cavitation will occur; in fact, the lower the value of σ, the more severe the cavitation.

It has been confirmed experimentally that, in a given system, cavitation will begin at a specific σ_I, no matter which combination of pressure and velocity yields that σ_I. Since, in theory, a system having a given geometry will have certain σ_I, despite differences in scale; σ_I is a useful concept in model studies.

26.4 CAVITATION DAMAGE

When cavitation bubbles grow and travel with the flow to an area where local pressure is higher, they can no longer be sustained and collapse. When a cavitation bubble collapses or implodes close to or against a solid boundary, an extremely high pressure is generated that acts on an infinitesimal area of the surface for a very short time period. Falvey (1990) has described the mechanism of collapse of an individual bubble. The bubble collapse consists of phases in which the bubble diameter decreases, reaches a minimum, and then grows or rebounds, as shown in Figure 2. The process is repeated for several cycles, with the bubble diameter decreasing during each cycle until it finally becomes microscopic in size. During the rebound phase, a shock wave forms, with a velocity equal to the speed of sound in water. It has been estimated that the pressure intensity due to this shock wave is about 200 times the ambient pressure at the collapse site. Countless impacts due to such collapses erode the metal and concrete, which is known as cavitation pitting.

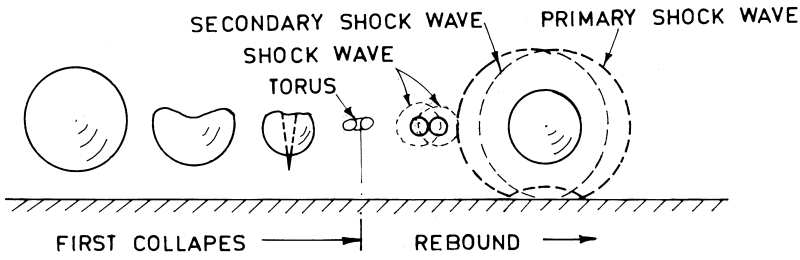

Figure 2 Collapse of an individual bubble near a boundary. (Shown in Falvey 1990.)

The damage mechanism in concrete is more complicated due to the presence of microfissures in the surface and between the mortar and coarse aggregates. Compression waves in water fill such interstices and may produce tensile stresses that loosen pieces of the material. The elastic rebounds from a sequence of such blows may cause and propagate cracks and other damage, causing chunks of material to break loose.

Once cavitation damage has substantially altered the flow regime, other mechanisms begin to act on the surface. These are mechanisms such as high water velocities striking the irregular surface and mechanical failure due to reinforcing steel vibrations. At this point, cavitation is only a minor contributor to the ensuing damage. The erosion may then continue through the whole mass or over the foundation.

This discussion is mainly concerned with the cavitation on spillway chutes, stilling basins, and other structures such as sidewalls, buckets, and energy dissipating appurtenances.

26.5 CAVITATION ON SPILLWAY SURFACES

Examples of cavitation damage on spillway surfaces have been well documented. Falvey (1990) has discussed in detail the damage that occurred to the free-surface tunnel spillways of Blue Mesa, Glen Canyon, Hoover and Yellowtail Dams, U.S.A., and the design of aerator slots used as remedial measures. Galperin (1979) has described cases of cavitation damage on some Russian dams including Bratsk and Krasnoyarsk Dams. Wang and Chou (1979) have discussed cavitation damages on the spillway surfaces of Feng Man and Liu Jia Xia Dams of China. Aksoy and Ethembabaoglu (1979) have reported cavitation damage to the spillway channel of the Keban Dam, Turkey. Beichley and King (1975) have described cavitation damage of some outlet works. Ball (1976) has discussed in detail several

examples of cavitation damage initiated by various types of irregularities on spillway and outlet surfaces.

The figures associated with the cavitation damage are very eloquent. Some examples;

Hoover Dam (USA, 1941): damage volume $L \times B \times H = 35 \times 9 \times 14$ cum
Infiernillo Dam (Mexico, 1964): 1200 cum
Yellowtail Dam (USA, 1967): $L = 38$m, $H = 2.5$m
Bratsk Dam (Russia) $10.5\text{m} \times 7.5\text{m} \times 1.2\text{m}$
Supkhun Dam (Korea) 1100 cum
Nagarjunsagar Dam (India, 1974) $15\text{m} \times 10\text{m} \times 3\text{m}$
Guri Dam (Venezuela, 1978) A bucket dislodged, several cum of rock dislodged
Karun Dam (Iran, 1977) Removal of concrete lining of spillway channel, exposure of foundation rock

From a study of these dams, the principal causes of cavitation damage on spillway surface can be classified in structural or geometrical features such as inadequate design, mis-alignment of boundary, and surface roughness on the boundary associated with flow conditions involving flow separation and reattachment.

26.5.1 Inadequate Design

The designs that are conducive to separation of the flow and zones of negative pressures are under designed-crest profiles, gate grooves, and inadequate curvatures at the transitions.

The implications of operating the spillway for heads in excess of the design heads in terms of negative pressures, separation, and drop in coefficient of discharge have been discussed in Chapter 4. It is found advisable to design the crest profile for a head not less than 75% of the maximum operating head. The cavitation potential of siphon spillways has been discussed in Chapter 7.

If curvature away from the flow is too abrupt or severe, low-pressure areas and cavitation can result. In the earlier designs of chute spillways, the convex curvature at the change of grade used to be in the form of a combination of circular arcs. Theoretically, such a transition is a trajectory as described by Equation 25, Chapter 5. The damage caused due to inadequacy in transition can be somewhat like that shown in Figure 3. Damage on the spillway face of the Grand Coulee Dam, U.S.A., can be cited as an example. Transverse grooves in flow surfaces are represented by gate slots, gate grooves, stoplog slots, etc. The flow action and damage locations are indicated in Figure 4.

Gate slots disrupt the smooth boundary lines of flow. Flow separation at the downstream corner creates a negative pressure zone. Cavitation damage may take place on the downstream side, both on the sides and floor. Such damages

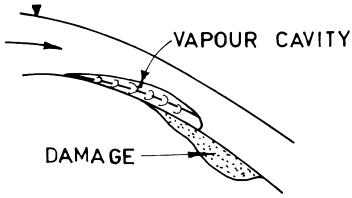

Figure 3 Cavitation damage due to abrupt curvature away from the flow.

occurred on the spillway gate slot of Bonneville and Parker Dams, USA. Banks et al. (1990) have reported cavitation damage to the crest of Hugh Keenleyside Dam spillway, Canada. Ball (1959) studied the hydraulic characteristics of gate slots and developed a geometric configuration for preventing cavitation. Ethembabaoglu (1979) has also proposed configurations of gate slots for eliminating cavitation.

26.5.2 Misalignment

One of the prime and early examples of the type of damage due to cavitation is that which occurred in the lower vertical bend of the Arizona spillway tunnel of the Hoover Dam, USA. The damage was reported as due to cavitation caused by a slight misalignment of the tunnel a few meters upstream of the damaged area, which consisted of a hole 35m long and 9m wide at the bottom of the tunnel, and erosion of the seven-year-old concrete lining to depths of 14 meters.

A view of the damaged area is shown in Fig 5. The flow velocities causing the damage was reported to be about 45 m/s. The repairs required seventeen months and $250,000.

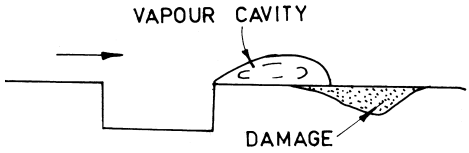

Figure 4 Cavitation damage due to void or transverse groove

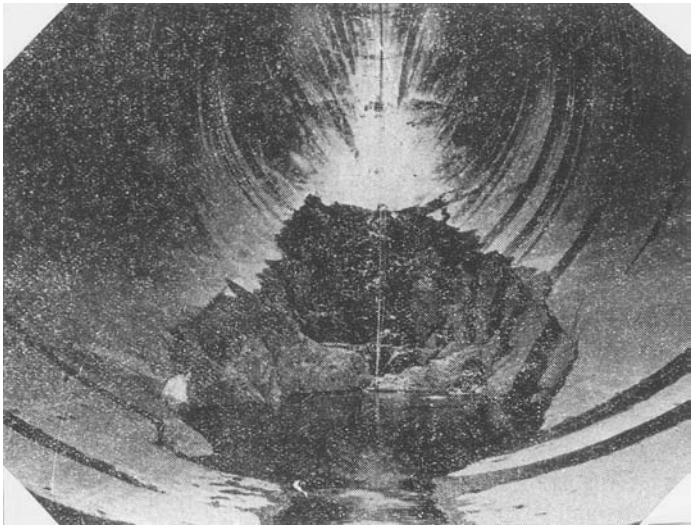

Figure 5 Damage to Hoover Dam spillway tunnel, USA. (Shown in Falvey 1990.)

Another example of similar cavitation damage is that which occurred to the invert of the center sluice of Libby Dam, USA, as reported by Regan et al. (1979) The damaged area was located between 41 m and 57 m downstream of the control gate and covered about 2 m widths on both the sidewalls and went to a depth of about 80 cm. A view of the damaged area is shown in Fig 6. Detailed investigations led to the theory that the damage was the result of the underdesigned trajectory profile of the invert coupled with a noticeably unsmooth and misaligned trajectory. The surveys showed that the invert profile ''as-built'' departed as much as 9 cm from the ''design profile.''

26.5.3 Surface Roughness

Surface roughness can be either isolated or uniformly distributed (Falvey, 1990). Isolated roughnesses are also referred to as local asperities and include offsets into the flow, offsets away from the flow, abrupt curvature or slope away from the flow, void or transverse groove, roughened surface, protruding joint, and wavy surface. In each of these cases, cavitation forms in the shear zone produced by the sudden change in flow direction at the irregularity. Figure 7 shows typical isolated roughness elements and probable location of cavitation damage.

Uniformly distributed roughness refers to variations that occur over a relatively wide area. This type of roughness is caused, for example, by erosion of a

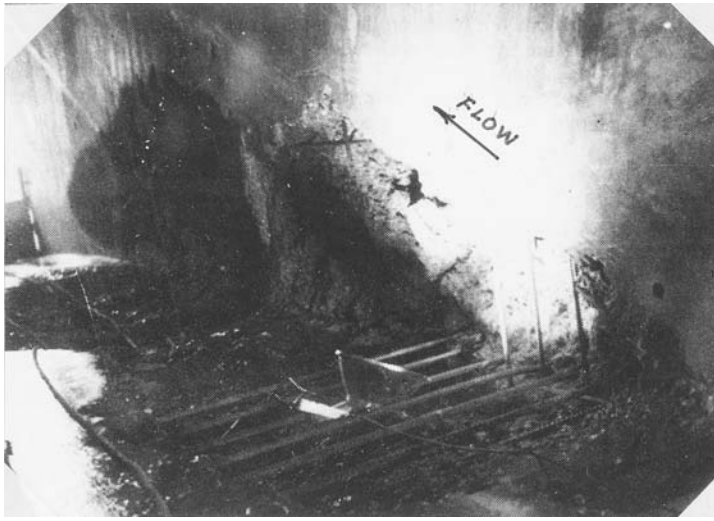

Figure 6 Damage to center sluice Libby Dam, USA. (Shown in Regan et al.1979.)

concrete surface due to abrasion or poor finishing of the surface during construction. In most cases, the absolute height of uniformly distributed roughness can be much larger than offsets on a smooth surface.

Ball (1976) has discussed in detail several examples of cavitation damage initiated by various types of roughness discussed earlier and has also presented relationships between pressures and velocities for cavitation inception. Falvey (1983) has compiled additional information in respect of champhered and elliptically rounded offsets, which also includes Arndt's (1981) investigations on the

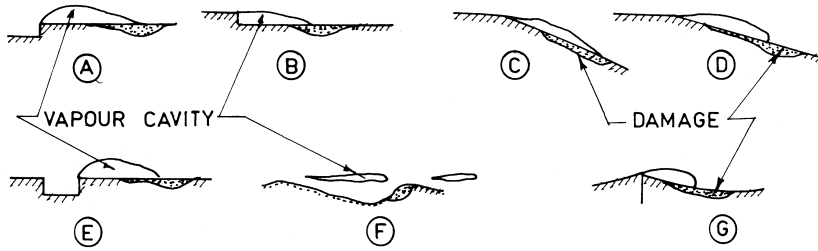

Figure 7 Typical isolated roughness elements and probable location of damage. (Shown in Falvey, 1990)

effects of boundary layer at into-the-flow offsets. Falvey (1990) has also presented a comprehensive treatment on various types of roughness.

A distinction must be made between the roughened flow surfaces and uniformly distributed roughness. The former may result from abrasion damage of the concrete surface, as happened in the case of the Davis Dam spillway, discussed by Ball (1976). Such surfaces may undergo extensive cavitation damage as revealed by specific investigations carried out for this case. On the other hand, a surface that has been made uniformly rough under controlled conditions may result in a higher cavitation index and lower damage potential, as demonstrated in the case of a comparison between two extreme values of rugosity, i.e., $k_s = 0.015$ mm and 1.5 mm for the Glen Canyon Tunnel spillway—as reported by Falvey (1990). With a uniformly roughened surface, the flow velocity will reduce and the depth of flow will increase, thereby increasing pressure; the combination results in a higher cavitation index and a lower damage potential.

The edges of forms for concrete surfaces may lack stiffness and thus cause the joints to be raised or to protrude into the flow. If the size of the forms were small, a wavy surface along the spillway face would result.

Applying the principles of conformal mapping, the cavitation potential of the wavy surface adjoining a high velocity flow can be described in terms of pressure difference, Δ_p from that prevailing without waviness, as in,

$$-\Delta_p = \frac{2\pi t H}{L} \tag{6}$$

Where projections of height, t, occur at an average spacing of L, and H is the effective head at the point under consideration. Zhuravliova (1983) has also obtained a relationship identical to Equation 6.

Figure 8 shows a view of a spillway surface damaged due to cavitation induced by wavy surface.

Application of Equation 6 to this spillway, where an actual survey of the surface gave $t = 75$ mm and $L = 5$ m, with $H = 104$ m (as shown in Figure 8) gives $\Delta_p = -9.8$ m of water.

With normal pressure (without waviness) corresponding to the depth of flow $= 2.5$ m, the pressure at the crest of the wave would be -7.3 m of water. Measurements with pressure transducers gave pressures as low as (-)9 m of water, which could have induced cavitation.

26.6 CAVITATION IN ENERGY DISSIPATORS

Energy dissipation at the base of a spillway is accomplished by abrupt distortions of flow: by transforming supercritical flow into subcritical flow to generate intense turbulence (as in a hydraulic jump), by splitting the high velocity jet against

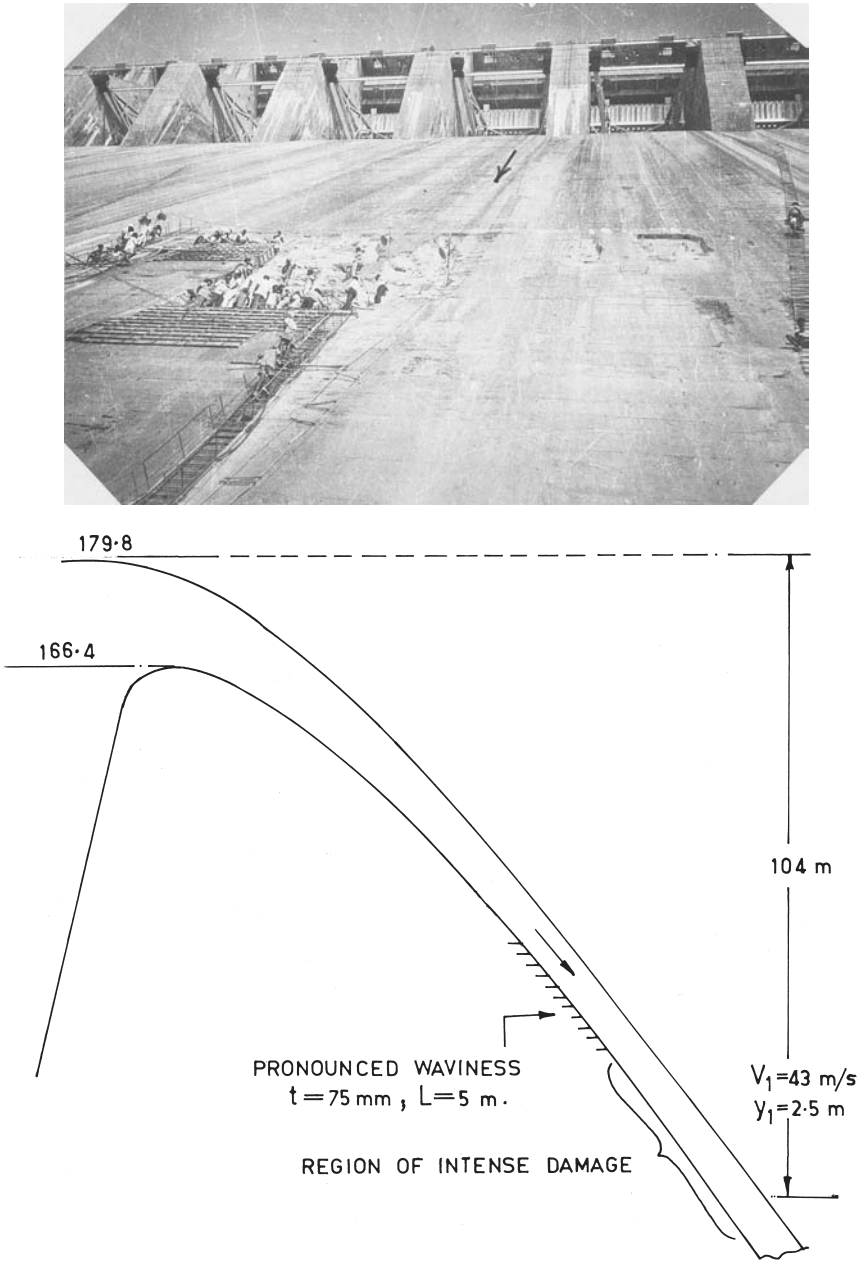

Figure 8 Damage due to waviness of surface.

obstacles (as with chute blocks, baffle piers, jet splitters, etc.), by deflecting the high velocity jet away from its normal direction (as in the case of deflectors, etc.), by suddenly contracting or expanding the high velocity flow. These flow conditions can result in fluctuating pressure depressions, flow separation, reattachment, sheared flows, and vortices leading to cavitation.

The most common elements of energy dissipators likely to be damaged due to cavitation are stilling basin floors, chute blocks, baffle piers, and flow splitters such as slots and teeth in the buckets.

26.6.1 Fluctuating pressure depressions

Intermittent inception of cavitation is caused by fluctuating pressure depressions whose magnitude may reach the vapor pressure as revealed by the studies of Lopardo et al. (1985) and Toso et al. (1988). It has been shown that the fluctuating depressions reaching the value of the vapor pressure in the initial reach of a hydraulic jump had a 0.1% probability of occurrence. Studies by Lopardo et al. (1985) for the Alicura Dam spillway indicated that the initial reach of hydraulic jump—between 0.1 y_2 and 0.3 y_2—was most vulnerable to such depression, which can cause intermittent cavitation inception.

An indication of inception of cavitation due fluctuating pressure depressions is generally based on the cavitation index relevant to the mean pressures derived from the fluctuating pressures, and then comparing that number to the critical cavitation index. Fattor et al. (2001) have, however, observed that the baffle piers of the stilling basin of Arroyito Dam, Argentina, were damaged due to cavitation, even when the cavitation indices based on the mean pressures were substantially higher than the critical cavitation index (of 0.7). It is argued that the cavitation index, σ, is not useful for macroturbulent flows because of the difficulty in obtaining the critical cavitation index, σ_c, from laboratory tests. They suggest that, in order to use conventional values of σ_c, it is necessary to use a new macroturbulence cavitation index, defined as σ'

$$\sigma' = \sigma \, (v^2 / V_1^2) = (p_\infty - p_v) \, (p - p_v) \, p' / (\rho V_1^2 / 2) \tag{7}$$

Where v′ is the velocity fluctuation.

They further suggest

$$\sigma - \sigma' = (2.23 - 1.12 \, S_w) \, C'_p \tag{8}$$

Where

S_w = Skewness of the probability density function of pressure fluctuation amplitude.

C'_p = Pressure coefficient relevant to a 0.1% probability of occurrence (see Ch. 20; shown in Lopardo et al. 1985.)

The skewness of the probability density function of pressure fluctuations is obtained from statistical analysis of the pressure–time series record. According to

experimental data, a negative value of S_w is indicative of flow separation, a positive value is indicative of stagnation, and a zero value is indicative of symmetrical Gaussian distribution.

Narayanan (1980) had published calculations for a stilling basin with a large incident Froude number showing the tendency of intermittent cavitation on floor slab. However, instances of cavitation damage on the floor slab, point to other reasons; for example, cavitation due to sheared layers or that result from the roughening of the surface by abrasion. Absence of cavitation damage could be attributed to the air entrainment by the hydraulic jump, as shown by the results of Rajaratnam (paragraph 20.2.5). However, appurtenances like chute blocks and baffle piers have suffered cavitation damage in several projects.

26.6.2 Flow Separation and Reattachment

Energy dissipating appurtenances like chute blocks, baffle piers, and flow splitters may be subjected to cavitation as a result of separation of high velocity flow from a surface and subsequent reattachment on the same surface. The formation of a wake is accompanied by intense pressure fluctuations below and above mean pressures.

A study to determine pressure distribution on chute blocks and to evaluate the effect of chute blocks on energy dissipation was conducted by Suryavanshi et al. (1973) They concluded that the chute blocks contributed little to the energy dissipation and that the risk of cavitation was too great for chute blocks to be used with confidence at high dams. However, the prototype experience with chute blocks subjected to the incoming velocities as high as 25 m/sec and analysis by Khatsuria et al. (2000) indicate that chute blocks could be used, provided the cavitation index does not fall below 0.50 or so.

Khatsuria (2001) has quoted examples of the spillways of Machhu II and Vir Dams, where baffle piers as per USBR basin III were used with the incoming velocities of up to 25 m/s. The baffle piers operating under a cavitation index of 0.33 have not experienced any damage, even after 30 years of operation. Their studies for distribution of hydrodynamic pressures on the baffle piers of standard design also revealed that cavitation index higher than 0.33 could be attained for an incoming velocity as high as 22 m/s.

Kuttiammu et al. (1951) have described use of T-shaped baffle blocks for the first time in the stilling basin of Lower Bhavani Dam spillway, India, under a total head of 35 m (velocity of about 27 m/s) (see Figure 4, Chapter 24). Their calculations, based on the critical cavitation index of 0.68, suggest that the blocks would be free from cavitation. The stilling basin has been functioning for the past four decades without any problem.

Literature contains many instances of flow conditions that have contributed to the cavitation damage. Pillai et al. (1967) and Berryhill (1957) highlight the

damage to baffle piers of Mc Nary, Bonneville and Glendo Dams as examples. One way to avoid heavy negative pressures on the sides of rectangular shaped baffle piers is to provide streamlining by rounding their edges, as done in the case of baffle piers of Glendo Dam. This, however, results in a reduction of their efficiency, since the coefficient of drag falls sharply with streamlining.

Since the sides of the baffle piers are the most vulnerable to cavitation damage, because of the separation of flow at the corners and subsequent reattachment, designs have been developed that ensure prevention of reattachment of the flow. This is done by:

Rounding the corners to eliminate the possibility of flow separation
Shaping the front of the pier so that the separated jet is spread obliquely to the direction of the flow
Recessing the sides inward so that the flow is unable to reattach on the sides

Early designs of baffle piers included rounding of the edges of the piers to effect streamlining of the flow and avoid separation altogether, as shown in Figure 9. This design, however, defeated the very purpose of providing the baffle piers—aiding the formation of hydraulic jump by introducing drag force resistance—and was soon discontinued.

Later designs envisaged separation of the flow at the corners but eliminated possibility of reattachment on sides. This was accomplished by spreading the separated jets laterally and recessing the sides inward.

Pillai et al. (1989) have proposed wedge-shaped baffle piers with a vertex angle of 150° cut back at 90° (Figure 9). However, there is no report of their adoption at prototype or performance.

In the other design, the emphasis is on recessing the sides inward to prevent re-attachment of the separating flow at corners. This baffle-pier design was compared to the standard-shape baffle piers (USBR basin III) and found to be superior. Baffle piers of this design have been utilized in the stilling basin of the Mangla Dam spillway, Pakistan. Pressure fluctuations at critical locations on the side might create intermittent depressions reaching vapor pressure. However, there is no report of any damage to the baffle piers.

There have been instances of cavitation damage to the teeth and downstream apron of slotted buckets. This damage is of particular interest in light of the fact that a spillway very similar to the Angostura Dam spillway, USA, with respect to head, discharge, and tail-water depths suffered cavitation damage, whereas no damage has been reported in the case of Angostura Dam. It is noteworthy that during the model studies for the development of the Angostura-type bucket with teeth and apron, piezometric pressures at most of the locations were highly positive, while three locations on the downstream sloping and vertical faces of the

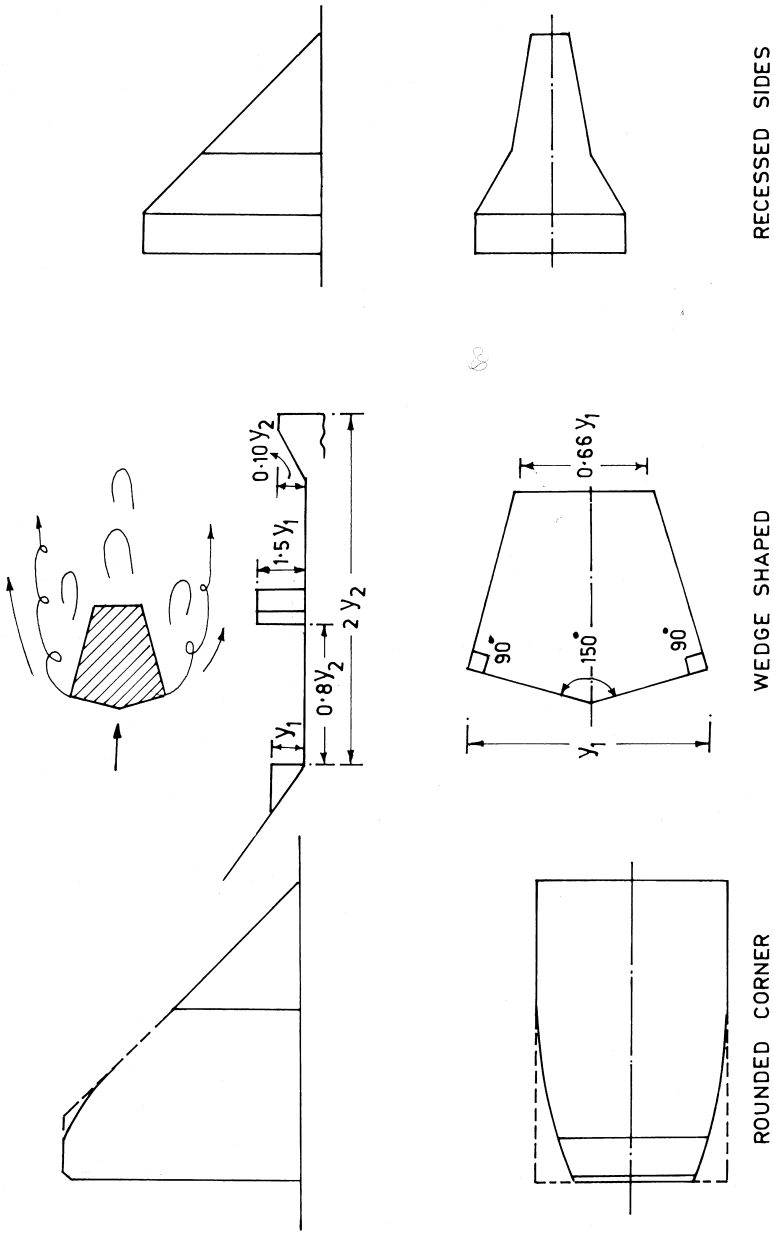

Figure 9 Modified designs of baffle piers.

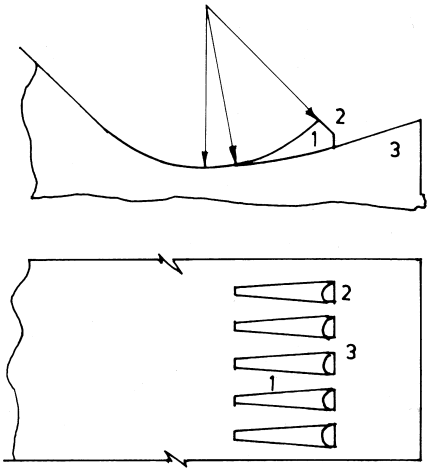

Figure 10 Cavitation-prone areas in a slotted bucket.
①Side of tooth ② D/s face of tooth and ③ D/s apron

tooth showed pressures fluctuating between negative and positive values. Pressures on the apron were not observed.

Repeated cavitation damages had taken place on the apron of the spillway. Model studies for the spillway were conducted to investigate probable causes of cavitation on the teeth and apron. Piezometric pressures at critical locations did not reveal subatmospheric pressures, which could lead to cavitation. Further studies employing piezoresistive pressure transducers revealed local pressure depressions up to -7 m of water, on the downstream face of teeth, even for normal tail-water conditions. Under the transient conditions of gate openings, the pressure depressions were still higher. Such conditions arise when the spillway starts overflowing due to a deficient water cushion in the downstream, and when some of the gates are closed all of a sudden, while other gates continue to pass the discharge. It was concluded that instantaneous pressure depressions were the cause of cavitation damage. Fig. 10 shows cavitation-prone areas indicated by the previous studies.

26.7 CAVITATION DUE TO SHEARED FLOW AND VORTICES

There is yet another source of damage to high-head spillways and outlets; The phenomenon of sheared flows of water plunging into a relatively deep and stag-

nant pool. If the velocities are sufficiently high, sheared flows can generate cavitating vortices capable of producing severe damage to concrete, even when the free-water surfaces are at atmospheric pressure. Unlike cavitation induced by inadequacies in the design, misalignment, or roughness, shear cavitation is most difficult to predict.

The studies conducted by Kenn and Garrod (1981) investigating the cause of cavitation damage to Tarbela tunnel indicated that it could have occurred due to the presence of severely sheared flows with a velocity exceeding 30 m/s in a stagnant or slowly moving water pool. As shown in Figure 11, the central intake gate to tunnel 2 was for sometime open (at first fully, later partly) while both side gates were closed. The evidence suggests that during this time, intense vorticity-induced cavitation was generated in the two essentially vertical planes of severely sheared flows leaving the inner walls of the adjacent piers. These cavities collapsed in the regions of high pressure further downstream and caused severe erosion of the concrete lining of the tunnel.

Pinto and Lemos (1967) have described cavitation damage to the sluice outlet portal of Bemposta Dam, Portugal, where, for the condition of both the sluice and spillway operating with a tail-water level near the roof of the portal, a horizontal axis vortex was forming at the outlet end (as shown in Figure 12)

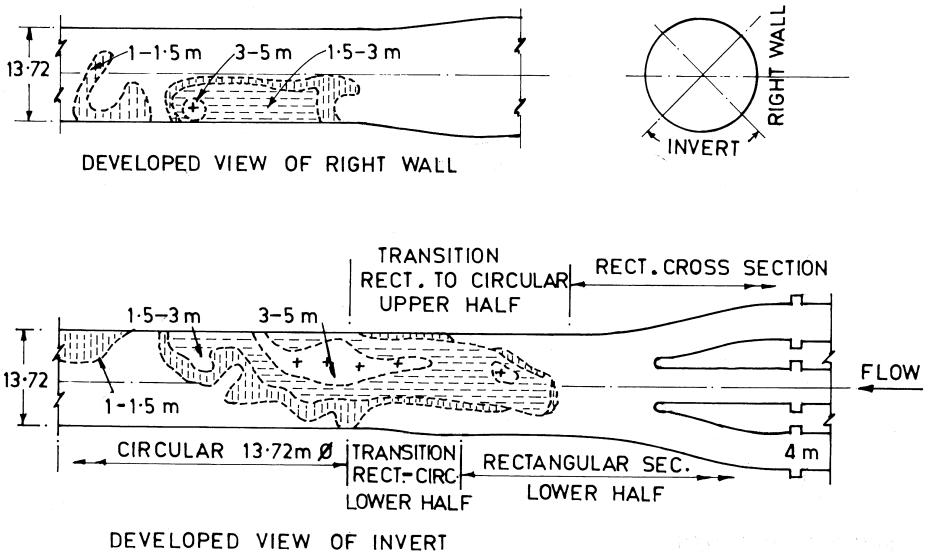

Figure 11 Cavitation damage to concrete lining—Tunnel 2, Tarbela Dam, Pakistan. (Shown in Kenn et al.1981.)

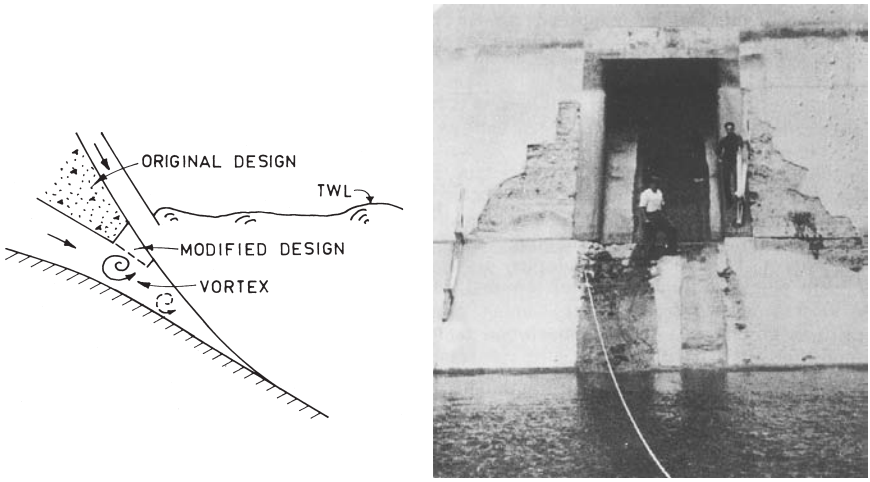

Figure 12 Cavitation damage to sluice outlet portal, Bemposta Dam, Portugal. (Shown in Pinto et al. 1967.)

and causing cavitation damage on the downstream slope. A modification, also shown in Figure 12, wherein the upper edge of the outlet end was extended downstream, resulted in a smaller vortex and reduction in damage.

Asymmetrical operation of spillway gates and sluice gates can result in a condition conducive to the formation of shear layers and cause cavitation. It is well known that equal and simultaneous opening of all the gates ensures better hydraulic conditions in the stilling basin and downstream. However, operating staff often prefer to open a single gate, starting from a central gate, adding on other gates as the discharge level increases. Conditions resulting from such operations—with potential to cause cavitation—are illustrated in Figure 13.

Burgess (1981) has described cavitation damage to the concrete floor and kicker block of the deep sluice-stilling basin of the Roseires Dam, Sudan, also believed to be a vortex-induced cavitation. The deep-seated sluice structure consists of five sluices 10.5 m high by 6.0 m wide equipped with radial gates. The overall head on the sluices is 44 m, resulting in a velocity of about 29 m/s. The basin floor and the kicker block (a high-end sill) in front of sluice number five were repeatedly damaged, as shown in Figure 14. It was found that sluice number 5 was operated most of the time while the other sluices were kept closed. Hydraulic model studies were conducted to study pressures at strategic locations in the damaged regions—also shown in Figure 14. It was revealed that potential cavity formation and collapse conditions occurred along the line of the intense-

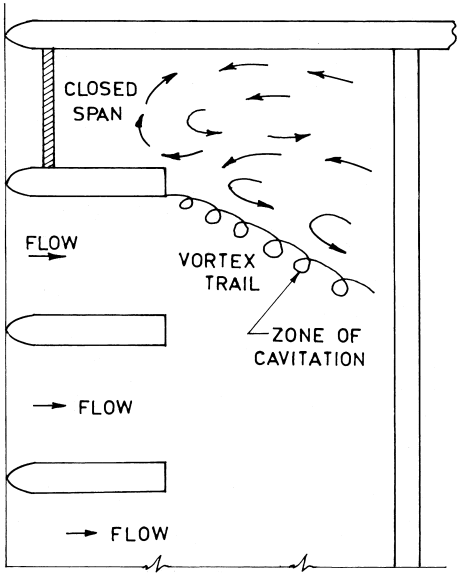

Figure 13 Flow separation and vortex trail due to asymmetrical operation of gates.

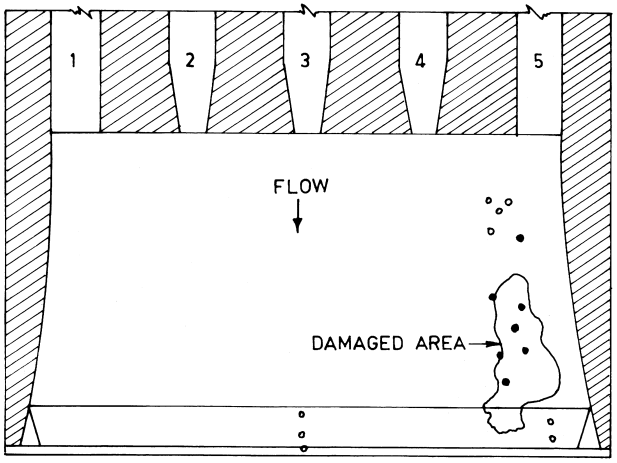

Figure 14 Damage to the basin floor and kicker block—Roseires dam, Sudan. (Shown in Burgess 1981.)
○ In all tests, pressures remained above the equivalent prototype vapor pressure
● Potential cavity formation and collapse condition recorded at least in one test

Table 1 Values of σ at the Beginning of Damage

Structure or type of irregularity	σ	Reference
Tunnel inlet	1.5	Tullis (1981)
Sudden expansion in tunnel	1.0*–0.19	Russel; (1967) Rouse (1966)
Baffle pier—		
Pyramidal shape	1.4–2.3	
Triangular (USBR basin III)	0.33	Khatsuria; (2000)
T-shaped baffle blocks (Bhavani-type stilling basin)	0.68	Kuttiammu (1951)
Spillway surfaces	0.20	Falvey (1982)
Gates and gate slots	0.20–3.0	Wagner; (1967) Ball (1976)
Abraded concrete—20 mm max depth of roughness	0.60	Ball (1976)
Slope into the flow	0.20	Ball; (1976) Arndt;(1977) Falvey (1982)
Slope away from the flow	0.20	–do–
Offsets (not exceeding 6 mm) into the flow	1.6	–do–
Offsets (not exceeding 6 mm) away from the flow	1.0	–do–
Endsills of stilling basins	1.05–1.75	
Jet splitters	0.15–0.70	

* Unusual definition of σ

shear boundary, indicating that the mechanism producing vapor pockets in the prototype was from vortex formation. The coinciding of the area of potential vapor-pocket formation and collapse with the area of damage substantiated the contention that the cause of the damage was collapse of vapor-cored vortices.

Information on critical values of σ for different types of appurtenances is scanty. A summary of literature on typical values of σ for various structures is summarized in Table 1. It is, however, suggested that the designer may use these numbers only after studying the relevant references. Some reasons for this are: the exact geometry and test conditions must be understood, authors use different locations for determining reference parameters and similitude in the model is difficult to achieve.

26.8 PREDICTION OF CAVITATION DAMAGE

It is recognized that cavitation damage is a function of cavitation index, flow velocity, surface construction material, and time of exposure. However, the rate of damage with respect to time is not constant and varies inversely with time.

Several attempts have been made to develop a parameter for quantitatively predicting cavitation damage. Falvey (1982) analyzed cases of cavitation damage (both minor and major) by cavitation index and hours of operation. The results are shown in Fig 15.

Wang and Chou (1979) define cavitation damage in terms of stabilized depth after a long period of operation. The method involves several parameters, some of which are difficult to determine without a model study.

Quantitative terms associated with cavitation damage are Damage potential and Damage index. Damage potential is expressed proportionality:

$$D_p \alpha \left(\frac{1}{\sigma_s}\right)\left(\frac{\sigma_s}{\sigma_f} - 1\right)\left(\frac{V}{V_r}\right)^6 \tag{9}$$

Where

D_p = Damage potential
σ_s = Cavitation index for the initiation of damage
σ_f = Cavitation index for the flow
V_r = Reference velocity
V = Flow velocity

The damage index is a quasi-quantitative measure of the severity of cavitation damage as a function of discharge and time and has been related to the damage potential as:

$$D_i = D_p \ln (t - t_0) \tag{10}$$

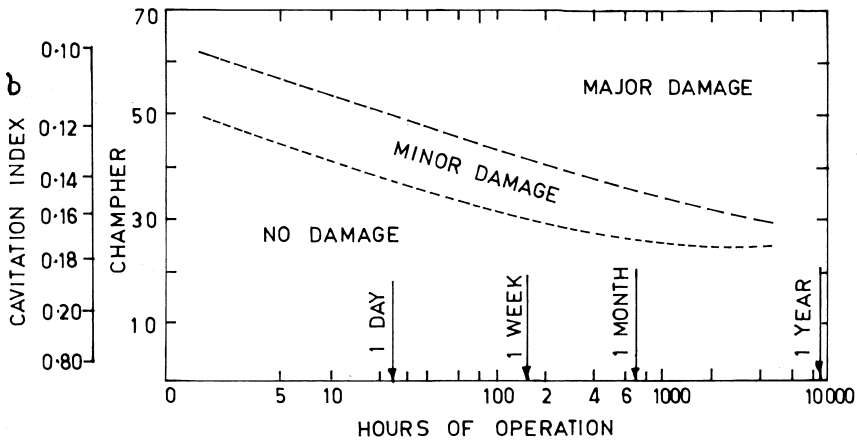

Figure 15 Cavitation damage experience in spillways. (Shown in Falvey 1982.)

Where

D_i = Damage index
t = Time
t_0 = Constant of integration

Falvey (1990) has discussed the evaluation of these parameters for determining the values for specific structures. He has also suggested design values relevant to chutes and spillways.

26.9 PREVENTION OF CAVITATION IN SPILLWAYS AND ENERGY DISSIPATORS

Measures for preventing cavitation damage should be considered at the design, construction, and operation stage of structures.

26.9.1 Design

Designs that are conducive to separation of the flow and creating zones of negative pressures are underdesigned crest profiles, gate grooves, and inadequate curvatures and transitions. Generally, the crest profiles should not be designed for heads less than 75% of the maximum depth of overflow. Sometimes, the portion of the crest upstream of the crest axis is widened in order to accommodate stop-log gates. However, such features have a detrimental effect on performance in terms of negative pressures and loss of discharging capacity. If, for any reason, such an arrangement is unavoidable, the design should be thoroughly studied in a model. Spillway crests normally have radial gates obviating the need for gate grooves. If vertical gates are to be adopted, the gate grooves should be designed with a recess on the downstream as recommended by Ball (1959) and (1979) Ethembabaoglu.

Abrupt grade-change transitions should be avoided, and the profile corresponding to the trajectory (Equation 25, Chapter 5) should be provided. In fact, a safety factor of 1.25 multiplied to the velocity has been suggested to prevent separation of the flow from the invert. (Regan et al. 1979)

It is generally recognized that, beyond a flow velocity of about 30 m/s and discharge intensity of 20 cumec/m, the surface finish required to withstand cavitation is not compatible, even with the best concrete finish and with all possible care taken. Therefore, use of cavitation-resistant liners and special materials like epoxy, fiber-reinforced concrete, etc., or provision of aerators is necessary in such situations.

Hydraulic-jump stilling basins and energy-dissipating appurtenances, like chute blocks, baffle piers, etc., are the most vulnerable to cavitation. Such appurtenances should not be used beyond the recommended velocity limit of 15–20 m/s or for cavitation indices smaller than that borne out by experience (Khatsuria, 2000). Alternatively, damage can be prevented by arranging the cavity's collapse well away from the boundary, as in the case of wedge-shaped supercavitating baffle piers.

Jet splitters at the end of the buckets have been damaged due to cavitation. Galperin et al. (1979) suggest that considerable improvement can be achieved by converging the two splitters instead of placing them parallel. This would create backpressure that can eliminate separation of the flow at the entrance to the splitters.

26.9.2 Construction

The precautions to be taken during construction pertain to:

- Monitoring the progress of construction as per design profile, avoiding misalignments and large scale irregularity such as undulating or wavy surface finish, etc.
- Controlling surface finish within the permissible tolerances specified in relevant standards

While the former could be accomplished by proper supervision during construction, the latter requires careful and extensive review.

A tolerance is defined as the range of variation allowed in a constructed dimension from the design dimension. The following three basic types of flow surface variations are present in hydraulic structures:

Offset: dimension of surface irregularities perpendicular to the flow is large relative to its dimension parallel to the flow

Slope: dimension of the surface irregularities parallel with the flow is large relative to the variation perpendicular to the flow

Uniformly distributed roughness: variation over a relatively large area. Absolute dimension of roughness element much larger than offset

USBR (1981) has designated three levels of tolerances for the offsets and slopes:

Tolerance, T	Offset, mm	Slope
T1	25	1:4
T2	12	1:8
T3	6	1:16

These tolerances have been associated with the cavitation index of the flow:

Cavitation index of the flow	Tolerance without aeration	Tolerance with aeration
>0.60	T1	T1
0.40–0.60	T2	T1
0.20–0.40	T3	T1
0.10–0.20	revise the design	T2
<0.10	revise the design	revise the design

The significance of the close tolerances can be best illustrated by the example of the Fontana Dam spillway tunnel, USA. Even with the flow velocity as high as 48 m/s, no cavitation damage has taken place, presumably due to the close tolerances in the surface finish and to correct alignments.

26.9.3 Operation of Structures

Structures that are not operated in accordance with the assumptions made in the design are likely to be damaged. A common example is the hydraulic jump stilling basin for a spillway having a number of gates. The design presupposes equal opening of all the gates; hence, the invert elevation of the basin is determined on this condition. A number of stilling basins have suffered damage due to abrasion, cavitation, and uplift as a result of asymmetrically operating the crest gates.

As shown in the cases of damage to Tarbela Tunnel, Bemposta Sluice outlet portal, and the deep sluice stilling basins of Rosiers Dam and other dams (see Figures 11 to 14), asymmetrical operations might induce shear cavitation in addition to producing flow conditions that are conducive to abrasion damage.

Prediction of such flow conditions and remedial measures can be best studied in hydraulic models.

26.10 REMDIAL MEASURES AND REPAIRS

For existing structures that suffer repeated cavitation damage, the cause of cavitation must be ascertained in order to determine remedial measures. Misalignments and surface irregularities can probably be rectified; such as design profile deviation, which can be corrected, or roughness, such as offsets, which can be grinded to permissible values. However, inadequacy in design and certain types of irregularities cannot be rectified. In such cases, aeration is the best remedial measure. Karun Spillway, Iran, is an example where aerators have been used after experiencing cavitation damage. Aerators that can be utilized on existing spillways are discussed in Chapter 27.

Conventional concrete typically performs poorly where the property of resistance against cavitation, abrasion, fatigue, and impact is important. Therefore, a variety of material and material combinations is used for the repair of concrete.

Installing stainless steel liner plates on concrete surfaces subject to high velocity flows has been a generally successful method for protecting against cavitation erosion. Stainless steel is found to be about four times more resistant to cavitation damage than ordinary concrete. The most preferred material is ASTM A 107 and S 30403, due to its excellent corrosion and cavitation resistance and weldability. Its drawbacks are high cost, sensitivity to vibration, and fatigue breakdown. There are several instances where steel plates have been ripped off, adding to the severity of the problem. Therefore, this alternative is gradually being replaced by special concretes such as epoxy, fiber-reinforced concrete, etc.

A major factor that is critical to the success of a repair is the relative volume change between the repair material and the concrete substratum. Many materials change volume as they initially set or gel; others change volume due to changes in moisture content or temperature. If a repair material's volume relative to the cocrete decreases sufficiently, cracks perpendicular to the interface will develop. In such situations, epoxy compounds that provide a durable bond between the fresh concrete and epoxy concrete are generally used. Epoxy compounds have been recently developed that bond to damp concrete, even to concrete under water. However, there is no unanimous opinion regarding the effectiveness of epoxy treatment against cavitation damage. For example, Lowe et al. (1979) reported unsatisfactory results from the application of epoxy mixes on the Tarbela spillway structure, yet they reported positive results from the application of fibrous concrete and polymerized fibrous concrete. Meanwhile, Corlin et al. (1979) reported that epoxy coating on the stilling basin of Morforsen Dam, Sweden, had a satisfactory performance.

Fiber-reinforced concrete (FRC) utilizes randomly oriented, discrete fiber reinforcement in the concrete mixture. The superiority of FRC in comparison to conventional and polymerized concretes has been demonstrated by Lowe et al., (1979) with the help of erosion tests on concrete specimen. It is claimed that FRC is resistant to the combined effects of cavitation and abrasion erosion.

Polymers are also incorporated into concrete to produce a material with improved properties. These are polymer-impregnated concrete (PIC), polymer-portland cement concrete (PPCC), and polymer concrete (PC). PIC is a hydrated portland cement concrete that has been impregnated with a monomer, which is subsequently polymerized *in situ*. PPCC is made by adding water-soluble polymer to fresh, wet concrete. PC is a mixture of fine and coarse aggregate with a polymer used as the binder. These materials are used as concrete repair materials for damaged surfaces.

ALAG anti-abrasion concrete is a recent advancement. This is a special concrete made of calcium aluminate cement and calcium aluminate reactive synthetic aggregate. Because both the cement and the aggregates have the same physical and mineralogical characteristics, two types of bonds, i.e., physical bonds as well as chemical bonds, are ensured to give it mechanical strength to resist abrasion. It has also been tested with velocities up to 110 m/s in cavitation conditions. However, more study is required to ascertain its suitability for protection against cavitation damage.

Notations

a = Height of undulation
$(C_p)_m$ = Maximum coefficient of pressure reduction
D_i = Damage index

D_p = Damage potential
H = Effective head
L = Average spacing between projection of undulations
p_a = Atmospheric pressure
p_c = Static pressure
p_{cr} = Critical pressure corresponding to cavitation inception
p_g = Piezometric pressure
p_v = Vapor pressure
p_o = Static pressure at location 1
t = Time
Projection height in undulated surface
t_0 = Constant of integration
V = Velocity of flow
V_{char} = Characteristic velocity over the smoothly undulated surface
V_r = Reference velocity
V_0 = Velocity at point 0
Z_0 = Elevation of point 0
Z_c = Elevation of point C
γ = Specific weight of fluid
Δ_{cp} = Pressure pulsation correction
Δ_p = Pressure deviation
σ = Cavitation index
σ_f = Cavitation index of the flow
σ_i = Cavitation index for incipient cavitation
σ_s = Cavitation index for initiation of damage
λ = Length of undulation

REFERENCES

1. Aksoy, S.; Ethembabaoglu, S. Cavitation damage at the discharge channels of Keban dam, 13th ICOLD, Q 50, R 21, 1979.
2. Arndt, R. E. A. Discussion on ''Cavitation from surface irregularities in high velocity''. ASCE Jnl of Hyd Div. April 1977, 103(HY4).
3. Arndt, R. E. A. T. Cavitation in Fluid Machinery and Hydraulic Structures, Annual Review of Fluid Mechanics, 1981.
4. Ball, J. W. Hydraulic Characteristics of Gate Slots. ASCE Jnl of Hyd Div. October 1959, 85(HY 10).
5. Ball, J. W. Cavitation from surface irregularities in high velocity. ASCE Jnl of Hyd Div. September 1976, 102(HY 9).
6. Banks, P. A.; Cass, D. E.; Yung, K. Y. C. Effects of spillway operarion on cavitation damage to Hugh Keenleyside dam spillway. ASCE Hyd Engg. 1990, II.
7. Beichley, G. L.; King, D. L. Cavitation Control by Aeartion of High-Velocity Jets. ASCE Jnl of Hyd Div. July 1975, 101(HY 7).

8. Berryhill, R. H. Stilling basin experiences of the Corps of Engineers. ASCE Jnl Hyd Div. June 1957, 83(HY3).
9. Burgess, J. S. Discussion on the paper –Cavitation damage and the Tarabela tunnel collapse of 1974, Proc Institution of Civil Engineers, Part I, Nov, 1981.
10. Corlin, B.; Larsen, P. Experience from some overflow and side spillway, 13th ICOLD, Q 50, R37, 1979.
11. Ethembabaoglu, S. Some characteristis of static prssures in the vicinity of slots, 13th ICOLD, Q 50, R 29, 1979.
12. Falvey, H. T. Predicting cavitation in tunnel spillways, Water Power and Dam Construction-, August 1982.
13. Falvey, H. T. Prevention of cavitation on chutes and spillways, Proc Conf on Frontiers in Hydraulic Engineering; ASCE, Cambridge, Mass: USA. 1983.
14. Falvey, H. T. Cavitation in Chutes and Spillways, USBR Engineering Monograph No 42, April 1990.
15. Fattor, C. A.; Lopardo, M. C.; Casado, J. M.; Lopardo, R. A. Cavitation by macroturbulent pressure fluctuations in hydraulic jump stilling basins, 29th IAHR Congress. Beijing, 2001.
16. Galperin, R. S. Cavitation in hydraulic structures. Moscow, 1979.
17. Kenn, M. J.; Garrod, A. D. Cavitation damage and the Tarbela tunnel collapse of 1974. Proc Instn of Civil Engrs, Part I. Feb 1981, 70.
18. Khatsuria, R. M.; Deolalikar, P. B.; Bhosekar, V. V.; Sridevi, M. I. Energy dissipator for a low head high discharge intensity spillway, 3rd Intnl R&D Conf; CBIP, Jabalpur, India. March 2000.
19. Khatsuria, R. M. Hydraulic jump stilling basins- Some unresolved issues, National Conf on Hydraulics and Water Resources Hydro 2001; Indian Society for Hydraulics, Pune. Dec 2001.
20. Kuttiammu, T. P.; Rao, J. V. Bhavani type stilling basin for large dams, 4th ICOLD, Q12, R 44, 1951.
21. Lopardo, R. A.; Henning, R. E. Experimental Advances on Pressure Fluctuations Beneath Hydraulic Jump, Proc 21st IAHR Congress. Melbourne, 1985.
22. Lowe III, J.; Bangash, H. D.; Chao, P. C. Some experiences with high velocity flow at Tarbela dam project, 13th ICOLD, Q 50, R 13, 1979.
23. Narayan, R.; Schizas, L. S. Force fluctuations on sill of hydraulic jump. ASCE Jnl Hyd Engg. April 1980, 106(No 4).
24. Pinto do Silva, D.; Lemos Olieira, F. Erosion in concrete and rock due to spillway discharges, Part III and IV, 9th ICOLD, Q 33, R 19. Istanbul, 1967.
25. Pillai, N. N.; Jayaraman, V. V. Cavitation on baffle piers in stilling basins, Symp on High Velocity Flows, Indian Institute of Science. Bangalore, 1967.
26. Pillai, N. N.; Goel, A.; Dubey, A. K. Hydraulic jump type stilling basin for low froude numbers. ASCE Jnl Hyd Engg. July 1989, 115(No 7).
27. Rajaratnam, N. An experimental study of the air entrainment characteristics of hydraulic jump, Publication No 14/1969, Indian Institution of Science. Bangalore, 1960.
28. Regan, R. P.; Munch, A. V.; Schrader, E. K. Cavitation and erosion damage to sluices and stilling basins at two high-head dams, 13th ICOLD, Q 50, R 11, 1979.
29. Rouse, H.; Jezdinsky, V. Fluctuations of pressures in conduit expansions. ASCE Jnl of Hyd Div. March 1966, 92(No HY 3).

30. Russel, S. O.; Ball, J. W. Sudden enlargement energy dissipator for Mica dam. ASCE Jnl of Hyd Div. July 1967, 93(HY 4).
31. Suryavanshi, B. D.; Vaidya, M. P.; Chowadhry, B. Use of chute blocks in stilling basins- An assessment, 11th ICOLD, Q 41, R 21. Madrid, 1973.
32. Toso, J. W.; Bowers, C. E. Exterme pressures in hydraulic jump stilling basins. ASCE Jnl Hyd Engg. Aug 1988, 114(No 8).
33. Tullis, J. P. Modelling cavitation for closed conduit flow. ASCE Jnl of Hyd Div. Nov 1981, 107(HY 11).
34. USBR Concrete Manual, 8th edition, US govt Printing Office. Washington, 1981.
35. Wang, Xi-Rui; Chou, Lin-Tai The method of calculation of controlling (or treatment) criteria for the spillway surface irregularities, 13th ICOLD, Q 50, R 56, New Delhi. 1979.
36. Wagner, W. E. Glen Canyon dam diversion tunnel outlets. ASCE Jnl of Hyd Div. Nov 1967, 93(No Hy 6).
37. Zhuravliova, A. G. Conditions of cavitation inception on smoothly-undulate surface of spillways, 20th IAHR Congress, Seminars. Moscow, Sept 1983.

27
Air Entrainment and Forced Aeration

27.1 INTRODUCTION

Air entrainment in spillways is both a problem and a remedy! High-velocity free-surface flows engulf air and become a bubbly mixture. This process is seen by the change in surface appearance from clear and glossy prior to entrainment to irregular, white, and bubbly. Knowledge of air concentration and the regions in which it exists is important to the designer since the flow of air-water mixture undergoes bulking when compared to a non-aerated flow and, therefore, requires adequate free board on training walls and side walls. Air entrainment is of great help in mitigating cavitation damage if the air can be kept close to the flow boundary. More recently, the flow conditions on spillways or chutes have been recognized for their contribution to the air-water transfer of atmospheric gases such as oxygen and nitrogen and the volatilization of toxic pollutants such as PCBs, mercury, etc. Air entrainment in open-channel flow or flow down a spillway begins when the turbulent boundary layer from the floor intersects the water surface. The flows in which the boundary layer creates air entrainment are referred to normally as self-aerated flows.

27.2 AIR ENTRAINMENT ON SPILLWAYS

Air entrainment on spillway chutes is a natural process; no external mechanism is needed to supply air. When water discharges from a reservoir over a spillway, its surface is smooth and glossy, as shown in Figure 1. Next to the spillway boundary, however, turbulence is generated. The turbulent boundary layer gradually grows toward the surface. When the boundary layer reaches the free surface, the surface becomes disturbed, and entrainment by the myriad vortices in the turbulent flow commences. This point is called the point of inception.

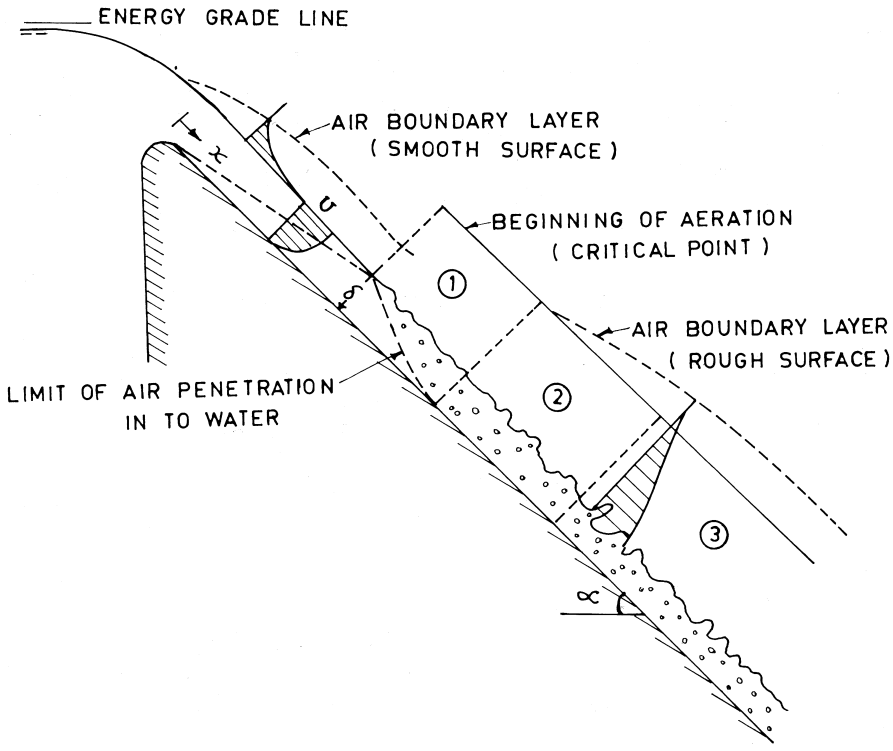

Figure 1 Air-entraining flow regimes on spillways.

Downstream from this point, a layer containing a mixture of both air and water gradually extends inside the flowing fluid. Its rate of growth is small. For small slopes, equilibrium is established before this layer reaches the spillway surface. However, for the steeper slopes, air reaches the lower boundary quicker. Measurements taken from the mixed layer show that the air-water mixture has a highly irregular wavy surface in which overturning waves continuously entrain air (Figure 1). This air is broken into bubbles that are dispersed by the intense turbulence. The flow near the surface is highly aerated (with air concentration in the range 0.5–0.9). The largest bubbles within the surface region are 10–20 mm in diameter. Away from the surface, the flow is less aerated and bubbles break down to 0.5–3 mm in diameter.

Above the wavy but reasonably continuous air-air-water mixture interface, water droplets of various sizes are present. This is spray, which may extend to

a considerable height above the main flow. However, it contributes little to the total discharge.

Far downstream from the point of inception, the flow becomes uniform. As with normal open-channel flow, this implies that, for a given discharge, measurements of the depth and the air concentration taken from fixed depths do not vary between distances along the spillway.

The flow in between the point of inception and uniform flow is the region that develops air entrainment; this region is a gradually varying flow. This regime is also divided into two sections. The first is a region where the aeration is developing but the air has not reached the bottom of the chute, and the second is a region where the air has reached the bottom of the chute but the air concentration varies along the length.

Falvey (1980) describes the vertical structure of the air-entrained flow in open channel with reference to the studies by Killen and Anderson (1969) as shown in Figure 2. It consists of four regions:

1. An upper zone of flying drops of water
2. A mixing zone where the water surface is very wavy but continuous
3. An underlying zone where air bubbles are diffused within the water body
4. An air free zone close to the bottom

The vertical structure can also be visualized as consisting of two layers only, i.e., entrained air and entrapped air as shown in Figure 3. Entrained air is the air that is being transported along with the flow in the form of air bubbles, which, at some point, have been pulled into the flowing water through the process of air entrainment. Entrapped air is the air that is being transported along with the flow because it is trapped in the surface roughness. Entrained and entrapped air together are the total conveyed air.

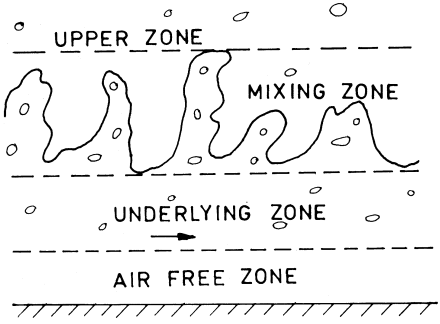

Figure 2 Vertical structure of air-entrained flow. (Shown in Falvey, 1990)

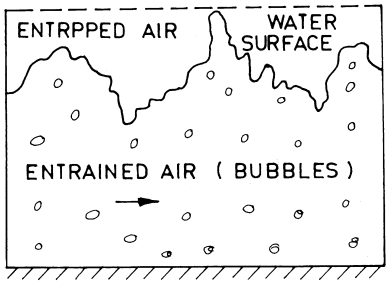

Figure 3 Concept of entrained and entrapped flow.

Total conveyed air is relevant when considering the bulking of the flow or flow features resulting from the plunging of an air-entrained jet into a pool of water. On the other hand, while evaluating cavitation prevention or characterizing gas transfer on the spillway face, the entrained air is of more significance than the entrapped.

However, it must be noted that the conceptual models are meant only for visualizing the process of air entrainment. Measured air concentration and velocity distribution show smooth continuous functions without discontinuity between the regions described earlier. The air-water behaves as a homogeneous mixture with varying concentration across the depth.

The following parameters are involved in the design concerning self-aeration on spillways:

Location of point of inception
Calculation of partially and fully developed aerated flow including mean air concentration and depth of aerated flows
Effect of air-entrained flow on stilling basin performance

27.3 LOCATION OF POINT OF INCEPTION

The point of aeration inception is generally accepted to be the point where the turbulent boundary layer emerges out of the flow surface and is identical to the point where ''white water'' begins to appear on the surface.

WES have evolved a relationship for the thickness of boundary layer δ on a spillway

$$\frac{\delta}{x} = 0.08\left[\frac{x}{k_s}\right]^{-0.233} \tag{1}$$

Where

x = Length measured along the spillway profile starting from the beginning of the curvature

k_s = Equivalent sand grain roughness, m

In order to locate the point of inception, values of δ for different values of x are obtained. The point of inception is located for that value of x where δ coincides with the free surface depth.

Falvey (1980) has described an early correlation between the boundary layer thickness, δ, and the unit discharge, q; free-stream velocity, U; and slope of the channel bottom, α; etc. He has also suggested a trial and error method for the calculation of the point of inception in accordance with Bormann's scheme that involves simultaneous solution of equations relating the local loss coefficient, C_f, boundary layer thickness, δ, and the distance Reynolds number.

The equations are:

$$\frac{1}{\sqrt{C_f}} = 3.85 \log\left[\frac{\delta u}{\nu}\right]^{1/2} + 3.67 \tag{2}$$

For a hydraulically smooth surface and

$$\frac{1}{\sqrt{C_f}} = 3.85 \log\left[\frac{\delta}{k_s}\right] + 6.45 \tag{3}$$

For a hydraulically rough surface.

The correlation between distance Reynolds number, R_x, and the local loss coefficient is given by

$$C_f = \frac{b_s}{(\log R_x)^{2.38}} \tag{4}$$

Where

C_f = Local loss coefficient

δ = Boundary layer thickness

u = Local velocity

ν = Kinematic viscosity of water

R_x = Distance Reynolds number

b_s = Empirical coefficient accounting for sand grain roughness

The value of b_s can be approximated as

$$b_s = 0.32 + 8.15\, k_s^{0.47} \tag{5}$$

Calculations are done by assuming a distance, x, where velocity, u, and depth, d, can be worked out. C_f is then calculated from Equation 2 or Equation 3, as the case may be; with the flow depth, d, taken as δ. C_f is also calculated using

Equation 4 with the values of R_x and b_s. If both the values of C_f are the same, the assumed distance, x, is the point of inception; otherwise, calculations are repeated with other value of x until the values of C_f match within the desired accuracy.

Keller and Rastogi (1977) used a mathematical model based on a two-dimensional form of time-averaged Navier-Stokes equations to compute the developing boundary layer and its intersection with the free surface. The results from their model were compared to the boundary-layer growth measurements taken in the laboratory and in the field; the agreement was excellent. Their analysis gave

$$\frac{X_I}{k_s} = \frac{X_S}{k_s} = 13.6\,(Sin\alpha)^{0.0796}\ F_b^{0.713} \tag{6}$$

$$\frac{d_I}{k_s} = \frac{0.233}{(Sin\alpha)^{0.04}} F_b^{0.643} \tag{7}$$

Where

X_I = Boundary layer development length

X_S = An approximation to the boundary-layer development length = $H_s/Sin\alpha$

α = Angle of chute with horizontal

F_b = A form of Froude number given by Equation 8

$$F_b = \frac{q}{\left(g\,S\,k_s^3\right)^{1/2}} \tag{8}$$

Where

S = Spillway slope expressed as Sin α

q = Unit discharge

Eliminating F_b from Equation 6 and Equation 7

$$\frac{\delta}{X_I} = 0.0212\left[\frac{X_s}{H_s}\right]^{0.11}\left[\frac{X_I}{k_s}\right]^{-0.10} \tag{9}$$

Or its alternate form

$$\frac{\delta}{X_I} = 0.0212\,(Sin\alpha)^{-0.11}\left[\frac{X_I}{k_s}\right]^{-0.10} \tag{10}$$

Where

H_s = Head at any point on spillway surface measured from total energy line

X_s = An approximation to the boundary-layer development length so that H_s/X_s = Sin α

α = Angle of the chute slope with horizontal

The above equations are applicable to the standard spillway shapes with constant slopes of 5 to 70 degrees. For spillways with varying slopes, the calculations can be carried out by noting that, at the point of inception, the discharge in the boundary layer, q_δ, equals the discharge over the spillway. Calculations can be done for a small distance, x, until q_δ matches the spillway discharge.

$$q_\delta = \frac{n}{n+1}\sqrt{2gH_s}\,\delta \tag{11}$$

Where n comes from the velocity distribution function $[u/U] = [y/\delta]^{1/n}$, with $n = 6.3$.

It is, however, argued that the points of inception and of the first occurrence of air entrainment are not identical. The air entrainment is believed to commence somewhat upstream, because the outer edge of the boundary layer is rough and irregular and extends about 1.2 times longer than the calculated depth. Therefore, $q_{1.2\delta}$ is considered, so that

$$q_{1.2\delta} = \frac{6n+1}{5(n+1)}\sqrt{2gH_s}\,\delta \tag{12}$$

Wood (1985) states that, for spillways with gradually varying flatter slopes, the boundary layer will be approximately in local equilibrium, and its growth rate can be obtained by differentiating Equation 7, thus

$$\frac{d\delta}{dx} = \frac{\delta}{x}\left[0.9 - 0.11\,X_I\,\mathrm{Cot}\,\alpha\,\frac{d\alpha}{dx}\right] \tag{13}$$

If the width of the spillway channel, W, is slightly converging or diverging,

$$\frac{d\delta}{dx} = \frac{\delta}{x}\left[0.9 - 0.11\,X_I\,\mathrm{Cot}\,\alpha\,\frac{d\alpha}{dx} - \frac{x}{W}\frac{dW}{dx}\right] \tag{14}$$

The calculations are done by dividing the length of the chute into smaller reaches, with the rates at the two sections calculated and averaged, and the new depth at each section calculated. The total depth of flow, y, can then be computed by applying the Bernoulli equation to obtain velocity outside the boundary layer, u_{fs} and then,

$$y = \delta + \{(q - q_\delta)/u_{fs}\} \tag{15}$$

If the first reach is that of a standard spillway crest and its rear face with a constant slope, Equation 9 or Equation 10 can be used for that reach. Subsequent numerical calculations using Equation 14 and Equation 15 do not depend on a constant spillway slope. The section where the discharge within the boundary layer given by Equation 12 is equal to the spillway discharge is the point of inception. All these computations can be done easily in a stepwise manner with a computer program.

Based on the analysis of published literature and their own laboratory experiments, Hager and Blaser (1998) proposed relationships for the draw-down curve

over spillway profile and turbulent boundary layer. These equations are valid only for standard spillways with constant slopes. The equations are:

$$\frac{\delta}{x} = 0.029\left[\mathrm{Sin}^2\,\alpha\,\frac{\mathrm{k_s}}{\mathrm{x}}\right]^{1/7} \tag{16}$$

Or its alternative form

$$\delta = 0.029\ (\mathrm{k_s}\ \mathrm{Sin}^2\alpha)^{1/7}\ \mathrm{x}^{6/7} \tag{17}$$

The location of the point of inception corresponds to the distance where the free-surface depth, d_I, given as

$$d_I = \frac{0.258\,\mathrm{y_c}}{\left[1.5625\left(\frac{\mathrm{y_c}\,Sin^3\alpha}{k_s}\right)^{0.1} - 1\right]} \tag{18}$$

Where y_c is the critical depth.

This can be determined from a graph of x Vs δ ($= d_I$).

Fernando et al. (2002) have analyzed available data and proposed the following relationships

$$X_I = \left[\frac{q}{0.056443\,k_s^{0.056}(Sin\,\alpha)^{0.34}}\right]^F \tag{19}$$

$$F = [1.46443\ k_s^{0.0054}\ \ (Sin\ \alpha)^{0.0027}]^{-1} \tag{20}$$

The analysis covered the following range of values:

$\alpha = 5°$ to $70°$; $q = 0.5$ to 20 m^2/s ; and $k_s = 0.001$ m to 0.003 m

Illustrative Examples

1) A standard spillway passes a discharge of 20 cumec/m. The spillway slope is 35 degrees and concrete roughness is $18\text{x}10^{-4}$ m. Find the location of the point of inception and flow depth at that point.

$$\text{Equation 1}\ \frac{\delta}{x} = 0.08\left[\frac{x}{18\times10^{-4}}\right]^{-0.233} \Rightarrow \delta = 0.0183\,\mathrm{x}^{0.767}$$

x	50	60	70	80	90	100
δ	0.37	0.42	0.47	0.53	0.58	0.63

from water surface profile L = 93 m corresponds to depth of flow of 0.59 m.

$$\text{Equation 6 and Equation 7}\ \frac{X_I}{k_s} = 13.6\,(Sin\,\alpha)^{0.0796}\,F_b^{0.713}$$

$F_b = q/(g\ \mathrm{Sin}\alpha\ \mathrm{k_s^3})^{1/2} = 11.04\mathrm{x}\ 10^4$

$\mathrm{X_I} = 92.3$ m ; $d_I = 0.233\ (Sin\alpha)^{-0.04}\ F_b^{0.643} = 0.717$ m

Equation 16 and Equation 18 $\delta = 0.029\ (k_s\ Sin^2\alpha)^{1/7}\ \mathrm{x}^{6/7}$ gives

X	50	60	70	80	90	100
δ	0.29	0.33	0.38	0.43	0.47	0.52

$$y_c = \left(\frac{q^2}{9.81}\right)^{1/3} = 3.44m \tag{20c}$$

$$d_1 = \frac{0.258\,\mathrm{y_c}}{\left[1.5625\left(\frac{\mathrm{y_c}\,\mathrm{Sin}^3\alpha}{k_s}\right)^{0.1} - 1\right]} \tag{20d}$$

$\delta = 0.49$ m is located at 94 m.

Equation 19 and Equation 20

$F = [1.46443\ \mathrm{k_s^{0.0054}}(\mathrm{Sin}\alpha)^{0.0027}]^{-1} = 0.708$ and

$$X_1 = \left[\frac{q}{0.056443\,\mathrm{k_s^{0.056}}(\mathrm{Sin}\,\alpha)^{0.34}}\right]^F = 93.7\ \mathrm{m} \tag{20e}$$

Results of Calculations

Method	Equation No.	Depth, δ, m	Length to the point of inception, m
WES	(1)	0.59	93
Keller-Rastogi	(6)(7)	0.717	92.3
Hager-Blaser	(16)(18)	0.49	94
Fernando	(19)(20)	0.708	93.7

It should be noted that although different relationships give almost identical values of $\mathrm{X_I}$, the depths of boundary-layer thickness vary considerably.

2) For the spillway shown in Figure 4, the depth of overflow is 6 m and coefficient of discharge is 2.2. The distance, x, from the crest, and the vertical distance, z, below the crest of points A,B,C,D and E are respectively (28,9),(55,27),(74,35), (136,44) and (185,62). Determine the approximate position of the point of inception. $\mathrm{k_s} = 0.0015$m.

An approximate and simplified procedure of calculation is indicated below, eliminating the trial and error method. This can be used for a preliminary assess-

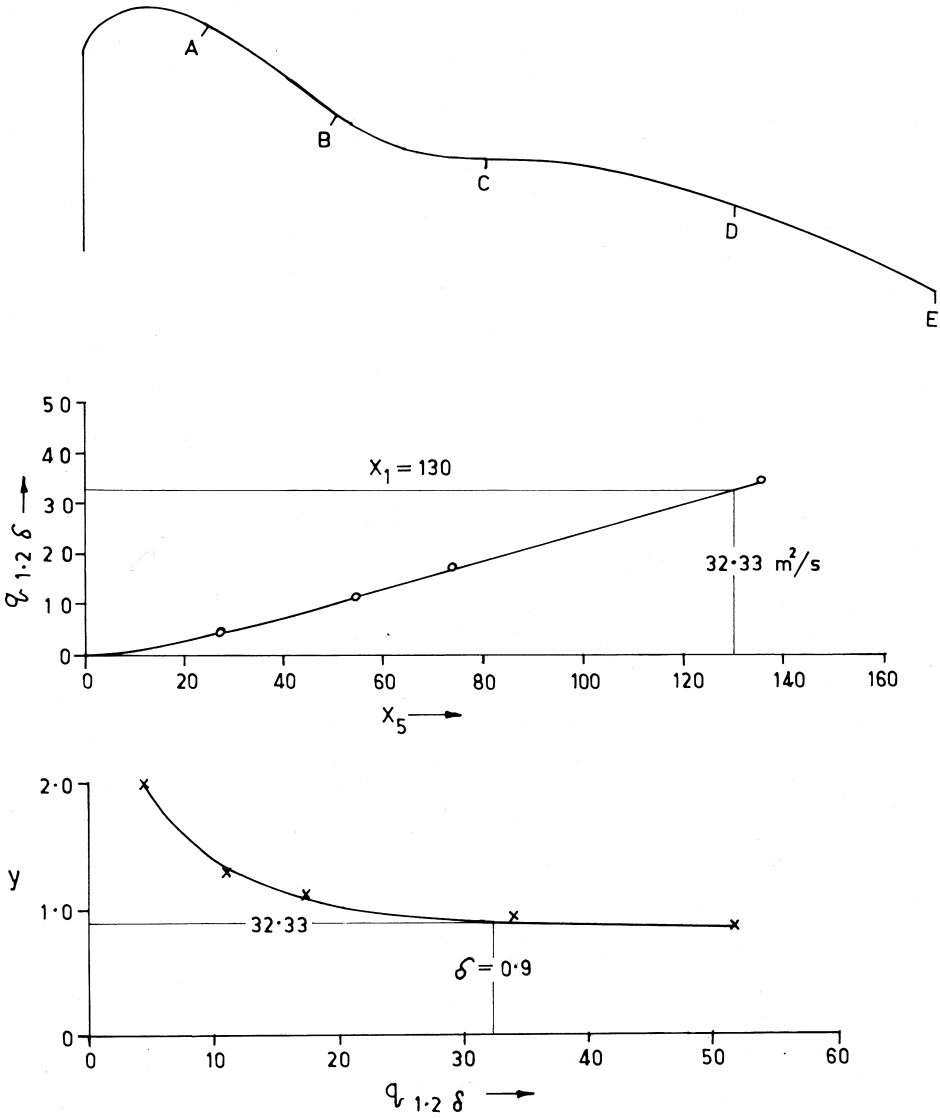

Figure 4 Illustrative example: locating the point of inception.

ment only. A more accurate solution described above (Equation 13, etc.) can best be obtained by programming on a computer.

$q = C_d\, h^{3/2} = 32.33$ cumec/m; when this discharge is contained within the boundary layer, the point of inception is reached.

Equation 12 $q_{1.2\delta} = \dfrac{6n+1}{5(n+1)}\sqrt{2gH_s}\ \delta$ reduces to

$$q_{1.2\delta} = 0.052\ X_S^{1.01} H_S^{0.39}$$

The depth of flow at various locations can be computed by applying the Bernoulli equation, neglecting the losses; $y\cos\alpha = H_S - \dfrac{u_{sf}^2}{2g}$ and $y = \dfrac{q}{u_{sf}}$, from which

$$u_{sf}^3 - (2gH_S)u_{sf} + (2gq\ \mathrm{Cos}\alpha) = 0$$

Point	X_s	Z	H_s	$q_{1.2\delta}$	y
A	28	9	15	4.33	2.02
B	55	27	33	11.64	1.29
C	74	35	41	17.09	1.16
D	136	44	50	34.15	0.95
E	185	62	68	52.36	0.89

Figure 4 shows the graph of $q_{1.2\delta}$ Vs x, from which the point of inception can be located at x = 130 m corresponding to the unit discharge of 32.33 cumec/m. The boundary layer thickness is approximately 0.9 m as read out from the graph of $q_{1.2\delta}$ Vs y.

27.4 PROPERTIES OF AERATED FLOW

Uniform aerated flow may occur asymptotically at the end of long prismatic chutes with a constant bottom slope. The location at which the flow fully develops aeration has not been studied in detail. The analysis by Afshar et al. (1994) indicates that the flow becomes fully developed when $x/d_I > 150$, where x is measured from the point of inception and where the depth of the non-aerated flow is d_I. This type of flow is not a common feature in most spillways with varying slopes and relatively large discharges. However, various characteristics of uniform flow such as air concentration, velocity distribution, etc., are relevant in understanding the characteristics of flow in the gradually varying flow as well.

Air Concentration

In the analysis of an air-entraining flow downstream from the point of inception, it is convenient to define a mean air concentration by the equation

$$(1 - \overline{C})y_{90} = y_w \tag{21}$$

$$y_w = \int_0^{\infty} (1 - \overline{C})\, dy \tag{22}$$

Where

$\overline{C}$ = average air concentration $q_a/(q_a + q_w)$
q_a = volume flow rate of air (m^2/s)
q_w = volume flow rate of water (m^2/s)
y_w = equivalent clear water depth
y_{90} = depth of flow where the air concentration is 90%

In a uniform flow, the depth-averaged mean air concentration, $\overline{C_e}$, remains the same for a given chute slope, discharge, and roughness, as shown by Wood (1985), based on his analysis of the results reported by Straub and Anderson (1958) who covered chute slopes from 7.5° to 75°. This is shown in Figure 5. Hager (1991) transformed the relationship (α Vs $\overline{C_e}$) as

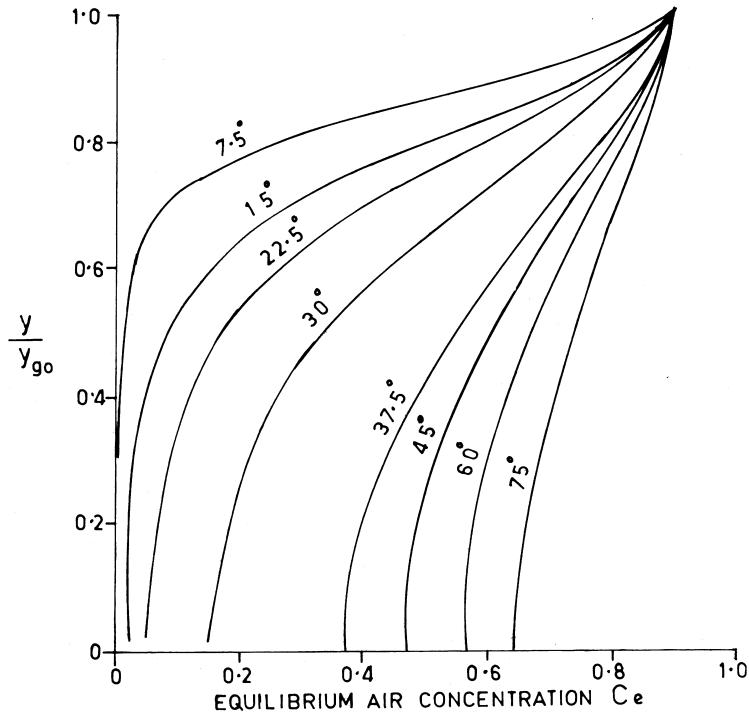

Figure 5 Equilibrium–air concentration distribution for various chute slopes. (Shown in Wood 1985.)

$$\overline{C_e} = 0.75\ (\text{Sin}\ \alpha)^{0.75} \tag{23}$$

Hager also analyzed the above data to obtain a normalized mean air concentration distribution across the depth for all the slopes as

$$c = 1.05 \exp\ [-0.54\ (y^* + 0.3)\ 2] \tag{24}$$

Where

c = relative air concentration with $0 \leq c \leq 1$
= $\overline{C_e}$-C_0)/(90-C_0) where C_O is bottom air concentration.
$y^* = (1\text{-}Y)\ Y_0$
$Y = y/y_{90}$ and $Y_0 = 2(\text{Sin}\ \alpha)^{-1/2}$

The above relationship is shown in Figure 6

Velocity Distribution

Wood (1985) on the basis of measuring velocity distribution in a developing region of flow on Aviemore Dam showed that

$$\frac{u}{u_{90}} = \left[\frac{y}{y_{90}}\right]^{1/6.3} \tag{25}$$

Chanson's (1989–a) analysis, however, indicated that the exponent might be 1/6 instead of 1/6.3. The experimental points on which the above results were based were obtained from curves with mean air concentrations in the range of 0–50%. This shows that the velocity distribution is independent of air concentration and, therefore, it is reasonable to expect that this will also apply to the uniform-flow region.

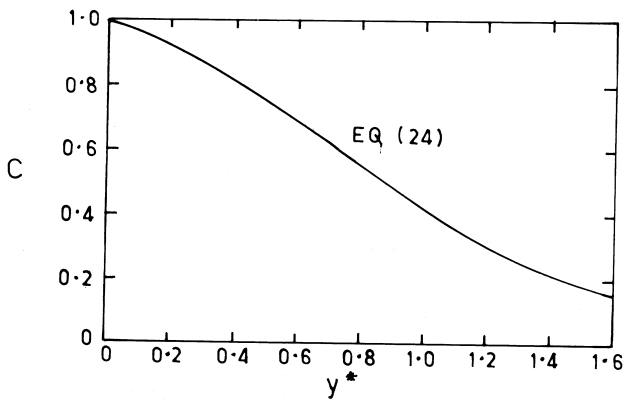

Figure 6 Normalized air concentration in uniform flow. (Shown in Hager 1991.)

Friction Factor

Presence of air close to the flow boundary is expected to reduce the shear stress, as well as the value of friction factor, f. Wood (1985) has shown that

$$f_e = \frac{8gSy_e^3}{q_w^2} = \left[\frac{y_e}{k_s}, R_e, \overline{C_e}\right] \tag{26}$$

$$\overline{C_e}, \overline{f_e}, = \phi\left[\frac{y_e}{k_s}, R_{e,} S\right] \tag{27}$$

Where f_e = Friction factor for equilibrium flow
y_e = Equilibrium clear water depth corresponding to $\overline{C_e}$

For flows under consideration, Reynolds number effects will be small and the variation in y_e/k_s will only be in a limited range. Therefore,

$$\overline{C_e}, f_e = \phi\,[S] \tag{28}$$

Wood's (1985) analysis of Straub and Anderson (1958) results is shown in Figure 7. Note that, until the mean air concentration reaches about 20%, the friction factor is not affected. This relationship can be expressed approximately as

$$\left[\frac{f_e}{f}\right] = \left[1 + 10\left(\overline{C}\right)^4\right] \tag{29}$$

Chanson's (2001) analysis based on his studies gives the relationship

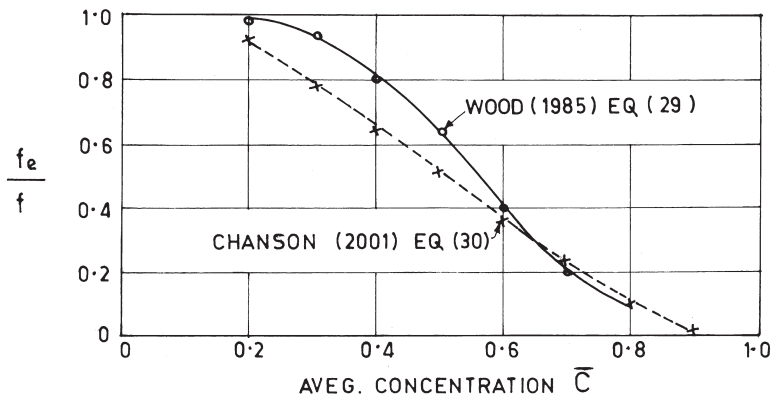

Figure 7 Effect of air entrainment on friction factor.

$$\frac{f_e}{f} = 0.5\left[1 + \text{Tanh}\left(0.628\frac{0.514 - \overline{C_e}}{\overline{C_e}\left(1 - \overline{C_e}\right)}\right)\right] \tag{30}$$

Which is also shown in Figure 7

Bulking of Flow

CBIP (1970) contains a discussion on the following relationship based on a large number of experiments conducted by various researchers and research institutes in India, relating the mean air concentration and non-aerated Froude number

$$1 - \overline{C_e} = [1 + \Omega F_w^{3/2}]^{-1} \tag{31}$$

Where

Ω = A factor accounting channel shape and roughness
= 1.35 n for rectangular channels, where n is Manning's roughness
F_w = Froude number of clear water flow
= $q_w/(g\ y_w^3)$

However, in their analysis, the clear-water depth, y_w, is defined as $y_w = (1 - \overline{C_e})\ y_{99}$, which is the depth corresponding to 99% air concentration.

Hager (1991) has shown that

$$Y_{99} = 1 + 1.35\left[\frac{\left(\text{Sin}^3\alpha\right) y_{99}}{n^2 g^3}\right]^{1/4}$$

Where $Y_{99} = y_{99}/y_w$

It is also shown that the above ratio of the mixture to clear-water depth also indicates bulking of the flow due to air entrainment by a factor $1.35\left[\frac{\left(\text{Sin}^3\alpha\right) y_{99}}{n^2 g^3}\right]^{1/4}$, which depends mainly on slope Sin α, moderately on roughness, and only slightly on clear-water depth.

Estimating Flow Parameters in a Uniform-Flow Regime

If the slope of the spillway chute, α, friction factor for non-entrained flow, and unit discharge are known, relevant flow parameters can be calculated from the relationships given above. The equilibrium mean air concentration, $\overline{C_e}$, corresponding to slope, Sin α, can be determined either from Equation 23 or Figure 5. The equivalent clear-water depth y_w can be calculated from

$$y_w = \left[\frac{q^2 f_w}{8gS}\right]^{1/3} \tag{33}$$

The average water velocity is $u_w = q/y_e$ and y_{90} is given by $y_w/(1 - \overline{C_e})$. The air concentration distribution can be obtained from Equation 24. Velocity distribution follows from Equation 25, with $u_{90} = 1.2\ u_w$.

27.5 THE REGION OF VARIED FLOW

Between the point of inception and the uniform flow region, the flow is characterized by a slow rate of air entrainment, a quasi-hydrostatic pressure distribution, and a slow variation of velocity. Wood (1985) observed that for a given mean air concentration, $\overline{C_e}$ (x), the air-concentration distribution would have a shape that is close to equilibrium concentration, which has been verified experimentally. This suggests that the entrainment velocity, V_e, will be a function of local conditions only, thus,

$$\frac{V_e(x)}{u_{90}} = \phi\left[F(x), \overline{C}(x)\right] \tag{34}$$

As with the entrainment of air, there is also simultaneous detrainment, which is given by $[V_T \text{ Cos } \alpha]\,\overline{C}(x)$, where V_T is the rise velocity of air bubbles. The equation for the continuity of airflow can then be written as

$$\frac{d}{dx} q_a = V_e(x) - \overline{C}(x) V_T \, Cos\alpha \tag{35}$$

Applying this equation in the region of uniform flow, where $\frac{d}{dx} q_a = 0$, yields

$$[V_e(x) - \overline{C}(x) V_T \text{ Cos}\alpha] = 0 \tag{36}$$

It is further suggested that on a spillway of long, uniform slope, the variation in the velocity, V_e, can be neglected, and, hence,

$$\frac{d}{dx} q_a = \left[\overline{C_e} - \overline{C}(x)\right] V_T \text{ Cos}\alpha \tag{37}$$

With $q_a = \frac{\overline{C}}{1-\overline{C}} q_w$, and by incorporating a variation in chute width (if any), the generalized form of the continuity of air flow equation can be written as

$$\frac{d\overline{C}}{dx} = \left(1-\overline{C}\right)\left[\frac{\left(V_T\right)_u Cos\alpha}{q_w}\left(k_e \overline{C_e} - k_T \overline{C}\right)\left(1-\overline{C}\right) + \frac{\overline{C}}{W}\frac{dW}{dx}\right] \tag{38}$$

Similarly, the equation of the energy of aerated flow has been developed by an extension of the normal gradually varied flow equation, treating the aerated flow as a continuous fluid with varying density and velocity,

$$\frac{dy_w}{dx} = \frac{Sin\alpha\left(1 + y_w \frac{d\alpha}{dx}\right) + E\frac{q_w^2}{g\,y_w^2}\frac{1}{W}\frac{dW}{dx} - 1}{Cos\alpha - \frac{E}{g}\frac{q_w^2}{y_w^3}} \tag{39}$$

Where

x = Distance along the chute from the point of inception
W = Chute width, if variable,
W = W(x)
y_w = Equivalent water depth
V_e = Entrainment velocity
V_T = Terminal bubble velocity in turbulent flow, usually taken as 0.17 m/s (Wood 1991)
$k_e = (V_e)/(V_e)_u$—Subscript u refers to the values of $\overline{C}$, Ve and
$k_T = (V_T)/(V_T)_u$—V_T in the uniform aerated zone
E = Kinetic energy correction coefficient, usually taken as 1.05
F = Roughness coefficient for the non-aerated flow
I = Friction slope = $q_w^2 f_w/4gy_w^3$—where f_w is the roughness coefficient for the equivalent flow, given by $f_w/f = 1/[1 + 10(\overline{C})^4]$

Numerical methods (finite difference) are used to solve the prior system of equations, and the average concentration $\overline{C} = \overline{C}(x)$ and equivalent depth $y_w = y_w(x)$ throughout the chute can be determined. The following simplifications are usually made: E = 1, $V_e = (V_e)_u$, $V_T = (V_T)_u$, and, hence, $k_e = k_T = 1$.

Ackers and Priestly (1985) have suggested a similar calculation procedure, where

$$f_w/f = 1 - 1.9(\overline{C})^2 \; for \; \overline{C} < 0.65 \tag{40}$$

$$\frac{L_m}{L_p} \geq \left[\frac{R_e}{F}\left(\frac{\mu_w/\rho_w}{\sqrt{g}}\right)\right]^{2/3} \quad fw/f = 0.2 \quad \text{for } \overline{C} > 0.65 \tag{41}$$

With an energy correction coefficient E = 1.09

Falvey (1990) has written a computer program in Microsoft–Fortran to calculate the hydraulic and cavitation properties of free-water surface flows. The output also includes an air concentration profile along the length of the chute. Air entrainment quantities are calculated using an empirical relationship

$$\overline{C} = 0.05F - \frac{(E_t\, Sin\alpha)^{1/2}}{6.3} \tag{42}$$

Where

F = Froude number = $V/(g\ y\ Cos\ \alpha/E)^{1/2}$
V = Flow velocity
Y = flow depth measured normal to channel depth

E_t = Eotvos number = $(g\rho_w y^2)/\sigma$
ρ_w = Density of water
σ = Interfacial surface tension

Chanson (2001) has proposed a continuity equation for air in the air-water flow in the uniform equilibrium regime based on an air bubble diffusion model, as

$$\frac{\partial}{\partial y}\left(D_t \frac{\partial C}{\partial y}\right) = (u_r)_{hyd} \operatorname{Cos}\alpha \frac{\partial}{\partial y}\left(C\sqrt{1-C}\right) \tag{43}$$

Where

D_t = Turbulent diffusion in the direction normal to the flow
$(u_r)_{hyd}$ = Rise velocity in hydrostatic pressure gradient

This leads to $C = 1 - \operatorname{Tanh}^2\left(K' - \frac{y/y_{90}}{2D'}\right)$

K' is an integration constant, and $D' = (D_t/(u_r)_{hyd} \operatorname{Cos}\alpha\ y_{90})$

It is stated that the above equation describes air concentration distribution as a function of two parameters only, i.e., y_{90} and D', and is in good agreement with model and prototype data.

27.6 EFFECT OF ENTRAINED AIR ON STILLING BASIN PERFORMANCE

Contrary to a common belief that air entrainment in the flow would contribute to energy loss, it is noted that, for all practical purposes, the conjugate depth of hydraulic jump could be determined from non-aerated flow equations. Falvey (1980) recommends that, in rectangular channels, conjugate depth y_2 can be calculated with sufficient accuracy from the classical jump equation, Equation 3, Chapter 20.

27.7 FORCED AERATION

With the increase in the flow velocity, the potential for cavitation damage increases in proportion to about the 6th power of velocity. For example, if damage occurs due to an offset of 3 mm in a velocity of 30 m/s, the same offset would create twice the damage if the velocity increases only to 33.7 m/s. If the velocity increases above a certain value, the surface finish required to protect the boundary exceeds the expected tolerances from the best-construction practice. In such a case, either a design modification to improve the cavitation index is required or, alternatively, remedial measures to prevent cavitation have to be taken.

A simple and effective method to prevent cavitation damage is the aeration of the flow. Experience shows that the mixture of air-water absorbs cavitation impacts. Experiments have shown that a relatively small concentration of air in flowing water significantly decreases the cavitation damage on concrete surfaces. It was shown that while an unaerated flow resulted into a cavitation weight loss of 5000 lbs, a 7% air concentration fully eliminated the cavitation loss.

The flow itself entrains air downstream from the point of inception, so the calculation procedure discussed previously could enable one to estimate the air contents that are dragged naturally by the flow. As a rule, self-aeration is sufficient only for relatively small discharge intensities. Based on prototype tests conducted on some spillways, it was found that self-aeration emitting a discharge intensity of 4 cumec/m would commence at a distance of 30 m from the crest, whereas self-aeration emitting a discharge intensity of about 18 cumes/m would commence at a distance of 100 m. When high discharges are released, the flow over the spillway surface does not entrain free air up to the boundary, which necessitates artificial aeration in order to introduce air into the flow near the boundary.

An aerator is a device that deliberately causes a large cavity or void to be formed on the underside of a high velocity jet, as shown in Figure 8. The void created is a negative-pressure region relative to the atmospheric pressure wherein air is drawn to the void via a vent connection. The types of devices that can be used to introduce air into the flowing water include deflectors or ramps, offsets, steps, grooves, and combinations therein, as shown in Figure 9. An aerator requires a passageway to admit air to the underside of the jet. Wall slots or recesses, lateral wall deflectors or wedges, and air intake conduits can be utilized. A schematic diagram of an aerator system with ramp, offset, and air intake shaft in various combinations is shown in Figure 10.

27.8 MECHANISM OF AERATION

The mechanism of an aeration device has been described by Falvey and Ervine, (1988) Bruschin, (1987) Pinto et al., (1982) Volkart and Rutschmann, (1986) and Chanson (1989–a). Basically, aeration develops through four zones in the vicinity of an aerator as shown in Figure 8. These are: the approach zone, transition zone, aeration zone, and de-aeration zone. The aeration zone is divided into three regions: the shear region, spray region, and mixing region.

In the approach and transition zones, the flow is in contact with the boundary, so natural aeration in the top layers of the flow may or may not take place. In the aeration zone, the top and bottom layers of the flow are detached from the boundary in the form of a high velocity jet. Local pressures in the bottom layers suddenly drop from a high value at the end of the transition zone to nearly atmospheric values at the beginning of the aeration zone, which induces a high

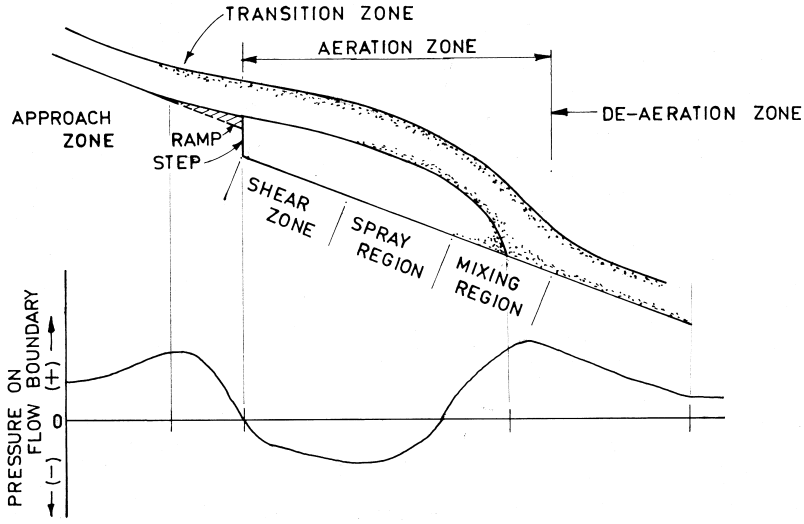

Figure 8 Typical aerator and zone describing mechanism.

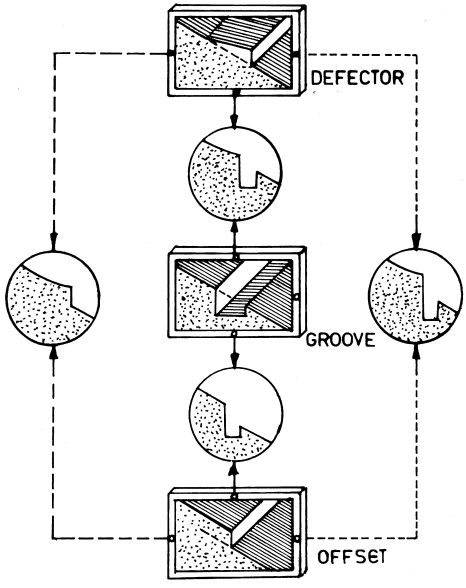

Figure 9 Basic aerator shapes. (Shown in Falvey 1990.)

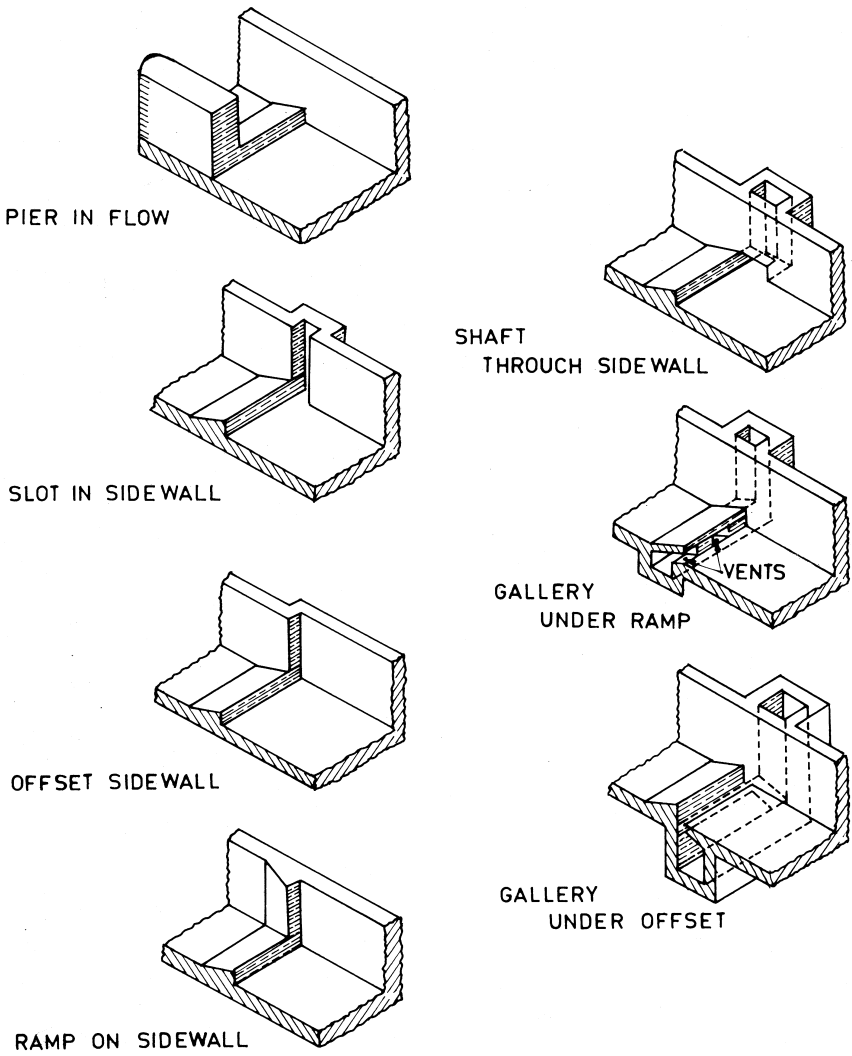

Figure 10 Aerator with various combinations of an air-inlet system. (Shown in Falvey 1990).

degree of turbulence responsible for aeration. In the shear zone, the flow is intact but in the (middle) spray region; the air entrainment is at a maximum. Downstream of this, the jet impacts on the chute floor, reestablishing a pressure gradient is by which air bubbles and water mix, resulting from the interaction of flow turbulence and gravity. This region extends downstream to the point where de-aeration begins. In the de-aeration zone, the air concentration in the bottom starts reducing, the air bubbles rise upward due to buoyancy, and the air bubbles interact with the self-aeration process occurring from the top downward. Finally, equilibrium is established with a small air-water ratio near the bottom and a large air-water ratio near the free surface. When the bottom concentration falls below acceptable level, another aerator is required.

27.9 DESIGN OF AN AERATOR SYSTEM

Designing an aerator system involves the following considerations:

a) Location of the first aerator
b) Type and size of the aerator
c) Volume of air entrained at the aerator
d) Type and size of the air supply system
e) Spacing between the aerators to maintain a given protection level

27.9.1 Location of the Aerator

In general, the aerator should be located first where the potential for cavitation damage is deemed possible. Referring to Figure 15, Chapter 26, shows this location to be where the flow-cavitation index is 0.20 or smaller. However, consideration should also be given to the characteristics of the flow at that location, i.e., depth and velocity—both of which are significant in estimating a reasonable length of the jet trajectory to facilitate proper aeration. Other recommendations specify magnitude of flow velocity, ranging from 20 to 30 m/s, which is where the first aerator should be located. A minimum Froude number equal to 6 has also been suggested. A velocity of 30 m/s with a Froude number of 6 gives an approximate cavitation index value of 0.22, which seems to be workable. Falvey, (1990), however, points out that the maximum discharge is not necessarily the flow rate that produces the lowest values of cavitation index. As shown in the Table 1, there could be a wide range of discharge proportions corresponding to the lowest cavitation index.

Falvey also states that, in addition to considering the cavitation index, curvature of the boundary should also be considered. While an aerator is desirable at a grade change, installing aerators in vertical bends that are concave upward should be avoided.

Table 1 Location of Aerator and Critical Discharge

Spillway	Cavitation index at aerator	Critical discharge (% of max)
Blue Mesa	0.22	30
Flaming Gorge	0.19	52
Glen Canyon	0.14	14
Hoover	0.18	19
Mc Phee	0.19	100
Yellowtail	0.13	16

Chanson (1995) suggests that the Froude number at the location of the aerator should be greater than 7–8 for an aerator with a ramp in order to ensure that the cavity does not get filled or drowned.

27.9.2 Types of Aerators

Ramps or steps inserted on the chute surface are the simplest and most practical devices used to cause natural aeration of flow near a boundary, as shown in Figure 9. The sudden discontinuity in the bottom alignment causes an air-water interface along which the high-velocity water drags air via the intense zone of spray below the cavity. This process requires continuous supply of air for which a transverse gallery or a recess can be added in order to improve conditions for air admission to the cavity below the jet, as shown in Figure 10.

27.9.3 Volume of Air Entrained by an Aerator

The simplest relationship about the volume of air entrained at the aerator is given by Hamilton (1983):

$$Q_a = C_1 \, V \, L \, W \tag{45}$$

Where

Q_a = Air-flow rate
C_1 = A coefficient varying from 0.01 to 0.04
L = Throw length of the jet trajectory
W = Spillway width at the aerator
V = Average velocity of water over the aeration ramp

Falvey (1990) quotes a similar relationship:

$$q_a = C_2 \, t_r \, V \tag{46}$$

Where

C_2 = A coefficient varying from 0.1 to 0.64
t_r = Height of the ramp or offset

Zagustin et al. (1982) suggest an empirical relationship L/y>3–5 in order to achieve an air concentration of about 40%, where y is the depth of flow at the ramp or step.

These equations ignore the effect of turbulence and the depression of the jet caused by the reduced pressure under the nappe.

It has been found that the trajectory length is affected by the pressure drop beneath the nappe, which in turn, is determined by the geometric and hydraulic characteristics of the air supply system. The calculation system must therefore involve all of these parameters together.

Falvey (1990) has described such a procedure for which an interactive computer program has been written and made available with the publication.

Rutschmann and Volkart (1988) discuss the concept of an aerator as a water-jet pump. Thus, the efficiency of an aerator mainly depends on two different systems:

The pumping device, that is, the air being dragged by the water flow, and
The air supply system, represented by the side inlets and the duct or space beneath the nappe

Dimensional analysis gives the air entraining capacity of the aerator by

$$\beta = \frac{q_a}{q_w} = K_1(F_r - K_2) - K_3 - \frac{\Delta_p}{\rho_w g\, y} \tag{47}$$

Where

$F_r = V/\sqrt{g\ y}$ is the Froude number of the flow at the aerator
K_1, K_2 and K_3 are constants depending mainly on the aerator and chute geometry
Δ_p = Subpressure under the nappe
y = Water depth at the beginning of aerator

As per this relationship, increase in subpressure reduces q_a for a given value of q_w.

The characteristics of the air supply system give the following relationship:

$$V_a = \left[\frac{2\,\Delta p\, g}{(1+\xi_{tot})}\right]^{1/2} \tag{48}$$

Where

V_a = Velocity of air in air intake shaft
ξ_{tot} = Total head-loss coefficient of the air supply system
Δ_p = Pressure at the spillway side wall

Rutschmann and Volkart (1988) suggest the following values of ξ_{tot}:

0.55 for an air inlet shaft with a bell mouth entrance and a rounded 90° bend at the outlet

1.0 for an inlet without a bell mouth but with a rounded 90° bend at the outlet

2.0 for an inlet without a bell mouth and without a rounded 90° bend at the outlet

Equation 48 shows that an increase in the subpressure increases the airflow rate.

For different values of $\Delta_p/\rho_w g$, values of q_a are worked out and curves representing the air demand of the aerator system and air supply system are plotted on the same graph. The intersection of the two curves is the operating point of the aerator system for a given water discharge. By repeating this process for different water discharges, the characteristics of the aerator system can be determined, as shown in Figure 11.

The subpressure under the cavity is not constant in the transverse direction. At the entrance to the main duct (i.e., the intersection of the sidewall and spillway surface) the pressure is subatmospheric by the amount equal to the head loss in the side duct and the velocity head. At the centerline of the main duct, the subatmospheric pressure is the head loss in the main and side ducts, with the velocity head being recovered and the friction losses in the main duct neglected. This is illustrated in schematically in Figure 11. A detailed procedure, including an algorithm for the calculations to determine subpressure distribution below the cavity, has been given by Rutschmann and Volkart (1988). Generally, an average value of the cavity subpressure, $\overline{\Delta_p}$, is considered in the calculations.

Another important consideration is the desirable air discharge entrained to achieve an air concentration of 40–45%, which effectively gives the desired bottom-air concentration to mitigate cavitation damage. Rules of thumb and empiric relationships based on the performance of existing aerator installations have been derived. One rule of thumb is that the air demand per unit width of an aerator should be around 10 cumec/m. Another relationship is

$$\beta = \frac{q_a}{q_w} = 0.015 + 0.464 \exp\left(-31.58\, F_q\right) \tag{49}$$

$$F_q = \frac{q_w}{\sqrt{g H_1^3}} \tag{50}$$

Where H_1 = Head above the aerator

Rutschmann and Hager (1990) have shown the effect of cavity subpressure on the air entraining capacity of an aerator as

$$\frac{\beta}{\beta_{\max}} = \left[\frac{2}{\pi}\tan^{-1}(3.10^{-3}\Delta E)\right]^{0.7} \tag{51}$$

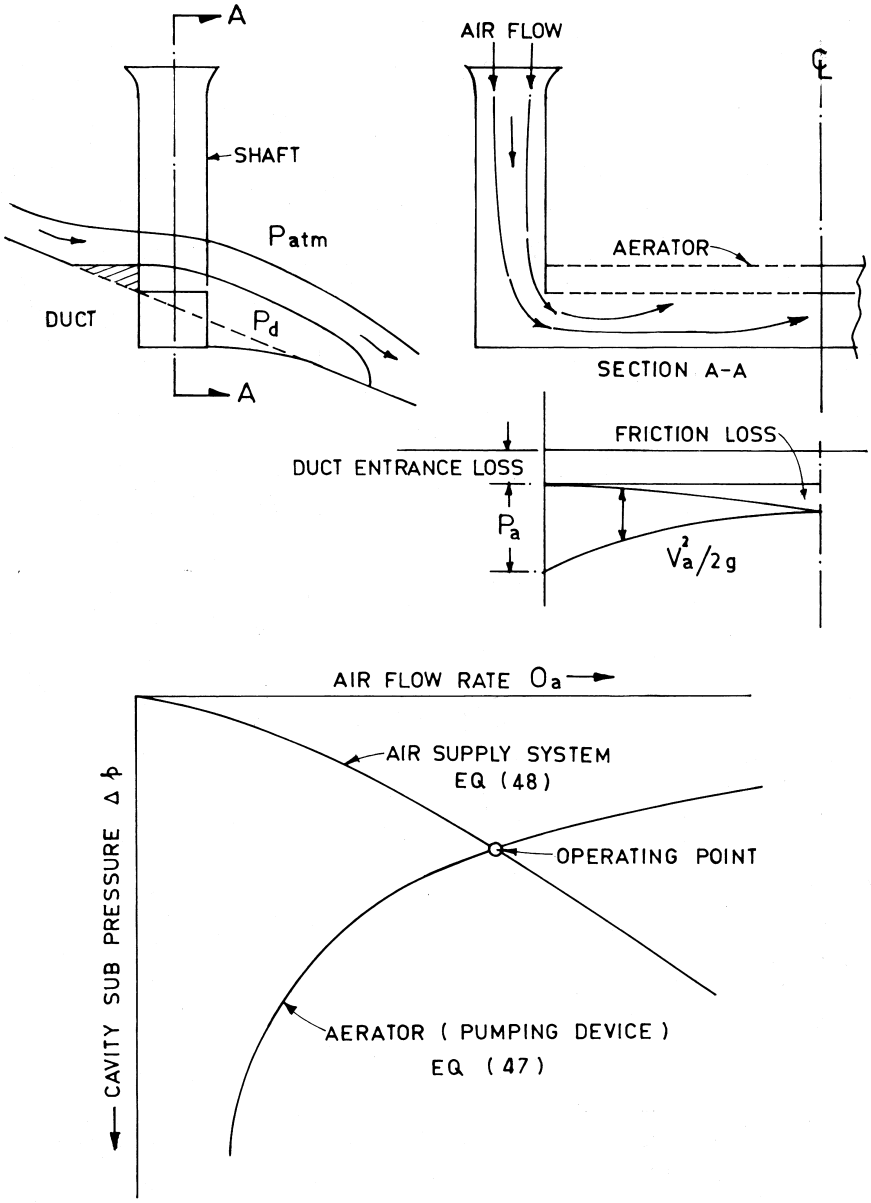

Figure 11 Schematic representation of an aerator operating point. (Shown in Rutschmann and Volkart 1988.)

Where $\beta_{max} = \beta\ (\Delta_p = 0)$ is the maximum air entrainment coefficient for zero subpressure. Also, $\Delta E = E - E_{min}$ is a difference–Euler number involving $E_{min} = E\ (\beta = 0)$ to represent the cavity subpressure at which the air entrainment vanishes. Expressions for E_{min} have been developed on the basis of limited set of data:

$$10^{-3} E_{min} = \frac{1}{2.3} (\tan \alpha)^{1.15} \exp\left[1.15\ (\tan \theta)^2\right] + \frac{1}{3} T_s^2 \tag{52}$$

Where

θ = Angle of chute with horizontal
α = Angle of ramp with chute surface
$T_s = t_s/y$—where t_s is the height of step and y is the depth of flow

They have also analyzed experimental data from various sources to relate the maximum air-entrainment coefficient, β_{max}, with the relative jet length, $\lambda j = L/y$, as

$$\beta_{max} = 0.030(\lambda_j - 5)\ (for\ F > 6) \tag{53}$$

The relative length of jet trajectory, assuming atmospheric pressure in the air slot, is given as

$$\lambda_j = \frac{L}{y} = \frac{\bar{\alpha} F^2}{Cos\,\theta} \left[1 + \left(1 + \frac{2T\ Cos\,\theta}{\left(\bar{\alpha} F\right)^2}\right)^{1/2}\right] \tag{54a}$$

Where $T = (t_r + t_s)/y$ is the relative height of aerator and $\bar{\alpha}$ is the effective take-off angle given by

$$\frac{\bar{\alpha}}{\alpha} = \left[Tanh\left(\frac{T_r}{y}\right)\right]^{1/2} \tag{55}$$

Where $T_r = (t_r/y)$. The above relations are valid for $T < 1$; $\tan \alpha < 0.15$; and $6 < F < 12$. Also, the chute should have no significant transverse slope, so a nearly two-dimensional flow should have established.

For an aerator having no ramp but an offset, i.e., $\alpha = 0$, Equation (54a) is

$$\lambda_j = F\left[\frac{2T}{\theta}\right]^{1/2} \tag{54b}$$

The other relationships include the average subatmospheric pressure below the jet

$$\overline{\Delta_p} = \rho_w \frac{V_w^2}{E} \tag{56}$$

and the air velocity in the intake system corresponding to $\overline{\Delta_p}$

$$V_a = \left[\frac{2\overline{\Delta_p}}{0.43\,(1+2\xi_{tot})\rho_a} \right]^{1/2} \tag{57}$$

Where

ξ_{tot} = Total head-loss coefficient of the air supply system (typically 0.55)
ρ_a = Mass density of air (typically 1.207 kg/cum)

The cross-sectional area, A_s of the air supply system, can thus be found as

$$A_s = \frac{Q_a}{V_a} \tag{58}$$

The maximum velocity in the air supply system may be up to 100 m/s to minimize the possibility of compression shocks and noise. It should be kept as small as possible.

One should bear in mind that, for protection against cavitation damage, the air concentration next to the bed—and not the mean air concentration—is important. The mean air concentration immediately after the impact zone can be estimated as $C_0 = q_a/(q_a + q_w)$. A well-designed aerator will produce higher air concentrations locally than those associated with the aeration equilibrium state. Thus, downstream of the aerator, the air concentration will decrease to that of the equilibrium state, $\overline{C_e}$. Chanson (1989–b) suggests that a steep spillway ($\alpha > 20°$), $\overline{C_e} > 30°$, will ensure that the bottom air concentration will be adequate to protect the downstream reach.

27.9.4 Air Supply Systems

Aerators should include a means by which air can be admitted to the jet cavity created by the ramp, offset, or step. A common means of providing the air supply is to connect a vertical air-intake conduit to a portal in the wall of the spillway chute. Air can also be supplied by means of a duct system located beneath the surface of the spillway chute, as shown in Figure 10. With this arrangement, an air gallery feeds several distribution ducts, which are connected to the downstream face of the aerator step or ramp. Such a system has been used at Guri, San Roque, and Tehri Dams. Air can also be supplied to an aerator cavity through the void created in the wake of pier tails for spillway gates.

The air duct cross-sectional area must be large enough to distribute the entrained air and not decrease the pressure under the nappe appreciably. The pressure drop between the atmosphere and the lower side of the nappe, Δ_p, can be calculated with Equation 57.

Keeping the air velocity in the duct as low as possible is preferable—generally not exceeding 50 m/s, although some investigators cite a maximum velocity of 120 m/s if compressibility effects are to be avoided. Falvey (1990) suggests a procedure to estimate the air velocity such that the pressure drop is limited to one-tenth of the critical pressure ratio.

27.9.5 Aerator Spacing

The required concentration of flow next to the boundary is about 8%. Taking into account that a part of the air migrates upwards and escapes through the free surface, it can easily be seen that the initial concentration just downstream of the aerator should be significantly higher. The loss of concentration along the spillway slope can be expressed as

$$C = C_0 - \alpha x \tag{59}$$

Where

C = Concentration of air at a distance x from the aerator
C_0 = Initial concentration at the point of impact of the jet
α = Coefficient of loss

Typical figures for α as indicated from the prototype measurements on some Russian dams are as follows:

0.15 to 0.20 per meter.....Straight zone
0.50 to 0.60 per meter.....Buckets
0.50 to 0 20 per meter.....Concave curve

If $C = 8$, the criteria for the distance S between the aerators is found as

$$S \leq (C_0 - 8)/\alpha \tag{60}$$

Based on the model studies conducted by Vischer et al. (1982), an approximate relationship can be expressed as

$$L_d = 1.1\ V \tag{61}$$

However, the above approaches do not consider the effect of self-aeration of the flow in the upper layers. Falvey (1990) suggests a procedure that considers the process of self-aeration and air concentration close to the bed. Chanson (1989–b) argues that, on a steep spillway ($\alpha > 20°$), the air concentration downstream of an aerator will tend toward the equilibrium air-concentration distribution where $C_e > 30\%$. This simulation is not possible in a hydraulic model because of the scale effects (see Ch. 28). If the average air concentration at the start of the downstream flow region is high enough ($\overline{C} > 25–30\%$), all the length downstream of the first aerator will be protected and no additional aerator will be required as long as $\alpha > 20°$. If the spillway slope becomes flatter than this, the flow may be de-aerated and an additional aerator will be required as soon as the average air concentration becomes less than 30%.

At Nurek spillway (Russia), eight aerators were spaced closely (10–15m). It is known that aeration was considered to be excessive and some aerators had to be eliminated.

Illustrative Example

A 100-m high gravity spillway has 5 spans, 15-m wide each, separated by 4-m thick piers. The spillway slope is 0.7H:1V. The maximum depth of overflow is 12.3 m to pass a unit discharge of 95 cumec/m. Determine whether

1) An aerator device would be necessary?
2) If so, the location of the first aerator, and
3) Broad design features of a ramp aerator with air supply shafts on both the sidewalls.

1) Calculating cavitation index at the base:

With H = 100 m, q = 95 cumec/m, θ = 55°; V = 43.81m/s; y = 2.17 m; F = 9.49

Cavitation index σ can be calculated form the general expression Equation 5, Chapter 26,

$$\sigma = \frac{y.Cos\theta \pm \dfrac{yV^2}{gR_c} + p_b - p_v}{\dfrac{V^2}{2g}}$$

which, with $R_c \rightarrow \infty$, gives σ = 0.113.

Since this value is considerably lower than the permissible value of 0.20 aeration is necessary.

2) Locating the first aerator:

The first aerator has to be located at the point where the cavitation index σ has reached the value of 0.20. Calculations have been carried out for different discharges and locations on the spillway slope in order to select a location meeting the various norms discussed earlier. The results are shown in Table 2.

The above results indicate that the first aerator should be located at 55 m below the FRL. However; the Froude number at this location, corresponding to the maximum discharge, is less than 6. One way to meet the various requirements would be to have the tip of the aerator ramp at an elevation 60 m below the FRL and to start the aerator ramp from an elevation approximately 5 m above the tip elevation, as shown in Figure 12.

3) Features of an aerator:

In the absence of any firm and definite guidelines, pertinent dimensions of the aerator are chosen by trial so as to suit the air slot, ramp, and air inlet configurations for a given structure, as shown in Figure 12. Starting with a ramp angle of 4° = 0.07 radian and a ramp height t_r of 0.35 m, $T_r = (t_r/y) = 0.123$. The effective take off angle is

$$\frac{\overline{\alpha}}{\alpha} = \left[Tanh\left(\frac{T_r}{y}\right)\right]^{1/2} = 0.068 \text{ rad}.$$

Table 2 Calculation of Cavitation Index

Head below FRL m	Unit discharge cumec/m	V_1 m/s	y m	F	Cavi. Index σ
50	95	30.32	3.13	5.47	0.24
	50	30.80	1.62	7.72	0.22
	25	31.06	0.80	11.05	0.21
	10	31.22	0.32	17.61	0.20
55	95	31.90	2.97	5.91	0.21
	50	32.40	1.54	8.32	0.20
	25	32.60	0.77	11.89	0.19
	10	32.75	0.30	18.92	0.18
60	95	33.50	2.84	6.35	0.19
	50	33.90	1.48	8.90	0.18

The relative jet length, Equation 54,

$$\lambda_j = \frac{L_j}{y} = \frac{\bar{\alpha}\, F^2}{Cos\theta}\left[1+\left(1+\frac{2T\,Cos\theta}{\left(\bar{\alpha}\,F\right)^2}\right)^{1/2}\right]$$

with T = 0.123, F = 6.35, works out to 11.11.

$\beta_{max} = 0.030(\lambda_j - 5) = 0.1833$ gives a maximum air discharge of 0.1833 × 95 × 91 = 1585 cumec.

E_{min}, Equation 52 gives

$$10^{-3} E_{\min} = \frac{1}{2.3}(\tan\alpha)^{1.15} \exp\left[1.15\,(\tan\theta)^2\right] + \frac{1}{3}T_s^2,\ E_{\min} = 212.86.$$

Calculation of ΔE requires determination of the ratio $\frac{\beta}{\beta_{max}}$, where β can be estimated from the criteria;

(1) Air discharge of about 10 cumec per unit length of the aerator, i.e., 91 × 10 = 910 cumec or $\beta = 0.105$ cumec/m.

OR

(2) Equation 49, $\beta = \frac{q_a}{q_w} = 0.015 + 0.464 \exp(-31.58 F_q)$, with

$F_q = 0.065$ gives $\beta = 0.074$ and $q_a = 7.04$ cumec/m

With an average value of Qa = 700 cumec or $q_a = 7.69$, thus $\beta = 0.081$ and hence $\frac{\beta}{\beta_{max}} = 0.442$, Equation 51 yields

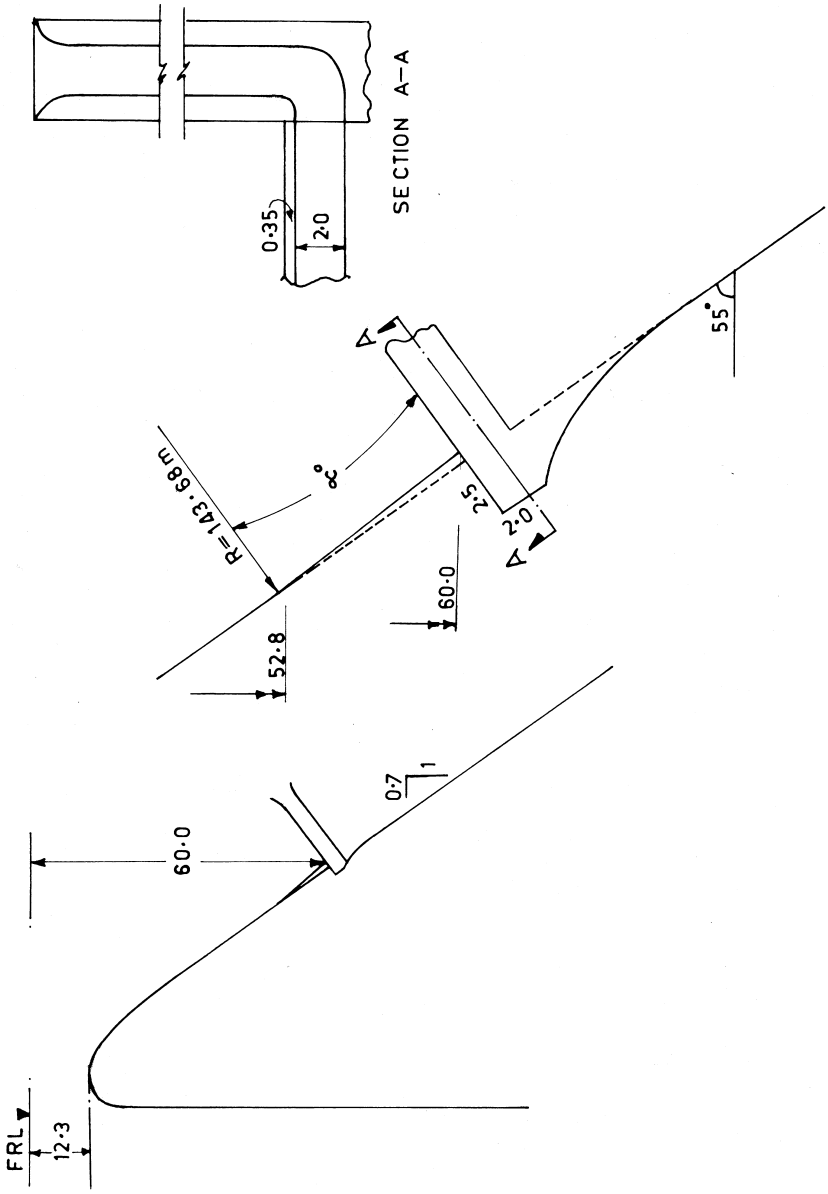

Figure 12 Design of an aerator: illustrative example.

$$\frac{\beta}{\beta_{\max}} = \left[\frac{2}{\pi}\tan^{-1}(3.10^{-3}\ \Delta E)\right]^{0.7} \text{ with } \Delta E = 177.4 \text{ and hence}$$

$$E = E_{\min} + \Delta E = 390.3$$

$$\text{Equation 56, } \overline{\Delta_p} = \rho_w \frac{V_w^2}{E} = 2873 \text{ Pa}$$

The velocity of air in the intake shaft, Equation 57

$$V_a = \left[\frac{2\overline{\Delta_p}}{0.43\,(1+2\xi_{tot})\rho_a}\right]^{1/2} = 72.6 \text{ m/ s}.$$

A value of $\xi_{tot} = 0.55$ has been chosen, assuming that the intake shaft will have a bell-mouth entrance and a 90° bend at the base.

4) Cross-Sectional Area of Air-Intake Shaft

$$A_{sd} = \frac{1}{2}\frac{Q_a}{V_a} = \frac{1}{2}\frac{700}{72.6} = 4.82 sqm.$$

A cross-section of 2.0 m × 2.5 m for the shaft as well as air slot below the ramp would be suitable, as shown in Figure 12. The design worked out is only a preliminary design, which should be refined on the basis of studies on a general comprehensive model with respect to flow conditions in the air slot, ramp and shaft, etc.

27.10 AERATORS FOR TUNNEL SPILLWAYS AND OUTLETS

Aerators for tunnel spillways and those to be located downstream of gates in outlets differ from the aerators on ogee and chute spillways with respect to size of ramps or offsets, slots, and air supply systems. This is because of the limited space available and relatively large depth of flow as compared to the cross-sectional area available. Unlike aerators for the ogee and chute spillways, those for the tunnel spillways and outlets have been developed completely from model studies, and no analytic or empiric means have been developed so far for their design.

The aerators for the open-channel type tunnel spillways of Blue Mesa, Flaming Gorge, Glen Canyon, Hoover and Yellowtail Dams, USA, were designed and constructed on the existing structures after experiencing severe cavitation damage, mainly in the region of vertical elbows. The locations where aerators were required were circular in section with diameters in the range of 7 to 15 m, and the depths of flow nearly two-thirds of the tunnel section. The access of air to the aerators was through downstream portal and along the free board over thewater surface. The circular section and the large depths of flow restricted the dimensions of ramp and air slots. It was required that the trajectory should not

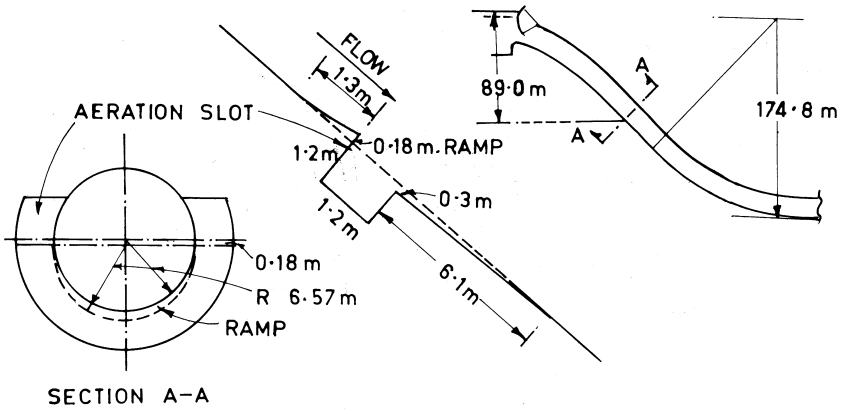

Figure 13 Aerator for Glen Canyon Dam–tunnel spillway. (Shown in Falvey, 1990)

hit the tunnel roof to block the flow passage and at the same time should not cause them to be filled at low flows. Falvey (1990) has described the design of aerators for the existing tunnel spillways. Figure 13 shows details of a typical aerator for the tunnel spillway of Glen Canyon Dam, USA. Generally, the ramp heights for such aerators varied from 0.1 m to 0.3 m and air slot sizes from 0.6 m $\times$ 0.6 m to 1.2 m $\times$ 1.2 m. Other alternatives developed by USBR are: a large offset away from the flow as shown in Figure 14, whereas, for the tunnels of horseshoe section, simpler method as shown in Figure 15.

The aerator designs of the outlet works of Palissades, Navajo, Pueblo, Crystal, and Teton Dams, USA, have been described by Beichley and King (1975)

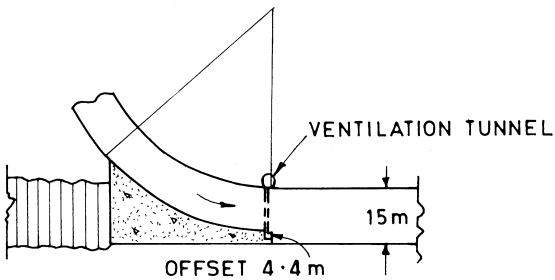

Figure 14 Aeration by large offset away from flow.

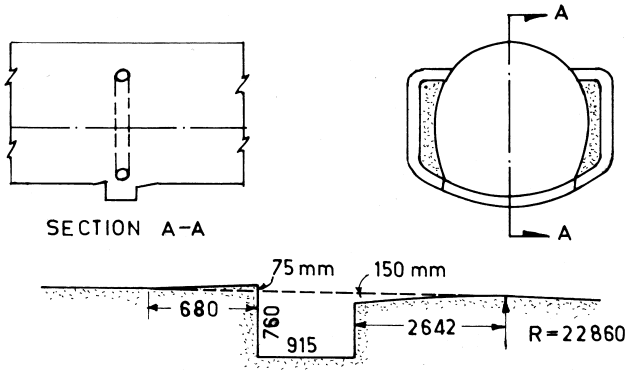

Figure 15 Aerator for horse-shoe section of a tunnel.

Air was to be introduced into the jet through wall and floor air vent slots in the existing structures and through wall and floor offsets away from the flow in the proposed structures. The aerators for the outlets were developed following cavitation damage to the floor immediately downstream of the gate of the Palisades Dam outlet. The design of the aerator was developed from the studies on a 1:19 scale model. Figure 16 shows details of the outlet works, as originally constructed, and recommended modifications to incorporate aerator system.

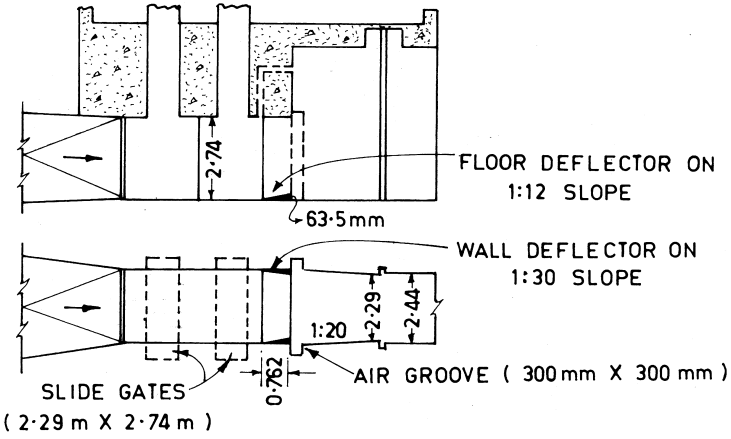

Figure 16 Aerator introduced in Palisades Outlet Works, USA. (Shown in Beichley et al. 1975.)

General guidelines for the size and dimensions of deflectors, offsets, and air slots have also been given in the article. However, model studies would be necessary for the finalization of the design, particularly the flow conditions with respect to jet trajectory and clearances.

27.11 AERATORS ON EXISITING STRUCTURES

If an existing structure is to be equipped with an aeration system, provision of ramp, air slot, and an offset or ramp or slot on the sidewalls may be possible. However, alternatives of providing aeration arrangement utilizing crest piers involve minimum structural modifications and are less expensive.

Oskolkove and Semenkov (1979) have described a ski jump aerator installed at the downstream ends of the crest piers of Bratsk spillway, as shown in Figure 17. With this arrangement, the flow leaving the crest piers gets constricted and lifted from the floor, creating an under-jet space. The access of air to the under-jet space is through the voids created at each end of the pier. This type of arrangement is suitable where the width of the spillway is large and hence slots or ramps in the sidewalls may not be effective in supplying air uniformly over the entire width.

In China, the arrangement of the Flaring Gate Piers (FGP) is popular. Details of a typical FGP aerator are shown in Figure 18. In this arrangement, the ends of the crest piers are flared so as to project into the waterway. The flow gets contracted, but there is no lifting in this case. The air entrainment occurs from the sides of the contracted flow.

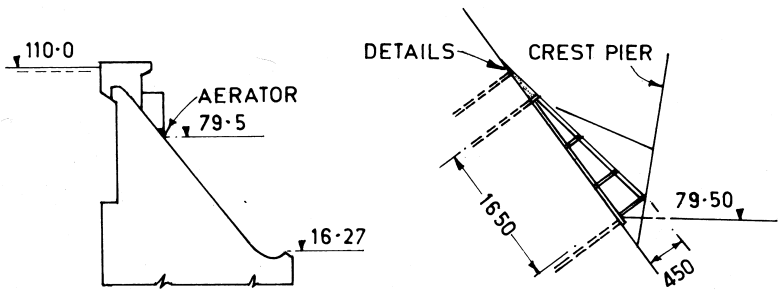

Figure 17 Aerator installed at the end of crest piers, Bratsk Dam, Russia. (Shown in Oskolkove et al. 1979.)

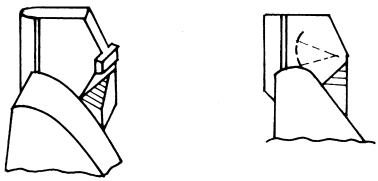

Figure 18 Aeration by flaring gate piers.

The ski-jump and FGP aerators can be provided further downstream in the case of high-head spillways, as well. In such spillways, the crest piers have to be extended upto the desired locations with their heights adequate enough to contain the flow depth with free board. Installation of ski-jump or flaring of the piers can then be made. However, this increases the cost substantially.

Notations

A_s = Cross-sectional area of the air-intake shaft
b_s = Empirical coefficient accounting for sand grain roughness
C = air concentration
C_1, C_2 } Coefficients of proportionality
$\overline{C}$ = Mean air concentration %
C_e = Mean equilibrium air concentration in uniform aerated flow, %
C_f = Local loss coefficient
C_o = Bottom air concentration
Mean air concentration immediately after the impingement of the trajectory
c = Relative air concentration $0<c<1$
D_t = Turbulence diffusivity in the direction normal to the flow
d_I = Depth of flow at which the boundary layer reaches the free surface
E = Kinetic energy correction coefficient
E_{min} = Euler number representing the cavity subpressure at which the air entrainment vanishes.
E_t = Eotvos number
F = Froude number given by $V/(g\ y\ \cos\alpha/E)^{1/2}$
Exponent in Fernando's equation
F_b = Froude number given by $q/(g\ S\ k_s^3)^{1/2}$
F_q = Froude number given by $q_w/(g\ H_1^3)^{1/2}$
F_r = Froude number of flow at aerator $V/(g\ y)^{1/2}$
F_w = Froude number of pure water flow $q_w/(g\ y_w^3)^{1/2}$

F_1 = Froude number of pre-jump flow $V_1/(g\ y_1)^{1/2}$
f = Roughness coefficient for non-aerated flow
f_w = Roughness coefficient for equivalent flow
H_1 = Head above the aerator
H_s = Head at any point on spillway surface measured from total energy line
I = Friction slope
K_1,K_2, K_3 = Constants depending on aerator and chute geometry
k_e = A constant
k_s = Equivalent sand grain roughness
k_t = A constant
L = Length of jet trajectory from an aerator
L_d = Projected length of de-aeration zone from an aerator
L_x = Slope distance downstream of aerator
L_I = Slope distance downstream from aerator to the beginning of aerator
n = Coefficient in velocity distribution function
Manning's roughness coefficient
q_a = Discharge of air entrained by the flow
q = Unit discharge
q_a = Volume flow rate of air per unit width
q_w = Volume flow rate of water per unit width
q_δ = Unit discharge within the boundary layer
R_e = Reynolds number
R_x = Distance Reynolds number
S = Spillway slope, Sin α
Distance between aerator spacing
$T = (t_r + t_s)/y$
T_r = Relative ramp height of aerator = (t_r/y)
t_r = Ramp height of an aerator
t_s = Step height of an aerator
U = Surface velocity at the point of inception
u = Local velocity
u_{fs} = Velocity of flow outside the boundary layer
u_{90} = Velocity corresponding to the depth y_{90}
V = Average velocity of flow over aerator ramp
V_a = Velocity of air in air intake shaft
V_e = Entrainment velocity
V_r = Ratio of viscosities of water and air
V_t = Rise velocity of air bubbles
V_1 = Velocity of pre-jump flow
W = Width of spillway/aerator
x = Distance
X_I = Boundary layer development length

X_s = An approximation to the boundary layer development length
$Y = y/y_{90}$
$Y_o = 2(\text{Sin } \alpha)^{1/2}$
$Y_{99} = y_{99}/y$
y = Flow depth
y_c = Critical depth
y_w = Equivalent clear depth of water
y_1 = Pre-jump depth
y_2 = Post-jump depth
y_{90} = Depth of flow corresponding to air concentration of 90%
y_{99} = Depth of flow corresponding to air concentration of 99%
α = Angle of spillway chute with horizontal
Coefficient of loss of aeration
$\bar{\alpha}$ = Effective take-off angle of aerator ramp
β = Air concentration q_a/q_w
δ = Thickness of boundary layer
ΔE = Difference Euler number
Δ_p = Difference in pressure between atmosphere and the cavity beneath aerator trajectory
ρ_a = Density of air
ρ_w = Density of water
λ_j = Relative jet length = L/y
σ = Interfacial surface tension
ξ_{tot} = Total-loss coefficient of the air-vent system
ν = Kinematic viscosity of water

REFERENCES

1. Ackers, P.; Priestley, J. Self aerated flow down a chute spillway, 2nd Intnl Conf on The Hydraulics of Floods and Flood Control, BHRA, Sept 1985.
2. Afshar, N. R.; Asawa, G. L.; Ranga Raju, K. G. Air concentration distribution in self aerated flow. Jnl of Hyd Research, IAHR, 1994, 32(No 4).
3. Biechley, G. L.; King, D. L. Cavitation control by aeration of high- velocity jets, ASCE. Jnl of Hyd Div, July 1975, 101(HY7).
4. Bruschin, J. Forced aeration of high velocity flows. Jnl of Hyd Research, IAHR, 1987, 25(No 1).
5. CBIP (India) Procedure to work out bulkage in air-entrained flows in chute spillways, Technical Report No 8, Nov, 1970.
6. Chanson, H. Study of air entrainment and aeration devices. Jnl of Hyd Research, IAHR, 1989(a), Vol 27(No 3).
7. Chanson, H. Flow downstream of an aerator, Aerator spacing. Jnl of Hyd Research, IAHR, 1989(b), 27(No 4).

8. Chanson, H. Predicting the filling of ventilated cavities behind spillway aerators. Jnl of Hyd Research, IAHR, 1995, 33(No 3).
9. Chanson, H.; Toombes, L. Experimental investigations of air entrainment in transition and skimming flows down a stepped chute, Research report No CE 158; The University of Queensland, Australia, July, 2001.
10. Falvey, H. T. Air-water flow in hydraulic structures, USBR Engineering Monograph 41, 1980.
11. Falvey, H. T. Cavitation in chutes and spillways, USBR Engineering Monograph 42, 1990.
12. Falvey, H. T.; Ervine, D. A. Aeration in jets and high velocity flows, Proc Intnl Symp on Model- prototype correlation of hydraulic structures; ASCE/IAHR, USA, Aug 1988.
13. Fernando, A. M.; Rio, J. R. On the incipient aerated flow in chutes and spillways. Jnl of Hyd Research, IAHR, 2002, 40.
14. Hager, W. H. Uniform aerated flow, ASCE. Jnl of Hyd Engg, 1991, 117(No 4).
15. Hager, W. H.; Blaser, F. Drawdown curve and incipient aeration for chute floe, Canadian. Jnl of Civ Engg, June 1998, 25(No 3).
16. Hamilton, W. S. Preventing cavitation damage to hydraulic structures, Water Power and Dam Construction, Part One, Nov 1983; Part Two, Dec 1983.
17. Keller, R. J.; Rastogi, A. K. Design chart for predicting critical point on spillways, ASCE Jnl of Hyd Engg, HY 12, Dec 1977.
18. Killen, J.; Anderson, A. G. A study of the air-water interface in air entrained flow in open channels, 13th IAHR Congress, Japan 1969.
19. Oskolkov, A. G.; Semenkov, V. M. Experience in designing and maintenance of spillway structures on large rivers in the USSR, 13th ICOLD, Q 50, R 46, 1979.
20. Pinto, N. L. D. S.; Neidert, S. H. Model prototype conformity in aerated spillway flow, Intnl Conf on Hydraulic Modelling of Civil Engineering structures, BHRA, 1982.
21. Rutschmann, P.; Volkart, P. Spillway chute aeration. Intnl Waterpower and Dam Construction, 1988, 40(No 1).
22. Rutschmann, P.; Hager, W. H. Design and performance of spillway chute aerators. Intnl Waterpower and Dam Construction, 1990, 42(1), 36–42.
23. Straub, L. G.; Anderson, A. G. Experiments on self-aerated flows on a spillway, ASCE. Jnl of Hyd Div, December 1958.
24. WES Hydraulic Design Criteria Chart 111-18, Spillway Energy Loss.
25. Vischer, D.; Volkart, P.; Sigenthaler, G. Hydraulic modelling of air slots in open chute spillways, Intnl Conf on Hyd Modelling of Civ Engg Structures, BHRA, 1982.
26. Volkart, P.; Rutschmann, P. Aerators on spillway chute: Fundamentals and Applications, Proc Specialty conf on Advancements in Aerodynamics; Fluid Mechanics and Hydraulics, Minn, USA, 1986.
27. Wood, I. R. Air-water flows: Keynote address, 21st IAHR Congress. Melbourne, 1985.
28. Wood, I. R. Air entrainment in free surface flows, Chap 3, IAHR design Mannual No 4; Balkema Publications, The Netherlands, 1991, © Swets & Zeitlinger.
29. Zagustin, K.; Mantellini, T. Some experience on the relationship between a model and prototype for flow aeration in spillways, Intnl Conf on Hyd Modelling of Civ Engg Structures, BHRA, 1982.

28

Hydraulic Modeling of Spillways and Energy Dissipators

28.1 INTRODUCTION

Studies on a physical hydraulic model are almost indispensable for a major spillway project. Although designs of various elements of spillway and energy dissipation structures have evolved through generalized model studies associated with theoretical analysis, specific model study may still become necessary because of some uniqueness in the design, layout, or operational aspect. Despite the advent of mathematical and numerical modeling, which is aided by high-speed computers and computational techniques, studies on physical models continue to be undertaken for the solution of problems, which are presently not amenable to other approaches. The purpose of this chapter is to bring out such areas in the design of spillways and energy dissipators along with the associated problems of scale effects and techniques of measurement, analysis, and interpretation of model findings. No attempt has been made to discuss the basic issues such as dimensional analysis, similitude, and hydraulic modeling theory, for which a number of standard books are available. However, a brief review of various dimensionless numbers involved in the process would be an appropriate starting point.

28.2 A REVIEW OF DIMENSIONLESS NUMBERS

In any fluid flow—regardless of free-surface or closed-conduit, laminar or turbulent, subcritical or super critical, etc.—at least four parameters are always involved: pressure, p, velocity, v, density, ρ, and characteristic length, l. A pressure differential, Δp, rather than the pressure, p, is more relevant when considering the origin of force. According to dimensional analysis, this will result in $(4-3)=1$

dimensionless number, $\frac{\Delta p}{\rho V^2}$, usually termed Euler number, Eu. Δp can also be substituted for head difference, Δh, or energy loss, ΔH. If this particular system is a closed-conduit flow, the force of gravity is not relevant; however, in a free-surface flow, gravity is an important parameter governing the flow pattern. For example, in the case of water flow over a spillway, there is no pressure difference between the water surfaces, upstream and downstream at a given point—both are exposed to atmospheric pressures. It is the difference between the elevations of the two surfaces that give rise to the velocity and flow pattern; in other words, gravity is the force causing this velocity. Inclusion of gravity, therefore, results in one more dimensionless number: the Froude number, or the ratio of inertia and gravity forces, most commonly expressed as:

$$F = \frac{V}{\sqrt{g\,L}} = \frac{V}{\sqrt{g\,y}} \tag{1}$$

Where the characteristic length is represented by the depth of flow, y.

It can be shown that other parameters also influence the flow over the spillway in the energy dissipator and in the river downstream, with the understanding that the parameters' relative magnitude may not be as predominant as that from gravity. Inclusion of these result in other dimensionless numbers:

$$\text{Viscosity, } \mu \text{ or } \nu \Rightarrow \text{Reynolds number } R_e = \frac{VL\rho}{\mu} = \frac{VL}{\upsilon} \tag{2}$$

$$\text{Surface tension } \sigma \Rightarrow \text{Weber number } W_e = \frac{V^2 L\rho}{\sigma} \tag{3}$$

$$\text{Elasticity E} \Rightarrow \text{Cauchy number } C_a = \frac{V^2 E}{\rho} \tag{4}$$

Or its square root, commonly known as Mach number:

$$\mathrm{M} = \frac{V}{\sqrt{E/\rho}} \tag{5}$$

The parameter, E, is reflected in different forms depending on the structural deformation due to fluid-structure interaction. For example, when elongation deformation of the fabric of a rubber dam is of interest, equality of Structural Merit number,

$$\mathrm{S} = \frac{L\gamma}{E} \tag{6}$$

is essential. If bending due to load is of concern, the Bending Stiffness number,

$$\mathrm{B} = \mathrm{E\ I} \tag{7}$$

has to be the same in the prototype and model, where I = moment of inertia.

28.3 HYDRAULIC MODELING AND SCALE EFFECT

The theory of hydraulic models emphasizes the equality of all of the above ratios (and, perhaps, others that may be of some significance, but are not included here) between the model and the prototype as the requirement for full dynamic similarity. In a practical situation, however, this requirement cannot be met, and, hence, models are a compromise.

In the case of spillways, etc., at least two requirements are mandatory between the prototype and its model: similarity of geometric form and the equality of Froude number. With the same fluid (i.e., water) in the prototype and model, equality of other numbers is not possible. In such a situation, a correction is made for those forces considered important, while those that are considered less important are ignored. This is the origin of the so-called ''scale effect,'' although, more appropriately, this should be termed ''scale defect''! Which forces are correctable and which ones are negligible? This depends on the situation being considered and relies heavily on the modeler's experience and judgment.

The most important scale effects encountered in the modeling of spillways and energy dissipators are those phenomena that cannot be adequately simulated in models:

Friction
Turbulence
Cavitation
Air entrainment and release
Fluid–structure interaction
Local scour below energy dissipators

28.3.1 Friction

The growth of a boundary layer is a function of the Reynolds number $\left(\frac{Vy}{\upsilon}\right)$ and the relative roughness of the boundary $\left(\frac{y}{k_s}\right)$, where y is the depth of flow and k_s is the equivalent sand grain roughness. The scale of roughness can be derived from Manning's equation,

$$V_r = \frac{R_r^{2/3} S_r^{1/2}}{n_r} \tag{8}$$

Where subscript, r, indicates the ratio of prototype to model quantity.

In a Froudian model,

$$V_r = L_r^{1/2};\ n_r = L_r^{1/6} \tag{9}$$

If one considers that Manning's ''n'' of a typical spillway concrete surface will be, say, 0.014, and the smoothest possible surface that can be used for modeling, such as plastic or glass, has n = 0.009, the scale of such a model would be:

$$L_r = \left(\frac{0.014}{0.009}\right)^6 \approx 14$$

This is quite difficult. Even if one tried to do so, it would only make the quantity y/k_s equal in the model and prototype. However, a lower value of the Reynolds number in the model will still produce a higher value of drag coefficient and frictional loss.

Therefore, it is apparent that a typical spillway model would always be rougher than its prototype. This difference would result in an underestimation of discharge capacity. It is expected, then, that as the size of the model increases, the error reduces.

Damle (1952) conducted studies of discharging capacity with a model of a high-coefficient weir (whose height in the prototype was about 2 m) using scales of 1:7.5, 1:6, 1:4.5, and 1:4, and extrapolated the results to prototype (scale 1:1), as shown in Figure 1.

As expected, as the size of the model increased, the error decreased. Although the error in this particular case was as much as 5%, the error, in most of the cases with high spillways, is not expected to be more than 1%, and, therefore,

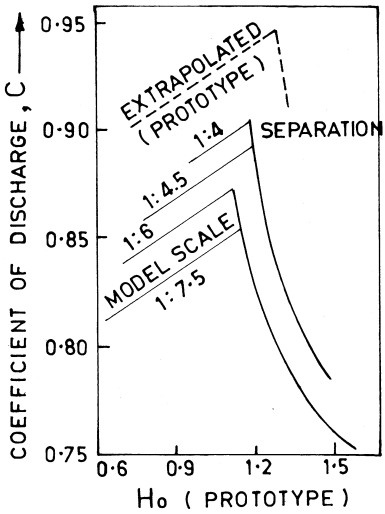

Figure 1 Scale effect in discharge characteristics. (Shown in Damle 1952.)

is generally not considered. However, the depth of overflow should always be more than 15 mm to eliminate the effect of capillary and surface tension.

In the case of long-crested weirs, where the boundary layer displacement thickness (δ^*) is significant, a correction has to be applied. Its magnitude in model, $(\delta^*)_m$, is calculated theoretically and replaced by that of the prototype, $(\delta^*)_p$, while scaling the results to prototype, as in Equation 6, Chapter 12.

Simulation of the friction in the flow channels and river reaches downstream of spillways is relatively easy. The free-surface flow is always turbulent, so the Manning's n is related to the length scale by Equation 9. However, in the closed-conduit flow, i.e., in a tunnel spillway under pressurized conditions, the situation is quite complicated. The Moody diagram representing the Colebrook-White equation (Figure 2) shows that the head loss h_f governed by friction factor f is a function of R_e and K_s/D:

$$f = \frac{2gD(h_f / L)}{V^2} = \Phi(R_e, k_s / D) \tag{10}$$

where

D = Diameter of tunnel
L = Length of tunnel

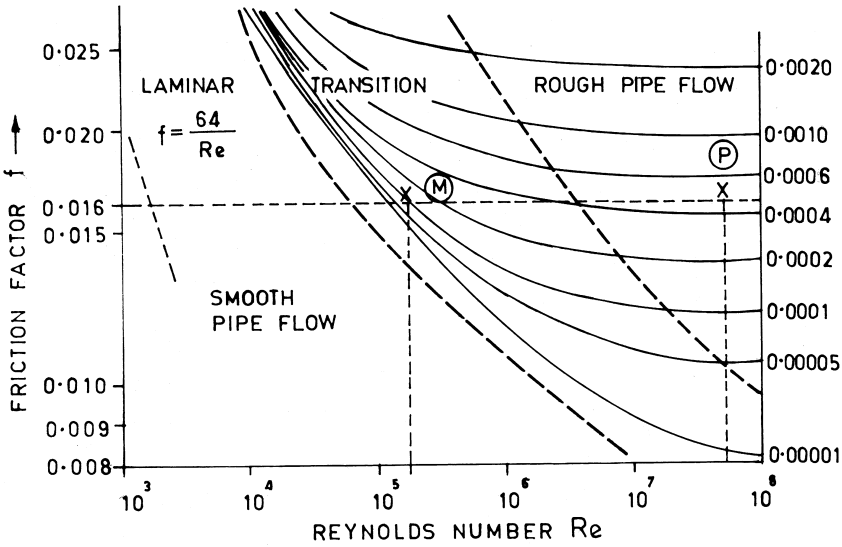

Figure 2 Simulation of friction.
(P) Prototype (M) Model

When the tunnel spillway model is operated under Froudian similarity:

$$D_r = y_r = V_r^2 \tag{11}$$

Thus, $f_r = \left(\frac{h_f}{L}\right)_r = 1$, has to be satisfied. This can be achieved only if:

$$(R_e)_r = 1 \text{ and } \left(\frac{k_s}{D}\right)_r = 1 \tag{12}$$

which is not possible in a Froudian scale. Yet, similarity of friction may be possible in some cases, as in, for example, a tunnel with diameter = 7 m, $k_s = 3$ mm, and flow velocity = 10 m/s, where prototype values are:

$$(R_e)_p = 10 \times 7 \times 10^6 \text{ and } \left(\frac{k_s}{D}\right) = \frac{0.003}{7} = 0.00043$$

giving f a value of 0.016. This zone is characterized by fully rough flow, which is represented by P on the diagram (Figure 2). The point, M, representing the model (to a scale 1:50) has:

$$(R_e)_m = \frac{10}{\sqrt{50}} \times \frac{7}{50} \times 10^6 = 2 \times 10^5$$

with the same f value of 0.016 falling in the transition zone between the smooth and rough flows, which gives $\left(\frac{k_s}{D}\right)_r = 0.0001$. This means that k_s in the model would be $\frac{7}{50}$ x 0.0001 = 0.014mm!

Equality of f and $\left(\frac{k_s}{D}\right)$ might still be possible by using very smooth material like plastic or glass for the model tunnel, but the flow regimes in the prototype and model would not be identical. Again, the earlier stated similitude would be valid for the velocity of $\left(\frac{10}{\sqrt{50}}\right)$m/s in the model. For a lower velocity, point P would move left and remain in the rough-flow regime, whereas point M moving left would approach the smooth pipe–flow region, requiring a smaller value of $\left(\frac{k_s}{D}\right)$.

An alternative would be to take measurements in the model to separate out frictional losses from form losses (i.e., losses due to bends, valves, etc). The latter may be assumed transferable from model to prototype in most of the cases. When assessing prototype performance, the measured frictional losses in the model may be replaced by the calculated full-scale losses.

Another problem of excessive friction in the model arises in the design of the hydraulic jump-stilling basin at the toe of a long chute spillway. In such a case, the energy of the flow entering the model's stilling basin would be lower than found in nature because of the excessive friction in the model. While this

may not be of much concern in the case of flip buckets, a hydraulic jump-stilling basin would be underdesigned. The true energy level to be expected at the toe in the prototype could be calculated; however, its simulation in the model would require a partial distortion of the chute structure, as shown in Figure 3. This would enable appropriate depth, velocity, and direction of the flow at the toe in order to study the stilling basin performance and downstream flow conditions for the design discharge.

28.3.2 Turbulence

Turbulence results from an interaction of viscosity and inertial reactions and, therefore, is characterized by Reynolds number. In Froudian models, the Reynolds number is always smaller than that derived from the prototype and, hence, the turbulent fluctuations are not expected to be correctly simulated. In order to evaluate this aspect, the interpretation of turbulence as a system of eddies of different magnitudes should be used. The main flow generates large eddies whose length scales are of the order f and whose main dimensions are of the flow field, such as water depth for open-channel flow. These large eddies usually are inertial eddies in which viscosity effects are negligible. The main flow conveys energy directly to them. This energy is transferred to smaller and smaller eddies until their size is so small that dissipation due to viscosity takes place. For a correct representation of turbulence in a hydraulic model, the large eddies have to be reproduced, because, through them, the energy is extracted from the main flow. It is irrelevant how the energy further cascades to the small eddies and whether the small viscous eddies, which dissipate the energy, are reproduced correctly, as long as the main flow is not altered. Because the large eddies in a turbulent flow are proportional to the main dimension of the flow field, their correct simulation is always ensured in a geometrically similar model, provided the microscale of turbulence, at which viscosity effects become important, is smaller than the macroscale in the model, so that alteration of large eddies due to viscosity is avoided.

In the models of spillways and energy dissipators, simulation of turbulence is mainly related to the study of fluctuating pressures/forces, which is a measurable outcome of turbulence. There are, however, differences in opinion regarding the capability of a Froude model to predict the fluctuations correctly. It has been shown that models can predict the mean values quite correctly if the value is large enough, but the prediction of RMS values and fluctuations in terms of energy spectrum and probability functions is not dependable. Some investigators believe that statistical properties of pressure fluctuations for low frequencies are independent of Reynolds number if $Re > 5 \times 10^5$. Lopardo et al. (1984) conducted studies with respect to model–prototype comparison comparing pressure fluctuations in the chute blocks and baffle piers of the stilling basin of the Salto Grande Dam, Argentina. The results obtained on a 1:50 scale model (where R_e

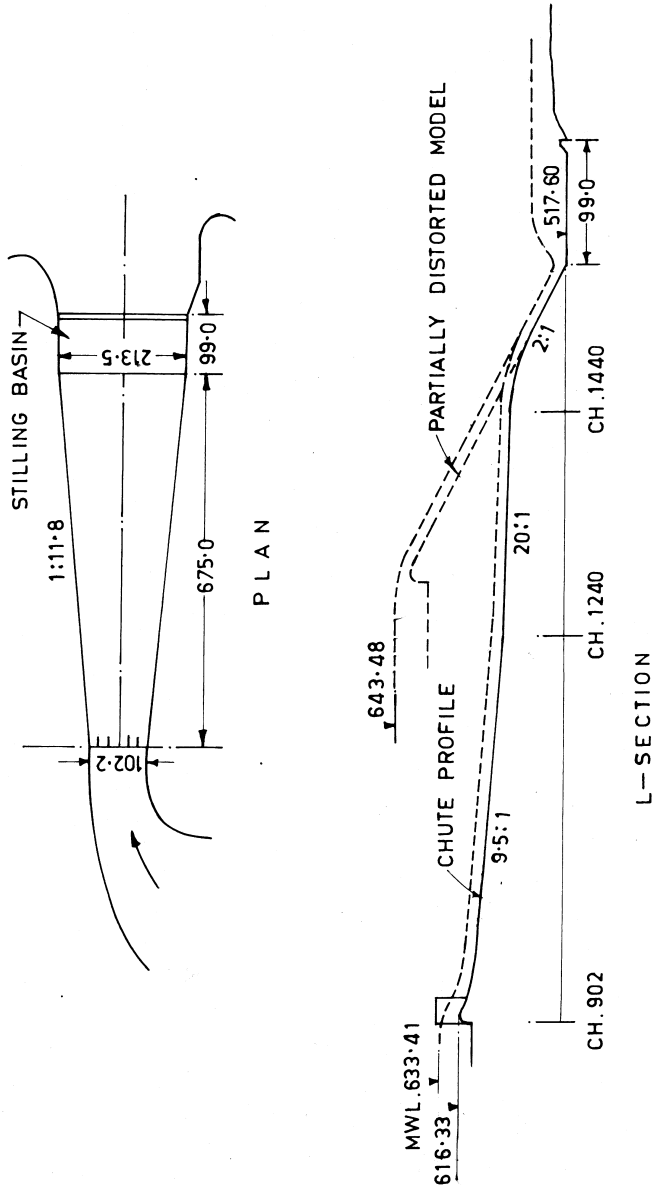

Figure 3 Scheme of partially distorted model.

in the model $= 6.3 \times 10^5$) were compared with thse observed at identical locations in the prototype. They observed satisfactory comparison in respect of mean and RMS values as well as energy spectrum and probability functions. It is still believed that with the increase in the size of the model and hence Reynolds number, the higher range of frequencies would be well simulated, whereas in the smaller models, these components are dampened by the viscosity. This question has not been resolved, but a model Reynolds number of at least 5×10^5 is the minimum that should be ensured while studying phenomena originated by turbulence.

28.3.3 Cavitation

The Euler number $\mathrm{E} = \dfrac{\Delta p}{\rho V^2}$ yields the same scaling condition as the Froude number, if the pressures are referred to atmospheric as datum. A Froudian model would thus give correctly scaled pressures in theory. In practice, however, there is a lower limit on pressure corresponding to vapor pressure of water, which is also dependent on temperature. This lower limit is not scaled down in a model and, therefore, a much lower pressure may exist and can be observed in the model than may be possible in the prototype without cavitation occurring. Cavitation phenomenon is therefore severely influenced by scale effects

For cavitation caused by intermittent pressure depression, Fattor et al. (2001) have proposed a macroturbulent cavitation index, (see 26.6.1 for details).

A useful approach in the study of cavitation potential is to use a special form of the Euler number, i.e., The cavitation index, σ, given by

$$\sigma_i = \frac{p_0 - p_v}{1/2 \rho V_0^2} \tag{13}$$

Cavitation index obtained from the measurement of mean pressures and velocities with reference to the altitude of the prototype, is compared to the incipient cavitation indices (Table 1, Ch. 26).

Cavitation tests may also be carried out using special equipment in which the ambient pressure is reduced below atmospheric pressure, thus encouraging cavitation to occur in the model. The special equipment for cavitation tests of this type (i.e., a cavitation tunnel) is elaborate, expensive to construct and maintain, and, hence, restricted to the problems of industrial applications, such as turbines, pumps, etc.

28.3.4 Air Entrainment and Release

The following parameters are involved in the process of entrainment of air and its release:

Physical properties of water and air:	density, viscosity, and surface tension
Flow properties:	velocity, depth, pressure differential
Geometrical properties:	shape, aspect ratio, etc.

Since density and viscosity ratios are the same in the model and prototype, the relation is expressed as

$$\beta = q_a/q_w = f\,(F, R_e, W, E_w, \textit{geometry}, \textit{shape factor})$$

This general relationship appears in different ways depending on the specific structure or flow condition. These are:

Chute spillways
Shaft spillways
Siphon spillways
Spillway aerators

Chute Spillways

Air entrainment is, in part, a turbulence phenomenon, and turbulence is influenced by both, inertial and viscous forces, as represented by Reynolds number. The entrainment of air on a chute spillway begins where the turbulence boundary layer reaches the water surface; however, there is a threshold turbulence level that is required for disrupting the surface tension skin. Thus, although there may be some dissimilarity between the model and prototype in the exact point where the boundary layer reaches surface, the major discrepancy arises because of surface tension not being scaled and is much more effective in restricting surface disruption and, hence, air entrainment in the model.

Once entrainment begins in the model, there is a further non-scalar effect because any air bubbles carried down into the body of the flow will be too large. This is primarily because of unsatisfactory simulation of bubble size; the maximum size of bubbles in the model not being very different from that in the prototype, both being controlled by the same value of the surface tension. These bubbles escape more rapidly in the model than in nature because of their non-scalar rise velocity. Consequently, air concentration in the model will be less than in the prototype. Empirical criteria for scaling have been suggested by some investigators. Kobus (1984) suggests a relationship that does not explicitly include the parameter of surface tension:

$$\frac{L_m}{L_p} \geq \left[\frac{R_e}{F}\left(\frac{\mu_w/\rho_w}{\sqrt{g}}\right)\right]^{2/3} \tag{14}$$

Where

R_e = Minimum Reynolds number in the model for fully turbulent flow $\approx 10^5$

F = Froude number of the flow at the location of entrainment

Sakhuja et al. (1984) state that a model larger than a 1:4 scale is necessary if air entrainment scale effects are to be negated for surface aeration. They also cite an empirical relationship for determining the approximate scale effect factor (SEF), which they suggest should be applied to the Froude scaling of model air entrainment data

$$\log_{10}(SEF) = 0.0048\,(L_r - 1) \tag{15}$$

Thus, the corresponding air-water discharge ratio could be estimated from $\beta_p = SEF\ x\ \beta_m$.

It would, however, be best to assess prototype air concentration by calculations, following notable contributions by Wood, Falvey, Chanson, and many others.

Shaft Spillways

The same major scale effects are present, as in the case of chute spillways, i.e., total entrainment scale effect, minimum velocity to entrain air and the air-transport scale effect, or minimum velocity to transport air. Studies by several investigators have established a minimum velocity of 0.8–1.1 m/s in the model at the location of air entrainment. The minimum outlet velocity to transport air bubbles is a function of impacting jet velocity, V_1, conduit diameter, D, jet thickness at the plunging point, d, and slope of the conduit. The details can be found in Chapter 8.

For horizontal or gradually sloping conduits, the vortex trapping parameter $\frac{V_1}{V_{br}} > 10-12$ applies where V_{br} is the air bubble rise velocity ≈0.25 m/s. For steep slopes, the transport parameter $V_1\left(\frac{d}{D}\right)^{1/2} > 0.8-0.9$ represents the threshold.

Siphon Spillways

Priming depth is the most important factor in the functioning of a siphon spillway. It is dependent on the air entrainment capacity of the flow at the crest. The empirical relationship developed by Ervine et al., Equation 12, Chapter 7,

$$\frac{Q_a}{Q_w} = 0.26\left(\frac{b}{p}\right)\left(\frac{H_1}{t}\right)^{0.446}\left(1-\frac{V_{\min}}{V}\right) \tag{16}$$

explains the scale effect inherent in the siphon models. Although, V_{min} is the same in the model and the prototype, the jet velocity in the model is reduced by a factor $\sqrt{L_r}$ and, hence, the factor $\left(1-\frac{V_{\min}}{V}\right)$ is smaller in the model, giving less air entrainment and delayed priming. It also explains why the priming depths differ between the models constructed to different scales.

If a siphon primes in a model at a given head, it will certainly prime in the prototype; however, if it does not prime in the model, it might still prime in the

prototype. Experiments by Casteleyn et al. (1977) on two models built to scales of 1:20 and 1:7 of the same siphon installation indicated that the air entrainment discharge was given by

$$q_{air} = \alpha\,(V_b - V_0)^3$$

Where

α is a function of h_a/D
h_a = Head over the siphon crest
D = Vertical dimension of the opening at the crest of the siphon
V_b = Velocity at the point of air entrainment
V_0 = Minimum velocity for air entrainment

The minimum velocity, V_0, was found to be 0.8–1.0 m/s. The model should therefore be designed such that a velocity in excess of 0.8–1.0 m/s is ensured near or about the crest of the siphon before priming.

For discussion on modeling of stepped spillways, see paragraph 6.7.

Aerators

Referring to the basic relationship,

$$\beta = q_a/q_w = f\,(F, R_e, W, E_u, \textit{geometry}, \textit{shape factor})$$

It should be noted that every parameter on the right-hand side has an influence on the functioning of an aerator.

Besides the geometric similarity of the flow pattern ensured by the equality of the Froude number, correct simulation of the air-entraining mechanism is necessary. This is mainly related to the spray formation at the air-water interface in the cavity formed below the jet. The air discharge is a function of cavity subpressure, which, in turn, depends on the characteristics of the air supply system, as demonstrated in Figure 9. On the other hand, the jet length may be influenced by the state of the flow on the ramp or step, which in the prototype would be rough turbulence, but may be in transition state in the model. Summarizing the conclusions from various studies:

- Artificially roughen the flow surface of the ramp and some length upstream so as to eliminate the laminar sublayer effect on the flow on the ramp
- A minimum flow velocity of 6–7 m/s over the ramp in the model is ideal
- Reynolds number in the model to be at least 10^5. If the Reynolds number is referred on the basis of jet length, $R_e = 3.5 \times 10^5$ or greater eliminating scale effect should be implemented.
- Arrangement in the model will vary due to cavity subpressure. It should be simulated in the model as per the magnitude expected in the prototype, which can be calculated. This will ensure similarity of $E_u = V / \sqrt{\Delta p / \rho}$.

- To overcome the surface tension scale effects, the Weber number in the model, defined in terms of cavity length, ($V\sqrt{L}/\sqrt{\sigma/\rho}$) should at least be 500, but preferably 1000 or so.

The relationship developed by Sakhuja et al. (1984) for applying correction, i.e., . Equation 15 is also relevant here.

Vischer et al. (1982) also suggest that for models smaller than 1:4 scale, surface air entrainment in a model will be less than in the corresponding prototype.

28.3.5 Sectional Models

The requirement of a length scale as large as 1:4 or even 1:10 presents practical difficulties in regard to space, pumping capacity, cost, etc. If the prototype is symmetrical or two-dimensional in shape, it is possible to restrict the simulation only to part of the width, instead of the full width, of the spillway, resulting in a so-called two-dimensional sectional model. Case studies of such models have been presented by Pinto et al., (1982) Vischer et al., (1982) and Zagustin et al. (1982).

However, general three-dimensional comprehensive models (although constructed to small size) may still be required to study general flow conditions in the vicinity of aerators, cavity length, or, possibly, of filling up the aerator groove, etc.

Bruschin (1987) and Kells, and Smith, (1991) have discussed at length the scaling and scale effects involved in the modeling of air entrainment and aerators.

28.3.5 Fluid-Structure Interaction

The phenomenon of fluid-structure interaction is manifested in the form of a response to the hydraulic forces. The physical properties of both the fluid as well as the structure especially density and elasticity plays an important role. The deformation of structure such as elongation, bending, etc., caused by the fluid forces can be studied on a Froude model if similarity of relevant dimensionless numbers involved in the process is ensured. The phenomena of interest in the case of spillways and energy dissipators are;

- Hydrodynamic forces such as impact, uplift, bending moment, and tendency of vibration of structures like sidewalls, divide walls, etc.
- Deformation of flexible structures like rubber dams caused by the fluid forces, such as elongation, bending, etc.

For studying deformation of rigid as well as flexible structures like sidewalls, divide walls, apron floors, rubber weirs, etc., for equality of Structural Merit number

$$S = \frac{L\gamma}{E} \tag{17}$$

is necessary.

For structures like sidewalls, divide walls, etc., equality of Structural Merit number results in a relationship $E_r = \rho_r L_r$. If the same fluid (i.e., water) is used in the model as well as prototype, then the equality applies to the material properties in the model and prototype. Generally, the prototype structure is RCC, which is constructed in acrylic perspex. For RCC, $E_p = 32.5 \times 10^9$ N/m^2 and $\rho_p = 2400$ kg/m^3. For perspex, $E_m = 2.8 \times 10^9$ N/m^2 and $\rho_m = 1200$ kg/m^3. Thus, $E_r = 0.0862$ and $\rho_r = 0.5$. This gives $L_r = (L_m/L_p) = 0.1724$, i.e., a 1:5.8 scale model! It is not possible to construct such a large model. Fortunately however, neither such a hydroelastically similar model is necessary; as useful inferences can be obtained from the measurement of pressures and forces on rigid models, provided Reynolds number in the model is at least 10^5. This aspect has been discussed later in this chapter.

While studying the deformation of flexible structures, like rubber dams, the following relationships would apply. Considering thickness of the fabric, t, as the characteristic length, the scaling relation derived from Equation 17 is

$$\frac{1}{L_r^2} = \frac{\gamma_p E_m t_m}{\gamma_m E_p t_p} \tag{18}$$

For similarity in bending, the bending stiffness parameter EI should be related as

$$\frac{E_m I_m}{E_p I_p} = \frac{1}{L_r^4} \tag{19}$$

Where I is the moment of inertia.

Jongling et al. (1999) have described a model study to determine the wave-induced response of a rubber barrier 8.5 m high, inflated partly by air and partly by compressed air. The structure responds to dynamic wave loads by varying its shape; meanwhile, the internal pressure fluctuates correspondingly. The following parameters involved in the process were identified:

- The stiffness of air inside, which is governed by the law $P_0\ V_0^{\Gamma} =$ constant. The stiffness factor $k_a = \dfrac{\Gamma P_0}{V_0}$ is non-linear and scaled as $(k_a)_p = (k_a)_m\ x\ L_r^2$, where P_0 is pressure, V_0 volume, and Γ is Poisson constant.
- The tension stiffness EA of the membrane in the circumferential direction, where A is the cross-sectional area of the membrane.
- Since the atmospheric pressure P_a is not scaled, the pressure scale $P_r = \dfrac{P_a + \Delta p}{P_a + \dfrac{\Delta p}{L_r}}$

The studies conducted on a 1:25 scale model with these simulations indicated that both the overpressure in the dam and the tension stiffness of the membrane were important parameters in the response of the dam.

Local Scour Downstream of Energy Dissipators

Scour of the bed comprising coarse granular material, like gravel, sand, cobbles, boulders, etc., is initiated by the shear stress caused by the flow, usually due to the residual energy leaving a stilling basin. In this situation, Shield's entrainment function $V_*^2/[(\gamma_s - 1)gd]$ defining incipient sediment motion is an appropriate criterion. Here, V* = shear velocity = $\sqrt{g_w R S_f}$, R = hydraulic radius, d is grain diameter and S_f is the friction gradient. This can also be expressed as

$$[y]_r [S_f]_r = [\gamma_s - 1]_r [d]_r \tag{20}$$

It can be shown that the appropriate scaling requirements are met by a geometrically similar model operated according to the Froude law, with same density sediment in model and prototype, with grading curve of the bed material scaled down by the linear model scale, provided the model material is coarse enough to be free of viscous effects. Shield's curve indicates that for this, the Reynolds number expressed as $(R_e)_* = \dfrac{V_* d}{\upsilon} > 400$. Generally, a model sediment diameter above 0.5 mm throughout its grading curve with d_{50} greater than about 1.5 mm would serve the purpose.

The mechanism of scour of rocky bed due to impact of the high velocity jet is different. Pressure fluctuations at the water–rock interface cause propagation of dynamic pressure into the rock joints. This causes hydrodynamic fracturing of closed-ended rock joints and splitting of rock in rock blocks. The disintegrated rock blocks are then ejected due to the dynamic uplift, broken down into smaller pieces due to the ball-milling effect, and then carried further downstream as sediment transport, resulting in a scour hole. Apparently, it is almost impossible to simulate the above series of events in a scale model, and, therefore, approximate and partial simulation is resorted to in the model depending upon the objective of the study.

The bed material is reproduced in its disintegrated form, which can be carried downstream by the flow forces. In most cases, the bed material selected is a mixture of sand and gravel—regardless of the size that would result from the disintegration of the rock in the prototype. This would result in what is termed, ''ultimate scour,'' which could take place at the given site and serves as a fairly reliable indicator for deciding on the protective measures necessary for the structure. It is observed that development of ultimate scour is inhibited by formation of a mound at the downstream periphery of the scour hole due to deposition of the scoured material. In some laboratories, it is a practice to artificially remove such mound in the model so that the scour reaches its ultimate state. This results in a regular, dish-shaped scour hole, irrespective of the river gorge configuration.

However, this method of simulation is not effective for the spillways located in narrow, steep gorges. In such situations, not only the ultimate scour but also

an indication of the areal extent of scour is necessary for designing protective works. The steep flanks, made up of loose granular material, scour out completely, and a huge mound of eroded material is formed downstream, resulting into an unrealistic scour development.

With a goal of obtaining the areal extent of scour and maintaining the steep erodible flanks, cementing material is mixed with fine sand-gravel to reproduce the erodible bed and flanks. Since cement gets hardened with time, material like bantonite, gypsum, etc., are found to be more suitable. The composition of the material (i.e., proportion of sand and binding material) is determined by trials on the model. The composition that gives the maximum depth of scour comparable to that obtained by applying various scour formulas is adopted for detailed studies.

28.4 DYNAMIC-FLOW MEASUREMENT

By the term, ''dynamic-flow measurement,'' a continuous measurement of time-varying parameters, such as pressure, force, uplift, bending moment, etc, that have their origin in turbulence is meant. Dynamic-flow measurement requires special types of equipment and methods for analyzing the results. Only a brief outline is intended here, i.e., the essential elements of dynamic flow measurement including analysis and interpretation of results, concerning the flow conditions in the energy dissipators of high-head spillways.

28.4.1 MEASUREMENT

Generally, the following parameters are required to be measured:

Parameter of measurement	Objective
Pressure	Estimation of force, cavitation susceptibility, tendency of vibration, etc.
Force	Estimation of force, vibration, etc.
Uplift	Estimation of uplift, pull-out of slab monolith
Bending moment	Design of sidewalls, divide walls, etc

Pressure

Since the size and dimension of elements in a scale model are small, specialized miniature pressure transducers are required. The most commonly used transducer

is a semiconductor-type piezoresistive pressure transducer. A number of products are commercially available in sizes up to 4 mm diaphragm diameter and 40 mm overall length. Such transducers have excellent sensitivity and frequency response and very low hysterisis and non-linearity for the turbulence flows encountered in models of energy dissipators.

It is advisable to use such transducers in a flush-mounted configuration and not through the piezometer in order to avoid distortion of signals. When the size of the structure does not permit fixing the transducer in a flush-mounting position, an arrangement of a small slot connecting the diaphragm and the flow can be employed without virtually any distortion of the signals. The author had successfully placed two miniature transducers, back to back, in a 3.1 cm thick model divide wall, as shown in Figure 4 (Gaikwad et al.) to assess the pressure differential across the wall.

Pressure measurements are carried out also for the estimation of hydrodynamic uplift of floor slab monoliths or pull out forces on the anchor walls of the stilling basins. For this, a matrix of measurement points (3×3, 4×4, etc.) is required, with simultaneous measurement on all the points, or at least for a pair of two points, in succession preferred. The force exerted is calculated by applying theory of correlation as discussed in Chapter 20.

Force and Uplift

Sometimes, direct measurement of force is preferred, which obviates the necessity of an elaborate arrangement of simultaneous measurements of pressures at a number of points, and a huge computational requirement for the analysis. Commercially available strain-gauge–type force transducers are suitable for such measurements with appropriate fixtures (Farhoudi et al. (1991); Bellin et al. (1995)).

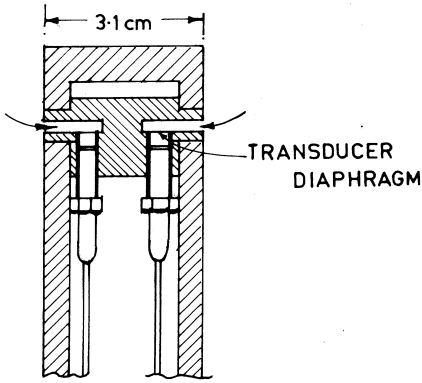

Figure 4 Mounted pressure inducers.

It is worth mentioning that identical results are obtained from both the approaches as borne out by the comparison of results obtained as shown in Table 2, Chapter 20. The measurement of pull-out force on a concrete-lined training wall, conducted by Khatsuria et al. (1992) and employing both of the approaches, also yielded excellent agreement.

Other force measurements generally pertain to the estimation of the hydrodynamic load on sidewalls in a stilling basin (Fletcher et al.–1988) and drag forces on baffle piers (Basco et al.–1971; Gomasta et al.–1977; and Nakato–2000).

Bending Moment

The divide walls in stilling basins and roller buckets are subjected to intense pressure fluctuations on both sides. The resulting net forces cause bending moments that are found to be far stronger than those calculated on the basis of hydrostatic pressures. The three-component force transducer of the type used by Nakato (2000) can be used for measuring the bending moment at the base of the divide wall. However, for obtaining distribution of the bending moment along the height of the wall, a special BM transducer would have to be designed and fabricated, as per the guide lines given by Khatsuria et al. (1994). Details of a typical BM transducer are shown in Figure 5. The transducer operates on the principle of a strain–bending moment relationship at the base of the thin web

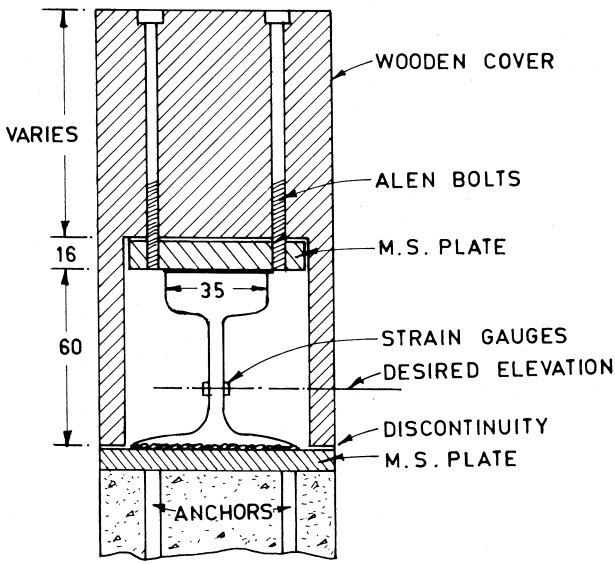

Figure 5 Details of typical BM transducer. (Shown in Khatsuria et al. 1994.)

plate to which the model divide wall is mounted. The strain is measured by affixing four strain gauges in a standard Wheatstone bridge circuit. For the transducer designed by the authors, a deflection of the web plate of about 1 mm (due to bending) gave about 160 microstrains and an output of 8 mV. The natural frequency of the transducer in water should at least be 3 to 4 times the dominant frequency of excitation by flow.

The results of a study conducted for assessment of the hydrodynamic bending moment on a submerged divide wall in a stilling basin have been discussed in Chapter 20.

28.4.2 Analysis of Results

The basic output from the measurement in respect of all the parameters above, will be a time-history record as typically shown in Figure 6.

This in itself conveys little useful information to the designer, except for giving a highest and lowest value of the parameter corresponding to the time of measurement. In order to derive useful inferences, the record must be subjected to further analysis. Statistical analysis of the time-varying phenomena is a powerful tool that enables a designer to decide on a rational design of a structure or its elements.

The various analyses are:

$$p(t) = \overline{p} + p' \tag{21}$$

Where the record is divided into two components: the mean $\overline{p}$ and fluctuating p′. The mean is the time-averaged mean expressed as

$$\overline{p} = \lim t \to \infty \frac{1}{t} \int_0^t p(t)\, dt \tag{22}$$

Where p is a parameter varying with time.

The fluctuating component is defined by standard deviation or root mean square (RMS) as

$$(p')_{rms} = \sqrt{\overline{(p')^2}} = \lim t \to \infty \left[\frac{1}{t} \int_0^t (p')^2\, dt \right]^{1/2} \tag{23}$$

A point, p(t), on the record can be assigned a probability of occurrence, as per the probability distribution plot shown in Figure 6. If the distribution is normal or Gaussian, the plot is symmetrical on both the sides with the mean $\overline{p}$ at the center. It could be skew, negative, or positive, as well. A cumulative probability plot can be derived with the y-axis showing the percentage of the probability of exceedance.

Figure 6 shows the results of analysis in terms of period or frequency corresponding to various amplitudes. The autocorrelation function, R(τ), is

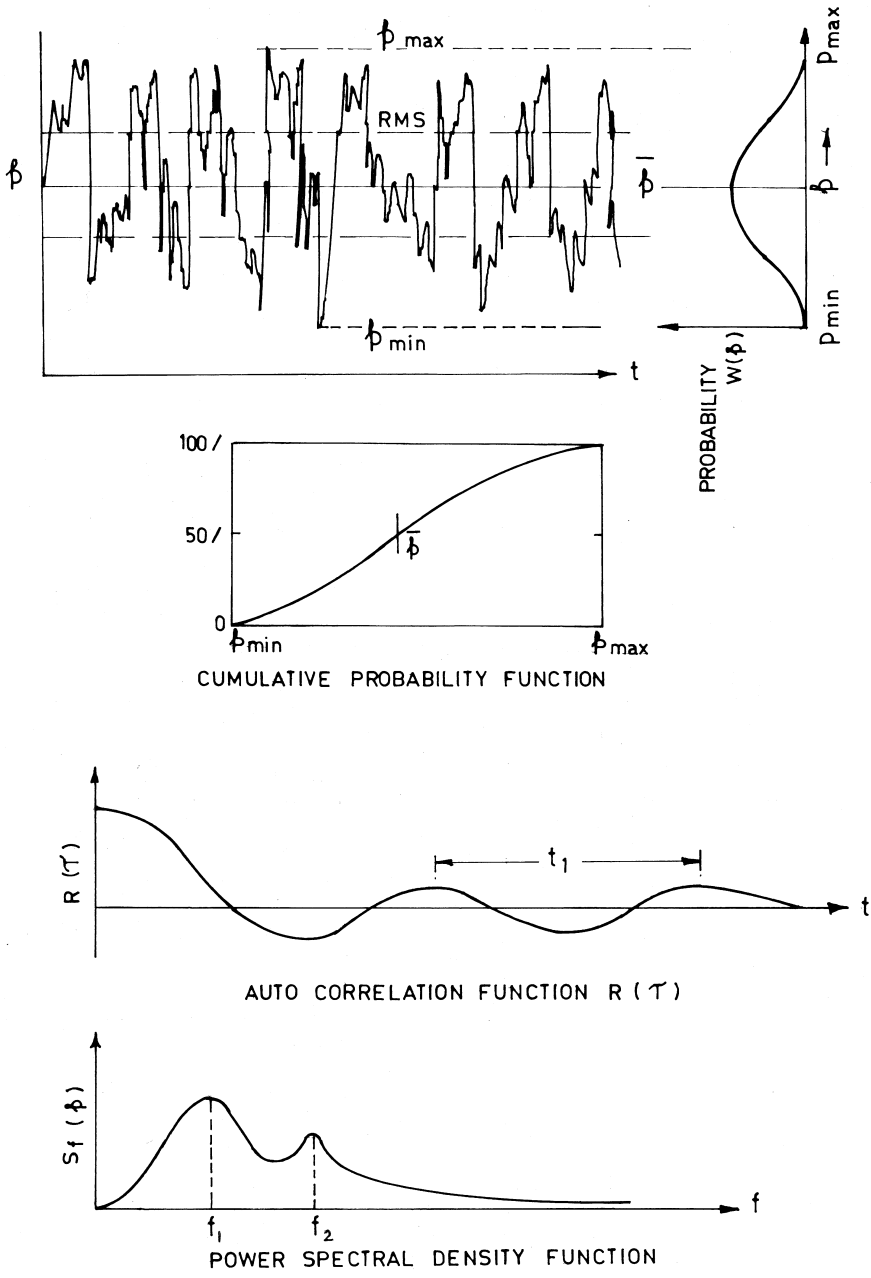

Figure 6 Analysis of time-history record.

$$R(\tau) = \lim t \to \infty \frac{1}{t} \int_0^t p(t).p(t+\tau)\, dt \tag{24}$$

The values of p at instants (t) and (t + τ) are multiplied instant to instant, and the product is averaged. This function, in time domain, indicates the randomness of the time history and points to a dominant period, if any.

The power-spectral density or mean-square spectral-density function,

$$S_f(p) = \left[\overline{(p')_f^2}\right] / \Delta f \tag{25}$$

also shown in Figure 6 represents the distribution of the mean square values of p′ over the frequency domain. This information enables the dominant frequencies of flow excitation and the corresponding amplitudes to be determined. Whether a structure would be subjected to resonant vibration can be determined by comparing the flow excitation frequency with the natural frequency of the structure as per standard formulas.

The spatial correlation of pressure/forces exerted on two points at distance, e, apart is expressed in terms of correlation coefficient R (e):

$$R(e) = \frac{\lim t \to \infty \frac{1}{t} \int_0^t (p'_z.p'_{(z+e)})\, dt}{[(p'_z)]_{RMS}.[(p'_{(z+e)})]_{RMS}} \tag{26}$$

As shown in Figure 7.

Correlation coefficient R(e) is the measure of the degree of association or correlation between the instantaneous values of a parameter at two points. It takes values between −1 and +1. A value of +1 represents a state of perfect correlation, −1 represents reverse correlation, and 0 represents no correlation at all.

All the analyses described previously can be performed conveniently with the standard, commercially available software packages.

28.4.3 Interpretation of Results

There are no standard methods for deriving useful and directly applicable inferences from the results of the analyses discussed earlier. Much depends on the requirement of the designer and his experience. The following case studies are presented here to show typical applications of the analysis.

Figure 8 shows the typical output of the measurement of a hydrodynamic bending moment on a divide wall. The hydrostatic bending moment calculated was 6700 kNm/m, whereas the hydrodynamic part varied from 14805 to 18986 kNm/m. The positive and negative signs have only directional sense, as indicated in Figure 8. The time-averaged mean was merely 1200 kNm/m. The question was—for what value of the bending moment, should the divide wall be designed?

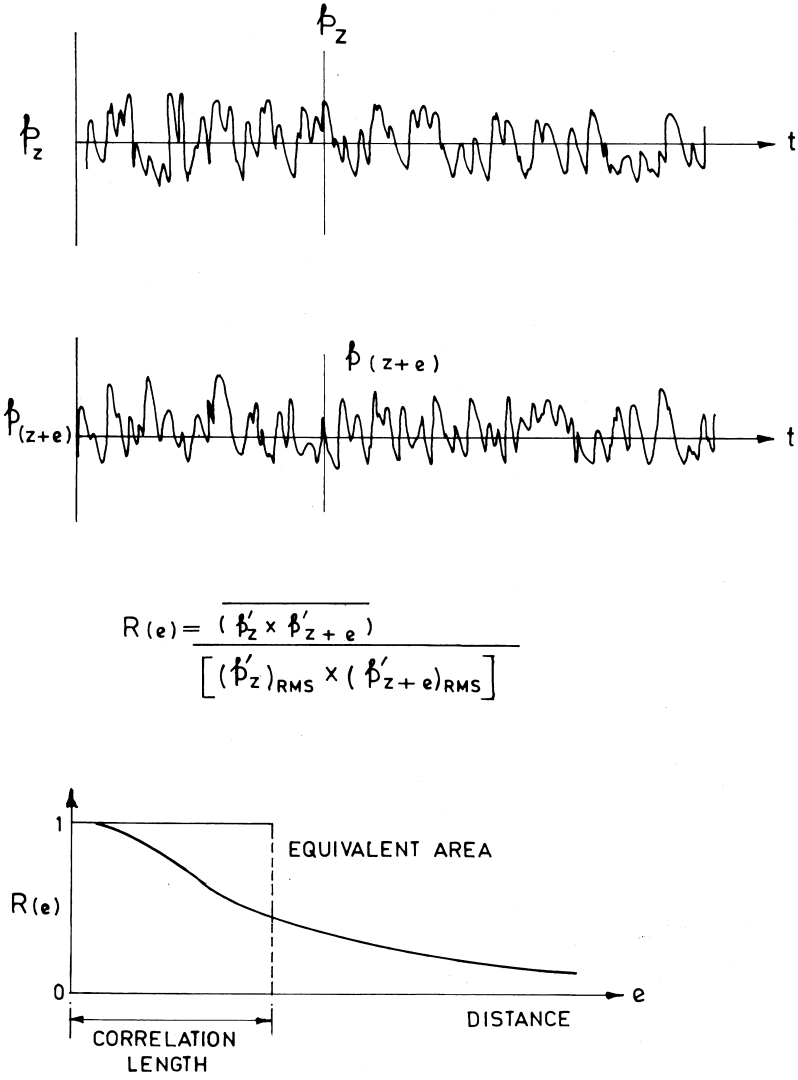

Figure 7 Correlation function.

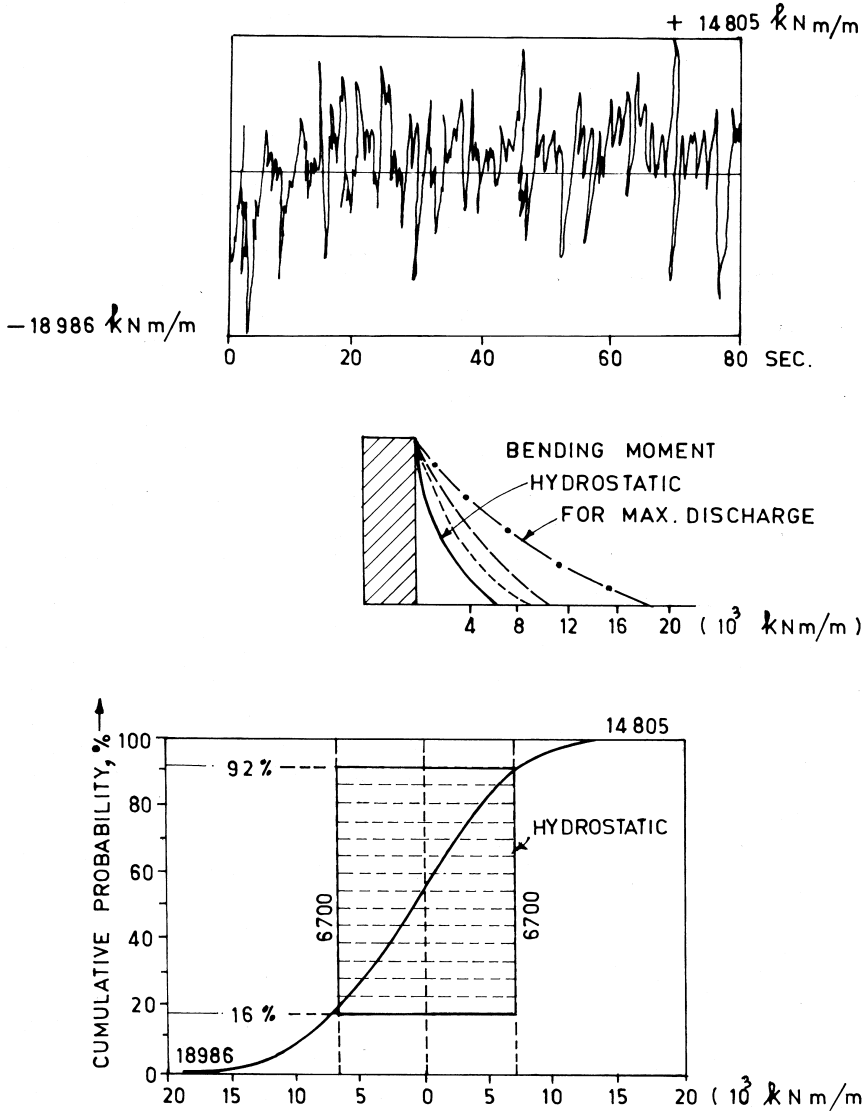

Figure 8 Cumulative probability distribution of hydrodynamic bending moment.

Obviously designing the divide wall for the hydrostatic value would be unsafe, as this value has been exceeded nearly 200%. On the other hand, designing for the maximum value of 18986 kNm/m, which occurs only for a fraction of a time, would result in a very conservative and expensive design. The analysis in terms of cumulative probability distribution is shown in Figure 8. It will be shown that the total time, the probability of the exerted bending moment exceeding the hydrostatic value of 6700 kNm/m, was about 24%. The designer took a comprehensive view of this information, along with the probability of different floods and reduction in the factor of safety, etc., to arrive at a design value.

The lip of a solid roller bucket was 16 m higher than the bucket invert. In order to assess the flow forces exerted on the lip, instantaneous pressures were recorded at two locations on the upstream face of the lip and two locations on

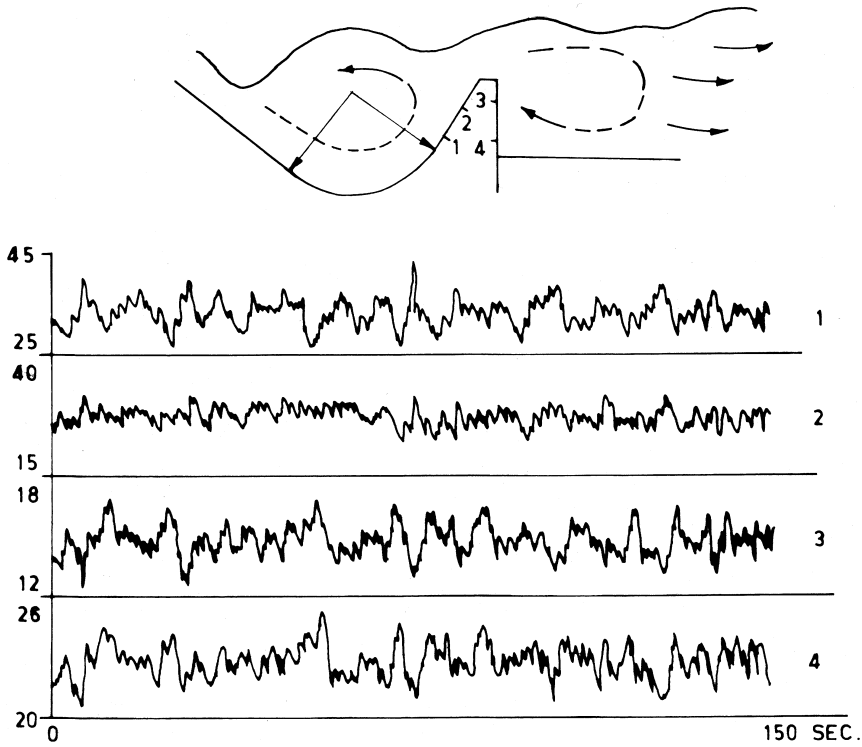

Figure 9 Application of correlation analysis.
R(1–2) 0.05 to 0.64, R(1–3) −0.34 to −0.57, R(1–4) −0.26 to −0.53
R(2–3) −0.03 to −0.30, R(2–4) 0 to −0.33, R(3–4) 0.94 to 0.96

the downstream face of the lip. The results are shown in Figure 9. This method would have required direct measurement of force or pressure distribution at a number of points and their correlation analysis on both the faces. However, this was not possible, given the size of the model. The pressure records were analyzed in terms of correlation coefficients between various pairs of locations. The results are also shown in Figure 9. It was indicated that the pressures on the opposite sides had negative correlations. This means that high pressure peaks on one side would occur at the instances when there are low pressure peaks on the opposite side. The structural design of the lip was based on the pressure differentials worked out on the basis of the above indications.

Notations

B = Bending stiffness number
D = Diameter of conduit
D = Grain size
Thickness of jet
E = Modulus of elasticity
E_u = Euler number
F = Froude number
f = Friction factor
h_a = Head over the siphon crest
h_f = Head loss
I = Moment of inertia
k_a = Stiffness factor
k_s = Equivalent sand grain roughness
L = Characteristic length
M = Mach number
n = Manning's roughness factor
p = Pressure
p_a = Atmospheric pressur
$\overline{p}$ = Mean pressure
p' = Fluctuating pressure
p_v = Vapour pressur
q_a = Air discharge
q_w = Water discharge
R = Hydraulic radius
R_e = Reynolds number
$R(\tau)$ = Auto correlation function
S = Structural merit number
Slope
S_f = Friction gradient

$S_f(p)$ = Power spectral density function
t = Time
Thickness of rubber fabric
V = Velocity
V_1 = Jet velocity
V_0 = Minimum velocity for air entrainment
V_{br} = Bubble rise velocity
W = Weber number
Y = Depth of flow
B = Ratio q_a/q_w
ΔH = Energy loss
Δh = Head difference
Δp = Pressure differential
δ^* = Boundary layer displacement thickness
Γ = Poisson constant
γ = Unit weight of water
γ_s = Unit weight of sediment
ρ = Density of water
μ = Dynamic viscosity of water
σ = Surface tension
ν = Kinematic viscosity of water

REFERENCES

1. Basco, D. R.; Adams, J. R. Drag forces on baffle blocks in hydraulic jump, ASCE. Jnl. of Hyd. Div., Dec. 1971, 97.
2. Bellin, A.; Fiorotto, V. Direct dynamic force measurement on slabs in spillway stilling basins, ASCE. Jnl. of Hyd. Div., Oct. 1995, 121(No.10).
3. Bruschin, J. Forced aeration of high velocity flows. Jnl of Hyd Research, IAHR, 1987, 25(No 1).
4. Casteleyn, J. A.; Kolkman, P. A. Air entrainment in siphons: Results of tests in two scale models and attempt at extrapolation – Proc. 17th Congress IAHR. Baden-Baden, 1977.
5. Damle, P. M. Role of hydraulic models in determining spillway profiles for low dams and anicuts, Symp on Role of models in the evolution of hydraulic structures and movement of sediment, CBIP. New Delhi, 1952.
6. Ervine, D. A.; Elsawy, E. M. Some scale effects in modelling air-regulated siphon spillways, Symp. on Design and operation of siphons and siphon spillways, BHRA, May 1975.
7. Farhaudi, J.; Narayanan, R. Force on slab beneath hydraulic jump, ASCE. Jnl. of Hyd. Engg., 117(1).
8. Fattor, C. A.; Lopardo, M. C.; Casado, J. M.; Lopardo, R. A. Cavitation by macroturbulent pressure fluctuations in hydraulic jump stilling basins, 29th IAHR Congress. Beijing, 2001.

9. Fletcher, B. P.; Saunders, P. E. Dynamic loading on sidewall monoliths of spillway stilling basins, Tech. Report HL-88-10, USWES.
10. Gaikwad, S. R.; Kumthekar, M. J.; Khatsuria, R. M.; Khurjekar, M. J.; Deolalikar, P. B.; Bhosekar, V. V. Consideration of macro-turbulent pressure fluctuations in design of divide walls of stilling basins – Intnl. Symp. on New Techniques in model testing in hydraulic research, CBIP, held at CWPRS. Pune.
11. Gomasta, S. K.; Mittal, M. K.; Pande, P. K. Hydrodynamic forces on baffle blocks in hydraulic jump, 17th Congress, IAHR, 1977, 4, C-56.
12. Jongeling, T. H. G.; Rovekamp, N. H. Wave induced response of inflatable barrier, 28th IHHR Congress, TUGRAZ, 1999.
13. Kells, J. A.; Smith, C. D. Reduction of cavitation on spillways by induced air entrainment, Canadian. Journal of Civ Engg, 1991, 18.
14. Khatsuria, R. M.; Deolalikar, P. B.; Bhosekar, V. V. Pull out forces on a concrete lined training wall in a stilling basin, 8th APD-IAHR Congress. Pune, 1992.
15. Khatsuria, R. M.; Deolalikar, P. B. Considerations on measurement of hydrodynamic bending moments on models of hydraulic structures, Proc. Ninth APD-IAHR Congress, August 1994.
16. Kobus, H. Local air entrainment and detrainment, Proc IAHR Symp on Scale effect in modeling hydraulic structures, Esslingen am Necker, 1984.
17. Lopardo, R. A.; De Lio, J. C.; Vernet, G. F. Model-prototype comparisons on pressure fluctuations in hydraulic jump energy dissipators, ibdi.
18. Nakato, T. Model tests of hydraulic performance of Pit 6 dam stilling basin, ASCE. Jnl. of Hyd. Engg, Sept. 2000, 126(No.9).
19. Pinto, N. L. D. S.; Neidert, S. H. Model prototype conformity in aerated spillway flow, Intnl Conf on Hydraulic Modelling of Civil Engineering Structures, BHRA, 1982.
20. Sakhuja, V. S.; Paul, T. C.; Singh, S. Air entrainment distortion in free surface flows, Proc IAHR Symp on Scale effect in modeling hydraulic structures,Esslingen am Necker, 1984.
21. Vischer, D.; Volkart, P.; Sigenthaler, G. Hydraulic modelling of air slots in open chute spillways, Intnl Conf on Hyd Modelling of Civ Engg Structures, BHRA, 1982.
22. Zagustin, K.; Mantellini, T. Some experience on the relationship between a model and prototype for flow aeration in spillways, Intnl Conf on Hyd Modelling of Civ Engg Structures, BHRA, 1982.

Index

about the book. . .

An unsurpassed treatise on the state-of-the-science in the research and design of spillways and energy dissipators, this reference compiles a vast amount of information and advancements from recent conferences and congresses devoted to the subject—highlighting developments in theory and practice and emphasizing topics related to scale effect, dynamic flow measurement, and the analysis and interpretation of model results.

Consolidates and compares the available information on various design approaches, procedures, and structure types to benefit practicing engineers.

Reflecting the author's nearly four decades of experience in the field, this handbook provides four broad sections on spillway design, flood estimation and selection, various types of spillways and energy dissipators, and topics of special interest…offers valuable case studies and illustrative examples to effectively highlight key topics in the text…includes chapters on crucial design elements such as cavitation, air entrainment, and aerators…and contains extensive discussions of spillway construction stages, dual purpose spillways, overtopping protection of earth dams used as spillways, unlined spillways, fuse plugs and fuse gate spillways, air entrainment and forced aeration, and protection against detrimental forces such as cavitation, uplift, and scour.

about the author. . .

R. M. KHATSURIA served as Additional Director, Central Water and Power Research Station, Pune, India, until his retirement in 2001. He joined the Central Water and Power Research Station in 1963 and was engaged in the research and design of hydraulic structures, based on hydraulic model studies. His special interests include spillways, energy dissipators, control and conveyance structures, and hydropower structures. He has completed nearly 150 projects pertaining to the above disciplines and has authored a number of technical papers and professional reports. He contributed towards the field standardization of overflow, non-overflow, and hydropower structures. He also served as the Senior Expert for WAPCOS (India) Ltd. (1989–90) for the planning and commissioning of the HLAB (hydraulics laboratory) at Al Taji, Baghdad, Iraq. He received the B.E. (1963) degree from Gujarat University, India, the M.E. (1975) degree from the University of Pune, India, and the M.S. (1981) degree from the University of Iowa, Iowa City.

Printed in the United States of America

DK1222

ISBN 0-8247-5789-0

90000

9 780824 757892

MARCEL DEKKER
NEW YORK